
GLASS SCIENCE

Second Edition

ROBERT H. DOREMUS

Rensselaer Polytechnic Institute



A Wiley-Interscience Publication

John Wiley & Sons Inc.

New York / Chichester / Brisbane / Toronto / Singapore

This text is printed on acid-free paper.

Copyright © 1994 by John Wiley & Sons, Inc.

All rights reserved. Published simultaneously in Canada.

Reproduction or translation of any part of this work beyond that permitted by Section 107 or 108 of the 1976 United States Copyright Act without the permission of the copyright owner is unlawful. Requests for permission or further information should be addressed to the Permissions Department, John Wiley & Sons, Inc., 605 Third Avenue, New York, NY 10158-0012.

Library of Congress Cataloging in Publication Data:

Doremus, R. H.

Glass science / by R. H. Doremus. -- 2nd ed.

p. cm.

Includes bibliographical references.

ISBN 0-471-89174-6

1. Glass. 2. Glass manufacture. I. Title.

TP857.D67 1994

666'.1--dc20

93-6343

10 9 8 7 6 5 4

Preface

Twenty years ago the first edition of *Glass Science* summarized the recent advances in the highly active field of amorphous solids, as well as the basics on the structure and properties of these materials. In the intervening years there has been much active research on glasses; perhaps this research can be considered as a consolidation of the rapid increases in knowledge reported in the first edition.

The purpose of this revision of *Glass Science* is to incorporate this expanding body of understanding into the base subject matter of the first edition. Certain areas have been particularly active recently, and are emphasized in the revision; among them are structure, chemical durability, and new processing methods.

As for the first edition, this volume is designed for several different audiences: as a reference source for students and glass technologists; as a stimulus to research workers in glass science; and as a textbook for advanced undergraduate and graduate students.

The advice of Professor Minoru Tomozawa, who has taught a course in Glass for many years with this book, is gratefully acknowledged, as well as his stimulating discussions on research on glass. I have also benefitted from interactions with numerous colleagues, especially members of the Glass Research Center at Rensselaer, Professors MacCrone, Moynihan, Schroeder, and Watson.

Mrs. Kathleen Curtice has dedicated much time and effort to preparing this manuscript for the printer, and her help is most appreciated.

CONTENTS

1	INTRODUCTION	1
	History of Glass Science / 2	
	Uses of Glass and Important Commercial Compositions / 4	
	Melting and Processing / 5	
	Books, Reviews and Journals / 10	
	Outline of the Book / 10	
	References / 11	
2	GLASS FORMATION	13
	Crystallization and Glass Formation / 16	
	Formation of Glasses from Simple Organic Liquids / 20	
	Glass Formation in Oxides / 20	
	Glass Formation and Material Properties / 22	
	References / 22	
3	STRUCTURE	25
	Ranges of Structural Order / 25	
	Experimental Methods / 28	
	Computer Simulation / 29	
	Specific Systems / 30	
	References / 44	

4	PHASE SEPARATION	48
	Phase Diagrams / 50	
	Theories of Immiscibility / 56	
	Nucleation / 60	
	Growth / 66	
	Morphology and Spinodal Decomposition / 67	
	Property Changes and Applications Related to Phase Separation / 69	
	References / 70	
5	CRYSTALLIZATION	73
	Nucleation / 75	
	Experimental Measurements of Nucleation and Growth Rates / 78	
	Nucleating Agents / 85	
	Morphology / 88	
	Growth / 89	
	Fluoride Glasses / 94	
	References / 96	
6	VISCOSITY	99
	Measurement / 101	
	Simple Glass-forming Oxides / 102	
	Multicomponent Oxides / 105	
	Nonoxide Glasses / 106	
	Temperature Dependence / 106	
	Theories / 109	
	References / 111	
7	GLASS TRANSITION	113
	Structural and Strain Relaxation / 116	
	References / 120	
8	MOLECULAR SOLUTION AND DIFFUSION IN GLASS	122
	Molecular Solubility of Gases / 122	
	Measurement of Molecular Permeation and Diffusion in Glass / 130	
	Effect of Temperature, Pressure, and Molecular Size on Molecular Diffusion in Glass / 132	

Molecular Diffusion and Chemical Reaction /	135
Effect of Glass Composition on Molecular Diffusion /	139
Diffusion from Contracting Bubbles /	142
Oxidation of Silicon /	144
Theories for Molecular Diffusion /	145
References /	147

9 FRACTURE 150

Experimental Results /	150
Fracture Criteria, Models, and Explanations /	160
References /	169

10 FATIGUE IN GLASS 172

Methods of Testing /	172
Results of Static Fatigue Tests on Glass /	173
Statistics of Fatigue /	177
Life Prediction /	178
Theories of Fatigue /	180
References /	183

11 SURFACES 184

Surface Energy /	184
Surface Structure /	185
Experimental Techniques /	189
Physical Adsorption /	190
Chemisorption and Surface Chemical Reactions /	192
Surface Conductivity /	194
Grinding and Polishing of Glass Surfaces /	194
References /	195

12 REACTIONS WITH GASES 198

Water /	198
Hydrogen /	201
Oxygen /	202
Carbon Dioxide /	208
Sulfur Dioxide /	208
Fining /	209
References /	212

13	CHEMICAL DURABILITY: REACTION OF WATER WITH GLASS	215
	Introduction / 215	
	Measuring Methods / 216	
	Experimental Results / 220	
	Interpretations / 232	
	Dissolution / 234	
	Influence of Reaction Layers on Kinetics / 235	
	Radioactive Waste Disposal / 236	
	Zirconium Fluoride Glass / 237	
	References / 237	
14	ION EXCHANGE AND POTENTIALS OF GLASS ELECTRODES	241
	Measurement of Ionic Distribution / 241	
	Experimental Results on Distribution Coefficients / 244	
	Selectivity Theories / 249	
	Potentials of Glass Electrodes / 252	
	Experimental Measurements of Potentials of Glass Electrodes / 256	
	Experimental Confirmation of Potential Equations / 257	
	References / 260	
15	ELECTRICAL CONDUCTIVITY AND IONIC DIFFUSION	263
	Measurement of Electrical Conductivity and Ionic Diffusion / 256	
	Relation Between Electrical Conductivity and Ionic Diffusion / 269	
	Dependence of Ionic Transport on Temperature and Pressure (Stress) / 271	
	Effect of Glass Composition on Ionic Transport / 277	
	Interionic Diffusion and Ion Size Effects / 279	
	Glasses with High Electrical Conductivity ("Fast Ion Conductors") / 283	
	Theories of Ionic Transport / 284	
	Conduction in High Fields / 285	
	References / 287	
16	DIELECTRIC AND MECHANICAL LOSS	291
	Experimental Measurement of Dielectric Loss / 291	

Effect of Frequency on Dielectric Loss /	293
Effect of Temperature on Dielectric Loss /	295
Effect of Composition on Dielectric Loss /	296
Measurement of Mechanical Loss /	297
Effect of Frequency and Temperature on Mechanical Loss /	298
Effect of Glass Composition on Mechanical Loss /	300
Theories of Dielectric and Mechanical Loss in Glass /	301
References /	303

17 OPTICAL ABSORPTION IN GLASSES **306**

Fused Silica /	307
Other Network-Forming Oxides /	310
Glasses Containing Alkali Oxide /	311
Transition Metal Ions /	313
Other Glasses and Ions /	314
Metallic Particles /	314
New Application of Glass in Optics /	315
References /	317

AUTHOR INDEX **321**

SUBJECT INDEX **335**

CHAPTER 1

INTRODUCTION

Glass is an amorphous solid. A material is amorphous when it has no long-range order, that is, when there is no regularity in the arrangement of its molecular constituents on a scale larger than a few times the size of these groups. For example, the average distance between silicon atoms in vitreous silica (SiO_2) is about 3.6\AA , and there is no order between these atoms at distances above about 10\AA . A solid is a rigid material; it does not flow when it is subjected to moderate forces. More quantitatively, a solid can be defined as a material with a viscosity of more than about 10^{15}P (poises).

Many glass technologists object to the above definition of a glass. These workers prepare a glass by cooling a liquid in such a way that it does not crystallize, and feel that this process is an essential characteristic of a glass. Many earlier writers insist on this criterion: "A glass . . . is a material, formed by cooling from the normal liquid state, which has shown no discontinuous change . . . at any temperature, but has become more or less rigid through a progressive increase in its viscosity," according to Jones (Ref. 1, p. 1), or, more succinctly, "glass is an inorganic product of fusion which has been cooled to a rigid condition without crystallization" as taken from the *ASTM Standards for Glass*. The difficulty with this view is that glasses can be prepared without cooling from the liquid state. Glass coatings are deposited from the vapor or liquid solution, sometimes with chemical reactions. Thus sodium silicate glass can be made by evaporating an aqueous solution of sodium silicate (water glass) and baking the deposit to remove water. The product of this process is indistinguishable from sodium silicate glass of the same composition made by cooling from the liquid. It seems wise to use the same name for materials with the same molecular structure and properties no matter how they are made;

consequently, the broader definition given here is preferred. Hutchins and Harrington² and Prins^{2a} use a similar definition.

Traditional glasses have been made of inorganic materials such as silica sand, sodium and calcium carbonates, feldspars, borates, and phosphates that react to form metallic oxides in the final glass. In recent years "glassy" polymers have been widely used and they are often called glasses in the technical literature, but there is little use of this term in everyday language. The ASTM definition of glass given above limits it to inorganic constituents, whereas Jones' definition does not. The present definition includes newer and more exotic materials such as "splat-cooled" metallic glasses, the electronically conducting glasses of the arsenic, sulfur, selenium, and tellurium halide families, and glasses of ionic salts and aqueous solutions, as well as oxide glasses and glassy organic polymers.

The word "glass" is derived from an Indo-European root meaning "shiny," which has also given us the words glare, glow, and glaze. The word "vitreous" comes from the Latin word for glass. No distinction is made here between the words glassy and vitreous.

The structure and properties of silicate glasses are emphasized in this book because these glasses are the most important commercially and have been studied more extensively than other types. In Chapters 2 and 3 an attempt is made to include information on the formation and structure of many types of glasses known at the time of writing. In the succeeding chapters, data on nonoxide glasses are included when this information is available and helps in understanding, or is of particular interest.

HISTORY OF GLASS SCIENCE

The history of glass is summarized in articles in the *Encyclopedia Britannica* and by Morey (Ref. 3, pp. 1 ff.). Natural glasses have been used by man from the earliest times for which there is archeological evidence. Glass and glazes were manufactured far back in human history. According to Sir W. M. Flinders Petrie, as quoted by Morey (Ref. 3, p. 4), the earliest known glaze dates from about 12,000 B.C. and the earliest pure glass from about 7000 B.C.; both were found in Egypt, and were probably brought there from Asia. At first glass was used only for decorative objects, but later it was molded or pressed into vessels. The invention of glass blowing in about the first century B.C. greatly increased the use of glass for practical purposes in Roman times, mainly for vessels but later for windows. In the West, glass manufacturing was dispersed to isolated sites after the fall of the Roman Empire, but was continued in Byzantium and later in the Middle East by the Arabs. Venice became the center of a resurgent glass industry in the West from about 1300 on. The art of glass making was summarized in 1612 by Neri in *L'Arte Vetraria*. Progress in techniques of glass manufacture and in the application of glass was subsequently rapid, in parallel

with many other areas of technology. Until the twentieth century most of these advances were made empirically, using common sense to guide experimentation. The application of basic scientific understanding to the improvement of manufacture and to new applications of glass has occurred only in the last few decades

Among the first to study glass in a more basic way was Michael Faraday. He described glass "rather as a solution of different substances one in another than as a strong chemical compound"⁴ which can still stand today as a characterization of a multicomponent glass. Faraday studied the electrolysis and conductivity of melts of various glasses,⁵ and found that some "decomposed" under the effect of a field and others did not. Apparently the glasses with higher conductivity or with easily reduced components were the ones that decomposed. Faraday was also the first to conclude correctly that the red color of a gold ruby glass was caused by very small gold particles in the glass,⁶ as described in Chapter 17. Also in the midnineteenth century, Buff studied the conductivity and electrolysis of glass,⁷ and later Warburg and Tegetmeier^{8,9} showed that the electrolysis of glass followed Faraday's law. About this time, Tammann initiated work on the viscosity of glass, the glass transition, the relationship of crystallization rate and viscosity, and the reasons for glass formation.¹⁰ Schulz¹¹ made a detailed study of exchange and diffusion of silver ions for sodium ions in a commercial glass that was unsurpassed until the last few years.

The understanding of glass strength received its greatest impetus from the theory of Griffith,¹² in which the fracture of a brittle solid results from the propagation of a surface flaw. At first this theory was considered by some to be a mathematical curiosity without application to real materials, but more recently it has provided the basis for much work and improved understanding of the strength of glass, as discussed in Chapter 9.

The Department of Glass Technology at Sheffield, England, under Professor W. E. S. Turner, was very active during the 1920s in measuring such properties as density, electric conductivity, chemical durability, viscosity, and thermal expansion of a wide variety of commercial and laboratory glasses.

In the 1930s the understanding of the reasons why certain molecules are glass formers, and of the structure of glass, was enlarged by the papers of Zachariasen¹³ and Warren.¹⁴ Since World War II the activity in glass science has grown sharply, along with all science and technology. The 1950s might be characterized as the "golden age" of metallurgical science. At that time physics and chemistry were intensively applied to the understanding of metallic behavior that had been found empirically and was previously understood only in terms of macroscopic phenomena. In a similar way, the 1960s could be described as a "golden age" of glass science because of the profitable application during this period of the basic science to understanding glass in terms of its structure and composition. It is curious that glass, which was in common use long before many other metals, polymers, colloids, solutions, solvents, and so on, should be one of the last to yield some of its mysteries to scientific

exploration. Perhaps the large variation in compositions and properties in glasses, coupled with the lack of long-range structure in a rigid material, has deterred systematic and broad characterization of glasses.

Some of the areas of glass science that have been most active in the last few years are sol-gel fabrication, zirconium fluoride glasses, optical wave guides, reactions of water with glass, nonlinear optical properties, and laser glass.

This brief survey of the history of glass science is not intended to be exhaustive, and many deserving names and studies have undoubtedly been omitted. The next decades should see a continued expansion of knowledge about glass and its useful application.

USES OF GLASS AND IMPORTANT COMMERCIAL COMPOSITIONS

The original use of glass was for decorative purposes. Next glass was used for containers, and this use is still the most important today. The production of flat glass, chiefly for windows in buildings and vehicles, is now the second largest item of glass manufacture. Lamp envelopes are another major area of use. There are many special applications of glass, some in small quantity, most of which have been developed over the past few decades. Some of these special applications are glass ceramics and surface-strengthened glass for higher strength, fiber glass, mirror blanks of fused silica, glass electrodes for alkali ions, and glass lasers. A good summary of uses of glass is given by Hutchins and Harrington.²

The most important commercial glasses are based on sodium calcium silicates. These glasses are cheap and weather well; they are easily melted and formed. Minor additions to the base compositions are made to improve certain properties: alumina for improved weathering and less devitrification (crystallization), borates for easier working and lower thermal expansion, and arsenic or antimony oxide for fining (removal of bubbles). Another important class of compositions is the borosilicates. They have lower thermal expansion and thus better thermal shock resistance, as well as improved chemical durability, for such applications as automobile headlamps, cookware, and laboratory apparatus. Aluminosilicate glasses are used for chemical durability, resistance to devitrification, higher temperatures, and greater strength in cookware, glass ceramics, fiber glass, and seals. Lead glasses are used for their high refractive index, easier working, and greater density as lamp envelopes, seals, optical glass, and "crystal" glass for art and tableware. Fused silica is especially valuable for its high-temperature stability, low thermal expansion and consequent high thermal-shock resistance, excellent chemical durability, purity, and good optical transmission in the ultraviolet. It is used for lamp envelopes, crucibles for melting silicon and germanium, optical components, and many special applications requiring its unique properties.

A vast number of other compositions, including nonsilicate glasses, has been

made for all sorts of applications. The infinite variability of glass compositions leads to a great variety of possible properties and consequent uses. Only a beginning has been made in exploiting this advantage of glass.

The compositions and properties of some of the most commonly used commercial silicate glasses are given in Table 1. Impurity concentrations and methods of making different types of vitreous silica (SiO_2) are given in Table 2. Tables of compositions and properties of commercial glasses, as well as binary and ternary silicate glasses, are given in Ref. 15.

MELTING AND PROCESSING

Melting

Raw materials for making silicate glasses are quartz sand, sodium carbonate or nitrate, calcium and magnesium carbonate, and oxides such as alumina, lead oxide, sodium borate, zinc oxide, and arsenic and antimony oxides. These materials have traditionally been mined directly, with little or no purification, so were cheap but of variable impurity content. Some deposits of quartz crystal and quartz sand are probably the purest of naturally occurring materials, having total impurity content less than about 100 parts per million by weight.

Glass has traditionally been melted in a "batch" in a pot or crucible of refractory ceramic material. Raw materials are mixed to the desired composition and either heated in the crucible or added to already molten glass. The low melting constituents (alkali oxides) melt and dissolve the higher melting constituents such as quartz and alumina.

Quantity production of glass, especially soda-lime and borosilicate compositions, is continuous in a large "tank" or furnace made of special refractory brick; a characteristic tank is 15×25 m in size, with glass 1.5 m deep, giving a daily production of as much as 700 metric tons of glass. The tank is heated by combustion of oil or natural gas across the glass surface. Melting temperatures are about $1200\text{--}1300^\circ\text{C}$. The furnace is separated into two positions by a refractory "wall" over which glass flows. The mixed raw materials are fed onto the top of the molten glass in the melting chamber; the molten glass flows across the wall into the refining chamber, in which the glass becomes more homogeneous and bubbles are removed.

In the refining chamber, the glass is "fined" by the removal of bubbles. The bubbles contain trapped air (oxygen and nitrogen) and decomposition products of the raw materials, mainly carbon dioxide. Large bubbles rise to the top of the melt, but most bubbles are too small to be removed in this way; the gases in them must dissolve in the melt to collapse the bubbles. This dissolution is aided by fining agents added to the glass batch. Arsenic and antimony oxides are common fining agents. They have two oxidation states, and increase dissolution rates of gases by changing the oxidation state of the melt. Sulfates

TABLE 1 Properties, Compositions, and uses of Important Commercial Silicate Glasses

Glass Type	Corning Number	Kimble Number	Approximate Composition (wt. %)								Relative thermal Expansion $10^{-7}/^{\circ}\text{C}$	Density (gms/cm ³)	Refractive index	Uses
			SiO ₂	B ₂ O ₃	Al ₂ O ₃	CaO	MgO	PbO	Na ₂ O	K ₂ O				
Soda lime	0080	R-6	72.6	0.8	1.7	4.6	3.6		15.2		92	2.47	1.51	Windows, lamps
"Pyrex" boro-silicate	7740	KG-33	81.0	13.0	2.0				4.0		33	2.23	1.47	Headlamps, cooking, and labware
Soda boro-silicate	7050	K-705	68.0	24.0	1.0				7.0		46	2.24	1.48	Sealing
Alkali lead	0010	KG-1	77.0			1.0		8	9.0	5.0	93	2.86	1.54	Lamp tubing, sealing
Alkaline earth	1720	EZ-1	64.0	4.5	10.4	8.9	10.2		1.3	0.7	42	2.52	1.53	High temperatures
Alumino-silicate														
"E" Fiber-glass			55.0	7.0	15.0	21.0			1.0	1.0	60	2.61	1.55	Fiberglass

TABLE 2 Different Types of Fused Silica

Type	Method of Manufacture	Maximum Impurity Conc. (ppm)									Manufacturers Designations				
		Al	Fe	Ca	Mg	K	Na	Li	Cl	OH	General Electric	Thermal Syndicate	Heraeus	Corning	Quartz et Silice
I	Electrical fusion of quartz crystal	150	7	12	7	4	12	12	≈ 50	4	101 204 125	IR Vitreosil	Infrasil		Pursil
II	Flame fusion of quartz crystal	uncertain										OG Vitreosil	Herosil Homosil Vitrasil		
III	Flame hydrolysis of SiCl ₄	10	6	4	3	2	2	I	60	1200*	151	Spectrosil	Suprasil I	7940	Tetrasil
IV	Vapor phase oxidation of SiCl ₄	similar to III													
									500	low		Spectrosil WF	Suprasil W	7943	

*Lower values of impurity concentrations are frequently quoted, but are questionable. For alkalis, see Ref. 32.

are also common fining agents; they also function by changing the oxidation state of the melt. The mechanism of fining is discussed in more detail in Chapter 12.

There is an article on glass melting in Ref. 16, p. 1986, by A. R. Cooper.

The rate of dissolution of silica in molten alkali silicate probably controls the overall rate of melting of silicate glasses. See p. 240 in the first edition of this book and Ref. 17 for discussions and additional references. The dissolution of other oxides in oxide melts is also usually controlled by transport in the melt, although there can also be a surface reaction that forms a new phase on the solid surface.¹⁷

Forming

Glass containers are formed from glass that flows out of the continuous furnace. A "gob" or portion of glass is placed in a mold where a first shape is formed by pressing or blowing. This initial shape is removed from the mold, reheated, and then placed in a second mold in which the final shape is blown. The continuous machine (IS or Individual Section machine) on which these steps are done rapidly produces a very large number of units; a usual cycle time for one container is 10–15s.

Lamp bulbs are made by blowing into a ribbon of glass emitting from the furnace on a "ribbon machine". Again a high rate of units is produced, up to 2000/min. A special nozzle blows glass in the ribbon into a mold.

Glass objects such as plates, tumblers and vases can be made by pressing molten glass in a mold with a metallic plunger. Patterns on the mold surface are imprinted into the glass and make it look more expensive than it is.

More than 100 years ago, window glass was made by hand by either the crown or cylinder processes. In the crown process, a glob of glass was blown into a sphere and one side flattened by pressing it against a plate. An iron rod was attached to the flat part and the blow pipe removed. The globe was then spun into a flat disc from which panes could be cut. In the cylinder process, the glass was formed into a large cylinder, which was split open and flattened.

Later, sheet glass was drawn directly from the melting surface, flowed through rollers, and then ground and polished. These processes are expensive. A new method of making more inexpensive flat glass of high quality was developed by Alistair Pilkington of the Pilkington Glass Company in England. In this float process, a continuous strip of glass from the melting furnace floats onto the surface of a molten metal, usually tin, at a carefully controlled temperature. The flat surface of the molten metal gives a smooth, undistorted surface to the glass as it cools. This process is continuous, and high production speeds are possible. Today most flat glass is made by this method.

There is an article on forming of glass in Ref. 16, p. 1818, by R. J. Ryder.

Fiber Glass

Glass fibers are finding increasing application in reinforcing polymer-matrix composites ("fiber glass"), which are used in automobile and boat bodies, aircraft, electronic circuit boards, and a variety of other ways. Fiber glass fabrics serve as protective apparel, industrial and decorative fabrics and tire cord. Short fibers are used in thermal insulation. A typical fiber glass composition is given in Table 1.

In making continuous fiber glass, molten glass from a melting furnace is fed to a drawing apparatus that consists of clusters of many holes called bushings. Each bushing has hundreds of holes or nozzles through which the glass is drawn into fibers of diameter about 10–100 μm . The fibers are cooled by a water spray, and a polymeric coating or "sizing" is applied to protect and lubricate the fibers. Instead of drawing glass directly from the furnace, glass can be cast into spherical "marbles" one or a few centimeters in diameter, which are then melted and fed into the heated bushings.

Short fibers can be formed either directly from glass from the melting furnace or from marbles. The molten glass is fed into a rotating cylinder through a large number of small holes in the walls of the cylinder, and inside the cylinder the glass streams are broken up by an axial high-velocity flow of gas. The short fibers formed in this way are sprayed with binder as they fall onto a collecting belt which carries them through an oven that polymerizes the binder.

There is an article on uses and manufacture of glass fibers in Ref. 16, p. 1974, by S. L. Mikesell and W. W. Wolf.

Sintering and Sol-Gel Methods

Several methods of melting and forming glass have been developed for special applications or properties. Glass powder can be pressed and sintered similar to powders of crystalline ceramics. This is expensive compared to more traditional methods of melting, but can be useful for making high-melting glasses and adding small amounts of desired impurities to them.

Sol-gel methods of glass making are finding increasing application in making highly pure and homogenous glasses or special shapes such as microshells. In one method, a mixture of liquid metal alkoxides is hydrolyzed, polymerized and then dehydrated to form a homogeneous glass at temperatures much below those ordinarily used for glass melting. The hydration and polymerization are carried out in acidic alcohol/water solution at temperatures up to 60°C; then the mixture can be formed or made to bulk gel by heating to somewhat higher temperatures; finally the gel is pyrolyzed and dehydrated by heating at temperatures from 500°C to 1000°C to form glass. Some superior products of this method are: homogeneous multicomponent glasses; composi-

tions hard to form into glasses by direct melting because of incomplete melting and crystallization on cooling; very pure glasses; and composites of glasses with other materials. Low forming temperatures save energy, allow less corrosion-resistant container materials, and allow formation of composites with materials not resistant to higher temperatures.

Special shapes such as fibers and thin films can be made by the sol-gel method. Glass microshells for laser targets have been made by dropping gel particles through a temperature gradient in a furnace tower; the organic compounds and water help to blow the glass into thin-walled shells.

A book by Brinker and Scherer¹⁸ and review article by Sakka¹⁹ give detailed discussions of sol-gel processing of oxides. Proceedings from a symposium are in Ref. 20.

BOOKS, REVIEWS AND JOURNALS

The *Handbook of Glass Properties*¹⁵ has chapters on vitreous silica and commercial glasses, with extensive lists of properties and compositions of commercial and optical glasses. There are short chapters on a wide variety of glass properties, with extensive tables of these properties for binary and ternary oxide glasses. The emphasis in the present volume is a more basic understanding of phenomena, rather than detailed listing and discussion of properties. A series of volumes contain data on properties of glasses taken directly from the original publications.²¹ Some other general books on various aspects of glasses are in Refs. 22–28. Other more specialized monographs are referred to in the appropriate chapters.

There is a series of short articles on many aspects of glass in Ref. 16.

Collections of review articles are in Refs. 29–31. Individual articles from these volumes are referenced in pertinent places.

OUTLINE OF THE BOOK

The following chapters can be grouped into sections on structure and microstructure (Chpts. 2–5), viscosity and structural relaxation (6 and 7), strength (9 and 10), chemical properties (8 and 11–14), electrical properties (15 and 16) and optical properties (17). These sections are a rough guide to classifying the subject matter; there is much overlapping. Areas of work that have been active recently are emphasized. For information and data on properties of glasses that are not discussed, such as density, surface tension, coefficient of thermal expansion, heat capacity, thermal conductivity, elasticity, hardness and refractive index, see Ref. 15. This reference also has more information on experimental techniques to measure properties.

REFERENCES

1. G. O. Jones, *Glass*, Methuen, London, 1956.
2. J. R. Hutchins and R. V. Harrington, in *Encyclopedia of Chemical Technology*, Vol. 1, 2nd edn., Wiley, New York, 1966, p. 533.
- 2a. J. A. Prins, in *Proc. Int. Conf. on Physics of Noncrystalline Solids*, J. A. Prins, Ed., North-Holland, Amsterdam, 1965, p. 1.
3. G. W. Morey, *The Properties of Glass*, edn., Reinhold, New York, 1954.
4. M. Faraday, *Philos. Trans. Roy. Soc.*, **49** (1830).
5. M. Faraday, *Experimental Researches in Electricity*, reprinted by J. M. Dent, London, 1914, pp. 38 and 115.
6. M. Faraday, *Philos. Mag.*, **14**, 401, 512 (1857).
7. H. Buff, *Liepzig Ann.*, **90**, 257 (1854).
8. E. Warburg, *Ann. Phys.*, **21**, 622 (1884).
9. E. Warburg and F. Tegetmeier, *Ann. Phys.*, **35**, 455 (1888).
10. G. Tammann, *Der Glaszustand*, Voss, Leipzig, 1933.
11. F. Schulze, *Ann. Phys. Liepzig*, **40**, 335 (1913).
12. A. A. Griffith, *Philos. Trans. Roy. Soc.*, **221A**, 163 (1921).
13. W. H. Zachariasen, *J. Am. Chem. Soc.*, **54**, 3841 (1932).
14. B. E. Warren and co-workers, *J. Am. Ceram. Soc.*, **17**, 249 (1934); **18**, 239 (1935); **19**, 202 (1936); **21**, 287 (1938).
15. N. P. Bansal and R. H. Doremus, *Handbook of Glass Properties*, Academic Press, San Diego, 1986.
16. M. B. Bever, Ed., *Encyclopedia of Materials Science and Engineering*, Pergamon Press, Oxford, 1986.
17. K. H. Sandhage and G. J. Yurek, *J. Am. Ceram. Soc.*, **73**, 3633, 3643 (1990).
18. C. J. Brinker and G. W. Scherer, *Sol-Gel Science*, Academic Press, San Diego, 1990.
19. S. Sakka, in *Treatise on Materials Science and Technology*, Vol. 22, M. Tomozawa and R. H. Doremus, Eds., Academic Press, San Diego, 1982, p. 129.
20. M. A. Aegerter, Ed., *Glasses and Ceramics from Gels*, *J. Non-Cryst. Solids*, **121**, (1989).
21. O. V. Mazurin, M. V. Strel'sina and J. P. Shvaiko-Shvaikovaskaya, Eds., *Handbook of Glass Data*, Elsevier, Amsterdam. Part A: Vitreous Silica and Binary Silicate Glasses, 1983; Part B: Single-Component and Binary Non-Silicate Oxide Glasses, 1985; Part C: Ternary Silicate Glasses, 1987.
22. C. L. Babcock, *Silicate Glass Technology Methods*, Wiley, New York, 1977.
23. T. S. Izumitani, *Optical Glass*, Kyoritsu Shuppan, Tokyo, 1984.
24. R. W. Douglas and S. Frank, *A History of Glass Making*, Foulis, Henley-on-Thames, 1972.
25. R. Zallen, *The Physics of Amorphous Solids*, Marcel Dekker, New York, 1983.
26. S. R. Elliot, *Physics of Amorphous Materials*, 2nd Edn., Longman, London, 1991.
27. J. Zarzycki, *Les Verres et l'État Vitreux*, Masson, Paris, 1982, see ref. 44, Chap. 3.
28. H. Scholze, *Glass*, Springer-Verlag, New York, 1990.

29. J. D. Mackenzie, Ed., *Modern Aspects of the Vitreous State*, Vols. 1–3, Butterworths, London, 1960, 1962, 1964.
30. M. Tomozawa and R. H. Doremus, Eds., *Treatise on Materials Science and Technology*, Vols. 12, 17, 22, and 26, Academic Press, San Diego, 1977, 1979, 1982, 1985.
31. D. R. Uhlmann and N. J. Kreidl, Eds., *Glass: Science and Technology*, Vols. 1–5, Academic Press, San Diego, 1980–1987.
32. R. H. Doremus, *Phys. Chem. Glasses*, **10**, 28 (1969).

CHAPTER 2

GLASS FORMATION

What materials can be glasses? In principle any substance can be made into a glass by cooling it from the liquid state fast enough to prevent crystallization. The final temperature must be so low that the molecules move too slowly to rearrange to the more stable crystalline form. Alternatively one can imagine building up the material onto a substrate, either by deposition or chemical reaction from the vapor, the substrate being so cold that rearrangement cannot take place. In actual practice, glass formation has been achieved with a relatively limited number of substances. After substances that have been made into glasses are listed, the question of why so few substances are amenable to glass formation is considered in subsequent sections.

Materials that have been made into glasses are listed in Tables 1 and 2. Undoubtedly these lists will be extended as new methods of more rapidly cooling melts and of deposition from vapor or solution are devised. Thus the lists show those materials most easily formed into glasses and are representative rather than exhaustive. Some of the glasses in the tables may contain fine crystals of size 100\AA or less. It is often difficult to be certain that small crystalline regions are absent, even with X-ray or electron diffraction measurements. A material containing crystallites of size from 20 to 100\AA can be mistaken for a glass even though it does not strictly fit the definition of a glass given in Chapter 1. The abstracts section of the *Journal of Physics and Chemistry of Glasses* under Glass Forming Systems and the Glass section of *Ceramic Abstracts*, published by the American Ceramic Society, should be consulted for additional information on new glass-forming systems.

The materials in Table 1 can be placed in several categories. The oxides are by far the most important commercially, as mentioned in the last chapter. Multicomponent oxide glass results from the mixing of other oxides with the

TABLE 1 Glasses Formed by Cooling from the Liquid

	Refs.
Elements	
S, Se	
Te(?)	1, 2
P	1, 3
Oxides	
B ₂ O ₃ , SiO ₂ , GeO ₂ , P ₂ O ₅ , As ₂ O ₃ , Sb ₂ O ₃	
In ₂ O ₃ , Tl ₂ O ₃ , SnO ₂ , PbO ₂ , SeO ₂	4
"Conditional" TeO ₂ , SiO ₂ , MoO ₃ , WO ₃ , Bi ₂ O ₃ ,	
Al ₂ O ₃ , Ba ₂ O ₃ , V ₂ O ₅ , SiO ₃ , Nb ₂ O ₅	1, 5
Sulfides	
As ₂ S ₃ , Sb ₂ S ₃	6
Various compounds of B, Ga, In, Te, Ge, Sn	
N, P, Bi	4, 7
CS ₂	9
B ₂ S ₃ -Li ₂ S, P ₂ S ₅ -Li ₂ S	8
Selenides	
Various compounds of Tl, Sn, Pb, As, Sb, Bi,	
Si, P	4, 10, 11
Tellurides	
Various compounds of Tl, Sn, Pb, As, Sb, Bi, Ge	1, 4
Halides	
ZnCl ₂ , multicomponent chlorides based on ZnCl ₂ ,	
CdCl ₂ , BiCl ₃ and ThCl ₄	1, 4, 14
BeF ₂ , AlF ₃ , ZrF ₄ , HfF ₄ , ScF ₃ , TiF ₄ as glass-	
formers and many other ions as intermediates	
and modifiers	14, 16
AgI-AgF-AlF ₃	17
Sb ₂ S ₃ -Ag ₂ S, Sb ₂ S ₃ -AgI, Sb ₂ S ₃ -Ag ₂ S-AgI	14, 17a
Cu(Cl, Br, I)	
Acetates	
Pb-K acetate, Ca-K acetate	17b
Nitrates	
KNO ₃ -Ca(NO ₃) ₂ and many other binary mixtures containing	
alkali and alkaline earths nitrates	1, 15
Sulfates	
KHSO ₄ and other binary and ternary mixtures	1
Carbonates	
K ₂ CO ₃ -MgCO ₃	1, 18

TABLE 1 (continued)

	Refs.
Simple organic compounds	
O-Terphenyl, toluene, 3-methyl hexane, 2,3-dimethyl ketone, diethyl ether, isobutyl bromide, ethylene glycol, methyl alcohol, ethyl alcohol, glycerol, glucose	9, 13
As droplets only: <i>m</i> -xylene, cyclopentane, <i>n</i> -heptane, methylene chloride	9
Polymeric organic compounds	
Example: polyethylene ($-\text{CH}_2-$) _n , and many others	19
Aqueous solutions	
Acids, bases, chlorides, nitrates, and others	20, 21
Metallic alloys by "Splat Cooling"	
Au ₄ Si, Pd ₄ Si	21a
Te _x -Cu ₂₅ -Au ₅	22

TABLE 2 Glasses Formed by Deposition or Reaction from the Vapor, and not included in Table 1

	Refs.
Elements	
Boron	24
Silicon, Germanium	23
Bismuth, Gallium	32
Oxides	
Aluminum(?)	25
Tantalum	25
Niobium	25
Water(?)	27, 28
Metals and alloys	26
Other compounds	
Silicon carbide	23
Indium antimonide	29
Various combinations of silicon, or germanium, with oxygen, sulfur, selenium, and tellurium	29
Magnesium with antimony or bismuth	30
Nickel, cobalt, or iron with phosphorous or sulfur	31

main "glass formers" SiO_2 , B_2O_3 , GeO_2 , and P_2O_5 . The "conditional" glass-forming oxides in Table 1 do not form glasses alone, but can do so in binary or multicomponent mixtures with other oxides.

A second category is the chalcogenide glasses based on sulfur, selenium, or tellurium. In chemistry, the term chalcogenide refers to compounds containing oxygen, sulfur, selenium, or tellurium; thus its use to describe glasses of these elements, excluding oxides, is unfortunate. Many of these glasses of commercial interest include halide elements. The root chalco- comes from a Greek word for copper, and the chalcogenide elements have traditionally been those that form strong compounds with copper. These glasses are primarily interesting because some are electronic conductors (semiconductors). They also soften at relatively low temperatures and transmit infrared radiation well.

Another category is the ionic glasses—halides, nitrates, sulfates, and carbonates. The latter three are quite similar because they form glasses only as binary or multicomponent mixtures. Angell has reviewed work on these glass formers.³³

Other categories are the simple organic compounds, the organic polymers, the aqueous solutions, and metallic alloys.

CRYSTALLIZATION AND GLASS FORMATION

Turnbull³⁴ has discussed the question of whether a glass is ever the most stable state of a solid below its melting point. He concludes that there is no rigorous proof that the most stable state of a substance at low temperature is crystalline rather than glassy, but that, with the exception of helium, it is found experimentally that the most stable forms of pure substances are crystalline. Furthermore the viscosities of liquids at their freezing points are invariably much lower than the 10^{15} P characterizing a rigid glass, the highest being silica with a viscosity of 10^7 P at the melting point of cristobalite.

Therefore, if a glass is formed from a liquid, it must be cooled below its melting point so fast that the supercooled liquid does not crystallize. Thus the rates of nucleation and growth of crystals in the liquid, together with the cooling rate, determine whether a glass is formed. Uhlmann and co-workers⁵² have treated the kinetics of glass formation in terms of the Avrami⁵³ equations for the volume fraction V_c/V crystallized, where V_c is the volume of crystalline material in a total volume V , and their treatment is followed here. The general transformation equation includes the possibility of time dependent rates of nucleation and crystallization. A simplification is to assume that these rates are functions of temperature only and not time. The result is

$$V_c/V = 1 - \exp(-\pi u^3 I t^4/3) \quad (1)$$

where I is the rate of nucleation of crystals per unit volume, u is the rate of crystallization (m/s), and t the time. Equations for these rates are discussed in Chapters 4 and 5. The exponential form in Eq. 1 allows for the possibility

of impingement of growing crystals; at short times, V_c/V is proportional to the term $\pi u^3 I t^4/3$.

If the rate of nucleation and crystallization are known as a function of temperature, the volume fraction of crystals at a particular temperature can be calculated as a function of time. It is assumed that crystallization is detectable at a certain fraction V_c/V ; then the time for detection as a function of temperature can be found. The resulting temperature–log time plot is called a time–temperature–transformation (TTT) curve, as shown in Fig. 1 for anorthite ($\text{CaO} \cdot \text{Al}_2\text{O}_3 \cdot 2\text{SiO}_2$), with $V_c/V = 10^{-3}$, from Ref. 54. The position of the curve is only weakly dependent on the value assumed for V_c/V . The rates of nucleation and growth are a maximum at a certain temperature (Chapters 4 and 5); the result is that the TTT curves have one or more minimum times, as shown in Fig. 1. This minimum results because of two opposing factors. As the temperature of the liquid is lowered below the melting temperature, the driving force for both nucleation and growth increases, leading to increased rates. Opposed to this increased is the decreased in transport rates (diffusion or viscosity) as the temperature is lowered, which decreases the rates of nucleation and growth. The result is a maximum in these rates and a minimum time for appreciable crystallization, as shown in Fig. 1.

The cooling rate to avoid crystallization and thus form a glass must be high enough to avoid the “nose” in the TTT curve. A rough estimate of this critical cooling rate R_c can be found by considering the temperature range over which the crystallization rate is appreciable. For the curve in Fig. 1, this temperature range is about 100°C at $2(10)^3/\text{s}$, so $R_c \approx 100/2(10)^3 = 0.05^\circ/\text{s}$. A cooling rate faster than this in the fast crystallization temperature range should prevent a crystallization volume fraction of more than 10^{-3} from being formed. This method of estimating R_c is somewhat different from that used by Uhlmann and Yinnon⁵²; they describe other methods for estimating R_c . For lunar sample 15286 Uhlmann et al.⁵² measured a critical cooling rate of $0.3^\circ/\text{s}$; from their

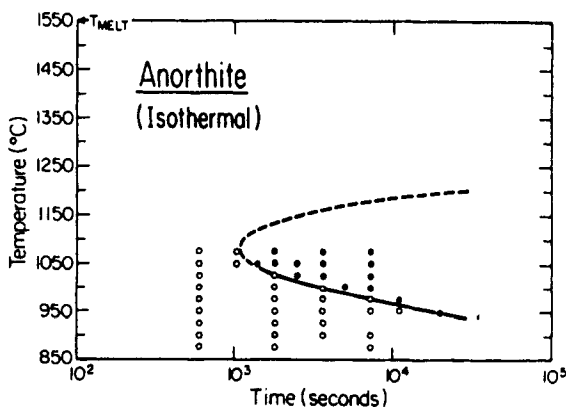


Fig. 1 Experimental isothermal time–temperature–transformation (T–T–T) diagram. Reprinted from Ref. 54 with permission from Elsevier.

TTT curve for this glass (MgO , FeO , Al_2O_3 silicate), the present method gives about $0.2^\circ/\text{s}$, in good agreement with the measured value.

Often measured nucleation and crystallization rates are not available. In that circumstance, it would be useful to be able to estimate nucleation and growth rates of crystals in a liquid to allow calculation of critical cooling rates and the tendency to glass formation. Estimates of these rates are described in Chapter 5; they are difficult. Problems are heterogeneous nucleation sites, which can increase nucleation rates, uncertainties in theoretical equations for nucleation and crystallization, and systems that do not follow equations. Uhlmann and Yinnon⁵² describe some estimation techniques; in some materials, estimation of critical cooling rates within an order of magnitude was possible. Ruckenstein and Ihm⁵⁵ have also calculated critical cooling rates for glass formation from nucleation and crystallization equations.

Crystallization rates are easier to measure than nucleation rates, and have been determined for many glass-forming systems. Maximum crystallization velocities as listed in Table 3. The rates of crystallization are lowest for substances easily cooled to glasses, such as silica and germania, whereas they are higher for alkali and alkaline earth compounds, which must be cooled more rapidly to avoid crystallization. From the table, one might guess that an upper limit for the crystallization rate of a material easily formed as a glass by cooling the liquid would be about 10^{-4} cm/s. With this rate, it is necessary to cool the glass through the temperature range of maximum crystallization rate in less than 0.01 s to prevent growth of crystals larger than 100 Å in diameter. This time is too short for most practical conditions, so the nucleation rates for materials with maximum crystallization rates above 10^{-4} cm/s must be low. For glasses such as silica, this low rate is enough to ensure glass formation for a wide range of cooling rates.

The velocity of crystallization of cristobalite from fused silica is shown as a function of temperature in Fig. 2, from the work of Wagstaff.³⁵ As the silica is cooled below the melting point of cristobalite, the rate of crystallization rises

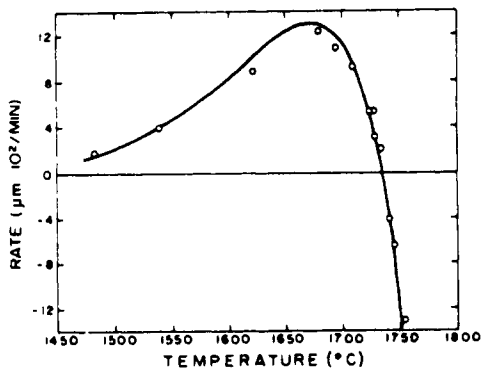


Fig. 2 The rate of crystallization of cristobalite from fused silica as a function of temperature.³⁵

TABLE 3 Crystallization Velocities and Viscosities of Glass-Forming Liquids

Material	Melting Point (°C)	Max Cryst. Velocity (cm/s)	Refs. for Velocity	Temp. of Max. ν (°C)	Log Viscosity at m.p. (P)	Refs. for Viscosity
Vitreous silica, SiO_2	1734	$2.2(10)^{-7}$	35	1674	7.36	36
Vitreous germania, GeO_2	1116	$4.2(10)^{-6}$	37	1020	5.5	38
Phosphorous pentoxide, P_2O_5	580	$1.5(10)^{-7}$	39	561	6.7	40
Sodium disilicate, $\text{Na}_2\text{O} \cdot 2\text{SiO}_2$	878	$1.5(10)^{-4}$	41,41a,42	762	3.8	42
Potassium disilicate, $\text{K}_2\text{O} \cdot 2\text{SiO}_2$	1040	$3.6(10)^{-4}$	41	930		
Barium diborate, $\text{BaO} \cdot 2\text{B}_2\text{O}_3$	910	$4.3(10)^{-3}$	43	849	1.7	44
Lead diborate, $\text{PbO} \cdot 2\text{B}_2\text{O}_3$	774	$1.9(10)^{-4}$	45	705	1.0	45
1,2-Diphenylbenzene	55.5	$2.5(10)^{-3}$	46	38	-0.46	46
1,3,5-Tri- α -naphthylbenzene	197	$9.3(10)^{-5}$	47	175	-0.34	47
Glycerol	18.3	$1.8(10)^{-4}$	48	-6.7	1.0	
Salol	43	$6.4(10)^{-3}$	49	20		
Polyethylene adipate	55	$9.5(10)^{-6}$	50	26		
Toluene	-95	> 0.5	51			
Ethyl ether	-116	> 0.13	51			
Methyl alcohol	-98	> 0.09	51			

to a maximum value and then decreases. At much lower temperatures (below about 900°C for pure vitreous silica) the rate of crystallization is so slow that even for long holding times, no appreciable amount of crystalline material is formed. Thus, if the silica is cooled rapidly enough from above the melting point to below 900°C, no appreciable amount of crystalline cristobalite is formed, and the silica becomes a stable glass.

FORMATION OF GLASSES FROM SIMPLE ORGANIC LIQUIDS

Several organic liquids listed in Table 1 can form glasses, even though they show rapid crystallization rates near their melting points and are quite fluid there. Different explanations have been proposed to account for this anomaly, but none is entirely satisfactory. This problem is considered in the following paragraphs.

The organic liquids that form glasses have relatively low melting points, and most have asymmetric molecules. Turnbull and Cohen⁵⁶ have pointed out that the ratio of the boiling temperature to the melting temperature (T_b/T_m) for these liquids is greater than 1.8, whereas it is less than this value for organic liquids that do not form glasses. They deduced that the temperature of glass formation is related to the cohesive energy of the liquid, which is proportional to the boiling point. Thus the closer the melting temperature is to the temperature of glass formation (the larger is T_b/T_m), the greater is the tendency to glass formation. Another qualitative way to view glass formation in these liquids is that they have lower melting temperatures because of the greater difficulty in rearranging their asymmetric molecules, and this difficulty, enhanced by the lower crystallization temperature, leads to reduced crystalline nucleation and growth and therefore to glass formation. These considerations explain the relative glass-forming tendency of the organic liquids with asymmetric molecules, but it is still difficult to account for glass formation in view of their relatively low viscosity and high crystallization rate near the melting points.

The viscosity of these liquids increases sharply below their melting points, and consequently the crystallization rate decreases.^{46,47,57} Stavely et al.⁹ found that they had to cool droplets of organic liquids to temperatures from 0.7 to 0.8 of the melting temperature before they crystallized. At this fraction of the melting temperature, the viscosity of the liquids with asymmetric molecules is so high that the rate of crystallization is low, and as droplets they form glasses. However, this reasoning does not explain why these liquids form glasses in the bulk, since many nucleation catalysts are present, in contrast to the droplets. It may be that these catalysts are ineffective because of the complex shapes of the organic molecules. Further work is needed to establish with certainty the reason for glass formation in these liquids.

GLASS FORMATION IN OXIDES

The most important commercial glasses are based on oxides, as described in the preceding chapter and listed in Table 1. Zachariasen⁵⁸ considered the relative glass-forming ability of oxides and concluded that the ultimate condition for glass formation is that a substance can form extended three-dimensional networks lacking periodicity with an energy content comparable with

that of the corresponding crystal network. From this condition, he derived four rules for oxide structure that allow one to choose those oxides that tend to form glasses. These rules were remarkably successful in predicting new glass-forming oxides as well as including such oxides known at the time of their formulation. The rules are the following:

1. An oxygen atom is linked to not more than two glass-forming atoms.
2. The coordination number of the glass-forming atoms is small.
3. The oxygen polyhedra share corners with each other, not edges or faces.
4. The polyhedra are linked in a three-dimensional network.

Oxides A_2O or AO , where A is a metal atom, do not satisfy the rules. Oxides A_2O_3 satisfy rules 1, 3, and 4 if the oxygen atoms form triangles around each A atom, and AO_2 or A_2O_5 satisfy these rules if the oxygen atoms form tetrahedra around each A. Higher coordination is apparently excluded by rule 2. From these considerations, Zachariasen concluded that the following oxides should be glass formers: B_2O_3 , SiO_2 , GeO_2 , P_2O_5 , As_2O_5 , P_2O_3 , As_2O_3 , Sb_2O_3 , V_2O_5 , Sb_2O_5 , Nb_2O_5 , and Ta_2O_5 . At the time of Zachariasen's research, only B_2O_3 , SiO_2 , GeO_2 , P_2O_5 , As_2O_5 , and As_2O_3 had been made into glasses, but since then glasses of several other oxides in his list have been prepared, as shown in Table 1. Oxides not listed either have not been made into glasses, or in a few cases are made as glasses only with difficulty.

Thus Zachariasen's rules are quite accurate in predicting glass formation, and it is interesting to question their relationship to the criteria for glass formation involving crystallization rates. The requirement that the oxide form a three-dimensional network means that viscous flow is relatively difficult because it requires breaking of primary chemical bonds. In fact, Sun⁵⁹ has shown that the glass-forming tendency of an oxide is directly related to the strength of the bonds between its oxygen and metal atoms. Glass formers have bond strengths above about 80 kcal/mole, and modifying ions that are not part of the oxide network have oxygen-metal bond strengths below this value. The requirement that the energy of the glass and crystal be close means that the heat of fusion for a glass former is less than that for other chemically similar materials. A lower heat of fusion in Eqs. 1 and 2 leads to lower rates of nucleation and crystallization; therefore for similar materials this factor may be of some significance in predicting the tendency to glass formation. However, it is much less important than factors influencing the viscosity of the liquid.

Other correlations of glass-forming tendency of oxides have been made. Stanworth⁶⁰ has suggested the following criteria:

1. the cation valence must be three or greater.
2. The tendency to glass formation increases with decreasing cation size.
3. The electronegativity should be between about 1.5 and 2.1 on Pauling's scale

Using these criteria Stanworth finds four groups of oxides: the strong glass formers, Si, Ge, As, P, and B; "intermediate" glass formers which form glasses only with "splat" cooling,⁶¹ Sb, V, W, Mo, and Te; other oxides that do not form glasses on rapid cooling, but do form them on oxidized surfaces of their metals or in binary combination with nonglass-forming oxides, Al, Ga, Ti, Ta, Nb, and Bi; and other oxides that do not form glasses. The second category includes most of the "conditional" glass-forming oxides in Table 1. Some oxides do not fit into this scheme, such as tin and chromium.

Poulain⁶² has suggested that glass formation in ionic systems occurs when a cation stabilizes the anion lattice, even if the field strength of the cation is not high. Thus in the zirconium fluoride glasses, zirconium ions stabilize the fluoride lattice.

GLASS FORMATION AND MATERIAL PROPERTIES

Uhlmann and Yinnon⁵² have summarized the relationship between liquid properties and the tendency to glass formation. The factors that favor glass formation are:

1. High viscosity at the nose of the TTT curve, since low transport rates lead to low rates of nucleation and crystallization;
2. Absence of heterogeneous nucleation sites;
3. A large crystal-liquid interfacial energy, which reduces the nucleation rate;
4. In multicomponent systems, a large concentration change between liquid and crystal.

In these multicomponent systems, it is often found that glass formation is favored by a "deep eutectic", because liquid compositions in low-temperature eutectics have higher viscosities and therefore lower nucleation and crystallization rates than at higher temperatures.

A low entropy of fusion also favors glass formation, as described above for oxides.

REFERENCES

1. H. Rawson, *Inorganic Glass-Forming Systems*, Academic Press, London, 1967.
2. R. Frerichs, *J. Opt. Soc. Am.*, **43**, 1153 (1953).
3. R. C. Ellis, *Inorg. Chem.*, **2**, 22 (1963).
4. A. Winter, *J. Am. Ceram. Soc.*, **40**, 54 (1957).
5. T. Sato Y. Koike, T. Endo and M. Shimada, *J. Mater. Sci.*, **26**, 510 (1991).
6. G. Tammann, *The States of Aggregation*, Van Nostrand, New York, 1925, p. 233.

7. A. Stock and K. Thiel, *Research*, **38**, 2719 (1905).
8. Z. Zhang and J. H. Kennedy, *Solid State Ionics*, **38**, 218 (1990).
9. H. J. deNordwall and L. A. K. Stavely, *J. Chem. Soc.*, **224** (1954).
10. A. Weiss and A. Weiss, *Z. Naturforsch.*, **8b**, 104 (1953).
11. P. L. Robinson and W. E. Scott, *Z. Anorg. Allg. Chem.*, **210**, 57 (1933).
12. K. H. Sun, *Glass Ind.*, **27**, 522, 580 (1946).
13. D. Turnbull and M. H. Cohen, in *Modern Aspects of the Vitreous State*, Vol. I, J. D. Mackenzie, Ed., Butterworths, London, 1960, p. 54.
14. Gan Fuxi, *J. Noncryst. Solids*, **123**, 385 (1990).
15. E. Thile, C. Wiecker, and W. Wiecker, *Silikattech*, **15**, 109 (1964).
16. M. G. Drexhage, in *Treatise on Materials Science and Technology*, Vol. 26, M. Tomozawa and R. H. Doremus, Eds., Academic Press, San Diego, 1985, p. 151.
17. T. Komatsu, H. Ur, and R. H. Doremus, *J. Noncryst. Solids*, **69**, 309 (1985).
- 17a. H. W. Sun, B. Tanguy, J.-M. Reau, J. J. Videau, and J. Portier, *J. Noncryst. Solids*, **99**, 222 (1988).
- 17b. M. D. Ingram, G. G. Lewis, and J. A. Duffy, *J. Phys. Chem.*, **76**, 1035 (1972).
18. R. K. Datta, D. M. Roy, S. P. Faile, and O. F. Tuttle, *J. Am. Ceram. Soc.*, **47**, 153 (1964).
19. P. C. Hiemenz, *Polymer Chemistry*, Marcel Dekker, New York, 1984, Ch. 4.
20. G. E. Vuilland, *Ann. Chim.*, **2**, 233 (1957).
21. C. A. Angell and E. J. Sayre, *J. Chem. Phys.*, **52**, 1058 (1970).
- 21a. P. Duwez, *Trans. ASM*, **60**, 605 (1970).
22. P. Duwez and C. C. Tsuei, *J. Noncryst. Solids*, **2**, 82 (1970).
23. M. H. Brodsky, *J. Vac. Sci. Technol.*, **8**, 125 (1971).
24. C. Feldman and K. Moorjanim, *J. Noncryst. Solids*, **2**, 82 (1970).
25. L. Young, *Anodic Oxide Films*, Academic Press, New York, 1961, p. 171, 212.
26. H. Endo, Ed., *J. Noncryst. Solids*, **117-118** (1990).
27. A. Hallbrucker, E. Mayer, and G. P. Johari, *Philos. Mag.*, **60B**, 179 (1989).
28. J. Yannas, *Science*, **160**, 298 (1968).
29. R. S. Allgaier, *J. Vac. Sci. Technol.*, **8**, 113 (1971).
30. R. P. Ferrier and D. J. Herrell, *J. Noncryst. Solids*, **4**, 338 (1970).
31. A. S. Nowich and S. R. Mader, *IBM J. Res. Dev.*, **9**, 358 (1965).
32. R. Hilsch, in *Noncrystalline Solids*, V. D. Frechette, Ed., Wiley, New York, 1960, p. 348.
33. C. A. Angell, *J. Phys. Chem.*, **70**, 2793 (1966).
34. D. Turnbull, *Contemp. Phys.*, **10**, 473 (1969).
35. F. E. Wagstaff, *J. Am. Ceram. Soc.*, **52**, 650 (1969).
36. G. Urbain, Y. Bottinga, and P. Richet, *Geochem. Cosmochim. Acta*, **46**, 1061 (1982).
37. P. J. Vergano and D. R. Uhlmann, *Phys. Chem. Glasses*, **11**, 30 (1970).
38. E. J. Fontana and W. A. Plummer, *Phys. Chem. Glasses*, **7**, 139 (1966).
39. R. L. Cormia, J. D. Mackenzie, and D. Turnbull, *J. Appl. Phys.*, **34**, 2239 (1963).
40. *Ibid.*, p. 2245.
41. A. Leontewa, *Acta Physicochem.*, USSR, **16**, 97 (1942).

- 41a. W. D. Scott and J. A. Pask, *J. Am. Ceram. Soc.*, **44**, 181 (1961).
42. G. S. Meiling and D. R. Uhlmann, *Phys. Chem. Glasses*, **8**, 62 (1967).
43. J. A. Laird and C. G. Bergeron, *J. Am. Ceram. Soc.*, **53**, 482 (1970).
44. P. Li, A. C. Shore, and G. Su, *J. Am. Ceram. Soc.*, **45**, 86 (1962).
45. J. P. DeLuca, R. J. Eagan, and C. G. Bergeron, *J. Am. Ceram. Soc.*, **52**, 322 (1969).
46. R. J. Greet, *J. Crystal Growth*, **1**, 195 (1967).
47. J. D. Magil and D. J. Plazek, *J. Chem. Phys.*, **46**, 3757 (1967); **45**, 3038 (1966).
48. M. Volmer and A. Maider, *Z. Phys. Chem.*, **154A**, 97 (1931).
49. K. Neumann and G. Micus, *Z. Phys. Chem.*, **2**, 25 (1954).
50. M. Takayangi, *Mem. Fac. Eng., Kyushu Univ.*, **16**, 111 (1957).
51. A. Van Hook, *Crystallization*, Reinhold, New York, 1961, p. 168.
52. D. R. Uhlmann and H. Yinnon, in *Glass: Science and Technology*, vol. 1, Academic Press, San Diego, 1983, p. 1.
53. M. Avrami, *J. Chem. Phys.*, **7**, 1103 (1939); **8**, 212 (1940); **9**, 177 (1941).
54. D. Cramer, R. Salomau, H. Yinnon, and D. R. Uhlmann, *J. Noncryst. Solids*, **45**, 127 (1981).
55. E. Ruckenstein and S. K. Ihm, *J. Chem. Soc., Faraday. Trans. 1*, **73**, 764 (1976).
56. D. Turnbull and M. H. Cohen, *J. Chem. Phys.*, **29**, 1049 (1958).
57. D. J. Denney, *J. Chem. Phys.*, **30**, 159 (1959).
58. W. H. Zachariasen, *J. Am. Ceram. Soc.*, **54**, 3841 (1932).
59. K. H. Sun, *J. Am. Ceram. Soc.*, **30**, 277 (1947).
60. J. E. Stanworth, *J. Am. Ceram. Soc.*, **54**, 61 (1971).
61. P. T. Sarjeant and R. Roy, *J. Am. Ceram. Soc.*, **50**, 500, 503 (1967).
62. M. Poulain, *Nature*, **293**, 279 (1981).

CHAPTER 3

STRUCTURE

The first section of this chapter is a discussion of the variation of glass structure as one goes from a central atom to successive ranges of surrounding atoms. Then some of the experimental techniques for probing glass structure are described, and finally a number of specific systems are discussed. Emphasis is on the silicate systems because of their practical importance.

RANGES OF STRUCTURAL ORDER

In Chapter 1, a glass was defined as an amorphous solid, an amorphous material being one with no long-range order but possibly with short range order. Some authors prefer to define a glass more narrowly as an amorphous solid that shows a glass transition.¹ The glass transition and the latter definition are discussed in Chapter 7. Here glass and amorphous solid are used synonymously.

In recent structural work on glasses, at least four ranges of structural arrangement are recognized,² as shown in Table 1. This scheme has been taken mainly from Ref. 2.

The first range is a central atom and its immediate neighboring atoms; for example, in silicates, silicon is the central atom and four oxygen atoms are its nearest neighbors, forming the corners of a tetrahedron. These tetrahedra have uniform bond angles and distances, and are the universal building blocks of silicates, both crystalline and amorphous. The first task in understanding the structure of a glass is to determine the coordination of the predominant glass-forming elements in the glass. In many glasses there is still debate about

TABLE 1 Ranges of Order for Amorphous Solids

Range	Name	Features
I	Basic building block Short range order	Central atom and its nearest neighbors
II	Interconnections of adjacent units	Packing of I units around central unit
III	Intermediate	Ordered arrangements several atom distances from a central atom
IV	Long range	Density and composition fluctuations
Examples		Characterization Parameters
I	SiO ₄ tetrahedron ZrF ₈ coordination polyhedron	Coordination number Bond length Bond angles
II	Packing of SiO ₄ tetrahedra, rings of atoms	Connection mode Connectivity Angles between structural units Ring constituents and dimensions
III	Ordered arrangements of modifier ions (alkalis, alkaline earths) in silicates	Small clusters of structural units Planes and chains and their dimensions
IV	Incipient phase separation and crystallization	Size and composition of fluctuations

these coordination numbers; for example, proposed structures of zirconium fluoride glasses include six, seven, eight and mixtures of fluoride ions around a central zirconium ion. Coordination of modifying ions such as alkalis and alkaline earths in silicate glasses is beginning to be explored³⁻⁶.

The next range of structural order is the organization of structural groups around the central one, in the silicates the bonding and packing of tetrahedral units around a central one, as shown in Fig. 1. This structural range also includes formation of units such as rings of atoms formed by linking adjacent tetrahedra, as shown in Fig. 2. This range includes the method of connecting or sharing bonds in structural units, such as corner sharing or single atom links, edge sharing (two linking atoms between units) and more rarely face sharing. In molecular glasses such as organics (glycerol, salol and toluene) and P₄Se₃,⁷ there are no strong atomic bonds between molecules. There can be considerable disorder in this range, for example in a distribution of Si-O-Si

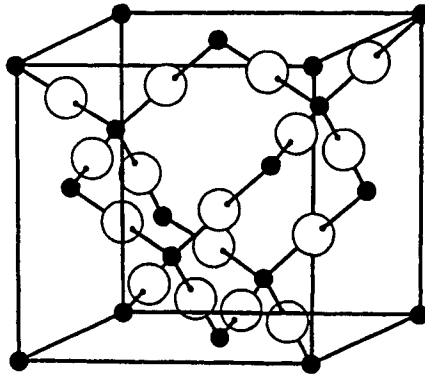


Fig. 1 The crystal structure of high cristobalite, showing the organization of tetrahedral units of silicon (black dots) and oxygen (O). Reprinted from Ref. 6a with permission from Elsevier.

angles in a three-dimensional silicate network and between structural units of different size, shape and composition in multicomponent glasses. Long-range order, meaning order over many (for example 20 or more) atoms apart, does not exist in glasses except in the form of density and composition fluctuations. However, there is evidence for some order in between long and short range, called intermediate range order. This type of order is exemplified by short

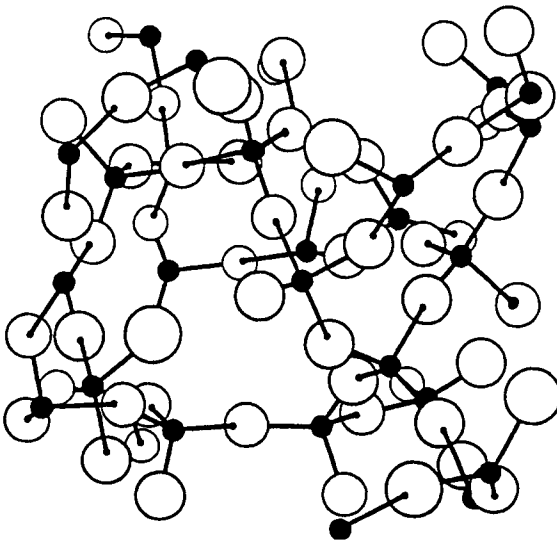


Fig. 2 A schematic diagram of vitreous silica, showing silica tetrahedra linked at corners to form a random network with rings and cages. Reprinted from Ref. 6a with permission from Elsevier.

planes or chains of modifying atoms such as alkali or alkaline earth ions in a multicomponent silicate glass.^{3,4,8}

EXPERIMENTAL METHODS

A wide variety of experimental methods have been used to explore glass structure, but only a few have proved to be of dominating importance. These are described briefly, and other methods are listed with references. In my view the most important methods are X-ray and neutron diffraction¹⁶ and infrared and Raman spectroscopy; more specialized and of increasing significance are nuclear magnetic resonance (NMR) and soft X-ray spectroscopy (EXAFS) or extended X-ray absorption fine structure.

X-Ray diffraction was the first technique that produced detailed insight into glass structure, as pioneered by Warren,⁹ and remains a highly valuable tool. The usual X-ray diffraction pattern from a glass is a broad peak with undulations at high angles. Detailed mathematical analysis of this pattern in terms of pair distribution functions leads to information on distances between atom pairs, both like and unlike, as shown in Fig. 3. The measured pair distribution function can be compared to distribution functions calculated from models of the glass structure, and the best fit adopted. In all methods of exploring glass structure, this procedure of choosing a model and comparing it to experimental results is followed. The obvious pitfall is that more than one model can be consistent with the measurements; then additional measurements

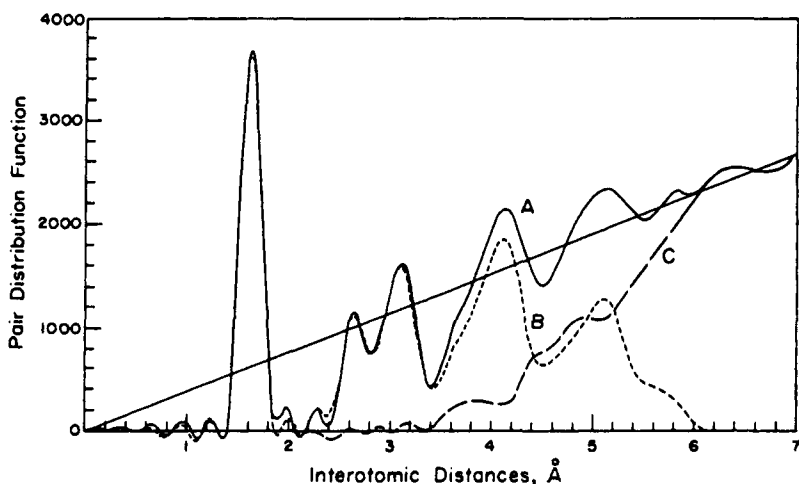


Fig. 3 The pair distribution function for fused silica, measured by Mozzi and Warren.³⁰ A is the measured curve, B is the sum of the calculated curves for the first six contributions: Si-O, O-O, Si-Si, Si-2nd O, O-2nd O, and Si-2nd, C is the difference between A and B.

must be invoked. This ambiguity is one reason for past and continuing debates about glass structure.

Neutron diffraction gives the same information on a pair distribution function as X-ray diffraction, and it has several advantages. The intensity of neutron diffraction varies irregularly with atomic number, so atoms close in the periodic table can have quite different intensities, allowing for better definition of atom-atom distances. Neutrons are also highly penetrating. The disadvantage of neutron diffraction is that a suitable source of neutrons requires a nuclear reactor, and only a few such sources are available.

Infrared and Raman spectroscopies give absorption spectra characteristic of motions of atom-atom bonds, as described more fully in Chapter 17. The resulting absorption bands are like fingerprints of particular structural arrangements. If the structures of crystalline solids close to the glass composition are known, their spectra can be compared to that of a glass, and the best fit helps to elucidate range I structure and sometimes range II structure.

In nuclear magnetic resonance (NMR), a sample is placed in a magnetic field and radio-frequency electromagnetic radiation is applied. Particular nuclei absorb this radiation at resonance frequencies, which are modified by neighboring atoms. The boron-11 atomic nucleus shows strong quadrupole coupling with a broad resonance line when it is in triangular coordination, whereas in tetrahedral coordination, the coupling is weak with a narrow resonance. These differences allowed Bray and co-workers to determine the fraction of three- and four-coordinated boron atoms in borate glasses.^{10,11} More recently, pulsed NMR spectrometers that use "magic angle spinning" have allowed exploration of coordination numbers and angular distributions in a variety of glasses.¹²⁻¹⁴

Improvements in soft X-ray spectrometers have led to availability of a wide range of X-ray wavelengths, up to 20 Å, that allow studies of the light atoms in silicate glasses.^{8,19} Pair distribution functions of like atoms of low atomic number can be isolated and studied without the interference of scattering from other like and unlike atom pairs. Synchrotron radiation provides an intense and versatile source of soft X-rays, but requires special facilities available only at a few sites. Laboratory-scale sources are also possible.¹⁵ These EXAFS techniques should prove to be particularly valuable for studies of modifying ions in oxides and amorphous alloys.⁵

Other techniques that are being applied to studies of glass structure are fluorescence line narrowing,¹⁷⁻¹⁹ electron spin resonance,^{20,21} and Mossbauer spectroscopy.^{22,22a}

COMPUTER SIMULATION

Computer calculations provide a useful complement to experimental measurements of glass structure.²³ These simulations provide positions of all atomic species in three dimensions directly from the calculations, exposing the assumptions involved in the modeling. The models can be modified with respect to

factors such as bond lengths and angles and compositions to see the influence of these factors on structure. The most critical assumption in the calculation is the form of the interatomic potential; good agreement between calculations and experimental measurements suggest that realistic potentials have been used. More realistic directional potentials have been explored,^{24,25} as well as potentials derived from quantum mechanics.²⁶

These simulations assume that the glass structure can be approximated with a number of atoms small (hundreds to a few thousand) compared to bulk samples. Interatomic potentials are imposed along with periodic boundary conditions. The atomic configurations are determined by thermodynamic sampling (Monte Carlo Techniques) or numerically integrating the classical equations of motion (molecular dynamics techniques).

In spite of the usefulness of these simulations, they contain a number of hidden assumptions about atomic bonding and organization. The simulations assume quite local atomic interactions, which may be only partially correct. In the simulation, the glasses are usually rapidly "quenched" from a very high temperature to a rigid state. Soules discusses other assumptions.²³ Simulations can be helpful, but must always be compared to experiment; they are not a substitute for real materials.

SPECIFIC SYSTEMS

In the remainder of this chapter, the results of structural studies on a variety of special glass systems are summarized. Again emphasis is on silicates.

Vitreous Silica

The simplest of the silicate glasses is vitreous silica (SiO_2), and the study of its molecular structure has been fundamental to understanding the structure of other silicates. This understanding began with Goldschmidt's recognition of the importance of the tetrahedral arrangement of oxygen ions around silicon ions in silicates,²⁷ and Zachariasen's postulate of a three-dimensional network without periodicity, formed by the union of these tetrahedra at their corners.²⁸

In all crystalline silicates, the coordination number of silicon-to-oxygen ions is four; therefore the silicon-oxygen tetrahedron is the basic building block for silicate structures. These tetrahedra can be attached to none, one, two, three, or four other tetrahedra by silicon-oxygen bonds at their corners, depending on the concentration of other oxides present. In vitreous silica, each tetrahedron is attached to four others, giving a three-dimensional network. Zachariasen²⁸ proposed that this network lacked any symmetry or periodicity, and this random-network model is generally accepted as the best description of the structure of fused silica.

The initial X-ray diffraction study of Warren et al.²⁹ was consistent with the random-network model, and later work of Mozzi and Warren³⁰ has confirmed

this agreement. There were theoretical and experimental limitations in the early studies that have been removed in the later work. The strong Compton scattering at large values of $\sin \theta/\lambda$, where θ is the scattering angle and λ the wavelength of the X-radiation, limited the accuracy of the diffraction results at these values. The method of fluorescence excitation has largely eliminated this background scattering, and a new treatment in terms of "pair-distribution" functions allows the interatomic distances to be calculated directly from the peak positions on a distribution curve, and the areas under the peaks give the number of neighboring atoms.

The "pair-function distribution" curve measured by Mozzi and Warren is shown in Fig. 3. The first peak corresponds to the silicon-oxygen distance of 1.62 Å, and the second peak corresponds to an oxygen-oxygen distance of 2.65 Å. These distances are close to those found in crystalline silicates. The widths of these peaks are consistent with a tetrahedral distribution of oxygen atoms around each silicon atom, as shown by the calculated peaks in the figure. The third peak corresponds to the silicon-silicon distance of 3.12 Å, and is much broader than the other two peaks because of the distribution in silicon-oxygen-silicon bond angle. The fourth peak, at 4.15 Å, is the silicon-second oxygen contribution, and the fifth peak, at about 5.1 Å, is a combination of the oxygen-second oxygen and silicon-second silicon peaks. A sixth peak, at about 6.4 Å, could result from the silicon-third oxygen contribution. No more peaks would be expected from a random network, and none were found experimentally.

The shapes of the third, fourth, and fifth peaks were fitted by assuming a distribution in the silicon-oxygen-silicon bond angle, as shown in Fig. 4. The maximum of the distribution curve is at 144°, with a maximum angle of 180° and a minimum angle of 120°. Almost all the angles are within $\pm 10\%$ of the maximum. Although this distribution of bond angles is wide enough to distinguish the structure clearly from a crystalline arrangement, it is rather narrow compared to a completely random distribution of bond angles from 90 to 180°. Thus the structure of vitreous silica is quite uniform at a short range, although there is no order beyond several layers of tetrahedra.

Histograms calculated from physical models of the structure of vitreous silica, based on a random network and constructed in various ways,³¹⁻³⁴ agree well with the experimental results of Warren et al. and Mozzi and Warren.³⁰ Various properties of vitreous silica calculated from the random-network model are also in accord with experimental results. For example, the spectrum of atomic vibrations as measured^{35,36} by infrared absorption, Raman emission, and inelastic neutron scattering is consistent with the random-network model³⁷ and shows that, at most, only a small amount of crystalline material could be present in completely melted vitreous silica.

Some alternate models for the structure of vitreous silica have been advocated in which there are regions of order alternating with connecting regions of disorder. These crystallite models,^{38,39} where very small crystalline regions are connected by disordered material, were examined by Warren and

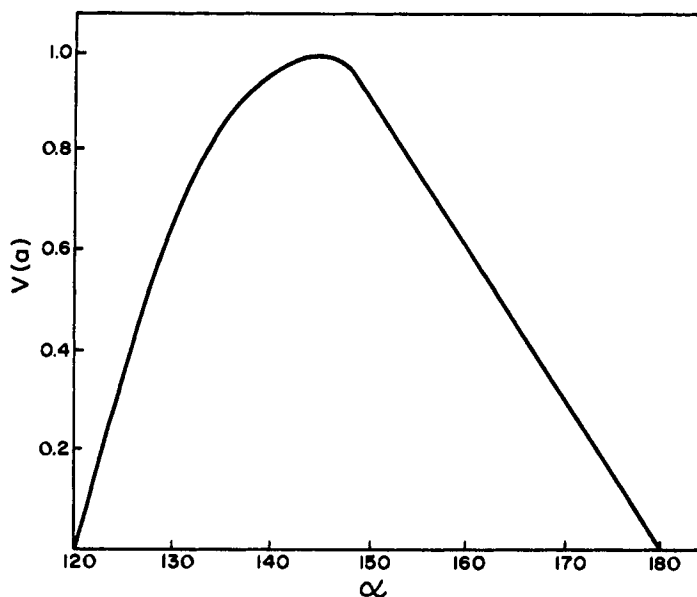


Fig. 4 The distribution of silicon-oxygen-silicon angles in fused silica assumed by Mozzi and Warren.³⁰ The function $V(x)$ is the fraction of bonds with angles α normalized to the most probable angle.

Briscoe.⁴⁰ They showed that the breadth of the first diffraction peak in vitreous silica required a crystallite size of no larger than 8 Å. At this size, the term crystal loses any meaning. Furthermore, vitreous silica showed little low-angle scattering of X-rays; any appreciable amount of fine nonuniformities would lead to such scattering.

More recent and highly refined neutron diffraction studies of vitreous silica are consistent with the random network model of Warren.⁴¹ There is perhaps some question about the exact distribution of silicon-oxygen-silicon angles (Fig. 4) because the experimental results are not sensitively dependent on this distribution. Nevertheless the random network model has withstood the test of intensive scrutiny, and in my opinion is still the best description of silica structure.

A careful study of thin slivers of different vitreous silicas by transmission in the electron microscope reveals no structure down to a resolution of about 20 Å.⁴² In dark-field electron microscopy coherently scattering regions 10–20 Å in size were revealed in thin films of silica, silicon, germanium, and germanium-tellurium alloys.⁴³ The authors concluded that their results were in better agreement with the random network model than with a microcrystalline model.

In a discussion of high resolution electron micrographs by Zarzycki,⁴⁴ he concludes that, for a variety of glasses, these micrographs are consistent with "completely disordered" structures.

The distribution of impurity ions in vitreous silica is not necessarily uniform. Optical nonuniformities are sometimes visible along the boundaries between regions that were crystalline grains.^{45,46} Because of the high viscosity of silica at its melting temperature, these regions are not mixed, even though fusion is complete. Impurities on the surface of the quartz starting material lead to a different refractive index. There is also evidence for a nonuniform distribution of sodium ions in synthetic silica,⁴⁷ and for chains or open cages of aluminum ions in vitreous silica.⁴⁸

Multicomponent Silicate Glass

Some ions can substitute for silicon in the silicon-oxygen network, either with charge-compensating ions (aluminum and phosphorous) or without them (germanium). The substitution of boron into the silicon-oxygen network with low alkali concentrations is difficult or impossible because of the three-coordinated planar structure of boron-oxygen (described below). Some evidence for this difficulty is given by the finding of Hair and Chapman that borate groups are not found in the silica phase of a phase-separated sodium borosilicate glass.⁴⁹

When an alkali or alkaline earth oxide reacts with silica to form a glass, the silicon-oxygen network is broken up by the alkali or alkaline earth ions, as evidenced by the much lower viscosity of these glasses compared to fused silica. As long as the number of A_2O or AO units, A being the metallic ion, is in less than a one-to-one ratio to the number of SiO_2 units, the silicon-oxygen network is preserved because each silicon-oxygen tetrahedron is linked to at least three other tetrahedra, and the glass-forming tendency of the mixture is retained. The backbone network of the glass is preserved, and probably is similar to the random network of fused silica. Thus the results of Warren and Bischoe⁵⁰ in an X-ray diffraction study of five different sodium silicate glasses were consistent with a random network of silicon-oxygen tetrahedra in which some oxygen ions were bonded to one silicon ion and some to two. They also were able to rule out the existence of discrete molecules such as SiO_2 , Na_2O , $Na_2O \cdot 2SiO_2$, and $Na_2O \cdot SiO_2$.

However, the distribution of alkali or alkaline earth ions in these glasses is uncertain. There is convincing evidence from X-ray diffraction studies that these ions are not uniformly distributed throughout the glass, but that their average separation is considerably less than for a uniform distribution.⁵¹⁻⁵⁴ Whereas there is a possibility of phase separation in some of these glasses, the nonuniform distribution seems to exist even when phase separation is not present.⁵⁴ This "clustering" of ions is perhaps not so surprising in view of the structure of the alkali disilicates, for example, lithium disilicate as shown in Fig. 5, after Liebau.⁵⁵ In these crystals there are layers of silicon-oxygen tetrahedra bonded together by the alkali ions, and the alkali ion distances in the layers are considerably less than if the ions had been uniformly distributed throughout the crystal. Thus in the alkali silicate glasses, one might expect a tendency for sheets of $Si-O-A$ layers to form with a shorter than uniform $A-A$ ion

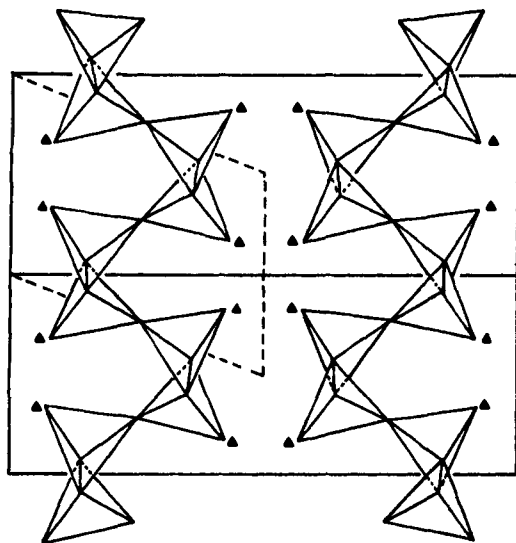


Fig. 5 Structure of crystalline lithium disilicate.⁵⁵ Small black triangles are lithium ions, and tetrahedra represent silicon oxygen groups. The projections of two unit cells are shown.

distance. Milberg and Peters⁵⁴ proposed a somewhat similar model of clusters of Si–O–Li groups to explain their results on thallium silicate glasses, and Domenici and Pozza⁵⁶ suggested that lithium silicate glasses have short range order similar to that in crystalline lithium disilicate. These models still retain the random-network structure at longer distances.

The above discussion of the structure of multicomponent silicate glasses was taken verbatim from the first edition of this book. It shows that intermediate range structure in these glasses was recognized and examined many years ago. From some recent publicity about the “discovery” of intermediate structure in silicate glasses, one might conclude that it had not been recognized before.

A detailed neutron diffraction study³ of the glass 48 mol% CaO, 49% SiO₂, 3% Al₂O₃ led to a model of planar units at the intermediate structural range (up to 1 nm or more). The structural units in planes were considered to be close-packed oxygen atoms with calcium ions in octahedral interstices. In crystalline CaSiO₃, the calcium ions are six-coordinated to oxygen, and these octahedra are arranged in planar arrays. A number of other studies of calcium aluminosilicates were summarized by Himmel et al.⁵⁷ These authors studied glasses of composition CaO · Al₂O₃ · 4SiO₂ and CaO · Al₂O₃ · SiO₃ with X-ray diffraction and computer simulation, and compared the results with various crystalline phases of anorthite, CaO · Al₂O₃ · 2SiO₃. Alternating silicon-oxygen and aluminum-oxygen tetrahedra are the building blocks of anorthite, and are also found in the glasses, with calcium associated with the alumina groups for charge balancing. In the glasses, the regular alteration of tetrahedra is inter-

rupted, and four- and six-membered rings exist. In small regions, there may be planar layers of tetrahedra. All of these intermediate range structures must be considered as tentative. Tetrahedral coordination of aluminum in calcium and magnesium aluminosilicates is confirmed with NMR⁵⁸ and infrared and Raman spectroscopy.⁵⁹ Aluminum in aluminosilicate^{59a} and fluorophosphate^{59b} glasses was found to have three different coordination numbers of four, five and six by NMR.

The coordination numbers of modifying ions in glasses can often be deduced from EXAFS studies. In a variety of sodium silicate glasses, the coordination number of sodium with oxygen was found to be about five.⁸ In crystalline alkali disilicates, the coordination number of the alkali ions with oxygen is four,⁵⁵ although the alkali ion is closely associated with one negatively charged oxygen ion. For many purposes, it may be best to consider the alkali ion coordinated with the one oxygen ion, for example when examining models for ionic transport and exchange, as discussed in Chapters 14 and 15. Furthermore, the infrared spectra of silicate glasses containing hydroxyl groups show the typical -OH absorption band, indicating that the hydrogen ions are closely bound to one oxygen ion.

As more alkali or alkaline earth oxide is added beyond the one-to-two ratio, the network becomes more and more disrupted as some tetrahedra are bonded to only two other tetrahedra. Glass formation becomes progressively more difficult because the rates of nucleation and crystallization in the glass become much more rapid as alkali or alkaline earth oxide is added. In the composition range between disilicate ($A_2O \cdot 2SiO_2$ or $AO \cdot 2SiO_2$) and metasilicate ($A_2O \cdot SiO_2$ or $AO \cdot SiO_2$) chainlike structures should exist, although direct evidence for them is lacking. At alkali concentrations above the metasilicate, isolated islands and rings, as well as chains, of silicon-oxygen tetrahedra should be the major structural features, although the evidence for them is indirect, coming from the studies of the melt.⁶⁰

Optical absorption spectra are valuable in determining the coordination number and configuration of higher valent ions such as those of the transition metals, which is discussed in detail in Chapter 17. In general these studies show that the immediate surroundings of these ions in a silicate glass are much like the surroundings in a corresponding crystal, or even in a solution with complexed ions. This finding is consistent with the picture of glass structure in which the short-range environment is quite regular, and the random characteristic of the glassy state occurs only over dimensions of several structural units.

Borate Glasses

Borate glasses are of little commercial importance because they react with atmospheric water and degrade. These glasses are of interest, however, because their structure and properties are quite different from the silicates, and boric oxide is used extensively in borosilicate glasses.

In crystalline oxides, boron occurs either in triangular coordination with three oxygen atoms or in tetrahedral coordination. Goubeau and Keller⁶¹ suggested that boroxol groups in B_2O_3 glass explain the sharp Raman line at 808 cm^{-1} . Krogh-Moe⁶² deduced from nuclear magnetic resonance, infrared and Raman spectra, and other physical properties that the boroxyl group is an important element in the structure of vitreous B_2O_3 . This group is a planar ring containing six members, alternatively boron and oxygen atoms. These rings are linked together in a three-dimensional network by boron-oxygen-boron bonds, as shown in Fig. 6.

The importance of the boroxol groups was confirmed by Mozzi and Warren⁶³ in an X-ray diffraction study, using the same fluorescence excitation method as for vitreous silica. In this study, the experimental "pair-distribution" curve showed peaks that could be assigned to different atom-atom distances. The first indicated a boron-oxygen distance of 1.37 \AA , which is the same as for triangular coordination in crystalline borates and less than the value of 1.48 \AA for tetrahedral coordination. The second peak gave an oxygen-oxygen distance of 2.40 \AA , close to the expected value of 2.37 \AA . A model of randomly oriented BO_3 triangular groups was inconsistent with the remaining peaks. The presence of definite peaks out to a distance of about 6 \AA required structural units larger than the BO_3 triangles. A model built up of boroxyl groups, as shown in Fig. 6, was capable of explaining the data. Within the six-membered rings, the boron-oxygen-boron bond angle was 120° . The boron-oxygen-boron bond between rings was assumed to have an angle of 130° , with a random orientation of the linked rings about this bond. This model of linked rings gave good agreement with the experimental X-ray curve; somewhat better agreement was possible by assuming that a small part of the BO_3 groups was linked randomly to the boroxyl groups and was not in rings.

This structure of linked rings is very different from the random network of

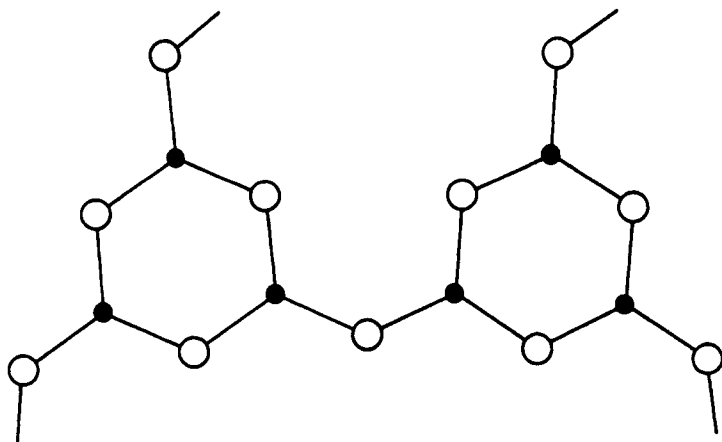


Fig. 6 Two boroxyl groups linked by a shared oxygen ●, boron; O, oxygen.

silicon-oxygen tetrahedra in vitreous silica. The space around any boroxyl group is not completely filled by linked neighbouring groups, and there is a low probability that two atoms near one another, for example, at 10-Å separation, are linked by a direct and unbroken path of B-O and O-B bonds. Mozzi and Warren suggest that this structural feature may be the reason for the low viscosity of glassy B_2O_3 compared to other glass-forming oxides, such as silica and germania. This structure is also very different from that of any crystalline form of B_2O_3 , which may be the reason for the difficulty in preparing crystalline B_2O_3 from the glass.

More recent results on the structure of glassy B_2O_3 are summarized in Refs. 64 and 65; see also Ref. 2. These authors concluded that vitreous B_2O_3 consists of a random network of equal numbers of B_3O_6 boroxyl groups and independent BO_3 triangles. A NMR study found a higher proportion of boroxyl rings.⁶⁶ Many multicomponent borates show wide ranges of glass formation.

The changes in the properties of alkali borates as more alkali is added are quite different from the changes in corresponding alkali silicates; this difference in borate properties is called the "boron oxide anomaly." The viscosity at certain temperatures can increase as alkali is added in some composition ranges, and the activation energy for viscous flow increases as alkali is added. In sodium borate, the coefficient of thermal expansion decreases as alkali is added to about 16% Na_2O . In contrast, the viscosity of the silicates decreases and the coefficient of thermal expansion increases as alkali is added, as one would expect from the simple picture of additional alkali breaking up the silicate network.

It seems likely that these anomalies are at least partially related to the change of coordination number of the boron with oxygen as alkali is added. This coordination number can be studied by nuclear magnetic resonance.^{67,68} The B^{11} nucleus shows strong quadruple coupling with a broad resonance line when it is in triangular coordination, whereas in tetrahedral coordination, the quadruple coupling is weak, with a narrow resonance. These differences allowed Bray and O'Keefe to determine the fraction of three- and four-coordinated boron in these alkali borates, as shown in Fig. 7.

Phosphate Glasses

As with the borate glasses, the phosphate glasses are of little commercial importance because of their reaction with atmospheric water. However, aqueous solutions of these glasses are important because of the complexing ability of the long phosphate chains, and P_2O_5 is an important constituent in a limited number of silicate glasses.

The basic building block in phosphate glasses and crystals is the phosphorous-oxygen tetrahedron. However, in contrast to the four-valent glass formers, the phosphorous has a double bond to one of its surrounding oxygen atoms. Thus the structure of glassy P_2O_5 is a three-dimensional network of these phosphorous-oxygen tetrahedra, each tetrahedron being bonded to three

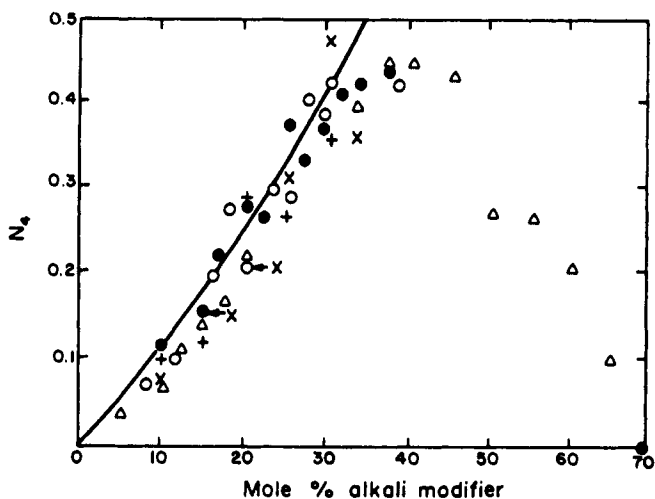


Fig. 7 The fraction N_4 of four coordinated boron atoms in alkali borate glasses.⁶⁷ ●, Na_2O ; ○, K_2O ; Δ, Li_2O ; +, Rb_2O ; , Cs_2O .

rather than four other tetrahedra as in vitreous silica, as confirmed by neutron diffraction.²

In metaphosphate glasses with a one-to-one molar ratio of alkali or alkaline earth oxide to P_2O_5 , each phosphorous-oxygen tetrahedron is linked to two other tetrahedra, and one oxygen ion per tetrahedron is associated with a metal ion. This structure leads to long chains of tetrahedra,⁶⁹ which are probably entwined in much the same way as long thin organic molecules are in polymers.

Other Oxide Glasses

Germania glass is built up of germanium-oxygen tetrahedra in a random network very much like that of silica glass, according to X-ray and neutron diffraction studies.^{2,70} This result is expected because of the similarity between the structure of many germanates and silicates.

Arsenous oxide (As_2O_3) glass has a three-dimensional network structure made up of corner-sharing AsO_3 pyramids.² Gallate, aluminate and titanate glasses were studied with X-ray diffraction, and four-coordinated network structures for them were deduced.⁷¹ Infrared and Raman spectra of a variety of simple oxide glasses are discussed in Ref. 72.

Chalcogenide Glasses

In Chapter 2, chalcogenide glasses were defined as those with any substantial amount of sulfur, selenium or tellurium. The structure of glasses of elemental

sulfur and selenium are discussed first, followed by consideration of a few select compound and multicomponent glasses.

The many forms of solid and liquid sulfur have been the subject of much study.^{73,74} From the melting point of about 114° to 160°C, liquid sulfur is made up of S_8 ring molecules. Above 160°C, the rings break up and form long chains of average length 10^5 – 10^6 sulfur atoms.⁷⁵ This structural change leads to a sharp rise in the viscosity by a factor of about 10^5 . At higher temperatures, the chains break down, causing a decrease in the viscosity. Glasses can be formed by quenching the liquid sulfur from above 160°C to below about –30°C. These glasses contain the entwined chains of the liquid, with chain lengths depending on the temperature from which they were quenched. Some S_8 rings also are present in the liquid and glass. Thus the structure of glassy sulfur is much like that of the metaphosphate glasses and the organic polymers, except for the presence of the rings.⁷⁶

Selenium forms a glass by cooling from above its melting point of 217°C to room temperature. Again the structure consists of long chains of selenium atoms.⁷⁶ Near the melting point, the average chain length in the liquid is about 10^4 atoms, and decreases as the temperature increases. Thus the structure is very similar to that of glassy sulfur, the chain length being determined by the quenching temperature. Some Se_8 rings are also present in the glass and liquid, but less than in sulfur. Sulfur-selenium glasses are also known, with chains of randomly arranged sulfur or selenium atoms, similar to organic copolymers, mixed with S_8 and Se_8 rings.⁷⁷

Zallen⁷⁸ suggested that the structure of vapor deposited arsenic trisulfide resembles the random packing of nearly spherical molecules (As_2S_3); as this material is heated, it transforms to a continuous random network. The intermediate structure of this glass presumably contains small regions of layer-like structure, similar to crystalline As_2S_3 . Arsenic selenide is similar.

In a detailed discussion of neutron diffraction and Raman spectra of $SiSe_2$, $GeSe_7$, and $GeSe_2$ glasses, Elliott described structural models for these materials.⁷⁹ These glasses have tetrahedral bonding, with rings at intermediate ranges. Elliott divides the intermediate or medium-range order in the distance range of 0.5–2 nm from the central atom into three sub-ranges: (1) connections between coordination polyhedra (corner, edge or face sharing); (2) aggregates of polyhedra to form rings or clusters; (3) local dimensionality of bonding: three-dimensional network, two-dimensional layers, chains, and isolated islands. $GeSe_2$ and $SiSe_2$ glasses are proposed to contain mainly edge-shared tetrahedra, with some corner sharing and “chain clusters”.

Silicon and Germanium

Amorphous silicon and germanium retain the tetrahedral coordination of the crystalline phases. There is much interest in the structure and properties of hydrided compounds of these elements; results are collected in Ref. 80.

Halides

Glasses based on zirconium or hafnium fluorides as glass formers with additional fluorides as glass modifiers are of special interest because of their good optical absorption in the infrared to $8\text{ }\mu\text{m}$ wavelength. These compounds are not expected to form glasses from Zachariasen's rules (Chapter 2) because the zirconium ions are coordinated to many (six to eight) fluoride ions. Almeida and Mackenzie studied the structure of binary BaZr fluoride glasses with infrared and Raman spectroscopy⁸¹ and concluded that zirconium was six-coordinated to fluorine. They proposed a glass structure of zigzag chains of ZrF_6 octahedra, cross-linked with barium ions. Lucas et al.⁸² calculated the radial distribution from X-ray scattering from $\text{BaF}_2 \cdot 2\text{ZrF}_4$ glass and deduced a coordination number of 7.5 fluorines to each zirconium, which was confirmed by a molecular dynamics simulation of the structure. They proposed a bipolyhedral structure, with one zirconium ion coordinate to eight fluorines and the other to seven. Inoue et al.⁸³ concluded that the best fit to radial distribution functions of $2\text{BaF}_2 \cdot 3\text{ZrF}_4$ and $\text{BaF}_2 \cdot 3\text{ZrF}_4$ glasses required eight coordination of fluorine to zirconium. Kawamoto et al.⁸⁴ used Raman spectroscopy, X-ray scattering and computer simulation to study barium, lead and strontium zirconium fluoride glasses, and proposed eight-fold coordination of fluorine to zirconium and a structure of ZrF_8 chains. More details of these models and structures of various barium zirconium fluoride crystals are given in Ref. 85.

The infrared absorption and Raman spectra of blown and crystallized thin films of various multicomponent barium-zirconium-fluoride glasses were measured.⁸⁵ From these measurements and the previous ones, we proposed a glass structure of eight-coordinated zirconium to fluorine units, bonded to other such units with corner sharing into a three-dimensional network. This structure is similar to that of $\beta\text{-ZrF}_4$; the infrared absorption of the glasses and this crystal were closely similar, whereas the spectra of other crystals, having structures similar to the others proposed for glasses, were quite different. The building block of this network structure is an Archimedean-antiprism of a zirconium ion surrounded by eight fluorine ions, as shown in Fig. 8. Four fluorines above and below the central zirconium ions are in squares; the bottom square is rotated 45° with respect to the top one.

The structures of crystalline modifications of beryllium fluoride, BeF_2 , are particularly curious in that they closely resemble those of silica. The structural unit of these crystals is a beryllium-fluorine tetrahedron with each beryllium ion coordinated to four fluorine atoms and each fluorine bonded to two beryllium ions. There are two crystalline forms of BeF_2 : a quartz form and a cristobalite form. The ionic sizes of the beryllium and fluoride ions are almost the same as those of the silicon and oxygen ions in silica, and the strength of the beryllium-fluorine bond is high. The four coordination of the beryllium ion and the bonding of the fluorides to two beryllium ions are quite unusual, in view of the strongly ionic character of these ions.

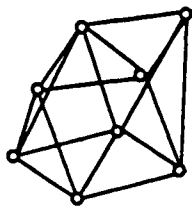


Fig. 8 Archimedean antiprism structure of zirconium coordinated with eight fluoride ions. Reprinted with kind permission of the Society of Glass Technology, from ref. 85.

The structure of glassy beryllium fluoride as derived from X-ray diffraction studies is built up of beryllium-fluoride tetrahedra,⁸⁶⁻⁸⁹ Presumably the tetrahedra are linked at their corners in the same random-network structure as vitreous silica.

There is a series of binary glasses of alkali or alkaline earth fluorides mixed with BeF_2 , and by analogy with binary silicates these glasses are expected to be based on a beryllium-fluoride network, broken up by the modifying metal cations. The viscosity of BeF_2 above its melting point is quite high and is reduced by addition of the alkali and alkaline earth fluorides, in analogy with the silicates.

Zinc chloride also forms a glass, although it is much less stable than the beryllium chloride glass. Apparently the zinc ions are surrounded by four chloride ions in tetrahedral coordination, giving a network structure like that of beryllium fluoride and the silicates,⁹⁰ although the zinc-chlorine bond is not as strong as that of beryllium and fluorine. The reason for this structure in zinc chloride is not clear.

Silicon Oxycarbide Glass

Silicone polymers pyrolyze to amorphous silicon oxycarbides that contain only silicon, oxygen and carbon.^{91,92} This glass is stable at very high temperatures; its viscosity is much higher than that of vitreous silica, and it remains amorphous to X-rays and transmission electron microscopy (TEM) at 1400°C.^{92,93} At higher temperatures (1500–1650°C), silicon carbide lines develop in X-ray diffraction and fine crystalline regions of silicon carbide and graphite appeared in TEM and electron diffraction,⁹³ as shown in Fig. 9. X-Ray photoelectron spectroscopy showed that silicon-oxygen bonds in the glass were similar to those in amorphous and crystalline silicates, and some silicons were bonded to both oxygen and carbon.⁹³ Carbon was bonded to either silicon or carbon; there were no carbon-oxygen bonds in the glass. Thus infrared spectra showed silicon-oxygen and silicon-carbon vibrations, but none from carbon-oxygen bonds. Solid-state nuclear magnetic resonance with “magic angle spinning” showed evidence for four different bonding groups around silicon.

The structure of silicon oxycarbide glass deduced from these results⁹³ is a random network of silicon-oxygen tetrahedra, with some silicons bonded to

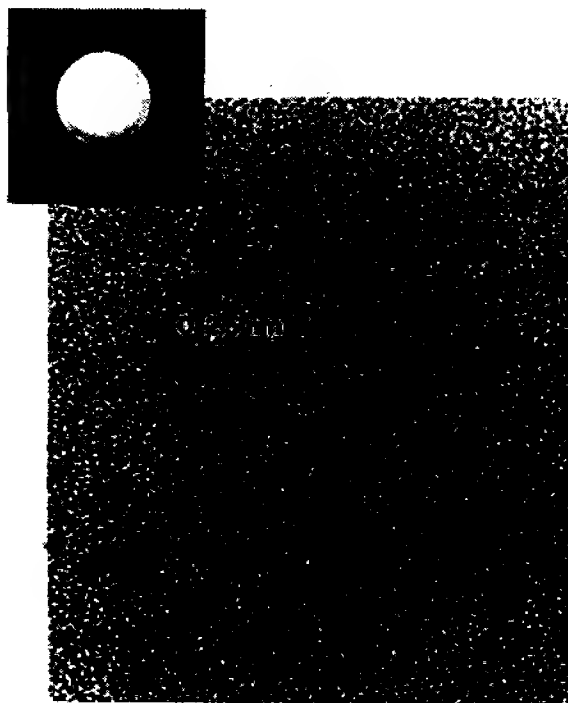
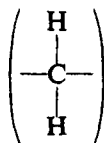


Fig. 9 Transmission electron micrograph of silicon oxycarbide glass hot pressed at 1650°C. The arrows point to SiC grains with 0.25 nm interplanar spacing; the diffraction pattern shows a corresponding ring.^{91,93}

one or two carbons substituted for oxygen; these carbons are in turn tetrahedrally bonded to other silicon atoms. Part of this structure is shown schematically in Fig. 10. There are very small regions of carbon-carbon bonds only, which are not bonded to the network. This “free” carbon colors the glass black. Multicomponent silicon oxycarbide glasses containing magnesium and aluminum have been reported.^{93a,b}

Organic Polymers

A great variety of organic polymers are known, based on carbon-carbon bonding. These simplest polymers are linear chains, such as polyethylene:



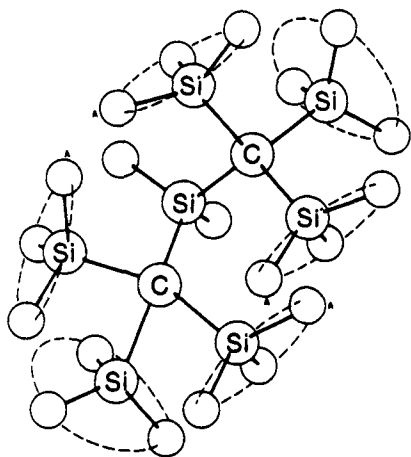


Fig. 10 Schematic representation of the structure of silicon oxycarbide glass.^{91,93}

The length of the carbon-carbon chain depends on the conditions of preparation. Many different side groups and branches can be attached to the backbone chain. Other atoms than carbon, such as oxygen or nitrogen, can also be linked in the chain, and copolymers with blocks of different molecules in the chain are possible.

In the melt, the chains are so entangled with one another that translational motion of the entire molecule is impossible, and thermal energy is manifested as Brownian motion of free segments of the chain. Different chains can be held together by Van der Waals forces at points or limited regions. If the melt is cooled rapidly the chains do not orient with respect to one another even partially, and a rigid glass results. However, with slower cooling small crystalline regions form, consisting of several chains precisely oriented. Thus most solid polymers consist of a mixture of very small crystalline regions in a matrix of entangled chains.

The chains can be tied together into a three-dimensional network if substituents on the side chains react and form covalent bonds. This cross-linking leads to substantial changes in the properties of the polymer, such as increasing the viscosity and softening temperature. A simple chain-like polymer is called thermoplastic because it softens as it is heated. A thermosetting polymer becomes more rigid as it is heated because of the formation of cross-links resulting from chemical reactions at the higher temperature.

Rubbers are cross-linked polymers that can be deformed elastically by large amounts. When a rubber is cooled sufficiently, it becomes a glass.

For those readers who wish more information on organic polymers than is contained in this brief sketch, a short bibliography is provided as a starting point.^{94,95} There are also many glassy polymers composed of combinations of carbon atoms with inorganic atoms.⁹⁶

Organic Liquids

A number of simple organic liquids form glasses, as listed in Chapter 2. Most of these liquids have asymmetric molecules. The bonding between these molecules should be weak, so the structure of the glasses probably consists of a random arrangement of these molecules, essentially a frozen liquid without much interaction between them. It is possible that some of the molecules have preferred orientations with respect to one another, giving rise to small crystal-like regions separated by disordered molecules. These conclusions are speculative because there has apparently been no direct study of the structure of these glasses.

Metallic Alloys

A variety of metallic alloys have been prepared as glasses by deposition techniques,^{97,98} or rapid cooling of the liquid.⁹⁹ Cargill¹⁰⁰ examined the X-ray scattering from electrodeposited nickel-phosphorous in the composition range Ni_3P to Ni_4P . He found that the results were inconsistent with the structures of crystalline Ni_3P . The radial distribution functions indicated more short-range order than in liquid noble metals. The results did agree well with the radial distribution function calculated for Bernal's dense random packing of hard spheres¹⁰¹ by Finney,¹⁰² and Cargill¹⁰⁰ proposed this packing as a model for the structure of glassy alloys. Polk¹⁰³ extended this model by proposing that the nonmetallic atoms fill holes in the dense random packing of metallic atoms. The structure is stabilized by the nonmetallic atoms, which interact strongly with the metal atoms.

Amorphous films of copper, nickel, gold and silver have been formed by vapor deposition on a substrate cooled to liquid nitrogen temperature.¹⁰⁴ The authors concluded that these films also had the structure of dense random packing of hard spheres, stabilized by gaseous impurities. Other results are discussed in ref. 105.

REFERENCES

1. S. R. Elliott, *Physics of Amorphous Materials*, 2nd Edn., Longman, London, 1990.
2. A. C. Wright, R. A. Hulme, D. J. Grimley, R. N. Sinclair, S. W. Martin, D. L. Prince, and F. L. Galeener, *J. Noncryst. Solids*, **129**, 213 (1991).
3. P. H. Gaskell, M. C. Eckersly, A. C. Barnes, and P. Chieux, *Nature*, **350**, 675 (1991).
4. R. Jeanloz and Q. Williams, *Nature*, **350**, 659 (1991).
5. P. H. Gaskell, J. M. Parker, and E. A. Davis, Eds., *The Structure of Noncrystalline Materials*, Taylor & Francis, London, 1983.
6. J. Colmenero and A. Alegna, Eds., *Basic Features of the Glassy State*, World Scientific, Singapore, 1990.
- 6a. T. F. Soules, *J. Noncryst. Solids*, **73**, 315 (1985).

7. D. J. Verrall, L. F. Gladden, and S. R. Elliott, *J. Noncryst. Solids*, **106**, 47 (1988).
8. G. N. Greaves and D. Raoux, in P. H. Gaskell, J. M. Parker, and E. A. Davis, Eds., *The Structure of Noncrystalline Materials*, Taylor & Francis, London, 1983, p. 55.
9. B. E. Warren, *X-Ray Diffraction*, Dover, 1969, p. 190.
10. P. J. Bray and J. G. O'Keefe, *Phys. Chem. Glasses*, **4**, 37 (1963).
11. H. M. Kriz, M. J. Park, and P. J. Bray, *Phys. Chem. Glasses*, **66**, 45 (1971).
12. R. F. Pettifer, R. Dupress, J. Farman, and U. Steinberg, *J. Noncryst. Solids*, **106**, 408 (1988).
13. C. M. Schramm, B. H. W. S. Dejong, and V. E. Parziale, *J. Am. Ceram. Soc.*, **106**, 4396 (1984).
14. R. Dupree, D. Holland, M. G. Mortuza, J. A. Collins, and M. W. G. Lockyer, *J. Noncryst. Solids*, **106**, 291 (1990).
15. K. Kadone, H. Kageyama, N. Kamijo, and H. Tanaka, *J. Noncryst. Solids*, **123**, 291 (1990).
16. A. C. Wright, *J. Noncryst. Solids*, **123**, 129 (1990).
17. M. Y. Weber and S. A. Brawer, *J. Phys.*, **C9**, 43, 291 (1982).
18. J. L. Adam, V. Ponçon, J. Lucas, and G. Boulon, *J. Noncryst. Solids*, **91**, 191 (1987).
19. S. R. Elliott, *J. Noncryst. Solids*, **123**, 149 (1990).
20. M. Nofz, R. Stösser, and F. G. Wihsmann, *J. Noncryst. Solids*, **129**, 249 (1991).
21. S. R. Elliott, *Physics of Amorphous Materials*, 2nd Edn., Longman, London, 1990, p. 284ff.
22. C. R. Kurkjian, *J. Noncryst. Solids*, **3**, 157 (1970).
- 22a. J. Jiang, J. Dezsí, Y. Gonser, and X. Lin, *J. Noncryst. Solids*, **124**, 139 (1990).
23. T. F. Soules, *J. Noncryst. Solids*, **123**, 48 (1990).
24. B. P. Feuston and S. H. Garofalini, *J. Chem. Phys.*, **89**, 5818 (1988).
25. P. Vashista, R. K. Kalia, J. P. Rino, and I. Ebbsjö, *Phys. Rev.*, **B41**, 12197 (1990).
26. R. Car and M. Parrinello, *Phys. Rev. Lett.*, **55**, 2471 (1985).
27. V. M. Goldschmidt, *Skrifter Norske Videnskaps Akad. (Oslo), Mat.-natur.*, **1**(8), 7 (1926).
28. W. H. Zachariasen, *J. Am. Chem. Soc.*, **54**, 3841 (1932).
29. B. E. Warren, H. Krutter, and O. Morningstar, *J. Am. Ceram. Soc.*, **19**, 202 (1936).
30. R. L. Mozzi and B. E. Warren, *J. Appl. Crystallogr.*, **2**, 164 (1969).
31. P. H. Gaskell and J. D. Tarrant, *Philos. Mag.*, **B42**, 265 (1980).
32. F. Ordway, *Science*, **143**, 800 (1964).
33. D. L. Evans and S. V. King, *Nature*, **212**, 1353 (1966).
34. R. J. Bell and P. Dean, *Nature*, **212m** 1354 (1966); *Philos. Mag.*, **25**, 1381 (1972).
35. M. Hass, *J. Phys. Chem. Solids*, **31**, 415 (1970).
36. A. J. Leadbetter, *J. Chem. Phys.*, **51**, 779 (1969).
37. R. J. Bell and P. Dean, *Discuss. Faraday Soc.*, **50**, 55 (1970).
38. E. A. Porai-Koshits, *J. Noncryst. Solids*, **123**, 1 (1990).
39. J. C. Phillips, *J. Noncryst. Solids*, **34**, 153 (1979); **43**, 37 (1981).
40. B. E. Warren and J. Bischoe, *J. Am. Ceram. Soc.*, **21**, 49 (1938).

41. D. J. Grimley, A. C. Wright, and R. N. Sinclair, *J. Noncryst. Solids*, **119**, 49 (1990).
42. A. M. Turkalo, General Electric Research Laboratory, unpublished results.
43. P. Chaudhari, J. F. Graczyk, and L. R. Herd, *Phys. Stat. Sol.*, **51b**, 801 (1972); *Phys. Rev. Lett.*, **29**, 425 (1972).
44. J. Zarzycki, *Les Verres et L'Etat Vitreux*, Masson, Paris, 1982, p. 159ff.
45. G. Hetherington and K. H. Jack, *J. Am. Ceram. Soc.*, **49**, 651 (1966).
46. R. Bruckner, *J. Noncryst. Solids*, **5**, 123 (1970).
47. R. H. Doremus, *Phys. Chem. Glasses*, **10**, 28 (1969).
48. R. H. Doremus, *J. Am. Ceram. Soc.*, **67**, C-150 (1984).
49. M. L. Hair and J. D. Chapman, *J. Am. Ceram. Soc.*, **49**, 651 (1966).
50. B. E. Warren and J. Biscoe, *J. Am. Ceram. Soc.*, **21**, 259 (1938).
51. C. Brosset, *Trans. Soc. Glass Tech.*, **42**, 125 (1958); *Phys. Chem. Glasses*, **4**, 99 (1963).
52. S. M. Ohlberg and J. M. Parsons, in *Physics of Noncrystalline Solids*, North-Holland, Amsterdam, 1965, p. 31.
53. S. Urnes, *Phys. Chem. Glasses*, **10**, 69 (1969).
54. M. E. Milberg and C. R. Peters, *Phys. Chem. Glasses*, **10**, 46 (1969).
55. F. Liebau, *Acta Crystallogr.*, **14**, 389, 395 (1961).
56. M. Domenici and F. Pozza, *J. Mater. Sci.*, **5**, 746 (1970).
57. B. Himmel, J. Weigelt, T. Gerber, and M. Nofz, *J. Noncryst. Solids*, **136**, 27 (1991).
58. C. J. Merzbacher, B. L. Sherriff, J. S. Hartman, and W. B. White, *J. Noncryst. Solids*, **124**, 27 (1991).
59. C. J. Merzhacher and W. B. White, *J. Noncryst. Solids*, **124**, 194 (1990).
- 59a. S. H. Risbud, R. J. Kirkpatrick, A. P. Tagliavore, and B. Montez, *J. Am. Ceram. Soc.*, **70**, C10 (1987).
- 59b. J. P. Fletcher, S. Risbud, and R. J. Kirkpatrick, *J. Mater. Res.*, **5**, 835 (1990).
60. B. O. Mysen, *Structure and Properties of Silicate Melts*, Elsevier, Amsterdam, 1988.
61. J. Goubeau and H. Keller, *Z. Anorg. Allg. Chem.*, **272**, 303 (1953).
62. J. Krogh-Moe, *Phys. Chem. Glasses*, **3**, 1 (1962).
63. B. L. Mozzi and B. E. Warren, *J. Appl. Crystallogr.*, **3**, 251 (1970).
64. P. A. V. Johnson, A. C. Wright, and R. N. Sinclair, *J. Noncryst. Solids*, **50**, 281 (1982).
65. A. C. Wright, D. J. Summer, and A. C. Clare, in *The Structure of Noncrystalline Materials*, P. H. Gaskell, J. M. Parker, and E. A. Davis, Eds., Taylor & Francis London, 1983, p. 395.
66. S. J. Gravina, P. J. Bray, and G. L. Petersen, *J. Noncryst. Solids*, **123**, 165 (1990).
67. P. J. Bray and J. G. O'Keefe, *Phys. Chem. Glasses*, **4**, 37 (1963).
68. H. M. Kriz, M. J. Parki, and P. J. Bray, *Phys. Chem. Glasses*, **12**, 45 (1971).
69. G. W. Brady, *J. Chem. Phys.*, **28**, 48 (1958).
70. A. J. Leadbetter and A. C. Wright, *J. Noncryst. Solids*, **7**, 37 (1972).
71. S. Sakka, H. K. Kozuka, K. Fukumi, and F. Miyaji, *J. Noncryst. Solids*, **123**, 176 (1990).
72. F. L. Galeener, *J. Noncryst. Solids*, **123**, 182 (1990).
73. B. Meyer, *Chem. Rev.*, **64**, 429 (1964).

74. A. F. Wells, *Structural Inorganic Chemistry*, Oxford, 1984, p. 700ff.
75. G. Gee, *Trans. Faraday. Soc.*, **48**, 515 (1952).
76. E. H. Henninger, R. C. Buchert, and L. Heaton, *J. Chem. Phys.*, **46**, 586 (1967).
77. A. V. Tobolski, G. D. T. Owen, and A. Eisenberg, *J. Colloid Sci.*, **17**, 717 (1962).
78. R. Zallen, *The Physics of Amorphous Solids*, Wiley, New York, 1983, p. 86ff.
79. S. R. Elliott, *Nature*, **354**, 445 (1991).
80. G. H. Bauer, W. Fuhs, and L. Ley, Eds., *J. Noncryst. Solids*, **137-138** (1991).
81. R. M. Almeida and J. D. Mackenzie, *J. Chem. Phys.*, **74**, 5954 (1991).
82. J. Lucas, D. Louer, and C. A. Angell, *Mater. Sci. Forum*, **6**, 449 (1985).
83. H. Inoue, H. Aseqawa, and I. Yasui, *Phys. Chem. Glasses*, **26**, 74 (1985).
84. Y. Kawamoto, F. Sakaguchi, and T. Horisaka, *J. Chem. Phys.*, **83**, 2398 (1985).
85. S. -H. Ko and R. H. Doremus, *Phys. Chem. Glasses*, **32**, 196 (1991).
86. B. E. Warren and C. F. Hill, *Z. Kristallogr.*, **A89**, 481 (1941).
87. J. Zarzycki, *Phys. Chem. Glasses*, **12**, 97 (1971).
88. A. J. Leadbetter and A. C. Wright, *J. Noncryst. Solids*, **7**, 156 (1972).
89. A. C. Wright, *J. Noncryst. Solids*, **123**, 129 (1990).
90. B. Brehler, *Naturwissenschaften*, **46**, 554 (1959).
91. G. M. Renlund, Ph. D. Thesis, Rensselaer Polytechnic Institute, 1989.
- 91a. A. F. Babonneau, K. Thorne, and J. D. Mackenzie, *Chem. Mater.*, **1**, 554 (1989).
- 91b. H. Zhang and C. G. Patano, *J. Am. Ceram. Soc.*, **73**, 958 (1990).
92. G. M. Renlund, S. Prochazka, and R. H. Doremus, *J. Mater. Res.*, **6**, 2716 (1991).
93. G. M. Renlund, S. Prochazka, and R. H. Doremus, *J. Mater. Res.*, **6**, 2723 (1991).
- 93a. J. Homeny and S. H. Risbud, *Mater. Lett.*, **3**, 432 (1985).
- 93b. J. Homeny, G. G. Nelson, and S. H. Risbud, *J. Am. Ceram. Soc.*, **71m** 386 (1988).
94. A. Bondi, in *Glass: Science and Technology*, D. R. Uhlmann and N. J. Kreidl, Eds., Academic Press, San Diego, CA, 1983, p. 339.
95. P. C. Hiemenz, *Polymer Chemistry*, Marcel Dekker, New York, 1984.
96. F. G. A. Stone and W. A. G. Graham, *Inorganic Polymers*, Academic Press, New York, 1962.
97. A. S. Nowick and S. Mader, *IBM J. Res. Dev.*, **9**, 358 (1965).
98. B. G. Bagley and D. Turnbull, *J. Appl. Phys.*, **39**, 5681 (1968); *Acta Met.*, **18**, 857 (1970).
99. P. Duwez, *Trans. ASM.*, **60**, 605 (1970).
100. G. S. Cargill, *J. Appl. Phys.*, **41**, 2248 (1970).
101. J. D. Bernal, *Proc. Roy. Soc.*, **280A**, 299 (1964).
102. J. L. Finney, *Proc. Roy. Soc.*, **319A**, 479, 495 (1970).
103. D. E. Polk, *J. Noncryst. Solids*, **5**, 365 (1971).
104. L. B. Davies and P. J. Grundy, *Phys. Stat. Sol.*, **8a**, 189 (1971); *J. Noncryst. Solids*, **11**, 179 (1972).
105. J. B. VanderSande and R. L. Freed, in *Glass: Science and Technology*, D. R. Uhlmann and N. J. Kreidl, Eds., Academic Press, San Diego, CA, 1983, p. 365.

PHASE SEPARATION

The separation of borosilicate glasses into two liquid phases has long been recognized¹ and is the basis of the Vycor process for the manufacture of 96% silica.² In this process, a sodium borosilicate glass is heat treated to separate the two liquid phases. Then the borate-rich phase is leached out with acid, leaving a honeycomb matrix of 96% silica. The channels in this matrix, which is sometimes called "thirsty glass", are a few hundred Ångströms or so in diameter, as shown in the electron micrograph in Fig. 1. This matrix sinters to a clear glass when it is heated to about 1000°C. Thus a glass similar to fused silica is produced without going to the high temperatures (above 1800°C) required to prepare fused silica.

Phase separation occurs in other commercially important glasses. For example, certain soda-lime silicate glasses can separate into two liquid phases after proper heat treatment,³ as shown in Fig. 2, and Pyrex borosilicate glass is phase separated on a very fine scale,⁴ as shown in Fig. 3. Phase separation can influence properties of glasses. Therefore a glass technologist must be aware of the possibility of phase separation; it can enhance the properties of his glasses, changing them adversely. Phase separation in a glass can sometimes bring about uniform crystallization in glass ceramics, as described in the next chapter.

Variations in glass composition often affect properties because of enhancement or elimination of phase separation. The addition of alumina to commercial soda-lime glass reduces the tendency to phase separation, thus reducing in turn weathering and devitrification (gross crystallization and consequent lower strength) of these glasses caused by a matrix phase high in soda.

Phase separation has been studied most intensively in the alkali silicates and borosilicates, and therefore the discussion deals mostly with these glasses.

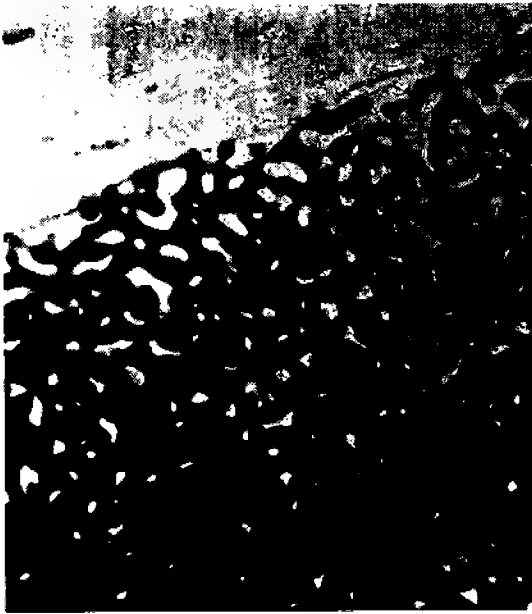


Fig. 1 Phase separation in a sodium borosilicate glass. The sodium borate phase was etched out with HCl. Transmission electron micrograph. Courtesy of Miss A. Turkalo. Magnification 26,000.

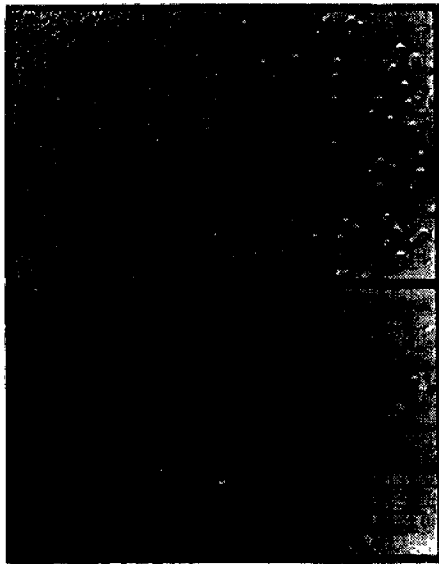


Fig. 2 Fracture surface of phase-separated glass (13% Na_2O , 11% CaO , and 76% SiO_2) after heating for different times at different temperatures.³



Fig. 3 Electron transmission photograph of Pyrex borosilicate glass in which silver ions have been exchanged for sodium ions to enhance contrast between the phases.⁴ Magnification 240,000.

Phase separation is also important in other glasses, such as the chalcogenides and beryllium fluorides.

In this chapter, experimental miscibility boundaries (phase diagrams) for phase separation in important glass systems are discussed first. Then some theories to explain these equilibrium properties are considered. Kinetic properties are treated next, with emphasis on nucleation and spinodal decomposition. An experimental test of nucleation theory for phase separation in a soda-lime silicate shows the validity of this theory. Finally the influence of phase separation on glass properties and some practical applications of phase separation in glasses are described. Reviews of phase separation in glasses are given in Refs. 5-8.

PHASE DIAGRAMS

Immiscibility in liquid solution is common. Many single-phase mixtures of organic liquids separate into two liquid phases as they are cooled. Certain liquid silicate mixtures also separate into two phases; examples of phase separation in alkaline earth silicates are shown in Fig. 4. The figure shows that the tendency to separate into two phases becomes greater as the cation becomes smaller; barium silicate mixtures do not show stable immiscibility. This correlation with ionic size has been the basis of certain explanations of phase separation in silicates and is discussed in the next section. In these explanations, the ratio of ionic charge Z to ionic radius r , called the "ionic potential," is used as a measure of the tendency to phase separation of silicates.

The ratio Z/r is plotted as a function of the width of the equilibrium immiscibility gap at its base for various binary silicate melts in Fig. 5. The temperature at the base is close to 1700°C for all the melts plotted, as shown in Fig. 4, so the base width should be an approximate measure of the tendency

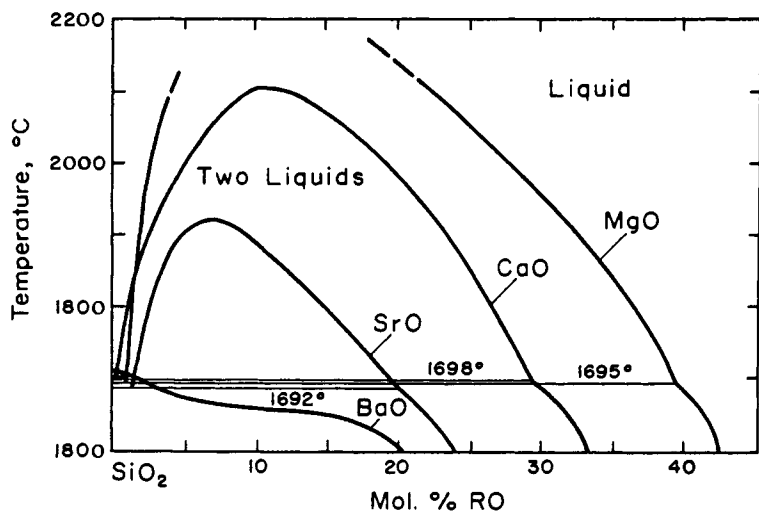


Fig. 4 Phase diagrams for binary alkaline-earth oxide-silica systems showing miscibility gaps.⁹

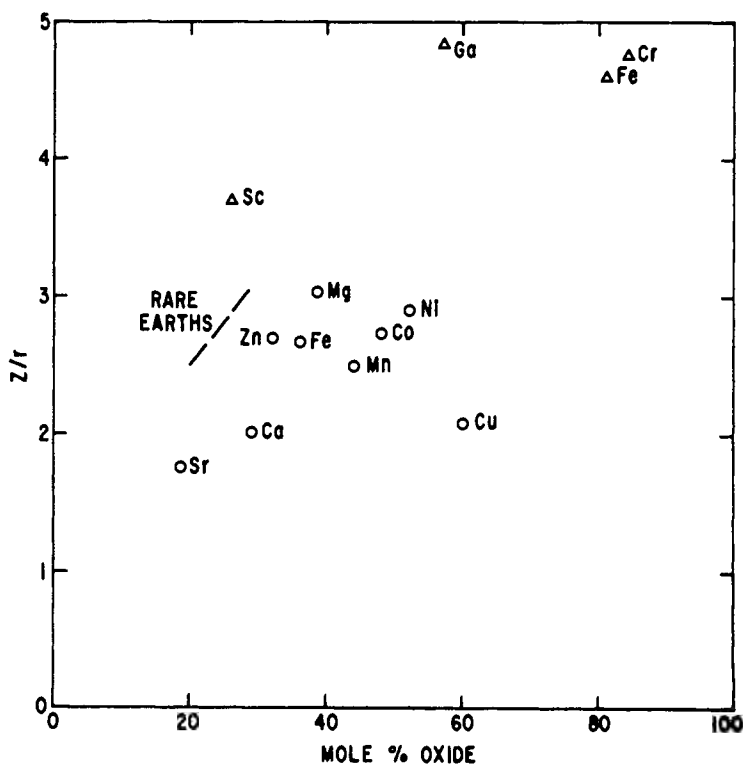


Fig. 5 Width of miscibility gap at its base for various binary silicate mixtures as a function of the charge over ionic radius (Z/r). O, two-valent ions; Δ , three valent ions; data on phase diagrams from Ref. 9.

to phase separation, as suggested by Glasser et al.¹⁰ The base widths were taken from phase diagrams in Ref. 9. If the tendency towards phase separation were determined by the Z/r ratio, all the points in Fig. 4 would fall on the same straight line. One could draw a line through the data for the divalent ions of Ca, Sr, Mn, Co and Ni, and a line from the Sr point to those for trivalent Fe and Cr does not deviate too much from the points for divalent Ca, Mn, Fe, Co, and Ni. However, the data for divalent ions Zn, Mg, and Cu do not fit with those already mentioned, and the trivalent rare earths together with scandium and gallium appear to form a separate group. Beryllium and lead silicates apparently show no stable separation possibly because these ions are tetrahedrally coordinated and act as glass formers at least in some concentration ranges. Several silicates of four-valent ions show stable two-liquid regions, but the extent of separation is less than would be expected from the Z/r ratio, especially for thorium, uranium, and zirconium silicates. Germanium and phosphorous silicates show no stable phase separation because they substitute for silicon in the silicon-oxygen network. Vanadium silicate with a high Z/r ratio shows no phase separation, although the similar niobium silicate separates into two liquids at 1695°C over most of the binary composition range. Therefore factors other than the charge and ion size can be quite important in determining the tendency of a binary silicate to separate into two liquid phases.

In binary alkali silicates there is no stable separation into two liquid phases. However, these silicates are easily cooled to glasses without crystallization, and some of them show liquid-liquid phase separation or immiscibility at temperatures below the liquidus temperature of crystallization. This type of phase separation is often called metastable, because crystalline phases are more stable than liquid ones at the temperatures of phase separation. The immiscibility curves for lithium and sodium silicates are shown in Fig. 6. There is some indication of phase separation in binary potassium silicates,^{11,12} but the immiscibility boundary has apparently not been determined. There is as yet no evidence for phase separation in binary rubidium and cesium silicates. The metastable immiscibility boundary for binary barium silicates is shown in Fig. 4.

Most of the data for these curves were found from the "clearing" temperature of the glasses, or the temperature above which the opalescent phase-separated glass becomes optically clear. This method is not entirely reliable, because the amount of light scattering depends on the size of the particles and the refractive index difference between the two phases. The light scattering per unit volume of particles is a maximum at an intermediate particle size. For particles very much larger or smaller than the wavelength of the incident light, the scattering is less. Thus if the size of the particles changes, or the refractive index difference changes as the composition difference between the particles and matrix changes, the clearing temperature may not always be at the phase boundary. The phase boundary can be determined most reliably from electron micrographs of quenched samples, if the quenching is fast enough to preserve the structure at the quenching temperature. If the composition of one phase is

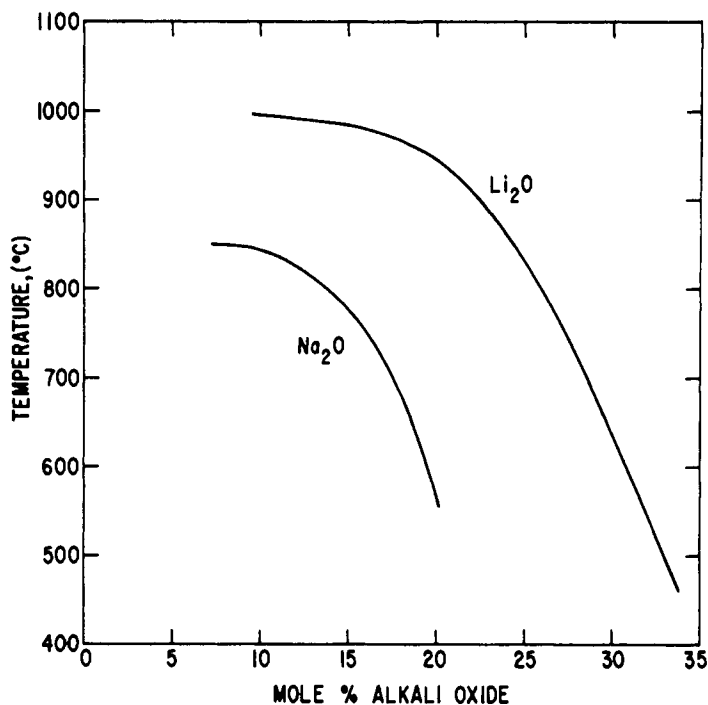


Fig. 6 Phase separation diagrams for lithium^{7,13,20} and sodium⁷ silicates.

known, the volume fractions of the separated phases as measured from the micrographs¹³ can also be used to calculate the phase boundary.

The metastable immiscibility boundaries of some alkali borates^{5,14} and borate-rich borate-silicates have been determined; however, there is evidence that only lithium borate among the binary alkali borates has an observable metastable miscibility boundary.¹⁶ The miscibility boundary of $\text{PbO-B}_2\text{O}_3$ has been determined.¹⁷

Burnett and Douglas have made a detailed study of phase separation in the commercially important ternary system of sodium calcium silicates,¹⁸ which form the soda-lime glasses. The addition of small amounts of soda to binary calcium silicates drops the immiscibility region below the liquidus temperature. No phase separation is observed below about 580°C because diffusional processes are too slow below this temperature. The maximum temperature of phase separation (consolute temperature) occurs at about 90 mol% SiO_2 for all ratios of the other components; in fact the consolute temperature in all alkaline earth and alkali silicates seems to occur at about 90% SiO_2 . The composition of the silica-rich phase in these glasses becomes almost 100% silica at temperatures not much below the consolute temperature.¹⁹

In both the soda-lime-silica¹⁸ and the soda-lithia-silica²⁰ systems, Douglas and his co-workers found that the reciprocal of the absolute immiscibility

temperature was linear with changing composition ratio of the nonsilicate ions, at constant silica composition. This relationship is probably valid for most multicomponent silicates. It provides a convenient means for finding immiscibility temperatures in complicated systems in which these temperatures for binary or ternary mixtures are known.

Burnett and Douglas also found that the composition c of the immiscibility curves for several binary and pseudobinary (ternaries with constant silica) silicate mixtures was related to the temperature T by the relation

$$|c_c - c| \propto (T_c - T)^n \quad (1)$$

where c_c and T_c are the composition and temperature at the critical consolute point, and n is a number usually between 1/4 and 1/2. Burnett and Douglas found n about equal to 1/2; theoretical estimates of n are given below.

Burnett and Douglas have also measured the immiscibility curves for the soda-baria-silica system;²¹ they are similar to the soda-lime-silica system except for the lower consolute temperature of the binary baria-silica system.

Another important commercial ternary system is that of sodium borosilicates. Results of several studies in this system have been summarized by Haller et al.^{22,23} and are shown in Fig. 7. There is some question about results in the silica-rich corner, and the positions of tielines.²⁴ As mentioned above, there is good evidence that silica-rich phases are nearly 100% silica in alkali and alkaline earth glasses. The results of Hair and Chapman²⁵ indicate that much of the boron that remains after leaching phase-separated borosilicate glass is on the internal surface of the leached glass and not in solution in the silica. Thus it seems likely that there is little solubility of borate in silicate, as would be expected from the different structures of these amorphous oxides described in the last chapter. Therefore, the silica-rich phases in sodium borosilicate glasses are also probably close to 100% silica.

The effect of small additions of "nucleating agents" such as TiO_2 and P_2O_5 , on phase separation in sodium and lithium silicates has been studied because these agents enhance nucleation of crystals in these glasses. James and McMillan concluded that P_2O_5 had only a small effect on the solubility of silica in the lithium-rich phase in lithium silicate glasses. Tomozawa²⁶ found that the "clearing temperature" of phase-separated sodium silicate glasses was increased by the addition of P_2O_5 , decreased slightly by the addition of TiO_2 , and remained unchanged when AlPO_4 was added. He explained the greater tendency to phase separation of P_2O_5 over TiO_2 as a result of the higher ionic potential (Z/r) of phosphorous than titanium ions, and the lack of an effect with AlPO_4 by the substitution of AlPO_4 for SiO_2 in the glass network.

Aluminum ion is known to have a strong tendency to reduce phase separation in silicates. For example, addition of 1.8 mol% Al_2O_3 to a sodium borosilicate glass of the consolute composition (in mol%, 70.5 SiO_2 , 27.7 B_2O_3 , 6.8 Na_2O) lowered the consolute temperature 111°C from 754°C.²⁷ The reason for this effect is uncertain.

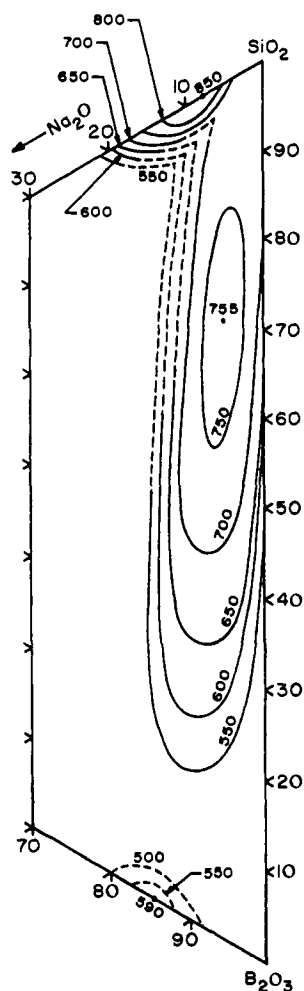


Fig. 7 Phase separation in the sodium borosilicate system.²² Dashed lines are uncertain.

The immiscibility range in alkaline earth silicates and borates is sharply reduced by the addition of alkali oxides. Shartiss et al.²⁸ made a detailed study of this reduction in borates. They showed that the effectiveness of alkali oxides in reducing phase separation was in the order $\text{Cs} > \text{K} > \text{Na} > \text{Li}$, which is the same order of decreased tendency to phase separation in the binary alkali silicates, and corresponds to a reduction in ionic size and increase in ionic field strength.

Phase separation has been found in several other of the glass-forming systems discussed in the last two chapters. Various alkali and alkaline earth fluoride-beryllium fluoride glasses show phase separation.^{5,29} A variety of chalcogenide glasses have regions of liquid-liquid immiscibility.³⁰ Some heavy-metal fluoride glasses show phase separation.^{31,32}

THEORIES OF IMMISCIBILITY

Various microscopic theories have been put forward to explain oxide miscibilities for different systems and compositions. In order to understand these theories, it is first useful to describe some thermodynamic parameters involved in the development of phase separation. This discussion is also important for an understanding of the proposed mechanism of spinodal decomposition for phase separation in glasses described in a later section.

The phase boundary between two liquid phases is related to the Gibbs free energies of the various possible phases. The free energy of two miscible components *A* and *B* as a function of composition is shown in Fig. 8a. The free energy of a single-phase mixture is always lower than the sum of the free energies of any two other phases. As the temperature is lowered, the single phase separates into two phases, and the free energy diagram has two branches, as shown in Fig. 8b. The compositions of the two phases in equilibrium correspond to the tangent points of the common tangent line. The shape of the free energy curve between the compositions of the equilibrium phases is uncertain because it is difficult to conduct experiments on the individual phases in the unstable region; they very quickly transform to the stable state. Two possible shapes of the free energy curves in the unstable region are shown in Figs. 8b and c.

Various theories can be used to derive free energy curves of the types shown in Fig. 8. The simplest is often called the regular solution or nearest neighbor model^{33,34} In this model, each component is assumed to be randomly distributed and coordinated with a certain fixed number *Z* of neighbors. In metallic alloys or mixtures of simple molecules such as organic liquids, the elementary mixing units are clearly the metal atoms or small molecules. However, in a network compound such as a silicate, it is often difficult to identify the mixing units that should be used for theoretical calculations, and this uncertainty leads to weakness in theoretical descriptions of miscibility in silicates, as described below.

The molar free energy of mixing, ΔG_m , is the free energy change when pure components are mixed to the desired composition, per mole of final mixture. In terms of the enthalpy and entropies of mixing,

$$\Delta G_m = \Delta H_m - T\Delta S_m \quad (2)$$

In this model it is assumed that the entropy change is the ideal entropy of mixing, or

$$\Delta S_m = -R(X_A \ln X_A + X_B \ln X_B) \quad (3)$$

where X_A is the mole fraction of component *A* and X_B is the mole fraction of component *B*.

The enthalpy change ΔH_m is assumed to equal the energy change ΔE_m . The total energy of the mixture is calculated from bond energies of nearest neighbors. It is also assumed that the bond energies are not a function of

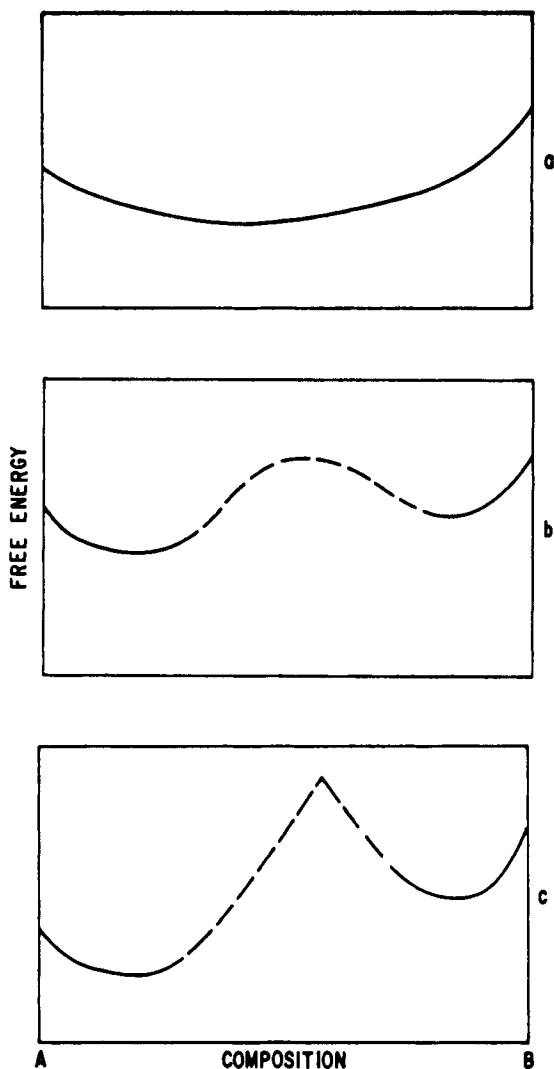


Fig. 8 Schematic diagrams of Gibbs free energy as a function of composition. (a) Complete miscibility; (b) separation into two phases; (c) separation into two phases, another possible functional dependence.

composition or temperature. In a mixture with A and B molecules, each with Z nearest neighbors, there are on average ZX_A molecules of A and ZX_B molecules of B around any given molecule in the mixture. Then if the total concentration of molecules in the mixture is c , the number of $A-A$ pairs per unit volume is $ZX_A^2c/2$, the number of $B-B$ pairs is $ZX_B^2c/2$, and the number of $A-B$ pairs is ZX_AX_Bc . If the energy of $A-A$ bonds is $-E_A$, $B-B$ bonds is

$-E_B$, and $A-B$ bonds is $-E_{AB}$, where the E s are positive quantities, then the total energy E per unit volume of the mixtures is

$$E = - \left(\frac{ZX_A^2 c E_A}{2} + \frac{ZX_B^2 c E_B}{2} + ZX_A X_B c E_{AB} \right) \quad (4)$$

or

$$E = - \frac{Zc}{2} \left[X_A E_A + X_B E_B + 2X_A X_B \left(E_{AB} - \frac{E_A + E_B}{2} \right) \right]$$

The first two terms in the brackets give the energies of pure A and B , so the energy of mixing is

$$\Delta E_m = - Zc X_A X_B \left(E_{AB} - \frac{E_A + E_B}{2} \right) \quad (5)$$

If the energy of $A-B$ bonds is greater (more negative) than the energy of $A-A$ and $B-B$ bonds, then $E_{AB} > (E_A + E_B)/2$, and ΔE_m is negative at all compositions. Under these conditions, the free energy function is as shown in Fig. 8a for all temperatures, and the two components are completely miscible at the temperatures where the equations apply. If, however, $E_{AB} < (E_A + E_B)/2$, then there is a tendency for like atoms to segregate, and below a certain temperature, the mixture separates into two different phases. The free energy as a function of composition is then given by Fig. 8b.

In applying these simple considerations to immiscibility in silicates there is uncertainty about the basic units for entropy considerations and about coordination numbers and bond strengths for energies. Warren and Pincus³⁵ made the following argument to explain the greater tendency of binary silicates to show immiscibility as the field strength (Z/r) of the cation increases. There are two tendencies for bonding in a binary silicate melt: one for the silicon ions to coordinate four oxygen ions tetrahedrally and the other for the other cation to surround itself with nonbridging (negatively charged) oxygen ions of the network. If the field strength of the cation is low its coordination is incomplete, and a single phase dominated by the silicon-oxygen network results. On the other hand, if the field strength of a cation is high, it is better able to coordinate nonbridging oxygens, and these groups then form a separate phase, the other phase being predominantly silica. Similar arguments were made by Levin and Block in their extension³⁶ of the work of Warren and Pincus. In terms of the nearest-neighbor theory, this point of view allows the coordination numbers of the different bond types to be different. Thus as the coordination number of the ion becomes larger in the mixture Z_{AB} can be considered to be larger, and the energy of mixing becomes positive, leading to phase separation. One can also consider the larger field strength of the modifier ion as leading to a larger bond strength E_{AB} , again favoring phase separation, as suggested by Rawson.³⁷ Thus the structural arguments of these authors involve the energetic contribution to the free energy of mixing. Understanding of the lack of phase separation

for ions that substitute for the network ions and more detailed calculations of energies are hampered by the uncertainty about just what units are mixing and bonding.

Charles³⁸ rejected the Warren-Pincus explanation of silicate immiscibility, at least in alkali and alkaline earth silicates, and substituted a description based on the deformation of the silica chains in the network. He argues that a more positive value of the energy of mixing ΔE_m as the cation concentration increases, required for immiscibility, results because of the distortion of the bridging silicon-oxygen bonds caused by the coulombic forces of the metal cations and negatively charged oxygen ions. The maximum energy occurs at some intermediate composition of cation determined by its field strength. Support for this view depends critically on the choice of the expression for the entropy of mixing. Charles asserts that the simple use of R_2O or RO and SiO_2 groups as the mixing entities is structurally unrealistic. He considered that the important mixing units are bridging and nonbridging oxygen ions, following a suggestion of Forland. The expression derived for ΔS_m from this model is

$$\Delta S_m = -R \left[X_A \ln \frac{X_A}{2X_B} + (2X_B - X_A) \ln \frac{2X_B - X_A}{2X_B} \right] \quad (6)$$

Whereas this equation seems more reasonable than Eq. 3 for a binary silicate, there is no direct experimental support for it, so that one must reserve judgement about Charles' approach until more experimental data on thermodynamic properties of silicate mixtures are available.

Charles also calculated the metastable immiscibility boundaries of the lithium and sodium silicate systems, shown in Fig. 5, from a subregular solution model.³⁹ In this model a more complicated equation for ΔE_m is used than Eq. 5, and the consolute temperature does not necessarily occur at the 50% composition (Ref. 34, pp. 196 ff.). Charles derived the activities of the components from the stable liquidus phase boundary. The consolute temperature of the immiscibility curve for sodium silicates was accurately predicted by Charles' treatment, but the predicted width was too small. The consolute temperature predicted for the lithium silicate system was 200°C too high, and the width was again too narrow. It seems likely that these discrepancies derive from the many simplifications implicit in the subregular solution model and also the uncertainties of deriving thermodynamic data at much lower temperatures from the liquidus phase boundary. McGahay and Tomozawa⁴⁰ have calculated the critical temperatures of a variety of "ionic" systems, including silicate glasses, organic polyelectrolytes, and exitonic silicon and germanium at temperatures near absolute zero, from an electrostatic model. They use the Debye-Hückel theory, which is valid for dilute aqueous solutions, to determine the thermodynamic properties of these systems. Their calculated critical temperatures were in good agreement with all of these systems. They assumed partial ionization of about 3%. It is surprising that the Debye-Hückel theory, which breaks down for concentrated aqueous solutions, can be used for these

dense solids. Perhaps the charges in them are highly screened from one another.

The exponent n of the miscibility line equation (Eq. 1) has been derived from quite general statistical considerations.⁴¹ One theory results from a three-dimensional Ising model as deduced from high temperature series, and the other from renormalization group methods. The former gives $n = 0.312$, the latter $n = 0.325$, and experiments⁴¹ seem to be closer to at 0.325. The value of 0.5 found for a soda-lime glass by Douglas and Burnett was a rough estimate based on few data. The results on lead borate glasses¹⁷ give a value of n of about $\frac{1}{3}$. The relationship between these statistical theories and the structural ones described above needs to be explored.

NUCLEATION

The rates of phase separation are important to the development of the morphologies of the phases and thus in some properties of phase-separated glasses such as electrical conductivity and chemical durability. In this and the next two sections various aspects of the kinetics of phase separation in glasses are considered and related to the morphology of the phase-separated structures. Also considered are the fundamentals of "classical" nucleation and growth for understanding kinetics of both phase separation and crystallization. In the following section, an alternative mechanism for phase separation, that of spinodal decomposition, is treated. In this discussion nucleation of a crystal from a pure liquid is first considered and then extended to nucleation of a second liquid phase or a crystal from a two-component liquid.

When a liquid is cooled below its melting point, small crystalline regions form by molecular fluctuations. However, the formation of these embryos is retarded because of the interfacial energy between them and the liquid. As the size of an embryo increases, its chemical potential decreases until it is less than that of the liquid, as shown in Fig. 9; then the embryo becomes a growing crystalline nucleus. The size at which the chemical potential of the embryo equals that of the liquid is called the critical size. The probability p of formation of an embryo of radius r is proportional to the exponential of the reversible work W_r done on the surroundings by the fluctuation to form the embryo:

$$p \propto \exp\left(\frac{W_r}{kT}\right)$$

where k is Boltzmann's constant and T the absolute temperature. The rate of formation I of growing crystalline nuclei is proportional to the probability of forming a critical nucleus, or

$$I = K \exp\left(\frac{W^*}{kT}\right) \quad (7)$$

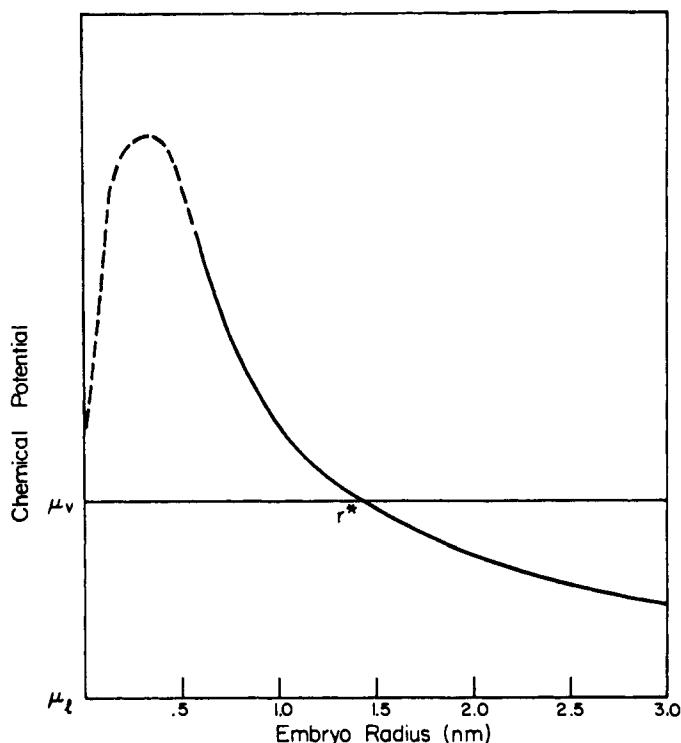


Fig. 9 Schematic drawing of the chemical potential of an embryo of phase B forming in phase A as a function of embryo size. From Ref. 44.

where W^* is the work done in forming the critical nucleus. A variety of methods of calculating the coefficient K have been suggested;⁴²⁻⁴⁴ the exponential term is usually predominant, especially in condensed systems. In this discussion, the dependence of K on composition and temperature is assumed to be negligible.

The work done in forming a spherical isotropic critical nucleus with isotropic surface energy γ is⁴⁵

$$W^* = -4\pi r^{*2}\gamma + \frac{4\pi r^{*3}\Delta P}{3} = -\frac{16\pi\gamma^3}{3(\Delta P)^2} \quad (8)$$

where ΔP is the pressure difference between the inside of the nucleus and the surrounding phase, and the radius of the critical nucleus r^* is given by

$$r^* = \frac{2\gamma}{\Delta P} \quad (9)$$

For a crystalline nucleus formed from a liquid of the same composition, the

pressure difference is equal to the free energy of fusion per unit volume at the temperature T of nucleation, and is approximately equal to

$$\Delta P \approx \frac{L}{vT_m} (T_m - T) \quad (10)$$

where T_m is melting temperature, L is the heat of fusion, and v is the molar volume of the liquid.

Equation 8 is valid for the homogeneous nucleation of a phase. In actual practice, nucleation is almost never homogeneous, but takes place on impurity particles, vessel walls, defects, or some other heterogeneity. These heterogeneities effectively lower the interfacial tension γ by a factor $f < 1$, so that

$$W^* = -\frac{16\pi(\gamma f)^3 v^2 T_m^2}{3L^2(T_m - T)^2} = -\frac{K_1}{(T_m - T)^2} \quad (11)$$

where K_1 is a coefficient approximately independent of temperature.

In condensed systems, the rate of formation of fluctuations can be limited by diffusion or viscous flow in the liquid. This transport limitation is particularly important in viscous systems such as glasses. It can be taken into account by adding a transport factor to Eq. 7 for the rate of nucleus formation. Then

$$I = K_2 \exp\left(\frac{W^* - Q}{RT}\right) \quad (12)$$

where Q is the activation energy for the transport process and K_2 is assumed independent of temperature. Without the transport limitation there is a very sharp increase in nucleation rate at some critical temperature below the melting temperature because of the $(T_m - T)^2$ factor in the exponential. However, with the transport factor there is a maximum in nucleation rate with decreasing temperature that can be quite broad, depending on the relative size of the two exponential terms.

Very similar considerations apply to nucleation of a liquid phase from a homogeneous liquid solution of two components. It is assumed that the nucleus forms with the equilibrium composition of one liquid phase and grows by accretion of material from the remaining matrix liquid. The composition of the nucleation phase, that is, the one forming discrete particles, is the equilibrium phase of composition furthest from the overall composition of the liquid. As an example, consider nucleation in lithium silicate glasses whose equilibrium phase-separation diagram is shown in Fig. 6. In a homogeneous glass containing 26 mol% LiO_2 and 74 mol% SiO_2 the silica-rich phase nucleates in the lithium-rich matrix below about 800°C because the equilibrium amount of the silica-rich phase is less than that of the lithium-rich phase. An electron micrograph of phase separation in this glass after heat treatment at 500°C (Fig. 10) shows silica-rich particles as raised circles because they etch more slowly in hydrofluoric acid than the lithium-rich matrix.

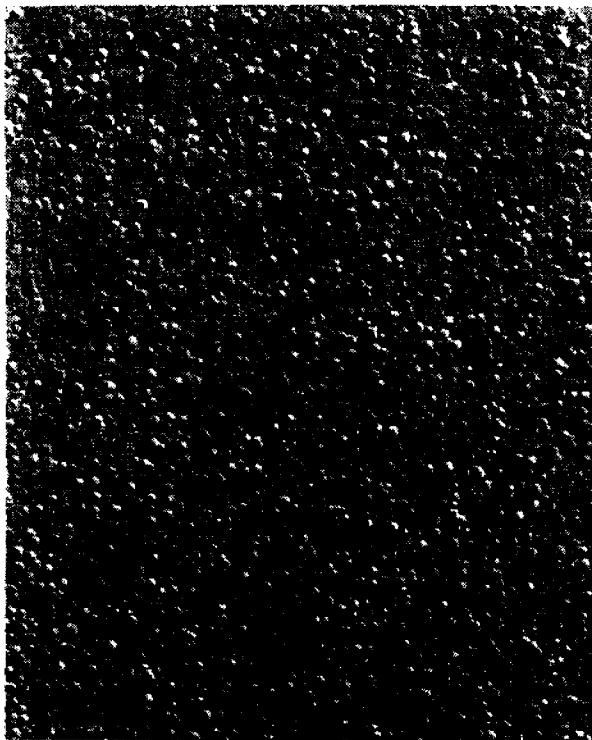


Fig. 10 Electron micrograph of phase separation in a 26 mol% Li_2O , 76% SiO_2 glass after 16 h at 500°C . Replica of fracture surface etched 5 s in 2% HF. Magnification 22,400.

In nucleation in a two-component system, the driving force ΔP for nucleation is a function of composition and is not given simply by Eq. 9. The expression for the driving force is (Ref. 42, p. 250)

$$\Delta P = G_1 - G_m - (c_1 - c_m) \left(\frac{\partial G}{\partial c} \right)_{cm} \quad (13)$$

where G_1 is the free energy of the nucleating phase of composition c_1 , and G_m is the free energy of the matrix of composition c_m (normally the bulk composition). The interfacial energy γ can also be a function of composition.

Hammel studied nucleation rates of silica-rich particles in a 13 mol% Na_2O , 11 mol% CaO , 76 mol% SiO_2 glass in detail.⁴⁶ The number of particles he measured as a function of time is shown in Fig. 11 for several different nucleation temperatures. The particles were measured from electron micrographs down to a radius of about 30 \AA ; since the radii of critical nuclei were in this size range, he apparently measured virtually all of the nucleated

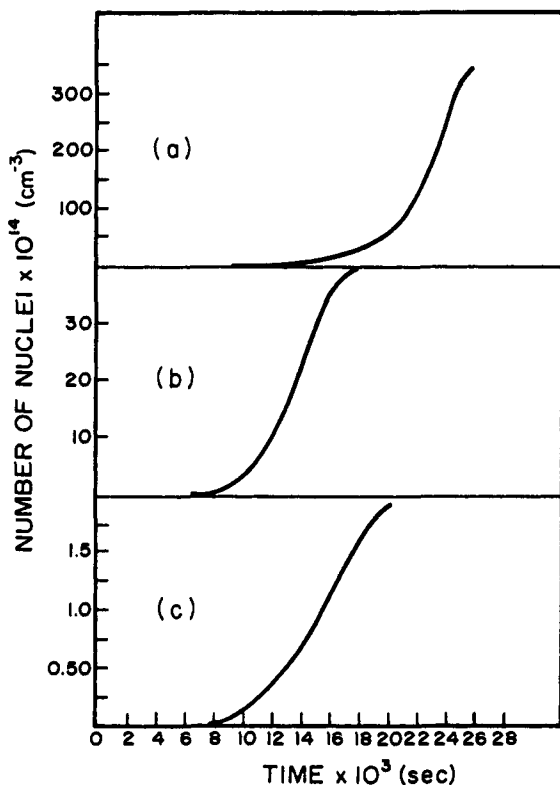


Fig. 11 Numbers of crystals in a 13 mol% Na_2O , 11% CaO , 76% SiO_2 glass as a function of time, measured by Hammel.⁴⁶

particles. Figure 11 shows that a constant rate of nucleation was achieved only after a period of time; this transient is discussed in more detail below. These constant rates are plotted as a function of nucleation temperature in Fig. 12.

In order to compare his results with the theory for homogeneous nucleation, Hammel measured the radius r^* of the critical nucleus at temperatures just below the miscibility gap. He made this measurement by holding a sample containing particles of a certain size in a temperature gradient and observing the temperature at which they neither grew nor dissolved, this then being the temperature at which the size was the critical size. If ΔP is proportional to the undercooling below the miscibility gap ΔT , a plot of $1/r^*$ against temperature should be a straight line; Hammel found this relationship. Then r^* at lower temperatures can be found by extrapolating the data at higher temperatures. To calculate the work W^* from Eq. 8 and r^* , it is necessary to know ΔP . Hammel calculated ΔP from the miscibility curve and various equations; the equation of Lumsden⁴⁷ seemed to give the best fit. As discussed in the last section, such calculations are rather uncertain. Hammel used the resulting value of W^* and $Q = 395 \text{ kJ/mol}$ as estimated from growth experiments

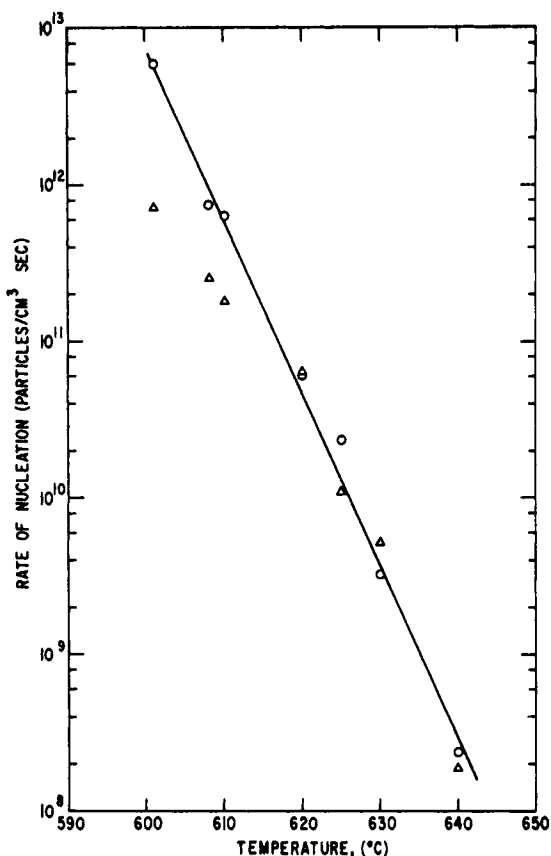


Fig. 12 Temperature dependence of the rate of nucleation of amorphous silica-rich particles in a 13 mol% Na_2O , 11% CaO , 76% SiO_2 glass. O, measured; Δ , calculated by Hammel.^{4,6}

described in the next section, together with a value of K_2 calculated from an equation of Turnbull⁴², to compute the nucleation rates shown in Fig. 12. The absolute values of calculated and measured rates are surprisingly close. This agreement between experimental and calculated nucleation rates, which is exceptional for nucleation experiments, provides evidence that the nucleation is homogeneous and supports the theory of nucleation outlined above.

The transient shown in Fig. 11 before reaching constant nucleation rate was also found by Burnett and Douglas¹⁸ in a study of nucleation in a glass containing 12.5 mol% Na_2O , 12.5 mol% CaO , and 75 mol% SiO_2 . These authors found that nucleation did not occur in their glass until it was at least 27°C below the miscibility temperature of 687°C. They studied nucleation by holding their glass at some lower temperature and then growing the nucleated particles at a temperature of 680°C where no more nucleation should occur. In

the early stages of nucleation before a constant rate of nucleation was achieved, the number of particles N followed the equation

$$N = K_3 \exp\left(\frac{-\tau}{t}\right) \quad (14)$$

so that the nucleation rate is given by

$$I = K_4 \exp\left(\frac{-\tau}{t}\right) \quad (15)$$

where K_3 , K_4 , and τ are parameters independent of time. Equations of this form were first derived by Zeldovich and subsequently by many other authors.^{44,48} Such a dependence of particle size occurs because the steady-state distribution of embryo sizes that is assumed in deriving Eq. 7 has not been set up yet, because of the slow diffusion in the condensed state. The parameter τ is related to the concentration of diffusing species and its diffusion coefficient.

GROWTH

In diffusion control, the rate of growth of a spherical particle of radius R is^{49,50}

$$\frac{dR}{dt} = \alpha \frac{D}{R} \quad (16)$$

where α depends only on concentrations, and D is a diffusion coefficient. The radius grows proportional to the square root of time.

At longer growth times, larger particles grow and smaller particles dissolve to decrease the total particle surface. This "Ostwald Ripening" or coarsening is often observed in phase-separated glasses, and occurs after the matrix has almost reached the equilibrium composition. The mathematical treatment for this process has been given by Lifshitz and Slyozov⁵¹ and Wagner⁵² based on earlier work by Greenwood.⁵³ The driving force for coarsening is provided by the higher solubility of the smaller particles, resulting in a transfer of material from them to the larger particles. The mean radius R of the particles is given by

$$R^3 - R_0^3 = \frac{8\gamma C_e D V_m t}{9KT} \quad (17)$$

in which R_0 is the mean particle radius when time $t = 0$, γ is the particle-matrix interfacial tension, C_e is the solute concentration, V_m is the molar volume of the particles, K is the gas constant, and T is the temperature. Thus the mean particle radius increases as $t^{1/3}$.

Hammel⁴⁶ studied the growth of phase-separated silica particles in a soda-lime silicate glass with 13 mol% Na_2O and 11 mol% CaO , the same composition used for his nucleation studies described above. He found that the particle radius increased proportionally to the square root of time, as required

for diffusion-controlled growth. He found an activation energy of growth of 395 kJ/mol, close to the activation energy of about 460 kJ/mol for viscous flow in glasses close to this composition, from diffusion coefficients calculated from Eq. 16. The solution was not dilute, so α was a function of composition as tabulated by Frank.⁵⁰ Hammel assumed that silica was the diffusing species. Burnett and Douglas¹⁸ also found that the particle size was proportional to the square root of time in the early stages of growth of silica particles in soda-lime glass.

In the later stages of growth, after the glass matrix is close to the equilibrium composition, the particles in phase-separated glasses grow by the coarsening mechanism of Eq. 17, as shown by proportionality of the particle radius to the cube root of time. From such measurements, Burnett and Douglas calculated an activation energy for diffusion of 247 kJ/mol for their glass containing 10 mol% Na₂O, 10% CaO, and 80% SiO₂, which is considerably smaller than the activation energy found by Hammel⁴⁶ for diffusion in a similar glass. The absolute values of the diffusion coefficients in the two studies were similar at 640°C: Hammel found $2.7(10)^{-15}$ cm²/s for growth, and Burnett and Douglas $0.6(10)^{-15}$ cm²/s for coarsening and $1.5(10)^{-15}$ cm²/s for growth.

This diffusion coefficient can be compared with that calculated from the viscosity η and the Stokes-Einstein equation

$$D = \frac{kT}{6\pi\eta R} \quad (18)$$

where R is the particle radius and k is the Boltzman's constant. For a D of $2.7(10)^{-15}$ at 640°C where the viscosity is about $2(10)^{11}$ P, the radius of the diffusing entity is 10^{-11} cm. Thus diffusion is apparently not directly related to viscous flow, in spite of the similarity between Hammel's diffusive activation energy and that for viscous flow.

Activation energies for diffusion have been calculated for other glasses from coarsening studies (composition in mol%): 10 Na₂O, 10 Li₂O, 80 SiO₂, 197 kJ/mol;²⁰ 1 K₂O, 26 Li₂O, 73 SiO₂, 297 kJ/mol.⁵⁴ 3 PbO, 97 B₂O₃, 343 kJ/mol;⁵⁵ 19 PbO, 76 B₂O₃, 5 Al₂O₃, 305 kJ/mol.⁵⁶ In all of these studies, as well as that of James and McMillan,¹³ the particle radius was proportional to the cube root of aging time, as required by Eq. 17.

MORPHOLOGY AND SPINODAL DECOMPOSITION

In the above studies, the volume fraction of particles was small and they grew as individual spheres. When the volume fractions of the two separating phases are not much different, the phases often separate into an interconnected structure, as shown in Fig. 1 (see also Ref. 57). Two explanations of this morphology have been advanced. The first explanation is that phase separation occurs by the mechanism of spinodal decomposition^{58,59} described below. The second is that particles nucleate and grow by the classical process described in

the last two sections, but then agglomerate to the connected structure because of their high volume fraction.⁶⁰

The theory of spinodal decomposition is based on the free energy diagram for a two-phase system shown in Fig. 8*b*. Vital to the theory is a region in which $\partial^2 G / \partial C^2$ is negative, where G is the free energy of the system and C is its composition. In such a region there is no barrier to phase growth, since any small fluctuation leads to a reduction in free energy. From this condition, Cahn derived the mechanism of spinodal decomposition.⁵⁸ In this mechanism, the transformation proceeds by a continuous change in the compositions of growing phases, whereas their extent remains constant. The composition changes take place in a regular three-dimensional array with a characteristic wavelength and grow until the compositions of the two phases reach the equilibrium values. This mechanism contrasts with the usual nucleation and growth process described above in which regions of constant composition (the equilibrium composition) nucleate and grow in size until the matrix also reaches the equilibrium value.

Cahn showed that the spinodal mechanism leads to an interconnected structure in an isotropic system such as one containing two liquid phases.⁶¹ Cahn and Charles⁵⁹ suggested that this mechanism was therefore the reason for the interconnected structure in glasses, since a computer solution of the spinodal equations gives a cross-section very similar to that found in glasses, such as shown in Fig. 1. The region of spinodal decomposition as estimated from various models agrees qualitatively with the compositions at which an interconnected structure is observed in glasses, except that this structure is usually not observed at temperatures just below the consolute temperature even for the consolute composition. This result may be caused by rapid agglomeration of the interconnected structure.

Several studies of the earliest stages of phase separation in the interconnected region have been made with small-angle X-ray scattering and compared to the spinodal equations.⁶²⁻⁶⁶ The height of the peak of scattered intensity as a function of angle is related to the composition difference between phases, whereas the angle at which the intensity is a maximum is related to the scale of the separation. Zarzycki and Naudin found that the angle of maximum intensity remained about constant with increase in aging time and height of the peak, as required by the spinodal mechanism, but this behavior was found only at the earliest aging times, as shown in Fig. 13. Stephenson⁶⁵ suggested that the influence of internal stress must be included to interpret small-angle scattering, and Yokota and Nakajima⁶⁶ concluded that relaxation of the glass changed the material transport as a function of time. It would be very desirable to have electron microscopic evidence to confirm these deductions from the small-angle X-ray work; until they become available, the evidence for the spinodal mechanism from this experimental technique remains tentative.

In support of the agglomeration mechanism of Haller, some electron micrographs have shown discrete particles agglomerating to an interconnected structure as they were aged.⁶⁷⁻⁶⁹ Thus it is possible for an interconnected

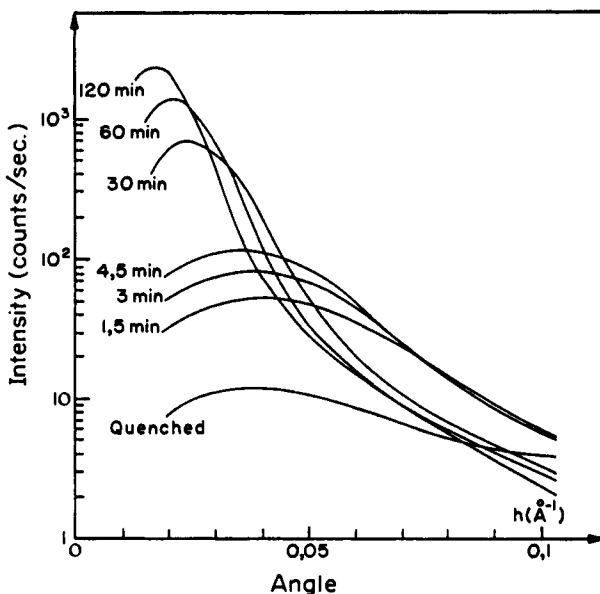


Fig. 13 Small angle X-ray diffraction spectra of a glass containing 76 wt% B_2O_3 , 19% PbO, and 5% Al_2O_3 , quenched from 1150°C and then heated to 450°C. From Ref. 55.

structure to develop from one with discrete particles; however, it is not proven that this is the way all interconnected structures in phase-separated glasses are formed.

The presence of a region in which $\partial^2 G / \partial C^2$ is negative for phase-separating glasses has not been established experimentally. Various theories of binary solutions, such as the one described above, lead to a free energy function with a continuous derivative, but this may be merely a mathematical convenience.

PROPERTY CHANGES AND APPLICATIONS RELATED TO PHASE SEPARATION

The viscosity of a phase-separated silicate glass is usually greater than that of a homogeneous glass of the same composition, because the separated silica-rich phase has high viscosity and dominates the flow behavior. The chemical durability of a glass can be increased by phase separation if the less durable phase is isolated from the corroding solution; if this phase is exposed to the solution, as in spinodal decomposition (see Fig. 1), the glass becomes less durable than if it were not separated. As Pyrex borosilicate glass is heated at 600°C, the scale of phase separation becomes larger, and the glass becomes less resistant to corrosion.⁷⁰

The electrical conductivity of a phase-separated silicate glass usually increases when the glass separates, if the higher conductivity phase is continuous.

Other properties, such as strength, density, and refractive index also change with separation, although not as much a viscosity and chemical durability.

The most important application of phase separation in glass has been the process of making high-silica Vycor glass, as described at the beginning of this chapter. The porous silica glass that is an intermediate step in this process can have pore sizes from 2 to 200 nm, and also has valuable applications, such as separation of biological substances of different sizes (viruses, proteins, cell component) by filtration.⁷¹ A porous surface layer produced by phase separation and partial leaching on a borosilicate glass provides an antireflection coating⁷² on the glass and can strengthen it with a compressive stress.⁷³ However, if too much stress is produced, the glass can fracture.⁷⁴

The size of pores in this glass can be changed by adding components to the original glass composition to alter the scale of the initial phase separation. Addition of molybdenum oxide to sodium borosilicate glass increases the scale of phase separation and thus of the resulting glass.⁷⁵ Molybdenum oxide also changes the scale of phase separation in other glass compositions.⁷⁶

REFERENCES

1. W. E. S. Turner and F. Winks, *J. Soc. Glass Tech.*, **10**, 102 (1926).
2. M. E. Nordberg and H. P. Hood, U. S. Patent 2, 106, 744 (1934).
3. S. M. Ohlberg, H. B. Golub, J. J. Hammel, and R. R. Lewchuk, *J. Am. Ceram. Soc.*, **48**, 178 (1965).
4. R. H. Doremus and A. M. Turkalo, *Science*, **164**, 418 (1969).
5. W. Vogel, *Glaschemie*, Translated into English, Am. Ceram. Soc., Columbus, OH, 1985.
6. M. Tomozawa, in *Treatise on Materials Science and Technology*, Vol. 17, Academic Press, San Diego, CA 1979, p. 71.
7. O. V. Mazurin and E. A. Porai-Koshits, Eds., *Phase Separation in Glass*, North-Holland, Amsterdam, 1984.
8. N. Kreidl, *J. Noncryst. Solids*, **129**, 1 (1991).
9. E. M. Levin, C. R. Robbins, and H. F. McMurdie, *Phase Diagrams for Ceramists*, American Ceramics Society, Columbus, OH, 1964; Supplement, 1969.
10. F. P. Glasser, J. Warshaw, and R. Roy, *Phys. Chem. Glasses*, **1**, 39 (1960).
11. Y. Kawamoto and M. Tomozawa, *J. Am. Ceram. Soc.*, **64**, 289 (1981).
12. J. M. Hyde and M. Tomozawa, *J. Noncryst. Solids*, **109**, 18 (1989).
13. P. F. James and P. W. McMillan, *Phys. Chem. Glasses*, **11**, 59, 64 (1970).
14. R. R. Shaw and D. R. Uhlmann, *J. Am. Ceram. Soc.*, **51**, 377 (1968).
15. R. J. Charles and F. E. Wagstaff, *J. Am. Ceram. Soc.*, **51**, 16 (1968).
16. E. A. Porai-Koshits, V. V. Golubhov, and A. P. Titov, in *Borate Glasses*, L. D. Pye, V. Frechette and N. J. Kreidl, Eds., Plenum Press, New York, 1977, p. 183.
17. J. H. Simmons, *J. Am. Ceram. Soc.*, **56**, 284 (1973).
18. D. G. Burnett and R. W. Douglas, *Phys. Chem. Glasses*, **11**, 125 (1970).

19. M. Yamane and T. Sakaino, *J. Am. Ceram. Soc.*, **51**, 178 (1968).
20. Y. Moriya, D. Warrington, and R. W. Douglas, *Phys. Chem. Glasses*, **8**, 19 (1960).
21. D. G. Burnett and R. W. Douglas, *Discuss. Faraday Soc.*, **50**, 200 (1970); *Phys. Chem. Glasses*, **12**, 117 (1971).
22. W. Haller, D. H. Blackburn, F. E. Wagstaff, and R. J. Charles, *J. Am. Ceram. Soc.*, **53**, 34 (1970).
23. G. Srinivasan, I. Tweer, P. B. Macedo, A. Sarkar, and W. Haller, *J. Noncryst. Solids*, **6**, 221 (1971).
24. O. V. Mazarin, M. V. Streltsina, and A. S. Totesch, *Phys. Chem. Glasses*, **10**, 63 (1969).
25. M. L. Hair and D. Chapman, *J. Am. Ceram. Soc.*, **49**, 651 (1966).
26. M. Tomozawa, in *Advances in Crystallization and Nucleation in Glasses*, American Ceramic Society, 1971, p. 41.
27. J. H. Simmons, P. B. Macedo, A. Napolitano, and W. K. Haller, *Discuss. Faraday Soc.*, **50**, 155 (1971).
28. L. Shartsis, H. F. Shermer, and A. G. Bestul, *J. Am. Ceram. Soc.*, **41**, 507 (1958).
29. W. Vogel and K. Gerth, *Glastech. Ber.*, **31**, 15 (1958); *Silikattech.*, **9**, 353 (1958).
30. E. Plumat, *J. Am. Ceram. Soc.*, **51**, 499 (1968).
31. M. J. Suscavage and O. H. el-Bayoumi, *J. Am. Ceram. Soc.*, **68**, C-259 (1985).
32. L. Boehm, K.-H. Chung, and C. T. Moynihan, *J. Noncryst. Solids*, **102**, 159 (1988).
35. A. H. Cottrell, *Theoretical Structural Metallurgy*, Edward Arnold, London, 1948, pp. 153 ff.
34. J. W. Christian, *The Theory of Transformations in Metals and Alloys*, Pergamon, London 1965, pp. 172 ff.
35. B. E. Warren and A. G. Pincus, *J. Am. Ceram. Soc.*, **23**, 301 (1940).
36. E. M. Levin and S. Block, *J. Am. Ceram. Soc.*, **40**, 95, 113 (1957); **41**, 49 (1958).
37. H. Rawson, *Inorganic Glass-Forming Systems*, Academic Press, New York, 1967, p. 123.
38. R. J. Charles, *Phys. Chem. Glasses*, **10**, 169 (1969).
39. R. J. Charles, *J. Am. Ceram. Soc.*, **50**, 631 (1967).
40. V. McGahay and M. Tomozawa, *J. Noncryst. Solids*, **109**, 27 (1989).
41. M. Levy, J.-C. Le Guillou, and J. Zinn-Justin, *Phase Transformations*, Plenum Press, New York, 1982 (see especially articles by D. Beyrens, p. 25 and J. V. Sengers, p. 95).
42. D. Turnbull, in *Solid State Physics*, Vol. 3, Academic Press, New York, 1956, p. 225ff.
43. J. W. Christian, *The Theory of Transformations in Metals and Alloys* Pergamon, Oxford, 1965, p. 377ff.
44. R. H. Doremus, *Rates of Phase Transformations*, Academic Press, San Diego, 1985, Ch. 5.
45. J. W. Gibbs, *Scientific Papers*, Dover, New York, 1961, p. 254.
46. J. J. Hammel, *J. Chem. Phys.*, **46**, 2234 (1967).
47. J. Lumsden, *Thermodynamics of Alloys*, Institute of Metals, London, 1952, p. 335.
48. D. Kashchiev, *Surf. Sci.*, **14**, 209 (1969).
49. C. Zener, *J. Appl. Phys.*, **20**, 950 (1949).
50. F. C. Frank, *Proc. Roy. Soc.*, **201A**, 586 (1950).

51. E. M. Lifshitz and V. V. Slyozov, *J. Phys. Chem. Solids*, **19**, 35 (1961).
52. C. Wagner, *Z. Electrochem.*, **65**, 581 (1961).
53. G. W. Greenwood, *Acta Met.*, **4**, 243 (1956).
54. R. A. McCurrie and R. W. Douglas, *Phys. Chem. Glasses*, **8**, 132 (1967).
55. J. Zarzycki and F. Naudin, *Phys. Chem. Glasses*, **8**, 11 (1967).
56. F. Naudin and J. Zarzycki, *Comptes Rendus*, **266**, 729 (1968).
57. R. J. Charles, *J. Am. Ceram. Soc.*, **47**, 559 (1964).
58. J. W. Cahn, *Acta Met.*, **9**, 745 (1961).
59. J. W. Cahn and R. J. Charles, *Phys. Chem. Glasses*, **6**, 181 (1965).
60. W. Haller, *J. Chem. Phys.*, **42**, 686 (1965).
61. J. W. Cahn, *J. Chem. Phys.*, **42**, 93 (1965).
62. J. Zarzycki and F. Naudin, *Comptes Rendus*, **265**, 1456 (1967); *J. Noncryst. Solids*, **1**, 215 (1969); **5**, 415 (1971).
63. G. F. Neilson, *Phys. Chem. Glasses*, **10**, 54 (1969).
64. M. Tomozawa, R. K. MacCrone, and H. Herman, *Phys. Chem. Glasses*, **11**, 136 (1970).
65. G. B. Stephenson, *J. Noncryst. Solids*, **66**, 393 (1984).
66. R. Yokota and H. Nakajima, *J. Noncryst. Solids*, **70**, 343 (1985).
67. T. P. Seward, D. R. Uhlmann, and D. Turnbull, *J. Am. Ceram. Soc.*, **51**, 634 (1968).
68. J. F. MacDowell and G. H. Beall, *J. Am. Ceram. Soc.*, **52**, 17 (1969).
69. R. H. Doremus, *Glass Science*, 1st Edn., Wiley, New York, 1973, p. 69ff.
70. M. Tomozawa and T. Takamori, *J. Am. Ceram. Soc.*, **62**, 370 (1979).
71. W. Haller, *Nature*, **206**, 693 (1965).
72. T. H. Elmer, *Am. Ceram. Soc. Bull.*, **58**, 1093 (1979).
73. M. G. Drexhage and P. K. Gupta, *J. Am. Ceram. Soc.*, **63**, 72 (1980).
74. G. W. Scherer and M. G. Drexhage, *J. Am. Ceram. Soc.*, **68**, 419 (1985).
75. H. Tanaka, T. Yazawa, and K. Euchi, *Yogyo-Kyokai-Shi*, **93**, 137, 700 (1985).
76. Y. Kawamoto, K. Clemens, M. Tomozawa, and J. T. Warden, *Phys. Chem. Glasses*, **22**, 110 (1981).

CHAPTER 5

CRYSTALLIZATION

Glass is metastable with respect to the crystalline phase at temperatures below its equilibrium liquidus temperature. The liquidus temperatures for commercial soda-lime glasses are usually between 900°C and 1000°C for crystallization of the compound “divitrite”, or $\text{Na}_2\text{O} \cdot 3\text{CaO} \cdot 6\text{SiO}_2$. In a zirconium fluoride glass, the liquidus temperature can be as low as 500°C. Glasses can form because the rate of crystallization is low, as discussed in Chapter 2.

Crystallization or “devitrification” of glass can lead to serious problems in glass manufacture because of the resultant changes in glass properties, such as viscosity and coefficient of thermal expansion. High stresses resulting from nonuniform contraction on cooling can cause fracture of the piece. Thus glass technologists have always been careful to avoid crystallization by not holding their glasses at temperatures where crystals grow rapidly. The proper conditions to avoid crystallization were found empirically, with the help of limited knowledge from phase diagrams. Recent experimental and theoretical studies on the crystallization of glass should be helpful in predicting crystallization rates in new compositions, and also in defining the limiting times and temperatures to which a glass piece can be subjected.

If crystals grow in the interior of a glass, its optical properties are changed because of light scattered by the crystals. This scattering can degrade desirable optical properties such as transparency; in an optical fiber for long distance transmission, even a small amount of crystals seriously degrades the transmission capability.

Opal glasses were among the first to be used for decoration, and have continued in this use to the present time. Their translucency derives from light scattered from internal crystals, resulting either from incomplete melting or from crystals that grew in the glass as it cooled. These glasses are often used

as glazes on decorative or practical objects; however, their low strength has limited wider application.

Some of the few really new materials developed recently are uniformly crystallized glasses or "glass-ceramics". These materials were first developed at the Corning Glass Works,^{1,2} and are made by special heat treatment of particular glass compositions to give a fine, uniform dispersion of crystals in the glass. These partially crystallized glasses can have many superior properties, such as high strength and impact resistance, low bulk and surface electrical conductivity, low dielectric loss, low chemical reactivity, low coefficient of thermal expansion, and a range of optical properties from clear to completely opaque or white resulting from light scattering from the crystals. Such glasses have been studied intensively since the original Corning discovery, and many companies now market them. Table 1 lists a few commercially available products with their enhanced properties and uses. Among other important uses not listed in the table are bearings, heat exchangers, reactor control rods, sealing, vacuum tube envelopes, substrates for electronic circuits, and capacitors. McMillan discusses these and other uses in his book entitled *Glass Ceramics*,³ as well as many other aspects of these materials. Beall⁴ has described new types of strong glass ceramics based on chain silicates such as enstatite; the microstructure of the enstatite glass ceramic is similar to that of natural jade ($\text{NaAlSi}_2\text{O}_6$).

Crystals usually form in glass by a nucleation and growth mechanism; a small region of the equilibrium crystal composition forms by nucleation and then grows. Sometimes metastable (nonequilibrium) phases nucleate. In this chapter, nucleation is discussed first, and then methods of measuring nucleation and growth rates along with results of these measurements and tests of nucleation theories are described. Then special agents added to the glass to form crystalline nuclei are considered and some morphologies of crystals in

TABLE 1 Properties and Uses of Some Commercial Glass-Ceramics

Glass Type and Company	Crystals	Properties	Uses
Corning 9606	$2\text{MgO} \cdot 2\text{Al}_2\text{O}_3 \cdot 5\text{SiO}_2$ (Cordierite)	Low expansion, transport to radar	Radomes
Corning 9608	β -Spodumene	Low expansion, chemical reactivity	Cookware
Owens-Illinois Cer-vit	β -Quartz	Very low expansion	Telescope mirrors
General Electric Re-X	$\text{Li}_2\text{O} - 2\text{SiO}_2$	Low electrical conduction high strength	Insulators

glass are shown. Finally rates of crystal growth in glasses are discussed in both silicate and fluoride glasses.

NUCLEATION

The theory of nucleation was first derived for formation of liquid drops from the vapor. Experiments in cloud chambers confirm the theory, with respect to temperature dependence, calculated values of surface energy, and absolute nucleation rates.⁵ Thus one has confidence in the ideas involved in the theory. To extend the theory to condensed phases, as described in the last chapter, uncertain assumptions are made about the mechanism of rearrangement of molecules in the matrix (liquid or glassy phase in the present case) to become part of the nucleating (crystalline) phase. The usual method is to assume that the rate of transferring molecules from one phase to another is proportional to the rate of diffusional jumping of molecules in the liquid. This assumption and the proportionality (geometric) factors in the pre-exponential are probably the most uncertain parts of nucleation equations for condensed phases.

Equations for the nucleation rate I of a phase were derived in the last chapter (see also refs. 5 and 6). For nucleation in a condensed phase, the rate I is

$$I = B \exp(-Q + W^*)/kT \quad (1)$$

where B is a constant not much dependent on temperature T , Q is the activation energy for molecular transport (or viscous flow) in the matrix phase, k is Boltzmann's constant, and W^* is the work to form a critical nucleus. For a spherical, isotropic nucleus

$$W^* = -16\pi\gamma^3/3(\Delta G_v)^2 \quad (2)$$

where γ is the interfacial energy between the nucleus and the matrix, and ΔG_v is the free energy change per unit volume for the transformation from matrix to critical nucleus. An approximate equation for ΔG_v for condensed phases is

$$\Delta G_v = L(T_m - T)/VT_m \quad (3)$$

where L is the heat of fusion, T_m is the melting temperature, and V is the molar volume of the matrix phase. Equation 3 assumes that the heat of fusion is not a function of temperature; a correction for its temperature dependence may be necessary for large undercoolings ($T_m - T$). The radius r^* of the critical nucleus is

$$r^* = 2\gamma/\Delta G_v \quad (4)$$

The above discussion is for homogeneous nucleation, in which a second phase forms in a matrix directly without interference of foreign particles, impurities, or defects. In liquids and solids, homogeneous nucleation is unusual, because it is difficult to remove nucleation catalysts. In glasses, these

catalysts for heterogeneous nucleation can be foreign particles, second phases, bubbles, surfaces, or defects. Segregation of dissolved impurities to interfaces can lower the interfacial energy, leading to a higher nucleation rate. An effective interfacial energy

$$\gamma_e = \sum_i f_i \gamma \quad (5)$$

where f_i is a correction factor for nucleation catalysts of a certain class i , can account for heterogeneous nucleation. In most situations, there are several different kinds of nucleation catalysts (values of f_i) that cause rapid nucleation at different undercoolings.

Figure 1 shows schematically the relative rates of nucleation and crystal growth as a function of temperature (undercooling). There is no barrier to growth, so it occurs at any undercooling. The barrier to nucleation results in very low nucleation rates until the undercooling is large enough; then the

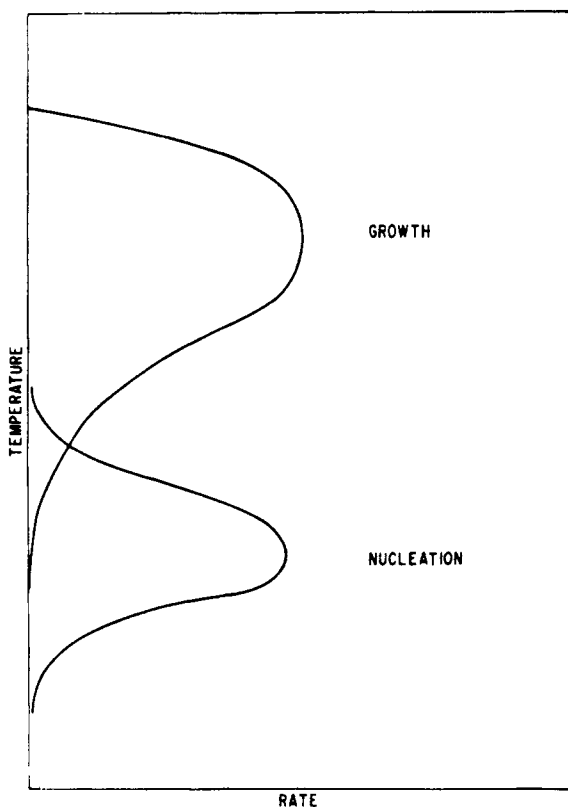


Fig. 1 Schematic representation of nucleation and growth rates of crystals in glasses.

nucleation rate increases rapidly with undercooling. The nucleation rates decrease at lower temperatures because molecular transport becomes slower.

In surface crystallization, impurities are the most important source of nucleation. On cooling from the melting temperature, dust particles adhere to the glass surface, giving preferred nucleation. Other impurities such as alkalis can corrode the surface, leading to lower glass-air surface tension and enhanced nucleation. The centers of cristobalite crystals growing on a vitreous silica surface when analyzed with the electron microprobe show impurities such as calcium or sodium. Thus the glass surface should be protected from dust and other impurities to prevent surface nucleation of crystals.

Impurity particles can nucleate uniform crystallization in glass. Fine metal particles grown in the glass can act as a center for crystallization. The platinum metals in concentrations of 0.001 to 0.1% catalyze crystallization in lithium silicate,⁷ lithium aluminum silicate, and alkali barium silicate glasses,⁸ and soda-lime glasses.⁹ The metal is added as a compound; it decomposes during glass melting and forms a very fine dispersion of metal particles, typically about 50 Å in diameter.⁶ The noble metals copper, silver, and gold, also act as nucleating agents in various lithium and barium silicate glasses, especially lithium aluminum silicates.² The noble metal can be added to the glass batch either as finely divided metal or as a compound. It dissolves in the glass in the ionic form during glass melting, and remains in this form if the glass is cooled quickly.¹⁰ If the glass contains some antimony or arsenic oxide, the noble metal precipitates on reheating. The particles nucleate continuously at a constant rate;¹¹ the efficacy of antimony and arsenic as nucleation agents apparently is related to their having two oxidation states in the glass, but the exact mechanism of nucleation of the metal is uncertain.

The noble metal particles can also be nucleated by ultraviolet light or X-rays.¹² Cerium oxide in the glass improves the photosensitive nucleation of noble metals.¹³ Again the efficacy of cerium as a nucleating agent is apparently related to its two oxidation states in the glass, and to its absorption band at 0.314 μm .¹⁴ One mechanism proposed was that the radiation caused electrons to be ejected from Ce^{3+} ions, and the electrons then reacted with the noble metal ions to form atoms, which agglomerated to a nucleus of a growing metal particle.^{10,11} However, it is possible to reduce gold ions to atoms with hydrogen in a photosensitive glass, and yet these atoms do not form particles without irradiation.¹⁵ Thus the nucleation mechanism is more subtle than a simple reduction process, and apparently involves an activated cerium ion¹⁴ as a nucleation agent. The noble metal ions must be reduced at some stage of the growth process, but this reduction can occur either before or during growth.¹⁵

Lithium metasilicate crystals formed in different configurations on metal particles in photosensitive glasses can be etched out to make useful shapes. This "chemical machining" is possible because the lithium metasilicate is much more soluble in hydrochloric acid than is the base glass. Tolerances of $\pm 50 \mu\text{m}$ are possible in Corning's "Fotoform" glass by this method. After machining, the remaining glass can also be crystallized to give better strength and

stability at high temperatures. These glasses have been used in printed circuit boards, dielectrics, and fluid amplifiers.

Lithium disilicate crystals in a 26 mol% Li_2O , 74% SiO_2 glass containing no added nucleating agent are shown in Fig. 2. The crystals are growing from an impurity particle, whose composition was not identified; it has flattened faces, implying that it is crystalline; perhaps it is platinum from the platinum melting crucible. Such a particle was found at the center of every cluster observed in this glass.¹⁶

Phase separation has been suggested as a precursor to uniform crystallization in glass. Often phase separation gives one amorphous phase that is more easily crystallized than the bulk glass. For example, in a sodium borosilicate glass, phase separation leads to one silica-rich phase and another sodium borosilicate phase containing less silica than the glass as a whole. This sodium borosilicated phase crystallizes during heat-treatment at relatively low temperatures, as shown in Fig. 3.

EXPERIMENTAL MEASUREMENTS OF NUCLEATION AND GROWTH RATES

The best way to measure nucleation rates is to observe the nucleated particles in a microscope after they have grown above the critical size (Eq. 4). However,

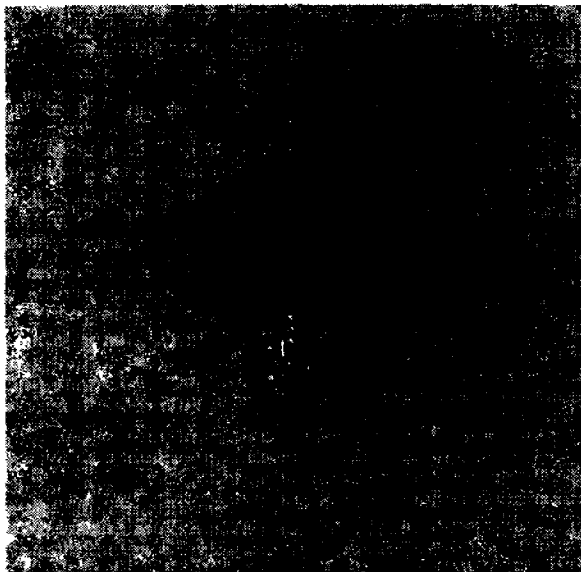


Fig. 2 Transmission electron micrograph of a cluster of lithium disilicate crystals growing in a 26 mol% Li_2O , 74% SiO_2 glass, heated for 243 min at 500°C. Unetched thinned section. Magnification 34,000.



Fig. 3 Replica electron micrograph of a phase-separated sodium borosilicate glass (49.7 wt% SiO_2 , 45.5% B_2O_3 , and 4.9% Na_2O) showing crystals growing in the borate-rich phase.

the critical sizes are extremely small, usually only a few tens of nanometers or less, so the crystals must be grown to a much larger size to be observed in the light microscope. Crystals near the critical size should be observable in thinned sections in the electron microscope, but this method has apparently not been used. Growth to larger sizes has been accomplished in two different ways. After nucleation at a particular temperature, the glass is held at the same temperature for a long time to grow the particles. This method gives reliable results, but often is not possible because growth rates are very slow at nucleating temperatures (see Fig. 1).

To overcome this difficulty, the second method is used: after nucleation at a particular temperature, the glass is heated to a higher temperature at which further nucleation is negligible and growth rapid (Fig. 1). If the difference between nucleating and growth temperatures is not too great, this method can give reliable counts of nucleated particle.^{17,18} However, for larger undercoolings, it is possible that some nucleated particles become subcritical at the higher temperature and dissolve. Equations 3 and 4 show that the size of a

critical nucleus, that is, a nucleus that is stable, decreases with greater undercooling. Thus a nucleus that forms at a low temperature is smaller than the critical size at a higher temperature, and can dissolve.

Experimental nucleation rates in a lithium disilicate glass as measured^{18,17} by the two-step process are plotted in Fig. 4. From Eqs. 1, 2 and 3 the temperature dependence of the nucleation rate I can be expressed as

$$\log I\eta = K/T(\Delta T)^2 \quad (6)$$

in which η is the viscosity of the glass matrix, K is a temperature independent parameter, and ΔT is the undercooling $T_m - T$. In Fig. 4, $\log I\eta/T$ is plotted as a function of $1/T(\Delta T)^2$; the factor of T in the logarithmic term results from a factor of T assumed to be in the pre-exponential coefficient B . A straight line on this plot agrees with Eq. 6; above about 440°C, such a line was found,¹⁸ but at lower temperatures, lower values of the nucleation rates were found than expected. It seems likely that these low rates resulted from dissolution of subcritical nuclei at the growth temperature of 560°C. Similar results were found in another study.¹⁹ From the slope of the line in Fig. 4 and Eqs. 1, 2 and 3 and the known heat of fusion and activation energy Q for viscous flow, one can calculate an interfacial energy of about 0.2 J/m² between lithium disilicate crystals and the melt of the same composition. There is no independent measurement of the interfacial energy.

The value of the pre-exponential factor B in Eq. 1 as calculated from these experiments on lithium disilicate glass is about twenty orders of magnitude

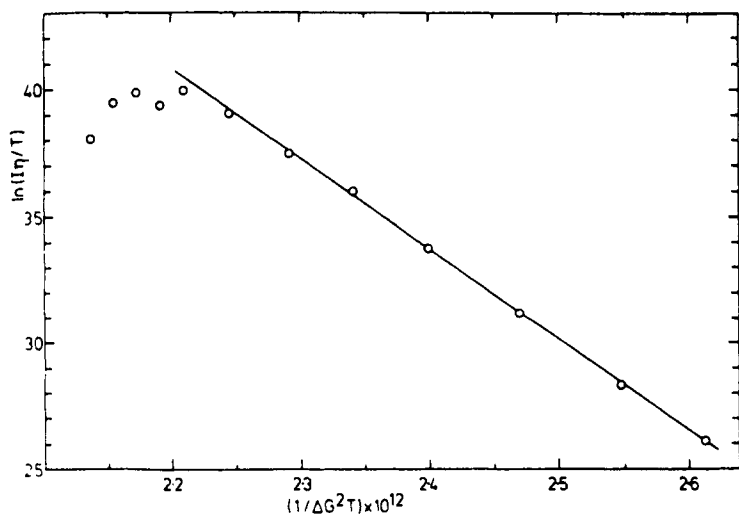


Fig. 4 Nucleation rates I in a $\text{Li}_2\text{O} \cdot 2\text{SiO}_2$ glass of $\text{Li}_2\text{O} \cdot 2\text{SiO}_2$ crystals. $\ln(I\eta/T)$ is plotted as a function $1/T\Delta T^2$; see Eq. 6: Reprinted from Ref. 18 with permission from Elsevier.

higher^{18,20,21} than expected from the theoretical value from Eq. 12, Ch. 4. James,¹⁸ showed that this discrepancy could be explained by a temperature dependence of the interfacial free energy resulting from small negative interfacial entropy: $\gamma = 0.029 + 0.16(10)^{-3} T$ in J/m², T in °K. Greer and Kelton analyzed the measured nucleation rates and time lags in lithium silicate glasses from refs. 17 and 19 with classical nucleation theory, and also found reasonable agreement if the interfacial free energy was temperature dependent.²² However, they found $\gamma = 0.094 + 7(10)^{-5} T$ J/m², which is quite different from that of James. Greer and Kelton also found that their calculated interfacial energies increased sharply from this relation below about 440°C, confirming the conclusion drawn above from Fig. 4 that nucleation measured rates at these lower temperatures were probably low. In metals the solid-vapor interfacial energy decreases as the temperature increases as expected from a positive interfacial entropy (Ref. 5, p. 38). It is also possible that the simple geometrical factors for interfacial rearrangement are not valid for this system.

Nucleation rates of BaO · 2SiO₂ and Na₂O · 2CaO · 3SiO₂ crystals in glasses of the same composition by two-step development and direct counting also gave the temperature dependence expected from Eqs. 1, 2 and 3 and values of interfacial energy of 0.13 and 0.18 J/m², respectively.^{18,21} The pre-exponential factors calculated from these rates were again much higher than calculated theoretically. Again this discrepancy can be removed by postulating a temperature-dependent interfacial energy.

Another method of calculating nucleation rates is from measurements of the crystallized volume of a glass as a function of time and independent measurements of the rate of crystal growth G , assumed to be constant with time. The radius of a spherical particle that has grown for a time t is then Gt , and the volume of the particle $V = 4\pi G^3 t^3 / 3$. If the rate of nucleation I per unit volume per unit time is constant (steadystate), then the volume fraction w_x of the glass crystallized is (Ref. 5, p. 25)

$$w_x = \int_0^t VI \, dt = \frac{4\pi G^3 I}{3} \int_0^t (t - \tau) \, d\tau = \frac{\pi G^3 I t^4}{3} \quad (7)$$

Equation 7 is valid before the individual crystals grow into one another; after collision, the volume fraction is²³

$$w = 1 - \exp(-w_x) \quad (8)$$

If the nucleation rate I is not constant but is a function of time, the time dependence of the volume fraction w is approximately

$$w = 1 - \exp(-Kt)^n \quad (9)$$

where K is a constant. If nucleation is rapid compared to growth and takes place on a fixed number of sites, the number of particles is constant with time and $n=3$, because

$$w = NV = 4\pi NG^3 t^3 / 3 \quad (10)$$

where N is the constant number of particles per unit volume. If the nucleation rate I decreases with time, $3 < n < 4$; if it increases with time, $n > 4$. Equations 8 and 9 are often called the Avrami equations.

If the growth of the particles involves diffusion in the melt, for example when the glass composition is different from that of the crystals, then lower exponents n are expected.⁵

Equation 7 has been used to calculate nucleation rates in sodium disilicate²⁴ and anorthite²⁵ ($\text{CaO} \cdot \text{Al}_2\text{O}_3 \cdot 2\text{SiO}_2$). The temperature dependence was that expected from the theory, and interfacial energies of 0.055 and 0.19 J/m² were calculated. The pre-exponential factor was found to be close to that expected theoretically. However, in later work, the bulk (homogeneously nucleated) phase in the anorthite work was found to be metastable.²⁶ It is not clear why the pre-exponential in these studies was that expected, whereas in the other systems a temperature-dependent interfacial energy was required to give agreement.

The kinetics of crystallization can be followed in a differential scanning calorimeter (DSC), which measures the temperature difference between a standard and a sample. In an isothermal measurement in the DSC, a phase transformation gives a peak in the output, which is a measure of the rate of transformation dW/dt as a function of time, as shown in Fig. 5. Integration of the area under the curve for different times, gives the fraction of transformation W as a function of time, and a plot of $\ln[-\ln(1 - W)]$ versus \ln time, as shown

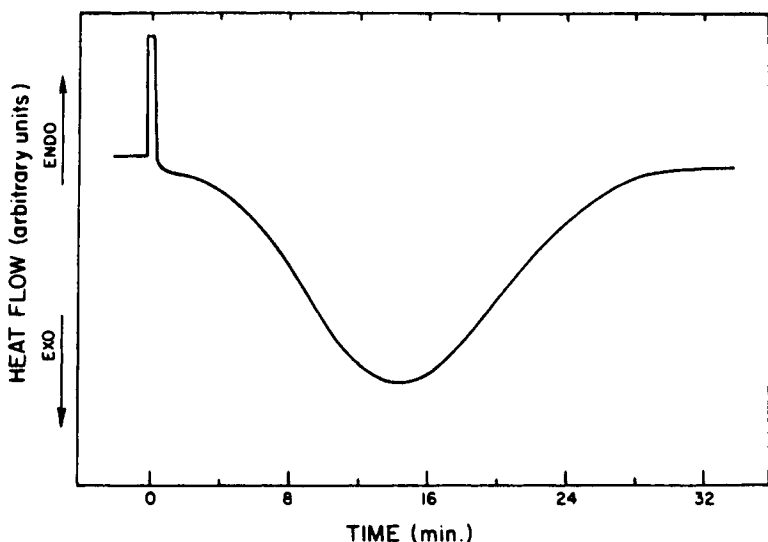


Fig. 5 DSC curve for isothermal crystallization of ZBL fluoride glass at 362°C (see Table 2 for glass composition). Reprinted from Ref. 30 with permission from the American Ceramic Society.

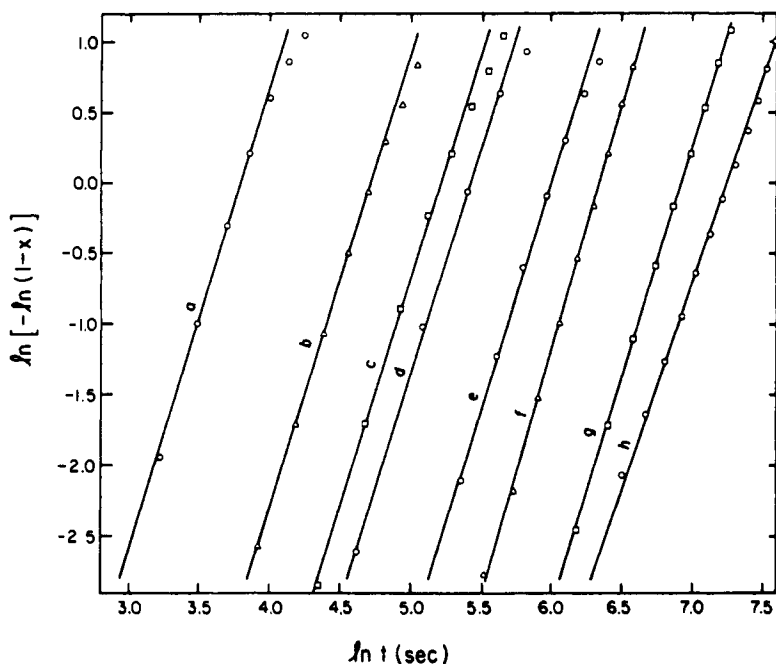


Fig. 6 Isothermal crystallization of ZBL fluoride glass, plots from Eq. 8 at temperatures °C: (a) 397; (b) 387; (c) 382; (d) 377; (e) 372; (f) 367; (g) 362; (h) 357. Reprinted from Ref. 30 with permission from the American Ceramic Society.

in Fig. 6, gives a straight line with slope n . The value of K for each temperature can be plotted as a function of temperature to find the activation energy Q :

$$K = v \exp(-Q/RT) \quad (11)$$

where v is a constant, R is the gas constant, and T the absolute temperature.

The DSC can also be used to measure Q and n from nonisothermal (constant heating or cooling rate α) experiments.²⁷⁻³¹ A series of crystallization peaks at different heating rates are shown in Fig. 7. The temperature at the peak maximum T_p and the activation energy Q are related in the equation³⁰

$$\ln(T_p^2/\alpha) = \ln(Q/R) - \ln v + Q/RT_p \quad (12)$$

Thus the activation energy Q can be found from a plot of $\ln(T_p^2/\alpha)$ versus $1/T_p$ for different heating rates. The exponent n can be found from the width of the DSC curve δ at half the maximum temperature²⁸

$$n = \frac{2.5 RT_p^2}{\delta Q} \quad (13)$$

The above treatment of nonisothermal DSC measurements is valid both for diffusion and interface controlled crystallization rates, as long as the tempera-

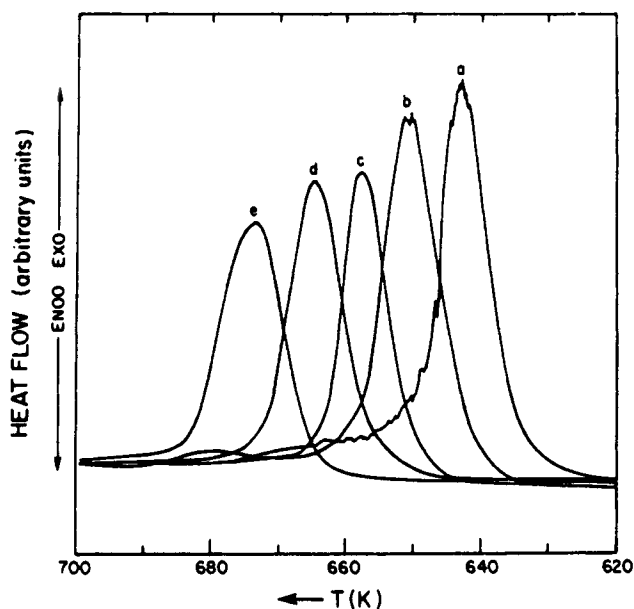


Fig. 7 DSC crystallization for ZBL fluoride glass at constant heating rates of (a) 1.25; (b) 2.5; (c) 5.0; (d) 10.0; (e) 20.0 K/min. Reprinted from Ref. 30 with permission from the American Ceramic Society.

ture dependence of K is given by an Arrhenius relation (Eq. 1). Effectively one assumes that the transformation is a function of W and temperature only; this assumption is sometimes called the "concept of additivity".^{32,33} In addition, Eq. 11 implies that growth is controlled by the transport-related interface process that is dominant at large undercoolings (see section on growth). At small undercooling, the growth rate increases as the temperature decreases (factor of ΔT), reaches a maximum and then decreases at larger undercooling, because of the influence of the reduction in transport (viscosity or diffusion in liquid) (see Fig. 1). It is only in this lower temperature range that Eq. 11, and consequently the above treatment of nonisothermal growth, are valid. If the DSC crystallization peak occurs close to the melting temperature, a more complicated temperature dependence must be used.

If the number of particles is not constant, but increases because of continued nucleation (n values > 3 for interface control), the temperature dependence must also include that of nucleation. If the experiment is being conducted on the low temperature side of the nucleation maximum (see Fig. 1), the temperature dependence of the nucleation rate is probably the same as for crystallization (see nucleation section), so Eq. 11 with a single activation energy can be used. However, if the crystallization temperature is near or above the temperature of maximum nucleation rate, the temperature dependence of the total

crystallization process becomes more complicated than given by Eq. 11, and the above treatment cannot be used for nonisothermal DSC measurements.

DSC measurements have been used to study crystallization in zirconium fluoride glasses, as described in the section on growth. They have also been used for crystallization studies in binary lithium silicate and lithium silicate glass ceramics, as described in the next section.

NUCLEATING AGENTS

The addition of "nucleating agents", such as titanium dioxide, phosphorous pentoxide, zirconium dioxide, and fluorides, to certain glasses leads to enhanced rates of uniform crystalline nucleation. The mechanism of nucleation by these agents is uncertain in most cases, although much work has been done on them and many mechanisms proposed.

The most widely used nucleating agent is titanium dioxide, TiO_2 . This agent was used in much of the early work on glass-ceramics in such glasses as lithium aluminum silicates and magnesium aluminum silicates.² TiO_2 is quite soluble in silicate glasses and lowers their viscosity considerably. In yttrium aluminum silicate, no nucleating agent is needed.³⁴

Phosphorous pentoxide, P_2O_5 , has been used successfully as a nucleating agent in various lithium silicate and magnesium aluminum silicate glasses by McMillan and his co-workers.³ Small amounts of P_2O_5 can influence crystalline nucleation rates strongly.

A number of other oxides have been used as nucleation agents.^{3,35} Among these are zirconium, chromium, vanadium, tungsten, molybdenum, iron,³⁶ zinc, and nickel. All the other nucleating agents except the last two have metallic ions with a high valence and field strength. This correlation may have some connection with the importance of field strength in bringing about phase separation, as described in the preceding chapter.

Fluorides have been used as nucleating agents in alkaline earth and alkali aluminosilicate glasses^{3,37} and soda lime glasses.³⁸ This use follows from the traditional application of fluorides in opal glasses and glazes.

Mixed cadmium sulfide and selenide acts as a nucleation catalyst in various glasses;³ the glass must be melted under reducing conditions to prevent oxidation of the sulfur or selenium, and the resulting glass ceramic is yellow or orange.

The heat-treatment of glasses containing nucleation agents is often carried out in two stages. First the glass is given a "nucleation treatment" at a temperature just above the annealing temperature; it is then crystallized at a higher temperature. The separation between these two processes is not sharp since some crystallization probably occurs during the nucleating treatment.

At least three different mechanisms have been proposed for the action of nucleating agents. They can be classified as agent crystallization, catalysts of

phase separation, and reduction of interfacial tension. Each is discussed in turn.

As discussed above, metal particles can act as nuclei for uniform crystallization, so the first idea was that nucleating agents act by precipitating from the glass as fine crystals during the nucleation heat treatment; they then serve as sites for crystallization of the main crystalline phase at the higher "growth" temperature. However, for most nucleation agents there is little or no evidence supporting this mechanism. Cadmium sulfide or selenide probably crystallizes as a uniform colloidal dispersion in glass that could catalyze nucleation. A fluorosilicate phase crystallizes first in alkaline earth aluminosilicate glasses,³⁷ but it is not certain that this phase nucleates the major phase. For the common nucleating agents such as TiO_2 and P_2O_5 , there is not much evidence that a crystalline phase containing them is the first phase to precipitate during heat-treatment to form a glass ceramic. Crystals containing these agents usually grow at temperatures much higher than the nucleating temperature in glasses containing them as nucleation catalysts

The sequence of phase separation and subsequent crystallization in a magnesium aluminosilicate glass containing titania has been found in one of the few definitive studies of the mechanism of a nucleation agent.³⁹ The sequence of events was followed with light scattered from inhomogeneities in the glass, which indicated that the glass separated into two phases upon cooling from its melting temperature. Treatment at about 750°C increased the anisotropy of the separated particles, which was interpreted as resulting from crystallization in them. X-Ray diffraction showed the presence of magnesium titanate, $\text{MgO} \cdot \text{TiO}_2$. Subsequent treatment at higher temperatures leads to the major crystalline phases of cordierite ($2\text{MgO} \cdot 2\text{Al}_2\text{O}_3 \cdot 5\text{SiO}_2$) and cristobalite. Thus in this glass, the sequence is phase separation, then crystallization in the titania-rich phase, whose crystals then act as nuclei for the major crystalline phases. Apparently the titania does not act as a catalyst for phase separation, but rather concentrates in one of the separated phases in which it crystallizes uniformly to very fine crystals, which then catalyze further growth.

In some uniformly crystallized glasses there is good evidence that phase separation does not precede crystallization of the major phases, even if nucleating agents are present. Barry et al. found that β -eucryptite and $\text{Li}_2\text{O} \cdot \text{Al}_2\text{O}_3$ crystals formed in various lithium aluminum silicate glasses containing TiO_2 before any crystalline titanate phases were present.⁴⁰ Figure 8 shows lithium disilicate crystals that grew in a multicomponent lithium disilicate glass which showed no phase separation either just after quenching or after various nucleating and crystallizing treatments. Thus in many, if not most, glass-ceramics, the nucleation agent does not enhance phase separation.

The crystallization of the lithium silicate glass shown in Fig. 8 was studied by nonisothermal DSC, using Eq. 12 to calculate the activation energy for crystallization.⁴¹ The crystals of lithium monosilicate ($\text{Li}_2\text{O} \cdot \text{SiO}_2$) were nucleated by Li_3PO_4 crystals at about 650°C ; at higher temperatures of about 850°C , the $\text{Li}_2\text{O} \cdot \text{SiO}_2$ crystals transformed to lithium disilicate ($\text{Li}_2\text{O} \cdot 2\text{SiO}_2$) by reaction with silica from the glass.



Fig. 8 Replica electron micrograph of lithium disilicate crystals growing in a multi-component lithium silicate glass, heated 1 h at 654°C and 4 h at 850°C. Magnification 26,000.

In many glasses with nucleating agents, neither phase separated regions nor crystals seem to be the nucleating sites. What is the mechanism of nucleation? After rejecting other possibilities, Hillig⁴² suggested that these agents lower the interfacial tension ν between the crystal and the glass, thus increasing the rate of nucleation by Eqs. 1 and 2. This idea has been confirmed by measurements of crystal numbers as a function of time in lithium aluminosilicate glasses containing different amounts of titania as a nucleating agent.⁴³ The change in numbers of nuclei could be explained only by a reduction in the work w^* of Eq. 2. The activation energy Q for viscous flow was independent of titania concentration. The change in titania concentration was too small to change the heat of fusion appreciably, so the increase in nucleation rates must result from a reduction in the interfacial energy γ . Ions of high field strength can possibly act as "surface active agents" to lower the interfacial energy. Barry et al.⁴⁰ have extended this idea in developing a detailed model for the enhancement of crystalline nucleation by titania in lithium aluminum silicate glasses. They argue that the Ti^{4+} ions associate with nonbridging oxygen ions, causing these

ions and alkalis to concentrate at the edge of domains enclosing bridging oxygens. With this model, Barry et al. explain some effects of composition on nucleation rate in their glasses. Their model is speculative, but it shows that the postulate of reduction of interfacial tension by nucleation agents is plausible.

MORPHOLOGY

When crystals grow from a glass surface they often form a flat front progressing into the interior on the glass. However, this growing front can have an irregular shape and contain crystals of varied morphologies.⁴⁴

In a binary lithium silicate glass the lithium disilicate crystals grew as spherical clusters, as shown in Figs. 1 and 9 in transmission electron micrographs.¹⁶

If a spherulite is defined as a spherical collection of crystals growing out of



Fig. 9 Transmission electron micrograph of a cluster of lithium disilicate crystals in 26 mol% LiO_2 , 74% SiO_2 glass, heated for 1034 min at 500°C. Unetched thinned section. Magnification 30,000.

a common center, then these clusters of lithium disilicate crystals could be called spherulites. However, many so-called crystalline spherulites in polymers, liquid crystals, and minerals have a complex structure.^{45,46} One characteristic feature of these complex spherulites is a cross-like figure in the polarizing microscope. These spherulites are often composed of helical, twisted strands of crystallites emanating from their center. In the early stages of growth, the morphology is sometimes similar to a sheaf.

Barry et al.⁴⁰ found some polarization figures somewhat like those in polymers in composite crystals of lithium metasilicate, $\text{Li}_2\text{O} \cdot \text{SiO}_2$, and β -eucryptite in lithium aluminosilicate glasses. However, most of these figures are not cross-like, but show some radial bands and other irregularities. Their complexity is undoubtedly related to the filamentary interwoven structure of the composite crystals, which may be similar to that of other complex spherulites, but probably also has unique features. Dendritic composite crystals also grow in these glasses.

When about 5 mol% alumina is added to a lithium silicate glass, the morphology of the lithium silicate crystals growing in it is sharply changed from spherical clusters to a laminar or micaceous structure, as shown by comparing Figs. 8 and 9. The reason for this change is not clear because the crystals apparently have the same composition in the two glasses.

In the sodium barium silicate system, barium disilicate crystals grow as spherulites at undercoolings of greater than 100°C according to Burnett and Douglas.⁴⁷ At smaller undercoolings, a platelet form of crystal grew either from the crucible wall or the glass-air surface. At an undercooling of about 100°C , the platelets developed perturbations that grew into fibrils at a size of about 1 mm. When the barium disilicate spherulites were aged for long periods, the spherulites broke up into a lath-like structure. The reason for this change in morphology is not clear; it could simply result from a reduction in surface energy from the spherulitic to lathlike form.

In a magnesium aluminosilicate glass with 7% zirconia, α -cordierite ($2\text{MgO} \cdot 2\text{Al}_2\text{O}_3 \cdot 5\text{SiO}_2$) crystallized at the glass surface as well as rods of tetragonal zirconia.⁴⁸ These crystals grew into the glass with the zirconia rods oriented perpendicular to the cordierite-glass interface, somewhat similar to "cellular" precipitation in metals. At longer times, the zirconia rods broke into particles. With 15% zirconia in the glass, the zirconia crystals grew as dendrites.

GROWTH

The rate of growth of a crystal from a melt of the same composition, also called freezing or solidification, is controlled both by heat flow and rearrangement process at the melt-crystal interface. It is difficult to be certain that heat flow is not a factor in experimentally observed crystallization rates. Here is a rough

estimate of the crystallization velocities above which heat flow can be important. The heat flux J generated during freezing is

$$J = u A \rho \Delta H_f \quad (14)$$

where A is the area of the growing crystal-liquid interface, ρ is the density of the crystal, u is the rate of crystal growth, and ΔH_f is the heat of fusion per unit mass of crystal. The heat flux also is proportional to the temperature gradient dT/dX ;

$$J = AK \frac{dT}{dX} \quad (15)$$

where again A is the area of heat generation and K is the thermal conductivity. Equating Eqs. 14 and 15 gives a relation for the temperature gradient in terms of known quantities. For a binary alkali silicate glass, using the parameters $K = 3(10)^{-2} \text{ W/cm K}$, $L\rho = 10^3 \text{ J/cm}^3$, $u = 10^{-4} \text{ cm/s}$, then $dT/dX = 3^\circ/\text{cm}$. Thus in a bulk sample with dimensions in centimeters, the crystal-glass interface can be 3° higher than the temperature of the external face when the crystallization rate is 10^{-4} cm/s . Therefore one might expect to find heat-flow effects in crystallization in glasses with growth rates higher than about 10^{-4} cm/s .

Maximum crystallization rates for a number of glasses are listed in Table 3 of Chapter 2. Those rates for silica, germania, phosphorous pentoxide, and the organic polymer polyethylene adipate are well below 10^{-4} cm/s , so it is probable that heat-flow effects are not important in crystallization in these materials. For the alkali disilicate and the borate glasses in the table, the rates are above 10^{-4} cm/s , so heat flow can be important in these glasses, depending on sample geometry.

If the rate of crystal growth is determined by the rate of incorporation of molecules into the crystal (interface control), then these rates should be influenced by interface structure. Some theories of solid-liquid interface structure are reviewed in Ref. 50, and computer simulations of the interface described in Refs. 51 and 52. Interface instabilities are reviewed in Ref. 53. These studies support the importance of the entropy of fusion in determining the interface structure and its influence on crystal growth. Jackson⁵⁴ first emphasized the importance of the entropy of fusion in his factor α :

$$\alpha = \Delta H_f / RT_m \quad (16)$$

When $\alpha < 2$, Jackson found a "rough" interface in which liquid molecules can transform to solid ones throughout the layer. For $\alpha > 2$, the interface is "smooth", so that molecules from the liquid can only be incorporated into the solid at steps in the solid surface.

Empirically the factor α is valuable in distinguishing between types of crystal growth from the melt. For $\alpha > 2$, growth is found to be anisotropic and faceted, whereas for $\alpha < 2$, growth is isotropic without facets. Furthermore, the simple

kinetic model to be described below fits crystallization rates for $\alpha < 2$ but not for $\alpha > 2$.

As the temperature of a liquid is lowered under its freezing point its rate of crystallization first rises to a maximum and then decreases, as shown in Fig. 1 of Chapter 2 for fused silica. This maximum can be understood qualitatively as follows. As the temperature difference from the freezing temperature becomes greater, the driving force for crystallization is increased, increasing the rate. However, the rate of motion of the molecules becomes slower as the temperature is lowered, decreasing their rate of incorporation into the crystals. The net effect of these two competing processes is a maximum in the growth rate.

Theories of varying complexity have been proposed to explain growth of crystals from the melt.⁵⁵⁻⁵⁷ However, their validity is still a matter of considerable controversy. In this discussion a simple equation is first compared to the experimental results of glasses, and then some of the more esoteric ideas that have been invoked for crystallization from the melt are discussed.

Consider a crystal growing into a melt of the same composition. The rate of crystallization should be proportional to two factors: a gradient of a driving force and a coefficient that is the unit force needed to bring about the rearrangement of liquid to solid. Fluxes in kinetic processes are usually linearly related to two such factors; H. A. Wilson suggested such a relation for crystallization velocity many years ago.⁵⁸ The driving force for crystallization from the melt at a temperature T is the difference in Gibbs free energy between the liquid and crystal,

$$\Delta G = \Delta H_f (T_m - T) / T_m \quad (17)$$

where ΔH_f is the heat of fusion at the melting point T_m . Equation 17 is valid when the heat capacities of the liquid and crystal are about equal. The velocity of crystallization u is the gradient in ΔG divided by a force f ,

$$u = \frac{\Delta H_f (T_m - T)}{f \lambda T_m} \quad (18)$$

f is the force required to rearrange the amount of material from liquid to crystal needed to give unit velocity, and λ is the thickness of the transition layer between liquid and crystal. The force to move a particle of diameter d through a medium of viscosity η at unit velocity is $3\pi\eta d$. If this force is the same as the force f in Eq. 18, and d is about the same size as λ , then

$$u = \frac{\Delta H_f (T_m - T)}{3\pi \lambda^2 \eta T_m} \quad (19)$$

Equation 19 has frequently been used to compare with solidification data. Equation 17 for the driving force should be reliable, and one would expect the rearrangement of molecules from liquid to crystal to be related to the viscosity.

Thus the temperature dependence of crystallization velocity and the dependence on ΔH_f and η should be given by Eq. 19. A convenient way to test the validity of the temperature dependence of Eq. 19 is to plot the product $u\eta$ as a function of temperature. Such a plot for crystallization and melting of germania⁵⁹ shows the linear dependence of $u\eta$ on ΔT and the continuity between crystallization and melting rates. Similar plots result for silica⁶⁰ and P_2O_5 glasses.⁶¹ See also Fig. 1, Ch. 2. Values of $u\eta/\Delta T$ calculated from Eq. 19 and measured are compared in Table 2, using $\lambda = 0.3$ nm. The calculated values are ten to twenty times lower for SiO_2 and GeO_2 and about equal to that measured for P_2O_5 . The discrepancies result from uncertainties in geometrical factors in Eq. 19, in the use of the force-velocity equation (sometimes called the Stokes-Einstein equation), and in values of λ and d . Nevertheless these comparisons suggest that the most important factors determining the crystallization rates in these oxides have been identified, especially for the temperature dependence.

Values of α in Table 2 are below two for SiO_2 and GeO_2 (rough interface) and above two for P_2O_5 . Consistent with the above discussion, growth of SiO_2 and GeO_2 crystals is isotropic, whereas P_2O_5 is faceted.

For many other glass-forming systems with large values of α (four or greater), the temperature dependence does not fit Eq. 19,⁵⁷ nor are melting and crystallization rates similar. The reason for these deviations from the simple theory are not clear.

Impurities and defects can markedly modify crystallization rates in glasses. These effects are usually related to changes in viscosity of the glass. For

TABLE 2 Comparison of Measured and Calculated Rates of Crystallization of Glasses

Glass	Crystal	$u\eta/\Delta T$ in cm P/sec °K		Reduced Entropy of Fusion L/RT_m
		Measured	Calculated	
Constant $u\eta/\Delta T$ at all undercoolings				
SiO ₂	Cristobalite	0.14	0.008	0.46
GeO	Hexagonal GeO ₂	0.21	0.02	1.3
P ₂ O ₅	Tetragonal P ₂ O ₅	0.035	0.036	3.1
17Na ₂ O, 12CaO	Divitrite			
2Al ₂ O ₃ , 69SiO ₂	Na ₂ O · 3CaO · 6SiO ₂	0.008		
Constant $u\eta/\Delta T$ at larger undercoolings only				
K ₂ O · 2SiO ₂	K ₂ O · 2SiO ₂	0.06		
Na ₂ O · 2SiO ₂	Na ₂ O · 2SiO ₂	0.05		3.7
Salol	Salol	$1.2(10)^{-4}$		> 3.0

example, fused silica crystallized much more rapidly in the presence of water or oxygen than without them.⁶² These gases are known to lower the viscosity of fused silica. Crystal growth in slightly reduced germania is faster than in stoichiometric material,⁵⁹ again paralleling a reduction in viscosity. Sodium impurity in germania also increases the growth rate; the effect may be intensified by concentration of the sodium ahead of the growing interface. Various transition metal ions, such as iron, zinc, and vanadium, at concentrations of a few percent were found to increase crystallization rates in alkaline earth aluminosilicate glass, whereas chromium ions decreased the rate of crystal growth.⁶³

The crystallization of organic polymers⁶⁴⁻⁶⁷ is a specialized subject not treated in depth here. The rate of growth of polymer crystals is often modeled by a "secondary" nucleation process at the growing crystal-liquid interface. The crystallization velocity for this kind of process fits an equation of the form

$$u = C \exp \left(\frac{-B}{RT} \right) \quad (20)$$

where B and C are coefficients constant with temperature. Such an equation was found by Hillig to be valid for growth in the c -direction of ice.⁶⁸ Hillig interpreted this functionality to result from the continued nucleation of new ice layers on the growing crystal.

An alternative model of polymer crystallization involves attachment of short polymer segments to the edge of a flat crystal.^{66,67} Sites on the top and bottom of the crystal are pinned by hooks and folding chains, so these surfaces do not grow. This model also seems to fit the temperature dependence of polymer growth rates.

In growth of crystals from the vapor phase, steps on the crystal surface sweep across it to add material. This "layer spreading" mechanism was confirmed by experiments on the growth of filamentary crystals or "whiskers".⁶⁹ This mechanism also can be important in crystal growth from the melt on "smooth" interfaces ($\alpha > 2$),⁵⁶ as shown by the elegant experiments of Sears on the melting and freezing of *p*-toluidine.⁷⁰ How widespread this mechanism is in crystal growth from the melt is not certain.

A suspension of colloidal particles about 0.2 μ m in diameter serves as a hard sphere model of crystallization in simple liquids and glasses; and of the glass transition.⁷¹ Such a suspension was studied as a function of volume fraction of the particles. Up to a volume fraction of 0.574, the simulated "crystallization" of these particles was analogous to classical nucleation and growth. Above this volume fraction, the "mechanism" of crystallization changed, and large asymmetric crystals formed. The authors identified the range of volume fractions from 0.574 to 0.581 with the glass transition. These particles with minimal interaction forces may be a reasonable model for molecular glasses such as glycerol, but it is not clear that they are valid models for network glasses such as silicates.

FLUORIDE GLASSES

Crystals in fluoride glasses can degrade the optical properties of these glasses and reduce their value for many applications in fiber optics and as optical components. Crystallization in these glasses has been described in reports from conferences on halide glasses.⁷²⁻⁷⁴ In this section, results of some studies at Rensselaer are discussed as an example of crystallization of these glasses. Compositions of some of the glasses studied are given in Table 3.

In zirconium barium based fluoride glasses, the main crystallizing phases are $\text{BaF}_2 \cdot \text{ZrF}_4$ and $\text{BaF}_2 \cdot 2\text{ZrF}_4$, both of which have α and β structural modifications. The heat of fusion of $\beta\text{-BaZr}_2\text{F}_{10}$ is estimated to be about 7800 J/mol from crystallization experiments with the DSC glass.⁷⁵ The melting temperature of this crystal is about 570°C, so $\alpha = 1.1$. This result agrees with the nonfaceted morphologies of surface crystals,⁷⁶ although spherulites were observed by Neilson et al.⁷⁷

The crystallization of a ZBL glass isothermally and at different heating rates was studied in the DSC by Bansal et al.³⁰ They found values of the activation energy Q and exponent n , calculated as described in the experimental section, within experimental error in the two methods. Thus one can use the nonisothermal method of calculating the kinetics parameters with confidence, with the condition that Eq. 11 gives the correct temperature dependence. In these experiments, the coefficient n was within experimental error of three, suggesting that the particles are all of the same size (rapid initial nucleation) and grow at a constant rate. Bansal et al.³⁰ found a final crystallite size of about 60 nm by X-ray line broadening, corresponding to a crystallite density of about $5(10)^{15}/\text{cm}^3$. Nucleation was probably homogeneous to give such a high, uniform density.

Measurements of kinetic parameters from DSC experiments for a variety of

TABLE 3 Acronyms and Batch Compositions of the Heavy Metal Fluoride Glasses

Glass	Glass Composition (mol%)						
	ZrF_4	BaF_2	LaF_3	AlF_3	LiF	NaF	PbF_2
ZB	65.0	35.0					
ZBL	62.0	33.0	5.0				
ZBLA	58.0	33.0	5.0	4.0			
ZBLLi	58.0	15.0	6.0	—	21.0		
ZBLN	58.0	15.0	6.0	—	—	21.0	
ZBLPb	58.8	31.4	4.8	—	—	—	5.0
ZBLAN	55.8	14.4	5.8	3.8	—	20.2	—
ZBLALi	50.7	20.7	5.2	3.2	20.2	—	—
ZBLALiPb	49.83	16.96	5.06	3.16	20.09	—	4.09

fluoride glasses are summarized in Table 4 (from Ref. 72, p. 434). These results show agreement between isothermal and constant heating rate measurements. For the ZB, ZBL, ZBLPb, and ZBLALi glasses, the exponent n is within experimental error of three, suggesting a constant number of particles growing at a constant rate (interface control). The ZBLA, ZBLLi, ZBLALiPb and ASYM fluoride glasses have n values significantly below three, suggesting some contribution of diffusion control in these glasses. Neilson et al.⁷⁷ measured the growth of crystals in ZBLA glass directly, and found that the radius of the particles grew proportional to the square root of time, as expected for diffusion control.

The activation energies for crystal growth in Table 4 are consistent with the activation energies for viscous flow in these glasses. The activation energy for viscous flow at the low temperatures is in the range from 1000 to 1500 kJ/mol, whereas at the higher temperatures, it is about 100 kJ/mol. The activation energies for crystallization are between these two values, and are about what one would expect for viscous flow at the crystallization temperature if a smooth curve is drawn between viscosity data at the two temperature extremes.

At 390°C, surface crystals on a ZBL glass grew at a rate of about $7(10)^{-7}$ cm/s. The bulk crystallization velocity v as calculated from DSC measurements and X-ray measurements of R_f , was about $4(10)^{-8}$ cm/s, or more than an order of magnitude lower. These results can be compared with a crystallization rate of 390°C calculated from Eq. 19. Estimates of the required parameters are: $\Delta H_f = 7.8$ kJ/mol, $T_m = 560^\circ$, $\Delta T = 170^\circ\text{C}$, $\eta = 2000$ Pa-s, $\lambda = 3(10)^{-10}$ m. Then u is about $1.5(10)^{-8}$ cm/s, which is in surprisingly good agreement with the measured value.

Crystallization in the system of BaZnYbTh fluoride glasses shows a complex series of crystalline phases, including a BaYbTh fluoride phase that decomposes to BaThF₆ and YbF₃ phases as the temperature increases, and partial dissolution of a zinc fluoride phase.⁷⁸

TABLE 4 Crystallization Parameters in Fluoride Glasses from Isothermal and Constant Heating Rate Measurements in the DSC

Glass	n		Q(kJ/mol)
	Isothermal	Constant Heating Rate	
ZB	3.1		374
ZBL	3.2	3.4	315
ZBLA		1.8	
ZBLALi	3.3	3.2	182
ZBLPb	2.9	2.8	320
ZBLLi	2.5	2.3	236
ZBLALiPb	2.2	2.3	190

REFERENCES

1. S. D. Stookey, U. S. Patents 2, 920,971 and 2, 933,857, 1960.
2. S. D. Stookey and R. D. Maurer, in *Progress in Ceramic Science*, J. E. Burke, Ed., Pergamon, New York, 1962, p. 77.
3. P. W. McMillan, *Glass-Ceramics*, 2nd edn., Academic Press, London, 1979.
4. G. H. Beall, *J. Noncryst. Solids*, **129**, 163 (1991).
5. R. H. Doremus, *Rates of Phase Transformations*, Academic Press, Orlando, FL, 1985, Ch. 4 and 5.
6. J. H. Simmons, D. R. Uhlmann, and G. H. Beall, Eds., *Nucleation and Crystallization in Glasses*, American Ceramic Society, Columbus, OH, 1982.
7. G. E. Rindone, *J. Am. Ceram. Soc.*, **45**, 7 (1962).
8. British Patent No. 863,569, 1961; see Ref. 3, p. 65.
9. C. J. R. Gonzalez-Oliver and P. F. James, in J. H. Simmons, D. R. Uhlmann, and G. H. Beall, Eds., *Nucleation and Crystallization in Glasses*, American Ceramic Society, Columbus, OH, 1982, p. 49.
10. S. D. Stookey, *J. Am. Ceram. Soc.*, **32**, 246 (1949).
11. R. D. Maurer, *J. Appl. Phys.*, **29**, 1 (1958).
12. R. N. Dalton, U.S. Patent, 2, 422,472, 1947.
13. S. D. Stookey, U.S. Patent 2, 515,275, 1940.
14. J. S. Stroud, *J. Chem. Phys.*, **35**, 844 (1961); **37**, 836 (1962).
15. R. H. Doremus, in *Symp. on Nucleation and Crystallization in Glasses*, American Ceramic Society, Columbus, OH, 1962, p. 119.
16. R. H. Doremus and A. M. Turkalo, *Phys. Chem. Glasses*, **13**, 14 (1972).
17. P. F. James, *Phys. Chem. Glasses*, **15**, 95 (1974).
18. P. F. James, *J. Noncryst. Solids*, **73**, 517 (1985).
19. K. Matusita and M. Tashiro, *J. Noncryst. Solids*, **11**, 471 (1973).
20. G. F. Neilson and M. C. Weinburg, *J. Noncryst. Solids*, **34**, 137 (1979).
21. P. F. James, in J. H. Simmons, D. R. Uhlmann, and G. H. Beall, Eds., *Nucleation and Crystallization in Glasses*, American Ceramic Society, Columbus, OH, 1982, p. 1.
22. A. L. Greer and K. F. Kelton, *J. Amr. Ceram. Soc.*, **74**, 1015 (1991).
23. M. Avrami, *J. Chem. Phys. I*, **7**, 1103 (1939); **8**, 212 (1940); **9**, 177 (1941).
24. L. C. Klein, C. A. Handwerker, and D. R. Uhlmann, *J. Cryst. Growth*, **42**, 47 (1977).
25. D. Cranmer, R. Salomaa, H. Yinnon, and D. R. Uhlmann, *J. Noncryst. Solids*, **45**, 127 (1981).
26. A. Hishinuma and D. R. Uhlmann, *J. Noncryst. Solids*, **94&96**, 449 (1987).
27. H. E. Kissinger, *J. Res. Natl. Bur. Stand.*, **57**, 217 (1956).
28. J. A. Augis and J. E. Bennett, *J. Thermal Anal.*, **13**, 283 (1978).
29. K. Matusita and S. Sakka, *J. Noncryst. Solids*, **38-39**, 741, (1980).
30. N. P. Bansal, R. H. Doremus, A. J. Bruce, and C. T. Moynihan, *J. Am. Ceram. Soc.*, **66**, 233 (1983).
31. X. J. Xu, C. S. Ray, and D. E. Day, *J. Am. Ceram. Soc.*, **74**, 909 (1991).
32. J. W. Christian, *The Theory of Transformation in Metals and Alloys*, Pergamon Press, Oxford, 1965, p. 492ff.
33. D. R. Macfarlane, M. Matecki, and M. Poulain, *J. Noncryst. Solids*, **64**, 351 (1984).
34. J. H. Arita, D. L. Williamson, and G. R. Purdy, *J. Am. Ceram. Soc.*, **75**, 3315 (1992).
35. I. Sawai, *Glass Technol.*, **2**, 243 (1961).
36. P. S. Rogers and J. Williamson, *Glass Technol.*, **10**, 128 (1969).

37. S. Lyng, J. Markali, J. Krogh-Moe, and N. H. Lundberg, *Phys. Chem. Glasses*, **11**, 6 (1970).
38. S. P. Mukherjee and P. S. Rogers, *Phys. Chem. Glasses*, **8**, 81 (1967).
39. R. D. Maurer, *J. Appl. Phys.*, **33**, 2132 (1962).
40. T. J. Barry, D. Clinton, L. A. Lay, R. A. Mercer, and R. P. Miller, *J. Mater. Sci.*, **4**, 496 (1969); **5**, 117 (1970).
41. W. F. Hammetter and R. E. Loehman, *J. Am. Ceram. Soc.*, **70**, 577 (1987).
42. W. B. Hillig, in *Symp. on Nucleation and Crystallization in Glasses and Melts*, American Ceramic Society, Columbus, OH, 1962, pp. 77.
43. U. Schiffner and W. Panhorst, *Glastech. Ber.*, **60**, 239 (1987).
44. H. R. Swift, *J. Am. Ceram. Soc.*, **30**, 165 (1947).
45. A. Keller, in *Growth and Perfection of Crystals*, R. H. Doremus, B. W. Roberts, and D. Turnbull, Eds. Wiley, New York, 1958, p. 499.
46. H. D. Kieth and F. J. Padden, *J. Appl. Phys.*, **34**, 2409 (1963).
47. D. G. Burnett and R. W. Douglas, *Phys. Chem. Glasses*, **12**, 117 (1971).
48. M. McCoy, W. E. Lee, and A. H. Heuer, *J. Am. Ceram. Soc.*, **69**, 2921 (1986).
49. W. Vogel, *Glas-chemie*, VEB/Deutscher Verlag für Grundstoffindustrie, Leipzig, Germany, 1979.
50. D. W. Oxtoby and A. D. Haymet, *J. Chem. Phys.*, **76**, 6262 (1982).
51. G. H. Gilmer, *Science*, **208**, 355 (1980).
52. D. Frenkel and J. P. McTague, *Annu. Rev. Phys. Chem.*, **31**, 491 (1980).
53. J. S. Langer, *Rev. Mod. Phys.*, **52**, 1 (1980).
54. K. W. Jackson, in *Growth and Perfection of Crystals*, R. H. Doremus, B. W. Roberts, and D. Turnbull, Eds., Wiley, New York, 1958, p. 319.
55. J. W. Cahn, W. B. Hillig, and G. W. Sears, *Acta Met.*, **12**, 1421 (1964).
56. K. A. Jackson, D. R. Uhlmann, and J. D. Hunt, *J. Cryst. Growth*, **1**, 1 (1967).
57. D. R. Uhlmann, in J. H. Simmons, D. R. Uhlmann, and G. H. Bell, Eds., *Nucleation and Crystallization in Glasses*, American Ceramic Society, Columbus, OH, 1982, p. 80.
58. H. A. Wilson, *Philos. Mag.*, **50**, 238 (1900).
59. P. J. Vergano and D. R. Uhlmann, *Phys. Chem. Glasses*, **11**, 30, 39 (1970).
60. F. E. Wagstaff, *J. Am. Ceram. Soc.*, **52**, 650 (1969).
61. R. L. Cormia, J. D. Mackenzie, and D. Turnbull, *J. Appl. Phys.*, **34**, 2239 (1963).
62. N. G. Ainslie, C. R. Morelock and D. Turnbull, in *Symp. on Nucleation and Crystallization of Glasses*, American Ceramic Society, Columbus, OH, 1962, p. 97.
63. J. Williamson, *Mineral Mag.*, **37**, 759 (1970).
64. L. Mandelkern, *Crystallization of Polymers*, McGraw-Hill, New York, 1964.
65. A. Keller, *Rep. Prog. Phys.*, **31**, Pt. 2, 623 (1968).
66. D. M. Sadler and G. H. Gilmer, *Polymer*, **25**, 1446 (1984); *Phys. Rev.*, **B38**, 5684 (1988).
67. G. Goldbeck-Wood, *J. Polym. Sci., Polym. Phys.*, **B31**, 61 (1993).
68. W. B. Hillig, in *Growth and Perfection of Crystals*, R. H. Doremus, B. W. Roberts and D. Turnbull, Eds., Wiley, New York, 1958, p. 350.
69. G. W. Sears, *Acta Met.*, **1**, 457 (1957).
70. G. W. Sears, *J. Chem. Phys.*, **23**, 1630 (1955).
71. W. Van Megan and S. M. Underwood, *Nature*, **362**, 616 (1993).
72. M. G. Drexage, C. T. Moynihan, and M. Robinson, Eds. *Mater. Sci. Forum*, **19-20**, 429 (1987).
73. M. Y. Yamane and C. T. Moynihan, Eds., *Mater. Sci. Forum* **32-33**, 185 (1988).

- 74. G. H. Frischat and C. T. Moynihan, Eds., *Mater. Sci. Forum* **67-68**, 187 (1991).
- 75. N. P. Bansal and A. J. Bruce, R. H. Doremus, and C. T. Moynihan, *SPIE*, **484**, 51 (1984).
- 76. N. P. Bansal and R. H. Doremus, *J. Am. Ceram. Soc.*, **66**, C-132 (1983).
- 77. G. F. Neilson, G. L. Smith, and M. C. Weinberg, *Mater. Res. Bull.*, **19**, 577 (1984).
- 78. R. Garcia, R. H. Doremus, N. P. Bansal, S. H. Ko, and T. Margraf, *J. Matls. Res.*, **3**, 989 (1988).

CHAPTER 6

VISCOSITY

The viscosity of a glass is one of its most important technological properties. It determines the melting conditions, the temperatures of working and annealing, fining behavior (removal of bubbles from the melt), upper temperature of use, and devitrification rate. The viscosities of different glasses vary enormously with composition and are strong functions of temperature.

When a shearing force is applied to a liquid, it flows and the viscosity is a measure of the ratio between the force and rate of flow. If two parallel planes of area A , a distance d apart, are subjected to a tangential force difference F , the viscosity η is defined as

$$\eta = \frac{Fd}{Av} \quad (1)$$

where v is the relative velocity of the two planes. The most common viscosity unit is the poise (P), which is a dyne-second per square centimeter or a gram per centimeter per second. In most literature, viscosity is reported in poises. The SI unit of viscosity is the pascal-second or Pa-s; 1 Pa-s = 10 P. The viscosity of most common fluids such as water and organic liquids is about one hundredth of a poise at room temperature.

The viscosity can also be defined in terms of a strain rate corresponding to an applied stress. For example, if a rod or fiber is pulled by a stress S , and it deforms at a rate dL/dt , where L is the length of the rod and t is the time, then

$$\eta = \frac{SL_0}{dL/dt} = \frac{S}{de/dt} \quad (2)$$

where L_0 is the initial length of the rod, and de/dt is the strain rate. This

relation is strictly valid only for the limiting deformation rate at the beginning of deformation. See Ref. 1 for a more complete discussion of the definition of viscosity, and Refs. 1 and 2 for consideration of viscoelasticity, the combination of elastic deformations and viscous flow.

The working point of a glass is defined as the temperature at which it has a viscosity of 10^4 P. At this temperature, the glass can be readily formed or sealed. The softening point of a glass is the temperature at which it has a viscosity of $10^{7.6}$ P. At this viscosity, a rod about 24 cm long and 0.7 mm in diameter elongates 1 mm/min under its own weight. The annealing point is the temperature at which the viscosity is $10^{13.4}$ P, and the strain point, the temperature at which the viscosity is $10^{14.6}$ P. The thermal expansion curve of an annealed glass begins to deviate considerably from linearity at a viscosity of about 10^{14} or 10^{15} P. At the annealing temperature, a rapidly cooled silicate glass becomes reasonably strain-free in about 15 min.

The viscosities of several commercially important silicate glasses are compared in Fig. 1, as a function of temperature. The working, softening, and

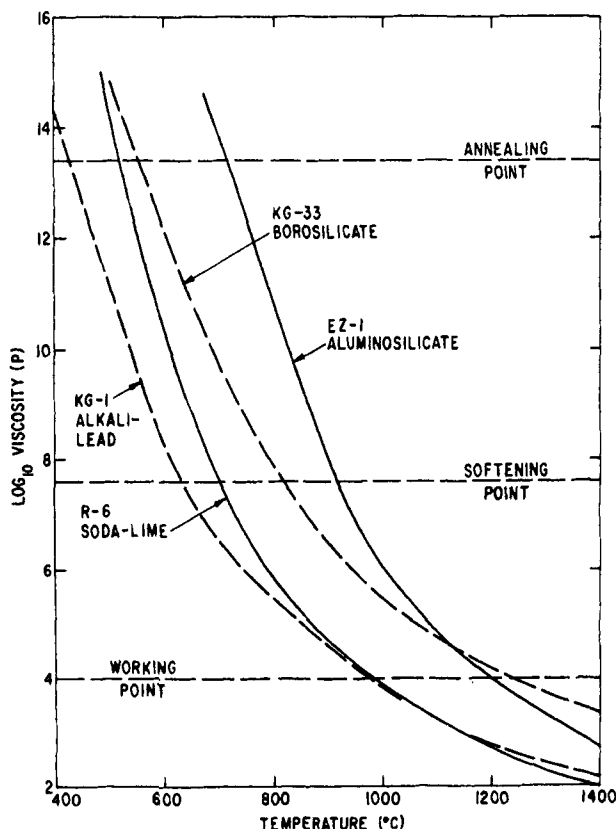


Fig. 1 Viscosity of some commercial silicate glasses listed in Chapter 1 Table 1.

annealing points are marked on the plot. Some other properties of these glasses and their approximate compositions are given in Chapter 1, Table 1.

MEASUREMENT

Two methods are most frequently used to measure viscosity in glass: one at low viscosity and the other at high viscosity. At low viscosity (up to 10^8 P), the rotating cylinder or crucible method appears to be the most reliable. In this method, the relative rate of rotation of two concentric cylinders is measured at a constant torque, and the viscosity is inversely proportional to the rate of rotation. Usually the viscometer is calibrated with liquids of known viscosity, but with care, absolute measurements can be made. Higher viscosities are measured by the rate at which a glass rod elongates under a fixed force. The viscosity is then given by the formula

$$\eta = \frac{Lmgf}{3\pi R^2 v} \quad (3)$$

where L is the length of the glass rod, R is its radius, m is the mass hanging on it, g is the gravitational constant, v is an instrumental reading proportional to the rate of elongation, and f is a calibration factor for the instrument.

Two problems arise in measuring the viscosity of viscous materials: one is the variation of viscosity with time, and the other is its variation with the force applied. Many investigators have found that the measured viscosity is not a function of applied force or velocity of flow,³ implying that glass is a Newtonian liquid in which the flow rate is directly proportional to the shearing stress. At high stresses, roughly above 50–100 MPa for silicate glasses, the apparent viscosity becomes smaller than at lower stresses at temperatures of 50–100°C above the glass transition temperature.^{4,5} At low stresses and high viscosities, elastic and anelastic (delayed but recoverable) deformations can interfere with viscosity measurements.^{2,6}

The deviations from Newtonian flow at high stresses possibly result because the glass melt develops a flattened or layered structure at these stresses,⁷ as also suggested by computer simulations of flow.⁸

Lillie studied the change of viscosity of glasses with time at the measuring temperature.⁹ He found that above a viscosity of about 10^{16} P, the viscosity of samples cooled quickly from a higher temperature initially appeared to be low, and asymptotically approached some higher value with time of holding at the measuring temperature. The same asymptotic "equilibrium" viscosity was found when a sample was held at a lower temperature for a long time and then raised to the measuring temperature. The deviation of the initially measured viscosity from the equilibrium viscosity became progressively greater at higher viscosities until, above about 10^{16} P, it was not possible to measure the equilibrium viscosity even after very long times at the measurement temperature. Thus this viscosity of 10^{16} P should be considered as the upper limit of

measurable values, and any viscosity measured higher than this cannot be considered an equilibrium value. These results and conclusions of Lillie have been confirmed in a more recent study of commercial soda-lime silicate glass rods and tubes in bending.¹⁰

The variation of viscosity with time of a quenched sample involves a structural change from a state characteristic of a higher temperature to that of a lower temperature. The change is slow because the structural elements of the glass rearrange slowly, as reflected in the high viscosity. The exact structural nature of this rearrangement is uncertain. As a rough model one can think of the glass network as being progressively broken up as the temperature increases. When a glass sample is cooled quickly from a higher temperature, the network flows more easily because it has more broken bonds than at equilibrium at the lower temperature. As these bonds heal with holding at the lower temperature the viscosity increases to the equilibrium value. This model, as well as stress relaxation and viscoelasticity, is discussed further in the next chapter on glass transition.

SIMPLE GLASS-FORMING OXIDES

As with many transport properties, the viscosity η fits an Arrhenius-type equation over some ranges of temperature:

$$\eta = \eta_0 \exp\left(\frac{Q}{RT}\right) \quad (4)$$

where Q and η_0 are temperature-independent coefficients called the activation energy and the pre-exponential factor, respectively.

Figure 2 shows the logarithm of viscosities of various simple glass-forming oxides as a function of reciprocal temperature. The activation energies for viscous flow of these glasses are given in Table 1.

The data for silica and germania were carefully selected from those of many workers as being the most reliable. The viscosity is decreased by the presence of small amounts of impurities, as discussed below; this is one of the main reasons for errors. Hetherington et al.¹¹ showed that at lower temperatures silica must be held for long times at the measuring temperature before a reproducible value of viscosity can be measured. Hofmaier and Urbain¹² suggested that the higher activation energies found by many investigators at lower temperatures resulted from mixtures of liquid and crystals. However, Hetherington et al. took their samples from the center of a silica block, and since only surface crystallization occurs in a pure sample, they should have avoided crystallization. Hofmaier and Urbain claimed that the measurements of Fontana and Plummer¹⁸ at low temperatures gave activation energies close to their high temperature values, but the absolute values of Fontana and Plummer agree closely with those of Hetherington et al., still implying a low activation energy at higher temperature. Some authors have stated that the

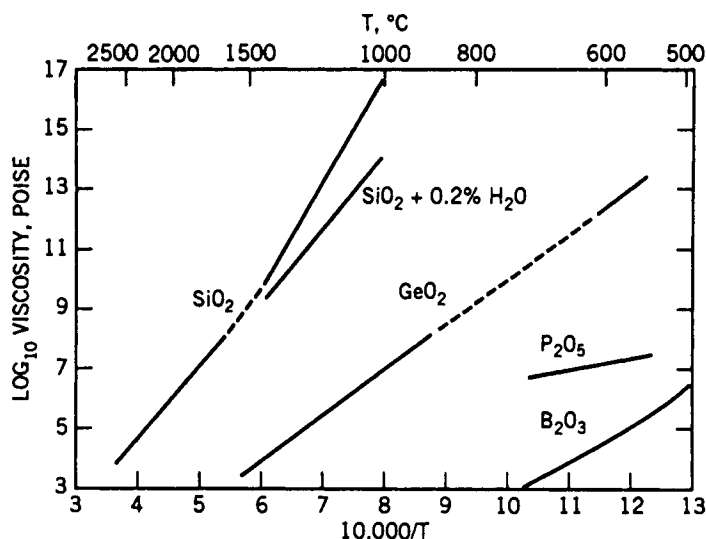


Fig. 2 Viscosities of various glass-forming oxides as a function of reciprocal temperature. Dashed lines show interpolations where data were not taken.

activation energy for flow of vitreous silica is constant, but this discussion and the data in Fig. 2 and Table 1 show that for pure water-free silica, the activation energy changes substantially over the temperature range from 1100°C to 2500°C.

The data of Kurkjian and Douglas¹³ on vitreous germania show a constant activation energy over a factor of 10^{10} change in viscosity. However, the data on vitreous silica definitely show a change in activation energy with temperature, and the results for B_2O_3 show a large change in activation energy with temperature. Also, multicomponent silicate glasses for which viscosity data are plotted in Fig. 1, and the organic glasses shown in Fig. 4, have changing

TABLE 1 Activation Energies for Viscous Flow of Various Glasses

Glass	Activation energy (kcal/mol)	Temperature range (°C)	Refs.
Vitreous silica	170	1100–1400	11
	123	1600–2500	12
Vitreous germania	75	540–1500	13
Vitreous P_2O_5	41.5	545–655	14
Vitreous B_2O_3	83–12	26–1300	15, 16, 17

activation energies for viscous flow as a function of temperature. From calorimetric measurements of the glass transition temperature of P_2O_5 , Martin and Angell¹⁹ concluded that the activation energy for its viscous flow from 317°C to 636°C at least was constant.

The strengths of oxygen-central atom bonds in the simple oxides such as SiO_2 , GeO_2 , P_2O_5 , and B_2O_3 are about 100 kcal/mol. The very great difference in viscosity of these oxides shown in Fig. 2 is, therefore, quite surprising, since the mechanism of flow undoubtedly involves breaking of oxide bonds. The melting points of the crystalline oxides parallel the variations in viscosity: SiO_2 (cristobalite) 1710°C; GeO_2 (hexagonal), 1116°C; P_2O_5 , 580°C; B_2O_3 , 450°C. The differences indicate that the detailed structure of the oxide network is also important in determining the ease of viscous flow. The linked-ring structure of B_2O_3 , described in Chapter 3, is the probable reason for the low viscosity of this oxide, since the bonds between rings should be weaker than those in the rings. This structure also provides an explanation for the strong temperature dependence of the activation energy. The bonds between the rings should have a spectrum of strengths leading to a change in the effective activation energy for flow as a function of temperature. The P_2O_5 network possibly contains sheets of PO_4 tetrahedra, as mentioned in Chapter 3; each tetrahedron is bonded to three others instead of four as for SiO_2 and GeO_2 . The lower viscosity and melting point of P_2O_5 may result from this structure.

Judged by their structure GeO_2 and SiO_2 should have a similar viscosity and melting point, since each apparently forms a random three-dimensional network in the rigid state (see Chapter 3). The great difference between both the absolute viscosity and its temperature dependence leads to doubt about the structural similarity. The random-network structure for vitreous silica is well established, as described in Chapter 3; thus there may be some subtle weakness in the germania network. Germania may also be more susceptible to impurity effects than silica, although there is no direct evidence for this contention.

The viscosities of the simple oxides decrease sharply with the addition of most impurity ions. Such impurities as water, in the form of -OH groups, and alkali oxides are particularly effective in lowering viscosity. For example, the addition of 0.1 wt% hydroxyl ion lowers the activation energy of flow for vitreous silica at temperatures from 1000 to 1400°C from 170 to 122 kcal/mol. The actual viscosity is lowered about three orders of magnitude at 1000°C by this addition, but is not too different from the value for water-free silica at 1400°C, as shown in Fig. 2. It is strange that the activation energy for silica containing water at lower temperatures is about the same as for water-free silica at higher temperatures, and extrapolates to about the same absolute values for the water-free material. Is this correspondence a coincidence? The answer is not clear. The addition of 0.165 mol% Na_2O to germania lowers the viscosity by a factor of about 46 at 1000°C, and also causes a decrease in the activation energy of flow and a change in the activation energy with temperature.¹³

The viscosity of germania (GeO_2) unexpectedly decreases with increasing

pressure at 1425°C by a factor of about five for a pressure of 9.5 kbar, compared to atmospheric pressure.²⁰

MULTICOMPONENT OXIDES

The addition of other oxides to silica invariably lowers its viscosity. The lowering is greatest with addition of alkali oxides and least with alkaline earth oxides and alumina. At higher temperatures, the effect of alumina is less than for other oxides. Zinc and boric oxides among the multivalent oxides are particularly effective in lowering the viscosity of silicates. Morey³ has collected data on the viscosity of many different silicate glasses and has given factors for the calculation of viscosity in soda-lime and soda-lead silicate glasses when other oxides are added to them. Additional viscosity data on commercial silicate glasses and binary and ternary silicates have been collected in Refs. 21 and 22.

The activation energy for viscous flow in multicomponent silicate glasses decreases as the temperature is increased.^{9,10,23} At low temperatures where the viscosity is above 10^{12} P, the activation energy for flow of sodium silicate glasses is about 100 kcal/mol, and it decreases to 50 kcal/mol or less at high temperatures where the viscosity is about 100 P. The value of 100 kcal/mol at low temperatures is much less than the low-temperature activation energy for flow in fused silica. The silicate lattice is broken up by the alkali oxide, making flow easier. With increasing temperature, the activation energy decreases relatively more rapidly in sodium silicates than in fused silica, apparently because the lattice is already broken up by the alkali ions. A similar, more rapid, decrease of activation energy with temperature occurs in B_2O_3 , again because of some weaker bonds.

The high-temperature activation energy of multicomponent silicates depends on the amount of oxides other than silica in the glass. For binary alkali silicates, this activation energy decreases from about 50 kcal/mol with 10% alkali oxide to 20 kcal/mol with 50% alkali oxide.²⁴ For binary alkaline earth silicate, the activation energy for viscous flow at high temperatures is about 40–50 kcal/mol for 25–50% alkaline earth oxide.²⁴

Bockris and co-workers^{24,25} have proposed a model of liquid binary silicates to explain these results and those of thermal expansion. At the orthosilicate composition (2 mol of metal oxide per mol of SiO_2) the liquid consists of metal cations and SiO_4^{4-} anions. As more silica is added, the anions polymerize to larger units, making flow more difficult. Among the larger units in these anions are rings and chains of silica tetrahedra. "Islands" of three-dimensional silica in the melt are proposed in a related model.²⁶ While silicate melts must undoubtedly contain polymerized units of silica tetrahedra, there is no direct evidence for any of the particular anions proposed, so these models remain speculative.

The viscosity of B_2O_3 also decreases when other oxides are added, but much

less than for SiO_2 . This result is expected because of the lower viscosity of B_2O_3 , resulting from some weaker bonds already present in the pure oxide. A summary of viscosities and other properties of borate melts is given by Mackenzie.²⁷

NONOXIDE GLASSES

Viscosities of heavy-metal (mainly zirconium) fluoride glasses have been discussed by Drexhage,²⁸ and there are data on nitrate, sulfate, chloride and chalcogenide glasses. Especially curious is the viscosity of liquid sulfur, which is low at the melting point, decreases with increasing temperature up to 160°C , where it abruptly increases by a factor of about 10,000 over a temperature range of 20°C , and then decreases again at higher temperatures. At the melting point, the liquid contains S_8 rings; at about 160°C , these rings break up and polymerize to long chains, causing the rise in viscosity. At higher temperatures, the chains decrease in length, again lowering the viscosity.^{30,31}

Miller³² has discussed and given references to earlier work on viscosities of glassy polymers.

Viscosity data on a number of organic glasses have been collected by Ling and Willard.³³ The activation energy for flow is constant with temperature above a viscosity of about 10^4 P. These activation energies are in the range from 12 to 35 kcal/mol. Since these measurements are at low temperatures (75–200 K), the viscosity drops very sharply as a function of temperature at these viscosities. For example, the viscosity of 2-methylpentane increases eight orders of magnitude in about 15°C . At higher temperatures where the viscosity is above 10^4 P, the activation energy for flow decreases with increasing temperature.

TEMPERATURE DEPENDENCE

The viscosities of four very different materials as measured over a wide viscosity range are shown in Figs. 3 and 4. In each case, the Arrhenius relation for the exponential dependence of viscosity on the reciprocal of temperature (Eq. 4) is obeyed at the highest viscosities, and in some cases at the lowest, with an activation energy changing with temperature in between.

The temperature dependences of viscosities of different glasses can be compared by plotting^{34,35} \log viscosity as a function of T_g/T , where T_g is the temperature at which the viscosity is 10^{13} P.

From this plot, glasses can be sorted into roughly four different types, as listed in Table 2, which perhaps correspond to different structures.³⁵

1. Strong network liquids show linear or nearly linear behavior (fit Eq. 3)

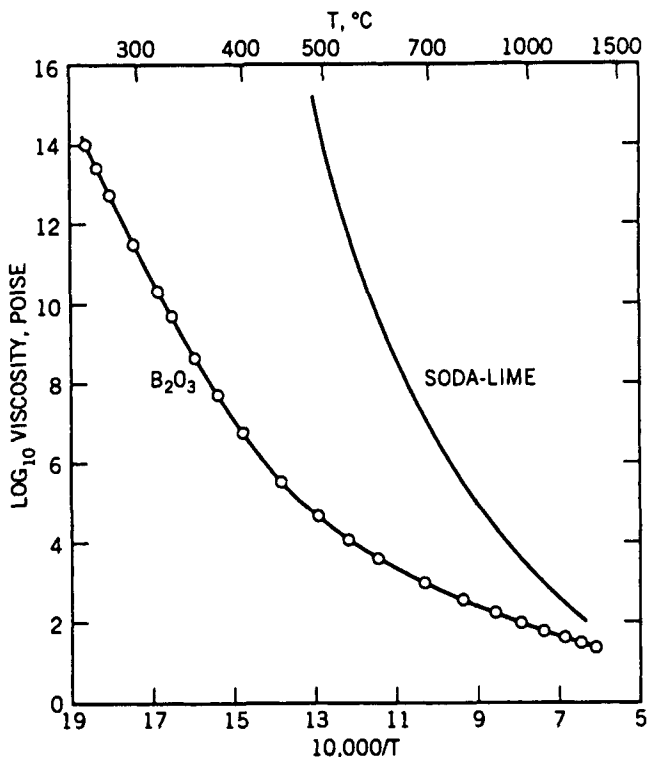


Fig. 3 Viscosity of boron trioxide³⁴ and a soda-lime glass³ (70 wt% SiO₂, 21% Na₂O, and 9% CaO) as a function of reciprocal temperature.

in the plot. The network structure resists thermal degradation as the temperature is raised above the glass transition temperature.

- Partially broken three-dimensional networks, as typified by alkali silicates, are less resistant to thermal degradation, but the silicon-oxygen network is still strong. Arsenic trisulfide perhaps is in this category because it has an ordered structure in two dimensions. It is possible that alkali-rich regions in alkali silicate glasses have a planar structure.
- Liquids in this category have a more severely distorted structure; calcium in the aluminosilicate anorthite ($\text{CaO} \cdot \text{Al}_2\text{O}_3 \cdot 2\text{SiO}_2$) apparently distorts the silicon-oxygen network, and zinc chloride and hydrogen-bonded organic liquids are perhaps less ordered on a short range than the network liquids of classes one and two.
- Completely ionic and molecular glasses such as the zirconium fluorides, alkali-alkaline nitrates, and nonhydrogen bonded organics, have bonds that are more easily exchanged between the first and second coordination shell, and therefore their viscosity decreases even more rapidly as a function of increasing reduced reciprocal temperature T_g/T .

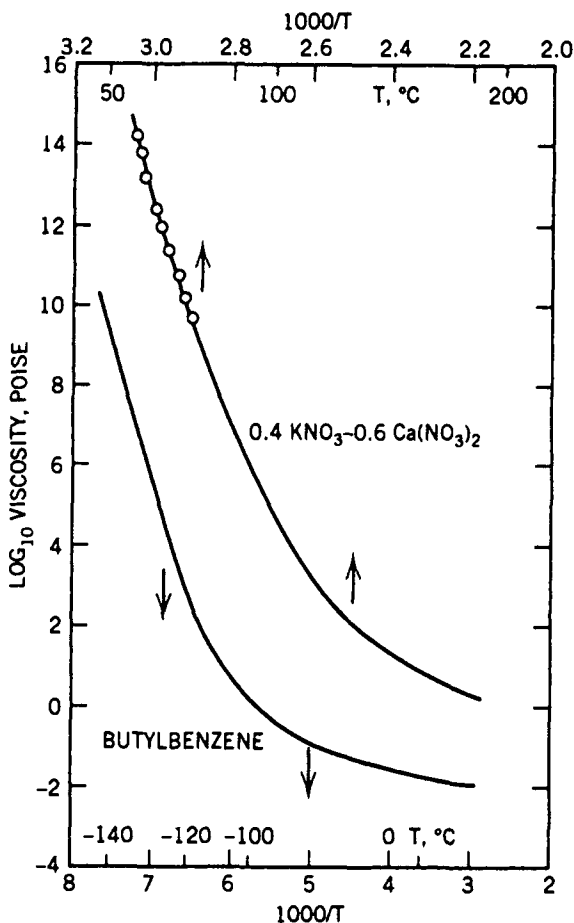


Fig. 4 Viscosities of glass-forming fused salt, $0.4\text{KNO}_3-0.6\text{Ca}(\text{NO}_3)_2$ ⁴⁸ and *N*-butylbenzene.³³

TABLE 2 Classification of Viscous Liquids by Temperature Dependence

1	2	3	4
SiO_2	Alkali silicates	$\text{CaAl}_2\text{SiO}_8$ (anorthite)	Heavy metal fluorides
GeO_2	Soda-lime silicates	Alkali phosphates	Multi-anion chlorides
P_2O_5	As_2S_3	ZnCl_2	$0.4\text{KNO}_3-0.6\text{Ca}(\text{NO}_3)_2$
$\text{NaAlSi}_3\text{O}_8$		n-Propanol	
BeF_2			Butylbenzene

Angell³⁵ suggests that these categories lead from "strong" glasses (one) with rigid networks to "fragile" glasses with molecules or ions that easily change their coordination numbers (four).

The viscosities of glycerol³⁶ at high pressure and of confined organic liquids³⁷ have been measured.

THEORIES

Theories for the viscosity of monomolecular liquids have the form of Eq. 4, where η_0 is a complicated function of various parameters, but usually varies much less with temperature than the exponential term, and to a first approximation Q is temperature-independent.³⁸ In a treatment based on the molecular theory of liquids, Q is equal to the mutual potential energy of a pair of molecules,³⁸ and in the transition state theory it is the height of the potential barrier to mutual rotation of neighboring molecules.³⁹ The mutual potential energy of molecules is at least calculable in principle, but the factors controlling the heights of potential barriers in all but the simplest cases are quite uncertain. Extension of these concepts to more complicated liquids, with strongly bonded molecules, is very difficult and has not been successfully accomplished. Thus other simpler approaches to the viscosity of glasses have been tried.

The empirical equation

$$\eta = \eta_0 \exp\left(\frac{B}{T - T_0}\right) \quad (5)$$

where η_0 and B are temperature-independent, has been found to fit viscosity data for glasses over certain temperature ranges.⁴⁰⁻⁴² This equation is the basis for two theories of viscosity: one based on "free volume" and the other on entropy.

In the simplest form of the free-volume treatment,⁴³⁻⁴⁵ the viscosity is given by the equation

$$\eta = \eta_0 \exp\left(\frac{B_1}{V - V_0}\right) \quad (6)$$

where V is the specific volume of the liquid and V_0 is its close-packed specific volume. If the expansion coefficient is independent of temperature, Eq. 6 is equivalent to Eq. 5, since then $V - V_0$ is proportional to $T - T_0$. This free-volume treatment can be thought of crudely as follows. At some temperature T_0 , the molecules are packed together with the specific volume V_0 , and in this condition no molecular motion is possible. As the temperature increases, some excess or free volume $V - V_0$ develops in the liquid, providing "space" for molecular motion and ultimately for flow. More elegant descriptions of this model are given by Bueche⁴⁶ and by Cohen and Grest⁴⁷.

In the entropy approach,⁴⁸ it is assumed that the liquid consists of regions

that rearrange as units when they experience a sufficient fluctuation in energy. Thus there is a barrier in potential energy to the rearrangements of the units. The sizes of the units are functions of temperature and are determined by the configurational entropy of the liquid. As this entropy decreases, the sizes of the units increase until at zero configuration entropy, the size is infinitely large and the liquid can no longer rearrange itself.

Quantitatively

$$\eta = \eta_0 \exp\left(\frac{B_2}{TS_c}\right) \quad (7)$$

where S_c is the configurational entropy. This equation is equivalent to Eq. 4 when $S_c = \Delta C_p (T - T_0)/T$, and ΔC_p , the relaxational part of the specific heat, is constant with temperature.

In Eq. 5, a third parameter T_0 is introduced to account for the changing of activation energy with temperature. Thus to establish more than empirical significance for the equation, one must find some significant correlation for values of T_0 . Williams et al.⁴⁴ and Adams and Gibbs⁴⁸ found that T_0 was about 50°C lower than the glass transition temperature T_g for many glasses. The glass transition temperature in these correlations was defined as the temperature at which there was a discontinuity in the coefficient of thermal expansion (see the following chapter for a discussion of transition temperature).

Goldstein compared the free-volume and entropy theories of viscosity and concluded that the entropy theory was superior,⁴⁹ chiefly because the free-volume theory cannot explain the pressure dependence of the glass transition temperature.

However, the most serious defect of any theory that results in Eq. 5 for the viscosity is that this equation is inconsistent with experimental data on glass-forming liquids at high viscosities. In a variety of different glasses, the activation energy for viscous flow becomes temperature-independent at high viscosities (see Refs. 17 and 33, and Figs. 3 and 4) just where Eq. 5 would predict it should vary most sharply. Equation 4 provides an empirical fit to data at intermediate temperature with some correlation between T_0 and the temperature at which other properties change, but the theoretical significance of T_0 for viscous flow is unclear. In at least two glasses, P_2O_5 and GeO_2 , T_0 is zero, since Eq. 4 is valid over the whole viscosity range in which measurements were made.

Two more recent theories emphasize the importance of defects in the melt structure as they affect viscosity. Mott⁵¹ suggested that the concentration of broken Si-O bonds in vitreous silica increases as the temperature increases, and provides for easier flow. Mott showed that motion of the broken bonds around an Si-O ring would lead to flow; he discusses other possibilities such as the breaking of two or four neighboring bonds, and concludes that the latter may be the most likely mechanism.

Brawer⁵² has proposed a change in coordination number of a glass constituent as the defect likely to result in flow, or at least in structural

relaxation. These defects were suggested by computer simulations of flow in melts, for example of calcium fluoride. The distribution of coordination numbers is a function of temperature, pressure and glass composition. The changes in coordination number result in density fluctuations in the melt. Flow under a stress takes place by changing the distribution of the low density region, although the total density is not changed. A detailed calculation of viscosity from this model remains to be worked out.

All these theories need more development and testing before the mechanisms of viscous flow in glasses are understood.

REFERENCES

1. G. W. Scherer, *Relaxation in Glass and Composites*, Wiley, New York, 1986.
2. J. D. Ferry, *Viscoelastic Properties of Polymers*, Wiley, New York, 1970.
3. G. W. Morey, *The Properties of Glass*, Reinhold, New York, 1954, pp. 140ff.
4. G. H. Li and D. R. Uhlmann, *J. Noncryst. Solids*, **3**, 127 (1970).
5. J. H. Simmons, R. K. Mohr, and C. J. Montrose, *J. Appl. Phys.*, **53**, 4075 (1982).
6. G. B. Bartenev, in *Physics and Noncrystalline Solids*, J. A. Prins, Ed., North-Holland, Amsterdam, 1965, p. 461; *The Structure and Mechanical Properties of Inorganic Glasses*, Wolters-Nordhoff, Groningen, 1970, pp. 141ff.
7. S. M. Rekhson, D. M. Heyes, C. J. Montrose, and T. A. Litovitz, *J. Noncryst. Solids*, **38-39**, 403 (1980).
8. T. F. Soules and R. F. Busby, *J. Chem. Phys.*, **78**, 6307 (1983).
9. H. R. Lillie, *J. Am. Ceram. Soc.*, **16**, 619 (1983).
10. F. R. Gauthier, M. S. Thesis, Rensselaer Polytechnic Institute, 1975.
11. G. Hetherington, K. H. Jack, and J. C. Kennedy, *Phys. Chem. Glasses*, **5**, 130 (1964).
12. G. Hofmaier and G. Urbain, in *Science of Ceramics*, Vol. 4, British Ceramics Society, 1968, p. 25.
13. C. R. Kurkjian and R. W. Douglas, *Phys. Chem. Glasses*, **1**, 19 (1960).
14. R. L. Cormia, J. D. Mackenzie, and D. Turnbull, *J. Appl. Phys.*, **34**, 2245 (1963).
15. G. A. Parks and M. E. Spaght, *Physics*, **6**, 69 (1935).
16. J. D. Mackenzie, *Trans. Faraday. Soc.*, **52**, 1564 (1956).
17. P. B. Macedo and A. Napolitani, *J. Chem. Phys.*, **49**, 1887 (1968).
18. E. H. Fontana and W. A. Plummer, *Phys. Chem. Glasses*, **1**, 139 (1966).
19. S. W. Martin and C. A. Angell, *J. Phys. Chem.*, **90**, 6736 (1986).
20. S. K. Sharma, D. Virgo, and J. Kushiro, *J. Noncryst. Solids*, **33**, 235 (1979).
21. N. P. Bansal and R. H. Doremus, *Handbook of Glass Properties*, Academic Press, Orlando, FL, 1986.
22. O. V. Mazurin, M. V. Streltsina, and T. P. Shvaiko-Shvaikovskaya, *Handbook of Glass Data*, Parts A, B and C, Elsevier, Amsterdam, 1983, 1985, 1987.
23. G. S. Meiling and D. R. Uhlmann, *Phys. Chem. Glasses*, **8**, 62 (1967).

24. J. O. Bockris, J. D. Mackenzie, and J. A. Kitchener, *Trans. Faraday. Soc.*, **51**, 1734 (1955).
25. J. W. Tomlinson, M. S. R. Heynes, and J. O. Bockris, *Trans. Faraday. Soc.*, **54**, 1833 (1958).
26. J. O. Bockris, J. W. Tomlinson, and J. T. White, *Trans. Faraday. Soc.*, **52**, 299 (1956).
27. J. D. Mackenzie, in *Modern Aspects of the Vitreous State*, Vol. 1, J. D. Mackenzie, Ed., Butterworths, London, 1960, p. 188.
28. M. G. Drexhage, in *Treatise on Materials Science and Technology*. Vol. 26, M. Tomozawa and R. H. Doremus, Eds., Academic Press, Orlando, FL, 1985, p. 189ff.
29. H. Rawson, *Inorganic Glass Forming Systems*, Academic Press, London, 1967.
30. R. E. Powell and H. Eyring, *J. Am. Ceram. Soc.*, **65**, 648 (1943).
31. G. Gee, *Trans. Faraday. Soc.*, **48**, 515 (1952).
32. A. A. Miller, *J. Polym. Sci.*, **A2**, 1094 (1964); *J. Chem. Phys.*, **49**, 1393 (1968).
33. A. C. Ling and J. E. Willard, *J. Phys. Chem.*, **72**, 1918, 3349 (1968).
34. W. T. Laughlin and D. R. Uhlmann, *J. Phys. Chem.*, **76**, 2317 (1972).
35. C. A. Angell, *J. Noncryst. Solids*, **73**, 1 (1985).
36. C. A. Herbst, R. L. Cook, and H. E. King, *Nature* **361**, 518 (1993).
37. S. Granick, *Science* **253**, 1374 (1991).
38. A. Bondi, in *Rheology*, F. R. Eirich, Ed., Academic Press, New York, 1956, p. 321.
39. R. E. Ewell and H. Eyring, *J. Chem. Phys.*, **5**, 726 (1937).
40. H. Vogel, *Phys. Z.*, **22**, 645 (1921).
41. G. S. Fulcher, *J. Am. Ceram. Soc.*, **77**, 3701 (1925).
42. G. Tamman and W. Hesse, *Z. Anorg. Allg. Chem.*, **156**, 245 (1926).
43. A. K. Doolittle, *J. Appl. Phys.*, **22**, 1031 (1951); **23**, 236 (1952).
44. M. L. Williams, R. F. Landel, and J. D. Ferry, *J. Am. Ceram. Soc.*, **77**, 3701 (1955).
45. M. H. Cohen and D. Turnbull, *J. Chem. Phys.*, **31**, 1164 (1954).
46. F. Bueche, *J. Chem. Phys.*, **30**, 748 (1959).
47. M. H. Cohen and G. S. Grest, *J. Noncryst. Solids*, **61 & 62**, 749 (1984).
48. H. Tweer, N. Laberge, and P. B. Mocedo, *J. Am. Cer. Soc.*, **54**, 121 (1971).
49. G. Adam and J. H. Gibbs, *J. Chem. Phys.*, **43**, 139 (1965).
50. M. Goldstein, *J. Chem. Phys.*, **39**, 3369 (1963); **43**, 1852 (1965); **51**, 3728 (1968).
51. N. F. Mott, *Philos. Mag.*, **B56**, 257 (1987).
52. S. Brawer, *Relaxation in Viscous Liquids and Glasses*, American Ceramic Society, Columbus, OH, 1985.

GLASS TRANSITION

As a glass-forming liquid is cooled, some of its properties change sharply in a narrow temperature range.¹ In Fig. 1 the specific volumes of a soda-lime silicate glass and glassy B_2O_3 are shown as a function of a temperature; an abrupt change in the slope of the curve, which is equal to the coefficient of volume expansion, occurs at a certain temperature. Other properties, such as the heat capacity (see Fig. 2 and Refs. 6–9) and electrical conductivity (Chapter 15), also change abruptly at about the same temperature. This temperature is called the glass transition or transformation temperature.

It is significant that the viscosity does not show an abrupt change at the glass transition temperature. This result suggests that the viscosity determines the rate at which a property relaxes to some equilibrium value, but may not be related to the magnitude of property changes under different conditions. Therefore a theory for the viscosity probably will not result from consideration of changes in properties of the glass, but only from study of the details of the flow mechanism itself; hence the failure of the viscosity theories described in the last chapter that were based on the free volume or entropy of the glass.

Kauzmann¹ showed that glass transitions occur for many of the types of glasses listed in Chapter 2. It has been suggested that some amorphous solids do not show a glass transition temperature, but this result has not been established with any certainty.

It is reasonable to associate the glass transition temperature with the slowing down of rearrangements in the glass structure. When these rearrangements occur rapidly during the time of experimental measurements, the glass has the properties of a liquid; when the rearrangements are slow, the glass structure is “frozen” and it behaves like a solid. In fact, the specific volumes and their temperature dependencies of the glasses shown in Fig. 1 are quite

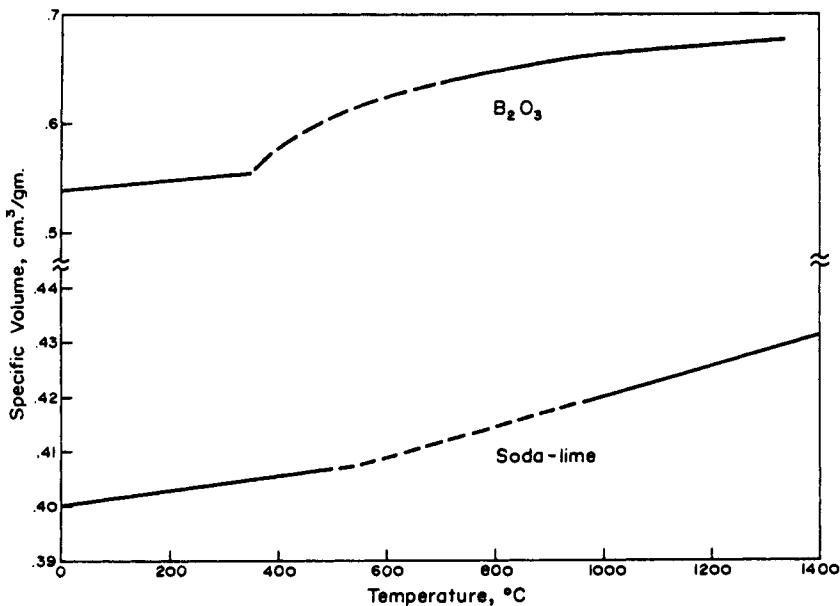


Fig. 1 Specific volumes of a soda-lime silicate glass (74% SiO₂, 16% NaO, and 10% CaO) and glassy B₂O₃ as a function of temperature.²⁻⁴

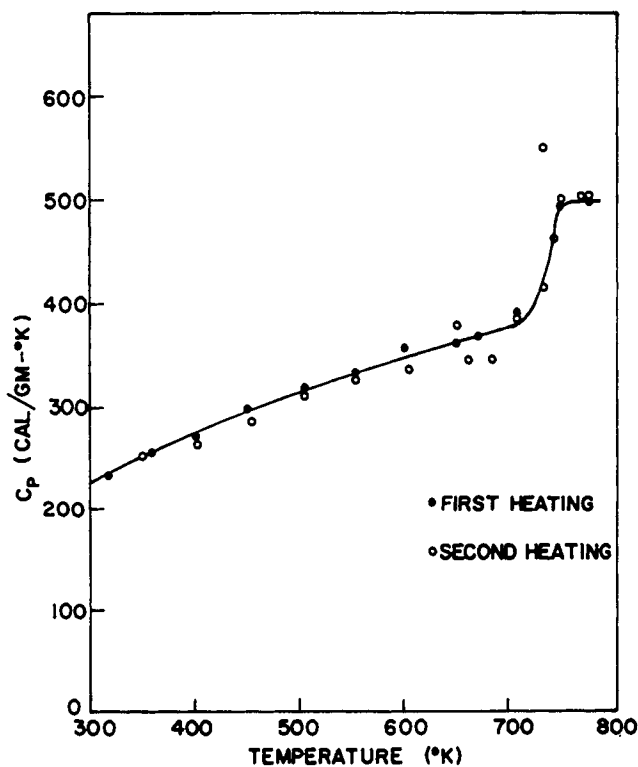


Fig. 2 Heat capacity of 0.15 Na₂O, 0.85 B₂O₃ glass as a function of temperature.⁵

close to those of the corresponding crystalline solids below the glass transition temperature. The rate of these molecular rearrangements should be closely associated with viscous flow, and indeed the glass transition temperature occurs at a viscosity of about 10^{13} P.

Thus the presence of a glass transition results from the slowing down of viscous relaxation in a liquid. Estimates of the relaxation time at a viscosity of 10^{13} P are in the range of minutes to a few hours, in reasonable accord with the usual times of experiments.

Since the transition temperatures determined from specific volume and heat capacity are nearly the same,¹ the molecular motions involved in changing these properties with temperature changes are probably similar. Alternatively, the same apparent transition temperatures for these two properties may result because the relaxation rate of glasses changes so rapidly with temperature. This rapid change is shown in the high activation energies for viscous flow at high viscosities, as described in the last chapter.

Other properties of glasses show changes at the glass transition temperature. There is some evidence that the elastic modulus of glasses changes sharply at the glass transition temperature,^{10,11} although it is difficult to measure a meaningful value of the modulus much above the glass transition temperature. As this temperature is approached from below, the delayed elasticity of glasses increases rapidly, as shown in Chapter 16. This change is a manifestation of the increasing ease of molecular motion and consequent change in elasticity with time at a particular temperature. An increase in hydrostatic pressure apparently increases the transition temperature.¹ This result might be expected because of the reduction in relaxation rates with increasing pressure. Changes in the absorption spectra of nitrate glasses occur at the glass transition.

Kauzmann¹ showed that the dielectric relaxation of several organic glasses changes abruptly at the glass transition temperature. The dielectric relaxation times are about 30 min at the transition temperature, consistent with the estimates mentioned above. It is known that the molecular motions in dielectric relaxation of liquids are related to their viscosities, so a correlation of dielectric relaxation with transition temperature is expected. This sort of dielectric relaxation should not be confused with other dielectric losses in ionic glasses, including oxides. These losses are associated with ionic motion, as discussed in Chapter 16.

Kauzmann¹ extrapolated the entropy of a supercooled liquid of the "fragile" type (strongly non-Arrhenius viscosity, large difference in heat capacity between crystal and liquid) and found that at some temperature below the glass transition temperature, the entropy of the supercooled liquid becomes less than that of the crystal. Since the liquid is less ordered than the crystal, this result is unexpected and has been called Kauzmann's paradox. Stillinger^{11a} examined this paradox with a statistical model for a liquid of small molecules. He concluded that the correct extrapolation of the entropy of the supercooled liquid does not become less than that of the crystal, but only approaches it asymptotically. Furthermore Stillinger concluded that the viscosity equations

of the Tammann–Vogel–Fulcher type that predict infinite viscosity at some temperature below T_g are unlikely to be correct.

STRUCTURAL AND STRAIN RELAXATION

When a glass is cooled rapidly from a temperature above the transition region into this region, it retains some properties of the higher temperature, and those properties “relax” to those characteristic of the lower temperature as a function of time. An example of this process was given in the last chapter in describing the change of viscosity with time at high viscosity. The time to reach a stable or equilibrium state is, of course, longer at lower holding temperature.

If a piece of glass is cooled rapidly from a temperature above the transition region, nonuniformities in its temperature during cooling lead to stresses in the glass. For example, as a rod or plate is cooled, the outer layers of glass become rigid first. Then as the inside cools, it tries to shrink, but is restrained by the rigid outer layers. These stresses can weaken the piece, and change its properties, so it is desirable to remove them by heating the piece at an appropriate temperature in the transition region. At this “annealing” temperature, the stresses are removed as the glass relaxes. The rate at which annealing goes on is important in preparing glasses for use and so has been much studied. Good empirical relations for annealing have been devised, and in particular it has been found that the rate of annealing is closely related to the viscosity of the glass, hence the designation of the temperature where the viscosity is $10^{13.4}$ P as the annealing point, since at this viscosity, most stresses are removed in about 15 min.

The relaxation of the glass structure from one set of properties to another after a rapid temperature change in the glass transition region is called structural relaxation. When a glass is subjected to a stress (strain) in this region, the deformation changes with time; this process is stress or strain relaxation. The rates of these relaxations are of practical importance, and have been studied intensively in the last few years. Two monographs by Scherer¹¹ and Brawer¹² provide extensive reviews of this work, and the proceedings of a meeting include discussions of recent experimental and theoretical work.¹³

When glass is stressed in the transition region, several different types of deformation can occur (see also Chapter 9):

1. Elastic: instantaneous and reversible, strain proportional to stress;
2. Anelastic: reversible, takes time to reach final value or relax;
3. Viscous: permanent flow, rate proportional to stress.

The combination of these various kinds of deformation is often called viscoelastic strain or relaxation. If the different types of strain are independent and additive, the deformation is called linearly viscoelastic.

It is important to characterize the initial state of the glass carefully before

studying the kinetics of property changes in the transition region. One way to start with a known state is to anneal the glass carefully at the temperature of the experiment. Then, if some force is imposed on the glass, such as a shearing stress, rates of changes under this force can be studied starting from a known condition. This procedure was followed by Kurkjian¹⁴ in studying stress relaxation in a soda-lime silicate glass. Since relaxation of stress is the aim of annealing, this type of experiment gives insight into the annealing process.

To study the stress relaxation, Kurkjian rapidly twisted an annealed glass rod a certain amount with a known stress. The stress in the rod at this fixed twist and at a constant temperature was then measured as a function of time. The "instantaneous" initial stress S_0 was used to normalize the stresses at different temperatures. When this was done, the stress relaxation at different temperatures in the transition range fitted on the same master curve, as shown in Fig. 3, where the normalized stress S/S_0 is plotted as a function of time. The existence of such a master curve shows that a single mathematical function describes the relaxation data at all temperatures. Kurkjian fitted his stress S as a function of time to a sum of six exponential terms of the form

$$S = \sum_i \epsilon_i M_i \exp\left(\frac{-t}{\tau_i}\right) \quad (1)$$

where ϵ_i is the initial strain, and M_i is the modulus for a process with relaxation time τ_i . In these terms, one can say that the spectrum of relaxation times was the same for the different temperatures of the experiment. A material that

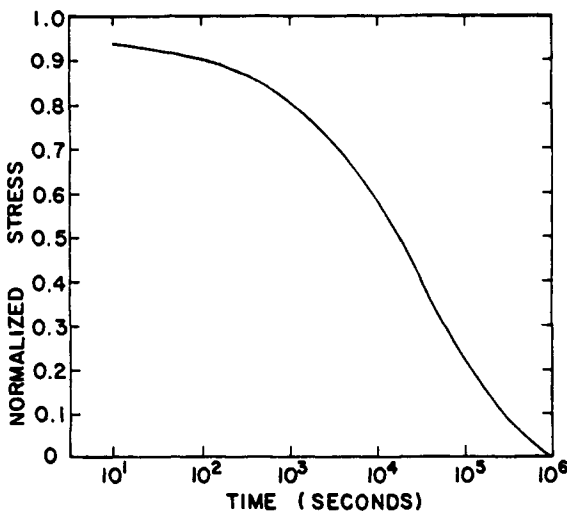


Fig. 3 Stress relaxation of a soda-lime silicate glass as a function of time.¹⁴ Data at different temperatures are normalized to 473°C using an activation energy of 150 kcal/mol.

exhibits this property of having the same relaxation spectrum at different temperatures is called thermorheologically simple.

A simpler function often fits the relaxation spectra of glasses:

$$S = S_0 \exp [-(t/\tau)^b] \quad (2)$$

in which S_0 is the initial stress before relaxation and b and τ are time-independent constants. Equation 2 has been given the names of various research workers, but since it has been used for more than 150 years, Scherer¹¹ suggests calling it the "b" equation. In glasses, b is often between 0.5 and 0.7 for structural and stress relaxation. For example, DeBast and Gilard found $b = 0.5435$ for uniaxial stress relaxation in a soda-lime silicate glass.¹⁵

Tool¹⁶ introduced the interesting idea of a fictive temperature as a parameter for characterizing the state of a glass. The fictive temperature of the glass is the temperature that corresponds to the state of the glass. For example, if a glass is rapidly cooled from a temperature above the transition region, it retains the properties characteristic of this temperature, which is therefore its fictive temperature. The fictive temperature changes as a function of time during annealing until it becomes the annealing temperature. The difficulty with this approach is that the same value of properties, such as the specific volume, can be attained in a glass by two quite different heat treatments, implying that a single parameter is not sufficient to characterize the state of a glass. Thus, whereas the idea of a fictive temperature has value in certain simple types of experiments and perhaps as a technological characterization, it is not sufficiently precise for a detailed description of the state of the glass sample (see also Refs. 11 and 17).

Structural relaxation was defined above as the change of a property value p as a function of time after a temperature change of the material. Because the relaxation times in Eqs. 1 and 2 are functions of time during structural relaxation, it can be nonlinear. If the temperature of the sample is changed from T_1 to T_2 , the relaxation function M at T_2 of a property p is

$$M = \frac{p - p_f}{p_0 - p_f} \quad (3)$$

where p is the property at time t , p_f is the final value of the property after it has completely relaxed, and p_0 is its initial value at T_2 . Equation 2 does not describe M for structural relaxation, because τ is time dependent.

To account for the time dependence of τ , Narayanaswamy¹⁸ introduced a reduced time u (often given the symbol Greek ξ) such that

$$u = \int_0^t \frac{dt'}{\tau} \quad (4)$$

Then he derived the following equation:

$$p = p_f - \alpha_s \int_0^t M(u - u') \frac{dT}{du'} du' \quad (5)$$

where α_s is the difference between the temperature dependence of the property in the glassy (solid) phase well below the transition range and in the liquid phase

$$\alpha_s = \left. \frac{dp}{dT} \right|_{\text{liquid}} - \left. \frac{dp}{dT} \right|_{\text{glass}} \quad (6)$$

The temperature dependence of the relaxation time was assumed to be

$$\tau = \tau_0 \exp \left[\frac{x}{T} + \frac{1-x}{T_f} \right] \frac{Q}{R} \quad (7)$$

where τ_0 and x are constants, T is the measurement temperature, T_f is the (time dependent) fictive temperature, Q is the activation energy, and R the gas constant. The fictive temperature T_f is given by

$$T_f = \frac{p - p_f}{\alpha_s} + T \quad (8)$$

Since Tool introduced the idea of a fictive temperature, this treatment is often called the Tool-Narayanaswamy model. It is discussed in more detail in Refs. 11-13.

This model has been fit to relaxation data on glasses in a variety of ways. In one approach, the changes in a property after a small temperature jump either up or down are measured to determine τ from the b function¹⁹

$$M = \exp [-(u/\tau)^b] \quad (9)$$

The fitting parameters from the model equations are b , τ_0 , x and Q . In another approach, the relaxation of enthalpy (heat capacity) is measured with a differential scanning calorimeter at different heating and cooling rates; the analysis in terms of Eqs. 4-9 is described in Refs. 20 and 21.

A large amount of relaxation data have been successfully analyzed by this model.^{11-13, 19-25} In almost all glasses studied, the activation energy Q is close to that for viscosity in the same temperature range. b values in Eq. 9 range from 0.5 to 0.85, and x from 0.25 to 0.70, although x is usually about 0.5. There are no independent theoretical estimates of b and x .

In spite of these successes, there are a number of questions about this model, and some failures of the model to fit data, especially at large excursions from equilibrium. Questions involving the b relaxation function of Eq. 9 and the form of Eq. 7 for the temperature dependence of the relaxation time are explored in detail in many articles, for example in Ref. 13, p. 420. The conclusion is that the Tool-Narayanaswamy model is a valuable first step in describing relaxation in glasses, but has deficiencies that require further study.

Moynihan and Schroeder²⁴ have analyzed time-dependent light scattering results^{25,26} from glasses in the glass transition region, and shown that they are consistent with a model of relaxing regions in the glass of nanometer size. In their model, the relaxation rates of these regions of about constant size depend

on their density, with regions of higher density relaxing more slowly than those of lower density. This distribution of relaxation times of the regions is then correlated with the macroscopic distributions of relaxation times of various properties.

Hansen²⁷ has reviewed application of theories of liquids, including "mode-coupling" theory and molecular dynamics simulation, to the glass transition, emphasizing glasses that have a sharp increase of viscosity near the glass transition (type four from Chapter 6, or highly "fragile" glasses). He distinguishes between a kinetic and a calorimetric glass transition, and concludes that the connection between them for these glasses is still an open problem.

REFERENCES

1. W. Kauzmann, *Chem. Rev.*, **43**, 219 (1948).
2. M. Coenen, *Glastech. Ber.*, **39**, 81 (1966).
3. P. B. Macedo, *J. Chem. Phys.*, **44**, 3357 (1966).
4. P. C. Li, A. C. Ghose and G. J. Su, *Phys. Chem. Glasses*, **1**, 198 (1960).
5. D. R. Uhlmann, A. G. Kolbeck, and D. L. DeWitte, *J. Noncryst. Solids*, **5**, 426 (1971).
6. C. T. Moynihan, A. J. Eastal, D. C. Tran, J. A. Wilder, and E. P. Donovan, *J. Am. Ceram. Soc.*, **59**, 137 (1976).
7. C. T. Moynihan, P. B. Macedo, J. D. Aggarwal, and V. E. Schnaus, *J. Noncryst. Solids*, **6**, 322 (1972).
8. S. S. Chang and A. B. Bestal, *J. Chem. Phys.*, **55**, 933 (1971); **56**, 503 (1972).
9. N. P. Bansal and R. H. Doremus, *Handbook of Glass Properties*, Academic Press, San Diego 1986, Ch. 7.
10. G. S. Parks and J. D. Reugh, *J. Chem. Phys.*, **5**, 364 (1937).
11. G. W. Scherer, *Relaxation in Glass and Composites*, Wiley, New York, 1986.
- 11a. F. Stillinger, *J. Chem. Phys.*, **88**, 7818 (1988).
12. S. Bräwer, *Relaxation in Viscous Liquids and Glasses*, American Ceramic Society, Columbus, OH, 1985.
13. K. L. Ngai and G. B. Wright, Eds., *Relaxations in Complex Systems*, *J. Noncryst. Solids*, **131-133**, 1991.
14. C. K. Kurkjian, *Phys. Chem. Glasses*, **4**, 128 (1963).
15. J. DeBast and P. Gilard, *Phys. Chem. Glasses*, **4**, 117 (1963).
16. A. Q. Tool, *J. Am. Ceram. Soc.*, **29**, 240 (1946).
17. H. N. Ritland, *J. Am. Ceram. Soc.*, **39**, 403 (1956).
18. O. S. Narayanaswamy, *J. Am. Ceram. Soc.*, **54**, 491 (1971).
19. S. M. Rekkson and O. V. Mazurin, *J. Am. Ceram. Soc.*, **57**, 327 (1974).
20. C. T. Moynihan, A. J. Eastal, M. A. DeBolt and J. Tucker, *J. Am. Ceram. Soc.*, **59**, 12, 16 (1976).
21. S. N. Crichton and C. T. Moynihan, *J. Noncryst. Solids*, **102**, 222 (1988).
22. O. V. Mazurin, *J. Noncryst. Solids*, **25**, 130 (1975).

23. S. M. Rekkson, *J. Noncryst. Solids*, **95 & 96**, 131 (1987).
24. C. T. Moynihan and J. Schroeder, *J. Noncryst. Solids*, **160**, 52 (1993).
25. N. A. Bokov and N. S. Andreev, *Fiz. Khim. Stekla*, **15**, 424 (1989).
26. J. Schroeder L. G. Hwa, X. S. Zhao, L. Busse and I. Aggarwal, *Mater. Sci. Forum*, **67 & 68**, 471 (1991).
27. J. -P. Hansen, *Phys. World*, **4**, 32 (1991).

CHAPTER 8

MOLECULAR SOLUTION AND DIFFUSION IN GLASS

Gases can dissolve molecularly in glass because of its open structure. If the gas molecule is small, it can diffuse rapidly in a simple glass such as fused silica. The permeability of fused silica and other glasses to helium has been known for many years; Barrer¹ reviewed earlier work back to 1900. The different permeabilities of glass for different gases can be used to separate and purify gas mixtures. Molecular diffusion is also important in "fining" or removal of bubbles from glass melts, oxidation of silicon and the oxidation state of a glass.

Gases such as hydrogen, oxygen, and water, which dissolve molecularly in glass, can also react with the glass network. These reactions affect certain properties of the glass, for example, optical absorption, viscosity, and electrical conductivity, and are important in fining glass. Such reactions are discussed below and in Chapter 12 on reactions of gases in glass.

In this chapter experimental results and theories of molecular solubility in glass are first discussed, followed by sections on the methods of measuring molecular diffusion in glass, the effects of temperature and molecular size on molecular diffusion, chemical reactions, the influence of glass composition on molecular diffusion, and theories for this diffusion. Reviews on diffusion and solubility of gases in glass are in Refs. 2 and 2a.

MOLECULAR SOLUBILITY OF GASES

Several different methods have been used to measure gas solubilities in glass. The simplest technique involves saturating the glass, usually in the form of fibers or powder, with gas at a certain temperature and then pumping out the gas at a higher temperature and measuring the amount given off.³⁻⁵ The

pressure drop of a gas in a vessel containing glass samples also gives a measure of the solubility.⁶ The most common method⁷⁻¹² employed is to combine measurements of the permeation coefficient K and the diffusion coefficient D , since the solubility is equal to the ratio K/D , as shown in the next section.

The solubility is defined here as the ratio C_i/C_g , where C_i is the concentration of gas dissolved in the glass, and C_g is the concentration of molecules in the gas phase. This solubility is unitless, and is sometimes called the "coefficient of solubility," after Ostwald. Other definitions of solubility are S , the volume of gas at standard temperature and pressure dissolved per unit volume of glass per unit of external gas pressure, and the number of molecules of gas dissolved per unit volume of glass per unit external pressure. These solubilities are proportional to C_i ; $S = (273/T)(C_i/C_g)$. The ratio C_i/C_g is preferred to the other definitions because it does not depend on external gas pressure, and because its temperature dependence gives directly the energy of interaction between the gas and the solvent (glass), as shown below, whereas the temperature dependence of S gives the enthalpy of interaction.

The solubilities of helium, neon, hydrogen, deuterium, and argon in fused silica are shown in Figs. 1-3. There are some rather surprising discrepancies between results of different investigators, particularly for helium and hydrogen. The high values of hydrogen solubility found by Shackelford⁶ may have resulted because he used a fused silica container, which can contribute an

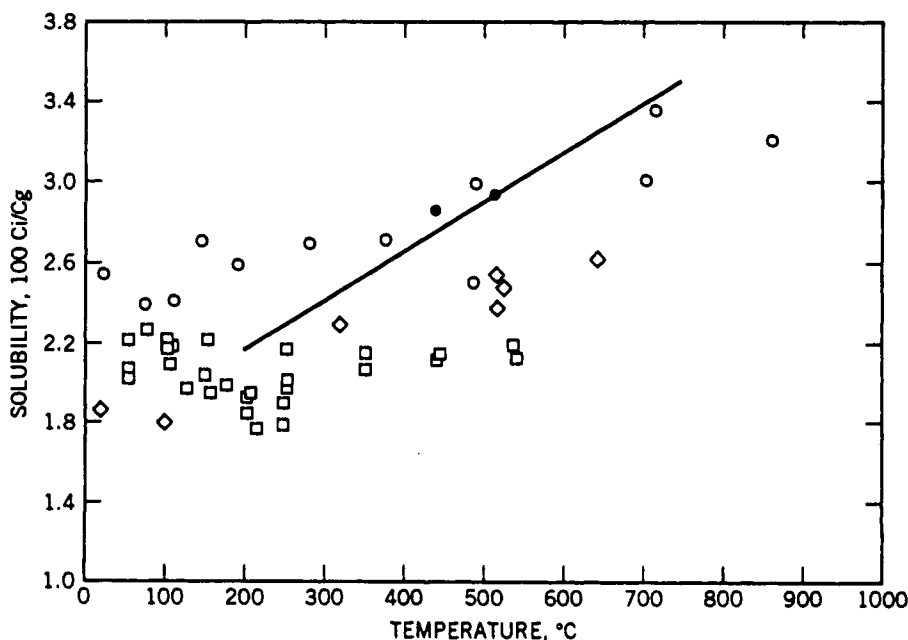


Fig. 1 Solubility ratio C_i/C_g for helium in fused silica. ■, Williams and Furguson;⁴ ★, Swets et al;⁷ ◇, Woods and Doremus;⁵ □, Shackelford;⁶ —, Shelby.¹¹

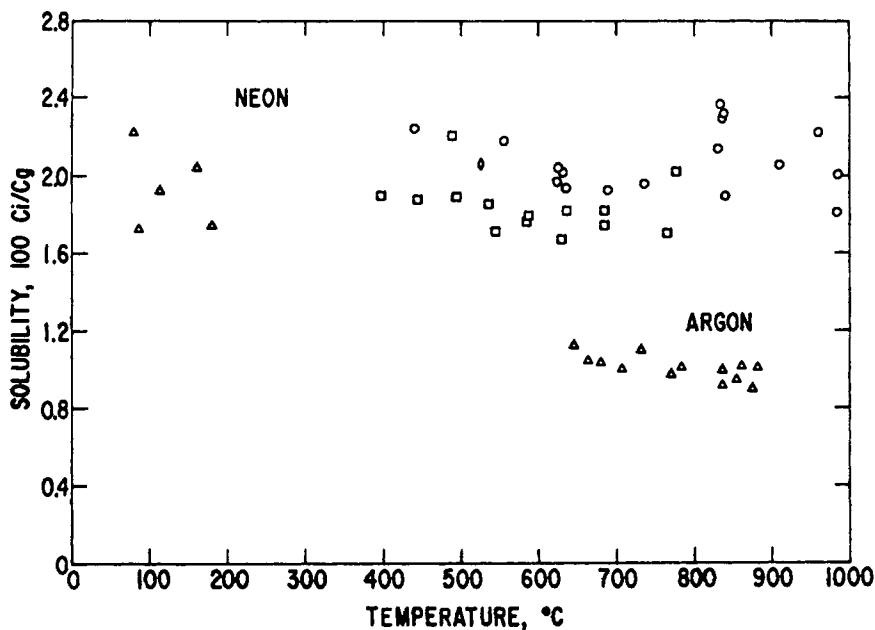


Fig. 2 Solubility ratio C_i/C_0 for neon and argon in fused silica, \circ , Frank et al;⁸ \diamond , Woods and Doremus;⁵ \triangle , Perkins and Begeal;¹⁰ \square , Shackelford.⁶

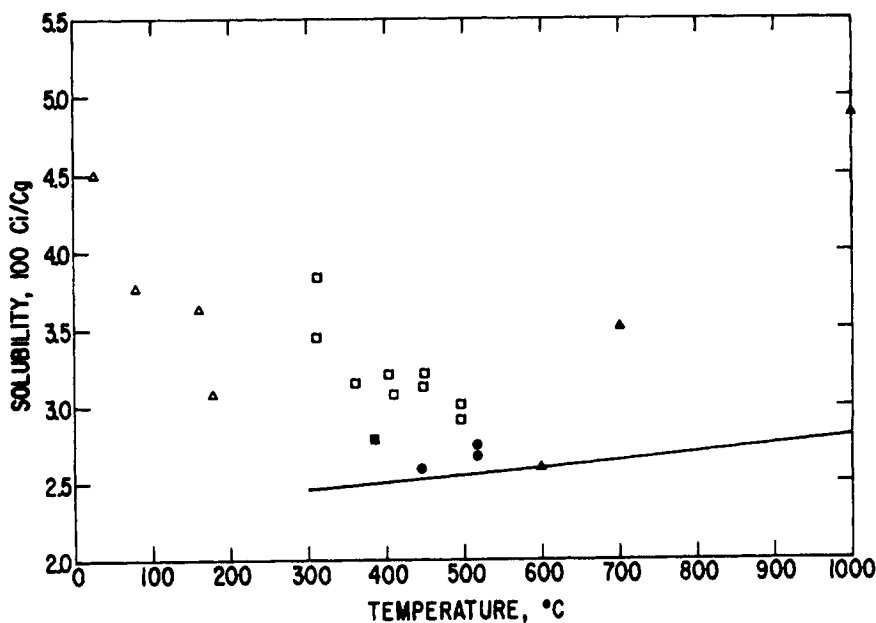


Fig. 3 Solubility ratio C_i/C_0 for hydrogen and deuterium in fused silica. Hydrogen: \blacksquare , Wustner;³ \bullet , Williams and Furguson;⁴ \square , Shackelford.⁶ Deuterium: \triangle , Perkins and Begeal;¹⁰ \blacktriangle , Beauchamp and Walters;¹⁹ —, Lee and Fry.²³

uncertain background. However, there are some striking generalities that can be made. The first is the small temperature dependence of the solubility, which is constant within experimental error from 80 to 1000°C for neon and increases only slightly, if at all, with temperatures over this range for helium. There appears to be some increase in solubility of hydrogen at low temperatures, but the results of different investigators differ widely in this region, so that this increase may result from experimental problems. A second interesting finding is the similarity of the solubility of different gases. The rough average values for all investigators are 0.024 for helium, 0.019 for neon, and 0.03 for hydrogen. Argon is appreciably lower at about 0.01; the data of Perkins and Begeal¹⁰ were confirmed in a recent study by Nakayama and Shackelford¹² who found little temperature dependence of the Ostwald solubility of argon, and slightly higher solubilities. Norton¹³ found a solubility of about 0.01 for oxygen in vitreous silica; the molecular diameter of oxygen is about the same as for argon.

The solubilities of inert gases in different glasses at 300°C are compared in Table 1. The solubilities in widely different glass types are remarkably similar; particularly striking are the values for the zirconium fluoride glass, which has a very different structure and anionic groups compared to the oxide glasses. There was little or no temperature dependence of solubility for all the systems in Table 1.

Shelby¹¹ found no appreciable difference in the solubilities of helium in several different types of fused silica with different impurity levels, for example, for a water concentration from a few parts per million up to 0.1%. He also found¹⁷ little change of the solubility of helium in a series of SiO_2 - TiO_2 glasses containing up to 10% TiO_2 .

The solubility of helium and neon in the tridymite crystalline form of silica is about the same as in vitreous silica, but the solubility of these gases in the cristobalite crystalline form is about a factor of four lower than in tridymite or fused silica.¹⁸

The solubility of helium in Pyrex borosilicate glass (81% SiO_2 , 13% B_2O_3 , 4% Na_2O , 2% Al_2O_3) is about 0.017 at 200°C, and appears to increase

TABLE 1 Ostwald Solubilities of Inert Gases in Various Glasses at 300°C

Gas	Molecular Diameter (Å)	Vitreous Silica (see Figs. 1 and 2)	Vitreous B_2O_3 ¹⁴	Vitreous GeO_2 ^{5,16}	Zirconium Fluoride ¹⁵	Sodium Borosilicate ^{5,a}
Helium	2.0	0.024	0.023	0.013	0.014	0.013
Neon	2.4	0.019	0.023	0.013	0.013	0.010
Argon	3.2	0.010	0.012		0.0054	
Krypton	4.2		0.015			

^a60% SiO_2 , 30.5% B_2O_3 , 9.5% Na_2O .

somewhat with increasing temperature.^{4,20-22} Deuterium solubility is 0.033 at 100–300°C, and decreases to 0.012 at 465°C.^{21,23} Shelby found somewhat different values.²²

Shelby^{2a} has summarized a number of measurements, mostly his own, of helium solubility in binary and ternary oxide systems. He found substantial decreases in solubilities as the amount of alkali oxide in the glasses increased. The amount of decreases was about the same with lithium, sodium, and potassium oxides.

Kohli and Shelby¹⁴ found that the solubilities of gases in boron oxide (see Table 1) were about constant with temperature below 300°C, but increased above this temperature, which is close to the glass transition temperature in this glass. At 800°C solubilities were: He, 0.110; Ne, 0.095; Ar, 0.084; Kr, 0.048. The solubility of nitrogen²⁴ in this glass at 550°C of about 0.03 is somewhat less than that of Krypton¹⁴ at this temperature.

Two different models have been proposed for the molecular solubility of gases in glass. In one model, the gas is considered to dissolve in an inert material with a certain amount of free volume that is available for solution of gas.²⁵ This volume is constant with temperature and pressure as long as the glass is not appreciably affected by these variables.

The free volume is given directly by the ratio C_i/C_g . This relation can also be derived from statistical equations, such as those of Fowler and Guggenheim²⁶ for the chemical potential of an ideal gas μ_g and of this gas dissolved in a condensed phase μ_i :

$$\mu_g = RT \ln \phi + RT \ln C_g \quad (1)$$

$$\mu_i = -E + PV + RT \ln \phi + RT \ln C_i - RT \ln v_f \quad (2)$$

where ϕ is a function involving the translational and internal degrees of freedom of the molecules, $-E$ is a potential energy resulting from interactions between the dissolved gas and the solvent liquid, P is the total pressure, R is the gas constant, T is the absolute temperature, V is the partial molar volume of the solute gas, and v_f is the fractional free volume available to the dissolving gas. At equilibrium these two chemical potentials must be equal in order to give a relation for C_i/C_g in terms of the free volume. In deriving this relation, it is assumed that the function ϕ is the same in the gaseous and dissolved states. This is equivalent to assuming that the dissolved molecule preserves three degrees of translational freedom. Then

$$\ln \frac{C_i}{C_g} = \frac{+E - PV}{RT} + \ln v_f \quad (3)$$

The total volume of the glass does not change appreciably as gas is dissolved in it; therefore $V = 0$, and the small temperature dependence of C_i/C_g shows that $E = 0$. Consequently, the free volume is equal to C_i/C_g , and is about 3% for fused silica.

This result can be compared with the free volume calculated by other methods. The free volume is often given by

$$V_f = 1 - \frac{V_0}{V} \quad (4)$$

where V is the bulk molar volume of the material, and V_0 is the volume of a mole of its molecules, these molecular volumes being calculated from the dimensions of the individual molecules. It is difficult to calculate the molecular volumes of the SiO_2 groups in fused silica. From the relative densities of fused silica (2.2) and coesite (3.0), a dense crystalline form of silica, one would expect a free volume of about 27%, far greater than the value calculated from the gas solubilities. Even using the density of quartz to calculate the molecular volumes gives a free volume of 13%. Therefore only a part of this kind of free volume in fused silica is available for solution of gas.

The free volume can be considered in terms of the detailed molecular structure of fused silica. It seems likely that the gas molecules dissolve in holes or interstices in the fused silica. Such interstices exist in cristobalite, which has a density close to that of fused silica. Molecular size, up to a molecular diameter of about 3 Å, appears to have a small effect on the gas solubility; then, if the oxygen and argon values are reliable, solubility decreases. Therefore it seems reasonable to assume that the average diameter of the interstices is about 3 Å. The total number of interstices for a free-volume fraction of 0.03 is then about $10^{21}/\text{cm}^3$. The largest gas concentration measured experimentally (by Wustner in hydrogen at 850 atm) is about $1.7(10)^{20}$ molecules/ cm^3 , which is still below the estimated number of interstices.

The discrepancy between the free volume calculated from the relative densities of fused silica and coesite or quartz and that for gas solubility is perhaps understandable in terms of the solution of gas molecules in interstices. There can be free volume in the fused quartz structure that is not in the form of interstices and thus is not available to the dissolving gas, either because it is not connected to the main network of interstices or because each part of it is too small to contain a gas molecule.

The number N_r of interstices of radius greater than the minimum radius r_0 can be estimated from the usual statistical equation

$$\frac{N_r}{N} = \exp\left(\frac{-W}{RT}\right) \quad (5)$$

where N is the total number of interstices and W is the energy of formation of an interstice of radius r from one of radius r_0 . An estimate for W comes from the equation of Frenkel²⁷ for the elastic energy to enlarge a spherical cavity of radius r_0 to a radius of r :

$$W = 8\pi G r_0 (r - r_0)^2 \quad (6)$$

The shear modulus is G , which is about $3(10)^{11}$ dyn/ cm^2 for fused silica. Using

$r_0 = 1.5 \text{ \AA}$, about 3% of the interstices have a diameter of 3.4 \AA at 600°C . Thus a certain distribution of hole sizes above the minimum size is expected. The lower solubility of oxygen and argon may be caused by such a distribution, resulting in a smaller free volume being available to the larger molecules. It is possible that the distribution of hole sizes is fixed at higher temperatures where the viscosity of the silica is lower and is frozen in at lower temperatures.

A second model for the molecular solubility of gas in glass has been developed from statistical mechanics.^{2a,6,12,18,29,30} For a dissolved molecule with three degrees of translational freedom, and localized in a site, the following equation was derived,²⁸ in the present notation:

$$\frac{C_i}{C_g} = N_s V_s \exp \left(\frac{E}{RT} - 1 \right) \quad (7)$$

where N_s is the number and V_s is the volume of solubility sites. Since $N_s V_s$ is equivalent to v_f , Eq. 7 is the same as Eq. 3 except for a factor of e . However, all of these authors preferred to consider the dissolved gas molecules as harmonic oscillators. Then for three degrees of vibrational freedom in the dissolved state, the following equation is found:

$$\frac{C_i}{C_g} = \left(\frac{kT}{\nu} \right)^3 \frac{N_s}{(2\pi m kT)^{3/2}} \exp \left(\frac{E}{RT} \right) \quad (8)$$

Here m is the mass of a molecule of the dissolving gas, k is the Boltzmann constant, and ν is the vibrational frequency of the dissolved gas molecules. Equation 8 is an approximation valid when $(h\nu/kT) < 1$, where h is Planck's constant, and is equivalent to Eq. 3 if the vibrational frequency is considered to equal $(kT/2\pi m)^{1/2}(\nu_f)^{-1/3}$. Thus the two models are formally very similar, and present experimental results cannot readily distinguish between them. Shackelford⁶ found that his vibration frequency ν was about inversely proportional to the molecular mass, giving a constant ν_f for different atoms. Thus the use of one model or the other is a matter of taste; I prefer the free-volume model because of its simplicity and more direct physical interpretation. Beauchamp and Walters¹⁹ and Perkins and Begeal¹⁰ have also given reasons for considering molecules dissolved in glass as having translational rather than linear oscillator character. Theoreticians and statistical mechanics may prefer the vibration model.

Shackelford³⁰ has extended the model of Eq. 8 by considering a log normal distribution of solubility site sizes. Nakayama and Shackelford describe this distribution in the following way.¹² Of the approximately $2.2(10)^{28}$ interstitial sites per m^3 in vitreous silica, $2.3(10)^{27}$ are accessible to helium atoms, $1.3(10)^{27}$ to neon atoms, and $1.1(10)^{27}$ to argon atoms, in line with the increasing molecular size of these atoms (see Table 1).

In comparing results of the vibrational model with experimental data, ν and E were treated as adjustable parameters. For fused silica, ν in the range from

$(10)^{12}$ to $7(10)^{12}$ vibrations/s was found, which is reasonable. Values of E of about 1–3 kcal/mol were computed; Barrer and Vaughan¹⁴ calculated similar values from a model of helium–oxygen interactions. In the free-volume model, the gas–glass interaction is considered to be small, and changes in C_i/C_g resulting from different glass structures are attributed to changes in the volume available for solution, rather than to changes in the vibration frequency of dissolved molecules.

At low gas pressures (near atmospheric and below), the solubility C_i/C_g is constant with pressure change, which states that the concentration of dissolved gas is proportional to the gas pressure. At higher gas pressures, the fugacity of the gas rather than its pressure (concentration) must be used to provide a constant solubility. At pressures above about 100 atm, the number of dissolved molecules is an appreciable fraction of the interstices available for them. The solubility can then be described by a Langmuir adsorption isotherm to account for competition for the sites.^{18,29,31} In this model, the equilibrium constant K for gaseous and adsorbed molecules is related to the fraction of adsorption sites θ by

$$K = \theta/F(1 - \theta) \quad (9)$$

where F is the fugacity of the gas. This equation can be derived from statistical mechanics (Ref. 26, p. 427). To apply this model to gas solubility, θ is given by C_i/N , where N is the number of interstices per unit volume for gas dissolution. Then

$$C_i = KFN/(1 + KF) \quad (10)$$

Data on helium and neon solubilities in cristobalite and tridymite up to 5000 atm¹⁸ and in vitreous silica,³¹ as well as hydrogen and deuterium in silica,^{32,33} fit Eq. 10. The number N of solubility sites in vitreous silica is found to be one to two times $(10)^{27}$ per m³ in this model, close to the number accessible to these gases in Shackelford's calculations, and those from the free volume model.

The experimental findings of little temperature dependence of solubility, a pressure dependence following Eq. 10, solubilities depending on molecular size, and similar solubilities in glasses with similar free volume but very different chemical composition and structure (Table 1) are all consistent with molecular solubility and very little gas–glass interaction. The dissolving molecules lodge individually in interstices of molecular size; the experiments of Hartwig³² on hydrogen and deuterium in vitreous silica with Raman spectroscopy show that the dissolved molecules are isolated from one another at pressures up to several hundred atmospheres. Even reactive gases such as oxygen, hydrogen, water, and nitrogen dissolved molecularly in the interstices without much interaction with the glass network, because their solubilities are about what is expected from their molecular size. These gases can react with the network, as described at the end of this chapter, but apparently unreacted molecules do not interact much with the glass network. There is some indication of increased hydrogen

and deuterium solubility at temperatures below 500°C, perhaps because of some gas-glass interaction at these temperatures.

As the glass becomes more dense, as in alkali-silicates, or in certain crystal forms, the solubility decreases because fewer interstices are available for dissolution.

Solubilities, diffusion coefficients, and permeation constants of gases, especially helium and water, in many different binary and ternary silicate glasses are summarized in Refs. 34 and 35 and in nonsilicate oxide glasses in Ref. 35, Vol. II.

MEASUREMENT OF MOLECULAR PERMEATION AND DIFFUSION IN GLASS

The permeation and diffusion of a gas through glass have usually been measured in two different ways: with a glass membrane (in the form of a tube or a bulb) or in a powder. Thin membranes of many different glasses can be made by blowing or polishing, but sometimes it is difficult to seal them into a vacuum system, in which case the powder technique is useful.

Adsorption of a gas on the glass surface has been considered to be a necessary prelude to its solution and diffusion in the glass; however, the amount of gas dissolved in glass is proportional to the gas pressure at pressures far above that required for saturation of surface adsorption sites. Thus it seems likely that the gas molecules can dissolve directly in the glass without surface adsorption. Equilibrium between the gas and gas dissolved at the glass surface occurs rapidly for molecular solubility, and surface adsorption and reactions are not involved.

A glass membrane is mounted in a vacuum system to measure permeation and diffusion of a gas through it. First the spaces on both sides of the membrane are pumped out, and then the permeating gas is introduced on one side at the desired pressure. The amount of gas that appears on the other side of the membrane is then measured with time. The amount of gas that permeates the glass is kept so low that the drop in pressure on the inlet side is negligible and the pressure on the outlet side is small. Under these conditions, the concentrations of gas dissolved in the membrane at its two surfaces are constant, being equal to some value C_i on the inlet side and zero on the outlet side. Since thin-walled tubes or bulbs of comparatively large diameter are used in these experiments, the diffusion equation for a slab applies without appreciable error. The flux J of diffusing gas, which passes through unit surface area of the membrane of thickness L in unit time under the boundary conditions $C = C_i$ when $x = 0$, $C = 0$ when $x = L$, $C = 0$ when $t = 0$, is³⁶

$$J = \frac{DC_i}{L} \left[1 + 2 \sum_{n=0}^{\infty} \cos n\pi \exp \left(\frac{-Dn^2\pi^2 t}{L^2} \right) \right] \quad (11)$$

where t is the time after emission of the gas. Holstein²⁰ has shown that this equation can be transformed to

$$J = 2C_i \left(\frac{D}{\pi t} \right)^{1/2} \sum_{n=0}^{\infty} \exp \left[\frac{-L^2(2n+1)^2}{4Dt} \right] \quad (12)$$

where the series converges rapidly for small t . For long times ($t \gg D/L^2$), these equations reduce to $J = DC_i/L$, which is the "steady-state" solution and implies a constant gradient throughout the membrane.

The measured pressure p of gas on the outlet side is related to J by the equation

$$J = \left(\frac{V}{ART_p} \right) \left(\frac{dp}{dt} \right)$$

where V is the volume on the outlet side where p is measured, A is the surface area of the glass membrane, R is the gas constant, and T_p is the temperature at which the pressure is measured. The results of permeation measurements in the steady state are usually expressed in terms of a permeation velocity K , which is defined as

$$K = \left(\frac{VL}{\Delta p A} \right) \left(\frac{dp}{dt} \right) = \frac{LRT_p J}{\Delta p}$$

where Δp is the pressure difference across the membrane. The units of K generally used are cm^3 of gas at stp per cm^2 of glass area per s per atm of gas pressure difference per cm of glass thickness. If the outlet pressure is negligible $\Delta p = C_g RT$, where C_g is the concentration of gas on the inlet side in mol/cm^3 , and T is the temperature of the diffusion experiment. Then, since $J = DC_i/L$, $K = DT_p C_i / C_g T$, where T_p is 273 K. The solubility S is defined as the volume of gas (at stp) dissolved in unit volume of glass per atm of external gas pressure:

$$S = \frac{C_i T_p}{C_g T} \quad \text{and} \quad K = DS \quad (13)$$

The units of K are also cm^2/s , since S is dimensionless. A discussion of the units of K and S is given by Rogers et al.²⁰ in an appendix to their article.

In the early stages of permeation, D can be calculated from the measured change in pressure with time (dp/dt) in the outlet side. For this purpose, Eq. 12 is useful, since for short times only the first term of the series is needed, so that a plot of $\log [t^{1/2} dp/dt]$ against $1/t$ is linear, because J is proportional to dp/dt ; the slope of the line is equal to $L^2/4D$, from which D can be calculated since L is known. This method was suggested by Rogers et al.²⁰ and gives the most accurate values of D from permeation data. The intercept of this line with the $\log [t^{1/2} dp/dt]$ axis ($1/t \rightarrow 0$) can also be used to calculate the solubility S if D is known. When the outlet pressure p_0 is plotted against time, the curve

becomes linear at long times (this is also the steady-state region), and the diffusion coefficient can also be found from the intercept t_c of this line with the pressure axis from the relation $D = L^2/6t_c$, as shown by Barrer.¹

If the gas on the inlet side is pumped out rapidly after the steady state is attained, the diffusion coefficient can be calculated from the rate at which the dissolved gas diffuses out of the membrane. The initial concentration for this desorption is given by $C = C_i(1 - x/L)$, and the boundary conditions are that $C = 0$ at both surfaces. The flux at the outlet is then³⁶

$$J = \frac{2C_i D}{L} \sum_{n=0}^{\infty} \cos n\pi \exp\left(\frac{-Dn^2\pi^2 t}{L^2}\right) \quad (14)$$

Thus the diffusion coefficient and solubility can be calculated from permeability data in a variety of ways, and comparisons between the various calculations should give some idea of the reliability of the results.

In the powder method, the diffusion coefficient is calculated from the amount of gas absorbed or desorbed from a powdered sample, and the solubility is found from the total amount of gas absorbed or desorbed per unit weight of glass. For desorption from spheres of radius R , the amount of gas desorbed Q is^{5,18}

$$\frac{Q}{Q_{\infty}} = \frac{6(Dt)^{1/2}}{\pi R} - \frac{3Dt}{R^2} \quad (15)$$

where Q_{∞} is the total amount of gas desorbed. A comparison of the experimental curve with Eq. 15 gives a measure of D where t , R , and Q_{∞} are known.

EFFECT OF TEMPERATURE, PRESSURE, AND MOLECULAR SIZE ON MOLECULAR DIFFUSION IN GLASS

The most extensive measurements on diffusion of molecules in glass have been made on fused silica, since this glass is one of the most permeable to gases. Few measurements of permeation of gases other than helium or hydrogen have been made in other glasses.

The diffusion coefficient of helium through thin fused silica tubes was measured by the membrane technique from room temperature to 1000°C by Swets, Lee, and Frank.⁷ In a plot of $\log D$ versus $1/T$, these authors found two straight line portions; however, a plot of $\log D/T$ versus $1/T$ gives a good straight line,³⁷ as in Fig. 4. These diffusion results are among the few taken over a wide enough temperature range and are of sufficient accuracy to determine whether a pre-exponential factor of temperature is needed in the Arrhenius equation,

$$D = D_0 \exp\left(\frac{-Q}{RT}\right) \quad (16)$$

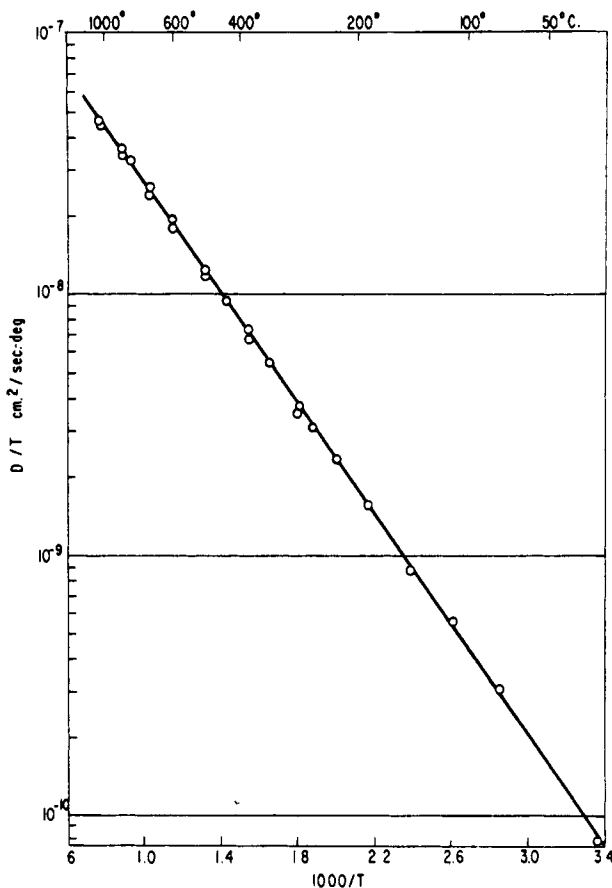


Fig. 4 Diffusion of helium in fused silica.⁷

Shelby^{2a} and Shelby and Keaton⁴² confirmed in more extensive measurements that a pre-exponential factor of temperature T^n with $n = 1.06 \pm 0.11$ in this equation gives the best fit for helium and neon diffusing in fused silica. The data of Frank et al.⁸ on neon diffusion in fused silica from 400 to 980°C are combined with those of Perkins and Begeal¹⁰ in Fig. 5. Perkins and Begeal used a thin film of silica formed on porous Vycor for their membrane. The neon data also fit well on a $\log D/T$ versus $1/T$ plot and show distinct curvature on a $\log D$ versus $1/T$. Therefore it seems likely that the pre-exponential factor of temperature in Eq. 16 is valid for all molecular diffusion in fused silica and perhaps in other glasses as well.

The size of the diffusing ion affects molecular diffusion in fused silica quite strongly, in contrast to the small dependence of solubility on size. The diffusion coefficients at 25 and 1000°C and the activation energies for diffusion for a

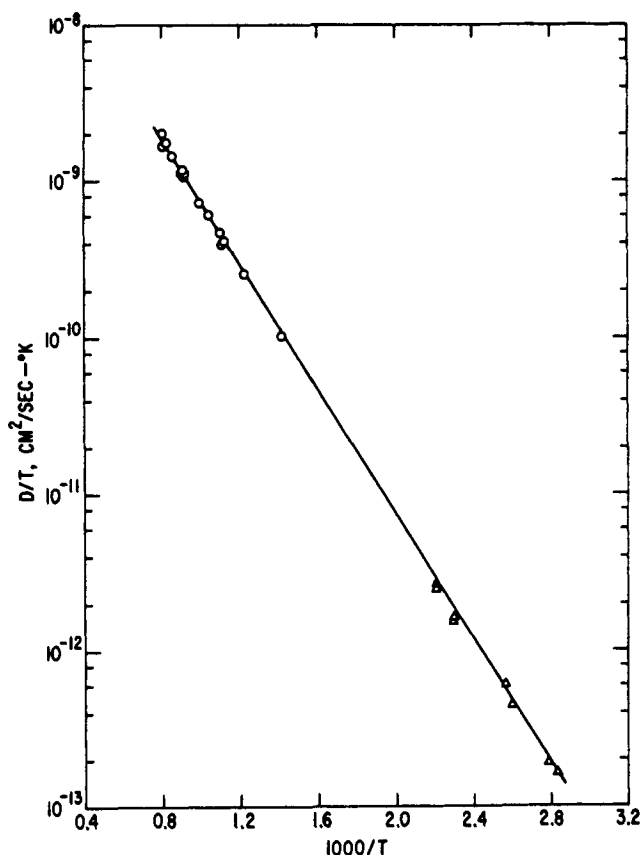


Fig. 5 Diffusion of neon in fused silica. \circ , Frank et al.,⁸ \triangle , Perkins and Begeal.¹⁰

number of molecules in fused silica are given in Table 2. The activation energies Q' have been calculated from an equation of the form

$$D = D' T \exp \left(\frac{-Q'}{RT} \right) \quad (17)$$

where Q' and D' are temperature-independent. This equation agrees well with experimental data and leads to a simple activation energy over the whole range of temperatures of the measurements, as mentioned previously. The molecular diameters in the table were estimated from the gaseous viscosities at 700°C; the water value was extrapolated. The diffusion coefficients and activation energies for helium, neon, argon, and hydrogen have been measured by several different workers and are considered quite reliable. The diffusion coefficient for oxygen as measured by Norton should be dependable, but the activation energy was determined from only two different measurements and therefore is less certain.

TABLE 2 Molecular Diffusion in Fused Silica

Molecule	Diameter (Å)	Diffusion coefficient (cm ² /s)		Activation energy Q' (kcal/mol)	Refs.
		25°C	1000°C		
Helium	2.0	$2.4(10)^{-8}$	$5.5(10)^{-5}$	4.8	7
Neon	2.4	$5(10)^{-12}$	$2.5(10)^{-6}$	8.8	8, 10
Hydrogen (deuterium)	2.5	$2.2(10)^{-11}$	$7.3(10)^{-6}$	8.5	9, 10
Argon	3.2		$1.4(10)^{-9}$	2.6	10, 12
Oxygen	3.2		$6.6(10)^{-9}$	25	13
Water	3.3		$\approx 2(10)^{-7}$	17	38, 39
Nitrogen	3.4			26?	1, 40
Krypton	4.2			≈ 46	10
Xenon	4.9			≈ 72	41

The activation energies for nitrogen and krypton were estimated from permeation measurements since no diffusion measurements have been made on these gases. The values for water are complicated by reaction with the silica lattice, as discussed later. The strong dependence of activation energy on molecular size is discussed further in the section on theories.

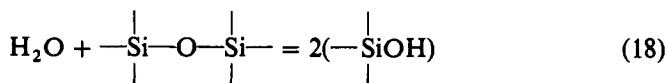
The diffusion coefficients of molecularly dissolved species show little dependence on gas pressure up to pressures of at least 1000 atm. Shelby^{2a} has discussed some deviations from simple behavior at high pressures.

Annealing stressed glasses reduces the rate of helium permeation in them, and increases the activation energy for diffusion.^{2a,43} Similar effects are found in ionic diffusion, as described in Chapter 15; these changes probably result from the decrease in density of the glasses with annealing.

MOLECULAR DIFFUSION AND CHEMICAL REACTION

Experiments on the diffusion of water, hydrogen and oxygen in silica are complicated by reactions of these gases with the silica lattice. These reactions will be considered again in the chapter on chemical reactions in glass; here only their interference with diffusion is treated.

Water reacts with silica glass to form -OH groups in the following way:



The rate at which these groups build up in fused silica in contact with water vapor has been studied extensively by Roberts and co-workers.^{38,44-46} They

avored a mechanism for diffusion of water into silica in which a proton jumps from an SiOH group to a neighboring Si-O-Si bridge, followed by a jump of the hydroxyl group. This mechanism is unlikely³⁹; it requires a much higher activation energy than the 18 kcal/mol found by Moulson and Roberts³⁸ because the silicon-oxygen bonds that must be broken in this mechanism have energies of over 100 kcal/mol. If a lattice diffusion mechanism were valid, one would expect a similar diffusion coefficient of water in crystalline quartz, but at 1000°C, where water diffuses readily into fused silica, there is no indication of its diffusion into quartz.⁴⁷

Therefore a more likely model of water diffusion in fused silica is one in which the water molecules dissolve molecularly in the glass and subsequently react with the silicon-oxygen lattice by Eq. 18.³⁹ Crank (Ref. 36, pp. 326 ff.) has treated simultaneous diffusion and reaction. The one-dimensional equation for diffusion plus reaction is

$$\frac{\partial C}{\partial t} = D \frac{\partial^2 C}{\partial X^2} - \frac{\partial S}{\partial t} \quad (19)$$

in which C is the concentration of dissolved material and S is the concentration of reacted (immobilized) material. If the concentration of diffusing material is much lower than the concentration of reaction product, diffusion takes place with an effective diffusion coefficient

$$D_e = 4D \left(\frac{S}{K^2} \right) \quad (20)$$

where D is the diffusion coefficient of dissolved species (molecular water), and K is an equilibrium constant. There is an extra factor of 2 in Eq. 20, because each water molecule gives two SiOH groups. The relation between S , the concentration of SiOH groups, and C_i , the concentration of molecularly dissolved water, is

$$S = K(C_i^{1/2}) \quad (21)$$

since each water molecule reacts to form two SiOH groups. This square-root relationship between the amount of SiOH groups and C_i , and consequently the ambient water vapor pressure, was found by Moulson and Roberts.³⁸

The effective diffusion coefficient of Eq. 20 is directly proportional to the concentration of S of SiOH groups; the solution of the diffusion equation for this dependence was found by Wagner⁴⁸ (see also Ref. 36, p. 162). This solution is compared with the profile of SiOH groups found by Roberts and Roberts⁴⁵ in Fig. 6. The fit is good, confirming the model of molecular diffusion and reaction of water. The activation energy and diffusion coefficient of water given in Table 2 were calculated from this comparison, assuming a solubility C_i/C_0 for water of about 0.01 and using the value of K in Eqs. 19 and 20 calculated from the data of Ref. 38.

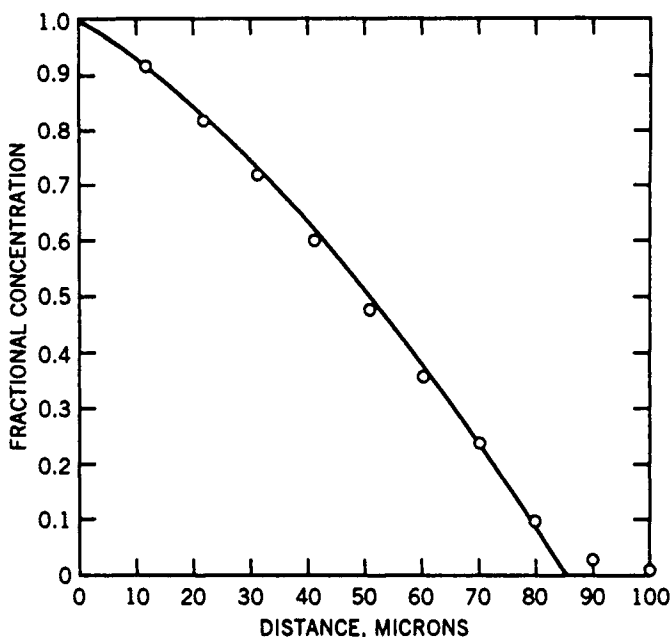


Fig. 6 Profile of water diffusing into fused silica at 1100°C. —, calculated from the diffusion coefficient of Eq. 17; O, smoothed data from Ref. 36.

There has been a great deal of confusion about the diffusion of oxygen in vitreous silica. Two types of experiments have been done. In the first, the permeation and diffusion of oxygen through a glass membrane was measured by Norton,¹³ as described above for other gases. Norton found the same behavior for oxygen as found for molecular solubility of inert gases, as described above and shown in Tables 1 and 2; the solubility was proportional to the pressure, and was of comparable magnitude for a molecule with the diameter of oxygen, and the diffusion coefficient and activation energy of diffusion were those expected for a molecule the size of oxygen.

The second kind of experiment involves diffusion and exchange of isotopically labeled oxygen into the glass.^{49,50} The ^{18}O concentration in the gas phase can be followed with a mass spectrometer⁴⁹⁻⁵² and the profile of ^{18}O in the network oxygen can be measured⁵³⁻⁵⁹ with a nonresonant nuclear reaction or secondary ion mass spectroscopy (SIMS). Much of the profiling work was done on thin silica films growing on silicon.^{53,54,56} This work was valuable for demonstrating that molecular oxygen was the diffusing species during oxidation of silicon (see below), because ^{18}O accumulated at the silicon-oxide interface.

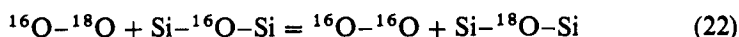
The following processes probably contribute to the tracer depletion in the gas phase and tracer profiles in the oxide:

1. Molecular diffusion of oxygen;
2. Network diffusion of oxygen;
3. Exchange of isotopic tracer between the molecularly dissolved oxygen and the oxygen in the silicon-oxygen network;
4. Traces of water;
5. A slow surface exchange reaction.

These mechanisms are listed in rough order of their experimental support.

Molecular diffusion in silica, as measured by Norton¹³ and described above, is clearly involved in all these isotopic tracer measurements. The ingenious interdiffusion tracer experiments of Mikkelsen⁵⁵ demonstrate diffusion of lattice oxygen at temperatures from 1200 to 1400°C with an activation energy of 453 kJ/mol. The extrapolated lattice diffusion coefficient at 1000°C is $6.7(10)^{-19}$ cm²/s, or about ten orders of magnitude smaller than the diffusion coefficient of $6.6(10)^{-9}$ cm²/s of molecular oxygen as measured by Norton at 1000°C. The high activation energy and low absolute value are good evidence that Mikkelsen was measuring a lattice diffusion coefficient; he cautiously claimed that his measured values were only an upper limit, and could possibly have been influenced by traces of dissolved molecular water or oxygen, although he took great care to remove them.

The tracer profiles^{53,54,56-59} indicate that appreciable exchange between dissolved and lattice oxygen takes place above 900–1000°C. There are considerable differences between calculated exchange rates by different experimenters, possibly because of different lattice defects in the silica or different trace amounts of water that could act as a catalyst for the exchange. The exchange reaction can be written as



and at equilibrium is governed by the relation

$$K_x = (C_0 - C)(S)/(S_0 - S)(C) \quad (23)$$

where C is the concentration of dissolved molecular $^{16}\text{O}-^{18}\text{O}$, C_0 is the total concentration of dissolved oxygen, S is the concentration of lattice ^{18}O , and S_0 is the total concentration of lattice oxygen. If it is assumed that the isotopic ratio at equilibrium is the same in the dissolved and lattice species, then $K_x = 1$, and from Eq. 23,

$$C_0 \frac{dS}{dt} = S_0 \frac{dC}{dt} \quad (24)$$

Then from Eq. 19, the diffusion is controlled by an effective diffusion coefficient D_e ,

$$D_e = D/(1 + S_0/C_0) \approx DC_0/S_0 \quad (25)$$

where D is the diffusion coefficient of dissolved species. At 1000°C , C_0 is $9.5(10)^{-8}$ mol/cm³, and S_0 is 0.0733 mol/cm³, so $D = 7.8(10)^5 D_e$. The experimental diffusion coefficients measured in Refs. 49, 50 and 52 are all about six orders of magnitude less than those measured by Norton, suggesting that in these experiments there was dissolved to lattice exchange to equilibrium. Possibly the equilibrium was encouraged by traces of water in these experiments; when great care was taken to exclude water,^{53,54,56-59} it appears that the exchange did not go to equilibrium. More work is needed to understand these exchange experiments better, and to determine the relative importance of factors 1-5 above.

EFFECT OF GLASS COMPOSITION ON MOLECULAR DIFFUSION

Shelby¹¹ examined the diffusion of helium in a variety of types of fused silica with different amounts of impurities. For example, the hydroxyl concentration varied from 5 to 1300 parts per million, and one sample had 8 ppm of chlorine. The silicas were made in different ways: electrical or flame fusion of quartz powder, and oxidation of SiCl_4 in an oxyhydrogen or a water-free plasma. Within the relatively small error of his measurements, Shelby found no differences in the diffusion or solubility of helium in these glasses. Thus changes in impurities and methods of manufacture normally encountered for fused silica apparently do not affect molecular diffusion, in spite of some earlier reports of such effects.

The diffusion of helium and neon were measured in vitreous germania by Woods and Doremus,⁵ and of helium in this glass by Shelby.⁶⁰ Woods and Doremus found for helium and neon, respectively, activation energies of 4.9 and 8.9 kcal/mol and pre-exponential factors of $6.1(10)^{-6}$ and $5.6(10)^{-6}$ cm²/s. The activation energies were close to those for fused silica, without the pre-exponential temperature term, but the actual values of the diffusion coefficient at room temperature were $2(10)^{-9}$ for helium and $2(10)^{-12}$ for neon, thus about an order of magnitude lower than the helium value in Table 2, but only a factor of about 2.5 lower than the neon value. Shelby found an activation energy of 8.0 kcal/mol and a pre-exponential factor of about $1.5(10)^{-3}$ cm²/s for helium in germania with somewhat higher diffusion coefficients than Woods and Doremus. Apparently the larger germanium atom leads to a more "filled up" lattice than silica, even though the specific volume per mole of germania is somewhat larger than that of silica.

Shelby found that the diffusion coefficient of helium in vitreous B_2O_3 was about four times greater than for fused silica, although the activation energies for the two glasses were about the same.⁶⁰

Norton⁶¹ reported a slightly higher permeability of Vycor glass (96% SiO_2 , 4% B_2O_3) to helium than fused silica, and Lee and Fry²³ found a slightly

higher diffusion coefficient for deuterium in Vycor than in fused silica. Apparently the Vycor process (see Chapter 4) leads to a glass with a slightly more open structure than that of fused silica.

In many studies of the effect of composition on molecular transport in glass, only the permeation rates, and not the diffusion coefficients, were measured. The results of Norton⁶¹ for the permeation of helium in different glasses are shown in Fig. 7. The compositions of some of these glasses are given in Chapter 1, Table 1. As more network modifying ions are added, the permeation rate decreases and the activation energy increases. Two later more extensive studies of the permeation of helium through silicate glasses, particularly borates, gave similar results.^{62,63} Shelby (unpublished) analyzed the results of these latter two authors by plotting the permeation rate at 300°C as a function of the sum of concentrations of network formers (SiO_2 , B_2O_3 , and P_2O_5) in these glasses, as shown in Fig. 8. There is a good correlation between the amount of network former, or alternatively the amount of network modifier ions, and the permeation rate. Shelby^{2a} has summarized his experiments on helium permeation in binary alkali silicate and borate glasses. As the amount of modifier increases in the glass, the permeation rate decreases sharply. In binary, modifier-free glasses such as $\text{B}_2\text{O}_3\text{--GeO}_2$, $\text{TiO}_2\text{--SiO}_2$, and $\text{Al}_2\text{O}_3\text{--SiO}_2$, Shelby found that the compositional dependence of molar volume indicates the change of permeation with composition. Shelby^{2a} also summarized other results on permeation of helium in multicomponent silicate glasses.

The data of Eschbach⁶⁴ on diffusion and solubility of helium in six different silicate glasses indicate that a good part of the changes in permeation rates shown in Fig. 8 are caused by changes in solubility. At 60% network former, Eschbach found a diffusion coefficient about twenty times smaller than that of fused silica, whereas the permeation rate was about 6000 times smaller.

Barton and Morain measured the permeation of hydrogen in various silicate glasses from the rate of reduction of silver in the glass by hydrogen penetrating into it. They found that in soda-lime glasses the calcium was more effective in reducing hydrogen permeation than sodium in glasses with the same silica content. Furthermore, the smaller the alkaline earth ion in glasses with the same sodium-alkaline earth-silica compositions, the higher was the permeation rate of hydrogen, except in barium and strontium glasses, which showed about the same rate of hydrogen permeation. These results indicate that hydrogen permeation would not show as good a correlation with only network concentration as does helium, as shown in Fig. 8, perhaps because the larger hydrogen molecule is more strongly influenced by changes in the size and charge of network modifying ions.

The rate of growth of small gold particles in glass can be controlled by diffusion of gold atoms in the glass to the growing particle.^{65,66} The activation energy for diffusion of gold atoms in a glass containing 72% SiO_2 , 23% Na_2O , 4% Al_2O_3 , and 1% ZnO changes in the glass transition region, but the diffusion coefficient does not show as large a change as it does for ionic diffusion, as shown in chapter 15.

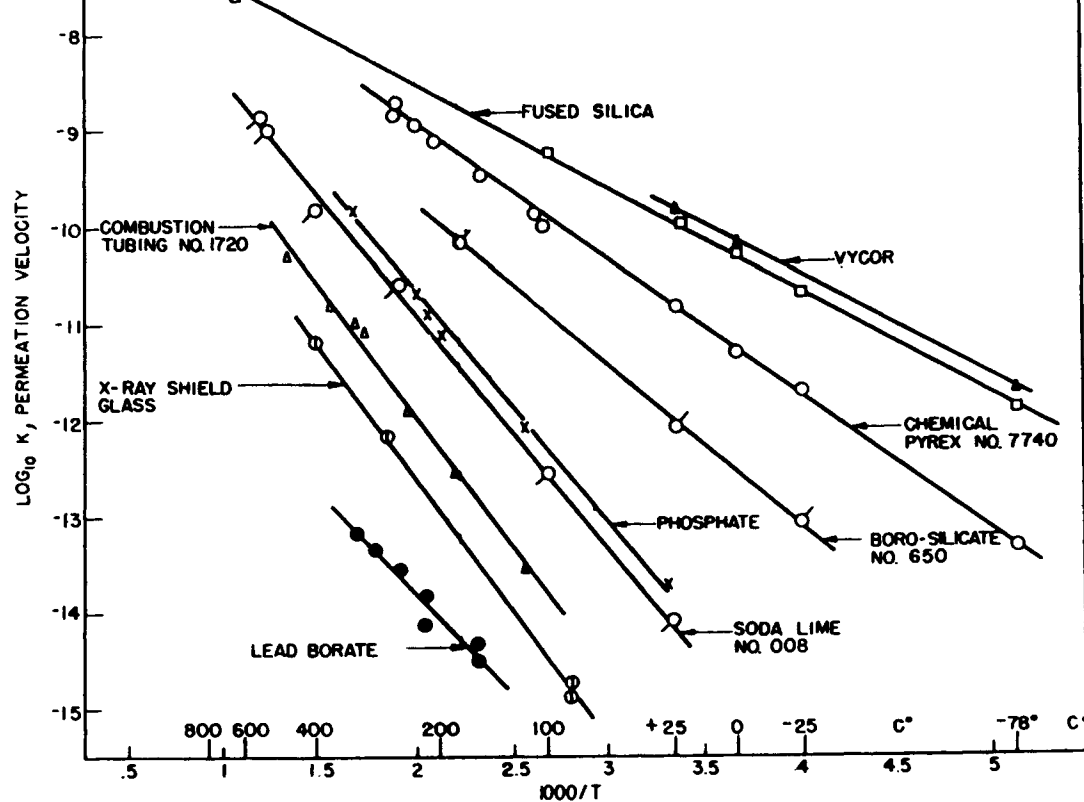


Fig. 7 Permeation rates for helium in various glasses as a function of temperature, measured by Norton.⁶¹ Permeation units are cm^3 of gas at STP per s per cm^2 area per mm thickness per cmHg pressure.

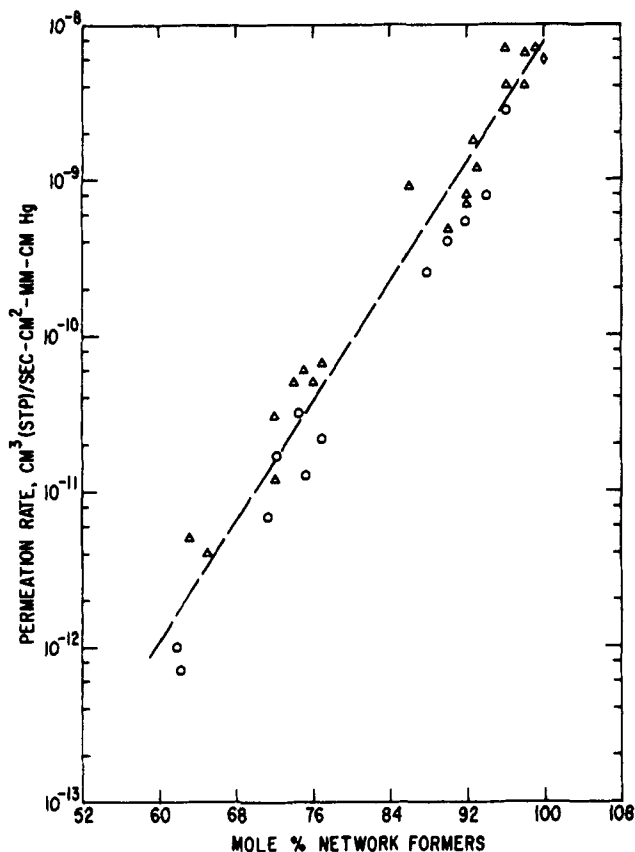


Fig. 8 Permeation rates for helium in various glasses at 300°C as a function of the % of network former ($\text{SiO}_2 + \text{B}_2\text{O}_3 + \text{P}_2\text{O}_5$) in the glass. \triangle , Altemose;⁶¹ \circ , Vostrov et al.⁶²

DIFFUSION FROM CONTRACTING BUBBLES

The diffusion of gas out of a bubble can control its rate of contraction, and is therefore important in removal of bubbles from glass melts (called “fining”, see Chapter 12). The rate of shrinkage of a bubble can also be used to calculate the diffusion coefficient of gas in the glass melt.

A simple equation for the diffusion flux J from an isolated bubble is^{67,68}

$$J = \frac{(c_e - c_i)D}{R} \left(1 + \frac{R_0}{\sqrt{\pi Dt}} \right) \quad (26)$$

where c_i is the concentration of gas in the glass melt at $t = 0$ and far from the bubble, c_e is the equilibrium concentration of gas in the glass at the bubble surface, R is the bubble radius at time t , R_0 is the radius when $t = 0$, and D is

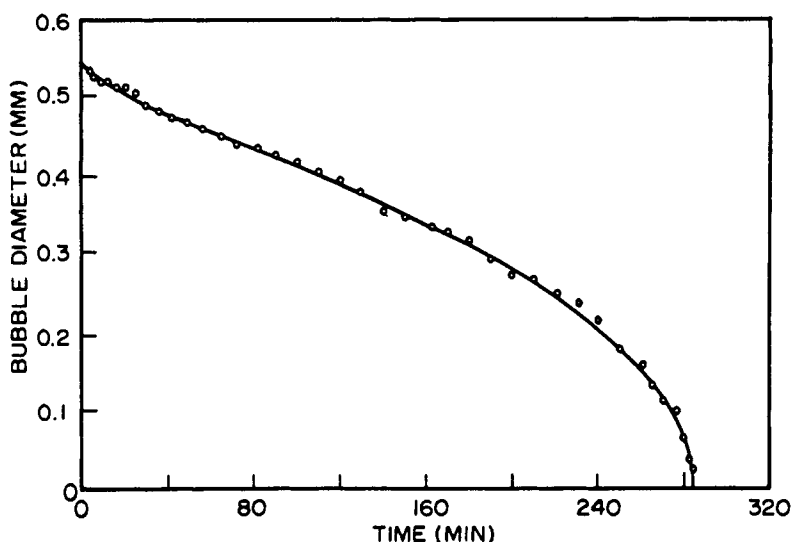


Fig. 9 Diameter of an air bubble in molten B_2O_3 as a function of time at $550^\circ C$. Points, experimental data, line from eq. 27 with $D = 2.3 \times 10^{-7} \text{ cm}^2/\text{s}$ and $B = 0.058$. Reprinted from Ref. 24 with permission from the American Ceramic Society.

the diffusion coefficient of gas in the melt, assumed independent of gas concentration. Since $J = (c_p - c_e)(dR/dt)$, where c_p is the gas concentration in the bubble,

$$R_0^2 - R^2 = \frac{2(c_e - c_i)dT}{c_p - c_e} \left(1 + \frac{2R_0}{\sqrt{\pi Dt}} \right) \quad (27)$$

A comparison between Eq. 27 and the shrinkage of a bubble of air (effectively nitrogen) in a boric oxide melt is shown in Fig. 9, from Ref. 24. The

TABLE 3 Diffusion Measurements from Contracting Bubbles in Molten Glass

Gas	Glass	Diffusion coefficient at $100^\circ C$ (cm^2/s)	Q	Refs.
O_2	Ba-Al-alkali Silicate	$8(10)^{-7}$	24	67-69
	Soda-lime silicate	$1.4(10)^{-7}$	53	67-69
	Borosilicate	$2.8(10)^{-6}$	32	67-69
He	Soda-lime silicate	$5(10)^{-5}$	13.4	70
Ne	Soda-lime silicate	$3(10)^{-6}$	13.4	70
H_2O	Soda-lime silicate	?	36	71

excellent agreement between Eq. 27 and the measurements shows that this equation is valid for these measurements (see also ref. 69a).

Diffusion coefficients calculated⁶⁷ from Eq. 27 and the shrinkage measurements of oxygen bubbles by Greene and co-workers^{68,69} are shown in Table 3, along with results of other measurements on contracting bubbles in glass.^{70,71}

OXIDATION OF SILICON

The formation of insulating oxide layers on silicon is a critical element in the processing of integrated semiconductor circuits. The oxide formed on silicon is pure vitreous silica, and experiments show that the oxide grows from the silicon-oxide interface, so that the oxidant (oxygen or water) must diffuse through the silica layer to reach the silicon. There is a vast literature on this subject because of its great technological and scientific interest; there are reviews in Refs. 72-74, and new papers appear frequently.

At high temperatures (above 1100°C) and for some silicides, the oxidation kinetics follow a parabolic equation

$$L^2 = Bt \quad (28)$$

where L is the film thickness after time t . For diffusion control, the parabolic rate coefficient B is given by

$$B = 2DC_0/\rho \quad (29)$$

where D is the diffusion coefficient of molecular oxidant in the film, C_0 its concentration dissolved in the glass at the oxide-gas surface, and ρ the concentration of oxygen in the film. When Eq. 29 is followed, the product DC_0 is just that measured by Norton¹³ for molecular oxygen, or that deduced³⁹ from the measurements of Moulson and Roberts³⁸ for molecular water.^{75,76}

At lower temperatures on pure silicon, the measured parabolic coefficient B becomes lower than that calculated from the data of Norton. One possible reason is strain in the oxide, which reduces the rate of oxidant diffusion through the film.⁷⁷ At these temperatures, the growth kinetics become linear-parabolic⁷⁹

$$L^2 + AL = Bt \quad (30)$$

where A is an additional parameter. One possible reason for the change from Eq. 29 to 30 is the strain of the silicon-oxide interface.⁷⁷ Other workers have claimed that the linear term results from a slow interfacial oxidation reaction, but this reaction is probably fast.⁷⁸

THEORIES FOR MOLECULAR DIFFUSION

In a random-walk treatment of diffusion, the diffusion coefficient has the form

$$D = \gamma \bar{\lambda}^2 \Gamma \quad (31)$$

where γ is a geometrical constant, $\bar{\lambda}^2$ is the average of the squares of step lengths, and Γ is the average number of steps per unit time. An expression for Γ is given by the transition state theory of kinetic processes:²

$$\Gamma = \frac{kT}{h} \exp\left(\frac{\Delta S}{R} - \frac{\Delta H}{RT}\right) \quad (32)$$

where k , h , and R are Boltzmann's Planck's, and the gas constant, respectively, and ΔS and ΔH are the entropy and enthalpy of activation. ΔH is thus equal to the activation energy Q' of Eq. 17.

A method of calculating the activation energy for molecular diffusion was proposed by Anderson and Stuart.⁸⁰ They assumed that this activation energy is the energy required to deform the silica network enough to allow the atom to pass from one interstice to another. The interstices were considered to be connected by "doorways" of average radius r_D ; the activation energy is then the elastic energy required to enlarge the doorway to the radius r of the diffusing molecule, assuming it to be incompressible. This energy was estimated from the equation (Eq. 6)

$$Q' = 8\pi G r_D (r - r_D)^2 \quad (33)$$

derived by Frenkel²⁷ for the elastic energy to dilate a spherical cavity from the radius r_D to r . G is the elastic modulus on the glass. From Eq. 33 the square root of the activation energy should be a linear function of the diameter of the diffusing molecule. Figure 10 shows this functional dependence for the data on molecular diffusion in fused silica recorded in Table 2. The doorway diameter is equal to 1.1 Å from the diameter extrapolated to zero activation energy. The elastic modulus calculated from Eq. 33 and slope of the line in Fig. 9 is about $1.2(10)^{11}$ dyn/cm², which is less than the value of $3(10)^{11}$ dyn/cm² for fused silica. This difference may result because the strain energy in the loose network structure of silica is less than in a close-packed liquid, for which Eq. 33 was derived. In any event, the functional dependence of activation energy on molecular diameter, as given in Eq. 33, describes well the activation energies for diffusion of molecules in fused silica, and the doorway diameter calculated from the equation is reasonable.

The entropy of activation can be estimated from experimental D' values (Eq. 17) and Eqs. 32 and 33. If $\gamma = \frac{1}{6}$ and $\gamma \approx 5.5$ Å for molecular diffusion in fused silica the entropies of activation are negative and become more negative as the size of the diffusing molecule increases. Perkins and Begeal¹⁰ found the same result with a slightly different pre-exponential factor in Eq. 32.

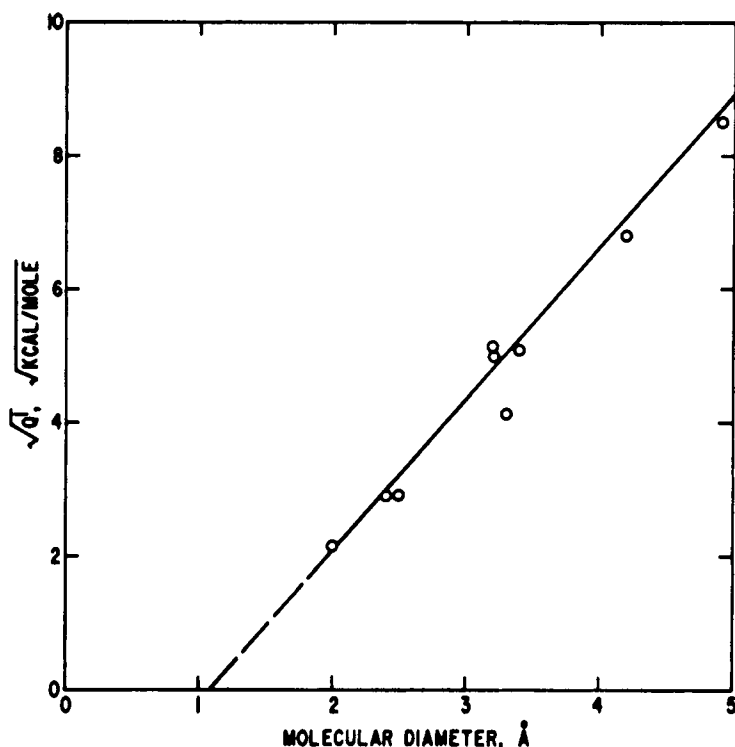


Fig. 10 Square root of the activation energies for molecular diffusion in vitreous silica as a function of molecular diameter. Data from Table 2.

Zener⁸¹ has shown that the entropy change ΔS should be proportional to the negative of the temperature coefficient of the elastic modulus of a substance if diffusion in it involves only straining its lattice. The elastic moduli for fused silica increase with temperature, in contrast to the decrease found for ordinary silicate glasses and metals; this positive temperature coefficient is consistent with the negative values of ΔS .

If it is assumed that $\gamma \approx 5.5$ Å for other glasses, then $\Delta S/R$ is negative for the diffusion of helium in Pyrex in the temperature range 25–350°C; in this range, the elastic moduli of Pyrex increase with temperature. The values of $\Delta S/R$ are positive for the diffusion of gold in a soda-alumina glass and argon in a potash-lime glass, and the elastic moduli of these glasses decrease with increasing temperature. These correlations probably cannot be extended to higher temperatures because, in the annealing range, the bulk elastic moduli will not be directly related to molecular transport, since the glass structure is changing with temperature. Thus there is the correct qualitative correlation between ΔS and the temperature dependence of elastic moduli, which is in agreement with the suggestion that the main contribution to the free energy of

activation of molecular diffusion in these glasses involves the elastic strain of the glass network.

Other theories have been proposed⁸²⁻⁸⁴ but they do not seem to replace Eq. 33.^{2a}

REFERENCES

1. R. M. Barrer, *Diffusion In and Through Solids*, Cambridge University Press, Cambridge, UK, 1941, pp. 117 ff.
2. R. H. Doremus, in *Modern Aspects of the Vitreous State*, Vol. 2, J. D. Mackenzie, Ed., Butterworths, London, 1967, pp. 1 ff.
- 2a. J. E. Shelby, in *Treatise on Materials Science and Technology*, Vol. 17, Academic Press, San Diego, 1979, p. 1.
3. H. W. Wüstner, *Ann. Phys.*, **46**, 1095 (1915).
4. G. A. Williams and J. B. Ferguson, *J. Am. Chem. Soc.*, **44**, 2160 (1922).
5. K. N. Woods and R. H. Doremus, *Phys. Chem. Glasses*, **12**, 69 (1971).
6. J. F. Shackelford, Ph. D. Thesis, University of California, 1971; see also J. F. Shackelford, P. L. Studt, and R. M. Fulrath, *J. Appl. Phys.*, **43**, 1619 (1972).
7. D. E. Swets, R. W. Lee, and R. C. Frank, *J. Chem. Phys.*, **34**, 17 (1961).
8. R. C. Frank, D. E. Swets, and R. W. Lee, *J. Chem. Phys.*, **35**, 1451 (1961).
9. R. W. Lee, *J. Chem. Phys.*, **38**, 448 (1963).
10. W. G. Perkins and D. R. Begeal, *J. Chem. Phys.*, **54**, 1683 (1971).
11. J. E. Shelby, *J. Am. Ceram. Soc.*, **55**, 61 (1972).
12. G. S. Nakayama and J. F. Shackelford, *J. Noncryst. Solids*, **126**, 249 (1990).
13. F. J. Norton, *Nature*, **191**, 701 (1961).
14. J. T. Kohli and J. E. Shelby, *Phys. Chem. Glasses*, **31**, 93 (1990).
15. J. M. Jewell and J. E. Shelby, *Phys. Chem. Glasses*, **29**, 67 (1988).
16. J. E. Shelby, *J. Appl. Phys.*, **43**, 3068 (1972).
17. J. E. Shelby, *J. Am. Ceram. Soc.*, **55**, 195 (1972).
18. R. W. Barrer and D. E. W. Vaughn, *Trans. Faraday Soc.*, **63**, 2275 (1967).
19. E. K. Beauchamp and L. C. Walters, *Glass Technol.*, **11**, 139 (1970).
20. W. A. Rogers, R. S. Burlitz, and D. Alpert, *J. Appl. Phys.*, **25**, 86 (1954).
21. H. M. Laska, R. H. Doremus, and P. J. Jorgensen, *J. Chem. Phys.*, **50**, 135 (1969).
22. J. E. Shelby, *J. Chem. Phys.*, **45**, 2146 (1974).
23. R. W. Lee and D. L. Fry, *Phys. Chem. Glasses*, **7**, 19 (1966).
24. R. B. Brown and R. H. Doremus, *J. Am. Ceram. Soc.*, **59**, 510 (1976).
25. R. H. Doremus, *J. Am. Ceram. Soc.*, **49**, 461 (1966).
26. R. H. Fowler and E. A. Guggenheim, *Statistical Thermodynamics*, Cambridge University Press, Cambridge, UK, 1939, pp. 81, 373.
27. J. Frenkel, *Kinetic Theory of Liquids*, Oxford University Press, London, 1946, pp. 10-11.
28. P. L. Studt, J. F. Schackelford, and R. M. Fulrath, *J. Appl. Phys.*, **41**, 2777 (1970).

29. J. F. Shackelford and J. S. Masaryk, *J. Noncryst. Solids*, **30**, 127 (1978).
30. J. F. Shackelford, *J. Noncryst. Solids*, 229 (1982).
31. J. E. Shelby, *J. Appl. Phys.*, **47**, 135 (1976).
32. C. M. Hartwig, *J. Appl. Phys.*, **47**, 956 (1976).
33. J. E. Shelby, *J. Appl. Phys.*, **48**, 338 (1977).
34. N. P. Bansal and R. H. Doremus, *Handbook of Glass Properties*, Academic Press, San Diego, CA, 1986.
35. O. V. Mazurin, M. V. Streltsina, and T. P. Shvaiko-Shvaikovskaya, *Handbook of Glass Data*, Vols. 1-3, Elsevier, Amsterdam, 1983, 1985, 1987.
36. J. Crank, *Mathematics of Diffusion*, 2nd edn., Oxford University Press, London, 1975.
37. R. H. Doremus, *J. Chem. Phys.*, **34**, 2186 (1961).
38. J. Moulson and J. P. Roberts, *Trans Faraday Soc.*, **57**, 1208 (1961).
- 38a. J. E. Shelby, *J. Am. Ceram. Soc.*, **54**, 125 (1971).
39. R. H. Doremus, in *Reactivity of Solids*, J. W. Mitchell, R. C. Devries, R. W. Roberts, and P. Cannon, Eds., Wiley, New York, 1969, p. 667.
40. J. Johnson and R. Burt, *J. Opt. Soc. Am.*, **6**, 734 (1922).
41. H. Matzke, *Phys. Stat. Sol.*, **18**, 285 (1966).
42. J. E. Shelby and S. C. Keaton, *J. Appl. Phys.*, **45**, 1458 (1974).
43. L. C. Walters, *J. Am. Ceram. Soc.*, **53**, 288 (1970).
44. T. Drury and J. P. Roberts, *Phys. Chem. Glasses*, **4**, 79 (1963).
45. G. J. Roberts and J. P. Roberts, *Phys. Chem. Glasses*, **5**, 26 (1964); **7**, 82 (1966).
46. I. Burn and J. P. Roberts, *Phys. Chem. Glasses*, **11**, 106 (1970).
47. A. Kats, Hydrogen in alpha-quartz, Thesis, Delft, 1961.
48. C. Wagner, *J. Chem. Phys.*, **18**, 1229 (1950).
49. R. Haul and G. Dumbgen, *Z. Electrochem.*, **66**, 636 (1962).
50. E. W. Sucov, *J. Am. Ceram. Soc.*, **46**, 14 (1963).
51. W. C. Hagel and J. D. Mackenzie, *Phys. Chem. Glasses*, **5**, 113 (1964).
52. E. L. Williams, *J. Am. Ceram. Soc.*, **48** 191 (1965).
53. L. D. Major, M. S. Thesis, Case Western Reserve University, Cleveland, OH, 1977.
54. R. Rochet, B. Agius, and S. Rigo, *J. Electrochem. Soc.*, **131**, 914 (1984).
55. J. C. Mikkelsen, *Appl. Phys. Lett.*, **45**, 1187 (1984).
56. C. J. Han and C. R. Helms, *J. Appl. Phys.*, **59**, 1767 (1986).
57. J. D. Cawley, J. W. Halloran, and A. R. Cooper, *Oxid. Met.*, **28**, 1 (1987).
58. J. D. Cawley and R. S. Boyce, *Philos. Mag.*, **B58**, 589 (1988).
59. J. D. Kalen, R. S. Boyce, and J. D. Cawley, *J. Am. Ceram. Soc.*, **74**, 203 (1991).
60. J. E. Shelby, *J. Appl. Phys.*, **43**, 3068 (1972).
61. F. J. Norton, *J. Am. Ceram. Soc.*, **36**, 90 (1953).
62. V. O. Altemose, *J. Appl. Phys.*, **32**, 1309 (1961).
63. G. A. Vostrov and O. J. Bolchakov, *Prib. Tech. Eksp.*, **2**, 112 (1966).
64. H. L. Eschbach, in *Advances in Vacuum Science and Technology*, E. Thomas, Ed., Pergamon, London, 1960, p. 373.

65. R. D. Maurer, *J. Appl. Phys.*, **29**, 1 (1958).
66. R. H. Doremus, in *Symp. on Nucleation and Crystallization in Glasses and Melts*, M. K. Reser, Ed., American Ceramic Soc., Columbus, Ohio, 1962, p. 119.
67. R. H. Doremus, *J. Am. Ceram. Soc.*, **43**, 655 (1960).
68. C. H. Greene and R. F. Gaffney, *J. Am. Ceram. Soc.*, **42**, 271 (1959).
69. C. H. Greene and J. Kitano, *Glastech. Ber.*, **32K**, V, 44 (1959).
- 69a. R. S. Subramanian and M. C. Weinberg, *AIChE Jour.*, **27**, 739 (1981).
70. G. H. Frischat and H. J. Oel, *Glastech. Ber.*, **38**, 156 (1965); *Phys. Chem. Glasses*, **8**, 92 (1967).
71. L. N. Nemer, *Glass Tech.*, **10** 176 (1969).
72. C. R. Helms and B. E. Deal, Eds., *The Physics and Chemistry of SiO₂ and the Si-SiO₂ Interface*, Plenum Press, New York, 1988; Vol 2, 1993.
73. E. A. Irene, *Crit. Revs. in Solid State and Materials Sci.*, **14**, 175 (1988).
74. N. F. Mott, S. Rigo, F. Rochet, and A. M. Stoneham, *Phil. Mag.*, **B60**, 189 (1989), and other papers in this volume.
75. R. H. Doremus, *J. Phys. Chem.*, **80**, 1773 (1976).
76. R. H. Doremus, in Ref. 72, p. 17.
77. R. H. Doremus, *Thin Solid Films*, **122**, 191 (1984).
78. R. H. Doremus, *J. Appl. Phys.*, **66**, 4441 (1989).
79. S. C. Kao and R. H. Doremus in ref. 72, Vol. 2, p. 23 (1993).
80. O. L. Anderson and D. A. Stuart, *J. Am. Chem. Soc.*, **37**, 573 (1954).
81. C. Zener, in *Imperfections in Nearly Perfect Crystals*, Wiley, New York, 1952, p. 289.
82. J. S. Masaryk and R. M. Fulrath, *J. Chem. Phys.*, **59**, 1198 (1973).
83. L. van Caugh, *Silic. Ind.*, 295 (1975).
84. W. W. Brandt, *Phys. Stat. Sol.*, **30**, 263 (1975).

CHAPTER 9

FRACTURE

Mechanical failure of glass at temperatures below the glass transition is caused by brittle fracture. In this chapter strength and fracture of glass are discussed in two parts; first a discussion of experimental measurements and results, and second their interpretation.

EXPERIMENTAL RESULTS

Testing Methods

In brittle materials, failure usually takes place at much lower tensile stresses than compressive. In principle, the simplest test is to pull a rod, putting a uniform tensile stress on it. In practice, there are difficulties in gripping the sample, and except for fine fibers one must make the central length of the rod smaller in diameter to be certain that failure does not occur at the grips. Making such samples is difficult and expensive, so other tests are used in which the stress distribution is not as simple as in a tensile test. For long fibers, the direct tensile test is the simplest and most frequently used since gripping problems can be overcome in a variety of ways.¹⁻⁴

The most common tests are in bending (flexure), with either three or four points of stress application. Rod samples are much better than bars because chips at the corners of the bars can initiate fracture. In the bending of a rod with four points, the tensile stress parallel to the sample axis is maximum on a line on the sample surface opposite and between the inner points. The stress S along this line for small strains is given by the simple bending formula

$$S = 8P/\pi D^3 \quad (1)$$

where P is the force at each contact point and D is the sample diameter. The stress on the sample surface decreases with the angle θ with the midplane,

$$S_s \approx \cos \theta \approx S(1 - 2\theta/\pi)^{1/2} \quad (2)$$

and the stress decreases approximately linearly from the surface to the sample axis. Thus the bend tests favor failure starting at the sample surface, where the tensile stress is higher. The four-point bend test is preferable to the three-point test because the former samples more of the specimen surface and is less prone to failure at the contact points.

The diametral compression test provides an attractive alternative to bend tests for some materials.^{5,6} In this test, a right circular cylinder is compressed along its diameter by two flat plates, giving a maximum tensile stress normal to the loading direction across the loading diameter, and also from one face of the cylinder to another, so that both surface and volume failures are possible. A pad of material softer than the compressing plates must be inserted between the sample and plates to prevent failure at the plates.

Compressive tests are sometimes used for glass, but failure usually takes place at a corner contact of the sample with the compressing plates. Presumably, failure is caused by a tensile stress that is difficult to calculate, so these tests give scattered and unreliable results.

Units of stress (strength) are particularly troublesome. Much older work is reported in pounds per square inch (psi); the SI units are Pascals (Pa) or Newtons per square meter. The conversion is

$$1.45 \times 10^{-4} \text{ psi} = 1 \text{ Pa} \quad \text{or} \quad 6.70 \times 10^3 \text{ Pa} = 1 \text{ psi}$$

Strength Distributions

When the failure stress of a number of glass samples is measured under identical conditions of sample preparation and loading, the failure stresses vary over a wide range of a factor of 2 or more, as shown in Fig. 1. It is desirable to express this distribution of strengths in statistical terms. The strengths are often distributed symmetrically, as is approximately so in Fig. 1, so they can be described by a normal (Gaussian) distribution,

$$P = (1/d\sqrt{2\pi}) \exp[-(S - S_m)^2/2d^2] \quad (3)$$

where P is the probability of finding a sample of strength (failure stress) S , S_m is the strength of greatest probability ($P_m = 1/d\sqrt{2\pi}$), and d is a measure of the spread of the distribution (called the standard deviation) and is equal to the root mean square of deviations from the mean strength. The integral of Eq. 3 gives the fraction F of samples that break below the stress S

$$F = \frac{1}{2} \{1 + \text{erf}[(S - S_m)/\sqrt{2}d]\}$$

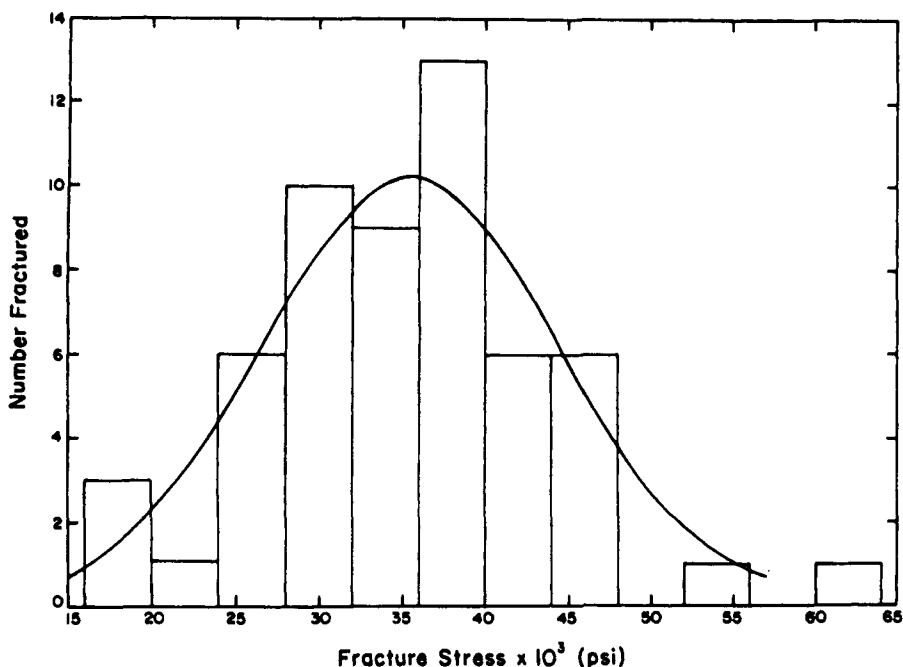


Fig. 1 Distribution of fracture strengths of rods of Pyrex borosilicate glass 3 mm in diameter in four-point bending at -196°C . Line from Eq. 3 with $S_m = 35.5 \times 10^3$ psi and $d = 8.9 \times 10^3$ psi. Ref. 48.

where erf is the error function

$$\text{erf } x = \frac{2}{\sqrt{\pi}} \int_0^x \exp(-\lambda^2) d\lambda$$

Recently, another distribution function called the Weibull distribution has become quite popular in describing strength distributions

$$F = 1 - \exp[-S/S_0]^m] \quad (4)$$

where S_0 is a scaling factor and m is a measure of the spread of the distribution; smaller m , broader distribution. For m larger than about 3, the Weibull distribution is nearly symmetrical and closely resembles the normal distribution.

A convenient way to examine the fit of strength data to a Weibull distribution and to calculate m is to transform Eq. 4 to

$$\log[-\ln(1-F)] = m \log S - m \log S_0 \quad (5)$$

A least-squares fit of the related equation gives values of m and S_0 . If the correlation coefficient R^2 of the fit is close to 1 (≥ 0.95), which means the data

fit the Weibull distribution well, these values are statistically acceptable; however, if the fit is poorer, especially for $R^2 < 0.9$, then a reasonable approximation to m and S_0 can be found only with the maximum likelihood procedure.⁷ The data of Fig. 1 are plotted according to Eq. 5 in Fig. 2; the Weibull parameters for the fit in Fig. 2 are $m = 5.5$ and $S_0 = 262$ MPa (3.8×10^4 psi). Weibull parameters and correlation coefficients calculated from a regression analysis of Eq. 5 for different glass compositions, surface treatments, and temperature are summarized in Table. 1. Compositions of the glasses are given in Chapter 1.

Strengths of glass fibers carefully drawn are much higher than for ordinary glass; E-glass has a strength of from $(1-4) \times 10^9$ Pa at room temperature,² and silica fibers have even higher strengths.^{1,3,4} The distributions of strengths of these fibers in short lengths can be quite narrow,^{8,9} with a coefficient of variation (standard deviation divided by mean strength) of 1-2%. On the other hand, flame-polished or etched glass rods with high strengths can have very broad and nonuniform distributions,¹⁰ as shown in Fig. 3.

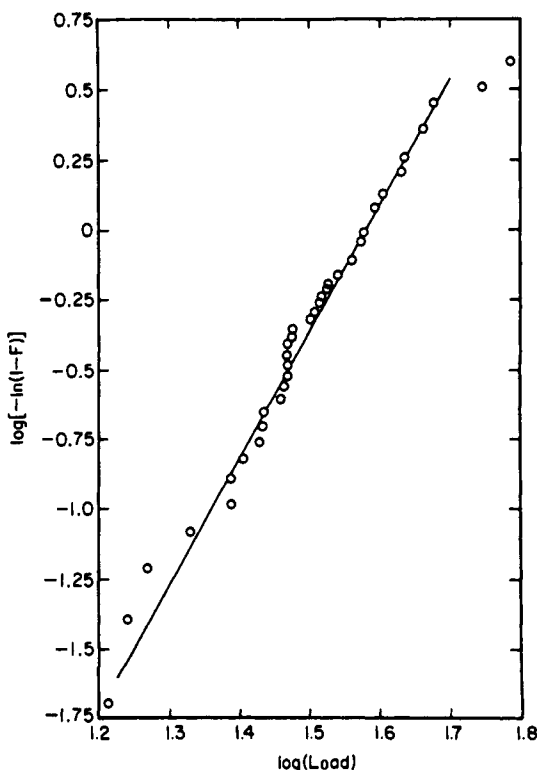


Fig. 2 Weibull plot (Eq. 3) of data in Fig. 1. Not all points are shown. Ref. 48.

TABLE 1 Mean Strength and Weibull Modulus for Strengths of Glasses

Run	Abraded	Number of Samples	Temperature (°C)	Crosshead Speed (cm/min)	Mean Strength (MN/m ²)	Coefficient of Variation (%)	m^a	R^2 for Weibull Fit ^b
<i>Soda-lime silicate</i>								
1	No	57	-196	0.13	245	25	4.5	0.98
2	Yes	49	-196	0.13	137	16	6.6	0.87
3	Yes	29	-196	0.13	236	17	6.5	0.86
4	Yes	104	23	0.13	135	20	6.4	0.96
5	Yes	58	23	0.025	132	18	5.9	0.96
6	Yes	90	23	0.013	112	18	6.7	0.94
7	Yes	123	23	0.0013	103	20	6.2	0.94
8	No	37	23	0.13	166	28	4.2	0.95
<i>Pyrex borosilicate</i>								
9	No	87	-196	0.05	246	21	5.5	-
10	No	21	23	0.25	134	17	6.4	-
11	No	21	23	0.051	123	15	6.0	-
12	No	21	23	0.013	118	20	6.4	-
13	Yes	85	23	0.127	117	14	7.8	-
<i>FN borosilicate</i>								
14	Yes	100	-196	-	102	6.9	7.3	-

^aLeast-squares fit to Weibull distribution calculated from Eq. 5.^bCalculated from Eq. 5.

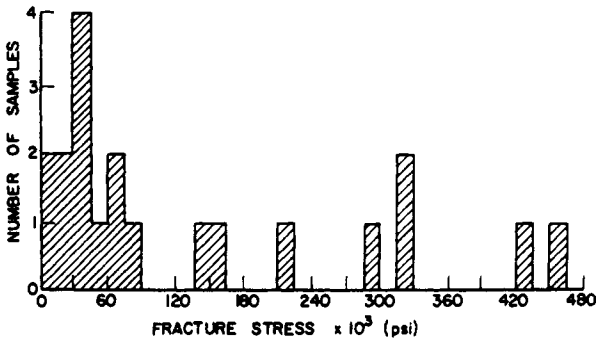


Fig. 3 Distribution of fracture strengths of rods of soda-lime glass 3 mm in diameter in four-point bending at -196°C after removing $9.4\text{ }\mu\text{m}$ by etching with dilute HF. Ref. 48.

Effect of Surface Area on Strength

One of the most interesting experiments on the influence of sample diameter on glass strength was carried out by Griffith.¹¹ He drew glass fibers of different diameters and compared their strengths at the same stressed length in simple tension; he had to age the fibers at ambient conditions and break short lengths ($\sim 5\text{ cm}$ long) under tension to obtain reproducible results. Griffith fitted his results with the equation

$$S = 154(110 + D)/(1.5 + D) \quad (7)$$

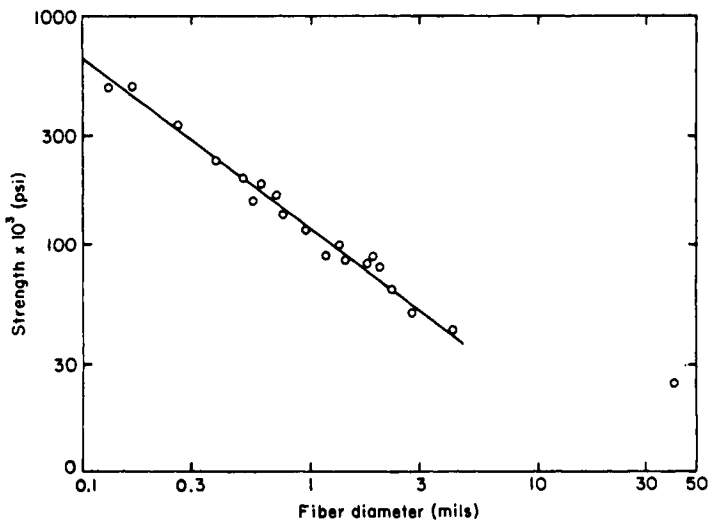


Fig. 4 Fracture strengths of fibers of soda-lime glass 5 cm long, as a function of diameter. Data from Griffith.¹¹

where D is the fiber diameter in micrometers and S is the failure stress in Pascals. Many other investigators have confirmed that as the stressed area of glass surface increases, the strength decreases.¹² If Eq. 7 is extrapolated to very small fiber sizes, a limiting strength of about 1.1×10^{10} Pa is found, which is about half the calculated theoretical strength of the glass (see below). Griffith's data can also be plotted as log breaking strength against log diameter, as shown in Fig. 4. Except for the one point at the largest diameter, the relation is linear. Fused-silica fibers also showed a linear relation between log S and log D below 25 μm diameter, with higher expected strengths at larger diameters.¹³

Otto¹⁴ reported no change in the strength of glass fibers from about 1 to 3 μm in diameter, and Thomas^{8,15} found no change in strength from a diameter of 1 μm to about 30 μm .

Effects of Surface Treatment on Strength

When a glass surface is abraded or bombarded with particles, the strength of the glass is reduced. Different treatments give quite different strengths.¹⁶

If glass samples are carefully prepared and kept "pristine", they have very high strengths. Many results up to 10^{10} Pa have been reported^{12,18}, and Hillig^{12,18} measured strengths of up to 1.5×10^{10} Pa at -196°C for fused-silica rods 1 mm in diameter. These samples were flame-drawn from larger rods and carefully protected from contact with solids. It is spectacular to bend a 1-mm rod of glass into a closed loop (Ref. 18, Fig. 16). Bimodal strength distributions were found for such fibers. If one so much as touched the fiber lightly with a finger tip, it broke at much lower stress.

The strength of ordinary or abraded glass can be substantially increased by etching with hydrofluoric acid.^{19,21} The distribution of strength after etching is shown in Fig. 3. Etching leads to some samples with very high strengths, but samples etched in HF are highly sensitive to damage by handling, and many samples have strengths lower than before etching. As the experimenter becomes more skilled, fewer low-strength samples result.

A soda-lime glass held in water for a few hours after being abraded has up to 1.5 times higher strength than if it is tested immediately after abrasion.^{21,22a} Immersion in water for a short time increases the strength considerably. If Vycor glass is tested in different organic liquids just after abrasion, it has different strength depending upon the liquid; the more polar the liquid, the greater the reduction in strength. All these results show that the strength of a glass is almost always determined by the condition of its surface.

Influence of Temperature and Glass Composition on Strength

The strength of soda-lime glass as a function of temperature was determined by Ernsberger²² for failure at oblate bubbles inside the glass as shown in Fig. 5. The strengths of other high-strength glasses have a similar temperature

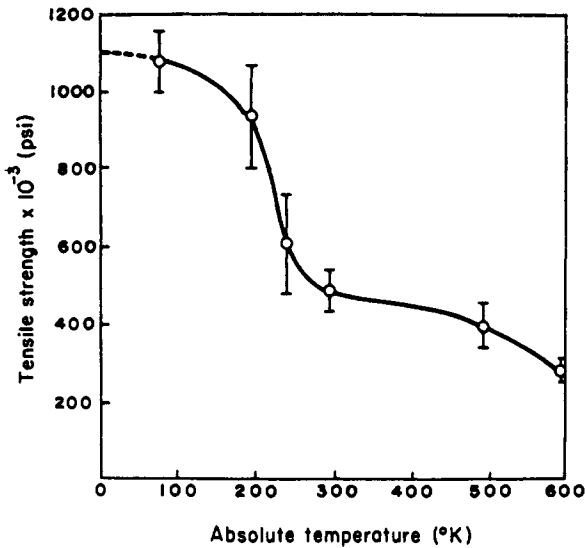


Fig. 5 Temperature dependence of the fracture strength of soda-lime glass at bubbles inside the glass.²²

dependence.^{1,2} However, abraded glasses of low strength often show little temperature dependence of fracture strength. These temperature effects are probably caused by the same mechanism as delayed failure, as discussed in the next chapter. Hillig¹⁸ found no difference in glass strength between -196°C and 268°C ; at these temperatures delayed failure is absent.

The glass composition can influence the strength indirectly through surface chemical reactions, introduction of surface stresses, and other secondary effects. However, there is no evidence that direct effects of glass composition on strength, for example, as a result of changes in bonding in the silicon-oxygen network, have been measured. Other results on the influence of surface damage, temperature, and glass composition on strength were reviewed by LaCourse.²³

Observations of Fracture Surfaces and Origins

Markings on fracture surfaces can give information about the origin and direction of fracture propagation, as well as about material inhomogeneities and local stress effects. The study of these markings is called fractology, and is discussed on the scale of the optical microscope by Frechette.²⁴ The determination of the macroscopic origin of fracture, directions of fracture propagation, and stress distributions is not discussed here.

A fracture surface on glass shows several characteristic regions: an origin usually on the glass surface; a smooth region called the mirror; a misty region outside the mirror; and finally a region of coarse surface roughness, called hackle, as shown in Fig. 6. The distance R from the fracture origin to the



Fig. 6 Fracture surface of soda-lime silicate glass, broken in bending at 25° C. Ref. 48.

mirror-mist boundary (or the distance to the mist-hackle boundary) is related to the fracture strength S by the empirical equation²⁵⁻²⁸

$$S\sqrt{r} = A \quad (8)$$

where A is a constant for a particular brittle material and temperature. Values of about $2 \times 10^6 \text{ N/m}^{3/2}$ were found for A for glass at room temperature. Apparently, A is not significantly dependent on temperature or glass composition, although it can depend on sample history.^{28a}

Equation 8 is of considerable practical value because it allows one to make an accurate estimate of fracture stress without having to measure it directly. Thus for pieces with complex shapes where a stress analysis is difficult, or where load measurements are not possible, Eq. 8 is invaluable.

Fracture origins in glass often look like that shown in Fig. 7, although quite different shapes are also possible.^{27,29,30}

A variety of special figures can develop on a fracture surface, depending upon the initial state of stress. For example, lath-like regions of constant thickness start at a particular distance on a fracture front in a tension-torsion sample.³¹ On the lines separating the laths, tiny "lances" separate from the glass surface.

Observations of Surface Damage

Different chemical treatments, such as sodium vapor or a molten lithium salt, give visible crack patterns on a glass surface; these cracks can result from the treatment and do not represent prior damage to the surface.³² Etching a glass surface with hydrofluoric acid reveals elongated pits resulting from surface cracks.¹²



Fig. 7 Origin of fracture in soda-lime glass, scanning electron micrograph. Upper surface is the original glass; fracture surface lower.³⁰

If a hard sphere is pressed against a glass surface, a crack around the contact region first develops and then grows into the glass in a conical shape.^{33,34} These cracks are called Hertzian cracks because the elastic stress distribution for contact of a hard sphere on a plate was calculated by Hertz.³⁵ Other papers on this subject are listed in Refs. 36 and 37.

If the indenter is sharp rather than spherical, the crack pattern is entirely different.^{37,38} A "median vent" crack propagates into the glass directly under the indenter during loading. When the load is released, wing-like cracks ("lateral vents") propagate radially from the contact region. A region of the glass directly under the indenter is deformed in a particular way that is discussed in more detail in the section on plastic deformation in glass.

The impact of a hard spherical projectile gives damage with features of both spherical and sharp indenters.³⁹ At low impact velocities, Hertzian cone cracks are formed, but at higher velocities the cone cracks turn up at their ends and finally resemble the radial wing-like cracks; at high velocities median cracks also propagate down into the glass. Liquid impacts cause crack growth and branching.⁴⁰

When a hard object such as a diamond indenter is dragged across a glass surface, median and lateral cracks form along its track much as under an indenter.⁴¹⁻⁴³ Abrasion of a hard surface against the glass also gives this kind of linear damage.

Velocity of Fracture Propagation

The velocity of fracture propagation in glass has been measured by a variety of methods.^{43,44} Velocity measurements from line markings on the mirror surface known as Wallner lines were developed by Smekal⁴⁵ and Shand²⁵. An example of such experimental results is shown in Fig. 8. Fracture velocities can also be measured from ripple marks on the fracture surface resulting from

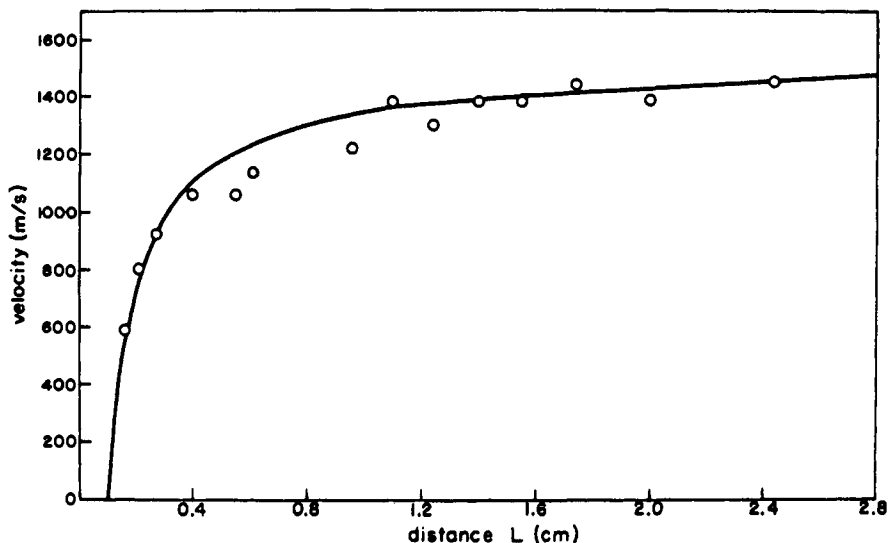


Fig. 8 Velocity of a propagating crack in soda-lime glass versus crack length. Fracture stress 6.7×10^6 Pa; points from Field (Ref. 44, Fig. 11), line from Eq. (33).

ultrasonic waves introduced perpendicular to the fracture face. Various techniques of high-speed photography, such as rotation-mirror and multiple-spark cameras, can be used to measure crack velocity. Another method is to measure the electrical conductivity of metal strips painted on the glass as they are progressively broken by the fracture front.

FRACTURE CRITERIA, MODELS, AND EXPLANATIONS

Fracture Criteria

The experimental results described above provide strong evidence that the surface condition of a glass determines its strength, and that flaws in the surface reduce the strength. These results therefore led to a model of surface cracks as the origin of brittle fracture. It is difficult to observe these cracks directly, and there still is uncertainty about their size, depth, and shape. Inglis^{46a} solved the elastic problem of an elliptical crack subjected to a tensile strength S . He showed that the stress σ along the inside crack surface is given by

$$\frac{\sigma}{S} = \frac{1 + 2c/a - (c + a)^2 x^2 / a^4}{1 + (c^2 - a^2) x^2 / a^4} \quad (9)$$

where c is the depth of the crack (semimajor axis of the ellipse), a is the half-width of the crack (semiminor axis of the ellipse), and x is the distance

from the crack tip parallel to the sample surface. Right at the tip ($x = 0$), the stress is

$$\sigma/S = 1 + 2c/a \quad (10)$$

In terms of the radius of curvature $\rho = a^2/c$ of the crack tip

$$\sigma/S = 1 + 2\sqrt{c/\rho} \approx 2\sqrt{c/\rho} \quad (11)$$

If the crack is not elliptical in shape, it can be shown that Eq. 11 is still the proper form. Thus if the crack is deep and has a sharp tip, the stress at the tip can be much higher than the applied stress. It seems reasonable that various types of surface damage on glass could give rise to cracks with different depths and tip radii, resulting in the influence of surface treatment on strength found experimentally. Equation 9 shows that the stress drops off very sharply away from the tip $x = 0$. The complete elastic solution also shows that the stress drops off sharply into the glass away from the crack tip. Thus the stress is near the maximum value given by Eq. 11 in only a very small volume of the glass.

A term called the stress intensity factor K is often used; for a small, deep, thin crack subjected to a tensile stress $K = S\sqrt{\pi c}$. K is sometimes considered to be a measure of the stress at the crack tip. The above discussion shows that this use is incorrect because the maximum stress at the crack tip is given by Eq. 11, and the crack tip radius must be included to determine this stress. The use of K as a fracture criterion is often justified from energy considerations; the discussion below on cracks and energy shows that this method is valid only in a limiting case, again because the influence of the crack tip radius is neglected. See ref. 48 for approximate stress functions.

One model of the crack tip is a cusp, giving a zero radius of curvature of the crack tip. However, this model cannot correspond to physical reality. A zero crack tip radius would give a high tip stress and crack propagation at any finite applied stress; the experimental results of failure at various high stresses show that the crack tip radius has a definite nonzero value. Even if the tip radius is of atomic dimensions, the bonds holding the atoms together will correspond to an effective nonzero tip radius. The discussion below, based on thermodynamics, suggests that the minimum tip radius for fracture is about ten atomic distances; if the tip radius is smaller than this value, the tip atoms rearrange to form a larger tip radius when the crack is subjected to a tensile stress.

Experiments show that glass samples with cracks of the same length but with different treatment (e.g., freshly abraded or abraded and aged in water) have different strengths, again showing the importance of the crack tip radius.⁴⁶

Equations 9–11 are derived for linearly elastic conditions. It is sometimes suggested that these equations must be modified for nonlinear elastic or plastic behavior at high stresses. The discussions in subsequent sections on plastic deformation show that such deformation probably does not take place in glass in tension at room temperature, and nonlinear elastic effects are small.

Theoretical Strength and Elasticity at High Strains

The results described above show that glass samples can have widely different strengths; design strengths for glass parts are usually less than about 30 MPa (4500 psi), but strengths up to 1.5×10^{10} Pa have been measured for vitreous silica at -196°C . Thus the intrinsic strength of vitreous silica must be greater than the latter value, and it is important to estimate how much greater. In this section theoretical calculations of intrinsic strength are compared, and the experimental behavior of glass at high stresses and strains discussed.

Glass is held together by a network of silicon-oxygen bonds. Therefore to calculate the force needed to tear apart planes held together by these bonds, some model of the forces between atoms is needed. A reasonable interatomic potential for covalently bonded atoms is the Morse potential;⁴⁷ the theoretical cohesive strength σ or ultimate strength of a material calculated from this potential is⁴⁸

$$\sigma^2 = E\gamma/4a \quad (13)$$

in which E is Young's modulus, γ is the surface energy, and a is the interatomic spacing in the glass. Equation 13 shows that the ultimate strength of a material is related to its stiffness and to the potential energy per unit surface area at equilibrium separation. Since each of these factors is proportional to the bond strength, the ultimate strength is proportional to the bond strength.

The surface energy γ can be approximately calculated from the bond free energy G_b and atomic density N of a solid,

$$\gamma = \frac{1}{4}G_b N^{2/3} Z \quad (14)$$

where Z is the coordination number. For silicon-oxygen bonds, $G_b \approx 6.6 \times 10^{-19}$ J/bond, and $\gamma \approx 5.2$ J/m² for vitreous silica and 3.5 J/m² for commercial soda-lime glass.

Young's modulus for vitreous silica is 7.2×10^{10} Pa and $a = 1.6 \times 10^{-10}$ m, so from Eq. 13, $\sigma_i \approx 2.4 \times 10^{10}$ Pa (3.5×10^6 psi); this estimate of ultimate strength is about 60% higher than the highest measured strength for silica. For soda-lime glass, the ultimate strength is about 1.6×10^{10} Pa (2.3×10^6 psi), reflecting the lower bond density and somewhat lower bond strength⁴⁹ of soda-lime glass. The estimate for fused silica is close to the value calculated by Nardy-Szabo and Ladik⁵⁰ using the Morse potential function in quite a different way.

At stresses above about 0.5×10^{10} Pa (strains above 7%), Hillig¹² found that vitreous silica deviates from Hooke's law and becomes stiffer (has a higher effective modulus) than at lower stresses. Krause et al.⁵¹ confirmed this result and found similar results for vitreous germania; vitreous B_2O_3 and As_2S_3 and commercial soda-lime glass also showed deviations from Hooke's law but in the opposite sense. These differences between glass compositions probably correspond to the increase (silica and germania) and decrease (other glasses) of modulus with temperature found for these glasses.

The tensile deformation of glasses at high stresses is entirely reversible and instantaneous, so there is no evidence for any plastic deformation in these tests.

Plastic Deformation in Glass

In contrast to tensile and bend tests of glasses, indentation of glass with a sharp point leads to regions of deformation under the indenter that do not recover when the load is removed.^{52,53} This deformation in fused silica is apparently a "densification" that recovers completely on heating. In glasses with modifiers (alkali and alkaline earth oxides), this deformation can be partly a densification,⁵⁴ but only a small part of the deformation recovers upon heating.⁵⁵⁻⁵⁷ More detailed examination of this deformed region under a sharp indenter showed that it is made up of flow or fault lines between which there are only elastic strains.⁵⁸⁻⁶¹ Some concise definitions will perhaps help to clarify the discussion of "plasticity" in glass and distinguish between the following different kinds of deformation:

1. Elastic: instantaneous and completely recoverable upon removing the load;
2. Anelastic: recoverable but requiring a measurable time for deformation after application or removal of the load;
3. Viscous: the uniform nonrecoverable flow of a liquid or amorphous solid subjected to a shearing stress; the rate of deformation is usually directly proportional to the load;
4. Plastic: the nonrecoverable nonuniform deformation of a crystalline solid; Occurs preferentially on certain lattice planes and in certain lattice directions, and results from dislocation motion; can occur at low stresses;
5. Faulting: nonrecoverable nonuniform deformation along certain planes in a solid that are determined by the applied loads; occurs only under a compressive stress close to the ultimate strength of the solid.

It is also useful to define

6. Crack: a flaw or defect in a solid, usually planar, in which solid planes are separated by a few or more lattice distances over a certain area.

With these definitions, the shear deformation of glass under a concentrated compressive load is distinguished from other types of deformation and is called faulting, in analogy to geological faulting. The excellent studies of Hagan⁶¹ show that this deformation has the following additional characteristics:

1. The fault lines are extremely narrow, probably no more than a few atomic distances thick.

2. The fault lines meet at 110° , instead of the 90° required by the traditional ideal elastic-plastic behavior.
3. Kinks at intersections of flow lines show that the fault planes are not cracks (see definition above) with free surfaces.
4. The fault lines can act as nucleation sites for cracks.

In view of these characteristics, these fault lines resemble geological faults and are quite different from slip in plastic deformation of crystals. Thus it seems important to distinguish this faulting deformation from plastic deformation in ductile crystals.

Viscous flow is much too slow in glass to cause appreciable deformation at ambient temperatures. The viscosity of commercial soda-lime glass at 490°C is about 10^{15} P, with an effective activation energy of greater than 400 kJ/mol; the activation energy increases with decreasing temperature.^{62,63} Thus the viscosity at room temperature is greater than 10^{59} P.

It is perhaps of interest to try to invent some atomic models for some of the deformations in glass. **Densification** is anelastic deformation by the definitions above. It occurs by bending and twisting but not breaking of the silicon-oxygen bonds in the glass network as they respond to a compressive stress. Since the bonds are only distorted but not broken, they return to their original configuration when they are heated to a temperature at which they can unwind. Densification is preferred in fused silica, in which the lattice is not broken up by modifier ions.

In silicate glasses with modifier ions, shear displacements occur at high compressive stresses because the silicon-oxygen lattice is partially broken up, possibly by planes of modifier ions. The fault planes resulting from these displacements can be modeled as being at most a few atoms thick and consisting of distorted regions of broken modifier and lattice bonds. These planes are not like regions over which dislocations have moved since the latter re-form more or less into the original lattice.

Scanning electron micrographs of glass surfaces after scoring with diamond points show shapes that resemble those from metalworking.^{58,59} Nevertheless, these deformations are very different from plastic deformation in metals and other ductile materials, since they arise only from sharp points and do not occur with large-scale stressing in tensile and bending modes. They probably result from a combination of densification and shear faulting. Likewise, furrows and pile-up after scribing⁶⁴ are probably combinations of these modes of deformation; in none of these cases is there any viscous flow or plastic deformation in the sense of the above definitions.

What is the significance of densification and faulting deformation in glass to the elastic solutions around a crack? Since crack propagation under normal conditions occurs as a result of applied tensile stress at the crack tip, there is not reason to expect densification or faulting under these conditions, and the elastic solutions should be valid.

Cracks and Energy

An applied tensile load is enhanced at a crack tip, as shown by the elastic solution of Inglis and Eqs. 10 and 11. There has been no direct experimental test of these relations; in some limited tests there is evidence for the dependence of failure stress on the square root of crack length¹¹ and on tip radius.⁴⁶ Because it has not been possible to observe the crack tip directly, there have arisen fracture criteria in which changes in its radius are ignored.^{11,65} These criteria are based on Griffith's calculation of the strain energy change in a stressed material caused by a crack. Griffith derived the equation

$$S_f^2 = 2E\gamma/\pi c \quad (15)$$

for the fracture stress S_f in a material with a crack depth c , surface energy γ , and Young's modulus E . This criterion is different from that of Inglis (Eqs. 10 and 11). In a treatment of crack energies and fracture criteria in terms of thermodynamic laws,⁶⁶ I concluded that the Griffith equation provides a necessary but not sufficient condition for fracture, and that the Inglis equations provide the correct criterion for fracture. The second law of thermodynamics shows that the fracture stress cannot be less than that given by Eq. 15, but can be greater.

If the applied stress is high enough to cause propagation by Eq. 11, but propagation cannot occur because S_f is lower than calculated from Eq. (15), what happens? The stress at the crack tip will be higher than the theoretical ultimate strength σ_t of the material, so it is reasonable to assume that the material at the tip will fluctuate to a larger tip radius so that the tip stress is reduced below σ_t . This reasoning from the second law of thermodynamics, therefore, predicts that fracture will occur only when the tip radius is larger than some critical minimum value ρ_m . A measure of ρ_m can be gained by comparing Eqs. 11 and 15 for the fracture stress. Then,

$$\rho_m = 8E\gamma/\pi\sigma_t^2 \quad (16)$$

is the tip radius for fracture. From Eqs. 13 and 16,

$$\rho_m = 32a/\pi \quad (17)$$

Thus the minimum tip radius for fracture is about ten times the interatomic spacing and is independent of other parameters.

Surface energies of brittle solids have been calculated from fracture measurements in several different ways.⁶⁷⁻⁶⁹ In all of these methods, the Griffith relation (Eq. 15) is assumed valid. In one method, the stress needed to fracture a material with a crack of depth c is measured, and the surface energy γ is calculated from Eq. 15. In the present view, the stress needed to propagate a crack of length c will be greater than or equal to the value calculated from Eq. 15. Thus one might expect values of γ calculated by these methods to be larger than the theoretical values and scattered. These are the results actually found experimentally for a variety of brittle solids.⁶⁶ For example, for soda-lime glass

the measured values of γ vary from 3.4 to 11 J/m², the lowest value being close to the value calculated from Eq. 14. This is just the result expected if Eq. 15 is a necessary but not sufficient condition for fracture.

Quite different views of crack shape and fracture processes in glass are held.^{69a}

Nucleation of Cracks

The flaw model successfully explains most features of brittle fracture and is generally accepted. This model assumes that fine cracks already exist in a material. How do these cracks get into the material? As described above, pressing a hard sphere against a glass surface causes a ring crack and then a cone crack. In some cases the ring cracks appear to start at pre-existing flaws and then propagate.³⁴ However, indenting a flaw-free surface of fused silica can nucleate a ring if the load is high enough.⁶¹ In soda-lime glass, sharp indenters and projectiles give median and radial cracks and scribing gives median and lateral cracks, as described previously. These types of damage are probably common in glass surfaces as a result of ordinary handling and contact with other solids.

Hagan and Swain⁷⁰ proposed that these median, radial, and lateral cracks are formed as a result of the fault lines described above. They suggested that median cracks are formed by the need to accommodate strains at the intersection of two flaw lines just like crack nucleation from dislocations on two intersecting slip planes. The lateral and radial cracks start at the boundary between the faulted region and the rest of the glass or along the fault lines and nucleate by unloading residual compressive stresses. In fused silica, even under a sharp indenter, there is only a densified region with no fault lines. Cone cracks nucleate directly, and median cracks form during loading because of the expansion of the boundary between compacted and elastic glass.⁶¹ Lateral cracks arise from mismatch of strain at the boundary.

This discussion shows that the nucleation of flaws in a pristine glass surface can be understood qualitatively as resulting from the stress and deformation caused by colliding projectiles, indentations, and scribing that are involved in handling the glass surface.

Apparently, chemical reactions at the glass surface can cause crack nucleation when a stress is applied. Just touching the surface of a pristine silica rod lowers its strength drastically, and fracture origins in high-strength silica show impurities, e.g., sodium chloride, by electron microprobe analysis. The detailed mechanism by which these chemicals lead to cracks is uncertain.

Effect of Surface Treatment on Glass Strength

From the flaw model, the increase in strength of glass that results from etching with hydrofluoric acid is explained by the removal of surface flaws. The

strength does not increase much when the etch depth is less than about $2\text{ }\mu\text{m}$, showing that the tip radius is not appreciably etched, probably because the etching solution in the cracks becomes rapidly saturated with reaction products.¹⁰ As the etch depth becomes greater, some samples show high strengths of up to $3 \times 10^9\text{ Pa}$ (see Fig. 3), presumably because some surface areas are etched free of all but the shallowest defects. A simple model of the etching process is that material is removed uniformly from the sample surface with no etching at the tip. For a crack depth c perpendicular to the surface, the etch depth is $c_0 - c$, where c_0 is the depth before etching. Then from Eq. 11, the fracture strength S after etching to a depth $c_0 - c$ is

$$S/S_0 = \sqrt{c_0/c} \quad (18)$$

where S_0 is the strength before etching.

After etching with HF, the surface of glass shows pits resulting from the cracks etched away. Thus a more accurate model of the etching process is that there is still no etching at the tip, but some etchant penetrates into the top of the crack, widening it.

Crack depths can be estimated from a comparison of Eq. 18 and strengths of etched glass. As the etch depth approaches c_0 , the initial crack length, the strength increases sharply. Samples of soda-lime glass were found to have a crack depth of about $6\text{ }\mu\text{m}$ with a strength at -196°C before etching of about 130 MPa . Then from Eq. 11 and the theoretical strength of about $1.6 \times 10^{10}\text{ Pa}$ for soda-lime glass, the tip radius is calculated to be about 1.6 nm or about ten lattice spacings, close to the estimate of Eq. 17 for minimum tip radius.

The increase in the strength of freshly abraded soda-lime glass after it is treated in water for several hours can be understood as resulting from the broadening of the tip radius by uniform corrosion of the glass at the tip. The etching method described above can be used to show that the crack length is not changed by soaking the glass in water.⁴⁶ This experiment also demonstrates a situation where the Griffith criterion Eq. 15 fails, since it predicts that the strength should be the same if the flaw depth is unaltered.

Fracture Origins and Velocity of Crack Propagation

The depths of surface features such as that in Fig. 7 have been taken as the depths of the crack-initiating flaws.^{27,29} However, many of the depths of these features are much greater than expected from other measurements of crack depths for comparable fracture strengths.^{10,16,71} It seems more likely that the initiating flaw was not nearly as deep as the semicircle in Fig. 7, and that this feature results from the early stages of crack propagation.

Figure 8 suggests a possible geometry for initiation of crack propagation in a sample such as the one in Fig. 7. A long, straight crack DF penetrates into the glass surface to a depth c much less than the crack length and is inclined

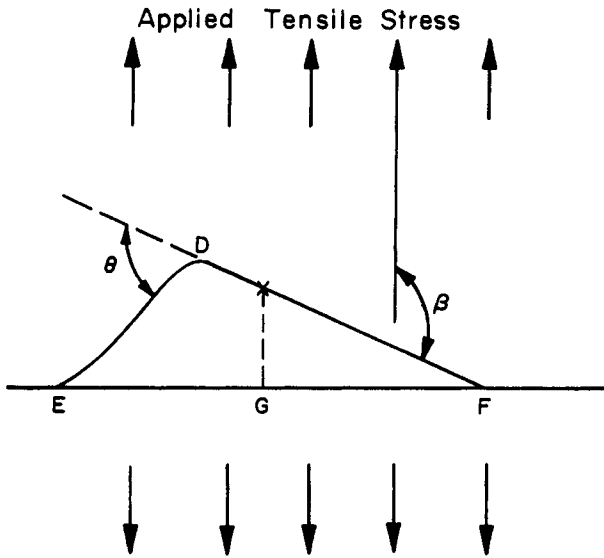


Fig. 9 Schematic plan view of a crack DF in a glass surface and its propagation path DE. EGF is the final fracture plane.³⁰

at an angle β to the applied stress. The highest tensile stress on the crack tip will occur somewhere along its length, usually not at the end, but at the point shown by a cross in Fig. 9.

After starting to grow at point X, the new crack front moves along the bottom of the initial crack DF and into the glass. At point D the crack turns along the line DF; a similar path was found for straight-through cracks in glass.⁷² A possible explanation for the circular trace of the initial propagation path with the final plane of fracture is that this plane is perpendicular to the applied stress and is defined by equal path lengths XE and XF on the glass surface, as well as the curved path XG down into the glass. If the crack propagates with the same velocity in all directions, the crack front will be circular when it reaches the final fracture plane EGF.

A simple equation for crack velocity v as a function of crack depth c is ⁷³⁻⁷⁵

$$v = v_m(1 - c_0/c) \quad (19)$$

where c_0 is the initial crack length, $v_m = m\sqrt{E/\rho}$ is the maximum velocity, E is Young's modulus, ρ is the density, and m is about 0.4–0.5. Equation 19 is compared with experimental results on the velocity of a crack in a soda-lime glass in Fig. 8, with $v_m = 1500$ m/s and $c_0 = 1$ mm. The fit is good for these data; Congleton and Petch⁷⁶ and Kerkhof and Richter⁷⁷ found poorer agreement between experiments and Eq. 19. Schardin⁷⁸ discussed the variation of v_m with glass composition.

REFERENCES

1. B. A. Proctor, I. Whitney, and J. W. Johnson, *Proc. Roy. Soc. London Ser. A*, **297**, 534 (1967).
2. N. M. Cameron, *Glass Technol.*, **9**, 14, 121 (1968).
3. R. D. Maurer, *Appl. Phys. Lett.*, **27**, 220 (1975).
4. C. R. Kurkjian, R. V. Albarino, J. T. Krause, H. N. Vazirani, F. V. DiMarcello, S. Torza, and H. Schonhorn, *Appl. Phys. Lett.*, **28**, 588 (1976); **29**, 712 (1976).
5. O. Vardar and I. Finnie, *Int. J. Fracture*, **11**, 495 (1975).
6. M. B. Thomas, R. H. Doremus, M. Jarcho, and R. L. Salsbury *J. Mater. Sci.*, **15**, 891 (1980).
7. R. H. Doremus, *J. Appl. Phys.*, **54**, 193 (1983).
8. W. F. Thomas, *Nature (London)*, **181**, 1006 (1958).
9. R. E. Mould, *J. Appl. Phys.*, **29**, 1263 (1958).
10. E. K. Pavelchek and R. H. Doremus, *J. Mater. Sci.*, **9**, 1803 (1974).
11. A. A. Griffith, *Philos. Trans Roy. Soc London Ser. A*, **221**, 163 (1921).
12. W. B. Hillig, in *Modern Aspects of the Vitreous State*, Vol. II, J. D. Mackenzie, Ed., Butterworths, London, 1962, p. 152.
13. F. O. Anderegg, *Ind. Eng. Chem.*, **31**, 290 (1939).
14. W. H. Otto, *J. Am. Ceram. Soc.*, **38**, 122 (1955).
15. W. F. Thomas, *Phys. Chem. Glasses*, **1**, 4 (1960).
16. R. E. Mould and R. D. Southwick *J. Am. Ceram. Soc.*, **42**, 542, 582 (1959).
17. R. E. Mould, in *Fundamental Phenomena in Materials Science*, Vol. IV, J. Bonis, J. J. Diega, and J. J. Gilman, Eds., Plenum, New York, 1964, p. 119.
18. W. B. Hillig, *J. Appl. Phys.*, **32**, 741 (1961).
19. B. A. Proctor, *Phys. Chem. Glasses*, **3**, 7 (1962).
20. C. Symmers, J. B. Ward and B. Sugarman, *Phys. Chem. Glasses*, **3**, 76 (1962).
21. E. K. Pavelchek and R. H. Doremus, *J. Noncryst. Solids*, **20**, 305 (1976).
- 22a. R. E. Mould, *J. Am. Ceram. Soc.*, **43**, 160 (1960).
22. F. M. Ernsberger, *Phys. Chem. Glasses*, **10**, 240 (1969).
23. W. C. LaCourse, in *Introduction to Glass Science*, L. D. Pye, H. J. Stevens, and W. C. LaCourse, Eds., Plenum, New York, 1972, p. 451.
24. V. D. Frechett, in *Introduction to Glass Science*, L. D. Pye, H. J. Stevens, and W. C. LaCourse, Eds., Plenum, New York, 1972, p. 433.
25. E. B. Shand, *J. Am. Ceram. Soc.*, **37**, 52, 559 (1954); **42**, 474 (1959).
26. W. C. Levengood, *J. Appl. Phys.*, **29**, 820 (1958).
27. J. J. Mecholsky, S. W. Freiman, and R. W. Rice, *J. Am. Ceram. Soc.*, **57**, 440 (1974).
28. H. P. Kirchner, R. M. Gruver, and W. A. Sotter, *Philos Mag.*, **33**, 775 (1976).
- 28a. W. T. Han and M. Tomozawa, *J. Noncryst. Solids*, **163**, 309 (1993).
29. J. R. Varner and J. Oel, *Glastech. Ber.*, **48**, 73 (1975).
30. R. H. Doremus and W. C. Johnson, *J. Mater. Sci.*, **13**, 855 (1978).
31. E. Sommer, *Eng. Fracture Mech.*, **1**, 539 (1969).
32. F. M. Ernsberger, *Proc. Roy. Soc. London Ser. A*, **257**, 213 (1960).
33. F. C. Roesler, *Proc. Phys. Roy. Soc. London Sect B*, **64**, 55, 981 (1956).

34. F. C. Frank and B. R. Lawn *Proc. Roy. Soc. London Ser. A*, **299**, 291 (1967).
35. H. Hertz, in *Hertz's Miscellaneous Papers*, MacMillan, New York, 1896, Ch. 5, 6.
36. B. A. Bilby, *J. Mater. Sci.*, **15**, 535 (1980).
37. B. R. Lawn and T. R. Wilshaw, *J. Mater. Sci.*, **10**, 1049 (1975).
38. K. Peter, *Glastech. Ber.*, **37**, 333 (1964).
39. C. G. Knight, M. V. Swain, and M. M. Chaudhri, *J. Mater. Sci.*, **12**, 1573 (1977).
40. M. V. Swain and J. T. Hagan, *J. Mater. Sci.*, **15**, 387 (1980).
41. F. M. Ernsberger, *Annu. Rev. Mater. Sci.*, **2**, 529 (1972).
42. B. R. Lawn, *Proc. Roy. Soc. London Ser. A*, **229**, 307 (1967).
43. F. Kerkhof, *Bruchvorgange in Glasern*, Verlag der Dt. Glastechn. Ges., Frankfurt, 1970.
44. J. E. Field, *Contemp. Phys.*, **12**, 1 (1971).
45. A. Smekal, *Glastech. Ges.*, **23**, 57 (1950).
46. R. H. Doremus and E. K. Pavelchek, *J. Appl. Phys.* **46**, 4096 (1975).
- 46a. C. E. Inglis, *Trans Inst. Naval Arch.* **55**, 219 (1913).
47. J. J. Gilman, in *The Physics and Chemistry of Ceramics*, C. Klingsberg, Ed., Gordon and Breach, New York, 1963, p. 240.
48. R. H. Doremus, *Fracture and Fatigue of Glass*, in *Treatise in Materials Science and Engineering*, Vol. 22, Academic Press, Orlando, FL, 1982, p. 170.
49. S. Sakka and H. Hotta, *J. Mater. Sci.*, **14**, 2335 (1979).
50. J. Nardy-Szabo and J. Ladik, *Nature (London)*, **188**, 226 (1960).
51. J. T. Krause, L. R. Testardi, and R. N. Thurston, *Phys. Chem. Glasses*, **20**, 135 (1979).
52. E. W. Taylor, *Nature (London)*, **163**, 323 (1949).
53. J. E. Neely and J. D. Mackenzie, *J. Mater. Sci.*, **3**, 603 (1968).
54. F. M. Ernsberger, *J. Am. Ceram. Soc.*, **51**, 545 (1968).
55. T. Izumitani and J. Suzuki, *Glass Technol.*, **14**, 35 (1973).
56. T. Izumitani, in *Treatise on Materials Science and Technology*, Vol 17, *Glass II*, M. Tomozawa and R. H. Doremus, Eds., Academic Press, New York, 1979, p. 115.
57. M. Imaoka, and I. Yasui, *J. Noncryst. Solids*, **22**, 315 (1976).
58. K. Peter, *J. Noncryst. Solids*, **5**, 103 (1970).
59. E. Dick, *Glastech. Ber.*, **43**, 16 (1970).
60. F. M. Ernsberger, *J. Noncryst. Solids*, **25**, 293 (1977).
61. J. T. Hagan, *J. Mater. Sci.*, **14**, 462, 2975 (1979); **15**, 1417 (1980).
62. R. H. Lillie, *J. Am. Ceram. Soc.*, **14**, 502 (1931); **15**, 418 (1932); **16**, 619 (1933); **19**, 45 (1936).
63. F. R. Gauthier, M. S. Thesis, Rensselaer Polytechnic Institute, Troy, New York, 1975.
64. D. M. Marsh, *Proc. Roy. Soc. London Ser. A*, **282**, 33 (1964).
65. G. R. Irwin, *J. Appl. Mech.*, **24**, 361 (1957).
66. R. H. Doremus, *J. Appl. Phys.* **47**, 1833 (1976).
67. J. J. Gilman, *J. Appl. Phys.* **31**, 2208 (1960).

68. J. Nakayama, *J. Am. Ceram. Soc.*, **48**, 583 (1965).
69. R. W. Davidge and G. Tappin, *J. Mater. Sci.*, **3**, 165 (1968).
- 69a. B. R. Lawn, *Fracture of Brittle Solids*, Cambridge Univ. Press, Cambridge, (1993).
70. J. T. Hagan and M. V. Swain *J. Phys. D.*, **11**, 2091 (1978).
71. S. M. Ohlberg, L. L. Sperry, J. M. Parsons, and H. R. Golob in *Advances in Glass Technology*, Part 2, Plenum, New York, 1962, p. 28.
72. F. Erdogan and G. S. Sih, *J. Basic Eng.*, **85**, 519 (1963).
73. N. F. Mott, *Engineering*, **165**, 16 (1948).
74. J. P. Berry, *J. Mech. Phys. Solids*, **8**, 194 (1960).
75. E. N. Dulaney, and W. F. Brace, *J. Appl. Phys.*, **31**, 2233 (1960).
76. J. Congleton and N. J. Petch, *Philos. Mag.*, **16**, 749 (1967).
77. F. Kerkhof and H. Richter, in *Fracture 1969*, P. L. Pratt, Ed. Chapman and Hall, London, 1969, p. 463.
78. H. Shardin, in *Fracture*, B. L. Averbach D. K. Felbeck, G. T. Hahn and D. A. Thomas., Eds., The Technology Press and Wiley, New York, 1959, p. 297.

FATIGUE IN GLASS

Fatigue in glass results when its strength deteriorates while it is stressed in an atmosphere containing water. This fatigue requires design strengths three or four times lower than if they retained their initial strength. In this chapter, fatigue in glass is discussed in the following sections: testing methods, experimental results, life prediction, and theories. A more extensive review is given in Ref. 1.

METHODS OF TESTING

The simplest method of studying fatigue in glass is a static test in which a constant load is imposed on a set of samples and the time of failure of each sample is recorded. Such tests can be done in bending, simple tension, or diametral loading; bending is easiest for rods and tubes and requires simple test equipment. Although static tests are the closest to practical situations and the least complicated in principle, they have some disadvantages. They require a large number of samples for each of several stresses to define the stress–failure time relationship, because of the large spread in failure times at a particular stress. Often it is difficult or expensive to obtain the required number of samples. Static tests must also be carried out over a large spread of times, leading to long delays in obtaining results.

Fatigue can also be measured with samples tested at different loading rates; the dependence of fracture strength on loading rate is related to the stress–failure time relation in static loading. This method requires fewer samples and less time, but a testing machine with a linear load application is needed.

Another method is to measure directly the velocity at which large (~ 1 cm) cracks propagate under different applied loads. This method has been widely used, but experimental and theoretical treatments suggest that results from this technique are not always directly comparable with the fatigue behavior of practical materials with much smaller flaws (a few micrometers long).

RESULTS OF STATIC FATIGUE TESTS ON GLASS

Failure times of Pyrex borosilicate glass rods in bending are shown in Fig. 1.² Each point represents the mean of many measurements, usually 40 or more. The results are plotted as log reduced stress S/S_N vs. log fracture time, where S is the maximum stress in four-point bending and S_N is the mean fracture stress in the same test at -196°C , where there is no fatigue. Similar fatigue results⁴ for a commercial soda-lime glass are shown in Fig. 2. Other results are given in Tables 1 and 2. Compositions of glasses referred to in this chapter are given in Chapter 1, Table 1, on viscosity. Other data are reviewed in Ref. 1.

Humidity strongly influences the failure time. Rods of soda-lime glass all

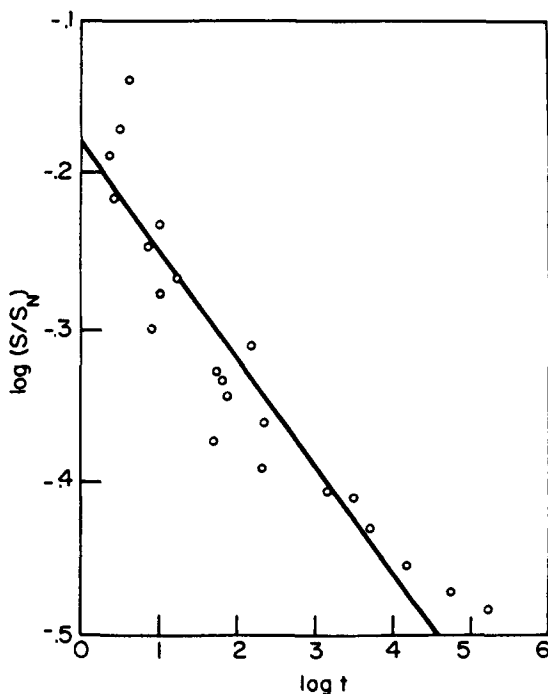


Fig. 1 Mean log failure times (in seconds) for Pyrex borosilicate glass rods held at constant relative stress S/S_N (static fatigue) at 60% relative humidity at 25°C . Line from Eq. 2; data from Ref. 2.

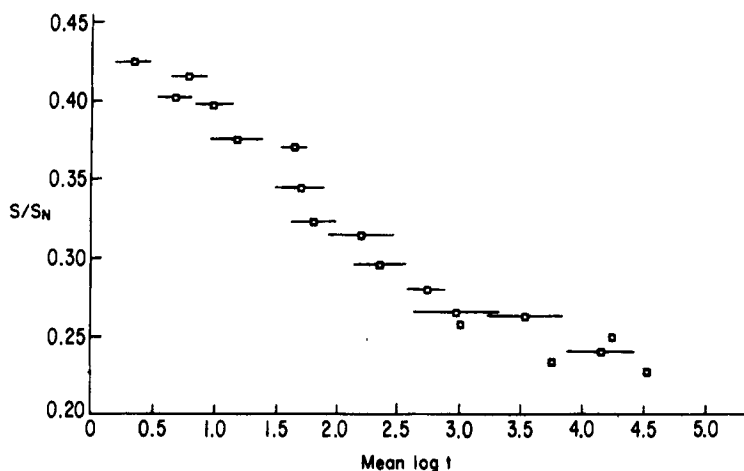


Fig. 2 Mean log failure times (in seconds) in 100% humidity at 25°C for soda-lime silicate (Kimble R-6) glass rods abraded and then aged 25 h in water before testing. Lines show 95% confidence limits for $\log-t$ values. From Ref. 4.

treated in the same way and all having a mean S_N of 86 MPa had mean failure times of 8.7, 200, 3470 s in water, 43% r.h. and 0.5% r.h. respectively, all at a stress $S/S_N = 0.5$.³ Log $t_{\frac{1}{2}}$ is about linear with relative humidity over this range of humidities.

Surface treatment and sample history strongly influence the failure times of glass tested at the same relative humidity and relative stress S/S_N . Values of $t_{\frac{1}{2}}$,

TABLE 1 Failure Times Measured for Soda-Lime Glass Rods in Static Bend Tests

Test Conditions, 50% r.h. ⁴	$t_{1/2}$ (s)	S_N (MPa)
Tested immediately after abrasion	304.0	118
Abraded, aged 24 h in water	3.4	160
Abraded, heated to 400°C for 1 h, held 24 h in water	37.0	187
Abrasion conditions, tested in water ³		
Severe grit blast	2.9	86
Mild grit blast	8.8	93
Perpendicular to stress		
600 grit paper	0.0043	134
320	0.149	95
150	0.56	70
Parallel to stress		
150 grit paper	0.14	165

TABLE 2 Comparison of Correlation Coefficients for Different Equations for Failure Times of Pyrex Glass at 60% Relative Humidity and 25°C

Equation Number	Correlation Coefficient R^2
1	0.805
2	0.869
3	0.917

the time of failure at $S/S_N = 0.5$, are given in Table 1 for soda-lime glass after different treatments. The failure times range over five orders of magnitude, and there is no simple connection with inert strengths S_N .

Fatigue in silica (SiO_2) glass has been of special interest because it represents a pure silicate glass without alkali and alkaline earth ions. Furthermore, the development of fiber optic waveguides made of fine silica glass fibers has emphasized the need for reliable information on the fatigue life of silica. Static fatigue data on abraded silica rods⁵ and pristine silica fibers⁶ are shown in Fig. 3. In both these studies, all samples were treated identically, and were chemically "clean" because of abrasion⁵ and fire drawing.⁶

Experimental results on strength and fatigue of very strong silica seem to be influenced by the chemical treatment of the silica surface. Just touching lightly

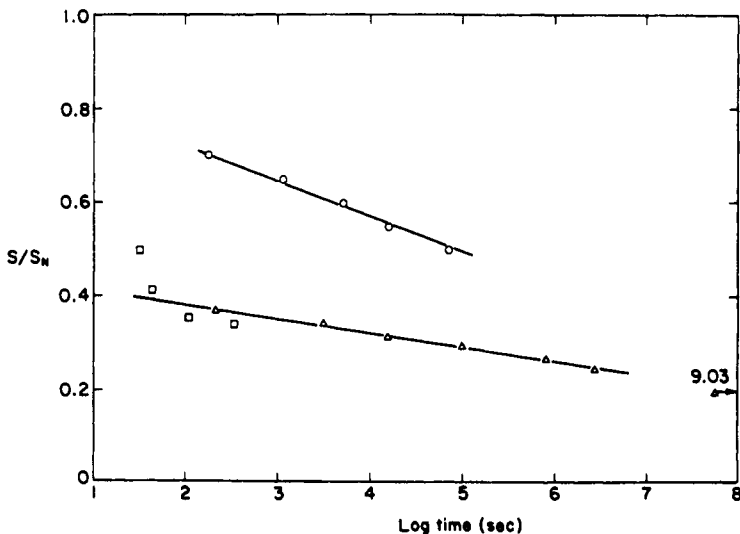


Fig. 3 Mean log failure times for silica glass held at constant reduced stress S/S_N . ○, rods, centerless ground, 50% relative humidity 23°C;⁵ △, fibers flame polished in room air and temperature;⁶ □, etched with 8% HF.

the surface of a pristine silica rod greatly lowers its strength. Fracture origins in strong silica tubes, when microanalyzed, show alkali or alkaline earth contaminants. Strong silica fibers, when stripped of their organic coatings, show transitions or nonuniform functional dependencies of failure time on stress.⁷

Silica fibers for use as waveguides are usually coated with an organic polymer to reduce their susceptibility to fatigue.^{7,9-12} These coatings reduce fatigue at short times, for example, a day at 22°C, but at longer times, higher temperatures,¹³ and in alkaline media¹¹ the coatings are attacked, and the fatigue becomes more like that of uncoated silica. When the coated fibers were treated in flowing distilled water at 90°C, the fatigue "drop" occurred at longer times than in static solution. All these results show the strong influence of chemical contamination on fatigue times of strong silica fibers.

The fatigue time decreases at higher temperatures.^{7,13,14} The temperature dependence of fatigue does not follow an Arrhenius relation; below about -100°C in soda-lime silicate glass, fatigue becomes very slow compared to experimental times.

Because of the large influence of sample history on fatigue, it is difficult to compare the fatigue response of different glass compositions. Some results for different glasses are listed in Table 3; unfortunately, the histories of the different

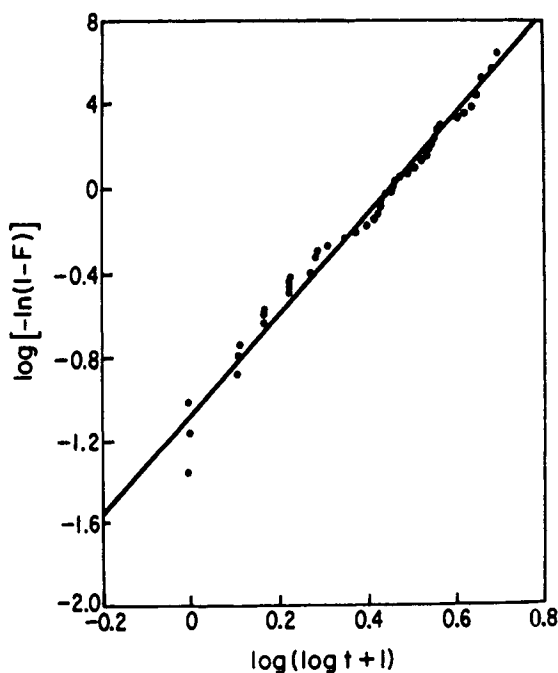


Fig. 4 Probability plot of log failure time as a function of fraction failing for Pyrex borosilicate rods at 65% humidity and 25°C.²

TABLE 3 Standard Deviation of Log Failure Time as a function of S/\bar{S}_N

S/\bar{S}_N	Mean log t	Standard Deviation	S/\bar{S}_N	Mean log t	Standard Deviation
<i>Fused silica, sets 100 samples⁵</i>					
0.70	0.22	0.76	0.531	1.102	0.902
0.65	3.06	0.74	0.504	0.924	0.863
0.60	3.57	0.63	0.489	1.182	1.239
0.55	4.04	0.97	0.471	1.731	1.065
0.50	4.73	0.93	0.466	1.829	1.337
			0.452	1.898	1.028
<i>FN borosilicate, sets of 100 samples⁵</i>					
			0.435	2.373	1.496
			0.425	1.740	1.253
0.550	0.77	0.78	0.408	2.374	1.300
0.525	1.20	0.83	0.394	3.214	1.634
0.500	1.51	0.85	0.398	3.573	1.540
0.475	2.02	0.86	0.371	3.744	1.484
0.450	2.67	1.00	0.352	4.261	1.106
0.400	3.96	1.39	0.337	4.811	1.177
			0.329	5.317	1.179
<i>Pyrex borosilicate²</i>					
			<i>Soda-lime silicate⁸</i>		
0.728	0.530	0.629			
0.673	0.390	0.715	0.461	1.80	0.75
0.647	0.289	0.783	0.424	2.40	1.1
0.608	0.447	0.882	0.378	2.98	1.1
0.583	1.040	0.845	0.332	4.00	1.2
0.568	0.887	0.995	0.298	5.36	2.4
0.542	1.296	0.994			

compositions were not all the same. Nevertheless, it appears that all the glasses except for fused silica have roughly the same fatigue sensibility. Abraded silica is less sensitive; however, pristine or etched silica has a lower log t_f (< 2.0), as shown in Fig. 2.

STATISTICS OF FATIGUE

The failure times of glass samples that are tested under identical conditions and that have identical treatments still show a large spread, as shown in Fig. 2 and Table 4. This spread is related to the spread in fracture strengths discussed in Chapter 9. These spreads can be treated in statistical terms, as discussed in Chapter 9. A plot of the distribution of log failure times for Pyrex borosilicate glass rods measured under identical conditions is shown in Fig. 4. In this example, the failure times had a range of five orders of magnitude. The plot is

TABLE 4 Comparison of $g\sigma/\bar{S}_N$ Values from Eq. 11

Glass	Calc. from g and σ/\bar{S}_N	Derived from σ versus \bar{S}_N/S Plots	References
Soda-lime	0.41	0.48	8
FN borosilicate	0.32	0.45	5
Pyrex	0.51	0.46	2
Fused silica	0.22	0.48	5
Soda-lime	0.47	0.36	4

on probability paper; a straight line on this plot suggests that the distribution of log failure times is a normal distribution, (Chapter 9, Eq. 3).

The mean of a sample of experimental measurements taken from a large population (for example, the log failure times for a series of samples held at a particular stress) is the "best" statistical measure of the "middle" of the distribution. It is the expected value and is unbiased and consistent (see statistical books such as Bhattacharya and Johnson¹⁵ and Bury¹⁶). The mean of the sample is therefore the best statistical estimate of the mean of the fictitious population of all log t values (the "true" mean). The distribution of the sample means has a standard deviation σ/\sqrt{n} , where σ is the standard deviation of the population and n is the number of measurements in the sample. The standard deviation σ of the sample is the best measure of the standard deviation of the population, so that σ/\sqrt{n} is a measure of the reliability of the mean value calculated for the sample.

What the statistical jargon of the last paragraph means in plain language is that the arithmetic mean of log failure times is the correct measure of the failure times measured under identical conditions. Furthermore, the reliability of this mean value increases as the square root of the number of measured times. Even if there is a large spread in measured failure times, as in Fig. 4, it is possible to obtain a reliable mean failure time by making enough measurements. It is also possible to predict how likely it is for a given measurement of failure time to be a certain amount away from the mean time from the distribution of measured times.

LIFE PREDICTION

An important practical problem is to predict the useful life of a stressed piece of glass. The mean value of failure time at a particular stress can be found if the functional dependence of failure time on stress can be determined, and mean failure times at some stresses are known. The likelihood of a particular failure at a particular applied stress can be assessed in terms of the known functional dependence, the known failure times, and a measure of the spread or standard deviation of failure times. In most treatments of life prediction of

glass, a particular functional dependence of failure time on stress is assumed, usually a power law dependence (Eq. 2); in many situations this assumption gives very inaccurate lifetime predictions; see Fig. 1.

Several different functional dependences of failure time on stress have been suggested; some are

$$\log t = 1 - bS/S_N \quad (1)$$

$$\log t = c - n \log (S/S_N) \quad (2)$$

$$\log t = d + gS_N/S \quad (3)$$

where the values of b , n , g , and p are positive. The theories discussed below introduce some minor differences into these equations, but they are not significant for choosing between the equations. Over the stress ranges studied experimentally, it is often difficult to choose from among Eqs. 1–3; yet if they are extrapolated to times of a few years, the sample lives predicted from each of the equations are very different. Thus it is important to choose the best equation if one wishes to extrapolate or to examine theories.

The simplest way to examine the equations is to calculate a regression equation by the least-squares method in the form of Eqs. 1–3 and compare the correlation coefficients from the regression.¹⁷ The mean $\log t$ values for Pyrex glass in Fig. 1 were examined in this way (see Table 2). There is a clear increase in goodness of fit in the order Eq. 1, 2, and 3.

Often data are not extensive or reliable enough to find any differences between correlation coefficients, and a more sensitive method is needed. If the equation for the cumulative number F of failures in a normal distribution is solved for the failure strength,

$$S_N = \bar{S}_N + \sqrt{2} \sigma \operatorname{erf}^{-1} (2F - 1) \quad (4)$$

where \bar{S}_N is the mean strength at -196°C , σ is the standard deviation of strengths at -196°C , and $\operatorname{erf}^{-1}(u)$ is the number whose error function is u , the value of S_N from Eq. 4 can then be substituted into Eqs. 1–3 to show the relation between the distributions of S_N and of $\log t$:

$$\log t = a - \frac{b S}{\bar{S}_N + \sqrt{2} \sigma \operatorname{erf}^{-1}(2F - 1)} \quad (5)$$

$$\log t = c - n \log \frac{S}{\bar{S}_N + \sqrt{2} \sigma \operatorname{erf}^{-1}(2F - 1)} \quad (6)$$

$$\log t = d + \frac{g}{S} \{\bar{S}_N + \sqrt{2} \sigma \operatorname{erf}^{-1}(2F - 1)\} \quad (7)$$

Thus only if Eq. 3 is valid should the $\log t$ values have the same distribution function as S_N . Eqs. 5–7 can all be written in the following approximate form:

$$\log t = \overline{\log t} + \sqrt{2} \sigma_t \operatorname{erf}^{-1}(2F - 1) \quad (8)$$

where $\overline{\log t}$ is the mean of $\log t$ values and σ_t is the standard deviation of the distribution of $\log t$ values. The following values of σ_t are calculated for each of Eqs. 1-3:

$$\sigma_1 = \frac{bS\sigma}{\overline{S_N}^2} \quad (9)$$

$$\sigma_2 = n\sigma/\overline{S_N} \quad (10)$$

$$\sigma_3 = g\sigma/S \quad (11)$$

where σ is the standard deviation of failure strengths at -196°C . Pavelchek and Doremus⁴ derived these relations by a somewhat different method. These equations show that the standard deviation of \log failure times changes differently with applied stress S depending upon which relation between $\log T$ and stress is valid (Eqs. 1-3). For the direct dependence of Eq. 1, σ decreases with decreasing stress; for the power law of Eq. 2, σ is not dependent on applied stress; and for the inverse relation of Eq. 3, σ increases with decreasing stress.

Standard deviations of distributions of \log failure times for different glasses are given in Table 3, and they all increase with decreasing stress, consistent with Eq. 3, and not with Eqs. 1 and 2. Thus the better fit to Eq. 3 demonstrated in Table 2 for Pyrex borosilicate glass is confirmed.

Long-time tests of Pyrex borosilicate glass² at $S/S_N = 0.253$ fit Eq. 3; both Eqs. 1 and 2 predict much too short mean failure times at this applied stress.

In fibers, variations in fatigue times may be related to differences in fiber diameter, as concluded by Matthewson and Kurkjian.¹¹ The variations are still a sensitive measure of the functional dependence of failure time on applied stress whether the variations result from differences in diameters, a spread in glass strength, or from some other cause.

This discussion shows that for prediction of fatigue lifetimes of glass beyond experimental times, Eq. 3 is much superior to either Eq. 1 or 2, even though Eq. 2 is widely used to analyze fatigue data. There is no evidence that glass samples with chemically clean surfaces show a sharp change in functional dependence of failure time on stress in different silicate glasses both strong and weak (Figs. 1-3). Alternatively chemical contamination or a change in a protective coating can cause more or less sharp changes in the functional dependence of failure times on stress.

THEORIES OF FATIGUE

The stress-enhanced reaction of water with the silicate lattice is generally agreed to be the reason for fatigue of silicate glasses. Hillig and Charles¹⁹ considered the reaction front at the tip of a crack and derived a theoretical relation between failure time and stress. The form of their results depends upon the reaction rate equation assumed. Hillig and Charles assumed that the reaction velocity v (rate of breaking of lattice structure) was

$$v = v_0 \exp \beta \sigma \quad (12)$$

where v_0 is the rate at zero tip stress, s is the tip stress, and β is a constant. Over a broad stress range, Eq. 12 leads to a linear dependence of log failure time on applied stress (Eq. 1).

Since Eq. 1 did not fit static fatigue data well, two other equations for v that leads to Eqs. 2 and 3 were introduced into the Hillig-Charles derivation.²⁰ They are the power law

$$v = As^n \quad (13)$$

and the exponential of reciprocal stress

$$v = v_\infty \exp(-\alpha/s) \quad (14)$$

where A , n , v_∞ and α are constants. With these relations the Hillig-Charles method gives

$$\frac{d\rho}{dt} = v(1 - 2n) \quad (15)$$

and

$$\frac{d\rho}{dt} = v \left[1 - \frac{2\alpha}{s} \right] \quad (16)$$

for Eqs. 13 and 14, respectively. These equations give the rate of change of the crack tip radius ρ with time t , and show that the rate of tip sharpening $d\rho/dt$ is much greater than the rate of lengthening of the crack, which is equal to the normal velocity v . For silicate glasses, $n \geq 15$ and $2\alpha/s \geq 14$, so that $-d\rho/dt$ is more than ten times greater than v . When integrated, Eq. 15 gives Eq. 2 and Eq. 16 gives Eq. 3, over a wide intermediate range of applied stress S .

Additional evidence²¹ that cracks sharpen rather than lengthen during fatigue come from observations of crack initiation sites. These sites look the same after failure at -196°C and 25°C and their sizes show no statistically significant difference between these two temperatures. If fatigue at 25°C caused crack lengthening, one would expect a changed appearance and larger sites at this temperature. A theory of crack tip blunting has extended the Hillig-Charles approach²² (see also ref. 27).

An equation for the rate constant k of a chemical reaction is

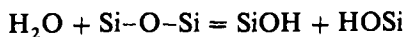
$$k = k_0 \exp(-\Delta G^*/RT) \quad (17)$$

where ΔG^* is the free energy of activation and k_0 is weakly dependent on temperature or pressure. If the pressure P is a variable as well as the temperature, Eq. 17 can be written

$$k = k_1 \exp[(-\Delta H^* + V^*P)/RT] \quad (18)$$

where V^* denotes the activation volume. Equation 17 or 18 fits the temperature dependence of many chemical reactions well, with ΔG^* or ΔH^* independent of temperature. However, the activation volume V^* is seldom independent of pressure.^{23,24} The application of Eq. 18 to solids has rarely been tested, and is even more uncertain. Therefore, Eq. 18 with V^* constant has no experimental basis for chemical reactions in solids.

Two different theories for the stress dependence of a chemical reaction give the functional dependence of reaction rate on stress of Eq. 14. Taylor²⁵ suggested that delayed fracture results from a time-dependent rearrangement of the structure of a material, and he derived an equation of the same form as Eq. 14. His ideas can be modified somewhat to gain some possible insight into the origin of Eq. 14 and parameters affecting α . The reaction of water with the silicate network leads to broken bonds and a change in the tip geometry



If the activation energy of this reaction is inversely proportional to the change in bond length Δa caused by a tensile stress σ , then

$$\frac{\alpha}{\sigma} = \frac{B}{RT\Delta a} = \frac{BE}{RT\sigma} \quad (19)$$

where B is a constant and E is Young's modulus. Thus α should be proportional to the activation energy of the rate of Eq. 19.

Gilman and Tong²⁶ derived an equation for the velocity of crack motion with the same dependence on stress as Eq. 14 from a quantum tunneling model of fracture. Their model does not explicitly include a chemical reaction, but extension of their ideas to stress-accelerated reactions should be possible.

There are striking differences between failure times of samples tested immediately after abrasion (see Table 1) and those aged in water before testing (a factor of 100 or more) even at the same relative humidity. The theory of Hillig and Charles and other theories of fatigue of glass give no explanation for this large difference in fatigue time.

In order to understand a possible origin of this difference, contributions of the statistical distribution of flaws, $g(S)$, must be considered. The stress at which a particular crack propagates depends upon at least three separate factors: its orientation (angle) θ to the applied tensile stress, the crack depth c , and the crack tip radius ρ . Each of these factors can be distributed over a range of values, so $g(S)$ is actually a product of at least three separate distributions

$$g(S) = T(\theta)R(\rho)K(c) \quad (20)$$

The distribution of each of these factors is strongly dependent on sample history and surface abrasion.

REFERENCES

1. R. H. Doremus, in *Treatise on Materials Science and Technology*, Vol. 22, *Glass III*, M. Tomozawa and R. H. Doremus, Eds. Academic Press, New York, 1982.
2. G. S. Friedman, K. Cushman, and R. H. Doremus, *J. Mater. Sci.*, **17**, 994 (1982).
3. R. E. Mould and R. D. Southwick, *J. Am. Ceram. Soc.*, **42**, 452 (1959).
4. E. K. Pavelchek and R. H. Doremus, *J. Noncryst. Solids*, **20**, 305 (1976).
5. J. E. Burke, R. H. Doremus, W. B. Hillig, and A. M. Turkalo, in *Ceramics in Severe Environments*, W. W. Kriegel and H. Palmour, Eds., Plenum Press, New York, 1971.
6. B. A. Proctor, I. Whitney, and J. E. Johnson, *Proc. Roy. Soc. London Ser. A*, **297**, 534 (1967).
7. J. T. Krause, *J. Noncryst. Solids*, **38 & 39**, 497 (1980).
8. K. Jakus, D. C. Coyne, and J. E. Ritter, *J. Mater. Sci.*, **13**, 2071 (1978).
9. T. T. Wang and H. M. Zupko, *J. Mater. Sci.*, **13**, 2241 (1978).
10. H. C. Chandan and K. Kalish, *J. Am. Ceram. Soc.*, **65**, 171 (1982).
11. M. J. Matthewson and C. R. Kurjian, *J. Am. Ceram. Soc.*, **70**, 662 (1987); **71**, 177 (1988).
12. J. E. Ritter, T. E. Service, and K. Jakus, *J. Am. Ceram. Soc.*, **71**, 988 (1988).
13. J. T. Krause and C. J. Shute, *Adv. Ceram. Mater.*, **3**, 118 (1988).
14. R. J. Charles, *J. Appl. Phys.*, **29**, 1549, 1554 (1958).
15. G. K. Bhattacharya and R. A. Johnson, *Statistical Concepts and Methods*, Wiley, New York, 1977.
16. K. V. Bury, *Statistical Models in Applied Science*, Wiley, New York, 1975.
17. N. R. Draper and H. Smith, *Applied Regression Analysis*, Wiley, New York, 1966.
18. R. H. Doremus, *J. Appl. Phys.*, **54**, 193 (1983).
19. W. B. Hillig and R. J. Charles, in *High Strength Materials*, V. F. Jackey, Ed., Wiley, New York, 1965, p. 682.
20. R. H. Doremus, *Eng. Fracture Mech.*, **13**, 945 (1980).
21. R. H. Doremus and W. C. Johnson, *J. Mater. Sci.*, **13**, 855 (1978).
22. T. Chuang and E. R. Fuller, *J. Am. Ceram. Soc.*, **75**, 540 (1992).
23. G. Kohnstam, in *Progress in Reaction Kinetics*, G. Porter, Ed., Pergamon, Oxford, 1970, p. 335.
24. C. A. Eckert, *Annu. Rev. Phys. Chem.*, **23**, 239 (1972).
25. N. W. Taylor, *J. Appl. Phys. Chem.*, **18**, 943 (1947).
26. J. J. Gilman and H. C. Tong, *J. Appl. Phys.*, **42**, 3479 (1971).
27. W. T. Han and M. Tomozawa, *J. Noncryst. Solids*, **163**, 309 (1993).

CHAPTER 11

SURFACES

Glass surfaces control strength, chemical durability, optical quality, and adhesion of glasses. These surfaces are the sites for a variety of chemical and physical processes important in processing and properties of glasses. In this chapter there is emphasis on surfaces of silicate glasses in the following sections: structure, measurement techniques, physical adsorption, surface chemical reactions, adsorption from solution, and surface conductivity. These topics involve the outer few molecular layers of the glass. Chemical reactions and ion exchange involving deeper penetration, and hence more of the bulk of the glass, are discussed in Chapters 12–14.

Surface properties of glasses have been reviewed in Refs. 1–4a.

SURFACE ENERGY

The surface energy γ at temperature T and pressure p can be defined as the reversible work dW_r to form a surface of area dA ,

$$\gamma = -(dW_r/dA)_{T,p} \quad (1)$$

For a liquid, surface energy and tension are equal. The units of surface energy are joules per square meter; $10^3 \text{ dyn/cm} = 1 \text{ J/m}^2$.

A number of measurements of surface energies of glass melts have been made by a dipping cylinder method developed by Shartsis and co-workers.⁵ In this method, the force F required to pull a small thin-walled platinum cylinder of radius R out of the melt is measured, and

$$\gamma = F/4\pi R \quad (2)$$

A correction factor is necessary for the most accurate work.

The surface energy decreases as the temperature increases; for most silicate glass melts this change is quite small (less than 10%) from 1200 to 1500°C.

The influence of composition on surface energy of silicate glass melts is not large. For most sodium silicate melts, the surface energy is about 0.3 J/m^2 at 1200°C, and this value is a reasonable approximation for the surface energy of most sodium-containing silicate glasses at this temperature.³ Measurements on surface energies of many binary and ternary silicate glass melts are summarized in Ref. 6. The surface energy of a molten zirconium-barium-lanthanum fluoride glass at 550°C was found to be $0.174 \pm 0.005 \text{ J/m}^2$ by a solidified pendant drop technique.^{6a}

Boric oxide (B_2O_3) has the low surface tension of about 0.085 J/m^2 at 800°C, and addition of alkali oxides raises the surface tension sharply.

These measurements of surface energy of melts refer to surfaces that have reacted with ambient water to form SiOH groups on the outer surface (see next section). The energy of a freshly fractured glass surface is much higher;^{7,8} for example, for a soda-lime glass it is about 3.4 J/m^2 . A fresh surface of this energy reacts very rapidly with low concentrations of water vapor to form SiOH groups and a much lower surface energy.⁹

Segregation of impurities to surfaces and interfaces is usually favored because it lowers the surface energy. Segregation and other aspects of surface thermodynamics are discussed in Ref. 10.

SURFACE STRUCTURE

The surface structure of oxides depends on the reactions of "dangling" oxide bonds. Thus in a silicate glass, formation of a surface leads to Si-O- and Si-bonds that are unsatisfied. These bonds react rapidly with atmospheric water to form SiOH groups. Therefore the surface of an oxide glass is normally composed of hydroxyl groups. The thickness and structural arrangement of the hydrated surface layer depend on the composition of the glass, its thermal history, humidity, and surface treatment after melting and cooling.

Extensive studies of silica (SiO_2) surfaces have been made because of the widespread use of silica gel as a catalyst and adsorbent. Results of these studies are discussed here because they help in the understanding of the surface structure of silicate glasses.

Hydroxyl groups on silica surfaces have been examined in detail by infrared spectroscopy.¹¹⁻¹⁵ In these studies, silica particles less than about $1 \mu\text{m}$ in diameter were pressed into thin porous disks for observation in the spectrophotometer. Spectra of such disks after different heat treatments are shown in Figs. 1 and 2. The broad band at about 3450 cm^{-1} and another at about 1250 cm^{-1} result from the OH vibrations in molecular water. Therefore the presence of these bands indicates physically absorbed molecular water. Consistent with this interpretation is the result that these bands disappear after

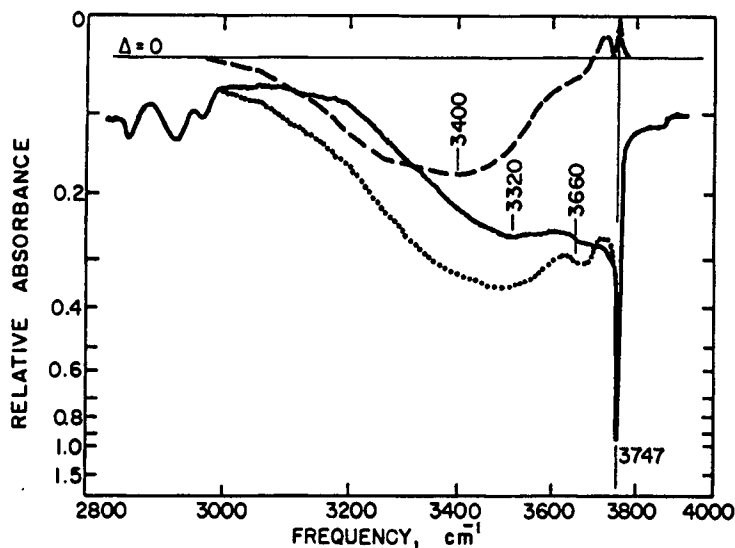


Fig. 1 Infrared spectra of SiOH groups on a cabosil silica. Dotted line, in air at room temperature; solid line, after 3 h in a vacuum at 30°C; dashed line, different between solid and dotted line. From MacDonald.¹¹

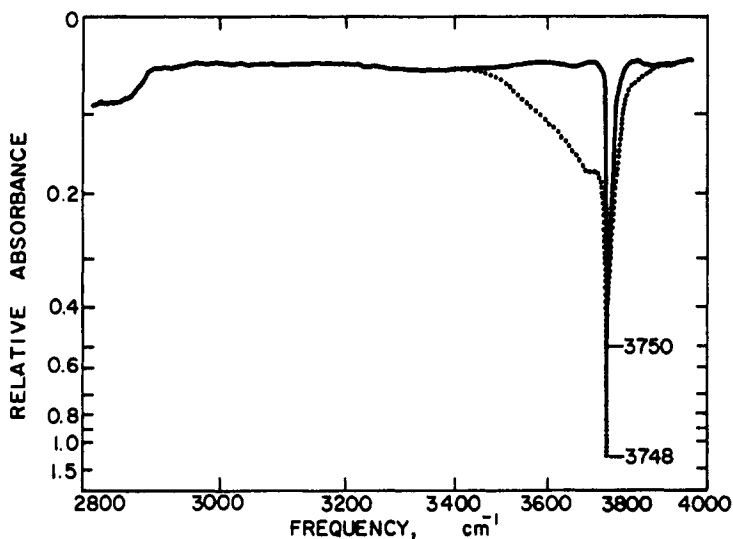


Fig. 2 Infrared spectra of SiOH groups on a cabosil silica. Dotted line, after 30 min in a vacuum at 500°C; solid line, after 8.5 h in a vacuum at 940°C. From MacDonald.¹¹

pumping at room temperature or heating to 150°C for a short time. These treatments reveal another band at 3660 cm^{-1} , in addition to the sharp band at 3747 cm^{-1} . As the temperature is raised above 150°C, the band at 3660 cm^{-1} slowly disappears, until at high temperatures only the sharp band at 3747 cm^{-1} remains. The latter band is attributed to isolated SiOH groups, whereas the one at 3660 cm^{-1} is considered to result from surface hydroxyl groups close enough together to be hydrogen-bonded. Schematic diagrams of these and other surface hydroxyl groups are given in Fig. 3.

Another type of silanol group exists near a silica surface, namely, internal SiOH groups.^{12,13,16,17} The presence of this group was originally inferred from deuterium exchange reactions on glass surfaces.¹³ At room temperature, only part of the hydroxyl groups reacted with D_2O vapor to form SiOD; the other groups were presumed to be somewhat beneath the surface and so inaccessible to the D_2O . This internal SiOH group results from the diffusion of water molecules into silica and their subsequent reaction with the silica lattice to form two SiOH groups, as described in Chapter 8. This process becomes important above about 100°C.¹⁷

The density of isolated SiOH groups on a silica surface has been calculated as 1.4 groups/100 \AA^2 and that of hydrogen-bonded groups as 3.2 groups/100 \AA^2 , or 1.6 pairs.¹⁸ Armistead et al.¹⁸ concluded that the surface corresponded to an array of different crystal planes, some of which contain widely separated hydroxyl groups and others with closer spacing that leads to hydrogen bonding.

There is evidence¹⁹⁻²¹ that some of the isolated surface hydroxyls groups on silica occur as pairs on the same silicon atom (Fig. 3c). Hair and Hertl²⁰ and Bermudez²¹ reached this conclusion from studies of reactions of chlorosilanes and boron trichloride with surface hydroxyls. They claimed that groups such as

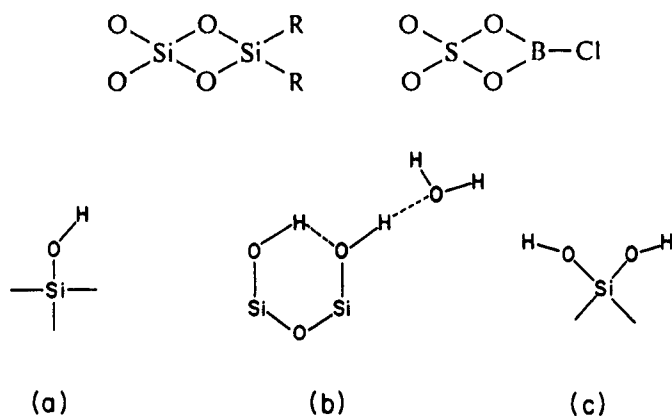
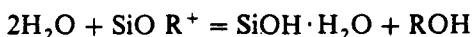


Fig. 3 Schematic diagrams of hydroxyl groups on a silica surface. (a) Isolated group; (b) hydrogen-bonded groups with an adsorbed water molecule; (c) two hydroxyls on one silicon atom.

are formed in reactions of these compounds with two hydroxyl groups on one silicon atom. However, such a four-membered ring is not often observed in silicate or borosilicate structures, and should be highly strained. Furthermore, Hair and Hertl found that all isolated hydroxyls were equally reactive; it would be surprising if the paired hydroxyls had the same reactivity as the single ones. These authors concluded that the reaction order of 1.5 for multichlorosilanes, as compared to 1.0 for monochlorosilane, showed the presence of paired groups. However, this different order for multichlorosilanes could also be caused by other reactions and mechanisms, such as the additional reaction of a chlorine on the bound silane to form a SiCl group. It is also possible to interpret the results of Bermudez without involving geminal hydroxyl groups (Ref. 21, footnote 41), so that more evidence for such groups is needed before their existence on a silica surface can be accepted.

To summarize, the following types of hydroxyl groups exist on silica surfaces: isolated SiOH groups, hydrogen-bonded SiOH groups, internal SiOH groups, and molecularly adsorbed water. The relative amounts of these different groups on silica depends on the thermal and atmospheric history of the glass, and the temperature and humidity at which it is being observed.

The surfaces of silicate glasses with additional components probably have the same types of groups as pure silica, modified by the following considerations. If other glass formers are in the glass network, they will also provide sites for hydroxyl groups. Thus AlOH, BOH, and POH groups are likely. Monovalent cations R^+ in a silicate glass can exchange with water by the following reaction:



This reaction gives rise to SiOH groups at the cation sites often with associated water; this combination can be considered to be a hydronium (H_3O^+) ion replacing the other cation. Reaction and exchange of silicate glasses with water are discussed in Chapter 13.

The surface of a glass can become depleted of volatile components during glass melting and cooling to room temperature. The alkali oxides are particularly volatile. Optical measurements of the surface refractive index sometimes show a lower index in a thin layer near the surface, indicating either a loss of alkali by volatilization or a hydrated layer.

From these considerations, one can conclude that the surface of a silicate glass containing only silicon as a glass former should be quite similar to that of pure silica. Dangling surface Si- or SiO- groups are hydroxylated, and any surface SiO alkali groups are also hydroxylated from ion exchange with water in the atmosphere. SiO groups bonded to higher valent cations may not exchange with hydrogen ions, but these cations are tightly bound to two or more SiO- groups, and so should not play a major role in surface reactions or adsorption. If other glass formers are present, different hydroxyl groups will occur on the glass surface. It is possible that one glass former or another will

appear preferentially at the surface, giving a distribution of surface hydroxyl groups different from what would be expected from the bulk composition.

EXPERIMENTAL TECHNIQUES

In recent years, a number of new techniques have been developed for examining solid surfaces. A summary of some of these techniques used to examine glasses is given in Table 1. There is not space to discuss these techniques in detail; reviews are given in Refs. 3, 4 and 22. There are references in the table to recent applications of these techniques on glasses; these references are

TABLE 1 Experimental Techniques for Examining Glass Surfaces

	Acronym	Approximate Depth of Sensitivity	References
<i>Chemical Analysis</i>			
Rutherford back scattering	RBS	1 μm	23
Resonant nuclear reaction	RNR	1 μm	24
Secondary-ion mass spectrometry	SIMS	1 μm	25
Electron microprobe		1 μm	
Ion beam spectrochemical analysis	IBSCA	1 μm	26
Electron energy dispersion	EDS	5 nm	
<i>Chemical and Bonding Analysis</i>			
Auger electron spectroscopy	AES	5 nm	27
Electron spectroscopy for chemical analysis, also called	ESCA	5 nm	4a, 27, 34
X-ray photoelectron spectroscopy	XPS		
<i>Surface Observation</i>			
Scanning electron microscopy	SEM	100 nm	28
Transmission electron microscopy	TEM		29
<i>Diffraction Techniques</i>			
Small-angle X-ray diffraction	SAXS		30
Low-angle electron diffraction	LEED		31
<i>Optical</i>			
Infrared absorption and reflection			32, 35
Ellipsometry			33

illustrative rather than comprehensive, and only serve as a starting point for further information.

Nuclear reaction techniques (RBS and RNR) give both the outer surface concentrations and the profile of concentration to a depth of about $1\text{ }\mu\text{m}$ without removing any of the sample. RBS can be used for atoms heavier than nitrogen; RNR is especially useful for hydrogen analysis. See Chapter 13 for more information on these techniques, which are nondestructive of the sample. SIMS is the most sensitive technique, with a detection limit of 10^{-16} gm , and it can be used for all elements including hydrogen. Profiling with SIMS, IBSCA, AES, and ESCA (XPS) requires sputtering off layers, because these techniques are sensitive only to the outermost atomic layers. The electron microprobe and EDS in the scanning electron microscope involve electron penetration into the sample to a depth of $1\text{ }\mu\text{m}$ or more, so they give an integrated analysis to this depth. An absolute concentration of elements can be calculated directly from the nuclear techniques (RBS and RNR); other techniques require standards for absolute concentrations, which are often quite unreliable.

AES and ESCA are quite difficult to use for quantitative surface analysis because they are especially sensitive to contamination and the chemical state of the elements being analyzed. The latter property can be used to advantage to give information on chemical bonding, coordination numbers, and defects in glass surfaces.

Diffraction techniques have not been used much to examine glass surfaces.

The value of infrared spectroscopy for examination of glass surfaces has already been demonstrated. Reviews of infrared experiments in glass surfaces are given in Refs. 3, 4, 4a, 14 and 15; optical absorption in the bulk of glass is discussed in Chapter 17.

PHYSICAL ADSORPTION

A favorite material for adsorption studies is "thirsty glass," a porous glass made by leaching a phase-separated borosilicate glass.^{14,36} Thirsty glass is an intermediate in the manufacture of 96% Vycor or silica glass, as described in Chapter 4. The surface of thirsty glass is heterogeneous and contains a high proportion of borate groups (B-OH), much more than would be expected from the bulk composition of 4% B_2O_3 .³⁶ Thus results of adsorption studies with this material are not directly comparable with those on silica, although there are many similarities in the surface behavior of the two materials.¹⁴

The nature of physical or chemical adsorption on glass is strongly dependent on the surface structure. The surface hydroxyl groups are the most important sites for adsorption and reaction, so the thermal history of a glass is important in its adsorption behavior.

Adsorption studies on pure silica can be related to the hydroxyl structure as described in the section on surface structure. McDonald found that the

3749-cm⁻¹ band on Aerosil 2491 silica was shifted by physical adsorption of a number of gases.³⁷ Since this band results from isolated SiOH groups on the silica surface, these shifts indicate that the gases are adsorbed on or near these hydroxyl groups. At low coverages at 83°K the shifts for argon, krypton, xenon, nitrogen, oxygen, methane, and perfluoromethane were small, the largest being 32 cm⁻¹ for methane. There was no direct relation between the band shifts and the polarizabilities of the adsorbed molecules. At higher gas pressures, the bands shifted more, indicating interaction of more than one adsorbed molecule with each group. In a detailed study of argon, oxygen, and nitrogen adsorption, McDonald found that much more of the latter gas was adsorbed at the same gas pressure than the other two gases. For nitrogen, the original 3749-cm⁻¹ hydroxyl band disappeared at a pressure several times lower than that for coverage with a "BET monolayer," indicating that the nitrogen molecules were preferentially adsorbed at the free SiOH groups, and that a monolayer on silica actually involves multiple adsorption at such a group.

Water, methanol, and benzene adsorbed on silica in appreciable amounts at room temperature, causing much greater band shifts.³⁷ Adsorption of these gases with hydrogen bonding is intermediate between physical and chemical sorption.³⁸ Cyclohexane also adsorbed at room temperature, but caused a shift about the same as for methane. Benzene adsorption on porous glass was studied in detail by Cusumano and Low,³⁹ who also reviewed earlier studies of adsorption of aromatics on silica and porous glass.

Physically adsorbed molecules are apparently bonded to the hydrogen atom on an SiOH group. Larger band shifts for water and methanol, indicating stronger hydrogen bonds with these molecules, are expected from their hydrogen bonding in the liquid state. A study of diethylamine adsorption on silica showed that it strongly preferred the isolated silanol groups to those groups hydrogen-bonded in pairs,³⁹ whereas water appears to prefer the adjacent (hydrogen-bonded) silanol groups.^{14,40}

A theoretical calculation was made of the band shift expected from nitrogen adsorption, considering the adsorbed molecule to be a quadrupole with its axis lying along the direction of the OH group, and rotating about an axis perpendicular to this group.⁴¹ Reasonable agreement with the experimental shift was achieved.

The studies above show that physical adsorption on silica takes place on particular sites, depending on the nature of the adsorbing molecule. The sites are hydroxyl groups, either isolated or hydrogen-bonded in pairs. Since neither of these types of sites fills the surface completely, the concept of a monolayer of adsorbed molecules loses significance. Thus absolute surface areas determined by the BET method are suspect because the density of isolated hydroxyl groups is about 1.4 groups/100 Å². If, for example, the area of an adsorbed nitrogen molecule is 16.2 Å²,⁴² then when one molecule of nitrogen is adsorbed per group, only about one-sixth of the surface is actually covered.

The variation of the amount of adsorbed gas as a function of the gas pressure is called an adsorption isotherm. A number of equations have been

proposed for these isotherms, both on an empirical and theoretical basis, but none is entirely satisfactory. Hydrated silica surfaces have been extensively studied as adsorbants, and over narrow pressure ranges a variety of equations fits the experimental isotherms. Thus such a fit is not conclusive evidence for the validity of the assumptions from which the isotherm is derived. At low pressures and therefore low surface coverage, the amount adsorbed should be proportional to pressure P , as governed by Henry's law

$$Q = kP \quad (4)$$

However, agreement with this functionality for adsorption on silicate glasses is found only at the lowest pressures,⁴ at which the amount absorbed is much less than a monolayer,^{42,44} as shown in Fig. 4 for Pyrex borosilicate glass. Perhaps the reason is different adsorption types on the glass surface. It is difficult to ascribe any theoretical or structural significance to empirical adsorption isotherms until the correspondence between adsorption and sites is resolved. Reviews of physical adsorption studies on silicates are given in Refs. 3, 4, 14, 42, 44, 46 and 47, and in the first edition of *Glass Science*.

CHEMISORPTION AND SURFACE CHEMICAL REACTIONS

Various gases react with the SiOH groups on a glass surface. Ammonia becomes hydrogen-bonded to the isolated SiOH groups, as shown by the strong perturbations of the SiOH vibrations after treatment of silica with

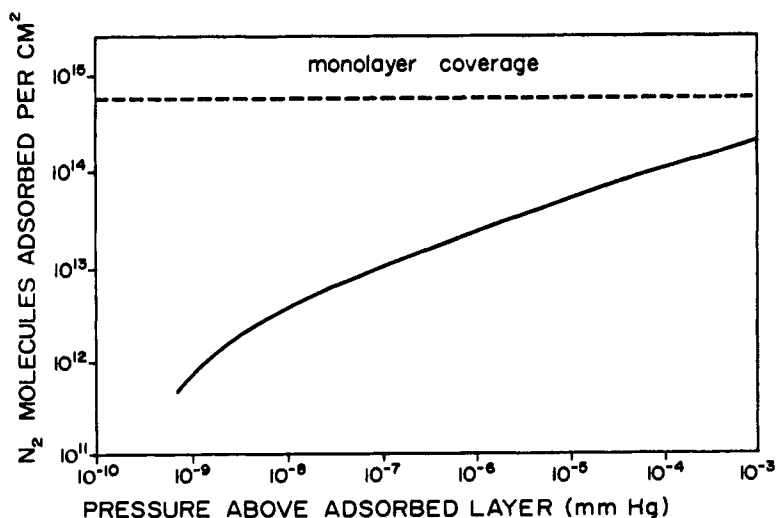


Fig. 4 Adsorption of nitrogen on Pyrex borosilicate glass. From Hobson.⁴³

ammonia.⁴⁴ Other chemisorption reactions on silica surfaces are reviewed in Refs. 3, 4, 14 and 15.

Surface hydroxyl groups can be replaced by halogen atoms, which change some surface properties substantially. A partial substitution of fluoride for hydroxyl groups is achieved by treatment with ammonium fluoride or hydrofluoric acid solutions. The latter, and probably the former, etch away the hydrated surface and also substitute fluoride ions for some of the hydroxyls. Heating this surface to 700°C causes complete removal of hydroxyl groups, and the resultant surface is hydrophobic.⁴⁰ Gaseous hydrofluoric acid also reacts with surface hydroxyls on silica, replacing all of them with fluoride ions at about 700°C.

A silica surface can be chlorinated by reaction with sulfuryl chloride (SO_2Cl_2) or silicon tetrachloride,⁴⁵ or by heating in chlorine at 700–950°C or carbon tetrachloride⁴⁴ at 350–600°C. Morrow and Devi have referred to many other studies of chemisorption of metallic halides on silica.⁴⁸ Other reactions are esterification, amination, carboxylation, etherification, and reactions with Grignard reagents, organosilicon compounds, diborane,¹⁴ and $\text{Al}(\text{CH}_3)_3$.⁴⁹

Glass surfaces can act as catalysts for various biochemical reactions,⁵⁰ for example, for rapid clotting of blood. They are also sometimes used as substrates for culturing cell growth.

The acid ionization constants of various surface hydroxyl groups on silica were found by Hair and Hertl from the frequency shifts of the OH band maxima when different molecules were adsorbed on them.⁵¹ BOH and POH groups were formed on the silica surface by reaction with BCl_3 and PCl_3 , respectively. Acid ionization constants $\text{p}K_a$ for ionization reaction



were found to be: SiOH, 7.1; BOH, 8.8; and POH, –0.4. They can be compared with values in aqueous solution of SiOH, 9.7 and POH, 2.0.

Reactions of carbon dioxide and oxygen with freshly formed silicate surfaces were studied in ultrahigh vacuum by Antonini and Hochstrasser.⁹ Fresh surfaces were obtained by fracturing or abrading glass samples inside the vacuum system. On a fresh silica surface, the energy of adsorption of carbon dioxide was about 11 kcal/mol, compared to the more usual heats of physical adsorption of about 1–2 kcal/mol. The desorption of gas was followed as the surface was heated; the increase in temperature was linear with time. A single desorption peak was found for fused silica and a calcium borosilicate glass, whereas for an alkali borosilicate and a sodium silicate (75% SiO_2 , 25% Na_2O) glass, two desorption peaks were found. The two peaks were taken to be evidence for two different types of adsorption sites, perhaps one being associated with unperturbed silicon atoms and the other with silicon perturbed by the presence of modifying ions, probably alkalis. This interpretation seems reasonable, but needs confirmation with other techniques.

These reactions were reversible as long as the sample was kept in the vacuum system at room temperature. Heating the samples to higher tempera-

tures progressively destroyed the active reaction sites, perhaps because of diffusion and reaction of atoms from the interior of the glass.

Antonini et al. found that oxygen reacted with the unpaired electron (dangling bonds) at silicon atoms on a fresh silica surface to form an Si^+O_2^- complex.⁹ The oxygen gas did not dissociate but retained its molecular form, although it was tightly bound with an adsorption energy of about 75 kcal/mol. The surface mobility of the adsorbed oxygen was immeasurably low. For an alkali borosilicate, a calcium borosilicate, and a sodium silicate glass the surface coverage was about the same as for silica, indicating a similar density of silicon dangling bonds for these glasses as for silica. The adsorption energy for the alkali borosilicate was somewhat lower than for silica.

Adsorption in glasses from solution is reviewed in Refs. 4 and 52 and *Glass Science*, first edition.

SURFACE CONDUCTIVITY

The surface resistivity of clean glass in dry air is very high: 10^{14} ohm/square or higher at room temperature.⁵³ Geddes found no appreciable surface leakage of freshly broken glass surfaces in clean dry air.⁵⁴ Since these results are at the limit of reliable resistivity measurements, the inherent resistivity of a dry glass surface is uncertain.

The surface resistivities of most glasses decrease rapidly as the relative humidity at room temperature increases above about 40%.⁵³⁻⁵⁵ However, the surface resistivity of fused silica, cleaned in chromic acid and then in distilled water, remains high even at quite high relative humidity.

These experimental observations can be explained in the following way. The inherent surface resistivity of a glass is very high. If there is any ionic contamination on the surface, it can conduct current in humid air, since physically adsorbed water reacts with these contaminants to provide mobile ions. Glasses containing monovalent cations can react with water by ion exchange forming metallic hydroxides on their surfaces.⁵⁶ These hydroxides react further with water, forming mobile ions on the surface. In some cases, the hydroxides absorb so much water that a liquid solution is formed on the glass surface, giving a highly conductive surface film. This possibility was first recognized by Faraday in his remarkable study of the electrical properties of glass.⁵⁷

GRINDING AND POLISHING OF GLASS SURFACES

Often the surface of glass must be smoothed, especially for optical applications. The smoothing process can be separated into three different stages, grinding, lapping, and polishing, in order of the rate of removal of material and the

TABLE 2 Smoothing of Glass

Process	Smoothing Material	Approximate Grain Size of Smoothing Material (μm)	Abrading Mechanism
Grinding	Diamond	10–80	Cracking (fracture) and scratching
Lapping	Alumina and liquid	20	Cracking (fracture) and scratching
Polishing	Cerium oxide and pitch polisher	10–50	Scratching and removal of hydrated layer

height of the roughness remaining, as summarized in Table 2. A review of grinding, lapping and polishing by Izumitani⁵⁸ is the basis for this discussion.

Grinding is the result of abrasion with a very hard substance such as diamond, either loose or bonded in metal. The diamond fractures the glass surface and chips away pieces of surface material. The rate of loss of glass by grinding is inversely proportional to the indentation hardness of the glass surface.

Lapping is the removal of material from the glass surface at a lower rate than during grinding, and by removing smaller chips. The glass surface is therefore partially smoothed by lapping. Water as a lapping medium increases the rate of lapping. The main mechanism of glass removal is cracking, as in grinding, and the rate of lapping is inversely proportional to the hardness. The influence of water suggests that surface hydration also plays a role; glasses more durable to water attack lap more slowly in water than less durable glasses, Izumitani⁵⁸ considers somewhat different mechanisms.

In polishing of a glass surface, roughnesses of micrometers are reduced by a factor of 100 or more. Softer solid grains, such as of Cerium oxide, are used in a water slurry with a polisher made of an organic material such as pitch, or felt. The grains remove the soft hydrated layer on the glass surface. The polisher holds imbedded polishing grains and transmits an applied load to the grains. The polisher must deform to fit to the glass surface, so it must be soft.

REFERENCES

1. L. Holland, *The Properties of Glass Surfaces*, Chapman and Hall, London, 1964.
2. F. M. Ernsberger, *Annu. Rev. Mater. Sci.*, **2**, 529 (1972).
3. H. H. Dunken, in *Treatise on Materials Science and Technology*, Vol. 22, M. Tomozawa and R. H. Doremus, Eds., Academic Press, Orlando, FL, 1982, pp. 1–74.

4. H. H. Dunken, *Physikalische Chemie der Glasoberfläche*, VEB Deutscher Verlag für Grundstoffindustrie, Leipzig, 1981.
- 4a. C. G. Patano, Ed., *J. Noncryst. Solids*, **120** (1990).
5. L. Shartis and S. Skinner, *J. Res. Natl. Bur. Stand.*, **46**, 385 (1951).
6. N. P. Bansal and R. H. Doremus, *Handbook of Glass Properties*, Academic Press, Orlando, FL, 1986, p. 101.
- 6a. N. P. Bansal and R. H. Doremus, *J. Am. Ceram. Soc.*, **67**, C-197 (1984).
7. J. J. Gilman, *J. Appl. Phys.* **31**, 2208 (1960).
8. R. H. Doremus, *J. Appl. Phys.* **47**, 1833 (1976).
9. J. F. Antonini, G. Hochstrasser and P. Aclouque, *Verres Refract.*, **23**, 169 (1969).
10. R. H. Doremus, *Rates of Phase Transformation*, Academic Press, Orlando, FL, 1985, p. 33.
11. R. S. MacDonald, *J. Phys. Chem.*, **62**, 1168 (1958).
12. G. J. Young, *J. Colloid Sci.*, **13**, 67 (1958).
13. V. Ya. Davydov, A. V. Kiselev, and L. T. Zhuravlev, *Trans. Faraday Soc.*, **60**, 2254 (1964), and earlier articles by these authors referred to in this paper.
14. M. L. Hair, *Infrared Spectroscopy in Surface Chemistry*, Marcel Dekker, New York, 1967.
15. L. H. Little, *Infrared Spectra of Adsorbed Species*, Academic Press, London, 1966.
16. A. J. Tyler, F. H. Hambleton, and J. A. Hockey, *J. Catal.*, **13**, 35 (1969).
17. R. H. Doremus, *J. Phys. Chem.*, **75**, 3147 (1971).
18. C. G. Armistead, A. J. Tyler, F. H. Hambleton, S. A. Mitchell, and J. A. Hockey, *J. Phys. Chem.*, **73**, 3947 (1969).
19. J. A. Hockey and B. A. Pethica, *Trans. Faraday Soc.*, **57**, 2247 (1961).
20. M. L. Hair and W. Hertl, *J. Phys. Chem.*, **73**, 2372 (1969).
21. V. M. Bermudez, *J. Phys. Chem.*, **75**, 3249 (1971).
22. W. A. Czanderna, *Methods of Surface Analysis*, Elsevier, Amsterdam, 1975.
23. W. A. Lanford, C. Burman, R. H. Doremus, Y. Mehrotra, and T. Wassick, in *Advances in Materials Characterization*, D. R. Rossington, R. A. Condra and R. L. Snyder, Eds., Plenum, New York, 1983, p. 549.
24. K. H. Schnatter, R. H. Doremus, and W. A. Lanford, *J. Noncryst. Solids*, **102**, 11 (1988).
25. T. Richter, G. H. Frischat, G. Brehardt, and S. Scherrer, *Phys. Chem. Glasses*, **26**, 208 (1985).
26. H. Bach, K. Grosskopf, P. March and F. Rauch, *Glastech. Ber.* **60**, 21, 33 (1987).
27. S. Myhra, J. C. Riviere, and A. M. Stewart *J. Noncryst. Solids*, **99**, 244, 255 (1988).
28. R. Garcia, R. H. Doremus, N. P. Bansal, S.-H. Ko, and T. Margraf, *J. Mater. Res.*, **3**, 989 (1988).
29. P. H. Gaskell and A. Saud, *J. Noncryst. Solids*, **106**, 250 (1988).
30. P. Lamparter and S. Stub, *J. Noncryst. Solids*, **106**, 137 (1988).
31. Y. Steinike, E. Mieller, J. Richter-Mendou, and H. P. Hennig, *Kristall. Tech.*, **29**, 795 (1980).
32. F. Geotti-Bianchini, L. DeRiu, G. Gagliardi, M. Guglielmi, and C. G. Patano, *Glastech. Ber.*, **69**, 205 (1991).

33. T. S. Chao, C. L. Lee and T. F. Lee, *J. Appl. Phys.* **73**, 1732 (1993).
34. N. Keshizaki, H. T. Akayanayi, and K. Kemmechi, *J. Noncryst. Solids*, **95&96**, 1111 (1987).
35. K. F. Ferris and L. R. Pederson, *Phys. Chem. Glasses*, **29**, 9 (1988).
36. M. J. D. Low and N. Ramasubramanin, *J. Phys. Chem.*, **70**, 2740 (1966); **71**, 730, 3077 (1967).
37. R. S. McDonald, *J. Am. Ceram. Soc.*, **79**, 850 (1957).
38. P. A. Sewell and A. M. Morgan, *J. Am. Ceram. Soc.*, **52**, 136 (1969).
39. J. A. Cusumano and M. J. D. Low, *J. Phys. Chem.*, **74**, 792 (1970).
- 39a. M. R. Basilo, *J. Chem. Phys.*, **35**, 1151 (1961).
40. T. H. Elmer, J. D. Chapman, and M. E. Nordberg, *J. Phys. Chem.*, **67**, 2219 (1963).
41. G. J. C. Frohnsdorff and G. L. Kinton, *Trans. Faraday Soc.*, **55**, 1173 (1959).
42. E. A. Flood, Ed., *The Solid-Gas Interface*, Marcel Dekker, New York, 1966.
43. J. P. Hobson, *Can. J. Phys.*, **37**, 300, 1105 (1959); *J. Chem. Phys.*, **34**, 1850 (1961).
44. J. B. Peri, *J. Phys. Chem.*, **70**, 2937 (1966).
45. M. Folman, *Trans. Faraday Soc.*, **57**, 2000 (1960).
46. A. Adamson, *The Physical Chemistry of Surfaces*, Wiley-Interscience, New York, 1990.
47. P. C. Hiemenz, *Principles of Colloid and Surface Chemistry*, Marcel Dekker, New York, 1986.
48. B. A. Morrow and A. Devi, *Trans. Faraday Soc. I*, **68**, 403 (1972).
49. R. J. Peglar, F. H. Hambleton, and J. A. Hockey, *J. Catal.*, **20**, 309 (1971).
50. P. B. Adams, *New Sci.*, **41**, 25 (1969).
51. M. L. Hair and W. Hertl, *J. Phys. Chem.*, **74**, 91 (1970).
52. F. Kepak, *Chem. Rev.*, **71**, 357 (1971).
53. H. L. Curtis, *Bull. Bur. Stand.*, **11**, 359 (1915).
54. S. Geddes, *J. Roy. Tech. Coll. (Glasgow)*, **3**, 551 (1936).
55. A. Ya. Kouznetzov, *J. Chem. Phys. USSR*, **27**, 657 (1953).
56. R. G. Pike and D. Hubbard, *J. Res. Natl. Bur. Stand.*, **59**, 127 (1957).
57. M. Faraday, *Philos. Trans., Part 1*, 49 (1830); *Experimental Researches in Electricity*, J. M. Dent, London, 1914, pp. 38ff.
58. T. Izumitani, in *Treatise on Materials Science and Technology*, Vol. 17, M. Tomozawa and R. H. Doremus, Eds., Academic Press, Orlando, FL, 1979, p. 115.

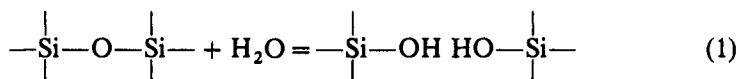
CHAPTER 12

REACTIONS WITH GASES

Certain gases such as water and hydrogen can react with the silicon-oxygen network of silicate glasses, breaking it up and consequently modifying such properties as strength and viscosity. Reactive gases in glass determine its oxidation state and can reduce or oxidize ions the glass. All these gases dissolve and diffuse in silicate glasses as molecules, as described in Chapter 8, and the rates of their reaction with the glass are determined by their diffusion coefficients in it.

WATER

Water reacts with the silicon-oxygen bond as follows:^{1-3,9}



forming pairs of adjacent silanol groups. These groups and the hydroxyl ions so formed are very immobile, even at temperatures as high as 1000°C (see Chapter 8 and Refs. 4 and 5). Thus water molecules must diffuse in and out of the silicate lattice to form or remove these hydroxyl groups.

The solubility of water in fused silica (Vitreosil and O.G. grades, Thermal Syndicate, Walland, England) was determined by Roberts and co-workers from the height of the infrared absorption peak resulting from Si-OH groups⁶ and from tracer diffusion studies.⁷ This solubility is proportional to the number of silanol groups formed by reaction per unit volume when the glass is in

equilibrium with water vapor of a fixed pressure. Below about 1000°C the solubility depended on the thermal history of the glass.⁸ For a sample heated at 1100°C the solubility was nearly constant from 1200 to 700°C⁸ at about $3 \times (10)^{-3}$ SiOH groups formed per SiO₂ group in the glass, with a water pressure of 700 mm/Hg. The solubility is not a function of impurity content in the fused silica, since Hetherington and Jack found the same solubility for a very pure silica (Spectrosil) and one containing more impurities, for example, about 60 ppm aluminum and 4 ppm sodium.⁹ The solubility is proportional to the square root of the water vapor pressure,^{3,6,9} as would be expected from reaction 1.

Equilibrium between the SiOH groups and dissolved water molecules gives the above solubilities. The insensitivity to impurities and the square root dependence on pressure suggest that there are a number of equivalent sites for reaction by reaction 1 in the silica; in fact, probably most of the Si-O-Si bonds in the glass are about equally susceptible to reaction 1.

The solubility of water in molten alkali silicates increases linearly with the alkali concentration,³ and also in the order Li < Na < K silicates.¹⁰ There is a slight increase in solubility with increasing temperature.^{10,10a} In molten B₂O₃ there is a decrease in solubility of water with increasing temperature.¹¹

In fused silica, the infrared spectrum of the silanol groups formed by reaction with water shows no indication of hydrogen bonding,¹ but in the alkali silicates, the number of hydrogen-bonded OH groups increases as the amount of alkali increases and also in the order Li < Na < K.³ The number of hydrogen-bonded hydroxyls decreases as aluminum oxide is added to the glass melt.³ Apparently the OH groups can form a hydrogen bond to nonbridging oxygen anions that have an associated alkali cation. As the bonding of the oxygen ion to the alkali ion becomes stronger (the smaller the alkali ion the stronger the bond), the tendency to hydrogen bonding is reduced. Addition of aluminum removes nonbridging oxygen ions, since each aluminum oxide tetrahedron has an associated alkali ion. The increased hydrogen bonding is perhaps at least partly responsible for the increased solubility in alkali silicates, and for the order of solubility among the various alkali silicates.

An additional factor in the water solubility is probably the reactivity of the silicon-oxygen bond. As alkali oxide is added to the silica structure, this bond is weakened, as shown by the greatly decreased viscosity resulting from such addition. The activation energy for viscous flow in fused silica in the temperature range 1100–1400°C is about 170 kcal/mol, whereas for binary sodium silicate glasses, it is about 100 kcal/mol in the transition region (450–600°C). Thus the greater reactivity of the bond pushes reaction 1 to the right, giving greater water solubility as the alkali ion concentration increases. Other structural interpretations of these results on water solubility have been given.^{3,12}

Water is always present in commercial silicate glasses in the range of about 0.01–0.1 wt%. It is possible to introduce water during melting by bubbling it through the melt.¹³ Changes in water content in these glasses has a strong

influence on their properties.¹⁴⁻¹⁷ Viscosity is strongly decreased by increasing water content; there is disagreement about the influence of water on electrical conductivity.^{11,15}

Substantial amounts (up to 20 wt% or more) of water can be introduced into certain multicomponent alkali silicate glasses from water vapor in an autoclave at temperatures above 100°C. The formation, analysis, and properties of these "hydrosilicates" were reviewed by Bartholomew.¹⁴ These glasses have "rubber-like" properties, and were first explored by Stookey.¹⁸ A typical composition is 76.9 mol% SiO₂, 10.8% Na₂O, 3.9% K₂O, 7.8% ZnO, and 1.3% Al₂O₃, although a wide range of silicate compositions can be made to a "hydrosilicate" state. Alkaline earth ions appear to inhibit the tendency to formation of these hydrosilicates, and durable commercial compositions such as soda lime silicates and Pyrex borosilicate do not form them under comparable conditions.

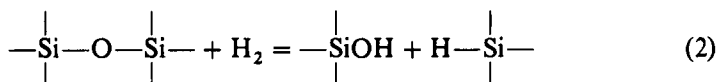
The water in these glasses is both in the form of SiOH and dissolved molecular water. Ernsberger¹⁹ showed the presence of molecular water in an autoclaved thin film of sodium aluminum borosilicate glasses from the infrared absorption band of molecular water at 6.2 μ m. The amount of SiOH in these glasses saturates at about 2 or 3 wt%, and as more water is added, it enters the glass as molecular water. The glass transition temperature and viscosity of these glasses decrease dramatically as the amount of water in them increases.¹⁴

It appears that the mechanism of formation of these hydrosilicates involves diffusion of molecular water into the glass and its reaction with the silicon-oxygen network by Eq. 1. As the network is progressively broken up by this reaction, the glass transition temperature decreases and the glass becomes more open, so the molecular water can diffuse into it more readily. At the same time as this deep penetration of molecular water takes place, there must also be ion exchange and interdiffusion between hydronium ions from the water vapor and alkali ions in the glass (see the next chapter). The depth of this exchanged layer is much less than the penetration distance of the molecular water, because the alkali concentration in the bulk of the glass remains at its initial value.

An intriguing question is why some silicate glass compositions form hydrosilicates and others do not. The diffusion of molecular water in the unaltered glass should be lower than in pure silica or Pyrex borosilicate (see Chapter 8), so faster diffusion cannot be the reason for hydrosilicate formation. Possibly the reason is the ease of reaction of dissolved molecular water with the silicon oxygen network. As mentioned above, the "solubility" of water, which is effectively the extent of reaction 1, increases in binary alkali silicates as the alkali concentration increases. Thus it appears that as the silicon-oxygen network is progressively broken up by alkali, the reaction of the network with water is more favorable, and the diffusion of molecular water becomes more rapid. Perhaps the presence of alkaline earth ions reduces the tendency to reaction or blocks the diffusion of molecular water, or both.

HYDROGEN

Hydrogen also reacts with silica to form hydroxyl groups.^{20,21} In fused silica containing 50–100 ppm of aluminum, the reaction becomes perceptible above about 700°C. In purer silica, it does not occur appreciably at these temperatures, but at higher temperatures or pressures hydrogen forms hydroxyl groups from Si–O–Si bonds. The reaction can be written as follows:

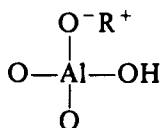


The presence of the SiH groups has been established from the growth of the SiH stretching band at 2250 cm^{-1} ($4.45 \text{ } \mu\text{m}$) in vitreous silica containing hydrogen.^{22,23} In this case the rate of introduction or removal of OH groups is controlled by the diffusion of hydrogen molecules,²⁰ which is much faster than the diffusion of the larger water molecules (see Chapter 8).

The rate of exchange of deuterium with SiOH groups in glass was studied by Lee.²¹ He found a first-order reaction for silica with low impurities in which all the hydroxyl groups were attached to silicon atoms. In a fused silica with about 100 ppm of aluminum, he found that the first-order reaction coefficient decreased with time, probably because both AlOH and SiOH groups were present in this glass, and the exchange rate was different for these two groups.

These results show that there can be at least three different types of hydroxyl groups in a silicate glass.²⁴

1. An aluminum hydroxyl group can be thought of as having the structure



where R^+ is either an alkali ion or another hydrogen ion, more or less associated with one of the oxygens bound to the aluminum. These groups result from the reaction of hydrogen with the Al–O–Si bond and are called “loosely bound” by Lee²¹

2. Hydroxyl groups in pairs are formed during melting or annealing of the glass by reaction with water:



These groups are introduced or removed by diffusion of water, which is slow compared to hydrogen diffusion.

3. Hydrogen ions are introduced by ion exchange with alkali ions, either by

interion diffusion or by electrolysis. These groups cannot be removed by gaseous diffusion because they are needed for electroneutrality.

Hydrogen can also reduce ions in various oxide glasses to the atomic state, for example, gold, silver, lead, bismuth, and antimony.²⁵⁻³¹ At lower temperatures, these reactions are often limited to layers of the glass near its surface because of the slow diffusion of hydrogen in the glass at these temperatures. In addition, hydrogen can reduce the valence of an ion in glass without reducing it completely to the atomic state. In this way, dissolved hydrogen affects the oxidation state of the glass. A study of fluorescence of terbium and europium in glass demonstrated the reduction of these ions from 3+ to 2+ valence;³¹ the rate of the reduction was controlled by diffusion of molecular hydrogen. Hydrogen can also form defect centers in glass; in silica-10% germania, a reduced center that absorbs ultraviolet light at a wave length of 0.19 μ m is formed in hydrogen at 500°C.³²

OXYGEN

The oxidation state of a glass is important in a variety of properties, such as optical absorption of coloring ions, chemical reactivity, and ease of fining (bubble removal). The oxidation state is directly related to the concentration of dissolved oxygen in the glass.

Oxidation-reduction reactions in glass can be examined by considering the equilibrium between different oxidation states of ions in the glass. For example, consider the equilibrium between solid phases of ferrous and ferric oxide:



The equilibrium constant K for this reaction is related to the standard free energy change for the reaction ΔG° by

$$\Delta G^\circ = -RT \ln K \quad (4)$$

and K is given by

$$K = \frac{[\text{Fe}_2\text{O}_3]^2}{[\text{FeO}]^4 P} \quad (5)$$

where the brackets denote thermodynamic activities with the pure oxide as the standard state, and P is the pressure of oxygen in equilibrium with the solid phase. Oxygen fugacity must be used if the gas phase is nonideal.

The phase rule for this system is

$$P_h + F = C + 2 \quad (6)$$

where P_h is the number of phases, F is the number of degrees of freedom in specifying the system and C is the number of components. The number 2 results from two environmental variables, pressure and temperature. In com-

plex systems, C is often difficult to determine. It can be defined³³ as "the minimum number of pure chemical substances that are required for the preparation of arbitrary amounts of all phases of the system". For the system of Eq. 3, there are two components and three phases, two solids and the oxygen gas. Thus from Eq. 6 there is one degree of freedom. This means that if the temperature is fixed, then the oxygen pressure has a particular value. This result can also be deduced from Eq. 5. In the pure form, the activities of the solid oxides are unity, so

$$P = \frac{1}{K} = \exp\left(-\frac{\Delta G^\circ}{RT}\right) \quad (7)$$

If the oxides are dissolved in a glass melt, there are three components because the glass adds an additional one, but only two phases, glass and gas. The result is three degrees of freedom, for example, temperature, oxygen pressure, and activity of one oxide in the glass; then the activity of the other oxide is fixed. Equation 3 still is valid with the understanding that the oxides are components dissolved in the glass, and Eq. 5 represents the reaction equilibrium with the activities of the oxides in the glass. If the temperature and oxygen pressure are fixed, the activity ratio (or the concentration ratio of an ideal solution) of iron plus three to iron plus two is fixed, and the total amount of iron in the glass is the third variable.

Oxygen molecules dissolve and diffuse in the relatively open structure of glass, as described in Chapter 8. At 1300°C the diffusion coefficient D of molecular oxygen in vitreous silica is about 5×10^{-8} cm²/s as extrapolated from the measurements of Norton;³⁴ similar or smaller values are expected for other silicate glasses. For a time t of 3 h, the mean diffusion distance ($\approx \sqrt{2Dt}$) is about 3 mm. Thus for usual melting times and temperature only a small depth of the glass surface comes to equilibrium with the oxygen in the gaseous phase. In this region, the thermodynamic activity of oxygen in the glass (P in Eq. 5) is determined by the partial pressure of oxygen in the gas phase. Deeper into the glass, however, the concentration of dissolved oxygen may not be in equilibrium with the surrounding atmosphere. In this region the chemistry of the glass batch influences the oxidation state of the glass. The following factors may be important:

1. Trapped gas in the powders of the batch (usually air).
2. Gases from decomposition of batch chemicals; examples are carbon dioxide from carbonates, nitrogen oxides from nitrates, and sulfur di- and tri-oxides from sulfates.
3. Constituents of the batch that can react with oxygen, such as organic substances either as impurities or purposely added.

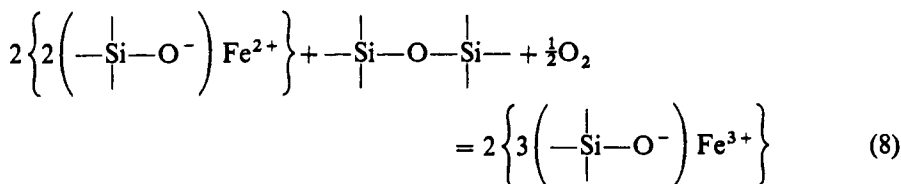
The result is that the oxidation state of a silicate glass is usually nonuniform and difficult to quantify. When the glass is cooled from the melting tempera-

ture, the diffusion coefficient of oxygen in it is substantially reduced, so the oxidation state in the melt is usually frozen in. It is possible to change this state at intermediate temperatures ($\sim 600^\circ$) by treatment in hydrogen, which diffuses much more rapidly than oxygen in silicate glasses (see Chapter 8).

Thermodynamic quantities for pure oxides are listed in standard references, for example Ref. 35. Often Eq. 4 for pure oxides is plotted as a function of temperature; this plot is called an Ellingham diagram and is a convenient source of data for pure oxides. There are Ellingham diagrams for oxides in many textbooks.^{36,37}

From Eq. 5, the ratio of Fe^{+3} to Fe^{+2} ion in the glass is proportional to the oxygen pressure to the $1/4$ power, for ideal solutions; in general this power is $n/4$, where n is the difference between valence states.³⁸⁻⁴⁰

The oxidation-reduction reactions of an ion in a silicate glass can also be written in terms of their lattice positions



to emphasize the coordination of the ion with oxygen in the lattice.

Douglas and co-workers studied the $\text{Cr}^{3+}-\text{Cr}^{6+}$, $\text{Fe}^{2+}-\text{Fe}^{3+}$, and $\text{Ce}^{3+}-\text{Ce}^{4+}$ equilibria in binary lithium, sodium, and potassium silicate glasses and reviewed earlier work on these systems in various glasses.^{41,42} They found that oxidation was more favorable as the alkali content of the glass increases, and as the ionic size increases in the order of lithium, sodium, and potassium.

From reaction 8 these composition effects can be interpreted as resulting at least in part from changes in the reactivity of the silicon-oxygen bonds, just as for water solubility as described above. As alkali is added to the glass the silicon-oxygen bonds are weakened, increasing the tendency to oxidation.

A more complicated situation arises if the ion has three oxidation states possible. Copper can occur in glass in the $+2$, $+1$ and atomic state. Reaction equations for the pure oxides are



Equilibrium constants K are

$$K_a = \frac{[\text{Cu}_2\text{O}]^2}{[\text{Cu}]^4 P} \quad (11)$$

$$K_{10} = \frac{[\text{CuO}]^2}{[\text{Cu}_2\text{O}] P} \quad (12)$$

For Eq. 11 there are three phases (gas, copper metal, and Cu_2O) and two

components, so there is one degree of freedom, and the same is true for Eq. 12. If all three pure solid phases are present there are four phases and three components and still one degree of freedom. If these constituents are dissolved in the glass as copper atoms, copper + 1 ions and copper + 2 ions, there are two phases and four components, so there are four degrees of freedom. If the copper atom concentration is greater than the solubility of bulk copper, copper metal particles will form. Then there are three phases and four components, giving three degrees of freedom; the concentration of dissolved copper atoms is fixed by the solubility of copper metal in the glass. Thus, for example, if temperature and oxygen pressure are fixed, there is one more degree of freedom, the total concentration of copper in the glass.

Douglas⁴³ discussed the thermodynamics of oxidation-reduction reactions in glass and their influence on ionic ratios and colors of ions (see Chapter 17). For example, he showed how the amount of different oxidation states of copper vary with the oxygen pressure, as shown in Fig. 1. At low oxygen pressure (concentration in the glass), copper metal is present and its solubility determines the concentration of dissolved copper atoms, which is independent of the oxygen concentration. Above a certain oxygen concentration, the concentration of dissolved copper atoms begins to decrease, and there is no copper metal present; the amount of monovalent copper increases to a maximum and then decreases. At high oxygen pressure, only divalent copper is present in appreciable amounts.

In discussing the oxidation state of a glass and other chemical properties, the concept of acidic or basic constituents is often used.^{45,45a} The glass-forming oxides such as silica and boric oxide are considered to be acidic, and the alkali and alkaline earth oxides basic. This designation can be justified in the "Lewis acid" sense from the negative charge on the glass-forming groups (SiO^-) that results from the reaction with a metal oxide, making the silica an electron

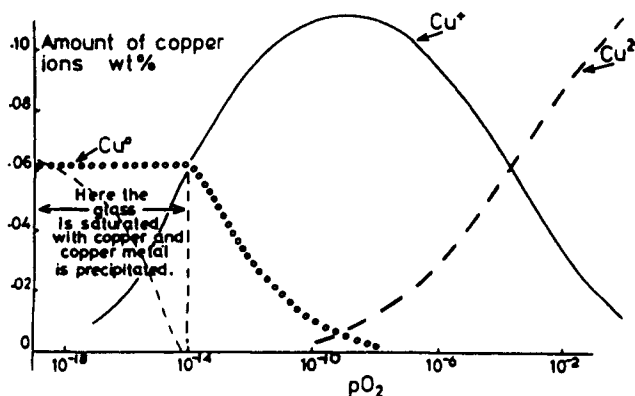
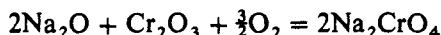


Fig. 1 The amount of copper in different oxidation states as a function of log oxygen pressure at 1000°C in a $0.3\text{Na}_2 \cdot 0.7\text{B}_2\text{O}_3$ glass with 0.124 wt% copper. From Ref. 43.

acceptor and the metallic cation an electron donor. Also when the glass-forming oxides are dissolved in water they form very weak acids, whereas the alkali and alkaline-earth oxides form strong bases. For oxides with higher valent cations, such as those of transition and refractory metals (TiO_2 , Ta_2O_5 , Nb_2O_5) the acid-base designation is not so clear. In acid-base terms the increase in ability to oxidize with increasing alkali concentration is considered to result from the increased basicity of the glass. A reaction such as



can be considered to result in the formation of chromate ion in the glass, and is enhanced by increasing the alkali concentration. It is not clear how a group such as Na_2CrO_4 is incorporated into the network structure of the glass.

Let us now consider the situation in which there are two different ions in the glass with two valence states. As an example consider iron (Eq. 3) and cesium:

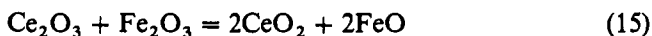


For pure oxides there are now five phases present (FeO , Fe_2O_3 , Ce_2O_3 , CeO_2 and oxygen gas) and three components, giving zero degrees of freedom. This result means that there is only one temperature and oxygen pressure at which both Eqs. 3 and 13 are at equilibrium; this condition is determined by the intersection of the lines for these two reactions on the Ellingham diagram.

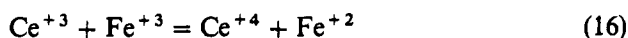
If these four ion species are dissolved in the glass, there are two phases and four components, giving four degrees of freedom. Two of these are normally the total amount of cesium and iron in the glass. If the temperature and oxygen pressure are fixed, the ratios of the two valent states of the two ions are independently determined by Eqs. 5 and 14:

$$K_{13} = \frac{[\text{CeO}_2]^4}{[\text{Ce}_2\text{O}_3]^2 P} \quad (14)$$

This conclusion is only valid if there is equilibrium between the melt oxygen concentration and the gas phase. As described above, this is rarely the case even at glass melting temperatures. If the glass is cooled to some intermediate temperature, for example 500°C , the oxygen concentration in the glass will be fixed by the melt condition ("frozen in"), and will not be in equilibrium with the gas phase. In this situation, the oxygen concentration in the glass will change as the ions in it are oxidized and reduced. The final oxygen concentration will depend upon the initial conditions from the glass melt, such as the amounts of the ions in different oxidation states, and cannot be predicted from thermodynamics. The oxidation-reduction reactions can be combined into one reaction by eliminating oxygen from Eqs. 3 and 13:



or



The equilibrium constant of the last equation is

$$K_{16} = \frac{[\text{Ce}^{+4}] [\text{Fe}^{+2}]}{[\text{Ce}^{+3}] [\text{Fe}^{+3}]} \quad (17)$$

Thus the ratios of the different states are interrelated, but their absolute values depend upon the actual oxygen concentration in the melt.

At lower temperatures still (for example, room temperature), the diffusion of oxygen is too slow to achieve equilibrium even between neighboring ions, and their oxidation states are determined by conditions at higher temperatures and quenching rates.

The relative ability to oxidize various ions in glass was calculated by Tress from thermodynamic data of the free oxides.⁴⁴ He found the order given in Table 1. Thus, of the pairs shown, chromium is the most easily reduced, and tin is the most easily oxidized.

Oxidation-reduction reactions in glass were discussed by Paul⁴⁵ and Schrieber^{45a} in somewhat different ways.

NITROGEN

Nitrogen can react with glass melted under reducing conditions, forming three Si-N bonds.^{46,47} In the presence of water or ammonia, N-H bonds are formed, as demonstrated by the 3- μm infrared absorption band. The solubility of nitrogen increases with temperature, but decreases as the amount of alkali in the glass increases.^{48,49} From an oxidation-reduction point of view this result is consistent with the finding of more reducing glasses as the silica content increases, and perhaps weakens the above explanations in terms of silicon-oxygen bond strengths.

Nitrogen can be incorporated in multicomponent silicate glasses, as reviewed in detail by Loehman.⁵⁰ The nitrogen increases the stiffness, viscosity, and chemical durability of the glass.⁵⁰⁻⁵²

TABLE 1 Oxidizing Tendency of Ions in Glass

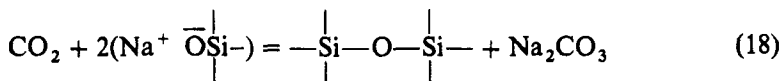
$\text{CrO}_3 = \text{Cr}_2\text{O}_3$
$\text{Mn}_2\text{O}_3 = \text{MnO}$
$\text{CeO}_2 = \text{Ce}_2\text{O}_3$
$\text{As}_2\text{O}_3 = \text{As}_2\text{O}_5$
$\text{Sb}_2\text{O}_3 = \text{Sb}_2\text{O}_5$
$\text{Fe}_2\text{O}_3 = \text{FeO}$
$\text{SnO}_2 = \text{SnO}$

The incorporation of nitrogen in B_2O_3 , $B_2O_3-SiO_2$ and B_2O_3-CaO glasses was studied;⁵³ the nitrogen substituted for oxygen in the borate-oxygen network and also dissolved molecularly in these glasses.

CARBON DIOXIDE

The solubility of carbon dioxide in sodium silicate glasses was found to increase rapidly below about 1100 or 1200°C, depending on the composition.^{54,55} Above these temperatures, the solubility did not change as much with temperature, and for several glasses was about 10^{-4} wt%/atm, which is roughly the amount of physical solubility expected. The logarithm of the solubility in wt% was linear with reciprocal temperature; the enthalpy of solution ΔH in binary alkali silicates ΔH was about -56 kcal/mol.⁵⁴

One possible way to write the reaction of carbon dioxide with a sodium silicate glass is



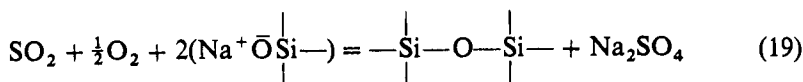
The entity formed in the glass is probably not a simple sodium carbonate molecule, but some more complex combination of these ions with the silicate lattice. Strnad⁵⁶ found that the solubility of carbon dioxide in a 30.3 mol% Na_2O , 69.7% SiO_2 melt was proportional to pressure below atmospheric pressure and at 1000°C was consistent with reaction 18. Both Pearce and Strnad found a large increase in solubility of carbon dioxide as the amount of Na_2O in the melt increased above 25%. The increase for melts above 35% Na_2O was much greater than proportional to the square of the Na_2O composition, as would be expected from reaction 18. Apparently in melts of higher Na_2O , the Na_2O activity increases sharply. This increase can also be deduced from the sharp increase in the volatility of soda in these melts.⁵⁷

Pearce also measured the reaction of carbon dioxide with sodium borate melts and found a similar increase in solubility as the temperature decreased; however, the enthalpy of solution was considerably lower than for the silicates. More recent studies of carbon dioxide in alkali borates are discussed in Ref. 59.

SULFUR DIOXIDE

Sulfur dioxide also dissolves in silicate melts. Its reaction to an alkali sulfate is complicated by the need for oxygen to form the sulfate from sulfur dioxide. Thus its solubility in alkali silicates increases as the alkali concentration increases,^{54,60-62} and decreases as the temperature increases; however, under

reducing conditions the solubility is much reduced. The reaction with alkali silcate can be written as



It has long been known that furnace gases are beneficial for the weathering properties of glass. These effects arise from the reaction of sulfur dioxide in the gases with the glass surface. Water and oxygen, as well as sulfur dioxide, must be present and the overall reaction can be written as



This "dealkalization" reaction is an ion exchange that is made possible by the removal of the sodium ion as sodium sulfate, as confirmed by Douglas and Isard.⁶³ They found that the rate of formation of sodium sulfate was proportional to the square root of time, and was controlled by the interdiffusion of hydrogen and sodium ions in the glass. The rate of weathering of a glass with a dealkalized layer is less because weathering requires ion exchange with sodium ions.

FINING

Fining, or the removal of bubbles from a glass melt, is one of the major technological problems in glass melting. It is usually solved by holding the glass for some time at a temperature somewhat below the highest melting temperature, and by adding certain minor constituents to the original glass batch. The mechanisms by which these additions aid bubble removal are discussed below.

Bubbles can be removed from a melt by either of two ways. They can rise to the surface or the gas in them can dissolve in the glass. The rate of rise is given by the following equation:

$$\frac{dh}{dt} = \frac{2\rho g R^2}{9\eta} \quad (20)$$

where ρ is the density of the glass, g is the gravitational constant, R is the bubble radius, and η is the viscosity of the glass. For a viscosity of 100 P, typical for melting temperatures, the rate of rise of bubbles 0.1 mm in diameter is about 10 cm/day, which is too small to eliminate them from a normal glass furnace. Thus small bubbles can be removed from glass melts only by dissolution of their gas into the glass melt, although larger bubbles can rise to the surface.

Arsenic oxide is a common fining agent added to glass to help remove bubbles. For many years it was thought that the arsenic released oxygen at

glass melting temperatures, which "swept out" the bubbles in the glass. However, the calculation above shows that such a mechanism would not eliminate small bubbles, and the elegant experiments of Greene and co-workers showed that arsenic enhances dissolution of oxygen bubbles in glass.⁶⁴⁻⁶⁶ Thus the importance of arsenic and antimony oxide additions to the glass is to aid in removal of fine bubbles, rather than to generate more gas.

The mechanism by which these agents enhance dissolution of gas from fine bubbles is still being debated. I suggested that the role of arsenic is to reduce the oxygen concentration in the glass.⁶⁷ At low temperatures arsenic oxide contains mostly pentavalent arsenic, but at higher temperature the As_2O_5 decomposes to As_2O_3 and oxygen. Thus a considerable portion of arsenic ion in glass is in the trivalent state, as has been confirmed by chemical analysis.^{68,69} This trivalent arsenic can react with oxygen physically dissolved in the glass, reducing its concentration and increasing the rate of oxygen diffusion into the glass. This hypothesis is confirmed by an analysis of the results of Greene and co-workers on the rate of shrinking of oxygen bubbles in different glasses. As the amount of arsenic in the glass increased, the amount of oxygen initially dissolved in the glass was reduced, and the rate of shrinking of the bubbles increased.⁶⁷ Thus in the case of oxygen bubbles the role of arsenic and antimony fining agents is to reduce the amount of oxygen dissolved in the glass.

In actual glass-melting practice, carbonates are the usual source of sodium and calcium oxides. Thus one would expect to find carbon dioxide in bubbles in glass as well as oxygen and nitrogen from air. A number of analyses of bubbles in glasses made from carbonates showed that these three are indeed the main gases found in the bubbles.^{70,71} The value of arsenic for dissolving oxygen from the bubbles is clear from the remarks above, but the elimination of the other two gases requires further consideration.

Cable et al. showed that the addition of arsenic to a glass batch increases the rate at which carbon dioxide diffuses out of bubbles at 1200°C in a soda-lime (73.5 wt% SiO_2 , 16.5% Na_2O , 10.0% CaO) glass.⁷² The solubility of carbon dioxide in this base glass is probably small, judging from results cited in the preceding section that show a decrease in solubility as the soda concentration decreases. Since it was shown by Greene's work that the arsenic in the glass lowered the concentration of oxygen in the glass, it is reasonable to relate this lowered oxidation state to the enhanced solubility of carbon dioxide. The decomposition of carbon dioxide to oxygen and carbon monoxide can be written as

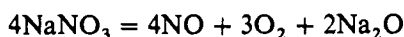


A decrease in the oxygen concentration or oxidation state of the glass would favor this decomposition. The smaller carbon monoxide molecule should diffuse more rapidly in the glass than carbon dioxide, so decomposing dissolved carbon dioxide should increase its rate of absorption from bubbles.

This hypothesis for the increase in rate of absorption of carbon dioxide by arsenic is speculative and needs confirmation with further experiments.

Fining by arsenic and antimony is improved if some of the alkali carbonates in the glass batch are replaced by nitrates. To explain this result it has been assumed that trivalent arsenic or antimony oxides react with the nitrate to form pentavalent oxides, which then release their oxygen at the glass-melting temperature to form larger bubbles. As mentioned above this mechanism is unlikely; furthermore, this reaction of these oxides with nitrates under the conditions of glass manufacture is improbable. Potassium and sodium nitrates decompose completely to the oxides between about 400 and 800°C, whereas in this same temperature range the arsenic and antimony oxides are in the pentavalent states as the result of reaction with oxygen.^{73,74} It is only above 900°C that the pentavalent compounds begin to decompose. Thus at no temperature above 500°C are the nitrates and trivalent oxides in the glass batch together.

The role of the added nitrates is probably to increase the amount of oxygen in the bubbles at the expense of nitrogen. The nitrates decompose before the glass becomes molten,



increasing the proportion of oxygen in the mixed batch materials and consequently in the bubbles of entrapped gas. Therefore it is suggested that arsenic and antimony increase the rate of fining in glass by decreasing the concentration of oxygen dissolved in the glass, which leads to increased rates of absorption of oxygen and carbon dioxide. Nitrates in the glass batch improve fining rates by replacing nitrogen in entrapped gas by oxygen.

Sulfates are often used as fining agents. Lyle showed that in soda-lime glasses, sulfate additions could either speed or retard fining, depending on the composition of the glass.⁷⁵ He found that when the ratio of soda to silica was greater than $0.45 + 0.20/W_s$, where W_s is the weight fraction of silica, fining was retarded, whereas for lower ratios it was enhanced, at least for silica concentrations from 69 to 76%. A very similar effect of soda-to-silica ratio was found on the color produced by carbon and sulfur in soda-lime silicate glasses. For production of a stable amber color, the soda-to-silica ratio had to be less than $0.5 + 0.22/W_s$; with a greater ratio the amber color was not stable and the glasses became blue-green.⁷⁶ Furthermore, it was found that bubbles in stable amber glasses were removed quickly, whereas the blue-green glasses foamed for a long time at 1475°C. These effects of composition are mainly related to the oxidation state of the glass.

Effects of composition on the oxidation state of glasses containing sulfur have been studied in detail in connection with the stability of the amber color.⁷⁷ This color is stable in equilibrium with a partial pressure of oxygen between about 10^{-10} and 10^{-8} atm.⁷⁸ The coloring group is ferric iron in tetrahedral coordination with one of the surrounding oxygen ions replaced by

sulfur.⁷⁹ As the concentration of soda in a soda-lime glass was increased, the glass became more oxidizing, and the optical absorption by the ferric sulfide group decreased, indicating a decreased concentration of these groups.⁷⁷

The presence of sulfide in the more reducing glasses means it can react with oxygen and carbon dioxide from bubbles and therefore enhance their removal from the bubbles.⁸⁰ Harding and Ryder found that an increase in the sulfate level in a soda-lime glass reduced the retention of nitrogen.⁸¹ However, when the sulfate was replaced by sulfide (more reducing conditions) nitrogen retention increased, again showing the effect of state of oxidation of the glass on reaction of nitrogen with it, and indicating that sulfide also helps to remove nitrogen from bubbles.

There are reviews of refining in glass in Refs. 82 and 83.

REFERENCES

1. R. V. Adams and R. W. Douglas, *J. Soc. Glass Technol.*, **43**, 147 (1959).
2. V. Garino-Canina, C. R., **239**, 705 (1954).
3. H. Scholze, *Glastech. Ber.*, **32**, 81, 142, 278 (1959).
4. V. Garino-Canina and M. Priqueler, *Phys. Chem. Glasses*, **3**, 43 (1962).
5. R. H. Doremus, in *Reactivity of Solids*, J. W. Mitchell, R. C. DeVries, R. W. Roberts, and P. Cannon, Eds., Wiley-Interscience, New York, 1969, p. 667.
6. A. J. Moulson and J. P. Roberts, *Trans. Faraday Soc.*, **57**, 1208 (1961).
7. T. Drury and J. P. Roberts, *Phys. Chem. Glasses*, **4**, 79 (1963).
8. G. J. Roberts and J. P. Roberts, *Phys. Chem. Glasses*, **5**, 26 (1964).
9. G. Hetherington and K. H. Jack, *Phys. Chem. Glasses*, **3**, 129 (1962).
10. H. Franz and H. Scholze, *Glastech. Ber.*, **36**, 347 (1963).
- 10a. J. Götz, *Glastech. Ber.*, **45**, 14 (1972).
11. H. Franz, *Glastech. Ber.*, **38**, 54 (1965).
12. R. Bruckner, *Glastech. Ber.*, **37**, 536 (1964).
13. P. W. McMillan and A. Chlebik, *J. Noncryst. Solids*, **38/39**, 509 (1980).
14. R. F. Bartholomew, in *Treatise on Materials Science and Technology*, Vol. 22, M. Tomozawa and R. H. Doremus, Eds., Academic Press, San Diego, CA, 1982, p. 75.
15. M. Tomozawa, *J. Noncryst. Solids*, **73**, 197 (1985).
16. H. Scholze, *Glass-Nature, Structure and Properties*, Springer-Verlag, Berlin, 1991.
17. J. M. Jewell, M. S. Shess, and J. E. Shelby, *J. Am. Ceram. Soc.*, **73**, 132 (1990).
18. S. D. Stookey, U.S. Patent 3,915,720 (1970).
19. F. M. Ernsberger, *J. Am. Ceram. Soc.*, **60**, 91 (1977).
20. T. Bell, G. Hetherington, and K. H. Jack, *Phys. Chem. Glasses*, **3**, 141 (1962).
21. R. W. Lee, *J. Chem. Phys.*, **38**, 448 (1963).
22. S. P. Faile and D. M. Roy, *Mater. Res. Bull.*, **5**, 385 (1970); *J. Am. Ceram. Soc.*, **54**, 533 (1971).
23. K. H. Beckman and N. J. Harrick, *J. Electrochem. Soc.*, **118**, 614 (1971).

24. R. H. Doremus, *J. Electrochem. Soc.*, **115**, 181 (1968).
25. R. H. Doremus, in *Symp. on Nucleation and Crystallization in Glasses and Melts*, American Ceramic Society, Columbus, OH, 1962, p. 119.
26. R. Zsigmady, *Dingler's Polytech. J.*, **226**, 364 (1887); **306**, 68, 91 (1897); *Sprechsaal*, **27**, 123, 147, 175, 201, 227 (1894).
27. A. W. Bastress, *J. Am. Ceram. Soc.*, **30**, 52 (1947).
28. J. T. Randall and R. E. Leeds, *J. Soc. Glass Technol.*, **13**, 16T (1929).
29. R. L. Green and K. B. Blodgett, *J. Am. Ceram. Soc.*, **31**, 89 (1948).
30. J. L. Barton and M. Morain, *J. Noncryst. Solids*, **3**, 115 (1970).
31. E. A. Weaver, K. W. Heckman, and E. L. Williams, *J. Chem. Phys.*, **47**, 4891 (1967).
32. K. Awaza, H. Kawazoe, and M. Yamane, *J. Appl. Phys.*, **68**, 2713 (1990).
33. F. T. Wall, *Chemical Thermodynamics*, San Francisco, CA, 1974, p. 219.
34. F. J. Norton, *Nature*, **191**, 701 (1961).
35. D. D. Wagman et al., *The NBS Tables of Chemical Thermodynamic Properties*, American Institute of Physics, New York, 1982.
36. R. A. Swalin, *Thermodynamics of Solids*, Wiley, New York, 1972, p. 116.
37. C. H. P. Lupis, *Chemical Thermodynamics of Materials*, North-Holland, Amsterdam, 1983, p. 134.
38. F. Irrmann, *J. Am. Chem. Soc.*, **74**, 4767 (1952).
39. E. J. Michal and R. Schuhmann, *J. Met.*, **4**, 723 (1952).
40. W. D. Johnston, *J. Am. Ceram. Soc.*, **48**, 184 (1965).
41. P. North and R. W. Douglas, *Phys. Chem. Glasses*, **6**, 197 (1965).
42. A. Paul and R. W. Douglas, *Phys. Chem. Glasses*, **6**, 207, 212 (1965).
43. R. W. Douglas, *10th Int. Congress on Glass*, The Ceramic Society of Japan, 1974, pp. 1-45 to 1-70.
44. H. J. Tress, *Phys. Chem. Glasses*, **1**, 196 (1960).
45. A. Paul, *Chemistry of Glasses*, Chapman and Hall, London, 1982, p. 148ff; *J. Noncryst. Solids*, **123**, 354 (1990).
- 45a. H. D. Schrieber, *J. Noncryst. Solids*, **84**, 129 (1986).
46. H. O. Mulfinger and H. Meyer, *Glastech. Ber.*, **36**, 481 (1963).
47. H. O. Mulfinger and H. Franz, *Glastech. Ber.*, **38**, 235 (1965).
48. J. Kelen and H. O. Mulfinger, *Glastech. Ber.*, **41**, 230 (1968).
49. E. L. Swarts, *J. Can. Ceram. Soc.*, **38**, 155 (1969).
50. R. E. Loehman, in *Treatise on Materials Science and Technology*, Vol 26, M. Tomozawa and R. H. Doremus, Eds., Academic Press, San Diego, CA, 1985, p. 119.
51. D. R. Messier, *Rev. Chem. Miner.*, **22**, 518 (1985).
52. M. Rajaram and D. E. Day, *J. Am. Ceram. Soc.*, **70**, 203 (1987).
53. T. Wakasugi, F. Tsukihashi, and N. Sano, *J. Am. Ceram. Soc.*, **74**, 1650 (1991).
54. M. L. Pearce, *J. Am. Ceram. Soc.*, **47**, 342 (1964).
55. C. Kroger and D. Lummerzheim, *Glastech. Ber.*, **38**, 229 (1965).
56. Z. Strnad, *Phys. Chem. Glasses*, **12**, 152 (1971).
57. E. Preston and W. E. S. Turner, *J. Soc. Glass. Technol.*, **18**, 143 (1934).

58. M. L. Pearce, *J. Am. Ceram. Soc.*, **48**, 175 (1965).
59. H. Zhang, S. Koritaka, K. Farooqui, R. Boekenhauer, D. Bain, S. Kambeyanda, and S. Feller, *J. Phys. Chem. Glasses*, **32**, 185 (1991).
60. C. J. B. Fincham and F. D. Richardson, *Proc. Roy. Soc.*, **A223**, 40 (1954).
61. E. T. Turkdogan and M. L. Pearce, *Trans. AIME*, **227**, 940 (1963).
62. H. Meier Zu Kocker and D. Chandra, *Glastech. Ber.*, **45**, 139 (1972).
63. R. W. Douglas and J. O. Isard, *J. Soc. Glass. Technol.*, **33**, 289T (1949).
64. C. H. Greene and R. F. Gaffney, *J. Am. Ceram. Soc.*, **42**, 271 (1959).
65. C. H. Greene and J. Kitano, *Glastech. Ber.*, **32K**, 44 (1959).
66. C. H. Greene and H. A. Lee, *J. Am. Ceram. Soc.*, **48**, 528 (1965).
67. R. H. Doremus, *J. Am. Ceram. Soc.*, **43**, 655 (1960).
68. E. M. Firth, F. W. Hodkin, and W. E. S. Turner, *J. Soc. Glass. Technol.*, **10**, 3T (1926); **11**, 190T (1927).
69. C. Kuhl, H. Rudow, and W. Weyl, *Glastech. Ber.*, **16**, 37 (1938).
70. V. T. Slavyanskii, *Gases in Glass*, Moscow, 1957.
71. M. Cable and M. A. Haroon, *Glass Technol.*, **11**, 48 (1970).
72. M. Cable, A. R. Clarke, and M. A. Haroon, *Glass Technol.*, **9**, 101 (1968); **10**, 15 (1969).
73. *Gmelin Handbuch der Anorganischen Chemie: Antimon*, System No. 18, Part B, Gmelin-Verlag GmbH., Clausthal-Zellerfeld, 1949, pp. 360–378.
74. *Gmelin Handbuch der Anorganischen Chemie: Arsen*, System No. 17, Verlag Chemie GmbH., Weinheim/Bergstrasse, 1952, pp. 258–276.
75. A. K. Lyle, in *Travaux du IV Congres Int. du Verre*, Imprimerie Chaix, 20, rue Bergere, Paris, 1957, p. 93.
76. A. K. Lyle, *J. Am. Ceram. Soc.*, **33**, 300 (1950).
77. F. L. Harding, *Glass Technol.*, **13**, 43 (1972); *J. Am. Ceram. Soc.*, **55**, 368 (1972).
78. D. Brown and R. W. Douglas, *Glass Technol.*, **6**, 190 (1965).
79. R. W. Douglas and M. S. Zaman, *Phys. Chem. Glasses*, **10**, 125 (1969).
80. C. H. Greene and D. R. Platts, *J. Am. Ceram. Soc.*, **52**, 106 (1969).
81. F. L. Harding and R. J. Ryder, *Glass Technol.*, **11**, 54 (1970).
82. *Symp. sur L'Affinage du Verre*, Union Scientifique Continentale du Verre, Charleroi, Belgium, 1956.
83. E. L. Swartz, in *Encyclopedia of Materials Science and Engineering*, Vol. 3, M. B. Bever, Ed., Pergamon, Oxford, 1986, p. 1768ff.

CHEMICAL DURABILITY: REACTION OF WATER WITH GLASS

INTRODUCTION

Silicate glasses are among the most chemically inert of commercial materials. They react with almost no liquids or gases at low (below $\sim 300^{\circ}\text{C}$) temperatures except hydrofluoric acid solutions and slightly with water. At high temperatures, above about 1200°C , there is also some reaction with strong reducing agents such as hydrogen or graphite. As a result of its durability, glass is useful as a container for corrosive fluids, as a liner for chemical reactors, as an electrical insulator, and in buildings and automobiles. In the last two decades glass has been introduced for encapsulating radioactive waste in a highly durable matrix. This use has led to a large number of studies of the reaction of glass with water and aqueous solutions, which are its potential corrosive agents in storage.

Because of its chemical inertness, the chemical durability of glasses is concerned almost entirely with their reactivity with liquid water, aqueous solutions, and water vapor, all of which are extremely slow. Thus this chapter is concerned with the reaction of water with glass. Reviews of early literature, especially from the viewpoint of practical applications of glass, are in Refs. 1–3. More emphasis on interpretation and chemistry of the reaction of glass with water are reviewed in Refs. 4–6.

A series of different processes can take place when liquid water reacts with glass. Among those well established experimentally are:

1. Dissolution of the glass into the water with the concentration ratios in the dry glass (congruent dissolution).

2. Ion exchange between alkali, and to some extent alkaline earth, ions in the glass with hydrogen-bearing ions from the water.
3. Diffusion of molecular water into the glass.
4. Formation of layers of reaction products on the glass surface. Included are preferential adsorption or precipitation of glass or solution constituents onto the glass surface or into a surface layer.
5. Reaction of water with the silicon-oxygen network (see Chapters 8 and 12).

In contact with water vapor processes 2–5 are possible.

The relative importance of these processes depends upon factors such as temperature, solution composition, especially pH, and glass composition. One goal of this discussion is to clarify conditions under which these various processes are significant.

The reaction of water with glass has been studied in a variety of ways. Many new techniques for probing the composition and structure of the glass surface layers have been developed. These methods and techniques are first reviewed below. Then some selected experimental results are reviewed; results that elucidate mechanisms and factors in them are emphasized. Finally interpretations and mechanisms are discussed. The emphasis is on silicate glasses because of their commercial importance and because they have been most studied; a few results on the new zirconium fluoride glasses are included.

MEASURING METHODS

The traditional way to study the chemical durability of glass was to immerse a glass powder in water or aqueous solution and measure its weight change with time. Weight change of bulk glass is still a convenient method, and can give valuable information on dissolution rates.⁷ If surface precipitates form, this method is less useful. Next, chemical analysis of the solution for glass constituents was adopted.⁸ This analysis gives information on processes such as preferential leaching and solution conditions. More recently a variety of methods for observing, analyzing and measuring profiles in glass surfaces have been developed. The most useful of these are described briefly.

There are different methods of reacting glass with liquid water and aqueous solutions. To keep solution conditions constant, dilute solutions have been used, and the amount of glass dissolved limited, so solution concentrations remain low. The solution pH can be held constant with buffers, the solutions refluxed (S Soxhlet extractor), or solution flowed through glass powder. In other experiments, the solution conditions have changed during the experiment ("static" test). Interpretation of this kind of test is difficult because solution conditions can change in complex ways; for example, the solution pH can rise to a maximum and decrease,⁹ as shown in Fig. 1. One reason for preferring static tests (or a flow test) may have been that they model the corrosion in

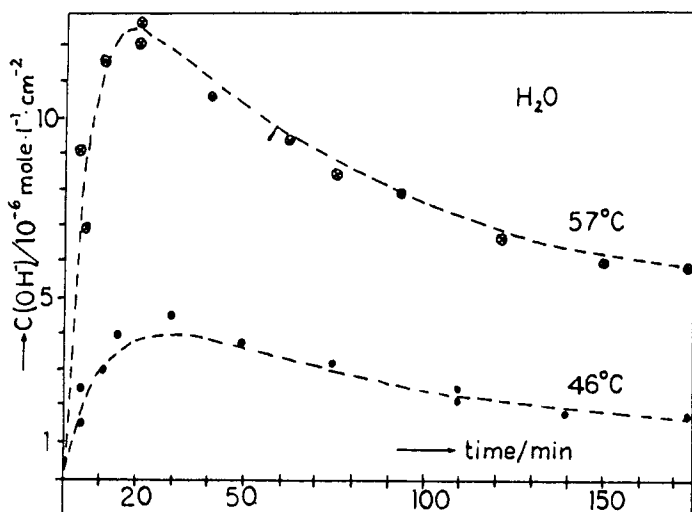


Fig. 1 Hydroxyl ion concentration as a function of time in water for 015 soda-lime silicate glass. Reprinted from Ref. 9 with permission from Elsevier.

natural conditions; this modeling is rarely reliable, however, because natural conditions vary so widely with location and time. In this chapter results with constant solution conditions are emphasized, because their interpretation is much more straightforward than for static tests.

Light and electron microscopy are valuable tools for revealing the morphology of a glass surface after it has reacted with water. An example is in Fig. 2, which shows crystals of zirconium fluoride that grew on the surface of a zirconium-barium fluoride glass in water.¹⁰

Several different methods are available to measure profiles of constituents in a glass surface. The glass can be etched with hydrofluoric acid solution and the solution analyzed.^{11,12} Non-destructive methods to a depth of about 1 μm are analysis by Rutherford backscattering (RBS) or nuclear reactions.^{13,14} In RBS the sample surface is bombarded with 2 MeV helium ions, and the energy of the backscattered ions measured; since the collisions with atoms in the glass are elastic, the absolute concentrations as a function of depth below the surface can be calculated from spectra such as that in Fig. 3. Each different atom in the glass shows an "edge" in the spectrum. This method is especially useful for heavy atoms; the spike for implanted xenon atoms is clearly shown in the figure. Resonant nuclear reactions are useful for analyzing particular atoms, especially hydrogen. If the sample is bombarded with ^{15}N ions, the reaction $^{15}\text{N} + ^1\text{H} = ^{12}\text{C} + ^4\text{H}$ emits 4.4 MeV gamma rays, and their yield is measured. Because there is a narrow isolated resonance with a large peak cross-section, this reaction will occur only when the ^{15}N ions are at the resonance energy of 6.405 MeV. If the sample is bombarded with ions of this energy, the yield of gamma rays is proportional to hydrogen on the sample surface. As the beam

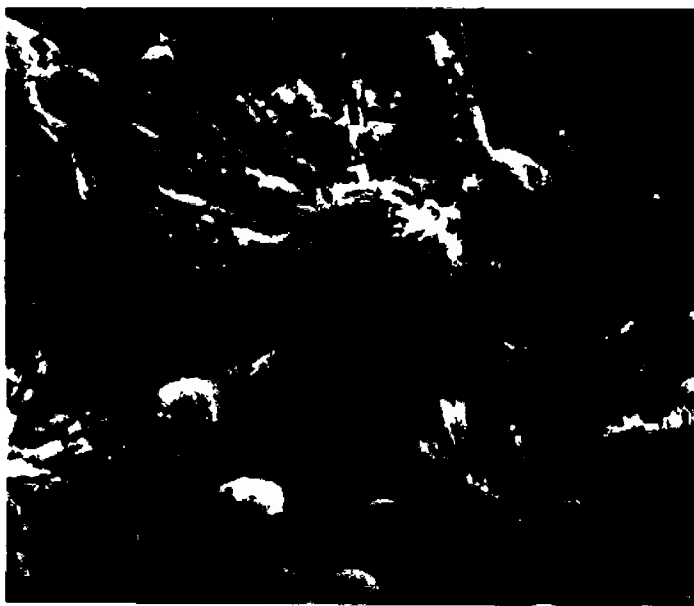


Fig. 2 Scanning electron micrograph of the surface of a Zr-Ba-La fluoride glass after 30 min in water at 25°C. 300 \times . Reprinted from Ref. 10 with permission from Chapman and Hall.

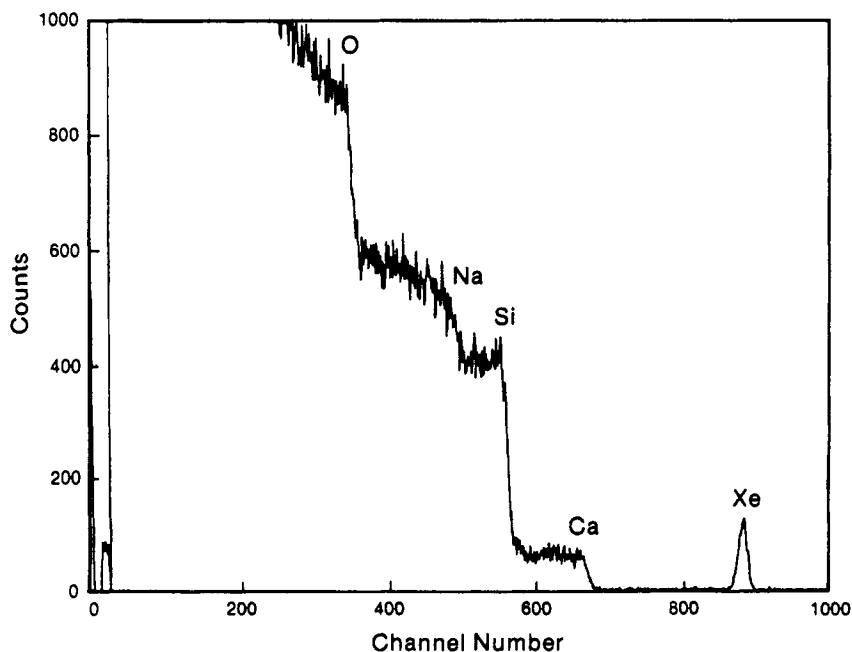


Fig. 3 Rutherford backscattering spectrum of R-6 soda-lime silicate glass after it was implanted with xenon ions, which have the spike on the right. Reprinted from Ref. 34 with permission from the American Ceramic Soc.

energy is raised, the ^{15}N ions penetrate into the sample and lose energy until their energy is 6.405 MeV, when they react with the hydrogen at this depth, which can be calculated from the density of glass constituents.

If the sample surface is sputtered away, the surface can be analyzed with secondary ion mass spectrometry (SIMS).^{15,16} This method has high sensitivity and can be used for light elements including hydrogen. A disadvantage is that the absolute concentration cannot be determined, only relative values. Profiles can also be determined on sputtered surface by spectrochemical analysis.¹⁷ Other methods of surface analysis are reviewed in Ref. 15.

Special care is needed to obtain reliable analysis of hydrogen in a glass surface. Water can outgas rapidly from a glass surface even at room temperature, especially if the surface has been "transformed" to a more open structure (see section on ion exchange below). To obtain a reliable hydrogen profile, that is, one characteristic of the profile while the glass is in water, the glass with a transformed layer must be cooled rapidly to well below 0°C , held at this temperature, and measured at this temperature.¹⁸ In Fig. 4 the profile of hydrogen in a soda-lime glass (015, see Table 1 for composition) after cooling rapidly, held at low temperature, and measured at low temperature is compared with the same glass after it was held in the vacuum system at room temperature. More than half of the hydrogen was removed by this treatment. The hydrogen level of 2.7×10^{-20} atoms/ cm^3 is about three times the

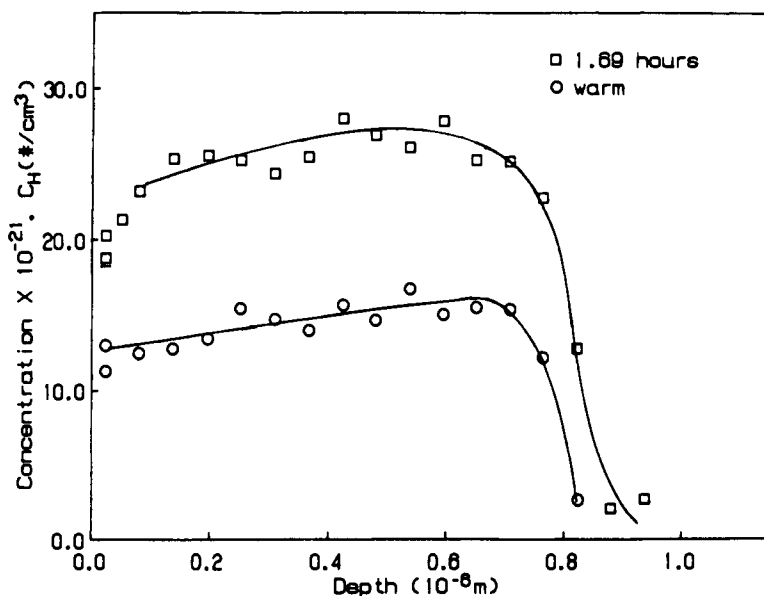


Fig. 4 Hydrogen concentration profiles in 015 soda-lime silicate glass, hydrated 1.69 h at 80°C , chilled, and measured chilled (\square); then held for 12 h in a vacuum at 25°C (\circ). Reprinted from Ref. 18 with permission from Elsevier.

concentration of sodium leached from this glass of 9.8×10^{-21} atoms/cm³.¹⁸ After the chilled sample was held in ambient air at 25°C for 1 week, the hydrogen level decreased to 2.2×10^{-20} atoms/cm³. These results show that most of the measurements of hydrogen profiles in silicate glasses reported in the literature are not reliable and are low because of outgassing of water. In certain durable compositions such as commercial soda lime glasses, it is not necessary to chill the glass to obtain reliable results, because outgassing of water is much slower in these "untransformed" glasses.¹⁸

EXPERIMENTAL RESULTS

In the next sections selected experimental results on reaction of silicate glasses in water and aqueous solutions are discussed under headings of the list of five different processes given in the introduction. Emphasis is on results in which solution conditions were held constant, because they are easier to interpret.

Ion Exchange

Alkali ions are preferentially leached from multicomponent silicate glasses containing alkali oxides. This leaching was first demonstrated by solution analysis of sodium and silicon.⁸ It has also been demonstrated by analysis of alkalis in the glass surface, which shows a layer of reduced sodium concentration near the glass-solution interface.^{5,7,11-19} An example of profiles of sodium and hydrogen in the surface of a commercial soda-lime glass (see Table 1 glass no. 4, for composition) as measured with resonant nuclear reactions is shown in Fig. 5. The pH of the distilled water used for leaching did not change from neutral (about 6) during the experiment. The concentration of hydrogen to about a depth of $0.3 \mu\text{m}$ was three times that of sodium in the glass. The sum of one-third the hydrogen concentration plus the sodium concentration was constant at the level of sodium in the dry glass. Hydrogen profiles in this glass after different leaching times in water are shown in Fig. 6, and the depths of hydrogen penetration at half the surface concentration are plotted versus the square root of time in Fig. 7. The plot is initially linear, and then the penetration depth becomes constant. The Rutherford backscattering spectra from this glass after leaching¹⁴ showed no evidence for preferential leaching of constituents other than sodium, and no formation of precipitation or layers of other constituents on the glass surface.

The leaching or ion exchange of alkali ions leaves a surface layer on the glass depleted of these ions, as shown in Fig. 5. The structure of this hydrated surface layer is critical in determining the rate of ion exchange and of dissolution of the glass. There is much experimental evidence that the surface layer can have either of two structures.²⁰ In a durable glass such as the commercial soda-lime glass containing 2% alumina, shown in Fig. 5, the

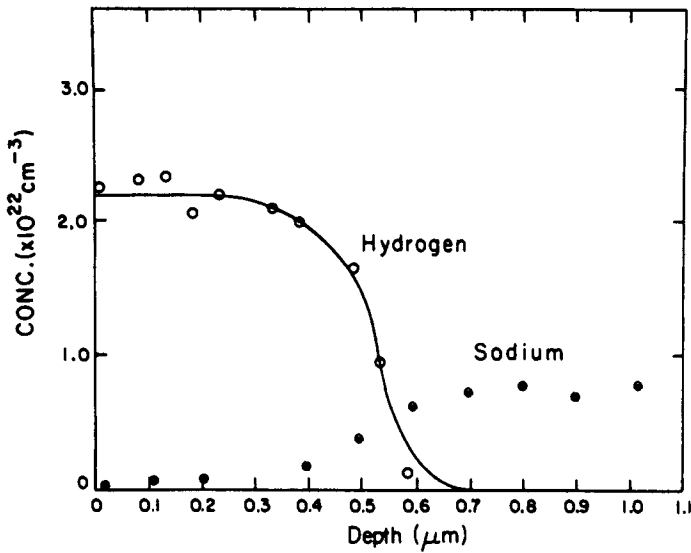


Fig. 5 Hydrogen and sodium concentration profiles in the surface of a commercial soda-lime glass (see Table 1, glass no. 4) held in water at 90°C for 404 h. Measured with resonant nuclear reactions. Reprinted from Ref. 13 with permission from Elsevier.

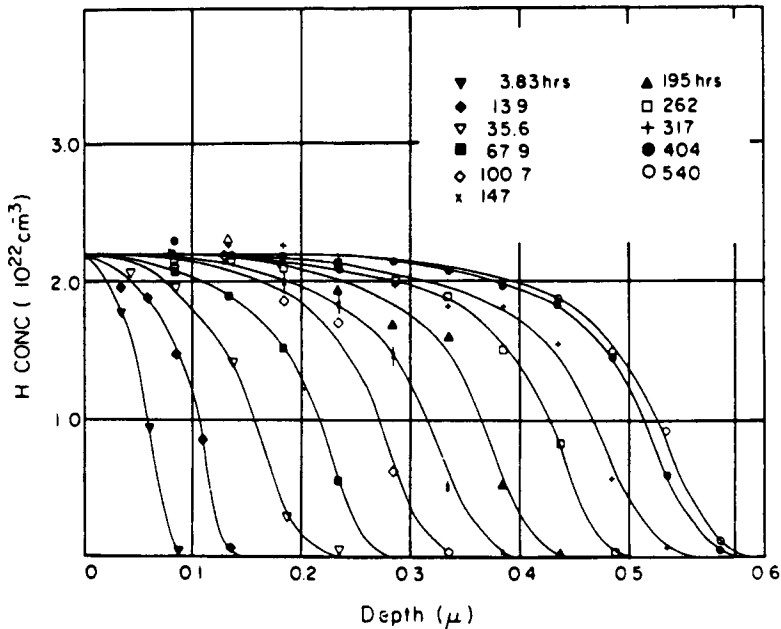


Fig. 6 Hydrogen profiles in a commercial soda-lime glass (no. 4 in Table 1) after hold in water at 90°C for different times, as measured with a resonant nuclear reaction.¹³ Reprinted from Ref. 13 with permission from Elsevier.

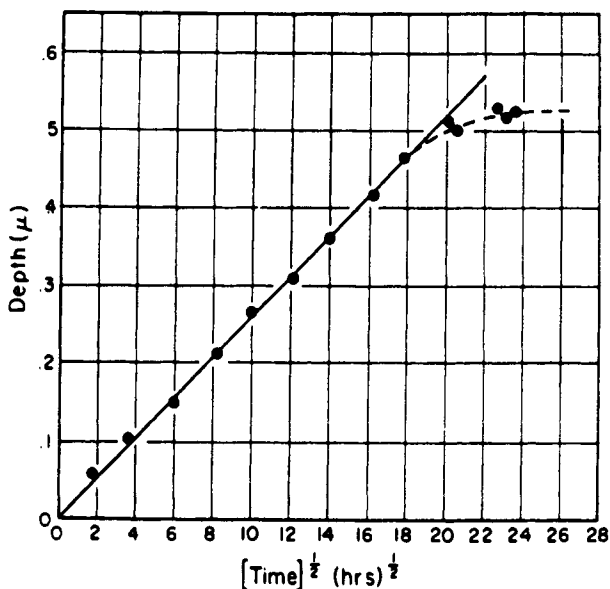


Fig. 7 The depth of hydrogen penetration versus square root time for the data in Fig. 6. Reprinted from Ref. 13 with permission from Elsevier.

silicon-oxygen network retains the configuration it has in the dry glass, and the diffusion in the layer is similar to that in the dry glass. In other less durable silicate glasses, the surface hydrated layer is transformed to a different more open structure in which diffusion is more rapid. Models for this transformation are described below in the interpretations sections. The experimental evidence for two different structures of the hydrated layer is:²⁰

1. Outgassing of water in a transformed layer is much more rapid than in an untransformed layer.^{18,20}
2. Ionic interdiffusion is more rapid in a transformed layer than in an untransformed layer.²⁰
3. The electrical resistance of a transformed hydrated layer is much less than that of an untransformed layer.^{21,22}
4. Infrared transmission spectra in the Si-O stretching region (9–11 μm) show much greater changes in glasses with transformed layers than in glasses without them.²³ Reflection infrared spectra of hydrated glasses with transformed layers also show substantial changes.²⁴
5. The surface of a glass with a transformed layer swells during hydration,^{25,26} whereas a glass with an untransformed layer does not swell.²⁵

Wikby measured the electrical resistance of glass bulbs as they were etched

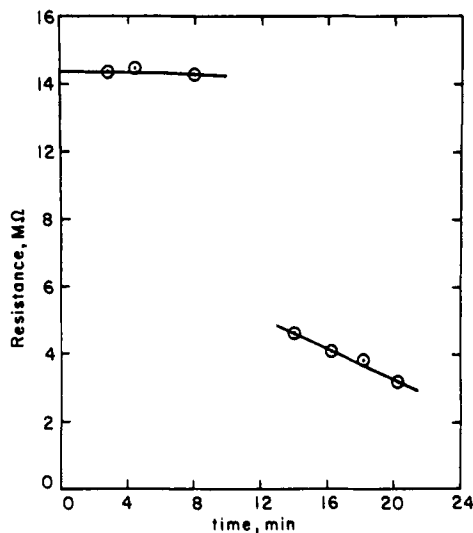


Fig. 8 Electrical resistance of a hydrated bulb of 015 soda-lime glass etched in 0.3% hydrofluoric acid.^{5,21}

with hydrofluoric acid.²¹ He used a pulse technique to avoid electrode polarization, and the glass was so thin that the resistance of the surface layer was an appreciable fraction of the resistance through the glass cross-section. The resistance as a function of etching time is shown in Fig. 8 for 015 soda-lime glass (see Table 1). The nearly constant initial resistance is evidence for rapid ionic motion in the transformed hydrated layer on this glass. Next, is a sharp drop of resistance and then a decrease that corresponds to the dry glass. See the interpretation section for further discussion.

In contrast to these results on a glass with a transformed hydrated layer,

TABLE 1 Composition of Glasses

Glass	Density (g/cm ³)	Composition (wt%)					
		SiO ₂	Na ₂ O	CaO	Al ₂ O ₃	MgO	B ₂ O ₃
Sodium trisilicate	2.44	75	25				
Corning 015 soda-lime	2.49	72	22	6			
PPG soda-lime	2.49	74	13.3	8.3	0.06	3.7	
Kimble R6 soda-lime (U)	2.45	74	12.9	6.8	1.8	4.5	
Pyrex borosilicate (U)	2.23	82	4		2		14
Obsidian ^a (U)	2.36	76	3.6	0.5	13		

^a4.8 wt% K₂O, 0.7 wt% FeO, 0.1 wt% TiO₂.

U, untransformed surface.

electrolysis of thin bulbs of a commercial soda-lime glass (Kimble R-6, Table 1) showed that mobilities in the hydrated layer were the same as in the dry glass,²² demonstrating that the glass network in the hydrated layer had the same structure as in the dry glass.

The infrared absorption bands from stretching, bending, and rocking vibrations of silicon-oxygen bonds in glass no. 6 in Table 1 were little affected by hydration.²³ In Pyrex borosilicate glass (Corning 7740, glass no. 4, Table 1) hydration did not change the positions or intensities of boron-oxygen and silicon-oxygen vibrational bands.²³ On the contrary, vibrational silicon-oxygen bands in a 70% SiO_2 -30% Na_2O glass and in 015 soda-lime glass shift and change intensity after hydration of these glasses. I conclude that the former glasses retain their network structure in the hydrated layer, whereas the hydrated layer in the latter glasses is transformed to a somewhat more open structure, consistent with the other evidence presented here.

The sum of all this evidence strongly supports the interpretation of a structural change in the hydrated layers of less durable silicate glasses and no structural change in these layers on durable glasses.

Measurements of lithium and sodium profiles in a variety of glass compositions show a similar S-shape to that in Fig. 5 (refs. 11, 14, 16, 18, 19, 20, 26-30 and references in these papers). Curiously, profiles of potassium in binary potassium silicate glasses have the shape of more traditional diffusion profiles.^{11,31} Interpretation of these results is given below.

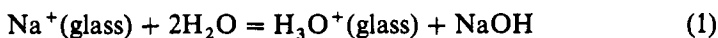
Solution conditions can influence the concentration level of alkali ion at the glass-solution interface. If the pH is basic and there are alkali ions in solution, the amount of alkali in the glass surface increases. Baucke studied the exchange equilibrium between lithium and hydrogen-bearing ions in a lithium silicate glass.³² Ion exchange equilibria in glass are discussed in the next chapter.

The reaction of glass with water vapor in the ambient air, instead of with

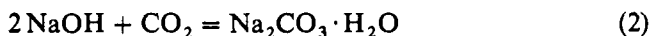
TABLE 2 Major Constituents of Glass for Radioactive Waste

Oxide Component	wt%			
	Swedish ABS	J-10 (Ref. 59)	LWR	DWPF
SiO_2	48.5	38.3	34.8	50.0
B_2O_3	19.1	11.8	12.9	8.0
Na_2O	12.9	20.3	5.5	8.7
CaO	—	6.4	2.0	1.0
Fe_2O_3	5.7	4.1	1.0	10.4
Al_2O_3	3.1	7.4	—	4.0
Waste oxides	10.7	14.0	21.3	—
Other oxides			22.0	17.9

liquid water or aqueous solutions, is called weathering. This reaction involves ion exchange but not congruent dissolution of the glass. The ion exchange can be written as



The form of the hydrogen-bearing species is discussed in the interpretation section. The sodium hydroxide remains on the glass surface, and reacts with ambient carbon dioxide:



The infrared spectra of the surface crystals on hydrated glass show they are sodium carbonate,²³ from absorption bands at 1450cm^{-1} and 230cm^{-1} ; sodium bicarbonate does not absorb at 1450cm^{-1} . An electron micrograph of surface crystals on a hydrated sodium silicate glass is shown in Fig. 9.

Dissolution of Glass in Water

In liquid water and aqueous solutions, silicate glasses dissolve congruently at a constant rate, concurrently with ion exchange and other processes. Since the ion exchange depth is proportional to the square root of time, as shown in Fig. 6, dissolution becomes the dominant process at long times, and is therefore the important process in determining the long-term durability of glass, for example, for encapsulating radioactive waste.

The rate of dissolution of glass can be measured in several different ways. Many workers have analyzed the solution for glass constituents, for example, silica.³³ This method is sometimes reliable, but if there is formation of precipitates or colloids in solution, or deposits or adsorption on the glass surface, it gives misleading results. Weight change is a useful method if there are no deposits on the glass surface.^{7,34} Two other methods involve the glass surface directly.

The first of these requires implantation of a heavy marker ion in the glass before dissolution.^{7,14} Then the depth of these implanted atoms, for example xenon, is measured with Rutherford backscattering, as shown in Fig. 3. Next, the glass is treated in solution, and some of it dissolves. The xenon is then not as deep in the glass; calculation of the depth with time gives the dissolution rate, which was constant in different glass compositions.^{7,14} The backscattering spectrum clearly shows whether there are deposits or adsorption or layers of modified composition on the glass surface. In Fig. 3, the spectrum shows edges and profiles for glass constituents as expected for uniform concentration right to the glass surface.

A second method involves protecting part of the glass surface from dissolution. The height of the step between this protected region and the dissolved region is measured with a profilometer stylus.⁷ This technique has vertical and lateral resolutions of less than 1 nm and 1 μm , respectively.



Fig. 9 Electron micrograph of crystals on the surface of a $\text{Na}_2\text{O} \cdot 2\text{SiO}_2$ glass after fracture. 42,000. \times

In a study of dissolution rates of a variety of silicate glasses,^{7,34} the results of these two techniques and weight change measurements agreed within experimental error, verifying the validity of the results, and showing that the implanted xenon does not influence the rate of dissolution. Dissolution rates for a wide variety of glasses at pH 7 as a function of $1/T$ are shown in Fig. 10, and rates of many glasses and activation energies are given in Table 3. The

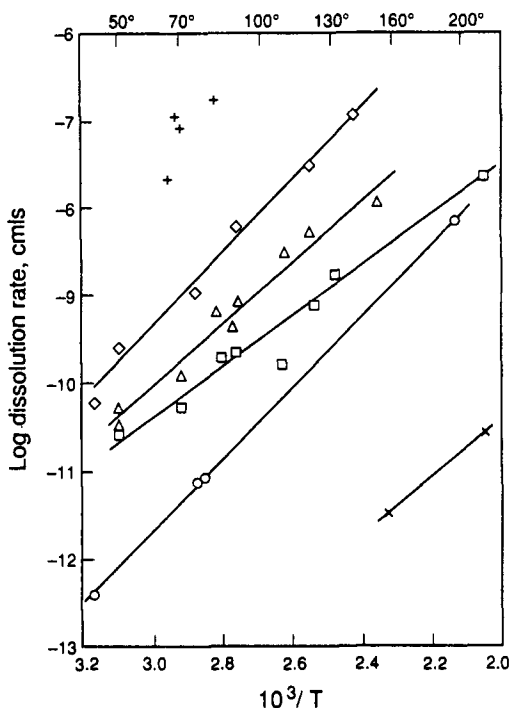


Fig. 10 Dissolution rates of different silicate glasses (Table 1) at pH 7 as a function of reciprocal temperature. +, $\text{Na}_2\text{O} \cdot 3\text{SiO}_2$; ◇, 015; △, PPG soda-lime; □, Pyrex borosilicate; ○, R-6 soda-lime; and ×, obsidian. Reprinted from Ref. 7 with permission from the American Ceramic Society.

rates of dissolution of Vycor and vitreous silicate glasses are about equal to those in Fig. 10 for commercial soda-lime glass containing alumina. Crystalline quartz³⁷ has a much lower dissolution rate than vitreous silica, and the rate for quartz is about the same as found for obsidian natural glass in this study.

TABLE 3 Rates of Dissolution of Different Glasses at 90°C^a and Activation Energies for Dissolution

Glass	$-\log v$ (v in cm/s)	Activation energy, Q (kJ/mol)
Sodium trisilicate	6.4 ^b	
Corning 015 soda-lime	8.18	84
PPG soda-lime	9.05	68
Pyrex borosilicate	9.64	54
Kimble R6 soda-lime	10.70	79
Obsidian	12.7 ^b	62

^aFrom Fig. 10.

^bExtrapolated.

A large number of minerals, mostly aluminosilicates, have rates of dissolution similar to those of quartz and obsidian,³⁸ with an activation energy of about 56 kJ/mol from 70 to 700°C.

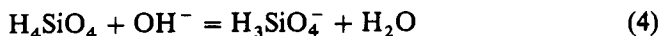
A commercial soda-lime silicate glass containing about 2% alumina dissolved much more slowly than a glass with a similar composition but without much alumina. Pyrex borosilicate glass has a surprisingly high rate of dissolution despite its use as a chemically durable glass. At room temperature and pH 7 Pyrex borosilicate glass dissolves about two orders of magnitude faster than commercial soda-lime glasses containing alumina.

Solution pH has a strong influence on the rate of dissolution of silicate glasses.^{1-6,33,34,39,40} It has long been known that these glasses dissolve more rapidly in basic solution. Boksay and Bouquet³³ found a minimum rate of dissolution of 015 soda-lime glass at pH 4, and vitreous silica^{34a} apparently has a minimum rate at somewhat lower pH. The rates of dissolution of glasses R-6, PPG float, and Pyrex borosilicate increased more than a factor of ten³⁴ between pH 4 and 9 (see also ref. 36, p. 73).

Build-up of the silica concentration in solution during dissolution of silicate glass reduces the rate of dissolution. The equilibrium solubility of amorphous silica in water at 25°C was found to be about 0.012 wt% by Alexander et al.,⁴¹ in close agreement with previous work cited in their article. The dissolved species was unionized monomeric silicic acid, H_4SiO_4 :



The solubility was about constant at pH values from 2 to 8, but decreases at lower pH (strongly acid solutions).⁴⁰ Above pH 8 the solubility rose sharply because of the ionization of the silicic acid:



However, the amount of unionized silica in solution remained constant, even though the total amount of dissolved silica increased by formation of H_3SiO_4^- ions.⁴¹ Between 25 and 200°C, the solubility of amorphous silica in water at pH 7 increased linearly with temperature to about 0.083 wt% at 200°C.

The influence of silica concentration on dissolution rates of PPG and Pyrex glasses (see Table 1) was measured in two different ways.⁴² In the first, the decrease of dissolution rate caused by the increase of silica in the solution from the dissolving glass was followed. In the second method, silica was added to the solution at different concentration levels and the dissolution rate measured. The dissolution rate approached zero as the silica reached its solubility limit in solution. A similar result was found for a simulated nuclear waste glass PNL 76-68 at 90°C from analysis of silica in the solution.⁴³ In both cases, the change of silica concentration in solution c fits a first-order reaction equation,⁴⁴

$$\frac{dc}{dt} = k_0 - k_r - R_r c \quad (5)$$

where k_0 is the rate of dissolution initially, k_r is the reverse reaction, and r is the concentration of silica in the glass. At high supersaturation, the reverse reaction (k_r) is anomalously high.^{34a}

Solubilities determined from these experiments⁴² are given in Table 4. The solubilities of silica for Pyrex borosilicate and soda-lime glasses at 140° and pH4 are not far from the silica values of $6(10)^4$ gm/cm³; at pH9 and 90°C, the solubility of silica is about five times higher than that measured for these glasses.

In highly acidic (pH 1 and below) and alkaline solutions above pH9, the rate of dissolution of silicate glasses becomes rapid and dominates ion exchange; the thickness of the leached layer becomes negligibly small, of atomic dimensions. The weight loss of several commercial glasses in sodium hydroxide is compared in Table 5. The first four glasses have about the same rate of loss, in spite of their different rates of dissolution at pH 7. At this pH, the weight loss is linear with time,⁴⁵ consistent with dissolution control. Zirconia in a silicate glass imparts substantial durability to alkaline attack, as shown in Table 5 corresponding to its strong resistance to alkali as the pure oxide.⁴⁸ A number of other oxides of multivalent cations impart some resistance to alkaline attack, but less than by zirconia; examples are oxides of aluminum, beryllium, lanthanum,⁴⁶ and transition metals such as iron,⁵⁰ manganese,⁵⁰ and chromium.^{46,51} The rate of dissolution of silicates at pH above about 7 is apparently related to surface charge.⁴⁹

Concentrated strong acids (HCl and H₂SO₄ above 1 M) attack soda-lime glass more rapidly than dilute acids or neutral solutions.⁵² There is an initial rapid attack and subsequent reduction of the rate of attack to zero.

Molecular Diffusion

As described in Chapters 8 and 12, water dissolves molecularly in vitreous silica and reacts with the silicon-oxygen lattice to form -SiOH groups. At temperatures above 100°C, water diffuses molecularly into certain alkali silicate glasses forming "hydrosilicates" as described in the last chapter; the reaction of

TABLE 4 Solubility of Silica from Commercial Soda-Lime and Pyrex Borosilicate Glasses

Glass	Temperature (°C)	pH	Solubility (g/cm ³ × 10 ⁴)	Method
Pyrex borosilicate	197	4	8.0	Saturation, Eq. 5
	140	4	3.4	Saturation, Eq. 5
	90	9	1.0	Saturation, Eq. 5
	90	9	1.0	Addition of silica
	70	9	0.2	Saturation, Eq. 5
Soda-lime	140	4	7.0	Saturation, Eq. 5
	90	9	1.0	Addition of silica

TABLE 5 Weight Loss of Different Silicate Glasses after 6h in 5% NaOH at 100°C

Corning no.	Glass	Weight loss, (mg/cm ²)
7900	96% silica	0.9
7740	Pyrex borosilicate	1.4
0080	Soda-lime	1.1
0010	Lead glass	1.6
7050	Sodium borosilicate	3.9
8870	High lead	3.6
1710	Aluminosilicate, low alkali	0.35
7280	Alkali resistant (with ZrO ₂)	0.09

<i>Approximate compositions (wt. %)</i>								
	SiO ₂	B ₂ O ₃	Al ₂ O ₃	CaO	MgO	PbO	Na ₂ O	K ₂ O
7740	81.0	13.0	2.0				4.0	
0080	72.6	0.8	1.7	4.6	3.6		15.2	
0010	77.0			1.0		8.0	9.0	5.0
7050	68.0	24.0	1.0				7.0	
1710	64.0	4.5	10.4	8.9	10.2		1.3	0.7

this water with the silicon-oxygen network causes a dramatic change in the mechanical properties of these glasses. During this molecular diffusion, the concentration of alkali in the bulk of the glass is unaffected, except by ion exchange just at the glass surface. There is no evidence for appreciable molecular permeation of molecular water in a durable glass such as a commercial soda-lime containing alumina below 100°C-except as part of the hydronium ion. The amount of hydrogen in the surface of such a glass is just three times the sodium concentration, as shown in Fig. 5, and expected from reaction 3. Even in less durable glasses, such as 015, soda-line, there is no evidence for more water than exchanges for sodium (Fig. 4). It is only at temperature above 100°C or in less durable glasses such as binary alkali silicates that there is evidence for molecular diffusion of water from liquid water.

At higher temperatures and in water vapor, it is likely that molecular permeation of water is appreciable in all silicate glasses. The penetration depth of water vapor in tektite glass⁵³ (aluminosilicate, see Table 1) at 200°C after 122 days was about 3 μ m. The effective diffusion coefficient of reacted water in vitreous silica measured by Moulson and Roberts⁵⁴ was about $D = 3.5 \times 10^{-14}$ cm²/s, extrapolated to 200°C; from the approximate relation $X = \sqrt{2Dt}$, where X is the penetration depth after time t , one expects penetration to about 6 μ m. Thus it is quite possible that the hydration front measured by Mazer et al.⁵³ resulted from diffusion of molecular water.

At higher temperatures of 650–950°C, the profiles of water in a rhyolitic obsidian glass^{55,56} were the same as in vitreous silica (Chapter 8, Fig. 6), so it is quite likely that the water diffuses and reacts in this glass in the same way that it does in vitreous silica. These aluminosilicates have relatively low amounts of alkali or alkaline earth oxides (see Table 1), so their structure may be more open, similar to vitreous silica.

Reaction Layers on Glass

Vitreous silica shows minimum formation of reaction layers on its surface. After strong hydration in acid, a thin (a few atomic layers) hydrated surface layer forms on vitreous silica on which there is enhanced adsorption; see first edition, p. 225. Other durable glasses, such as commercial soda-lime containing alumina, also show minimum tendency to form reaction layers in solution. The Rutherford backscattering spectra and infrared spectra of these durable glasses show no evidence for surface layers after hydration in water of neutral pH below 100°C. Less durable glasses show an increased tendency to form reaction layers with alteration of the structure of the silicon–oxygen network. A step towards these structural changes is the formation of a transformed hydrated layer described above and discussed in the interpretations section.

Some factors that favor the formation of reaction layers on silicate glasses are:

1. Treatment of the glass in water vapor, rather than liquid vapor. Products of ion exchange remain on the glass surface and react with it, whereas in liquid water they are dissolved away. Clay-like phases formed on the surface of an aluminosilicate tektite after hydration at 200°C for 122 days in water vapor;⁵³ clay-like phases also formed on nuclear waste glasses in water vapor.⁵⁷
2. Nondurable glasses are more likely to form structurally altered and reaction layers. Surfaces of binary sodium and potassium silicate glasses crack in acid solution.^{47,58} Certain sodium borosilicates have considerably altered network structures after leaching.⁵⁸
3. Higher temperatures (above 100°C) favor surface reactions and layer formation.
4. High solution concentrations of constituents of less soluble phases lead to precipitation on the glass surface. Zinc silicate was found on the surface of a nuclear waste glass after hydration at 90°C in static solution,⁴³ giving a final pH from 9 to 10.
5. Certain constituents of glasses are preferentially leached in acidic or basic solution. Boron is removed in acids, and aluminum in bases. Since the silicon–oxygen network is rapidly dissolved in basic solutions, most silicate glasses have close to the same dissolution rate in strong base, as shown in Table 5.

Murakami and Banba⁵⁹ studied surface layers formed on a simulated nuclear waste glass with a large number of components (glass no. J-10, Table 2). Many other authors also studied nuclear waste glasses.^{60,61} Murakami and Banba identified four different surface layers after treatment of the glass at 100°C for 200 days in refluxed water (Soxhlet test). The total layer thickness was about 0.55 mm. These authors found that alkali metals and molybdenum were depleted from surface layers, and that manganese, iron, nickel, zirconium, lanthanum, cesium and neodymium had about the same concentration in the surface layers as in the glass. Silicon, aluminum, and calcium had lower concentrations in the surface layers than in the glass. There were finely divided crystals in the layers of a layer silicate containing the elements that remained in the layers.

The possible influences of surface layers on the kinetic processes of ion exchange and dissolution are discussed below.

INTERPRETATIONS

There is strong experimental evidence that certain silicate glasses retain their network structure in a hydrated ion exchanged layer, as described above; these glasses with untransformed hydrated layers are designated with a "U" in Table 1. Outgassing of water from them is slow after hydration,^{13,18,20} even at temperatures up to 100°C and in a vacuum.

In ion exchange in these untransformed glasses, three hydrogen atoms replace each sodium, as shown in Fig. 5. This result is good evidence that hydronium ions exchange for alkalis (reaction 1). Even in less durable glasses, the ion exchange involves three hydrogen atoms for each alkali ion,¹⁸ as shown in Fig. 4, also suggesting hydronium exchange.^{62,63} Several previous workers have found less than three hydrogen atoms exchanged in these less durable glasses, and have questioned hydronium exchange; these lower hydrogen concentrations result because of outgassing of water from the transformed hydrated layers on these glasses, as established in Ref. 18, and are not representative of true hydrogen concentrations during hydration.

The dependence of hydration depth and sodium concentration in solution on the square root of time during ion exchange is evidence for a diffusion-controlled process. The S-shaped profiles found for ion exchange during hydration of silicate glasses show that the diffusion depends upon ionic concentration. The interdiffusion of two monovalent cations on fixed sites can be described^{64,65} by a concentration-dependent interdiffusion coefficient D ,

$$D = \frac{D_H D_A}{N_A D_A + N_B D_B} = \frac{D_A}{1 + b N_A} \quad (6)$$

where D_H and D_A are diffusion coefficients for individual ions and N_A and N_H are their ionic fractions; $N_A + N_H = 1$, and $b = (D_A/D_H) - 1$. As a first approximation, one can assume that the individual D_H and D_A values are not

a function of ionic ratio; then b is a constant. Experimentally variations in D_H and D_A are small compared to those in \bar{D} . Equation 6 applies to interdiffusion during hydration of glass with A and H alkali cation and hydrogen (hydronium ion), respectively.⁶⁶ Profiles calculated with the concentration-dependent interdiffusion coefficient of Eq. 6 are compared with experimental profiles in Fig. 5; the agreement is good. The diffusion coefficients of sodium and lithium ions in glasses with untransformed hydrated layers, obtained from the measured profiles, agree with diffusion coefficients calculated from Eq. 6.^{20,30} Also diffusion coefficients calculated from the Einstein equation (see Chapter 15, Eq. 11) and measured electrical conductivity agree with measured coefficients.²² This good agreement is strong evidence for the validity of the interdiffusion theory of the rate of ion exchange during hydration of these glasses. Some workers have suggested that the ion exchange rate is controlled by molecular diffusion of water into the glass. However, there is no experimental support for this idea.⁶⁷ The ionic interdiffusion control of ion exchange during hydrolysis is also confirmed by electrolysis experiments;²² the same ratio of ionic mobilities is found in these experiments as in the experiments without an electrical field.

In ion exchange in glasses with transformed surface layers, the mobilities of ions are much greater than in the dry glass.^{8,12,16,20,30,47,58} However, the profiles of ions are similar to those in the glasses with untransformed layers. The applicability of Eq. 6 in this case must be tested with independent measurements of ionic mobilities in the hydrated layers, which have not been carried out.

At the same time that diffusion-controlled ion exchange is taking place, the glass is dissolving congruently. To account for these two simultaneous processes, Boksay et al.¹¹ introduced a new distance variable $y = X - vt$, in which X is the distance from the initial glass-solution interface and y is the distance from the actual interface after dissolution at a constant rate v after time t . An equation for the concentration profile with a constant diffusion coefficient can be derived from this new variable;^{5,11} however, this profile does not have the required S-shape. With the concentration-dependent interdiffusion coefficient of Eq. 4, an analytical solution is difficult. At long times a steady-state is reached in which the thickness of the hydration layer is constant. In this steady-state regime, the concentration profile of alkali with a diffusion coefficient from Eq. 6 is⁶⁶

$$N_A = \frac{1 - \exp(-vy/D_H)}{1 + b \exp(-vy/D_H)} \quad (7)$$

Curves from this equation fit experimental profiles well.^{6,13,30}

In some nondurable glasses, cracks form on the surface during hydration, for example binary sodium silicate glasses.^{47,58} In this case, the amount of alkali in the solution can become linear with time while the thickness of the hydration is still increasing, presumably because water reaches deeper into the glass along the cracks.

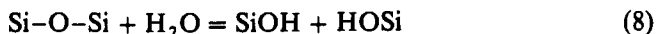
The increase in solution pH to a maximum in a static solution of limited volume⁹ is shown in Fig. 1. This pH change can be modeled with a series of differentials for the different reactions.^{9,68} Qualitatively these changes in pH can be understood as follows. At first the alkaline products of ion exchange (Eq. 1) build up in the solution, causing an increase in pH. This increase speeds the rate of lattice dissolution, including the formation of silicic acid by Eq. 3. This acid neutralizes the alkaline products, and because the amount of silica in the glass is greater than the other constituents, it eventually dominates and causes the pH to decrease. In some glasses containing less silica in solution of limited volume, the pH seems to reach a constant value.

The transformation of the hydrated glass layer to a somewhat more open structure in which outgassing and ionic mobilities increase is perhaps similar to separation into two fine phases, one in which water and ions can diffuse rapidly. Tomozawa and Capella found evidence for a two-phase structure in the surface of a hydrated sodium silicate glass with small angle X-ray scattering.⁶⁹

DISSOLUTION

Surface structure is an important factor causing different rates of dissolution from silicate glasses of different compositions. The higher dissolution (and ion exchange³⁰) rates of soda-lime silicate glasses without alumina compared to glasses with almost the same composition but containing a few % alumina result from the transformed hydrated surface layers in the former. Perhaps the alumina inhibits a phase separation of the type described in the last paragraph; alumina inhibits phase separation in silicates (see Chapter 4).

In vitreous silica, molecular water penetrates into the surface layers of the silicon-oxygen lattice and reacts with silicon-oxygen bonds.⁷⁰



There is evidence that a sequence of these bond-breaking reactions causes large molecular "islands" to dissolve from the silicate surface and slowly hydrolyze to monomeric silicic acid (eq. 3). Whatever the details of the dissolution process, the more open structure of the transformed layer provides easier access of water to the silicon-oxygen network and increases its dissolution rate. The binary alkali silicate glasses have more open transformed layers than the soda-lime glasses,⁶⁹ so they dissolve even more rapidly.

The dissolution of many aluminosilicate crystalline minerals, crystalline quartz, and obsidian natural glass are all about the same and much lower than vitreous silica and soda-lime with alumina.³⁸ Perhaps these low rates represent the rate of reaction of water with a relatively impenetrable surface, and are therefore the minimum possible for a silicon-oxygen network. The higher rates for R-6 soda-lime and vitreous silica may result because water can diffuse into

their surface layers more easily than into obsidian or quartz. This difference corresponds to the much greater permeation of gases into vitreous silica than an alumino silicate glass or quartz (Chapter 8, Fig. 7).

The rate of dissolution of vitreous silica is closely related to the surface charge on the silica,^{39,49} as determined by titration of surface silica groups.^{71a} The dissolution rate has a minimum at pH 2 or 3, which is close to the point of zero charge of amorphous silica. Perhaps the silicon-oxygen bonds on the silica surface become weaker as neighboring SiO^- groups are charged. Some authors have suggested that hydrogen or hydroxyl ions "catalyze" the hydration and dissolution reactions. It seems unlikely that attraction of specific groups or molecules is the mechanism of charge enhancement, because both positive and negative charges on the silica surface appear to enhance the rate of dissolution.

The extent of reactions 1, 3 and 4 and their relation to solution conditions such as pH can be related to the thermodynamic properties of reactants and products. Free energies of formation of compounds in these reactions are given in Ref. 5, in which there is discussion of these values and their use. The solubility of amorphous silica in water increases with temperature and pH. These increases correspond qualitatively with increases in dissolution rates of silicate glasses, but not quantitatively; for example, the solubility of amorphous silica is about seven times greater at 200°C than at room temperature, whereas the dissolution rates in Fig. 10 increases much more over this temperature range.

Durabilities of multicomponent glasses have been compared with thermodynamic properties of component oxides and silicates (e.g. calcium silicate).^{72,73} The influence of other components in a multicomponent glass on thermodynamic properties (activities) of a specific oxide is difficult to deduce; often mixtures are highly nonideal. This approach neglects the important role of surface structure on glass durability. For example, quartz dissolves much more slowly than amorphous silica, yet their free energies of hydration are almost the same. See Refs. 5, 7, 72 and 73 for discussion.

The chemistries of component ions in solutions can give clues as to the influence of these components on reactions with acidic and basic solutions. An amphoteric ion (one that forms both acids and bases) such as aluminum is likely to be soluble in both acids and bases, even if it is not soluble in neutral water. Certain ions form highly insoluble silicates in aqueous solutions, for example zirconium, thorium, beryllium and zinc. The first three impart increased resistance to corrosion in alkali as a glass constituent.

INFLUENCE OF REACTION LAYERS ON KINETICS

Silica in solution, either deliberately added or from the dissolution of glass, reduced the rate of congruent dissolution of the glass.⁴² This reduction follows

the first order kinetic equation of Eq. 5, and can render the dissolution rate negligible.

Some workers have suggested that surface reaction layers inhibit leaching from glass. There is no direct evidence for this idea. The layers are usually loose mixtures of amorphous and crystalline phases. It seems likely that water and ions can diffuse in these layers more or less easily. I suggest that the inhibition of dissolution results mainly from the increase of silica in the solution, causing a reduction in the dissolution rate (Eq. 5). This reduction is more likely to occur in solutions of limited volume, which is just the condition that favors layer formation. The ratio A/V of surface area of glass to solution volume is an important parameter for determining the build-up of silica concentration in solution.

The solubility of silica from different glasses can be considerably smaller than from vitreous silica, as shown in Table 4. In some compositions this reduction in solubility is related to the fraction of silica in the glass; in other glasses at pH 9, it is much greater than expected from the silica concentration in the glass. Apparently constituents of the glass in solution reduce the silica solubility.

RADIOACTIVE WASTE DISPOSAL

Large amounts of highly dangerous radioactive waste, generated from weapons development, are stored in liquid form in steel tanks, and large quantities of degenerated radioactive fuel are produced in commercial atomic reactors. Some of these tanks are beginning to leak. Thus it has been essential to develop a more stable form for the waste. Encapsulation in glass is being carried out in Europe, and a plant to incorporate radioactive waste in glass has been built at the Savannah River facilities in South Carolina. This plant represents a major technological achievement of remotely treating the waste and melting it into glass.

The glass compositions chosen for waste encapsulation are similar to those in Table 2. This composition was chosen because it can be melted at relatively low temperature, avoiding vaporization of radioactive material during melting. Unfortunately the compositions chosen, while durable compared to other materials, are not as durable as some other glasses. The rate of dissolution is not as low as desired to insure long-term (10^4 years or greater) durability of the glass, so methods of confining leach products and reducing the dissolution are being considered. One is to bury the waste in rock or remote sites such as Yucca Mountain in Nevada. These methods have led to wrenching controversies (Ref. 74, see also Refs. 36, 60 and 61 for discussions of waste disposal).

It was necessary and wise to start with a glass that was relatively convenient to process. It seems appropriate, however, to consider improving the durability of the glass to the point that it can be relied on entirely to confine the waste by dissolving slowly even under adverse conditions. The present discussion

shows that there is considerable possibility of reducing the dissolution rate of the encapsulating glass by judicious change in the glass composition.

ZIRCONIUM FLUORIDE GLASS

A variety of glasses based on zirconium fluoride have infrared transmission to $8\text{ }\mu\text{m}$ or beyond, and therefore have excellent potential for optical fibers and other optical components. In liquid water these glasses dissolve rapidly and congruently,⁷⁵ and crystals deposit on the surface as shown in Fig. 2. These crystals are zirconium fluoride,¹⁰ and they grow from solution near the glass surface. In water vapor these glasses are quite durable.⁷⁶ There is evidence from hydrogen profiles that water from solutions penetrates into the glass, perhaps increasing the ease of dissolution.⁷⁷ Glasses formed directly from the melt can be much more durable than cut and polished surfaces.⁷⁸

REFERENCES

1. R. W. Morey, *The Properties of Glass*, Reinhold, New York, 1954, pp. 101 ff.
2. F. R. Bacon, *Glass Ind.*, **49**, 438, 494, 554, 557 (1968).
3. V. Gottardi, Ed., *The Chemical Durability of Glass—A Bibliographic Review*, Int. Comm. on Glass, 1972.
4. A. M. Filbert and M. L. Hair, in *Advances in Corrosion Science and Technology*, M. G. Fontana and R. W. Stachle, Eds., Plenum Press, New York, 1976, p. 1.
5. R. H. Doremus, *Chemical Durability of Glass*, in *Treatise on Materials Science and Technology*, Vol. 17, M. Tomozawa and R. H. Doremus, Eds., Academic Press, San Diego, CA, 1979, p. 41.
6. H. H. Dunken, *Physikalische Chemie der Glasoberfläche*, VEB Deutscher Verlag für Grundstoffindustrie, Leipzig, Germany, 1981, p. 284 ff.
7. G. Perera, R. H. Doremus, and W. A. Lanford, *J. Am. Ceram. Soc.*, **74**, 1269 (1991).
8. M. A. Rana and R. W. Douglas, *Phys. Chem. Glasses*, **2**, 179 (1961).
9. H. H. Dunken and R. H. Doremus, *J. Noncryst. Solids* **92**, 61 (1987).
10. R. H. Doremus, N. P. Bansal, T. Bradner and D. Murphy, *J. Mater. Sci. Lett.* **3**, 484 (1984).
11. Z. Boksay, G. Bouquet and S. Dobos, *Phys. Chem. Glasses*, **9**, 69 (1968).
12. H. Scholze, *J. Noncryst. Solids*, **52**, 91 (1982).
13. W. A. Lanford, K. Davis, P. Lamarche, T. Laursen, R. Groleau, and R. H. Doremus, *J. Noncryst. Solids*, **33**, 249 (1979).
14. W. A. Lanford, C. Burman, R. H. Doremus, Y. Mehrotra and T. Wassick, *Advances in Materials Characterization*, D. R. Rossington, R. A. Condrate and R. L. Snyder, Eds., Plenum, New York, 1983, p. 549.
15. L. L. Hench, in *Characterization of Materials in Research, Ceramics and Polymers*, V. Weiss and J. J. Burke, Eds., Syracuse University Press, Syracuse, NY, 1975, p. 211.

16. B. M. J. Smets and M. G. W. Lommen, *Phys. Chem. Glasses*, **23**, 83 (1982).
17. H. Bach and F. G. K. Baucke, *J. Am. Ceram. Soc.*, **65**, 527, 533 (1985).
18. K. H. Schnatter, R. H. Doremus, and W. A. Lanford, *J. Noncryst. Solids*, **102**, 11 (1988).
19. F. G. K. Baucke, *J. Noncryst. Solids*, **14**, 13 (1974).
20. R. H. Doremus, Y. Mehrotra, W. A. Lanford, and C. Burman, *J. Mater. Sci.*, **18**, 612 (1983).
21. A. Wikby, *Electrochim. Acta*, **19**, 329 (1974).
22. R. H. Doremus, A. Babinec, K. D'Angelo, M. Doody, W. A. Lanford, and C. Burman, *J. Am. Ceram. Soc.*, **67**, 476 (1984).
23. R. D. Husung and R. H. Doremus, *J. Mater. Res.*, **5**, 2209 (1990).
24. D. E. Clark, M. F. Dilmore, E. C. Ethridge, and L. L. Hench, *J. Am. Ceram. Soc.*, **59**, 62 (1976).
25. D. Hubbard, E. H. Hamilton, and A. N. Finn, *J. Res. Natl. Bur. Stand.*, **22**, 339 (1939).
26. H. Scholze, D. Helmreich, and J. Bakardjico, *Glastech. Ber.* **48**, 237 (1975).
27. J.-C. Petit, G. Della Mea, J.-C. Dran, M. C. Magonthier, P. A. Mando, and A. Paccagnella, *Geochim. Cosmochim. Acta*, **54**, 1941 (1990).
28. B. M. J. Smets and M. G. W. Tholen, *Phys. Chem. Glasses*, **26**, 60 (1985).
29. T. Richter, G. H. Frischat, G. Borchardt, and S. Scherrer, *Glastech. Ber.*, **63**, 300 (1990).
30. T. A. Wassick, R. H. Doremus, W. A. Lanford, and C. Burman, *J. Noncryst. Solids*, **54**, 139 (1983).
31. S. Dobos, *Acta Chim. Acad. Sci. Hung.*, **68**, 371 (1971).
32. F. G. K. Bauke, in *Mass Transport Phenomena in Ceramics*, A. R. Cooper and A. H. Heuer, Eds., Plenum Press, New York, 1975, p. 337.
33. Z. Boksay and G. Bouquet, *Phys. Chem. Glasses*, **21**, 110 (1980).
34. G. Perera and R. H. Doremus, *J. Am. Ceram. Soc.*, **74**, 1554 (1991).
- 34a. B. A. Fleming, *J. Colloid Interface Sci.*, **110**, 40 (1986).
35. K. B. Harvey, C. D. Litke, and C. A. Boase, *Phys. Chem. Glasses*, **27**, 15 (1986).
36. D. E. Clark and B. K. Zoites, Eds., *Corrosion of Glass, Ceramics, and Ceramic Superconductors*, Noyes Pub., Park Ridge, N.J., 1992.
37. T. M. El-Shamy, J. Lewins, and R. W. Douglas, *Glass Technol.*, **13**, 81, 1972.
38. B. J. Wood and J. V. Walther, *Science*, **222**, 413 (1983).
39. G. S. Wirth and J. M. Gieskes, *J. Colloid Interface Sci.*, **68**, 492 (1979).
40. T. H. Elmer and M. E. Nordberg, *J. Am. Ceram. Soc.*, **41**, 517 (1958).
41. G. B. Alexander, W. M. Heston, and R. K. Iler, *J. Phys. Chem.*, **58**, 453 (1954); **61**, 1539 (1957).
42. G. Perera and R. H. Doremus, *Ceram. Trans.*, **20**, 41 (1991).
43. J. L. Means, E. D. Spinosa, A. J. Markworth, J. K. McCoy, N. E. Miller, R. E. Kurth, and H. C. Taylor, Report NUREG/CR-4795, BMI-2143, Battelle, Columbus, 1987.

44. T. L. O'Connor and S. A. Greenberg, *J. Phys. Chem.*, **62**, 43 (1958).
45. T. M. El-Shamy, J. Lewins, and R. W. Douglas, *Glass Technol.*, **13**, 81 (1972).
46. J. V. Rogogine and L. A. Zayonts, *10th Int. Glass Congr.*, Ceramic Soc. Japan, Kyoto, 1974, p. 9-63.
47. B. C. Bunker, G. W. Arnold, E. K. Beauchamp, and D. E. Day, *J. Noncryst. Solids*, **58**, 295 (1983).
48. F. A. Cotton and G. Wilkinson, *Advances Inorganic Chemistry*, Wiley, New York, 1988, p. 780.
49. P. V. Brady and J. V. Walther, *Geochim. Cosmochim. Acta*, **53**, 2823 (1989).
50. A. Paul and A. Youssefi, *J. Mater. Sci.*, **13**, 97 (1978).
51. H. Ohta and Y. Suzuki, *Am. Ceram. Soc. Bull.*, **57**, 602 (1978).
52. R. Wollast, P. Brennet, and A. Jelli, *Verres Refract.*, **24** 251 (1970).
53. J. J. Mazer, J. K. Bates, J. P. Bradley, C. R. Bradley and C. M. Stevenson, *Nature*, **357**, 573 (1992).
54. J. Moulson and J. P. Roberts, *Trans. Faraday Soc.*, **57**, 1208 (1961).
55. J. L. Karsten, J. R. Holloway, and J. R. Delaney, *Earth Planetary Sci. Lett.*, **59**, 420 (1982).
56. K. E. Lapham, J. R. Holloway, and J. R. Delaney, *J. Noncryst. Solids*, **67**, 179 (1984).
57. T. A. Abrajano, J. K. Bates, A. B. Woodland, J. P. Bradley, and W. L. Bourcier, *Clay Clay Miner.*, **38**, 537 (1990).
58. B. C. Bunker, D. R. Tallant, T. J. Headley, G. L. Turner, and R. J. Kirkpatrick, *Phys. Chem. Glasses*, **29**, 106 (1988).
59. T. Murahami and T. Banba, *Nucl. Technol.*, **67**, 419 (1984); **70**, 243 (1985).
60. *Scientific Basis for Nuclear Waste Management*, Vols. I-XV, Materials Research Society, Pittsburgh, PA, 1976-1992.
61. *Nuclear Waste Management*, Vol. I, 1984; Vol. II, 1988, American Ceramics Society, Columbus, OH.
62. J. S. T. Tsong, C. A. Hauser, W. B. White, A. L. Winterberg, P. D. Miller, and C. D. Moak, *Appl. Phys. Lett.*, **39**, 669 (1981).
63. F. M. Ernsberger, *J. Noncryst. Solids*, **38-39**, 557 (1980).
64. F. Helfferich and M. S. Plesset, *J. Chem. Phys.*, **28**, 418 (1958).
65. R. H. Doremus, *J. Phys. Chem.*, **68**, 2212 (1964).
66. R. H. Doremus, *J. Noncryst. Solids*, **19**, 137 (1975).
67. R. H. Doremus, *J. Noncryst. Solids*, **55**, 143 (1983).
68. H. H. Dunken and R. H. Doremus, *Mater. Res. Bull.*, **22**, 868 (1987).
69. M. Tomozawa and S. Capella, *J. Am. Ceram. Soc.*, **66**, C-24 (1983).
70. R. H. Doremus, in *Reactivity of Solids*, J. W. Mitchell, R. C. DeVries, R. W. Roberts and P. Cannon, Eds., Wiley, New York, 1969, p. 667.
71. S. S. Jorgensen, *Acta Chem. Scand.*, **22**, 335 (1968).
- 71a. R. P. Abendroth, *J. Colloid Interface Sci.*, **34**, 591 (1970).
72. A. Paul, *J. Mater. Sci.*, **12**, 2246 (1977).
73. C. M. Jantzen and M. J. Plodinec, *J. Noncryst. Solids*, **67**, 207 (1984).

74. E. Marshall, *Science*, **251**, 864 (1991).
75. C. J. Simmons, H. Sitter, J. H. Simmons, and D. C. Tran. *Mater. Res. Bull.*, **17**, 1203 (1982).
76. S. J. Loehr, K. H. Chung, C. T. Moynihan, G. Fonteneau, P. Chistensen, and J. Lucas, *Mater. Sci. Forum*, **19–20**, 327 (1987).
77. R. H. Doremus, D. Murphy, N. P. Bansal, W. A. Lanford, and C. Burman, *J. Mater. Sci.*, **20**, 4445 (1985).
78. C. Burman, W. A. Lanford, R. H. Doremus, and D. Murphy, *Appl. Phys. Lett.*, **44**, 845 (1984).

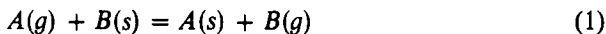
CHAPTER 14

ION EXCHANGE AND POTENTIALS OF GLASS ELECTRODES

Although glass is not usually thought of as an ion exchanger, many of the chemical properties of glasses are determined by ion exchange, as shown by the discussions in the preceding two chapters of hydrogen-alkali ion exchange in the reactions of water with glass. Ion exchange also gives rise to the potentials of glass electrodes, and the introduction of larger ions into glass by ion exchange results in a compressive surface stress, thus strengthening the glass (see Chapter 9). This chapter contains sections on measurements of the distribution of ions between glass and solutions, experimental results on distribution coefficients, theories of the selectivity of anionic groups in glass for different cations, potentials of glass electrodes, and tests of the ion exchange theory of glass electrode potentials. My review on ion exchange in glasses¹ should be consulted for more details on earlier work. Helfferich's treatise on ion exchange² emphasizes work on organic exchangers, but gives some discussions applicable to glasses.

MEASUREMENT OF IONIC DISTRIBUTION

An ion exchanger can be treated as a separate phase. The exchange of an ion B in a solution with an ion A in the exchanger (glass) is represented by the following equation:



where (s) represents the solution and (g) is the glass. At equilibrium the ions are distributed between the two phases in a fixed ratio. A number of coefficients

have been used to represent this equilibrium, as discussed in Ref. 2, pp. 152 ff. Here the thermodynamic equilibrium constant K is used whenever possible,

$$K = \frac{a_s b_a}{a_a b_s} \quad (2)$$

where the lower-case letters represent the thermodynamic activities of the A and B ions. The absolute value of K depends on the reference functions and states chosen to define the activities. For aqueous solutions, the most usual reference state is the concentration at infinite dilution. However, for fused salts, it is more convenient to use the mole fraction N of a component in the pure state; that is,

$$\lim_{N \rightarrow 1} \frac{a}{N} = 1$$

The latter reference state is also used for the glassy exchanger in this work. If the exchanger is homogeneous and has only one type of site, K is constant with changing composition at constant temperature and pressure. Inhomogeneous exchangers are considered in refs. 1 and 6.

The value of K reflects the selectivity of the exchanger. It is a quantitative measure of the preference of the exchanger for one ion over another in solution with it. The surface potential of a glass electrode also depends on K , as described below.

Two methods have been used to estimate K in glass. One technique is a direct measurement of the distribution of ions between the solution and glass; the second method is an indirect inference of the selectivity of a glass electrode from measurement of its electrical potential. The first method is preferable and can be used in a molten salt at higher temperatures, where considerable exchange takes place. When a glass electrode is used in aqueous solution, the region of exchange at the glass surface is limited and direct measurement of ionic concentrations becomes difficult. Therefore, almost all results on equilibria between glass and ions in aqueous solution come from potential measurements.

In making a direct measurement of K for exchange between a molten salt and a glass, powdered glass can be equilibrated with a salt bath of desired composition and then analyzed for the exchanging constituents. If the rate of diffusion in the glass is too slow for a bulk sample, such as a tube or rod, to come to equilibrium with the melt, it is still possible to find K by measuring the concentrations of the exchanging ions near the glass surface.^{1,3} To find the surface concentration, layers of the glass are etched off with hydrofluoric acid and analyzed for the exchanging ions. The concentrations are then plotted as a function of distance from the glass surface and extrapolated back to the surface. To ensure that the exchange process at the surface has reached equilibrium, measurements can be made at different times of immersion in the molten salt.

In some glasses such as fused silica the concentration of exchanging ions is so low that conventional analysis is difficult. In this case it is possible to calculate the exchange coefficient from the conductivity of the glass in equilibrium with melts of different concentration.⁴ The total conductivity σ_T of the glass is then made up of contributions from the two ions,

$$\sigma_T = N_A \sigma_A + N_B \sigma_B \quad (3)$$

where σ_i is the conductivity of the glass containing only one kind of ion, and N_i is the mole fraction of this ion ($N_A + N_B = 1$). In using this equation, it is assumed that the total ionic concentration in the glass is constant and uniform, and also that the mobility ratios of the ions do not depend on ionic concentration.

If the thermodynamic activities of the ions in the salt are known, tentative selectivity coefficients K' can be calculated from them and the measurements of the concentration ratio C_B/C_A in the glass:

$$K' = \frac{a_s C_B}{b_s C_A}$$

If the K' values are constant with changing solution concentration, the ionic activities in the glass should be equal to the concentrations, as required for an ideal solution. If the K s vary with solution concentration, the pairs of ions in the glass behave nonideally, and the calculated K s provide a measure of this nonideality.

To find exchange coefficients between aqueous solutions and the hydrated layer on glass, Eisenman measured the uptake of radioactive ions, as described in Ref. 1, p. 8, and Ref. 5, Chapter 5.

The potential of a glass electrode can also be used to examine the selectivity of a glass for different ions. The electrical potential V of a glass electrode immersed in a solution containing A and B ions with thermodynamic activities a and b is given by (see section on glass electrode below)

$$V = V_0 + \frac{RT}{F} \ln \left\{ a + K \left(\frac{u_B}{u_A} \right) b \right\} \quad (4)$$

when the ions in the glass behave ideally (activities can be equated to concentrations), and their mobility ratio, u_B/u_A , in the glass is constant with composition. In Eq. 4, R is the gas constant, T is the absolute temperature, F is the Faraday constant, and V_0 is invariant with the composition of the solution. The product $K(u_B/u_A)$ can be found from measurements of the glass electrode potential (membrane potential) as a function of ionic activities in solution. Since it is relatively easy to measure the potential of a glass electrode in aqueous solution, many such measurements have been made, and this dependence of potential on K has given information on K values in many systems for which no direct measurements are available. However, there are unknown factors in the relationship between potential and K , so these results

TABLE 2 Equilibrium Coefficients for Ionic Distribution Between Nitrate Melts and Glasses

Glass	Refs. to Table 1	Ion in Solution (B)	Ion in Glass (A)	Temperature (°C)	K	n	Remarks	Refs.
Soda-lime	A, B	Ag ⁺	Na ⁺	320	120.0	1.08	From surface conc.	3, 12
Soda-lime	B	K ⁺	Na ⁺	350	0.05			12
Sodium borate	D	Cs ⁺	Na ⁺	550	1.5(10) ⁻³		Ions dilute in NaNO ₃	13
Sodium borate	D	Sr ²⁺	Na ⁺	550	2(10) ²			
Sodium borate	D	Eu ³⁺	Na ⁺	550	4(10) ³			
Lithium aluminosilicate	E	Na ⁺	Li ⁺	400	0.28	1.9		14
Lithium aluminosilicate	E	Ag ⁺	Li ⁺	300	3.2	2.2		14
Sodium aluminosilicate	G	K ⁺	Na ⁺	500	0.94	3.2		14
Lithium aluminosilicate	F	Na ⁺	Li ⁺	400	0.27	3.2		14
Sodium borosilicate	H	Ag ⁺	Na ⁺	300	2.6	1.4		14
Fused silica (General Electric 204)		Ag ⁺	Na ⁺	337	2.1	1.0	From Eq. 3	15
Fused silica (General Electric 204)		K ⁺	Na ⁺	823	2.1		From Eq. 3	17
Sodium aluminoborate	K	Ag ⁺	Na ⁺	375	79.0	0.71		18, 19
Sodium silicate	L	Ag ⁺	Na ⁺	350	50.0			20
Sodium silicate	L	K ⁺	Na ⁺	350	0.08			20
Pyrex	C	Ag ⁺	Na ⁺	335	1.6		Two Phases	22
Pyrex	C	K ⁺	Na ⁺	380	1.1			23
				465	1.4			

TABLE 3 Ionic Radii

Ion	Radius (Å)	Ion	Radius (Å)
H ⁺	Small		
Li ⁺	0.68	Be ²⁺	0.33
Na ⁺	0.95	Mg ²⁺	0.67
Ag ⁺	1.26		
K ⁺	1.33	Ca ²⁺	0.99
Rb ⁺	1.48	Sr ²⁺	1.13
Cs ⁺	1.67	Ba ²⁺	1.35

The sequence of preference of soda-lime glass for ions from nitrate melts (Table 2) is $\text{Ag}^+ \gg \text{Na}^+ > \text{K}^+$. In lithium aluminosilicates, the order is $\text{Ag}^+ > \text{Li}^+ > \text{Na}^+$, with not nearly so strong a preference for silver. In borosilicates and fused silica, the preference for silver over sodium is further reduced.

In chloride melts, the attraction of the glass for silver is dramatically lower, undoubtedly because of the strong bonding between chloride and silver ions in the melt. From Stern's work¹⁶ the sequence in fused silica would appear to be $\text{Na}^+ > \text{Li}^+ \gg \text{Ag}^+$, but van Reenan et al.²¹ found sodium and lithium about equally favored by fused silica. This difference may result from the use by the latter authors of a zinc chloride melt, although the size of the difference is surprising. These authors also found the sequence $\text{Li}^+ > \text{K}^+ > \text{Na}^+$ for a soda-lime glass and Pyrex borosilicate glass. One questionable aspect of both studies of ionic distributions with chloride melts is that the authors apparently used solution concentrations in calculating their exchange coefficients; that is, they assumed the solutions were ideal and the activities were equal to the concentrations. This assumption is probably not valid and it may be responsible for some of the peculiarities of the results.

Results on the exchange of ions in Pyrex borosilicate glass were interpreted with a two-phase model because the calculated K values were not constant, nor did they fit Eq. 5, for silver-sodium exchange.²⁴ This glass separates into two phases as described in Chapter 4, in agreement with the two-phase model. Nicolsky et al. have also presented equations for ion exchange with two different sites in glass.^{25,26}

Eisenman (Ref. 5, Ch. 5) investigated the equilibrium between samples of a hydrated-soda aluminasilicate glass (glass G, Table 1) and solutions of potassium ions by the method described in the preceding section. He found K values of 90 and 102 (glass prefers potassium) for two different samples of about the same composition.

Baucke²⁷ measured the equilibrium between hydrogen-bearing (hydronium) ions and lithium ions in a lithium silicate electrode glass. The glass strongly preferred hydronium ions, with values of $\log K$ of -11.30 , -10.60 , and -9.88 at 25, 50, and 75°C. Equation 5 fit well at 25°, and progressively less well at

high temperatures,²⁸ with n values of 1.61, 1.60 and 1.43 at temperatures of 25, 50 and 75°C.

Since few direct measurements of K with aqueous solutions are available, it is important to try to supplement these data from estimates of K values from potential studies. As described above, the product $K(u_B/u_A)$, where the u is the ionic mobility, can be calculated from measurements of membrane potentials across glasses. The utility of this approach is dependent on knowledge of the value of u_B/u_A . From measurements of mobility ratios in dry glass, it seems likely that certain generalities about the properties of this ratio can be made. For example, the mobility ratios of sodium to potassium ions seem to be about the same in a variety of glasses whose only univalent cation is sodium (soda glasses). In lithia or potash glasses, this ratio is lower than in soda glasses. Thus the selectivity of different glass electrodes made of sodium silicates may be compared, but comparisons of these with glasses containing lithium or potassium ions should be less reliable. These conclusions are based on mobility measurements in dry glasses; mobilities in hydrated glasses are much higher, and it is quite possible that some of the differences in mobility ratios found in dry glass are reduced in hydrated glasses. A more definitive analysis awaits further mobility measurements on hydrated glasses.

Results of numerous measurements of selectivities of glass electrodes for ions in aqueous solution, mainly in connection with the "alkaline error" of pH electrodes, are reviewed in Ref. 5, particularly Chapters 3, 6, 7, and 9. Since most of these measurements were not specifically designed to examine the role of glass composition, discussion of this work is limited to the extensive experiments of Eisenman.¹¹

In Eisenman's experiments the conditions on one side of the glass were held constant. The potential on this side of the glass, the electrode potentials, and junction potentials of salt bridges are constant with changing ionic concentrations and contribute only to V_0 , so the experiments should provide a measure of the product $K(u_B/u_A)$. For an ideal solution in the glass, Eq. 4 applies. If the glass is not ideal and the activities are given by Eq. 5, the potential is (see section on electrode potentials below)

$$V = V_0 + \frac{nRT}{F} \ln \left\{ a^{1/n} + \left[K_{AB} \left(\frac{u_B}{u_A} \right) b \right]^{1/n} \right\} \quad (7)$$

Since hydrogen ions are always present in aqueous solution, Eisenman measured the selectivities of the glass for alkali ions by determining the potential as a function of pH for a constant concentration (0.1 M) of alkali cation B . At higher pH the potential becomes constant because the glass is sensitive only to the alkali ion; the difference between this constant potential and one at a pH where the glass is sensitive only to hydrogen ions is equal to $(RT/F)[\ln K_{HB}(u_B/u_A)]$. If ion B is different from the alkali ion in the glass (usually sodium), the system contains three cations. However, as long as this ion is not in the solution, it contributes only a constant additional diffusion potential to V_0 and does not affect this method of calculating $K_{HB}(u_B/u_A)$. The

selectivity of the glass for any pair of ions can be found from the results of these measurements, since

$$K_{AB} \left(\frac{u_B}{u_A} \right) = \frac{K_{HB}(u_B/u_H)}{K_{HA}(u_A/u_H)}$$

Results of this kind are presented schematically for a variety of glasses in Fig. 1, taken from Ref. 11. The results are plotted in terms of the sodium-potassium selectivity of the glasses, therefore the abscissa is $\ln K_{NaK}(u_K/u_{Na})$, and the ordinate is the same term for any pair of ions, ij , $\ln K_{ij}(u_j/u_i)$. At the right of the figure, the lines are plotted in terms of the cesium-potassium selectivity. Although the data scatter considerably, a definite qualitative pattern in the selectivity of the ions emerges. Eisenman analyzed these patterns into the 11 sequences shown in Fig. 1. The data in the figures fit almost entirely into these few sequences, out of the 120 (5!) that are possible for the five ions. Thus the sodium-potassium selectivity provides a basis for estimate of the selectivity sequences of the glass.

The selectivity sequences are related in a definite way to the composition of the glass. For example, data for silicate glasses without boron and aluminum fall off Fig. 1 to the left, whereas the borosilicates fall to the right of the figure. In the sodium aluminosilicates, the important factor determining selectivity is the sodium/aluminum atom ratio. The theoretical significance of these results is discussed below.

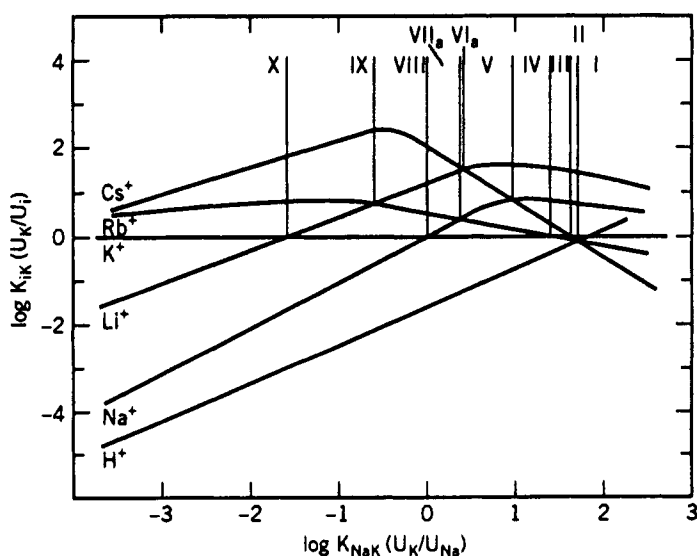


Fig. 1 Selectivity of sodium aluminosilicate glasses for monovalent cations. The roman numerals refer to selectivity sequences. A particular glass composition would be represented by a vertical line on the figure. From Eisenmann.¹¹

Other monovalent ions, such as silver, thallium, and ammonium, seem to fit into the selectivity sequences in a regular way.²⁹

Values for n from Eq. 5 and the potential data for hydrogen-alkali ion pairs were found to depend on the glass composition, and strongly on the cation, being higher (up to 6 for cesium) the larger the cation.

SELECTIVITY THEORIES

The simple empirical relation of Eq. 5 between activity and concentration of ions in the glass fits data on many different types of ion exchangers.^{8,9} Garrels has shown that this description is related to the solution theory of binary mixtures.^{1,30}

One of the simplest models of a binary solution results from quasichemical or nearest-neighbor assumptions about bonding in the solution. Somewhat more generally one can define a simple mixture as one that has a molar Gibbs free energy of mixing ΔG_m with the composition dependence.³¹

$$\Delta G_m = -EN_A N_B + RT(N_A \ln N_A + N_B \ln N_B)$$

where E is a net interaction energy that can depend on temperature, but not composition, and the N 's are the mole fractions. In terms of positive bond energies U , $E = U_{AB} - (U_{AA} + U_{BB})/2$. The second term results from the ideal entropy of mixing expression. From this equation, the activity coefficients gamma of the two components are given by³¹

$$\begin{aligned}\ln \gamma_A &= -EN_B^2/RT \\ \ln \gamma_B &= -EN_A^2/RT\end{aligned}\quad (8)$$

Here the reference state for activity is pure A for component A and pure B for B . Then the ratio of the activity coefficients is

$$\ln \frac{\gamma_A}{\gamma_B} = \frac{E(N_A^2 - N_B^2)}{RT} = \frac{E(N_A - N_B)}{RT}$$

To compare this with Eq. 5, it is assumed that the solution theory can be applied to the glass being considered as a rigid matrix with a mixture of A and B ions on the anionic sites. From Eq. 5,

$$\ln \frac{\gamma_A}{\gamma_B} = (n-1) \ln \left(\frac{N_A}{N_B} \right)$$

If the logarithm is expanded,

$$\ln \left(\frac{N_A}{N_B} \right) = 2 \left[(N_A - N_B) + \left(\frac{N_A - N_B}{3} \right)^3 + \left(\frac{N_A - N_B}{5} \right)^5 + \dots \right]$$

For N_A between 0.1 and 0.9, where most ion-exchange data are obtained, only

the first term in the brackets is important. A comparison of the two earlier equations gives

$$n = 1 + \frac{E}{2RT} \quad (9)$$

Thus the empirical Eq. 5 of Rothmund and Kornfeld has the same form as is derived from the simple solution model. When one or the other component is very dilute, the n representation of Eq. 5 is unrealistic for an exchanger with identical sites, since it requires the activity coefficient of the dilute component to be a function of its concentration even at great dilution. Under these conditions the simple solution equations should be used, but at intermediate compositions the simple n equation is often more convenient.

In the nearest-neighbor solution model a positive value of E denotes a net attraction between unlike atoms, whereas a negative value indicates repulsion. Since Eisenman,¹¹ Garfinkel,¹⁴ and Baucke²⁷ found n values greater than or equal to 1, their deviations from ideality in glasses were caused by attraction of the alkali and hydrogen ions. One would expect that as the size difference between the exchanging ions becomes greater, the nonideality or n value should become greater; this functionality was found, except for sodium-hydrogen exchange, which is nearly ideal ($n \approx 1$) for all glasses studied. Glasses with small selectivity between ions were closer to ideal than those with greater selectivity, possibly because the former are more hydrated. From this simple model one would expect more ideal behavior as the site density decreased; however, Fig. 5 of Ref. 11 does not seem to show any such dependence. Apparently the deviations from ideality depend on several factors in a complicated way.

The data of Eisenman, summarized in Fig. 1, show that the selectivity of glasses for ions has a definite dependence on the composition of the glass. The most important factor in this dependence is the type of anionic site in the glass. Thus the alkali silicate glasses containing no other glass former than silica show sequences X or XI (Fig. 1), with a strong preference for hydrogen and the smaller alkali ions. With aluminum or boron in the glass, however, the sequence is different and depends in a regular way on the glass composition. Eisenman proposed the following theory, based on the structure of the anionic sites in the glass, to explain these dependences.¹¹

The SiO^- anionic groups are more compact (the negative charge is less "spread out") than for the AlOSi^- site. Therefore the field strength, or attractive force for cations, is greater for the SiO^- site, giving it a smaller equivalent anionic radius. The interaction energies of these sites with alkali cations were calculated by Eisenman with a simple electrostatic model and compared to the free energies of formation of the hydrated ions in aqueous solution.¹¹ The SiO^- site showed the selectivity pattern XI, whereas the AlOSi^- site showed pattern I. It is therefore clear qualitatively why the glasses with only SiO^- sites prefer small ions, whereas the AlOSi^- sites (and similarly the BOSi^- sites) tend to show a preference for larger ions. Eisenman defined

the equivalent anionic radius of a site to be the radius which yields the same electrostatic energy with each cation as does the actual site. On this basis the silicate site has an effective radius of about 0.9 Å, whereas the aluminosilicate site has one of about 2.0 Å.

It is also possible to estimate the effective anionic radius of a group from the dissociation behavior of an acid containing it. For example, Eisenman observed that silicic acid is very weak, whereas the aluminosilicate group gives a strong acid. He calculated anionic radii comparable to those of the preceding paragraph by comparing the dissociation constants of these groups with those of halide acids.¹¹ Boric acid is quite weak, so the selectivity of sodium borate glass should be similar to that of sodium silicate glass. The attraction of borate glass for higher valent ions, as opposed to the behavior of silicate glasses, may possibly result from a shorter distance between neighboring anionic groups in the former. This behavior is also found in amorphous and polymeric phosphates. In borosilicates, on the other hand, the BOSi^- group appears to be similar to the AlOSi^- group.

Nicolosky et al.²⁶ showed that both the SiO^- and AlOSi^- sites contribute to the potentials measured in glass electrodes made with sodium aluminosilicate glasses containing less than about 3 wt% Al_2O_3 ; however, above this composition only the AlOSi^- sites seem to be effective. In hydrated glass the SiO^- site has H^+ , rather than Na^+ , associated with it. Apparently the presence of the AlOSi^- sites suppresses exchange of other ions with the $\text{SiO}^- \text{H}^+$ site or, in terms of Eisenman's model, increases the field strength of the silica site.

In comparing experimental data derived from electrode potentials with the calculations, the effect of changes in mobility ratio has been completely ignored. As mentioned previously, this assumption may be reasonable for certain groups of glasses, for example, for sodium silicates, but is uncertain for others. The qualitative success of Eisenman's considerations indicates that in hydrated glasses the equilibrium selectivity effects are possibly larger than changes in mobility ratios. In a more refined treatment, however, these changes in mobility ratio must be taken into account.

Eisenman's selectivity theory can also be applied to the results on distributions between glass and fused salts, although in this case data are not available for hydrogen, rubidium, or cesium ions. The strong selectivity of soda-lime glass for sodium over potassium results from the small anionic radius of the SiO^- groups, just as for hydrated glasses. Silver is anomalous for its size because of its strong polarizability, which causes it to be attracted strongly by the SiO^- anion.

In the aluminosilicates, the preference for silver is reduced because of the larger anionic radius of the aluminosilicate group. The selectivity of sodium over potassium found in the soda-lime glasses is lost, although the smaller lithium ion is still preferred over sodium. In the borosilicate phases there is little selectivity between silver, sodium, and potassium ions, again reflecting the larger anionic size of the borosilicate groups. In fused silica, the monovalent ions are associated with the alumina groups in the glass, so a greater relative

attraction of these groups for lithium than for sodium, and little selectivity between sodium and silver, is reasonable. In a sodium aluminoborate glass with no nonbridging oxygens, as determined for XPS spectra (see Chapter 12), silver from silver nitrate was still strongly preferred by the glass to sodium^{18,19} (see Table 1). However, in this glass the n value was less than 1, in contrast to all other results on silicate glasses. This result suggests that the silver and sodium ions in the glass have a net repulsion, rather than the net attraction found in all other ion exchange pairs. Surprisingly the silver-sodium equilibrium data fit the " n " equation 5 better than the full quasichemical expression, suggesting some strange behavior at both high and low silver concentrations in the glass.

Recent interest in new optical components such as gradient index lenses and optical waveguides has led to ion exchange as a method of introducing a gradient of refractive index in the surfaces of these optical components. This interest has led to a large number of papers in this area, which is discussed in Chapter 17. Introducing silver by ion exchange is attractive because silver changes the refractive index substantially, because of its high polarizability. In exchange with nitrate melts, the preference of the glass for silver is an asset for these applications (see Refs. 49 and 50 and other references in these papers and in Chapters 15 and 17).

POTENTIALS OF GLASS ELECTRODES

Until the 1960's the origin of potentials in glass electrodes was not well understood. However, recognition that the glass electrode is analogous to an ionic membrane, and studies of ionic behavior in glass in both aqueous solution and fused salts, have led to clarification of this problem. The historical development of the understanding of glass electrode potential is summarized in Ref. 5, Chapters 3 and 5, and Ref. 29. The treatment of the ion exchange theory given here is taken from Chapter 4 of Ref. 5, to which the reader is referred for further details.

The experimental arrangement that is used to measure electrode potentials is shown schematically in Fig. 2. A thin piece of glass separates two sources of ions. These sources could be gases, liquids, or solids; however, only two types of sources have been studied: aqueous solutions and mixed fused salts. These sources are referred to as solutions. A reference electrode is placed in each solution, and the total potential between these electrodes is read by an external instrument, such as a potentiometer or electrometer.

Two types of measurements are of interest here. In the first type, the conditions in solution 2 are held fixed, and the potential is varied by changing the conditions in solution 1. The potential between reference electrode 1 and solution 1 must also be constant under these changing conditions. Then the only changes in the system occur at the solution 1-glass interface. No attempt is made to interpret the absolute value of the potential measured; only its

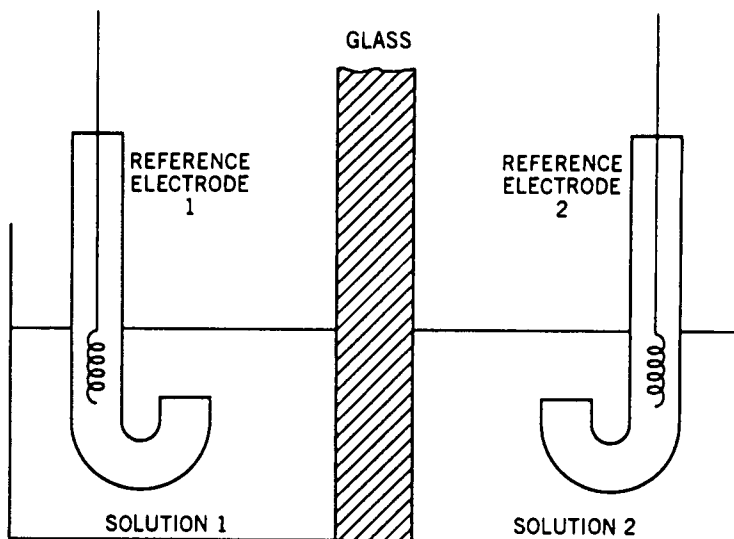


Fig. 2 Schematic diagram of a cell used to measure potential in glass.

changes with respect to an arbitrary value are considered. This is the type of measurement made in conventional pH meters and in most measurements of the concentrations of other ions with a glass electrode. In the pH application the glass is formed into a bulb, with solution and reference electrode 2 on the inside and solution and electrode 1 outside. Reference electrode 2 is usually a calomel or silver-silver chloride electrode, and solution 2 a buffered chloride solution.³² Reference electrode 1 can be a calomel electrode connected to solution 1 by a saturated potassium chloride salt bridge. Under these conditions, variations in the pH of solution 1 change the total cell potential by changing the conditions at the solution-glass interface.

In a second type of measurement, the absolute value of the cell potential is studied. Usually solvents 1 and 2 are the same, and the reference electrodes are also the same, therefore their potentials cancel or are calculable. Then the total membrane potential (measured directly or calculated) is that caused by different ionic concentrations in solutions 1 and 2, giving rise to different conditions at the two solution-glass interfaces.

The total membrane potential V of a glass electrode can be separated into two additive parts: the boundary or surface potential V_s and the diffusion potential V_D . To interpret measurements of the membrane potential, equations for both V_s and V_D are necessary. First the equations for the surface potential are described.

Consider an ionic solute in two different phases at constant temperature and pressure. If both positive and negative ions can exchange between the two phases, considerations similar to those for a molecular solute apply. However, if only ions of one sign can exchange between the two phases as with silicate

glasses, electrical fields can arise. At equilibrium between the two phases the total (or electro-) chemical potentials μ of the exchanging cations in them must be equal. However, this equality cannot be achieved by gross changes of the cation concentration in the glass because the concentration is fixed by the number of anionic groups in the glass network. As the cations leave or enter the glass, giving an excess or deficient total charge, an electrical-potential difference between the two phases builds up. At equilibrium this electrical-potential difference $(\chi' - \chi'')$ just balances the difference in thermodynamic activity of the cations between the two phases. In equation form,

$$\mu' - \mu'' = \phi' - \phi'' + RT \ln \left(\frac{a'}{a''} \right) + Z(\chi' - \chi'')F = 0$$

where F is the Faraday constant, Z is the valence (assumed to be $+1$) of the exchanging ions, ϕ is a function of temperature only and is often called the standard chemical potential, and one prime represents the solutions and two primes the glass.

In the experimental arrangement of Fig. 2, an equation of this type applies to both solution-glass boundaries, so the overall boundary potential V_s for the presence of one cation is

$$V_s = (\chi'_2 - \chi'_1) - (\chi''_1 - \chi''_2) = \frac{[(\phi'_1 - \phi'_1) - (\phi'_2 - \phi'_2)]}{F} + \left(\frac{RT}{F} \right) \ln \left(\frac{a'_1 a''_2}{a'_2 a''_1} \right) \quad (10)$$

where solution 2 is considered positive.

If the glass is uniform and homogeneous, $\phi'_1 = \phi'_2$ and $a'_1 = a'_2$. If both solvents are the same and the same reference state for activity of the ion is used for them, then $\phi'_1 = \phi'_2$, and

$$V_s = \left(\frac{RT}{F} \right) \ln \left(\frac{a'_1}{a'_2} \right) \quad (11)$$

so that the boundary potential is a direct measure of the activity ratio of the exchanging ion in the two solutions. In the normal use of glass electrodes, the conditions in solution 2 are held constant, and the relative variation of V_s then measures the activity of the ion in solution 1. If only one ion is present, there is no diffusion potential in the glass.

Purists may object to the individual ionic activities used in the above derivation, since they cannot be measured separately. However, if other components are carried along throughout the derivation, the results are the same. Only ratios of ionic activities, which can be measured, appear in the final results. A further discussion of this point is given by Helfferich (Ref. 2, pp. 140-369 ff.).

From Eq. 2, for both surfaces 1 and 2,

$$\frac{a'}{a''} = \frac{(a' + Kb')}{(a'' + b'')}$$

so from Eq. 10 the boundary potential is

$$V_s = \frac{RT}{F} \left(\ln \frac{a'_1 + Kb'_1}{a'_2 + Kb'_2} - \ln \frac{a''_1 + b''_1}{a''_2 + b''_2} \right)$$

If the sum of the activities in the glass is the same at both surfaces, the total boundary potential is related to the solution activities by

$$V_s = \left(\frac{RT}{F} \right) \ln \left[\frac{(a'_1 + Kb'_1)}{(a'_2 + Kb'_2)} \right] \quad (12)$$

However, if Eq. 5 is followed and n is not unity, the sum of the activities at the two faces is generally not the same, and the second term must be retained. An alternative form for this case is given by Eisenman,¹¹ and also below (Eq. 17), including the diffusion potential.

In the limit of small concentrations of either A or B in both solutions, Eq. 12 goes to Eq. 11. Similar, but more complicated expressions, are valid when more than two ions exchange.

Now equations for the diffusion potential are derived from the Nernst-Planck equations for interdiffusion of two ions, as described in Chapter 15. From Eq. 19, Chapter 15, the electrical field set up when two monovalent ions interdiffuse is

$$E = \frac{RT}{F} \frac{u_B - u_A}{c_A u_A + c_B u_B} \frac{\partial c_A}{\partial x} \frac{\partial \ln a_A}{\partial \ln c_A} \quad (13)$$

and the diffusion potential V_D is, again considering solution 2 positive,

$$V_D = \int_1^2 E dx = \frac{RT}{F} \int_{c_A(1)}^{c_A(2)} \frac{(u_B u_A) - 1}{c_B (u_B/u_A) + c_A} \frac{\partial \ln a_A}{\partial \ln c_A} dc_A \quad (14)$$

Therefore the diffusion potential depends only on the ionic concentrations at the two surfaces $c_A(2)$ and $c_A(1)$, the mobility ratio u_B/u_A , and the thermodynamic factor $\partial \ln a_A / \partial \ln c_A$. The latter can be written

$$\frac{\partial \ln a_A}{\partial \ln c_A} = 1 + \left(\frac{c_A}{\gamma_A} \right) \left(\frac{\partial \gamma_A}{\partial c_A} \right)$$

since the activity coefficient γ is defined by $a = \gamma c$. Therefore this term measures the change in activity coefficient with concentration; if this coefficient is constant, the term is unity. If the ion exchange follows Eq. 5, and a constant mobility ratio, Eq. 14 can be integrated to

$$V_D = \frac{nRT}{F} \ln \frac{c_A(2) + c_B(2)(u_B/u_A)}{c_A(1) + c_B(1)(u_B/u_A)} \quad (15)$$

where use is made of the constancy of the total ionic concentration $c_A + c_B$. The diffusion potential can be related to the ionic concentrations in the

external solution through the coefficient K of Eq. 2. For the same solvent in the two solutions and $n = 1(a''/b'' = c_A/c_B)$, the result is³³

$$V_D = \frac{RT}{F} \left[-\ln \frac{a'_2 + K(u_B/u_A)b'_2}{a'_1 + K(u_B/u_A)b'_1} + \ln \frac{a'_2 + Kb'_2}{a'_1 + Kb'_2} \right] \quad (16)$$

The total membrane potential V for $n = 1$, including both boundary and diffusion contributions, is the sum of Eqs. 12 and 16 (see Ref. 33):

$$V = \frac{RT}{F} \ln \frac{a'_1 + K(u_B/u_A)b'_1}{a'_2 + K(u_B/u_A)b'_2} \quad (17)$$

If the mobility ratio and thermodynamic term are functions of concentration, Eq. 14 cannot be integrated without knowledge of this functionality. However, even in this case the potential V_D is not a function of time, but only of the surface concentrations, for a given dependence of the mobility ratio and thermodynamic term on ionic concentration. Therefore as soon as equilibrium between the solutions and glass surfaces is established, the diffusion potential is fixed and does not change with time, independent of the concentration profile of diffusion ions in the glass. The diffusion potential should change with time only if there is some change in structure of the glass with time or position, giving changes of mobility ratio or thermodynamic factor with time and position. Examples of this kind of change are progressive hydration of the glass in contact with water, internal variations in the glass structure, and stress changes in the glass.

Various complications in potentials of glass electrodes are treated in the following references: multicationic systems (Refs. 6 and 34); pressure or stress gradients (Ref. 6); inhomogeneous glass (Refs. 6 and 34); and phase separation (Ref. 35).

EXPERIMENTAL MEASUREMENTS OF POTENTIALS OF GLASS ELECTRODES

A vast number of measurements of potentials of glass electrodes have been made, with objectives ranging from the development of practical analytical tools to the understanding of theories for the electrode potential. Earlier measurements are reviewed in Refs. 5, 32, 36 and 37. In this section, a few more recent measurements of special kinds are singled out for comment.

Changes of glass electrode potentials and electrical resistance in aqueous solutions as a function of time have been measured under a variety of conditions.³⁸⁻⁴⁰ These experiments are important in determining the time required before the electrodes are acceptably stable. Response times for glass electrodes have also been studied.^{41,42}

The selectivity of Pyrex electrodes to various ions in fused nitrate has been deduced from their potentials,^{43,44} and a selectivity sequence of

$\text{Na}^+ > \text{Ag}^+ > \text{Li}^+ > \text{K}^+ > \text{NH}_4^+ \approx \text{Tl}^+$ was found. However, these results represent changes in the product $K(u_B/u_A)$ and not in K itself, since the mobility ratios were not measured. These ratios can be quite different from unity in dry glass, so the above sequence must be considered tentative. Furthermore, ionic activities in molten ammonium nitrate, which was used as a solvent in some experiments, were not measured, leading to further uncertainties in the meaning of the selectivities found.

EXPERIMENTAL CONFIRMATION OF POTENTIAL EQUATIONS

Many theories, in addition to the ion exchange theory given above, have been suggested to explain the origin of potentials of glass electrodes.^{29,36,37,45,46} Dole classified the theories into phase-boundary, ion-adsorption, and diffusion-potential categories. In virtually all of these theories, it is found that the potential V of a glass electrode when it is sensitive to only one ion A is given by

$$V = V_0 + \frac{RT}{F} \ln a_s \quad (18)$$

where V_0 is independent of concentration, and a_s is the activity of the ion in solution in contact with the electrode. This equation is the same as Eq. 11 with $V_0 = -RT/2F \ln a'_2$. V_0 can be different from this value if electrode compartment 2 has different conditions (for example, if different ions are in it), but as long as conditions in this compartment are held constant, V_0 will be constant. In this single-ion case there is no diffusion potential. A large number of results agree with Eq. 18; for example, pH measurements with a glass electrode.

When another ion B also has influence on the potential, the following equation is derived in most theories when the glass phase is ideal (ions have constant activity coefficients in it):

$$V = V_0 + \frac{RT}{F} \ln(a_s + K'b_s) \quad (19)$$

where b_s is the activity of B in the solution, and K' is a coefficient independent of ionic concentration. This equation has the same form as Eq. 17 with conditions constant in one compartment and $K' = K(u_B/u_A)$. If the glass is not ideal, but activities in it are given by Eq. 5, then the potential is given by Eq. 7.

Several investigators have found agreement between Eq. 19 and data on electrode potentials and claimed this agreement was proof of the theory they espoused. However, since different theories can lead to Eq. 19, it is essential to test values of K' with independent data to decide which theory is preferable. Only a few such tests have been made. In the ion exchange theory derived above, $K' = K(u_B/u_A)$, the product of the equilibrium distribution coefficient and the mobility ratio of the ions.

Eisenman measured the potentials of hydrated glass electrodes selective to

sodium and potassium ions in aqueous solutions of these ions (Ref. 5, Chapter 5) and calculated values of $K(u_B/u_A)$ from these measurements. He also measured the mobility ratio and distribution coefficient independently from the penetration of radioactive tracer ions into the hydrated layer. The product $K(u_B/u_A)$ calculated in these two different ways was nearly the same, confirming the ion exchange theory for hydrated glass electrodes in aqueous solution.

The ion exchange theory was tested for dry fused silica electrodes immersed in molten nitrate mixtures at 333°C.⁴ Again Eq. 19 was obeyed for the membrane potentials, from which $K' = 0.18$ was calculated for sodium-silver nitrate ion solutions. The ratio of silver-to-sodium mobility was found to be 0.073 from the conductivities of the glass containing only one ion or the other, and K was measured from electrolysis experiments, as described in the first section, and was found to be 2.1, giving $K' = 0.15$ in good agreement with the value measured from membrane potentials. Thus the ion exchange theory is judged to be valid in this case also.

Measurements of K' for Pyrex glass tubes immersed in molten nitrates have also been made;^{23,35} however, the two-phase behavior of this glass complicates interpretation of the results. For concentrations of silver nitrate above about 10%, K' was calculated to be about 1.1 from measurements of the membrane potential, although these were deviations of up to 10 mV from the expected potential.³⁵ In this range of melt concentrations, $K \approx 2.0$, and the mobilities of silver and sodium were about equal, giving $K' = 2$. This agreement within a factor of two is further evidence for the validity of the ion exchange model.

Garfinkel measured membrane potentials, mobility ratios, and distribution coefficients for sodium-potassium nitrate melts exchanging with Pyrex glass.^{14,23,47} He found evidence for change in individual ionic mobilities as a function of concentration, as well as other concentration dependencies resulting from the two phases, and thus was unable to make an exact comparison between his result and the ion exchange theory.

van Keenan et al.²¹ measured membrane potentials of glass electrodes in zinc chloride melts containing sodium and lithium ions. Their results for ionic distribution coefficients and mobility ratios were derived from electrolysis measurements, and were somewhat uncertain because they did not take account of activity coefficient changes in the melt, as mentioned above. Furthermore, they neglected the two-phase nature of the glass. Nevertheless they achieved reasonable agreement between measured potentials and those calculated from the mobility ratio, which was a function of ionic concentration in the glass, and distribution coefficients. It seems likely that compensating errors in measurements of mobility ratios and distribution coefficients were at least partly responsible for this agreement, since the authors reported that these two factors seemed to be related and not independent. In spite of these uncertainties these results provide further evidence that the ion exchange theory is valid for glass electrodes.

Tadros and Lyklema found that the surface charge of hydrated sodium-

sensitive glass electrodes in solutions of various alkali chlorides was the same for several different cations (lithium, sodium, potassium, cesium, and tetraethyl ammonium).⁴⁸ The surface charge at a certain pH was calculated from the amount of acid or base that had to be added to a solution plus powdered glass to reach this pH, less the amount that had to be added to the same solution without glass to reach the desired pH. Thus the surface charge was actually a measure of the adsorption of monovalent cations on the surface, associated with the negatively charged SiO groups (see the section on adsorption from solution, 1st edition). These authors concluded that the surface potential V_s for all these ions was the same, since the affinity of the hydrated layer for the ions was the same. They therefore concluded that the value of K (with respect to hydrogen ion) for all these cations was the same, and differences in the selectivity of the glass resulted entirely from different mobility ratios and diffusion potentials, and not from differences in surface potentials. Such a result is not inconsistent with the ion exchange theory, but is contrary to Eisenman's finding that mobilities of sodium and potassium ions in the hydrated layer differed only by factors of five to twelve, and that most of the selectivity of these electrodes resulted from different K values and surface potentials.

The resolution of this discrepancy may reside in the distinction between adsorption just at the glass surface and the selectivity of groups inside the hydrated layer. The experiments of Tadros and Lyklema measured adsorption at the outermost portions of the glass surface, since in their experiments there was insufficient time for interdiffusion of ions very far into the hydrated layer. On the other hand, the equilibrium membrane potential of a glass electrode in a solution of two ions, both of which are present in appreciable amounts in the hydrated layer, results from the selectivity of the bulk of the hydrated layer, not from its surface groups. A longer time is required for these ions to interdiffuse and equilibrate some appreciable distance (several molecular layers) into the hydrated layer than for adsorption at its outer surface. This requirement for longer equilibration time is not contradicted by the rapid response time of a glass electrode in solutions of ions that the electrode selects strongly, for example, in pH electrodes. In this case the surface is saturated with the ion to which the electrode is responding, and when the concentration of this ion in solution changes, the electrode potential changes rapidly because no interdiffusion in the hydrated layer is necessary for establishment of the characteristic membrane potential. Thus Tadros and Lyklema were measuring selectivities of the outermost surface SiO groups for hydrated ions in solution, which can be very different from the selectivities for the unhydrated ions in the bulk of the hydrated layer on the glass.

Different amounts of surface adsorption do not affect overall membrane potentials as long as the adsorbed layer is in equilibrium with both the glass exchanger (hydrated layer) and the surrounding solution. If the adsorbed layer is at equilibrium, it can have no concentration gradients and therefore no diffusion potential, and this layer will contribute no additional phase boundary

potential to the measured membrane potential, since the electrochemical potential of ions at the membrane surface will still equal their potential in solution.

The insensitivity of membrane potential to surface adsorption was shown by experiments on fused silica membranes.²⁸ If the silica surface was treated with nitric acid its surface was highly hydrated, and it strongly adsorbed silver ions from nitrate melts containing silver ions, as shown by radioactive tracer measurements. When the silver surface was treated with dilute hydrofluoric acid, the hydrated layer was removed, and the adsorption of silver was negligible. However, in both these samples, the measured membrane potential was the same for the same contacting solutions, as was the coefficient K .

Baucke⁴⁶ put forward a theory of glass electrode potential that he describes as including a "dissociation mechanism". In this theory the equilibrium of ions at the glass surface (Eq. 12) is included, but not the diffusion potential. In his words: "Particularly, the correct pH response of protonated glass electrodes in alkali-free solutions excludes mechanisms which are based on an exchange of different ions between glass and solution, e.g. as assumed for the ion exchange theory." To the contrary, the above treatment shows that the internal diffusion potential must be included, even if there are alkali ions in solution. The ion exchange theory has been established to hold for glasses experimentally;^{4,5} the mobility ratio or internal diffusion potential must be included to obtain agreement between theory and experiment. Diffusion potentials also occur in organic ion exchange membranes; these potentials must be included to obtain experimental and theoretical agreement for these membranes (Ref. 2, p. 377 ff).

REFERENCES

1. R. H. Doremus, in *Ion Exchange*, J. Marinsky, Ed., Marcel Dekker, New York, 1969, p. 1.
2. F. Helfferich, *Ion Exchange*, McGraw-Hill, New York, 1962.
3. G. Schulze, *Ann. Phys.*, **40**, 335 (1913).
4. R. H. Doremus, *J. Phys. Chem.*, **72**, 2877 (1968).
5. G. Eisenman, Ed., *Glass Electrodes for Hydrogen and Other Cations*, Marcel Dekker, New York, 1967.
6. R. H. Doremus, in *Glass Electrodes for Hydrogen and Other Cations*, G. Eisenman, Ed., Marcel Dekker, New York, 1967.
7. F. Helfferich, *Ion Exchange*, McGraw-Hill, New York, 1962. pp. 193 ff., where there are other references.
8. H. F. Walton, in *Ion Exchange, Theory and Application*, F. C. Nachod, Ed., Academic Press, New York, 1949, p. 1.
9. E. Hogfeldt, *Acta Chem. Scand.*, **9**, 151 (1955).
10. V. Rothmund and G. Kornfeld, *Z. Anorg. Allg. Chem.*, **103**, 129 (1918); **108**, 215 (1919).

11. G. Eisenman, *Biophys. J.*, **2**, 259 (1969).
12. R. H. Doremus, unpublished work.
13. M. H. Rowell, *J. Inorg. Chem.*, **4**, 1802 (1965); **5**, 1828 (1966).
14. H. M. Garfinkel, *J. Phys. Chem.*, **72**, 4175 (1968).
15. R. H. Doremus, *Phys. Chem. Glasses*, **10**, 28 (1969).
16. K. Stern, *J. Phys. Chem.*, **74**, 1323 (1970).
17. O. R. Flinn and K. H. Stern, *J. Phys. Chem.*, **76**, 1072 (1972).
18. C. Kaps and W. Fliegel, *Glastech. Ber.*, **64**, 199 (1991).
19. C. Kaps, *Glastech. Ber.*, **64**, 235 (1991).
20. V. V. Moiseev, *J. Noncryst. Solids*, **42**, 589 (1980).
21. T. H. van Reenan, M. Niekerk, and W. J. deWet, *J. Phys. Chem.*, **75**, 2815 (1971).
22. R. H. Doremus, *Phys. Chem. Glasses*, **9**, 128 (1968).
23. H. M. Garfinkel, *J. Phys. Chem.*, **73**, 1766 (1969).
24. R. H. Doremus, *J. Phys. Chem.*, **72**, 2665 (1968).
25. B. P. Nicolovsky and T. A. Tolmacheva, *Zh. Fiz. Khim.*, **10**, 504 (1937).
26. B. P. Nicolovsky, M. M. Schulz, E. A. Materova, and A. A. Balijustin, *Akad. Nauk SSSR*, **140**, 641 (1961).
27. F. G. K. Baucke, in *The Physics of Noncrystalline Solids*, G. H. Frischat, Ed., Trans. Tech., Aedermannsdorf, Switzerland, 1977, p. 503.
28. R. H. Doremus, unpublished.
29. G. Eisenman, *Adv. Anal. Chem. Instrum.*, **4**, 305 (1965).
30. R. M. Garrels and C. L. Christ, *Solutions, Minerals, and Equilibria*, Harper and Row, New York, 1965, pp. 272 ff.
31. C. H. P. Lupis, *Chemical Thermodynamics of Materials*, North-Holland, Amsterdam, 1983, p. 235 ff.
32. R. G. Bates, in *Reference Electrodes*, D. J. G. Ives and G. J. Janz, Eds., Academic Press, New York, 1961, p. 231.
33. G. Karreman and G. Eisenman, *Bull. Math. Biophys.*, **24**, 413 (1962).
34. F. Conti and G. Eisenman, *Biophys. J.*, **5**, 247 (1965).
35. R. H. Doremus, *J. Elect. Soc.*, **115**, 924 (1968).
36. M. Dole, *Glass Electrode*, Wiley, New York, 1941.
37. K. Schwabe and H. D. Suschke, *Angew. Chem.*, **76**, 39 (1964), and earlier papers by Schwabe and co-workers.
38. M. J. D. Brund and G. A. Rechnitz, *Anal. Chem.*, **41**, 1788 (1968).
39. R. P. Buch, *J. Electroanal. Chem.*, **18**, 363 (1968).
40. A. Wikby and G. Johansson, *J. Electroanal. Chem.*, **23**, 23 (1969); **33**, 145 (1971).
41. G. A. Rechnitz and G. C. Kugler, *Anal. Chem.*, **39**, 1682 (1967).
42. A. E. Bottom and A. K. Covington, *Anal. Chem.*, **24**, 251 (1970).
43. N. Notz and A. G. Kennan, *J. Phys. Chem.*, **70**, 662 (1966).
44. A. G. Keenan, N. Notz, and F. L. Wilcox, *J. Phys. Chem.*, **72**, 1085 (1968).
45. M. Dole, *J. Am. Chem. Soc.*, **53**, 4620 (1931).
46. F. G. K. Baucke, *J. Noncryst. Solids*, **73**, 215 (1985); **129**, 233 (1991).

47. H. M. Garfinkel, *Phys. Chem. Glasses*, **11**, 151 (1970).
48. J. F. Tadros and J. Lykelema, *J. Electroanal. Chem.*, **22**, 9 (1969).
49. S. N. Houde-Walter and D. T. Moore, *Appl. Opt.*, **25**, 3373 (1986).
50. T. Poszner, G. Schreiter, and R. Mulli, *J. Appl. Phys.*, **70**, 1966 (1991).

ELECTRICAL CONDUCTIVITY AND IONIC DIFFUSION

In many applications, glass must serve as an electrical insulator or conductor, and therefore understanding of its electrical conductivity is important. Ionic transport plays a role in other applications and in manufacture of glass. Rates of chemical reactions in glass melting are often controlled by diffusion. Ionic motion in the amorphous silica layers on silicon devices can interfere with their performance and must often be suppressed.

In most oxide glasses, the electrical conductivity results from ionic motion. In certain special compositions containing multivalent oxides, such as vanadium pentoxide or iron oxide, the conduction is electronic. Most chalcogenide glasses, those containing pure or combined sulfur, selenium, or tellurium, are also electronic conductors; it is their semiconducting and switching properties that have excited interest in these glasses. The "salt"-type glasses of halides, nitrates, sulfates, and aqueous solutions are ionic conductors. Organic glasses can be either electronic conductors or show ionic conduction resulting from impurities.

The ionic conductivity of virtually all oxide glasses results from the transport of monovalent cations. In most commercial glasses the conducting ion is sodium. Faraday's law is found to hold for these glasses, and a number of electrolysis experiments,^{1,2} reviewed in detail in earlier publications,^{3,4} have established the ionic nature of the conduction process. Lithium ions also are quite mobile in oxide glasses. Potassium and hydrogen ions sometimes carry current, although their mobility is usually lower than that of sodium and lithium. Even in glasses with no nominal addition of monovalent ions, the conductivity results from transport of monovalent cations. In fused silica,

electrolysis experiments show that sodium and lithium ions are the conducting species, even though they are present only in quantities of a few parts per million.⁵

The conduction mechanism in various "alkali-free" silicate and borate glasses containing lead, aluminum, and alkaline earth ions is uncertain. Conduction does not result from sodium ion motion in sodium-lead silicate glasses containing less than 5 mol% Na_2O , 50% SiO_2 , and the balance PbO , as shown from electrolysis measurements.⁶ In a 50 mol% BaO , 50% SiO_2 glass the diffusion coefficient and concentration of sodium were too low to give the measured conductivity,⁷ as calculated from the Einstein equation, given in the section below on the relation between conductivity and diffusion. The electrical conductivity of 50 mol% CaO , 50% SiO_2 glasses was insensitive to sodium concentration in the range from 45 parts per million to 1.26 mol% Na_2O .⁸ Thus it appears that alkali ions do not carry the current in any of these glasses. The diffusion coefficient of oxygen in calcium aluminum silicate glasses is apparently too low to account for their conductivity;⁹ in calcium aluminum borate glasses, the contribution of oxygen is uncertain.^{9,10} In lead silicate and borate glasses, the diffusion coefficient of oxygen gives too high a conductivity from the Einstein equation, and the activation energy for oxygen diffusion, 11 kcal/mol, is much less than the 24 kcal/mol for conduction.¹¹ It therefore seems likely that these experiments measure the diffusion of molecular oxygen and its reaction with the lattice, as described in Chapter 8, and that the diffusion of lattice oxygen is much slower.

The electrical conductivity of lead silicate,⁶ calcium silicate,¹² and barium aluminum borate¹³ glasses was affected by the presence of $-\text{OH}$ groups. Thus it seems possible that hydrogen ions are carrying the electrical current in these glasses.^{6,12,13} In most silicate glasses, the mobility of hydrogen ions is about three to four orders of magnitude lower than the mobility of sodium ions,^{14,15} but it is possible that the mobility of protons is higher in the alkaline earth, lead, and aluminosilicate glasses. It is known that alumina groups lead to relatively less tightly bound hydrogen ions in silicate glasses,¹⁵ so a relatively high hydrogen ion mobility is particularly likely in aluminosilicate glasses.

In barium silicate glasses with 30 and 50 mol% barium oxide, Evstrop'ev and Kharyuzov⁷ found that the diffusion coefficient of barium ions and the electrical conductivity obeyed Einstein's equation; however, in calcium silicate glasses the diffusion coefficient of calcium is much too low to account for the electrical conductivity, and apparently hydrogen ions carry the current.¹² The diffusion coefficient of lead in lead silicate glasses gives about the right value of conductivity from the Einstein equation; however, electrolysis experiments show that the lead ion is not conducting.⁶ It is also possible that electrons carry part or all of the current in these glasses.

Trnovcová et al.^{15a} studied the electrical conductivity of alkaline earth aluminophosphate glasses and found that the conductivity increased as the water content of the glasses increased. They found that the diffusion coefficients of the alkaline earth ions and impurity sodium ions were too low to cause the conductivity, and concluded that protons were the dominant carriers.

Abe and co-workers¹⁶⁻¹⁸ have explored the electrical conductivity of alkali-free phosphate glasses. They found that the conductivity was directly related to the concentration of hydroxyl groups (OH) in calcium phosphate glass, and they also concluded that protons were the charge carriers in this glass and a variety of alkaline earth phosphates. Their published infrared absorption spectra show strong absorption of the base glass at the wave number where molecular water absorbs (1630 cm^{-3}), so it is not possible to tell whether the glass contains appreciable molecular water.

Ernsberger¹⁹ has concluded that bare protons are bound too tightly to oxygen ions in oxide glasses to have appreciable mobility, even at high temperatures. He suggested that hydrogen ion transport occurs only in association with a water molecule. A careful study of the infrared absorption band of molecular water at 1630 cm^{-1} in these glasses should help to decide upon the validity of this mechanism.

This chapter contains sections on the following subjects: methods of measuring ionic conductivity and diffusion; the relation between conductivity and diffusion; the effect of temperature, stress, and glass composition on ionic transport in glass; fast ion transport, interionic diffusion in glass; and finally theories of ionic transport. Earlier reviews on these subjects are given in Refs. 3, 4, 15, and 20-30.

MEASUREMENT OF ELECTRICAL CONDUCTIVITY AND IONIC DIFFUSION

The electrical conductivity of a solid ionic conductor can be measured with direct or alternating current. In a direct current (DC) measurement, a space charge is often set up in the glass because of partial blocking of the ionic current by the electrodes; then the current decreases rapidly with time, and its value must be extrapolated to zero time if an accurate value of conductivity is desired. To avoid this electrode polarization, alternating current is usually used, of a frequency from 10^3 to 10^6 cycles/s. Silicate glasses show dielectric losses at these frequencies, however, so care must be taken to make the measurements over a wide frequency range. If a constant sample resistance is found over several decades of frequency, one can be reasonably certain that an accurate value of conductivity is being measured. Such constancy is usually not found. The result of these difficulties is that many experimental measurements of electrical conductivity of glasses that have been reported in the literature are not reliable.

The type of electrode and preparation of the glass surface can have a strong influence on the measured conductivity, especially at frequencies below 10 cycles/s. Kim and Tomozawa found that evaporated gold electrodes showed fewer deviations from low frequency dielectric constants and conductivity than did gold paste electrodes.³¹ Polishing and etching the glass surface gave quite different results from the as-received glass. Kim and Tomozawa concluded that surface hydrated layers influenced the results, and that electrode and surface

effects resulted from space charge at the glass surface. These results show that blocking or partially blocking electrodes can cause misleading results of electrical conductivity measurements.²⁹ Electrode and surface hydration problems are more severe with less durable glasses (see Chapter 13).

A method that avoids these problems is to return to a DC measurement and to use electrodes of fused salts.^{5,32} In this way electrode reactions and frequency effects are eliminated. A simple experimental arrangement consists of a glass tube partially filled with molten salt in a molten salt bath. A variety of metallic electrodes can be inserted into the bath; if small currents are used, contamination of the bath by electrode reactions is minimized. The molten salt has a much higher conductivity than the glass, so nearly all the potential drop is across the glass. Care must be taken that the bath contains the ion conducting in the glass, usually sodium, in sufficient quantity to prevent depletion, and that other possible conducting ions, such as lithium, must be present in low enough quantity so that they do not cause any change in the conductivity of the glass by exchanging with the conducting ions in it. One difficulty with this method is to find stable salt melts for wide ranges of temperatures. Alkali nitrates have low melting points but decompose above about 450°C. Many other salts are hygroscopic; that is, they absorb moisture from the atmosphere, so that many of them can be used only in a dry atmosphere. Any fused salt should be purged with dry gas to remove residual water. In some salts, such water is tenaciously held, and they must be heated for long times at high temperatures to remove it. Even in fused salts there is some evidence of problems with surface resistance.³³

Stresses in glass can increase the conductivity up to a factor of 10. These stresses are removed by holding the glass at its annealing temperature for about 0.5 h and then cooling it slowly (1°C/min). All results reported here are on annealed glasses unless otherwise stated.

The specific resistivity ρ in ohm-cm is defined as the resistance of a sample of unit area A and unit thickness d , so $\rho = AR/d$, where R is the resistance of a platelike sample. The conductivity σ is the reciprocal of the resistivity: $\sigma = 1/\rho$.

Ionic diffusion can be studied with radioactive tracers; such diffusion, called "tracer diffusion," takes place without chemical changes or ionic gradients in the sample. The tracer can either be deposited on the sample surface from a solution to provide a concentrated source of tracer, or the tracer concentration at the sample surface can be maintained constant by a large dilute source such as a fused salt.

The diffusion coefficient D is defined by the equation

$$J = -D \frac{\partial c}{\partial x} \quad (1)$$

where J is the flux of diffusing species and $\partial c/\partial x$ is its gradient of concentration c in the x direction. From the equation of continuity

$$\frac{\partial c}{\partial t} = \frac{\partial(-J)}{\partial x} = D \frac{\partial^2 c}{\partial x^2} \quad (2)$$

where t is the time and D is independent of concentration.

If at time zero an amount Q of substance per unit area is added to one face of a semi-infinite solid containing none of this substance, then the solution of Eq. 2 is³⁴

$$c = \frac{Q}{\sqrt{\pi D t}} \exp\left(-\frac{x^2}{4Dt}\right) \quad (3)$$

where c is the concentration of diffusion substance at a distance x from the face after diffusion for a time t . To calculate the diffusion coefficient D from Eq. 3, only the slope of the log concentration against x^2 plot for a certain time of diffusion is needed, since Q and t are constants for these conditions. The boundary condition of Eq. 3 applies when material containing a radioactive or isotropic tracer of high specific activity is deposited on a solid. The concentration profile in the solid after diffusion for a certain time can be determined by removing successive layers of the solid and analyzing for the tracer with a counter or mass spectrometer.

Under certain conditions, Frischat found profiles of sodium tracer in glasses, measured as described in the preceding paragraph, that deviated from Eq. 3 close to the sample surface.³⁵ However, McVay and Farnum were able to eliminate similar effects by making the diffusion anneal in argon instead of atmospheric air.³⁶ It seems likely that the deviations resulted from introduction of hydrogen ions by reaction and ion exchange with water in the air. These results are further evidence of the possible interference of water in diffusion and conductivity measurements in glass, as mentioned above.

If the solute concentration at the face of a semi-infinite solid that contains no solute initially is maintained at c_i , then with D constant

$$c = c_i \operatorname{erfc}\left(\frac{x}{2\sqrt{Dt}}\right) \quad (4)$$

where

$$\operatorname{erfc} z = \frac{2}{\sqrt{\pi}} \int_z^\infty e^{-y^2} dy$$

The total amount of material M that has diffused into the solid after a time t is

$$M = 2c_i \left(\frac{Dt}{\pi}\right)^{1/2} \quad (5)$$

The functional form of Eq. 5 is preserved even if D is a function of the concentration of the diffusing material. This is so because the solute concentration c depends only on the variable $y = x/\sqrt{D_i t}$, where D_i is the diffusion

coefficient when $c = c_i (x = 0)$. Then the flux J_0 crossing the surface $x = 0$ is

$$J_0 = -D \left(\frac{\partial c}{\partial x} \right)_{x=0} = -\frac{\sqrt{D_i}}{\sqrt{t}} \left(\frac{\partial c}{\partial y} \right)_{y=0}$$

The derivative is not a function of x , t , or D_i , since y does not appear in it. The resulting expression for M is

$$M = \int_0^t J_0 dt = -2\sqrt{D_i t} \left(\frac{\partial c}{\partial y} \right)_{y=0}$$

Therefore M is proportional to \sqrt{t} regardless of the functional relation between D and solute concentration. This relation can usually be deduced from the profile of diffusing material. To determine this profile, the concentration of diffusing material as a function of penetration distance into the glass after a certain time of diffusion must be found. To do this, layers of glass can be removed, either by etching with acid, by grinding, or by sectioning, and the amount of diffusing material in each layer determined by chemical or tracer analysis.

If the electrical resistance of a glass is changed by the diffusing species, this change can sometimes be used to follow the progress of diffusion. Consider a solid sample of fixed cross-sectional area with flat faces and thickness L . The resistance R per unit cross-sectional area of the sample measured between its faces can be expressed as

$$R = \int_0^L \frac{dx}{\sigma}$$

where σ is the specific conductivity of the glass at the distance x from one face. If the penetration of diffusing material is limited to a thin layer of the sample throughout the diffusion process, there is a constant concentration c such that

$$R = \int_0^x \frac{dx}{\sigma} + R_0$$

throughout the diffusion, when x is the distance corresponding to c and R_0 is the initial resistance of the sample when it contains no solute. Since the penetration of diffusing material is limited to a thin layer, the equations for a semi-infinite solid apply. Thus, if the concentration of diffusing material is held constant at one face at c_i , the reduced solute concentration c/c_i at a distance x from the face is a function of $y = x/\sqrt{D_i t}$ only, in which D_i is the diffusion coefficient of solute at the concentration c_i . Then the above equation can be transformed to

$$R - R_0 = 2\sqrt{D_i t} \int_0^y \frac{dy}{\sigma} \quad (6)$$

Since y is constant with time, because c is constant, and σ varies only with y for a particular diffusion run at constant temperature, the integral is a constant throughout a diffusion experiment, and the resistance increment $R - R_0$ is proportional to \sqrt{t} . This equation was derived without assuming a relation between resistivity and concentration, or between the diffusion coefficient and concentration. To relate $R - R_0$ to D_i under conditions of changing temperature, the Einstein equation (Eq. 11) can be used for σ .

RELATION BETWEEN ELECTRICAL CONDUCTIVITY AND IONIC DIFFUSION

If the electrical current in a glass is carried by a single ionic species, the electrical conductivity of the glass is related to the diffusion coefficient of the ion by the Einstein equation. This equation can be derived as follows:³⁷ the driving force for ionic transport in the x direction is the negative of the gradient in total chemical potential ("electrochemical potential"):

$$\frac{\partial \mu}{\partial x} = \frac{RT}{c} \frac{\partial c}{\partial x} \frac{\partial \ln a}{\partial \ln c} + ZFE \quad (7)$$

where a is the thermodynamic activity, c is the concentration, Z is the ionic charge, F is the faraday, E is the electrical potential gradient, R is the gas constant, and T is the temperature. A generalized mobility can be defined as the average ionic velocity v per unit driving force. Then since the flux J of diffusing species is equal to cv , the mobility u^* for tracer diffusion is given by

$$u^* = \frac{-v}{\frac{RT}{c} \frac{\partial c}{\partial x}} = \frac{-J}{RT \frac{\partial c}{\partial x}} = \frac{D}{RT} \quad (8)$$

since there is no electrical potential gradient in tracer diffusion, and the term

$$\frac{\partial \ln a}{\partial \ln c} = 1 + \frac{c}{\gamma} \frac{\partial \gamma}{\partial c} \quad (9)$$

is unity because there is no gradient in activity coefficients. The tracer-diffusion coefficient is D . The electrical mobility u_e in an experiment measuring the electrical conductivity σ is

$$u_e = \frac{-v}{ZEF} = \frac{\sigma}{Z^2 F^2 c} \quad (10)$$

The Einstein equation is found by equating the electrical and diffusive mobilities,

$$\sigma = \frac{Z^2 F^2 D c}{RT} \quad (11)$$

In other derivations of this equation, thermodynamic expressions for a system in equilibrium are used, but these expressions are unsatisfactory, since in a transport experiment the system is not in equilibrium. Deviations from the Einstein equation in aqueous solutions because of the distortion of the electric field around a moving ion demonstrate this deficiency. The present derivation is based on a simple physical assumption, the equivalence of electrical and diffusive mobilities, and a deviation from the Einstein equation shows when this assumption is not valid.

In glasses, Eq. 11 is often not obeyed exactly; to give equality σ must be multiplied by a factor f of less than 1. Kelly et al.³⁸ have summarized experimental results on f factors, sometimes called the Haven ratio. In silicate glasses at alkali concentrations below about 5 mol%, several investigators find f values close to 1. At higher alkali concentrations, there is a wide scatter of results of different investigators even in glasses of the same composition varying from 1 to 0.2. In germanate glasses, there is better agreement between different investigators with f factors of 1 for alkali concentrations below about 2%, with a sharp decrease to 0.2 to 0.3 for higher (15–30%) alkali concentrations. In borate glasses, the results of two investigators are similar to those in the germanates. Earlier measurements are discussed in the first edition of this book, pp. 153–154.

The f factor can be measured in an experiment in which an electrical field moves tracer in a glass, first devised by Chemla for alkali halides.³⁹ The distance of motion is related to the electrical conductivity of the glass, and the spreading of the tracer in the glass to the diffusion coefficient. In three different research groups, results of this method for $\text{Na}_2\text{O} \cdot \text{SiO}_2$ were 0.69, 0.50 and 0.32 in refs. 40, 41 and 33, respectively. The origin of these differences is not clear. Ideas about transport mechanisms in glass have been based on values of f , but until the large differences in experimental results on silicate glasses by different investigators are resolved, this approach seems premature.

In spite of these problems, the Einstein equation is valuable in comparing results of conductivity and diffusion experiments. Thus the temperature dependences of these two processes are accurately related in Eq. 11, and so are other relative changes caused by stress, ion size, and glass composition. In the following discussions of these effects, no distinction needs to be made between conductivity and diffusion, since the trends apply to both processes.

Electrochemical experiments provide intriguing methods for measuring diffusion coefficients of ions in glass melts. Examples are chronopotentiometry,⁴² cyclic voltametry,⁴² and square-wave voltametry.⁴³ The principles behind these methods can be understood from a description of chronopotentiometry in fused salts.⁴⁴ In chronopotentiometry, a constant current flows through a melt at a potential difference of an electrode reaction of an ion in dilute solution in the melt (electrolyte). An experimental parameter is the transition time τ , which is the time after the start of constant current electrolysis when the surface concentration of the ion just reaches zero and a jump of electrode potential occurs, because the ion is depleted at the electrode.

The experimental value of τ can be related to the diffusion coefficient D of the ion in the melt with the assumption that the concentration gradient of diffusing ion in the melt at the electrode surface is equal to J/nFD , in which J is the constant applied current density, n is the number of electrons in the electrode reaction, and F is the Faraday. Then at the electrode surface, the ionic concentration c is⁴⁴

$$c = c_0 - \frac{2J}{nF} \sqrt{\frac{t}{\pi D}} \quad (12)$$

Since the transition time τ is the time when $c = 0$,

$$\tau = \left(\frac{c_0 n F}{I} \right)^2 \pi D \quad (13)$$

From this equation, the diffusion coefficient D can be calculated from known values of c_0 , F , I and τ . Application of an alternating current, instead of a constant current, avoids certain experimental problems. Analysis of these cyclic voltametry techniques is more complicated, but the principle for measuring a diffusion coefficient is based on Eq. 13, with modification for an alternating current. Square-wave voltametry^{45,46} gives good results in glass melts.⁴³ In this technique the glass, for example a soda-lime composition, serves as an electrolyte, and the ion of interest is melted with the glass at a level of about 0.5%.

DEPENDENCE OF IONIC TRANSPORT ON TEMPERATURE AND PRESSURE (STRESS)

The electrical resistivity of a glass containing about 26.5 wt% Na₂O and 73.5% SiO₂ is shown in Fig. 1 as a function of reciprocal temperature. The data were taken by Babcock⁴⁷ at higher temperatures and Sedden et al.⁴⁸ at lower temperatures on glasses of almost the same composition. Sedden et al. annealed their glass carefully and cooled it slowly to obtain reproducible measurements. The temperature dependence shown in the figure parallels that found by Johnson⁴⁹ for diffusion of sodium ions in binary sodium silicate glasses (see Fig. 6). A similar temperature dependence for diffusion or conductivity is found for other alkali silicate glasses, both binary and multicomponent, that have been measured.

At lower temperatures the resistivity fits an Arrhenius-type equation, with a pre-exponential factor ρ_0 and activation energy Q independent of temperature. This dependence shows the relative stability of the glass structure below the transition temperature. As the temperature approaches that where structural rearrangements become possible, the resistivity drops more rapidly with increasing temperature, leading to a second temperature region with a constant although higher activation energy than at lower temperatures. As the glass structure is further broken up with increasing temperature, the effective

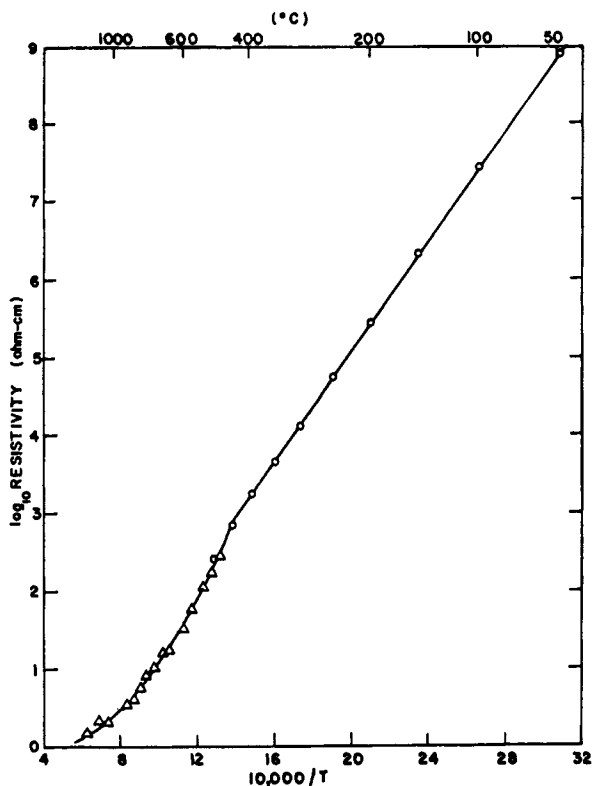


Fig. 1 Electrical resistivity of a 26.5 wt% Na_2O , 73.5% SiO_2 glass as a function of reciprocal temperature. \circ , Seddon et al;⁴⁸ \triangle , Babcock.⁴⁷

activation energy continuously decreases. At temperatures above the glass transition temperature, Q is constant over short temperature ranges, but $\log \rho$ versus $1/T$ is actually curved. For the glass in Fig. 1, the activation energy at low temperatures is 16.0 kcal/mol, about 23 kcal/mol just above the glass transition temperature, and about 8 kcal/mol from 1100 to 1500°C.

The intersection of the lines on the $\log \rho$ versus $1/T$ plot at low and intermediate temperatures has been used to determine a transition temperature. However, this temperature of about 430°C for the glass in Fig. 1 is considerably lower than the temperature of about 490°C, where the viscosity is 10^{13} P, which is the more conventional transition temperature. Thus it appears that ionic transport changes character at a lower temperature than thermal expansion, the more usual property used as a criterion for the transition temperature.

A constant Q for the resistivity implies, from Eq. 11, a factor of temperature in the pre-exponential term for the diffusion coefficient in an Arrhenius-type equation. However, the experimental data for diffusion and conductivity

in glasses are not accurate enough or taken over a wide enough range of temperature to tell whether a pre-exponential factor of temperature is needed for either property. Thus activation energies for both diffusion and conductivity are reported for Arrhenius equations with no pre-exponential temperature factor. The result is that activation energies for diffusion are somewhat (about 10%) lower than those for electrical conductivity.

The electrical conductivity and viscosity of glasses have been related by various empirical formulae.^{3,47} However, it seems unlikely that there is any quantitative relation between these properties because their temperature dependence is very different. The viscosity shows no unusual changes in the transition region, as discussed in Chapter 6, whereas ion transport is markedly affected at temperatures in the transition region. Furthermore, the Stokes-Einstein equation relating viscosity η and the diffusion coefficient D of a particle of radius r ,

$$D = \frac{RT}{6\pi\eta r} \quad (15)$$

gives ionic radii orders of magnitude too small for alkali ions diffusing in silicate glasses. Therefore, although both viscosity and ionic transport reflect changes in the glass structure with temperature, there is no general quantitative relation between them.

The temperature dependence of ionic transport in vitreous silica appears to be different from that in other silicates containing more transporting ion, perhaps because the transport properties of silica in the rigid state can be measured over such a wide temperature range. The diffusion coefficient of sodium in vitreous silica made from fusion of natural quartz crystals is shown in Fig. 2, from the measurement of Frischat.⁵¹ A further discussion of diffusion of sodium in vitreous silica is given in the next section on composition dependence.

In order to measure the electrical mobility of sodium ions in vitreous silica, it was necessary to electrolyze the glass in fused salt to remove other mobile ions from the glass and replace them with sodium. This was done for the sample shown in Fig. 3; initially it contained mobile lithium ions as well as sodium ions. This sample was also used to test the Einstein equation, as described in the preceding section for Frischat's measurements. The concentration of sodium was calculated from the time course of electrolysis;⁵ good agreement with the Einstein equation was found for the data in Fig. 3 and Frischat's results in Fig. 2.

At low temperatures, the activation energy for sodium ion conduction in vitreous silica was constant, as shown in Fig. 3. Similar results were found for lithium and potassium ions. As the temperature was varied above a certain temperature, which was different for the different ions, the activation energy started to decrease and continued to decrease slowly as the temperature was raised. For sodium, the activation energy for conduction at temperatures below

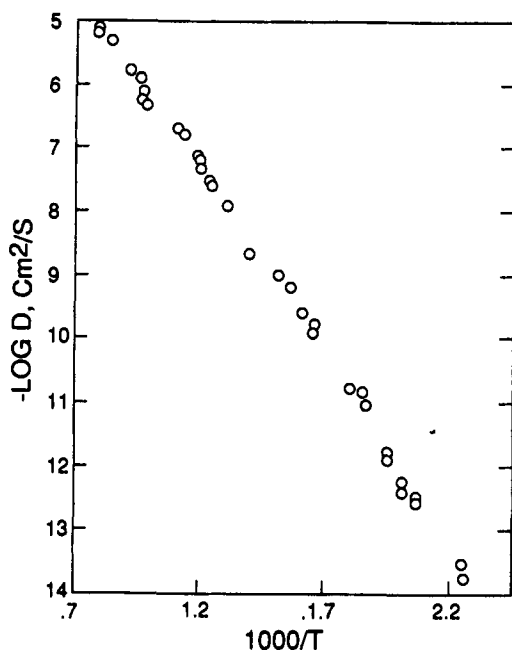


Fig. 2 Diffusion coefficient of sodium in vitreous silica as a function of reciprocal temperature, measured by Frischat.⁵¹

about 280°C was 35 kcal/mol, whereas above about 600°C the activation energy was down to about 24 kcal/mol.⁵² Veltri⁵³ measured the conductivity of vitreous silica from 1000 to 1800°C and found a constant activation energy of about 24 kcal/mol in this temperature range. Thus the activation energy for ionic transport is constant at high and low temperatures, but changes at intermediate temperatures. Diffusion coefficients of a variety of ions in amorphous silica at 1000°C are given in Table 1. The diffusion of several other ions in vitreous silica is complex. Boron and phosphorous diffusion depends strongly on ion concentration and the ambient atmosphere,^{67,68} and gallium, indium, and thallium (three-valent) appear to have two different diffusing states in silica.⁶⁸

Rüssel and co-workers⁴³ measured the diffusion coefficients and their activation energies for a number of ions in a melt of soda-lime glass with square-wave voltametry, which was described in the measurements section. In this glass of composition 74 mol% SiO₂, 16% Na₂O and 10% CaO, a variety of ions were included at a level of 0.5% in different samples. At 1000°C, the sequence of mobilities was Ag⁺ ≫ Cd²⁺ > Fe²⁺ > Ni²⁺ > Te⁴⁺ > Cr³⁺ > Sn²⁺ > Bi³⁺ > As³⁺ > Pb²⁺ ≈ Co²⁺ > Sb³⁺ > Sn⁴⁺ ≈ Ta³⁺ ≫ Cr⁶⁺, from 3.5 × 10⁻⁷ cm²/s for silver to 3.9 × 10⁻¹¹ cm²/s for Cr⁶⁺. The activation energies increased in roughly the same sequence, from 107 kJ/mol for silver to

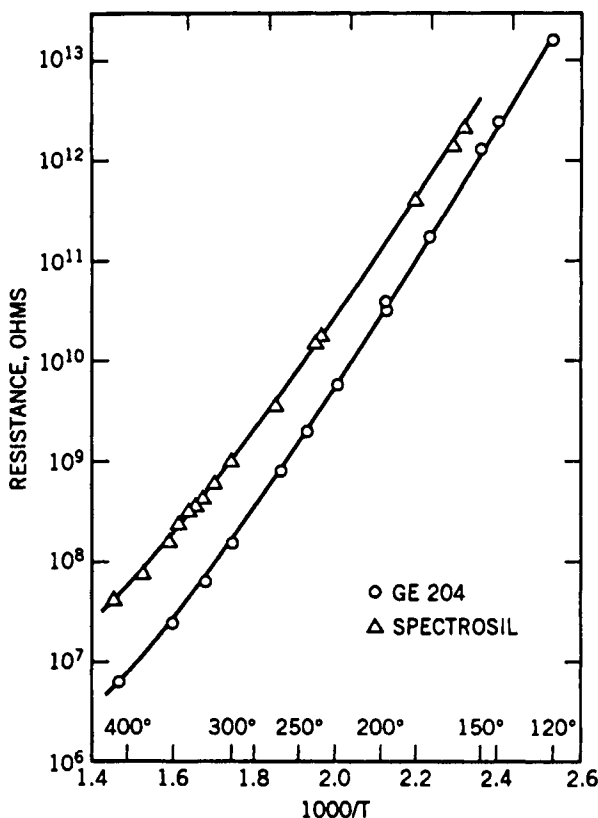


Fig. 3 Resistance of fused silica containing sodium ions, as a function of $1/T$. From Ref. 5.

327 kJ/mol for Cr^{6+} . Except for the end-members, this sequence is curious. There seems to be little relation between ion charge, size, or chemical character and mobility.

Stress has long been known to affect the electrical conductivity of glasses. A quenched glass has a higher conductivity than an annealed one. The effects of compaction by hydrostatic stress and expansion by quenching on a soda-lime glass are shown in Fig. 4 from the work of Charles.⁵⁵ The figure indicates a linear dependence of log conductivity on pressure, since for small volume changes this change is proportional to the pressure P . Thus

$$\sigma = \sigma_0 \exp \left(\frac{V^*P}{RT} \right) \quad (16)$$

where σ_0 and V^* , the "activation volume," are independent of pressure at constant temperature. Charles' results show that the effect of compressing the

TABLE 1 Diffusion Coefficients of Ions in Vitreous Silica at 1000°C

Ion	D (cm ² /s)	Ref.
Sodium	7.98×10^{-6}	51
Lithium	1.2×10^{-6}	5
Silver	6.5×10^{-7}	5
Potassium	1.6×10^{-8}	54
Rubidium	2.5×10^{-9}	54
Cesium	3.2×10^{-11}	66
Calcium	2.0×10^{-8}	66
Aluminum	1.3×10^{-13}	66
Arsenic	4.0×10^{-17}	68

glass with hydrostatic pressure has a much smaller effect on resistivity of glass for unit volume change than do the structural changes brought about by quenching a sample to put it in tension internally. A V^* of about 3.7 cm³/mol for hydrostatic compression is calculated from Fig. 4. Hamann⁵⁶ measured the effect of pressure on different alkali silicate glasses and found the following activation volumes in cm³/mol: lithium, 1.0; sodium, 3.4; potassium, 6.0. These results can be compared with the molar volumes of the ions as calculated from the ionic radius: lithium, 0.55; sodium, 2.2; potassium, 5.9. In crystalline solids the activation volume is usually about half the molar volume, whereas in liquids it is closer to the molar volume. Thus diffusion in glasses is between these extremes and changes with the size of the diffusing ion.

The presence of a stress gradient in a glass gives an additional driving force for ionic transport. In the presence of a stress gradient $\partial P/\partial x$, Eq. 7 for the gradient in chemical potential becomes

$$\frac{\partial \mu}{\partial x} = \frac{RT}{c} \frac{\partial c}{\partial x} \frac{\partial \ln a}{\partial \ln c} + ZFE + V^* \frac{\partial P}{\partial x} \quad (17)$$

Weber and Goldstein⁵⁷ devised an ingenious experiment to measure V^* from this effect. They bent a glass plate to give a stress gradient across the thickness of the glass and measured the current J_p that flowed as a result of the applied stress ΔP . Then from this current and the electrical current I in a conventional measurement of electrical conductivity with an applied potential V they calculated V^* from the relation

$$V^* = \frac{J_p}{I} \frac{VF}{\Delta P}$$

where F is the Faraday constant. For a soda-lime glass they found $V^* = 1.3$ cm³/mol, which is about one-third the value calculated from Charles' results. The reason for the difference is not clear.

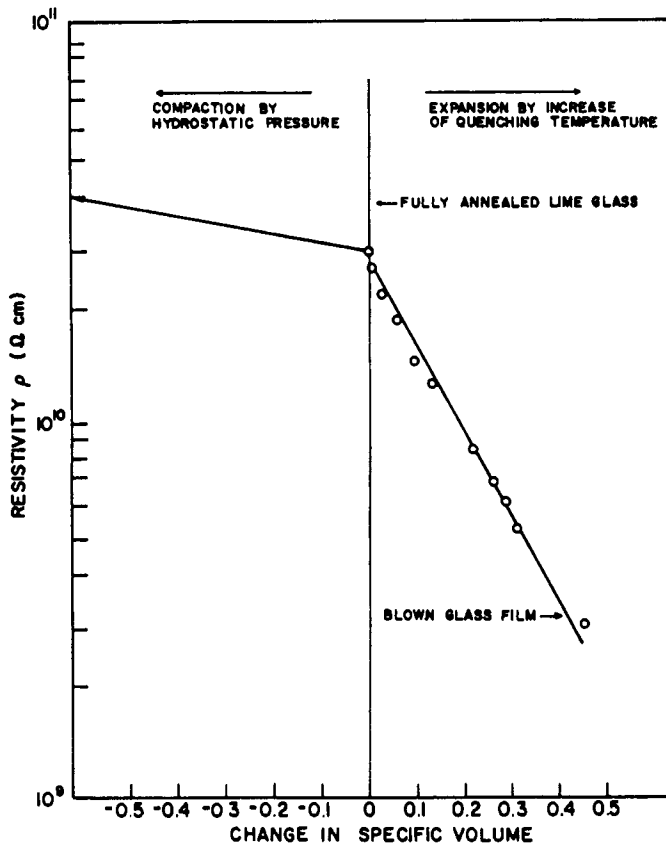


Fig. 4 Resistivity at 72°C of a commercial soda-lime glass (Corning No. 0080, see Chapter 1) as a function of changes in its specific volume caused by hydrostatic pressure or by quenching from various temperatures.⁵⁵

EFFECT OF GLASS COMPOSITION ON IONIC TRANSPORT

The electrical conductivity is proportional to the product of concentration of the current-carrying ion and its mobility or diffusion coefficient, as shown by Eq. 11. Thus in a comparison of glasses with different concentrations of ions, the diffusion coefficient is the more meaningful parameter. However, the activation energy for either property is not dependent directly on composition, and so it may be used to follow changes caused by, for example, changes in glass structure.

The tracer diffusion coefficient of sodium silicate glasses as a function of glass composition and temperature is shown in Fig. 5, from the measurements of Johnson.⁴⁹ The diffusion coefficient decreases as the concentration of sodium

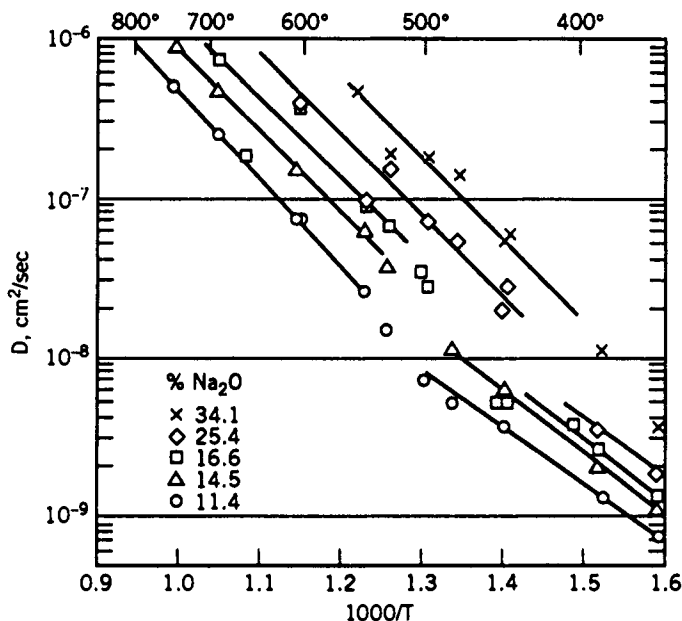


Fig. 5 Diffusion coefficients of sodium in binary sodium silicate glass, measured by Johnson.⁴⁹

ions decreases. Qualitatively the silica lattice is less broken-up the smaller the sodium concentration, making ionic transport more difficult. Similar trends are found for multicomponents silicate glasses, and in other alkali silicate glasses, the diffusion coefficient of the alkali ion also decreases as its concentration decreases.

The activation energy for electrical conduction in binary alkali silicates is about 15–17 kcal/mol above an alkali concentration of about 20 mol%, and increases at lower alkali concentrations.⁵⁸ The data of different investigators do not agree very well,⁵⁸ particularly for sodium silicates. Conduction in binary sodium and lithium silicates may be affected by phase separation in these glasses.

The addition of an oxide of a higher-valent metal ion to an alkali silicate leads to a decrease in the ionic mobility of the alkali ion. The decrease is related to the ionic size of the added ion for divalent ions; the largest change was found for barium ions, with a decreasing effect for lead, strontium, and calcium ions and a relatively small change for addition of magnesium, zinc, or beryllium oxides.^{4,24,59} Addition of aluminum oxide increases the ionic mobility and decreases its activation energy,²⁴ as discussed further in the section on theory.

When a second alkali oxide is added to an alkali silicate glass, the conductivities decrease sharply. This “mixed-alkali” effect is shown in Fig. 6 for mixed binary alkali silicate glasses.⁶⁰ Measurements of diffusion coefficients in

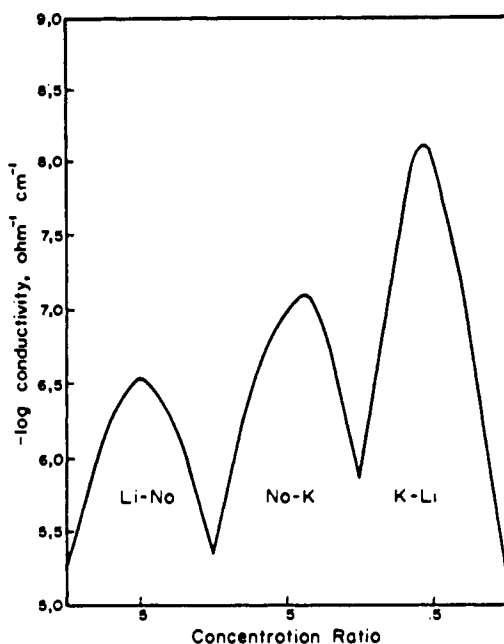


Fig. 6 The electrical conductivity of mixed binary alkali silicate glass containing 26 mol% alkali and 74% SiO_2 at 250°C , from Lengyel and Boksay.⁶⁰

such glasses show that the mobility of each ion is decreased by the addition of the other⁶¹⁻⁶³. The decrease in conductivity results from these reductions in mobility, but the reason for the mobility reductions in terms of the mechanism of diffusion is uncertain. Borate glasses also show a mixed alkali effect,⁶⁴ but in aluminosilicate with $R/\text{Al} = 1$, R being the alkali ion, there is no effect.⁶⁵ Additional data on diffusion of different ions in glass is summarized in Refs. 23, 24, and 69-71.

INTERIONIC DIFFUSION AND ION SIZE EFFECTS

If glass is placed in contact with a medium containing monovalent cations, such as a fused salt or an aqueous solution, these cations can exchange with monovalent cations in the glass and interdiffuse with them into the glass. The ionic equilibrium between the glass and solution is considered in Chapter 14, as are the electrical potentials that result from this exchange and are responsible for the operation of glass electrodes. In this section, the interdiffusion of like-charged ions is treated.

An alkali silicate glass can be considered as a matrix of immobile negative groups with associated mobile cations. An exchange cation normally has a

different mobility from the original ion; therefore as interdiffusion proceeds, one ion tends to outrun the other, and an electrical charge is built up. However, accompanying this charge is a gradient in electrical potential that slows down the fast ion and speeds up the slow one. To preserve electrical neutrality, the fluxes of the two ions must be equal and opposite, and the electrical potential ensures this condition in spite of the difference in mobility of the two ions. The mobility u in an experiment with both ionic and electrical gradient is found from Eq. 7 and the definition of mobility as the velocity v per unit driving force; the flux J per unit time and area equals cv in the ionic concentration, so that

$$J = -u \left(RT \frac{\partial c}{\partial x} \frac{\partial \ln a}{\partial \ln c} + ZcFE \right) \quad (18)$$

An equation of this form applies to each mobile cation in the glass. These flux equations are usually called the Nernst-Planck equations, and were derived here from the assumption that the driving force is the gradient of electrochemical potential, and the definition of the mobility.

If two monovalent cations A and B interdiffuse, each has a flux equation (Eq. 18), with $Z = 1$. The conditions of electroneutrality require that $J_A = -J_B$ and $\partial C_A / \partial x = -\partial C_B / \partial x$ because the number of negative groups is constant and immobile. From these four relations, the gradient E in electrical potential is

$$E = \frac{RT}{F} \frac{u_B - u_A}{C_A u_A + C_B u_B} \frac{\partial C_A}{\partial x} \frac{\partial \ln a_A}{\partial \ln C_A} \quad (19)$$

To develop this electrical potential, small deviations in electrical neutrality must occur in the ionic system. However, the number of ions involved in these deviations is negligible compared to the total ionic concentrations.

When Eq. 19 is substituted into Eq. 18, the flux for ion A is

$$J_A = -u_A RT \left(\frac{C_A u_B + C_B u_A}{C_A u_A + C_B u_B} \right) \frac{\partial C_A}{\partial x} \frac{\partial \ln a_A}{\partial \ln C_A} \quad (20)$$

The coefficient of the concentration gradient is the same for ion B ; if the activity coefficients are constant $\partial \ln a_A / \partial \ln C_A = 1$, and this interdiffusion coefficient \tilde{D} is

$$\tilde{D} = \frac{D_A D_B}{N_A D_A + N_B D_B} \quad (21)$$

where $N_i = C_i / (C_A + C_B)$, and Eq. 8 is used to relate the mobilities to the tracer diffusion coefficient D . This latter substitution amounts to assuming that the mobilities in a tracer diffusion experiment, in which there are no gradients in ionic concentration, are equal to those in an interdiffusion experiment. Even if the Einstein equation (Eq. 11) is not obeyed, the ratio D_A / D_B still equals u_A / u_B if the deviations from this equation are the same for the two ions.

The diffusion equations with the concentration-dependent diffusion coefficient of Eq. 21 have been solved for various ratios of D_A / D_B and different geometries by Helfferich and Plesset,^{72,73} with the assumption that the diffu-

sion coefficients D_A and D_B were concentration independent. In Fig. 7 their curve is compared to experimental data for silver-sodium interdiffusion in a soda-lime glass.³⁷ The tracer diffusion coefficients of sodium and silver were measured, and the ratio D_{Na}/D_{Ag} and the absolute value of D calculated from these tracer diffusion coefficients agreed well with those calculated from the data in Fig. 7. Furthermore, measurements of the total amount of diffused material and the change in resistance with time of diffusion gave agreement with the interdiffusion coefficient of Eq. 21 in Eqs. 5 and 6, respectively. Thus the assumptions leading to Eq. 21 are confirmed: the validity of the Nernst-Planck equations, the equality of mobility ratio for tracer and interdiffusion experiments, and especially the independence of the (tracer) diffusion coefficients D_{Na} and D_{Ag} with changing ionic ratio in the glass. The equivalence of the mobilities in the two types of experiments is additional evidence that the Einstein equation (Eq. 11) is obeyed in this system, as was deduced from measurements of electrical conductivity and tracer diffusion of sodium in the initial glass.

In certain other glasses, conditions are not so simple. For example, in Pyrex borosilicate glass, silver⁷⁴ and potassium⁷⁵ exchange for sodium are influenced by the two-phase structure of the glass. Silver ions are preferentially bound by one phase, so their effective diffusion coefficient is reduced at low silver ion concentrations.

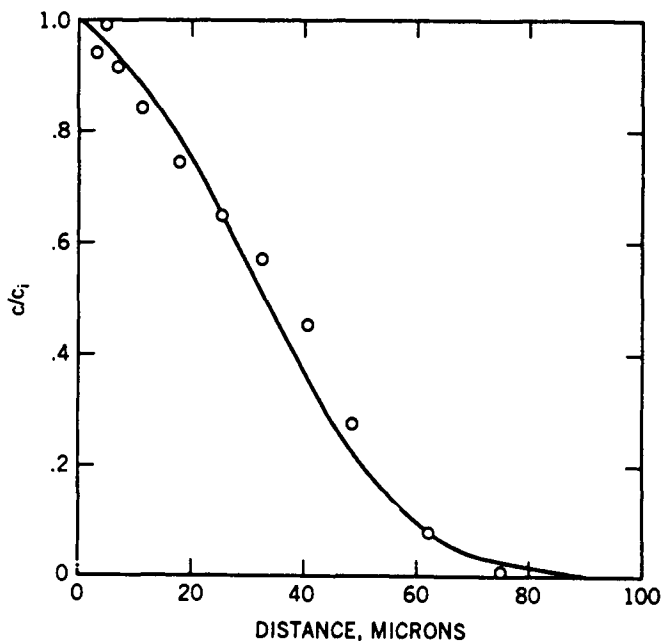


Fig. 7 Profile of silver that diffused from a silver nitrate melt into a soda-lime glass (Corning 0080, Chapter 9, Table 1) after 1097 min at 378°C. Line for $D_{Na}/D_{Ag} = 10$.³⁷

A careful distinction should be made between interdiffusion experiments done well below the transition temperature of the glass and diffusion in silicate glasses melted with different or mixed alkali ions. The structure of the glass is determined by the melting conditions, and interdiffusion well below the transition temperature does not alter it. Thus the result that the tracer diffusion coefficient of an ion is constant with varying ionic ratio cannot be compared with the results on mixed alkali glasses in which a change in the ionic ratio changes the tracer diffusion coefficient; in this case, the structure of the glasses is different.

Interionic diffusion experiments have been carried out at temperatures not too far below the transition temperature.^{76,77} In the sodium-potassium exchange of these experiments, large stresses arise in the glass because of the difference in the sizes of the ions. This stress slowly relaxes at these tempera-

TABLE 2 Ratios of Diffusion Coefficients of Monovalent Ions in Rigid Silicate Glasses

Glass type	Mol% M ₂ O	Temperature (°C)	Ions A-B	D_A/D_B	Refs.
Soda-lime	15.2 Na ₂ O	354	Na-Ag	4	32
			Na-Ag	12	37
			Na-K	500	79
	14.0 Na ₂ O	250	Ag-Li	2	80
	13.0 Na ₂ O	350	Na-H	1800	14
			Na-K	1400	14
Potash-lime	12.5 K ₂ O	350	Na-Rb	3.4(10) ⁵	14
			K-H	2	14
			K-Rb	190	14
Sodium binary	13 Na ₂ O	415	Na-K	25	61
	20 Na ₂ O	415	Na-K	39	61
	25 Na ₂ O	415	Na-K	48	61
Potassium binary	13 K ₂ O	415	Na-K	0.5	61
	20 K ₂ O	415	Na-K	0.5	61
	25 K ₂ O	415	Na-K	0.6	61
Sodium aluminosilicate (hydrated)	12.5 Na ₂ O	400	Na-K	~ 300	81
Lithium aluminosilicate	27 Na ₂ O	25	Na-K	3; 7	82
	5.2 Li ₂ O	415	Na-Li	1	83
Pyrex borosilicate	4 Na ₂ O	335	Na-Ag	1	74
		373	Na-K	~ 30	75
Vitreous silica (G.E. 204)	1.1(10) ⁻⁴ Na ₂ O	380	Na-Li	6.7	5
	3.4(10) ⁻⁴ Li ₂ O	380	Na-Ag	12	5
	?	380	Na-K	> 500	5
		380	Na-Li	33	5
(Spectrosil)	?	380	Na-K	1400	5
		1000	Na-H	~ 10 ⁴	84
(Vitreosil)	~ 5(10) ⁻⁴ Na ₂ O	1000	Na-H	~ 10 ⁴	84

TABLE 3 Ionic Radii

Ion	Radius (Å)	Ion	Radius (Å)
H ⁺	Small		
Li ⁺	0.68	Be ²⁺	0.33
Na ⁺	0.95	Mg ²⁺	0.67
Ag ⁺	1.26		
K ⁺	1.33	Ca ²⁺	0.99
Rb ⁺	1.48	Sr ²⁺	1.13
Cs ⁺	1.67	Ba ²⁺	1.35

tures, leading to a time-dependent change in the structure of the glass and also of the tracer diffusion coefficients of the ions. Thus interpretation of these experiments is difficult. When the stress is completely relaxed the diffusion coefficients have nearly the same dependence on ionic ratio as in the mixed alkali glasses melted with a range of ionic ratios.⁷⁸

In Table 2 the mobility ratios of diffusing ions in various rigid alkali silicate glasses are listed and can be compared with ionic radii in Table 3. In soda-lime glass, the maximum mobility is found for sodium and lithium ions, with a large decrease for smaller (hydrogen) and larger (potassium and rubidium) ions. For fused silica the sequence is similar, except that lithium is less mobile than sodium. Silver is somewhat more mobile in lime glass than would be expected from its size, probably because it is much more polarizable than the alkali ions.

Interest in making optical wave guides and gradient index lenses (see Chapter 17) by exchanging ions such as silver with alkalis to change the surface refractive index has led to a number of fresh studies of ionic interdiffusion in glass. The principles outlined in this section, especially Eq. 21 for the concentration-dependent diffusion coefficient, have been applied and confirmed in these studies. See Refs. 85–87 for reviews. In some cases in the most precise work it may be necessary to take into account small change of the individual diffusion coefficients D_A and D_B with ionic composition N_A .⁸⁸

GLASSES WITH HIGH ELECTRICAL CONDUCTIVITY ("FAST ION CONDUCTORS")

Electrolytes with high conductivity at temperatures below 300°C or even at room temperature are of interest for applications in batteries, sensors and display devices. Reviews of glasses with high conductivity are given in Refs. 26–29; Ref. 29 has 250 citations to work on ionic conductivity. In certain oxide glasses with high alkali ion concentrations, especially sodium and lithium, conductivities of about 10^{-3} (ohm-cm)⁻¹ are possible.⁸⁹ To obtain high conductivity at room temperature, silver halides have been added to a variety

of glasses. With about 50% silver iodide and 50% silver phosphate, selenide molybdate or chromate, glasses with conductivities of about $10^{-2} \text{ (ohm-cm)}^{-1}$ at 25°C have been reported. These glasses are probably related to the high electrical conductivity of crystalline α -silver iodide and mixed silver salts at room temperature. In some compositions, substitution of sulfur for oxygen increases the conductivity.²⁶ Many glasses with high copper or silver halide concentrations show high conductivity at room temperature.

One problem with these glasses is their lack of chemical durability. All are among the less durable glass compositions, and some are strongly attacked by water and acids. Practical applications of these glasses are presently possible only in chemical conditions in which they are durable.

THEORIES OF IONIC TRANSPORT

The diffusion coefficient D of Eq. 1 can be described in terms of a random walk of molecules in discrete steps. From the probability of finding a molecule at a certain place after a fixed number of steps

$$D = g\bar{\lambda}^2\Gamma \quad (22)$$

where g is a geometrical constant, $\bar{\lambda}^2$ is the average of the squares of the step lengths, and Γ is the average number of steps made in unit time. The jump rate Γ_m for ionic motion can be calculated from various models; its usual form is

$$\Gamma_m = \nu \exp\left(\frac{\Delta S}{R} - \frac{\Delta H}{RT}\right) \quad (23)$$

where ν is the vibration frequency of the diffusing atom, and ΔS_m and ΔH_m are the entropy and enthalpy of activation for the motion of an atom from one site to another. In some cases, it is found that the pre-exponential frequency term depends on the temperature. In the preceding chapter, results on diffusion of gases in glass showed such a dependence. However, the results on ionic diffusion have not been accurate enough or measured over wide enough temperature ranges to tell whether such a temperature factor is needed; therefore it will be ignored in this discussion.

The diffusion coefficients of monovalent cations in oxide glasses cannot be described by considering the glass to be a viscous liquid. Equation 13, the Stokes-Einstein equation, predicts much too low a diffusion coefficient, as described in the section on temperature effects. Furthermore, these cations diffuse much more rapidly than the lattice elements, such as silicon and oxygen, so the glass behaves like a rigid solid with mobile interstitial ions.

A variety of theories have been proposed for ionic motion in glass. Anderson and Stuart⁹⁰ considered the activation enthalpy ΔH for ionic transport of alkali ions to consist of two parts, one of electrostatic interaction with the immobile nonbonding oxygen ion, and the other a resistance to pushing the

ion through a "doorway" (Chapter 8, Eq. 33). This model gives a strong dependence of activation energy on ion size, with a minimum activation energy for an intermediate ion size.

A "weak electrolyte" theory has been proposed for glasses,⁹¹⁻⁹³ analogous to partially ionized molecules in aqueous solution. From Eq. 11, the electrical conductivity is proportional to the product of ionic concentration c and diffusion coefficient D . In the weak electrolyte theory, the concentration of carriers is much less than c , the total number of alkali ions, because most of them are held tightly to nonbridging oxygen ions:



Other theories have involved a combination of the Anderson-Stuart and weak electrolyte models,⁹⁴ defects (the first edition of this book, p. 171, and Ref. 29), a "cluster bypass" model, in which ions move through disordered regions between ordered regions,⁹⁵ a relaxation model,⁹⁶ in which the Charles idea of a defect with two alkali ions at a nonbridging oxygen is resurrected, a three configuration model,⁹⁷ and a relation between ionic motion and the thermodynamic state of the glass.⁹⁸ However, none of these models has been generally accepted. The conclusion of Greaves⁹⁹ seems apt: "Nevertheless, taken on their own, transport measurements remain inconclusive as to the precise diffusion mechanism occurring."

A number of explanations of the mixed alkali effects have been put forward, including ionic interactions,¹⁰⁰ defects, pathways, percolation, cluster bypass,²⁹ and thermodynamic state.¹⁰¹ None of these models has achieved widespread acceptance. Hyde and Tomozawa have shown that the mixed alkali effect becomes less marked at high frequency or at high fields, and they suggest that these limiting conditions can be explained from the theory of ionic interactions in an electrolyte.¹⁰²

Structural factors may be quite important in diffusion mechanisms in glass.⁹⁹ For example, in vitreous silica there is evidence that the alkali ions are associated with impurity aluminum ions. These aluminum ions may be arranged in cells or ribbons in a three-dimensional network, and not uniformly distributed.¹⁰³ These alumina cells may provide a preferred path for alkali transport in vitreous silica.¹⁰³

CONDUCTION IN HIGH FIELDS

Results on the ionic transport in very high electrical fields may shed some light on the mechanism of ionic transport in glass, although the correct interpretation of these results is still not entirely clear. If a Boltzmann distribution of energy exists among ions, their jump rate is given by Eq. 23. When an electric field E is imposed on them, jumps in one direction become more probable than

in the other, giving rise to the following equation for the conductivity:¹⁰⁴

$$\sigma = \frac{2gcF\lambda\Gamma}{E} \sinh \frac{FE\lambda}{2RT} \quad (24)$$

For low fields, $\sinh X = X$ and Eq. 24 becomes

$$\sigma = \frac{gcF^2\lambda^2\Gamma}{RT}$$

which is Eqs. 11 and 22 combined. When the fields are very high, Eq. 24 becomes, in terms of the current $I = \sigma E$

$$I = 2gcF\lambda\Gamma \exp\left(\frac{F\lambda E}{2RT}\right) \quad (25)$$

so that the current depends exponentially on the field. This exponential dependence at high fields has been found by several different workers for sodium silicate glasses.¹⁰⁴⁻¹⁰⁹ The hyperbolic sine law over the whole range of fields was found by Maurer¹⁰⁴ and Zagar and Papanikolau.¹⁰⁸ Maurer and Vermeer¹⁰⁷ found the expected temperature dependence of the pre-exponential and exponential factors of Eq. 25 from their low-field results on the same glasses. Maurer's jump distances calculated from Eq. 25 were high. However, when these λ values were corrected by using the effective local field E_L , calculated from the Lorentz-Lorentz relation

$$E_L = \left(\frac{\epsilon + 2}{3}\right) E$$

where ϵ is the DC dielectric constant, instead of the external field E_0 , reasonable values of λ (about 5 Å) were found. This correction has been questioned,⁴ but it probably is valid. This distance of 5 Å is not too different from the average separation of the sodium ions in this glass. Zagar and Papanikolau¹⁰⁸ calculated values of the jump distance for several different sodium silicates, soda-lime silicate, and sodium borosilicate glasses, and found an average value of 28 Å for all glasses, with little difference between glasses and no effect of temperature between -30 and 100°C. Again the high value could be corrected by the Lorentz-Lorentz relation to a more reasonable value.

Barton and Leblond¹⁰⁹ criticized Eq. 25 because of the high-jump distances calculated from it and the differences between these distances and those calculated from the low-field conductivity. However, the latter are uncertain because of uncertainties in the factor g and correlation effects. Barton and Leblond suggested that a better equation would be that of Poole and Frenkel, in which the log current is proportional to the square root of the field at high fields. However, this mechanism would require a change from Eq. 25 to this different dependence at some intermediate field. There is no evidence for such a shift from Eq. 25 in the data of Maurer, and Zagar and Papanikolau, which

agree with Eq. 25 at all fields. The jump distances calculated from the Poole-Frenkel equation are about 20 Å, and therefore are also higher than would be expected. Thus Eq. 25 still seems to be the best for representing conduction data at high fields.

REFERENCES

1. E. Warburg, *Ann. Phys.*, **21**, 622 (1884).
2. R. C. Burt, *J. Opt. Soc. Am.*, **11**, 87 (1925).
3. G. W. Morey, *The Properties of Glass*, 2nd edn., Reinhold, New York, 1954, p. 465.
4. A. E. Owen, in *Progress in Ceramic Science*, J. E. Burke, Ed., Macmillan, New York, 1963, p. 77.
5. R. H. Doremus, *Phys. Chem. Glasses*, **10**, 28 (1969).
6. K. Hughes, J. O. Isard, and G. C. Milnes, *Phys. Chem. Glasses*, **9**, 43 (1968).
7. K. K. Evstrop'ev and V. A. Khar'yuzov, *Dokl. Akad. Nauk USSR*, **136**, 140 (1961); Translation in *Proc. Acad. Sci. USSR*, **136**, 25 (1961).
8. M. Schwartz and J. D. Mackenzie, *J. Am. Ceram. Soc.*, **49**, 582 (1966).
9. W. G. Hagel and J. D. Mackenzie, *Phys. Chem. Glasses*, **5**, 113 (1964).
10. A. E. Owen, *Phys. Chem. Glasses*, **2**, 87, 152 (1961); **6**, 253 (1965).
11. H. A. Schaeffer and H. J. Oel, *Glastech. Ber.*, **42**, 493 (1969); *Z. Naturforsch.*, **25a**, 59 (1970).
12. M. Schwartz, Thesis, Rensselaer Polytechnic Institute, Troy, N.Y., 1969.
13. E. Gough, J. O. Isard, and J. A. Topping, *Phys. Chem. Glasses*, **10**, 89 (1969).
14. P. Ehrmann, M. deBilly, and J. Zarzycki, *Verres Refract.*, **18**, 164 (1964).
15. R. H. Doremus, in *Ion Exchange*, Vol. 2, J. A. Marinsky, Ed., Marcel Dekker, New York, 1969, p. 1.
- 15a. V. Trenovcova, E. Majkova, A. Bohun, J. Thurzo, and E. Mariani, *Proc. XIth Int. Congress on Glass*, Prague, CVTS-Dum Techniky Prague, Czechoslovakia, 1977, Vol. II, p. 405.
16. Y. Abe, H. Shimakawa and L. L. Hench, *J. Noncryst. Solids*, **51**, 357 (1982).
17. Y. Abe, H. Hosono, Y. Ohta, and L. L. Hench, *Phys. Rev.*, **B38**, 10166 (1988).
18. M. Kotama, J. Nakanishi, H. Hosono, Y. Abe, and L. L. Hench, *J. Elect. Soc.*, **138**, 2928 (1991).
19. F. M. Ernsberger, *Phys. Chem. Glasses*, **21**, 146 (1980); *J. Noncryst. Solids*, **38&39**, 557 (1980); *J. Am. Ceram. Soc.*, **66**, 747 (1983).
20. J. M. Stevels, in *Handbuch der Physik*, Vol. 20, Springer-Verlag, Berlin, 1957, p. 350.
21. R. H. Doremus, in *Modern Aspects of the Vitreous State*, Vol. 2, J. D. Mackenzie, Ed., Butterworths, London, 1962, p. 1.
22. R. H. Doremus, *J. Elect. Soc.*, **115**, 181 (1968).
23. P. Winchell, *High Temp. Sci.*, **1**, 200 (1969).
24. G. H. Frischat, *Ionic Diffusion in Oxide Glasses*, Trans. Tech., Bay Village, OH, 1975.

25. L. Pietroneco and A. Avogadro, *Solid State Ionics*, **3/4**, 7 (1981).
26. J. L. Souquet, *Annu. Rev. Mater. Sci.*, **11**, 211 (1981).
27. H. L. Tuller and M. W. Barsoum, *J. Noncryst. Solids*, **73**, 331 (1985).
28. C. A. Angell, *Solid State Ionics*, **18, 19**, 72 (1986).
29. M. D. Ingram, *Phys. Chem. Glasses*, **28**, 215 (1987).
30. S. W. Martin, *J. Am. Ceram. Soc.*, **74**, 1767 (1991).
31. C. Kim and M. Tomozawa, *J. Am. Ceram. Soc.*, **59**, 127, 321 (1976).
32. G. Shultz, *Ann. Phys. Leipzig*, **40**, 335 (1913).
33. P. Laborde, C. Kaps, H. Kahnt, and A. Feltz, *Mater. Res. Bull.*, **24**, 921 (1989).
34. J. Crank, *The Mathematics of Diffusion*, Oxford University Press, London, 1956, p. 26.
35. G. H. Frischat, *Phys. Chem. Glasses*, **11**, 25 (1970); *J. Am. Ceram. Soc.*, **53**, 285 (1970).
36. G. L. McVay and E. H. Farnum, *J. Am. Ceram. Soc.*, **55**, 275 (1972).
37. R. H. Doremus, *J. Phys. Chem.*, **68**, 2212 (1964).
38. J. E. Kelly, J. F. Cordaro and M. Tomozawa, *J. Noncryst. Solids*, **41**, 47 (1980); **51**, 345 (1982).
39. M. Chemla, *Annales de Physique*, **13**, 959 (1956).
40. J. Heinemann, Ph.D. Thesis, Technical University, Clausthal, Germany, 1986.
41. J. R. Engel and M. Tomozawa, *J. Am. Ceram. Soc.*, **58**, 183 (1975).
42. T. Takahashi and Y. Miuri, *J. Noncryst. Solids*, **95/96**, 119 (1987) and earlier papers by these authors.
43. C. Rüssel, *J. Noncryst. Solids*, **134**, 169 (1991) and earlier papers by this author and colleagues.
44. H. A. Laitinen and R. A. Osteryoung, in *Fused Salts*, B. S. Sundheim, Ed., McGraw-Hill, New York, 1964, p. 255.
45. J. G. Osteryoung and J. J. O'Dea, in *Electroanalytical Chemistry*, Vol. 14, A. J. Bard, Ed., Marcel Dekker, New York, 1986, p. 209.
46. J. G. Osteryoung and R. A. Osteryoung, *Anal. Chem.*, **57**, 101A, (1985).
47. C. L. Babcock, *J. Am. Ceram. Soc.*, **17**, 329 (1934).
48. E. Sedden, E. J. Tippet, and W. E. S. Turner, *J. Soc. Glass Technol.*, **16**, 450 (1932).
49. J. R. Johnson, R. H. Bristow, and H. H. Blau, *J. Am. Ceram. Soc.*, **45**, 135 (1951); see also J. R. Johnson, Thesis, Ohio, State University, 1950.
50. J. O. Bockris, J. A. Kirchner, S. Ignatowicz, and J. W. Tomlinson, *Trans. Faraday Soc.*, **48**, 75 (1952).
51. G. H. Frischat, *J. Am. Ceram. Soc.*, **51**, 528 (1968).
52. A. E. Owen and R. W. Douglas, *J. Soc. Glass Technol.*, **43**, 159 (1959).
53. R. D. Veltri, *Phys. Chem. Glasses*, **4**, 221 (1964).
54. S. J. Rothman, T. L. M. Marcuso, L. J. Nowicki, P. M. Baldo, and A. W. McCormick, *J. Am. Ceram. Soc.*, **65**, 578 (1982).
55. R. J. Charles, *J. Am. Ceram. Soc.*, **45**, 105 (1962).
56. S. D. Hamann, *Aust. J. Chem.*, **18**, 1 (1965).
57. N. Weber and M. Goldstein, *J. Chem. Phys.*, **41**, 2898 (1964).

58. R. M. Hakim and D. R. Uhlmann, *Phys. Chem. Glasses*, **12**, 132 (1971).
59. O. V. Mazurin and E. S. Borisovski, *J. Tech. Phys. Moscow*, **27**, 275 (1957); *Sov. Phys. Tech. Phys.*, **2**, 243 (1957).
60. B. Lengyel and Z. Boksay, *Z. Phys. Chem.*, **203**, 93 (1954); **204**, 157 (1955).
61. K. K. Evstrop'ev, in *The Structure of Glass*, Vol. II, Consultants Bureau, New York 1960, p. 237.
62. G. L. McVay and D. E. Day, *J. Am. Ceram. Soc.*, **53**, 508 (1970).
63. J. P. Lacharme, *C. R. Acad. Sci. Paris*, **270C**, 1350 (1970); **275C**, 993 (1972).
64. H. Jain, H. L. Downing, and N. L. Peterson, *J. Noncryst. Solids*, **64**, 335 (1984).
65. P. J. Hayward, *Phys. Chem. Glasses*, **17**, 54 (1976).
66. G. H. Frischat, *J. Am. Ceram. Soc.*, **53**, 625 (1969).
67. M. Ghezzeo and D. M. Brown, *J. Elect. Soc.*, **120**, 110, 146 (1973).
68. A. H. vanOmmen, *Appl. Surf. Sci.*, **30**, 244 (1987).
69. N. P. Bansal and R. H. Doremus, *Handbook of Glass Properties*, Academic Press, San Diego, 1986.
70. O. V. Mazurin, M. V. Streltsina, and T. P. Shviko-Shvaikovskaya, *Handbook of Glass Data*, Parts A, B, and C, Elsevier, Amsterdam, 1985.
71. P. Winchell, *J. Am. Ceram. Soc.*, **54**, 63 (1971).
72. F. Helffreich and M. S. Plesset, *J. Chem. Phys.*, **28**, 418 (1958).
73. F. Helffreich, *J. Phys. Chem.*, **66**, 39 (1962).
74. R. H. Doremus, *Phys. Chem. Glasses*, **9**, 128 (1968).
75. H. M. Garfinkel, *Phys. Chem. Glasses*, **11**, 151 (1970).
76. J. Tochon, *C. R. Acad. Sci. Paris*, **236C**, 829 (1966).
77. G. H. Frischat, *Glastech. Ber.*, **44**, 113 (1971).
78. G. H. Frischat, *J. Mater. Sci.*, **6**, 1229 (1971).
79. R. H. Doremus, unpublished results.
80. C. M. Hollabaugh and F. M. Ernsberger, unpublished results; see ref. 21, p. 33.
81. A. J. Burggraaf and J. Cornelissen, *Phys. Chem. Glasses*, **5**, 123 (1964).
82. G. Eisenman, in *Glass Electrodes for Hydrogen and Other Cations*, G. Eisenmann, Ed., Marcel Dekker, New York, 1967, p. 133.
83. M. H. Garfinkel and C. B. King, *J. Am. Ceram. Soc.*, **53**, 686 (1970).
84. G. Hetherington, K. H. Jack and M. W. Ramsay, *Phys. Chem. Glasses*, **6**, 6 (1965).
85. S. N. Houde-Walker and D. T. Moore, *Appl. Opt.*, **25**, 3373 (1986).
86. T. Findakly, *Opt. Eng.*, **24**, 244 (1985).
87. R. V. Ramaswamy and R. Srivastava, *J. Mod. Opt.*, **35**, 1049 (1988).
88. L. Tronev and I. Savatinova, *J. Mod. Opt.*, **35**, 919 (1988).
89. C. C. Hunter and M. D. Ingram, *Solid State Ionics*, **14**, 31 (1984).
90. O. L. Anderson and D. A. Stuart, *J. Am. Ceram. Soc.*, **37**, 573 (1964).
91. R. L. Muller, *Electrical Conductivity of Vitreous Substances*, Consultants Bureau, New York, 1971, p. 93.
92. D. Ravaine and J. L. Souquet, *Phys. Chem. Glasses*, **18**, 27 (1977); **19**, 115 (1978).
93. J. F. Cordaro and M. Tomozawa, *Phys. Chem. Glasses*, **21**, 74 (1980).

94. S. W. Martin and C. A. Angell, *Solid State Ionics*, **23**, 185 (1986).
95. M. D. Ingram, *Philos. Mag.*, **B60**, 729 (1989).
96. S. R. Elliott and A. P. Owens, *Philos. Mag.*, **B60**, 777 (1989).
97. A. Pradel, F. Henn, J. L. Souquet, and M. Ribes, *Philos. Mag.*, **B60**, 741 (1989).
98. M. Tomozawa, V. McGahay, and J. M. Hyde, in *Ceramics: Toward the 21st Century*, N. Soga and A. Kato, Eds., Ceramic Society of Japan, Tokyo, 1991, p. 580.
99. G. N. Greaves, in *Ceramics: Toward the 21st Century*, N. Soga and A. Kato, Eds., Ceramic Society of Japan, Tokyo, 1991, p. 793.
100. J. R. Hendrickson and P. J. Bray, *Phys. Chem. Glasses*, **13**, 43, 107 (1972).
101. M. Tomozawa and V. McGahay, *J. Noncryst. Solids*, **128**, 48 (1991).
102. J. M. Hyde and M. Tomozawa, *Phys. Chem. Glasses*, **27**, 147 (1986).
103. R. H. Doremus, *J. Am. Ceram. Soc.*, **67**, C-150 (1984).
104. R. J. Maurer, *J. Chem. Phys.*, **9**, 79 (1940).
105. H. Schiller, *Ann. Phys.*, **83M**, 137 (1927).
106. A. M. Venderovitch and V. J. Chenykh, *J. Tech. Phys. USSR*, **18**, 317 (1948).
107. J. Vermeer, *Physica*, **22**, 1257 (1956).
108. L. Zagar and E. Papanikolau, *Glastech. Ber.*, **42**, 37 (1969).
109. J. L. Barton and M. Leblond, *Verres Refract.*, **24**, 225 (1970); *J. Noncryst. Solids*, **4**, 220 (1979).

CHAPTER 16

DIELECTRIC AND MECHANICAL LOSS

In many substances mechanisms for dielectric and mechanical loss (internal friction) are entirely different. However, in nonmetallic solids and liquids, there is often a loss of both kinds that is related to the electrical conductivity of the material.

Various mechanisms have been suggested for this loss, but none has been universally accepted. Therefore, in this discussion experiments on each kind of loss are discussed separately with no interpretation in terms of mechanism. For each type, experimental methods and effects of frequency, temperature, and glass composition on the loss are considered. In the final sections the relation between these two types of loss and theories for them are treated. Reviews of dielectric relaxation in glass are in Refs. 1–10.

EXPERIMENTAL MEASUREMENT OF DIELECTRIC LOSS

The charge Q on a conductor is proportional to the potential difference V between this conductor and other conductors within the electric field of the charge, so that

$$Q = CV \quad (1)$$

where C is called the capacitance. The capacitance depends on the geometrical arrangement of the conductors and the material in between them called the dielectric and is measured in farads, which are coulombs/volt. The property of the material that determines the capacitance is called the dielectric constant ϵ . For a vacuum ϵ is called ϵ_0 , the dielectric constant of free space, and equals

8.85×10^{-12} F/m. If the conductors are flat plates of area A a distance d apart, the capacitance of this "condenser" or "capacitor" is given by

$$C = A \frac{\epsilon}{d} \quad (2)$$

If an alternating voltage is impressed across the plates of a condenser with a vacuum dielectric, the current in the circuit leads the voltage by 90° . If the dielectric is not a vacuum, the current often is not exactly 90° out of phase with the voltage, giving rise to a power loss. This property can be described by considering the dielectric constant to be a complex number with a real and imaginary part,

$$\epsilon^* = \epsilon' - i\epsilon'' \quad (3)$$

In this case the capacitance given by Eq. 2 can also be considered to be a complex quantity. The loss angle θ by which the current deviates from a 90° advance with the voltage is given by

$$\tan \theta = \frac{\epsilon''}{\epsilon'} \quad (4)$$

The complex dielectric constant is usually measured with an AC bridge, such as a Schering bridge.¹¹ A schematic diagram of such a bridge is given in Fig. 1. The variable capacitors C_N and C_B are alternatively adjusted until the detector shows a minimum current, first without the sample X and then with it. At low loss, the real part of the capacitance C' of the sample is just the difference between the two readings of C_N , and $\tan \theta$ is proportional to the difference between the readings of C_B and C_N . For $\tan \theta$ greater than about 0.1, these readings must be corrected by adding squared terms.¹¹ If the sample

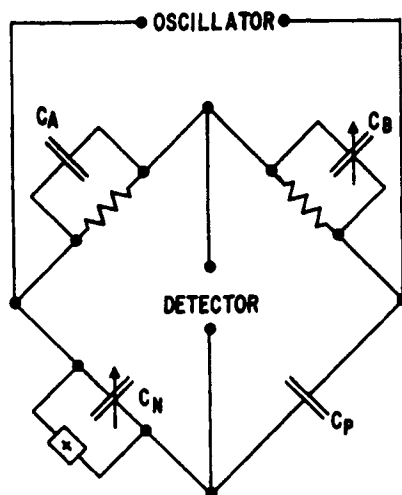


Fig. 1 Schematic diagram of a bridge circuit used to measure dielectric properties.

is the dielectric of a capacitor with plates of area A a distance d apart, then ϵ'' can be calculated from $\tan \theta$ and Eq. 4.

In recent years a variety of automated capacitance and conductance bridges have been developed and are available commercially, for example the Gen Rad Model 1615 and 1689 (Digobridge)[®] capacitance bridge, for frequencies between 12 and 100 kHz.¹²

The type of electrodes used in measuring the dielectric loss of glass can substantially influence the results. The usual type of electrodes have been films of metal deposited on the glass. With this type of electrode, it is necessary to make a correction for the contribution of the normal DC resistivity of the sample to the apparent value of ϵ'' . This correction is inversely proportional to the frequency, so that at low frequency it is much larger than the other losses in the glass, and makes results at these frequencies quite unreliable. Another disadvantage of the film electrodes is that surface conductivity can contribute to the loss. This contribution can be avoided by a third "ring" electrode, but this electrode leads to additional complications in the measuring circuit. Silver electrodes can also react with the glass.

Kim and Tomozawa¹³ studied the influence of different electrode materials, such as pastes and vapor-deposited silver and gold, and pretreatment of the glass surface, on dielectric measurements. They found large differences between measured dielectric constants and losses at lower frequencies, for example below about 10^4 Hz at 250°C for a soda-lime silicate glass. Paste electrodes showed the largest deviations but were not sensitive to surface preparation; evaporated electrodes were quite sensitive to surface preparation. Silver electrodes reacted strongly with a $\text{Li}_2\text{O} \cdot 2\text{SiO}_2$ glass at 400°C.

An alternative type of electrode is made of stainless steel disks, which are simply pressed against the flat glass sample.¹⁴ The electrodes and sample can be held in vacuum for measurements at high temperatures. With this arrangement, the glass is partially isolated from the electrodes, which are covered with a thin oxide layer. The DC resistivity of a sample between such electrodes was about three orders of magnitude lower than measured with silver electrodes painted on the same sample.

EFFECT ON FREQUENCY OF DIELECTRIC LOSS

At high frequencies (above about 10^6 cycles/s at room temperature), the real part of the dielectric constant changes little with frequency, and the imaginary part is small. However, at lower frequencies there is a loss peak, and ϵ' decreases with increasing frequency in the frequency range of the loss. Results at 253°C for an alkali borosilicate glass containing 7.2 wt% Na_2O , 8.7% K_2O , and negligible Li_2O and CaO , are shown in Figs. 2 and 3. These measurements were made as described above, with stainless steel electrodes.¹⁴ The increase in loss at low frequencies probably results from the DC resistivity of the sample, for which no correction was made. The values actually plotted are $(\epsilon' - \epsilon_\infty)/(\epsilon_s - \epsilon_\infty)$ and $\sqrt{2\epsilon''}/(\epsilon_s - \epsilon_\infty)$, where ϵ_∞ is the high-frequency dielec-

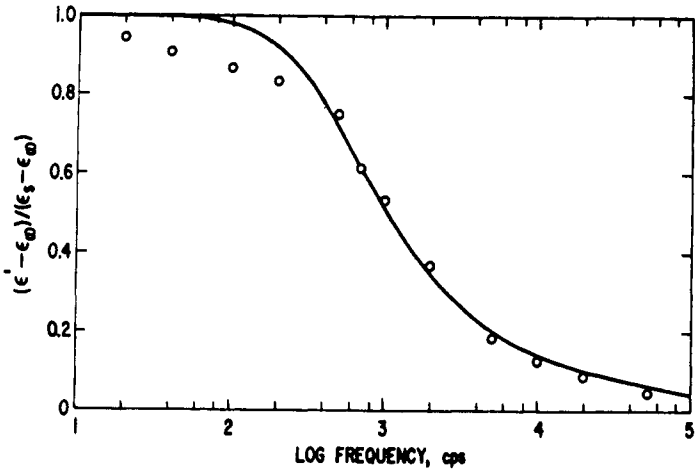


Fig. 2 Reduced real part of the dielectric constant for an alkali borosilicate glass. Points, experimental data; curve, theoretical.¹⁴

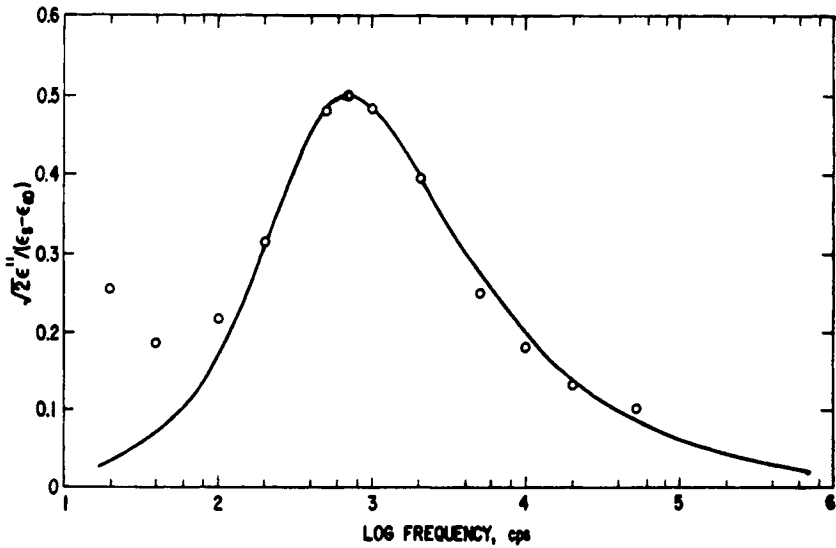


Fig. 3 Reduced dielectric loss as a function of frequency for an alkali borosilicate glass. Points, experimental data; curve, theoretical.¹⁴

tric constant, and ϵ_s is the estimated value of the "static" dielectric constant, or the real part at zero frequency.

A number of earlier measurements of dielectric loss of silicate glass as a function of frequency have been made.^{1-3,15,16} Taylor¹ found that his loss peaks for a number of soda-lime glasses and Pyrex borosilicate glass had about the same frequency dependence; an example is shown in Fig. 4. Charles¹⁵ found a similar loss curve for a commercial soda-lime glass. The loss peaks found by these investigators are somewhat broader than the one shown in Fig. 3. Taylor and Charles made their measurements on samples with painted silver electrodes. It is not certain whether the different experimental techniques are responsible for the differences in the shape of the loss curves. Isard¹⁷ found some change in peak shape for $\text{Na}_2\text{O} \cdot 4\text{SiO}_2$ glass as a function of temperature, using sodium amalgam electrodes, and he found an asymmetric peak, in agreement with Fig. 3. Asymmetric loss peaks have also been found for lithium¹⁸ and cesium¹⁹ silicate glasses.

Owen and Douglas measured some dielectric properties of fused silica. They found that the dispersion curves of ϵ' had the same shape at different temperatures and for different fused silicas. Their loss curves were narrower than those measured by Taylor and Charles, but similar to the one shown in Fig. 3.

EFFECT OF TEMPERATURE ON DIELECTRIC LOSS

The loss peak and dispersion curve shift to higher frequencies as the temperature is increased. If the peak shape remains the same as the temperature is

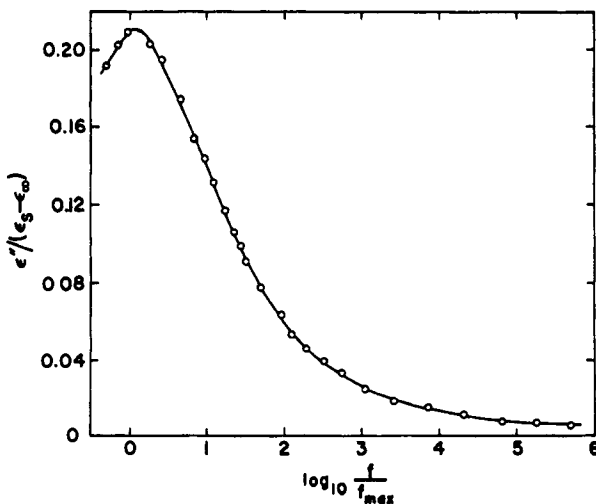


Fig. 4 Dielectric loss curve for a soda-lime glass, measured by Taylor.¹

changed, the shift of the peak maximum gives a measure of the temperature dependence of the loss. For glasses, the frequency at which the loss is a maximum increases exponentially with reciprocal temperature following the relation

$$f_m = A \exp \left(\frac{-Q}{RT} \right) \quad (5)$$

where Q is the activation energy, R is the gas constant, T is the temperature, and A is independent of temperature.

The activation energies of relaxation and electrical conduction for some commercial and laboratory glasses are shown in Table 1. The activation energy for relaxation was close to that for conduction for every glass examined including many not listed in Table 1.

Gough, et al.²¹ found a dielectric loss at high temperatures in alkali-free borate glasses (alkaline earth or lead aluminoborates) that was related to the electrical conductivity of the glasses, even if the conductivity was electronic, as for bismuth borate glasses. Except for these latter glasses, the conductivity is probably ionic and results either from the metal ions or residual hydrogen ions. Isard also concluded that dielectric loss in glass is related to conductivity, whether it is electronic or ionic.²² Mansingh et al.²³ found a dielectric loss in an electronically conducting vanadium phosphate glass.

EFFECT OF COMPOSITION ON DIELECTRIC LOSS

High-frequency dielectric constants and power factors (power factor = $\cos \theta \approx \tan \theta$) at room temperature are summarized by Navias and Green;²⁴ see also Ref. 6. The high-frequency reduced dielectric constants ϵ'/ϵ_0 of some different

TABLE 1 Activation Energies for Dielectric Relaxation and Electrical Conductivity

Glass type	Composition (mol%)			Activation energy (kcal/mol)		Refs.
	SiO ₂	Na ₂ O	CaO	Relaxation	Conductivity	
Soda-lime	74.2	15.3	10.5	20.6	19.8	1
Soda-lime	70.4	19.1	10.5	19.2	18.8	1
Soda-lime (commercial)	74.4	19.1	6.5	18.7	18.6	1
Pyrex borosilicate	80.0	4.1		23.9	22.2	1
Soda-lime (Corning 0080)	73.9	15.9	4.7	20.8	20.2	15
Fused silica (600–800°C)	100.0			23.0	22.0	20

glasses at 25°C are fused silica, 3.7; Pyrex borosilicate, 4.6; and commercial soda-lime (Corning 0080), 7.2. The dielectric constant usually increases as the amount of alkali in the glass increases. Factors for calculating the dielectric constant from the composition are given by Scholze,²⁵ as taken from Appen and Brecker.²⁶

The power factor ($\tan \theta$) also increases as the amount of alkali increases. Many measurements of $\tan \theta$ for glasses, particularly for small $\tan \theta$ values, are not very accurate.

MEASUREMENT OF MECHANICAL LOSS

When a stress is applied to a material there is an instantaneous deformation and sometimes a further deformation that increases with time. When the stress is released there is an instantaneous elastic relaxation, but some of the deformation may relax more slowly.

If a periodic stress $S = S_0 \cos \omega t$ of frequency $\omega/2\pi$ is applied to the material, the deformation lags behind the stress and is proportional to $\cos(\omega t - \delta)$ because of these time-dependent relaxations. The tangent of the lag angle δ is called the internal friction. Two different experimental methods have been used to measure this mechanical loss or internal friction in glass: the torsion pendulum and the crystal oscillator.

In the torsion pendulum, a fine glass rod is twisted and the damping of its oscillations observed. If there were no internal friction or external damping forces the pendulum would oscillate through the angle of the initial twist. However, internal friction causes this angle ϕ_1 to decrease to ϕ_2 in the subsequent cycle. The logarithmic decrement $\ln \phi_1/\phi_2$ is equal to one-half of the fractional energy loss $\Delta E/E$ per cycle. In turn $\Delta E/E$ is related to the internal friction $\tan \delta$:

$$\ln \frac{\phi_1}{\phi_2} = \frac{\Delta E}{2E} = \pi \tan \delta \quad (6)$$

Thus by measuring the deformation angles of a torsion pendulum after successive oscillations it is possible to calculate the internal friction. The frequency of the torsion pendulum usually is in the range from 0.05 to 10 vibrations/s.

The internal friction of glass can be measured at frequencies in the kilocycle range by a piezoelectric driver-gage method.²⁷ One quartz bar drives a composite oscillator of which the sample is a part, and another quartz bar acts at the gage. The total energy loss in the composite oscillator is proportional to the ratio of the voltage V_d on the driver crystal to the voltage V_g from the gage crystal, and if the angle δ is small, so that $\tan \delta \approx \delta$, then

$$\delta = K \frac{V_d}{V_g m_t f_t^2} \quad (7)$$

where m is the total mass of the oscillator and f_i is the resonant frequency of the composite oscillator. The proportionality constant can be measured from the half-width of the resonance peak. To find the internal friction of glass, two samples differing in length by one-half of a wave length are used. Then

$$\delta = \frac{(m_L \delta_L - m_s \delta_s)}{m_L - m_s} \quad (8)$$

where the m 's are the masses of the larger and smaller samples and the δ 's are the total losses calculated from Eq. 7, for the appropriate sample.

EFFECT OF FREQUENCY AND TEMPERATURE ON MECHANICAL LOSS

The internal friction of glass has been measured as a function of temperature at constant frequency because it is easier to change the temperature than the frequency in the techniques mentioned above. It is unfortunate that no measurements at constant temperature over a wide frequency range have been made, because many properties of glass change with temperature. Thus it is easier to compare theories of mechanical loss with measurements at constant temperature than with those at constant frequency.

The internal friction of sodium silicate and a sodium-aluminum silicate glass over a wide range of temperatures is shown in Fig. 5. At high temperatures the loss probably results from large-scale relaxations in the silicate network. The rate of these relaxations is related to viscous flow; they are discussed in more detail in Refs.²⁸⁻³⁰ Viscous flow and the glass transition are discussed in Chapters 6 and 7, respectively.

At intermediate temperatures two internal friction peaks appear that are related to ionic motion in the glass. These peaks are shown in Fig. 5 for a sodium disilicate glass. The peak at low temperature is related to alkali ion movement in the glass, whereas the peak at higher temperatures is related to hydrogen ions in the glass. The reasons for these assignments are enlarged upon in the next paragraphs.

The temperature for maximum internal friction can be measured for different frequencies. At two different frequencies f_1 and f_2 the temperatures T_1 and T_2 of maximum $\tan \delta$ are related by

$$\ln \frac{f_1}{f_2} = \frac{-Q}{R} \left(\frac{1}{T_1} - \frac{1}{T_2} \right) \quad (9)$$

where the activation energy Q is independent of temperature. The activation energies for the low-temperature peaks of a number of alkali silicate glasses are found to be close to those for electrical conductivity and alkali ion diffusion,³¹⁻³⁴ just as for the activation energies of the dielectric loss peaks. Furthermore, the height of the internal friction peak is related to the concen-

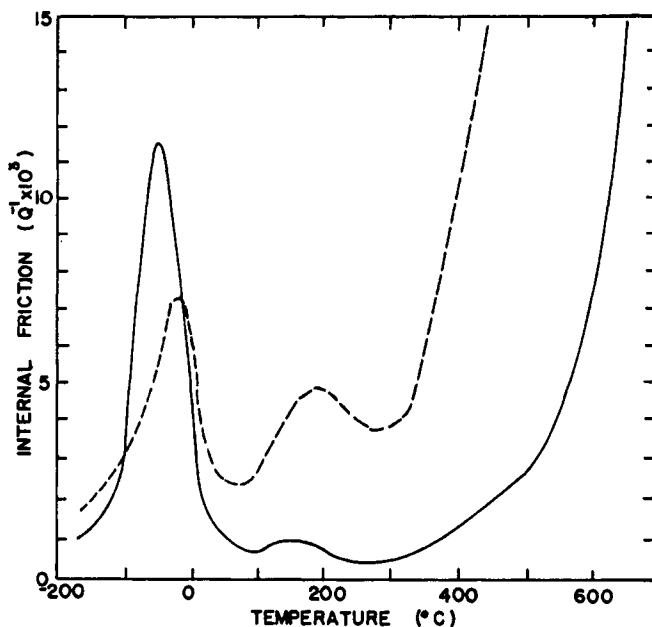


Fig. 5 Internal friction of a $\text{Na}_2\text{O} \cdot 3\text{SiO}_2$ glass (dashed line) and a $\text{Na}_2\text{O} \cdot \text{Al}_2\text{O}_3 \cdot 6\text{SiO}_2$ glass (solid line) at 0.4 cycles/s as a function of temperature, measured with a torsion pendulum.³⁷

tration of alkali ion in the glass, usually becoming smaller as this concentration becomes smaller, as described in the following section. Thus there appears to be a definite connection between alkali ion motion and the low-temperature peak. Mechanisms for this relaxation are discussed in the section on theories.

The internal friction peak at higher temperatures, sometimes called the "intermediate temperature" peak is probably related to the motions of hydrogen ions in the glass.³⁵ A number of experimental results point to the importance of hydrogen ions for this peak. First, there is a close correlation between the rate of weathering of a silicate glass and the occurrence of the peak. Glasses that weather rapidly show the peak, whereas those that are less reactive do not. Weathering results from the exchange of hydrogen ions from atmospheric water with alkali ions in the glass (see Chapters 13 and 14). The rate of weathering is controlled by the rate of interdiffusion of alkali and hydrogen ions in the glass. The addition of alkaline earth ions to the glass reduces the diffusion coefficient of alkali ions and consequently the rate of weathering. Aluminosilicates have a lower rate of weathering because the aluminosilicate groups in glass have a lower ratio of hydrogen-to-sodium ion affinity than do $-\text{SiO}$ groups. Therefore, on the aluminosilicate glasses the fraction of surface alkali ions that exchange with hydrogen ions is lower than for other alkali silicate glasses. The internal friction peak at higher tempera-

tures becomes smaller as more alkaline earth or aluminum oxide is added to an alkali silicate glass,^{36,37} and is absent in some commercial glasses containing these oxides and known for good weatherability.^{33,38,39}

Second, Vaughn et al.⁴⁰ showed that when a fine glass fiber reacts with the atmosphere an internal friction peak slowly develops at higher temperatures than the alkali peak. Their fibers were stored in a desiccator and measured in a vacuum, under which conditions this peak did not develop.

Third, DeWaal⁴¹ studied the internal friction of a sodium disilicate glass before and after exchange with hydrogen ions from a melt of NH_4HSO_4 . He treated the glass for 2.5 h at 275°C. At this temperature, the effective interdiffusion coefficient of sodium and hydrogen ions is about $1.3 \times 10^{-11} \text{ cm}^2/\text{s}$, so that the average distance of penetration of the hydrogen ions was about 5 μm . After this treatment DeWaal found a substantial increase in the height of the second internal friction peak at higher temperature, as would be expected if this peak resulted from motion of hydrogen ions.

Fourth, Abdel-Latif and Day⁴² were able to introduce a high-temperature peak in an $\text{Li}_2\text{O} \cdot \text{Al}_2\text{O}_3 \cdot 2\text{SiO}_2$ glass that should not contain nonbridging oxygen atoms. The original glass did not show this peak, but after hydrogen ions were introduced by ion exchange in molten ammonium acid sulfate for 21 h at 366°C such a peak appeared. Therefore the experimental evidence is in favor of a connection between hydrogen ion motion in the glass and the appearance of the high-temperature peak.

EFFECT OF GLASS COMPOSITION ON MECHANICAL LOSS

The effect of alkali ion concentration on peak height for number of different silicate glasses is shown in Fig. 6. There is considerable scatter in the results from one investigator to another for identical compositions, but for each investigator there is a consistent increase in peak height with alkali oxide concentration. These results show that the particular experimental technique used, and the history of the samples, can influence the background contributions to the peak height. Results on some glasses containing a third oxide are not consistent with those in Fig. 6; for example, in a glass containing 12.5 mol% Na_2O , 12.5% Al_2O_3 , and 75% SiO_2 , the peak height was about 12×10^{-3} ,³⁷ and in Pyrex borosilicate glass (4% Na_2O) it was about 10^{-3} .³⁸ In fused silica with about 5–10 ppm by weight Na_2O , the peak height was measured to be about 3×10^{-5} .²⁷

In sodium borate glasses with Na_2O concentrations greater than about 15 mol%, the alkali ion peak behaves much the same as in sodium silicates.^{31,45} The temperature of maximum loss decreases as the sodium concentration increases, as does the peak height, paralleling an increase in conductivity in the glass. Below about 15% Na_2O , the peak is obscured by background damping, since the temperatures approach the glass transition range.

The internal friction of sodium germanate glasses is quite similar to that of

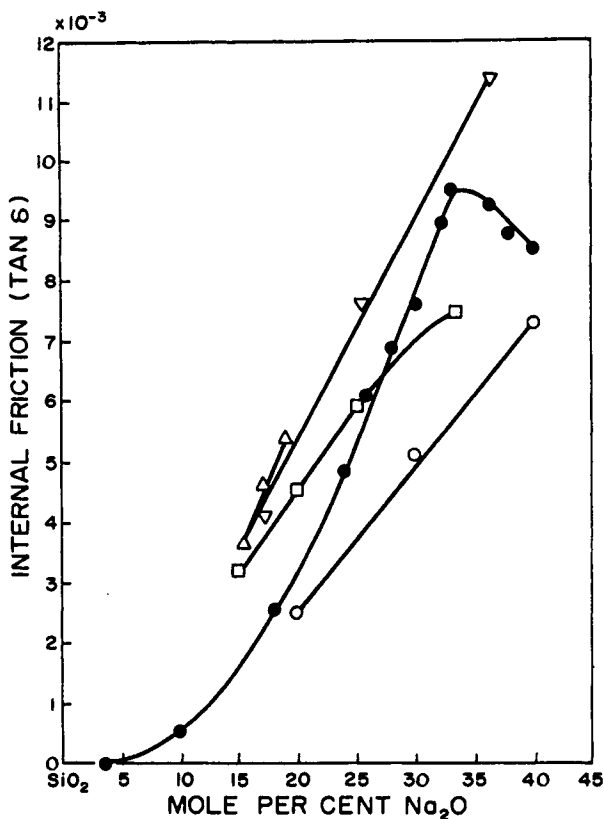


Fig. 6 Height of the internal friction peak in binary alkali silicate glasses as a function of alkali oxide concentration. ●, Coenen;³¹ ○, Deeg;⁴³ □, Jagdt;⁴⁴ △, Mohyuddin and Douglas;³⁴ ▽, Forry.^{44a} From Ref. 28.

sodium silicate glasses.^{46,47} The alkali ion peak has an activation energy close to that for electrical conductivity of the glasses and for sodium ion diffusion in them, and the peak height is related to the sodium ion concentration. A higher temperature peak is similar to the same peak in sodium silicate glasses, and is also probably related to hydrogen ions in the glasses.

A mechanical loss peak has been found in an iron phosphate glass; this peak has the same activation energy as the conductivity for the glass.⁴⁸ This result is curious because the conductivity in this glass is electronic rather than ionic.

THEORIES OF DIELECTRIC AND MECHANICAL LOSS IN GLASS

Most theories of the alkali ion peaks in dielectric and mechanical loss in glass have considered these peaks to result from short-range rearrangements of the alkali ions in the glass. In dielectric loss this rearrangement leads to an effective

dipole moment, and in mechanical loss it leads to a time-dependent change in modulus.

The dielectric properties are usually described in terms of the complex dielectric constant of Eq. 3. Alternative descriptions are the complex conductivity

$$\sigma^* = \sigma' + i\sigma'' \quad (10)$$

both real and imaginary parts can depend on frequency. The complex conductivity is related to the complex dielectric constant as

$$\varepsilon^* = \sigma^*/i\omega \quad (11)$$

Another representative is the complex modulus M

$$M = M' + iM'' = 1/\varepsilon^* = i\omega/\sigma^* \quad (12)$$

as introduced by Macedo et al.⁵⁰ This modulus emphasizes data at higher frequencies than the dielectric constant of Eq. 3, and therefore reduces problems with electrode effects and direct current conduction.

The shapes of the loss peaks can be calculated by assuming an exponential decay of current or deformation. For dielectric loss this assumption leads to a complex dielectric constant of the form

$$\varepsilon^* = \varepsilon' - i\varepsilon'' = \varepsilon_\infty + \frac{\varepsilon_0 - \varepsilon_\infty}{1 - i\omega\tau} \quad (13)$$

or

$$\varepsilon' = \varepsilon_\infty + \frac{\varepsilon_0 - \varepsilon_\infty}{1 + \omega^2\tau^2} \quad (14)$$

and

$$\varepsilon'' = \frac{(\varepsilon_0 - \varepsilon_\infty)\omega\tau}{1 + \omega^2\tau^2} \quad (15)$$

Here ε_0 is the static (DC) dielectric constant, ε_∞ is the dielectric constant at high frequency, ω is 2π times the frequency, and τ is a relaxation time.

For the internal friction $\tan \delta$ can be found, based on similar equations, to be⁴⁹

$$\frac{\tan \delta}{(\tan \delta)_{\max}} = \frac{2\omega\tau}{1 + \omega^2\tau^2} \quad (16)$$

Equations 15 and 16 give symmetrical loss peaks that are considerably narrower than those measured for dielectric and mechanical loss in glass. To explain the broader peaks, it is necessary to assume that there is a spectrum of relaxation times τ , rather than a single time. This broadening of the loss peaks can also be taken into account with the "b function" described in Chapter 7

for structural and strain relaxation. Instead of a simple exponential, the decay of the current or field follows the function

$$E = E_0 \exp(-t/\tau)^b \quad (17)$$

Theories of dielectric and mechanical loss are reviewed in Refs. 4, 5, 7–10, and 14. Elliott⁸ reviewed models of dielectric relaxation and data for amorphous chalcogenides, phosphorus and arsenic. Angell⁹ reviewed dielectric and mechanical relaxation of silicate and fluoride glasses. Especially intriguing are the trenchant comments of Dyre.¹⁰ He emphasizes that at high frequencies the real part of the conductivity σ' follows a power law with an exponent for 0.7–1.0, as found in several experiments;^{5,22,51,52} however, he finds that "... there is no basis for concluding that power laws are fundamental . . ." Dyre discusses models involving hopping charge carriers, and concludes that although they are simple and give reasonably good fits to experiments, other models may be more appropriate. He lists open problems and suggestions for future work: reliability of data, additional kinds of measurements, relation of loss to the scale of inhomogeneities, and the similarity between model predictions (see also ref. 50a).

Because there is a close correlation between dielectric and mechanical loss peaks and electrical conductivity, theories of conductivity (see Chapter 15) also are pertinent to loss mechanisms. For example, the relationship between high field conduction and dielectric relaxation was examined by Hyde and Tomozawa,⁵³ and they concluded that the weak electrolyte theory gave a qualitative but not quantitative description of the data. These authors also explored the relation between dielectric relaxation and thermodynamic nonideality⁵⁴ and the "b" function of Eq. 13 as applied to mixed alkali glasses.⁵⁵ Ngai et al.⁵⁶ relate traditional relaxation results to spin-lattice relaxation.

The conclusion is that there is no completely satisfactory explanation of dielectric and mechanical relaxation in glasses, and that uncertainties in measurements and interpretations remain.

REFERENCES

1. H. E. Taylor, *J. Soc. Glass Technol.*, **41**, 350 (1957); **43**, 124 (1959).
2. J. M. Stevels, in *Handbuch der Physik*, Vol. 20, Springer-Verlag, Berlin, 1957, p. 350.
3. A. E. Owen, in *Progress in Ceramic Science*, J. E. Burke, Ed., MacMillan, New York, 1963.
4. M. Tomozawa, in *Treatise on Materials Science and Technology*, Vol. 12, M. Tomozawa and R. H. Doremus, Eds., Academic Press, San Diego, CA, 1977, p. 283.
5. A. K. Jonscher, *Dielectric Relaxation in Solids*, Chelsea Dielectric, London, 1983.
6. N. P. Bansal and R. H. Doremus, *Handbook of Glass Properties*, Academic Press, San Diego, CA, 1986, Ch. 14, p. 450.

7. M. D. Ingram, *Phys. Chem. Glasses*, **28**, 215 (1987).
8. S. R. Elliott, *Adv. Phys.*, **36**, 135 (1987).
9. C. A. Angell, *Chem. Rev.*, **90**, 523 (1987).
10. J. C. Dyre, *J. Noncryst. Solids*, **135**, 219 (1991).
11. F. A. Laws, *Electrical Measurements*, McGraw-Hill, New York, 1938, p. 417.
12. Gen. Rad Corp., Bolton, MA, Instruction Manual, 1983.
13. C. Kim and M. Tomozawa, *J. Am. Ceram. Soc.*, **59**, 127, 321 (1976).
14. This book, first edition, p. 192.
15. R. J. Charles, *J. Appl. Phys.*, **32**, 1115 (1961); *J. Am. Ceram. Soc.*, **45**, 105 (1962).
16. J. Volger, J. M. Stevels and C. van Amerongen, *Philips Res. Rep.*, **8**, 452 (1953).
17. J. O. Isard, *Proc. IEEE (London)*, **109B**, 22, 440 (1961).
18. L. Heroux, *J. Appl. Phys.*, **29**, 1639 (1958).
19. D. R. Uhlmann and R. M. Hakim, *J. Phys. Chem. Solids*, **32**, 2652 (1971).
20. A. E. Owen and R. W. Douglas, *J. Soc. Glass Technol.*, **43**, 159 (1959).
21. E. Gough, J. O. Isard and J. A. Topping, *Phys. Chem. Glasses*, **10**, 89 (1969).
22. J. O. Isard, *J. Noncryst. Solids*, **4**, 357 (1970).
23. A. Mansingh, J. M. Reyes and M. Sager, *J. Noncryst. Solids*, **7**, 12 (1972).
24. L. Navias and R. L. Green, *J. Am. Ceram. Soc.*, **29**, 267 (1946).
25. H. Scholze, *Glass*, Springer-Verlag, Berlin, 1991, pp. 318–319.
26. A. A. Appen and R. J. Bresker, *J. Tech. Phys. USSR*, **22**, 946 (1952).
27. J. W. Marx and J. M. Sivertsen, *J. Appl. Phys.*, **24**, 81 (1953).
28. J. L. Hopkins and C. R. Kurkjian, in *Physical Acoustics*, Vol. II, Part B, Academic Press, New York, 1965, p. 91.
29. R. W. Douglas, P. J. Duke and O. V. Mazurin, *Phys. Chem. Glasses*, **9**, 169 (1968).
30. K. L. Ngai and G. B. Wright, Eds., *J. Noncryst. Solids*, **131–133** (1991).
31. M. Coenen, *Z. Elektrochem.*, **65**, 903 (1961).
32. H. Rötger, *Glastech. Ber.*, **19**, 192 (1941).
33. J. V. Fitzgerald, *J. Am. Ceram. Soc.*, **34**, 314, 339, 399 (1951).
34. J. Mohyuddin and R. W. Douglas, *Phys. Chem. Glasses*, **1**, 71 (1960).
35. R. H. Doremus, *J. Noncryst. Solids*, **3**, 369 (1970).
36. R. J. Ryder and G. E. Rindone, *J. Am. Ceram. Soc.*, **43**, 662 (1960).
37. D. E. Day and W. E. Steinkamp, *J. Am. Ceram. Soc.*, **52**, 571 (1969).
38. P. L. Kirby, *J. Soc. Glass Technol.*, **39**, 385 (1955).
39. G. J. Copley and D. R. Oakley, *Phys. Chem. Glasses*, **9**, 141 (1968).
40. L. Vaugin, J. C. Breton, P. Gobin, *Verres Refract.*, **23**, 174 (1969).
41. H. deWaal, *J. Am. Ceram. Soc.*, **52**, 165 (1969).
42. A. I. A. Abdel-Latif and D. E. Day, *J. Am. Ceram. Soc.*, **55**, 254 (1972).
43. E. Deeg, *Glastech. Ber.*, **31**, 1, 85, 124, 229 (1958).
44. R. Jagdt, *Glastechn. Ber.* **33**, 10 (1960).
- 44a. K. E. Forry, *J. Am. Cer. Soc.* **40**, 90 (1957).
45. K. H. Karsch and E. Jenckel, *Glastech. Ber.*, **34**, 397 (1961).

46. C. R. Kurkjian and J. T. Krause, *J. Am. Ceram. Soc.*, **49**, 134 (1966).
47. J. E. Shelby and D. E. Day, *Phys. Chem. Glasses*, **11**, 224 (1970).
48. R. A. Miller and K. W. Hansen, *J. Elect. Soc.*, **116**, 254 (1969).
49. C. Zener, *Elasticity and Anelasticity of Metals*, University of Chicago Press, 1948, pp. 6ff.
- 50a. R. H. Doremus, *J. Appl. Phys.*, **41**, 3366 (1970).
50. P. B. Macedo, C. T. Moynihan and R. Bose, *Phys. Chem. Glasses*, **13**, 171 (1972).
51. A. E. Owen, *J. Noncryst. Solids*, **25**, 372 (1977).
52. G. A. Niklasson, *J. Appl. Phys.*, **66** 4350 (1989).
53. J. M. Hyde and M. Tomozawa, *Phys. Chem. Glasses*, **27**, 147 (1986).
54. J. M. Hyde and M. Tomozawa, *J. Noncryst. Solids*, **109**, 18 (1989).
55. M. Tomozawa, J. M. Hyde, J. F. Cordaro, and M. Yoshiyagawa, *Phys. Chem. Glasses*, **33**, 69 (1992).
56. K. L. Ngai, Y. Strom and O. Kanest, *Phys. Chem. Glasses*, **33** 109 (1992).

OPTICAL ABSORPTION IN GLASSES

Optical absorption in glass in the visible spectral region colors the glass, leading to applications in optics and to many decorative uses. Absorption and transmission in the infrared and ultraviolet are important in optical uses in instruments. Absorption in all three regions can be used to study short-range structure of glasses, that is, the immediate surrounding of the absorbing atom.

In recent years there have been many new exciting applications of glasses in optics: optical fibers as waveguides, laser hosts and optical components, glasses that change absorption with light level (photochromic) and electric field (electrochromic), gradient index lenses, new glasses such as fluorides with different optical properties from silicates, planar wave guides, sensors, and glasses with nonlinear optical properties.

Data on the refractive indices of glasses as a function of glass composition, wavelength, and temperature are given in Refs. 1–8; Refs. 3 and 4 contain large numbers of references to sources of data. The optical constants n (refractive index) and k (extinction coefficient or absorption index) of a large number of solids over a wide range of wavelengths, with critical assessments, are given in Ref. 8. Included are the amorphous solids silica, silicon, silicon monoxide, silicon nitride, carbon and polyethylene.

In this chapter, the absorption of different glasses is discussed separately in the following order: fused silica, other network oxides, alkali and alkaline-earth oxides, transition-metal oxides, chalcogenides, and small metallic particles in glass. Then there are sections on the recent developments mentioned above.

FUSED SILICA

Fused silica is useful as an optical material because of its high transmission of visible and ultraviolet light. The transmission edge in the ultraviolet depends on the purity and state of oxidation (stoichiometry) of the silica, and therefore on its method of manufacture. Figure 1 shows the optical absorption at intermediate wavelengths of different fused silicas that are listed in Chapter 1, Table 3. The table also gives the methods of manufacture of the various types of fused silica and their approximate impurity contents. References to reviews on fused silica are given in Chapter 1.

The optical constants n and k are listed for amorphous silica for wavelengths from $0.05\text{ }\mu\text{m}$ to $500\text{ }\mu\text{m}$ by Philipp.⁹ He discusses measurement methods and evaluates the data critically.

The absorption edge for amorphous silica in the ultraviolet is at about $0.16\text{--}0.17\text{ }\mu\text{m}$ (about 8 eV). Absorption at longer wavelengths results from impurities in the silica, as described by Sigel;¹⁰ the most common impurities are alkalis, alkaline earths, and iron. There is a reduced center that causes absorption at about $0.24\text{--}0.28\text{ }\mu\text{m}$ in fused silicas melted in mildly reducing conditions, as for Type I silica in Fig. 1. This center probably is associated with an impurity in the silica such as aluminum.^{11,12} This band emits fluorescence radiation at 0.28 and $0.39\text{ }\mu\text{m}$ when it absorbs.

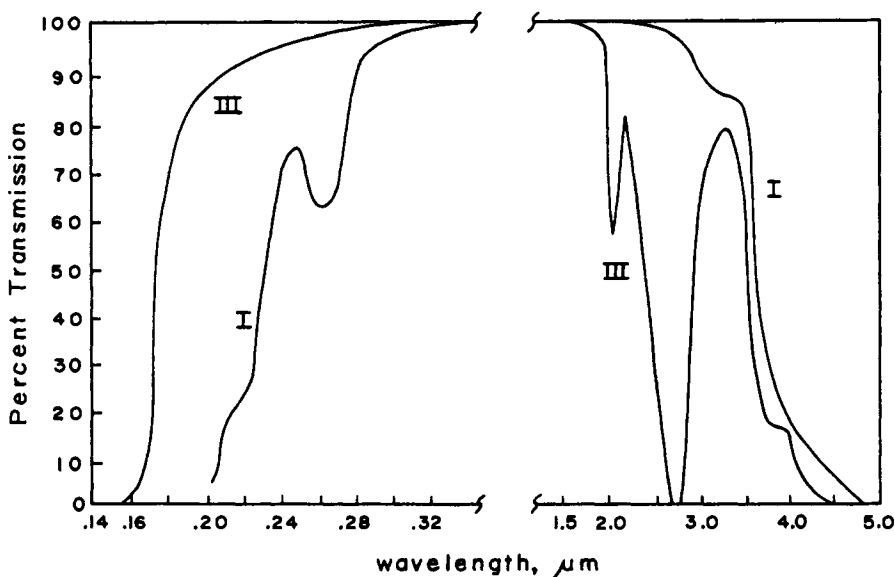


Fig. 1 Optical transmission of different types of fused silica (see Chapter 1, Table 2), in the near ultraviolet, visible, and near infrared. Sample thickness about one mm.

When silicates are irradiated with ultraviolet light, X-rays, or γ -rays ("ionizing" radiation) or atomic particles, defects are formed that absorb light in the ultraviolet and visible parts of the electromagnetic spectrum. These irradiation effects in glasses, especially silica, are reviewed by Frieble and Griscom in Refs. 13, 14 and 15.

The absorption band of fused silica in the near infrared at $2.7\mu\text{m}$ is associated with hydroxyl groups in the silica.^{16,17}

The absorption of vitreous silica in the infrared is shown in Fig. 2. The absorption bands are the same for different types of fused silica and can be considered to result from transitions of the silicon-oxygen network that are not disturbed by the impurities in fused silica. The band at about 1100cm^{-1} is not found in the Raman spectrum, and is attributed to the stretching vibration of the $-\text{Si}-\text{O}-\text{Si}-$ bond.^{10,18,19} The lack of a Raman band indicates conditions of high symmetry, in agreement with the structure of fused silica suggested in Chapter 3 in which there is considerable short-range order in the arrangement of the silicon-oxygen tetrahedra. The band at 465cm^{-1} has been assigned to "rocking" of the $\text{Si}-\text{O}-\text{Si}$ bond.²⁰ The lower-intensity bands at intermediate frequencies involve various bending modes mixed with the stretching and rocking modes of the $\text{Si}-\text{O}-\text{Si}$ bonds.

Absorption and reflection of vitreous silica in the ultraviolet at frequencies higher than the absorption edge (wavelengths below about $0.16\mu\text{m}$) have been measured by Loh,²² Philipp,^{9,23} Sigel,¹⁰ and Tarvio and Schnatterly.^{23a} The reflectance of fused silica and quartz at these higher energies is shown in Fig. 3. The similarity between these curves shows that optical absorption at these energies is determined by the short-range structure of the silicon-oxygen tetrahedra, which is the same in both amorphous and crystalline silica. This result is consistent with the random-network structure for fused silica discussed

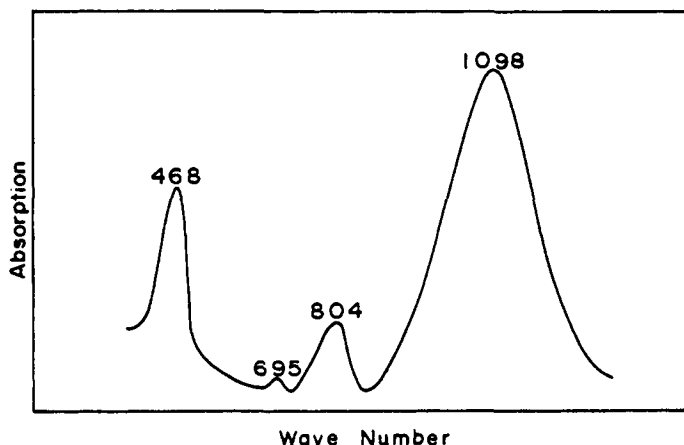


Fig. 2 Optical absorption of fused silica in the infrared.

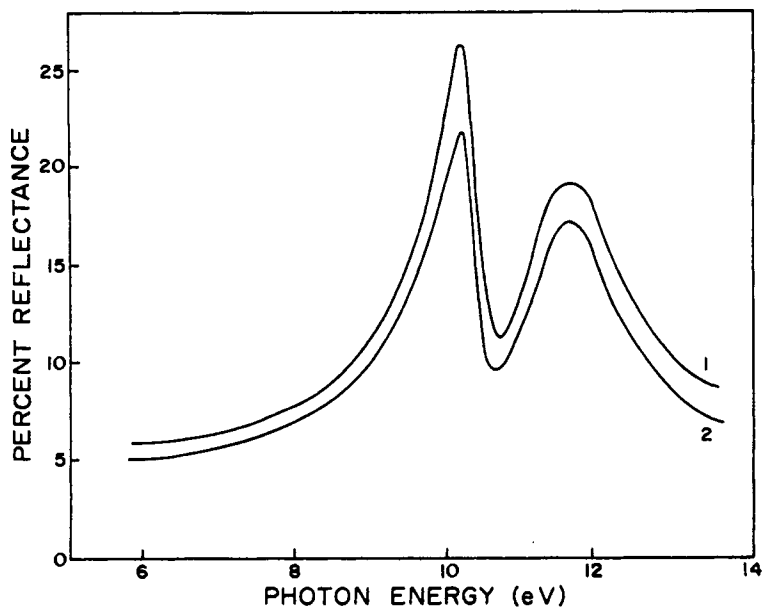


Fig. 3 The reflectance of fused silica and quartz in the ultraviolet.¹⁰ The values for fused silica have been lowered by 5%.

in Chapter 3, where it was shown that at short distances of the order of less than 10 \AA the crystalline and amorphous structures are virtually identical.

By studying silicate glasses containing various amounts of alkali, Siegel showed that the 11.5 eV band is characteristic of the silicon-oxygen network and is not affected by these additions.¹⁰ However, the band at 10.2 eV is apparently not present in silicate glasses of the disilicate composition ($67\% \text{ SiO}_2$, $33\% \text{ alkali oxide}$); in these glasses there is another band at 8.5 eV .

Theoretical calculations of the electronic structure of silica have employed valence band²⁴ and molecular orbital^{25,26} approaches. The 11.5 eV band is interpreted to result from band-to-band electronic transitions²⁴ or atomic-like electronic transitions.²⁵ Loh and Ruffa suggest that the 10.2 eV band results from an "exciton" (a bound electron-hole pair). Siegel discussed this assignment as a possible way to explain the shift of the 10.2 eV band to 8.5 eV , which could result from the change in the effective dielectric constant of the glass as alkali is added.¹⁰ Other calculations of SiO_2 electronic structure are given in Refs. 27 and 28.

From a study of the ultraviolet reflectance of mixed silicon and oxygen films, Philipp concluded that amorphous substances of all compositions between Si and SiO_2 can be formed, and that they are made up of random mixtures of Si-Si and Si-O bonds with the silicon atoms being four coordinated.²³ He found evidence that these materials are not mixtures of silicon and silica.

OTHER NETWORK-FORMING OXIDES

The approximate ultraviolet wavelengths at which the optical transmission drops sharply (the absorption edge) for simple oxide glasses in micrometers are SiO_2 , 0.16; B_2O_3 ,²⁹ 0.17; GeO_2 ,³⁰ 0.22; and P_2O_5 ,³¹ 0.27. The higher edge for P_2O_5 may occur because of the oxygen atoms doubly bonded to the phosphorous that are not part of the phosphorus-oxygen network.

The infrared spectrum of vitreous germania is similar to that of fused silica, but shifted to lower frequencies, with a strong absorption band at about 880 cm^{-1} resulting from $-\text{Ge}-\text{O}-\text{Ge}-$ stretching vibration and bands at lower frequencies corresponding to those in silica.³²⁻³⁵ The infrared spectrum of amorphous germania is similar to that of the hexagonal crystalline form, but different from that of the tetragonal crystalline form. This result is consistent with a germanium coordination number of four in amorphous germania, since in the hexagonal form germanium is four-coordinated, whereas in the tetrahedral it is six-coordinated.

The infrared absorption spectrum of amorphous anhydrous boron oxide (B_2O_3) has been measured by several workers.³⁶⁻³⁹ Strong absorption bands are found at 1260 cm^{-1} and 718 cm^{-1} , with a broad band at lower frequencies, and a shoulder on the 1260 cm^{-1} band at about 1370 cm^{-1} , as shown schematically in Fig. 4. The raman spectrum³⁸ shows a very intense band at

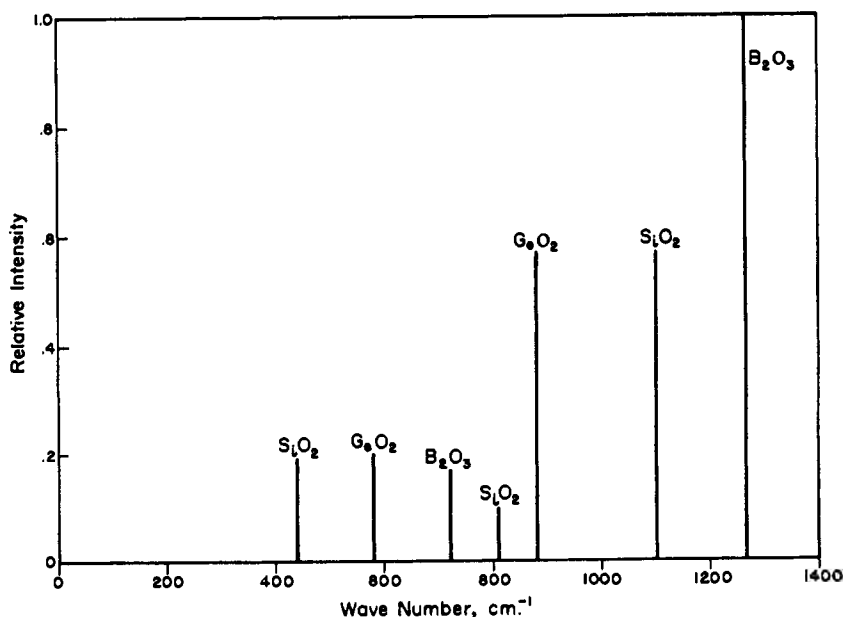


Fig. 4 Comparison of strong infrared absorption lines in vitreous silica, germania, and boric oxide.

808 cm^{-1} and a strong band at 1260 cm^{-1} . Krogh-Moe³⁹ has interpreted these results in terms of the boroxol structure of vitreous B_2O_3 , which from X-ray measurements appears to be the correct one (see Chapter 3). In this structure planar boroxol rings with three boron and three oxygen atoms are linked together by other B–O bonds. The band at 1260 cm^{-1} is assigned to the stretching vibration of the B–O bonds linking the boroxol groups. In the ideal case the vibration giving rise to this band should be inactive, but because of its coupling with its surroundings, the selection rules are relaxed. As water reacts with vitreous B_2O_3 the intensity of this band decreases.⁴⁰ The B–O bonds linking the boroxol groups should be the most reactive, consistent with this result.

The Raman line at 808 cm^{-1} has a degree of depolarization which indicates that it results from a symmetrical vibration.³⁹ This vibration is considered to be a “breathing” motion of the oxygen atoms in the boroxol ring;^{41,42} this vibration is inactive in the infrared. The band at 718 cm^{-1} is assigned to an out-of-plane vibration of the boroxol ring. These assignments are therefore consistent with the boroxol structure of vitreous B_2O_3 and strengthen the evidence for this structure.

The infrared spectrum of vitreous arsenic trioxide has been discussed by Wong and Angell.¹⁹

GLASSES CONTAINING ALKALI OXIDE

As alkali oxide is added to silica, the infrared absorption band at 1100 cm^{-1} decreases and new bands at 1075 and 940 cm^{-1} develop.^{10,19,43–48} The band at 940 cm^{-1} has been assigned to the Si–O stretching vibration when the oxygen is not bonded to another silicon (nonbridging oxygen), and the 1075- cm^{-1} band is the 1100- cm^{-1} Si–O stretching band shifted by the presence of SiONa^+ groups. A Raman band at 540 cm^{-1} can be assigned to bond-bending involving a nonbridging oxygen atom.⁴⁹

Similar results for the infrared spectra of the alkaline-earth silicates have been found,^{18,19} supporting the interpretation that the changes with respect to fused silica result from the introduction of nonbridging oxygen ions.

In the far infrared the absorption of a silicate glass (Corning 0211) was found⁵⁰ to increase with the square of the frequency in the range from 10 to 100 cm^{-1} . This absorption was interpreted to result from the excitation of lattice vibrations (phonons) by the alkali ions and other lattice-breaking ions in the glass. In fused silica the absorption in this frequency range is much lower and apparently results from charged defects, either associated with impurities or intrinsic in the silica lattice.⁵⁰

Sigel found that the optical density in the ultraviolet at wavelengths longer than the absorption edge (about 0.16 μm for fused silica) was directly proportional to the alkali concentration in the glass.¹⁰ The intensity of absorption increased in the order of lithium, sodium, and potassium for a given alkali

concentration. When aluminum was added to the alkali silicate glasses, the absorption decreased. These results indicate that this absorption is associated with the nonbridging oxygen ions introduced with the alkali ions; when aluminum is added these ions are associated with it, rather than increasing the number of nonbridging oxygens. The size of the alkali ions influences the electric field at the nonbridging oxygen ions, changing the absorption. It is not clear if this absorption results from broadening of the 8.5 eV band or represents formation of a new band.

At shorter wavelengths reflection spectra of alkali silicate glasses indicated absorption bands at 11.5 and 8.5 eV, as mentioned in the preceding section.¹⁰ The 11.5 eV band is also present in fused silica and is therefore interpreted to result from electronic transitions associated with the silicon-oxygen lattice. The 8.5 eV band is also found in alkaline-earth silicates, and its position is not much affected by the type lattice-breaking cation. This band could result from a shift of the 10.5 eV band in silica, as discussed in the preceding section.

References to measurements of infrared optical absorption of multicomponent alkali and alkaline-earth silicate glasses are given by Wong and Angell.¹⁹ They show no particularly different features from absorption of binary silicates.

When alkali oxide is added to boron oxide, the infrared band at 1260 cm^{-1} decreases in intensity and a new peak forms^{37,43} at about 1400 cm^{-1} . This change can be interpreted to result from the reaction of the boron-oxygen bonds linking the planar boroxol rings with alkali oxide to form boron atoms coordinated to four oxygen atoms, the excess charge of the boron being compensated by the alkali ions. This continuous change in the coordination number of boron with addition of alkali has been found with other techniques, as described in Chapter 3. Alkaline-earth borates show similar changes in the infrared spectrum as alkaline-earth oxides are added.¹⁹

When sodium oxide is added to boron oxide, the ultraviolet absorption edge is not much affected up to about 15 mol% Na_2O .²⁹ This result is consistent with the interpretation above of the changing boron coordination number with addition of alkali, and contrasts with the increase in ultraviolet absorption in silicate glasses caused by the introduction of nonbridging oxygen ions. In the borates all oxygens are linked to boron atoms and there are no nonbridging oxygen ions. Above about 15 mol% Na_2O , the ultraviolet absorption edge moves sharply to higher wavelengths. This increase in absorption is probably related to other changes in properties at this composition, known as the "borate anomaly."

The infrared spectra of a variety of alkali and alkaline-earth phosphates were very similar,¹⁹ indicating that the absorption bands resulted from the vibration of phosphorus-oxygen groups. These metaphosphates have a chain-like structure, and the spectra are consistent with calculations based on this structure.¹⁹ In the ultraviolet, the addition of alkali or alkaline-earth oxides to phosphorous oxide shifts the absorption edge to lower wavelengths, rather than higher as for other glass formers. This shift may occur because of tighter oxygen lattice.

The addition of alkali oxide to germanium induces a larger shift in the main

infrared absorption band than for the same addition to silica.³² The larger shift apparently results because the coordination number of germanium with oxygen is changing from four to six as alkali is added.

TRANSITION METAL IONS

A variety of colors in glasses are caused by transition metal ions in them, often in small concentrations. Thus the green color observed for thick slabs of most commercial glasses results from absorption of impurity ferric ions in the glass, and some absorption of this ion in the ultraviolet persists even when it is present in concentrations of less than 1 part/million. Other familiar coloring ions for glass are chromium for green, cobalt for blue, and manganese for purple.

The absorption bands for several different transition metal ions in glass are summarized in Table 1. Also given in the table are the most common colors

TABLE 1 Visible Optical Absorption in Soda-Lime Silicate Glasses of Transition Metal Ions

Ion	No. of <i>d</i> electrons	Abs. max. (μm)	Coordination No. with oxygen	Color of Glass	Remarks	Refs.
Cr^{3+}	1	0.66 0.45	6	Green		51, 62, 64
Ti^{3+}	1	0.57	6	Purple	Borosilicate glass	52
V^{4+}	1	1.12	6?	Red		53
V^{3+}	2	0.645 0.425	6	Green		53
Mn^{3+}	4	0.50	6	Purple		52
Mn^{2+}	5	0.435	4, 6?	Brown		52, 54, 55
Fe^{3+}	5	0.41	4?	Green	Potassium silicate	56-58
Fe^{2+}	6	1.10	4, 6?	Blue		56, 58
Co^{2+}	7	0.56	6	Blue	Low alkali borate	59-61
		0.60	4		High alkali borate	
Ni^{2+}	8	1.33 0.76 0.42 1.19 0.68-0.49	6 4	Purple, grey	Low alkali borate	59 60 61
					High alkali borate	
Cu^{2+}	9	0.79	6	Blue		53, 58

derived from each ion, its coordination number with oxygen, and the number of d electrons.

These visible absorption bands result from electron transitions of the $3d$ electrons of the ions. When the transition metal ions are coordinated with other ions, the energy levels of these d electrons are split by the electric field of the coordinating ions, instead of being degenerate as in the free ion. The d -electron orbitals are strongly directional, so the splitting is sensitive to the arrangement of the surrounding ions, and the electronic transitions and resulting absorption spectra can be used to study the coordination numbers of the central ions. The theory of these effects, called "ligand field" theory, was first developed by H. Bethe, and its application to glasses has been discussed in detail by Bates,⁵¹ and also in Refs. 10 and 19. Various experimental measurements on spectra of transition metal ions in glass are reported in Refs. 10, 19 and those in Table 1.

The assignment of coordination numbers given in Table 1 was mostly determined from the absorption spectra. In some cases (iron, cobalt, and nickel), both tetrahedral (4) and octahedral (6) coordination is possible, depending on the composition of the glass. Unequivocal determination of the coordination number from the optical spectrum alone is not always possible, for example, in the case of iron, so other techniques such as Mossbauer spectroscopy and electron spin resonance have been used to help in deciding on the correct coordination number.

OTHER GLASSES AND IONS

The optical properties of amorphous semiconductors are discussed in a series of articles in Ref. 76; see also Refs. 19, 77, and 78. Optical properties of halide glasses are reviewed in Ref. 79. Some recent studies of rare earth ions in glass are listed in Table 2. Tellurium in glass was described in Ref. 80, and neptunium in Ref. 81.

METALLIC PARTICLES

Small metallic particles dispersed in glass absorb light and can develop striking colors. Best known of these glasses is gold ruby glass, which has been known since the seventeenth century. Faraday recognized that the color of gold ruby glass resulted from finely divided gold particles.⁸² This glass is made by dissolving gold in the glass melt, as an ion, in which state the gold is retained when the glass is cooled rapidly.⁸³ To form the gold particles the glass is reheated to an intermediate temperature region. Certain agents, such as antimony oxide, in the glass aid nucleation of the particles, or they can be nucleated by ultraviolet, X-ray, or γ -radiation if a radiation-sensitive ion such

TABLE 2 Optical Studies of Rare-Earth Ions

Ion	Symbol	Refs.
Lanthanum	La	66
Cerium	Cr	63, 64
Praseodymium	Pr	67
Neodymium	Nd	19, 65
Samarium	Sm	68
Europium	Eu	65, 70
Gadolinium	Gd	71
Terbium	Tb	72
Holmium	Ho	73
Erbium	Er	74
Ytterbium	Yb	75

as cerium is present.⁸³ The growth of the particles takes place by diffusion of gold atoms or ions to the particles.⁸⁴

The color of gold ruby glass results from an absorption band at about $0.53\mu\text{m}$ as shown in Fig. 5. This band comes from the spherical geometry of the particles and the particular optical properties of gold.⁸⁵ It can be considered as a "plasma-resonance" band, in which the free electrons in the metal are considered as a bounded plasma. These electrons oscillate collectively at a particular frequency in the bulk metal, known as the plasma-resonance frequency. The spherical boundary condition of the particles shifts this resonance oscillation to lower frequencies (longer wavelengths).

The size of the gold particles influences the absorption. For particles larger than about 200\AA in diameter, the band shifts to longer wavelength as the oscillation becomes more complex.⁸⁵ For smaller particles, the bandwidth progressively increases because the mean free path of the free electrons in the particles is about 400\AA , and is effectively reduced.⁸⁶

Silver particles in glass color it yellow, resulting from a similar absorption band at $0.41\mu\text{m}$.⁸⁷ Copper has a plasma absorption band at $0.565\mu\text{m}$ for copper particles in glass.⁸⁸

NEW APPLICATION OF GLASS IN OPTICS

A large number of new uses of glass involve its optical properties. These are described briefly, with references.

The development of silica (SiO_2) glass fibers for long distance optical communication has been a major technological achievement, jointly worked out by America Telephone and Telegraph and Corning Glass. The fibers must be drawn to great lengths (kilometers) and must be extremely strong to prevent their fracture. Information on the making of fibers and their applications is

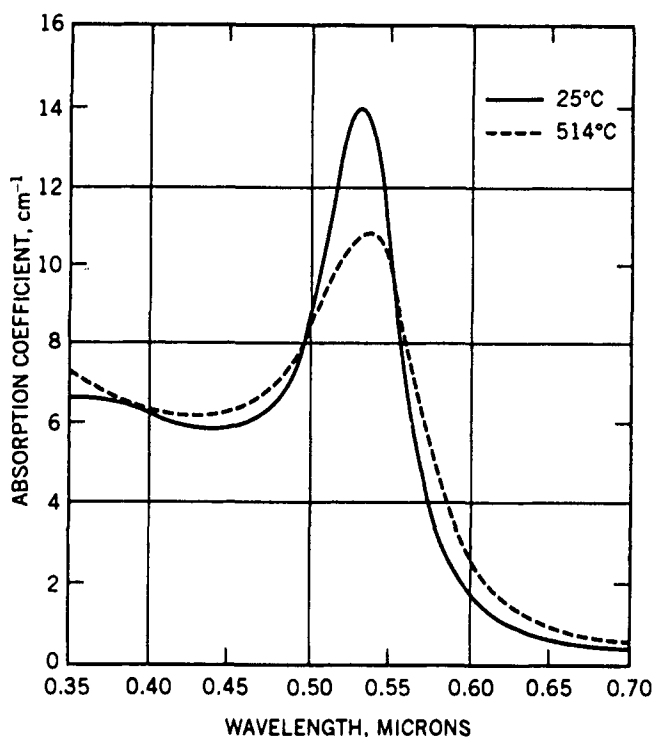


Fig. 5 Absorption spectrum of gold particles about 200 Å in diameter in glass.

given in Ref. 89; a review of optical propagation theory and its relation to fiber properties is given in Ref. 90; other reviews on fibers are given in Refs. 91, 92 and 92a.

Optical waveguides in bulk glass can be prepared by ion exchange in the glass surface, for example of silver ion for sodium, to change the refractive index in a surface layer.⁹³⁻⁹⁵ There has been considerable work on diffusion in ion exchange, both concentration and field driven, and the relation of the ionic concentration to the refractive index.⁹³⁻⁹⁵

Glass is an excellent laser host, and also can be used for active and passive optical components in laser systems.^{2,96}

Gradient index lenses result when the index of refraction of a material changes continuously in such a way as to focus light rays. Such an index gradient can be formed in a glass by exchanging ions; again exchange of silver for sodium ions in a glass is a favorite method for making the gradient, because such exchange results in a relatively large index change. There is a review in Ref. 97, and papers from meetings on these lenses have been published in *Applied Optics*.⁹⁸

Photochromic glasses that change their optical absorption when they are in

visible light are reviewed in Refs. 99 and 100. One example is a glass containing tiny silver chloride particles that are sensitive to light. Electrochromic glasses change their absorption in response to an electrical field;^{101,102} many are based on tungsten oxides.

The change in optical absorption or refractive index of a material with light intensity at high intensities is called nonlinear optical behavior. Such changes may lead to optical switches and other devices, and possibly to all-optical amplifiers, sensors, switches, rectifiers, and other circuits and devices. Certain components in a glass can give rise to enhanced optical nonlinearity; examples are small metallic and semiconductor particles, and heavy metal ions giving high refractive index in the glass, such as lead, bismuth, titanium, tantalum, tellurium and niobium. A review is given in Ref. 103.

REFERENCES

1. J. Fanderlik, *Optical Properties of Glass*, Elsevier, Amsterdam, 1983.
2. T. S. Izumitani, *Optical Glass*, Kyoritsu Shuppan, Tokyo, 1984; Translation American Institute of Physics, New York, 1986.
3. N. P. Bansal and R. H. Doremus, *Handbook of Glass Properties*, Academic Press, San Diego, 1985, p. 539.
4. O. V. Mazurin, M. V. Streltsina, and J. P. Shivaiko-Shaikovskaya, *Handbook of Glass Data*, Parts A, B, and C, Elsevier, Amsterdam, 1984–1987.
5. H. Scholze, *Glass*, Springer-Verlag, Berlin, 1991, p. 214ff.
6. D. R. Uhlmann and N. J. Kreidl, Eds., *Optical Properties of Glass*, American Ceramic Society, Westerville, OH, 1991.
7. W. Vogel, in D. R. Uhlmann and N. J. Kreidl, Eds., *Optical Properties of Glass*, American Ceramic Society, Westerville, OH, 1991, p. 1.
8. E. D. Palik, Ed., *Handbook of Optical Constants of Solids*, Vols. I and II, Academic Press, New York, 1985 and 1991.
9. H. R. Philipp, in E. D. Palik, Ed., *Handbook of Optical Constants of Solids*, Vol. I, Academic Press, New York, 1985, p. 749.
10. G. H. Sigel, in *Treatise on Materials Science and Technology*, Vol. 12, M. Tomozawa and R. H. Doremus, Eds., Academic Press, San Diego, CA, 1977, p. 5.
11. G. Hetherington, K. H. Jack, and M. W. Ramsay, *Phys. Chem. Glasses* 6, 6 (1965).
12. See also *Glass Science*, 1st edn., p. 320.
13. E. J. Friebele and D. L. Griscom, in *Treatise on Materials Science and Technology*, Vol. 17, M. Tomozawa and R. H. Doremus, Eds., Academic Press, San Diego, CA, 1979, p. 257.
14. E. J. Friebele, in D. R. Uhlmann and N. J. Kreidl, Eds., *Optical Properties of Glass*, American Ceramic Society, Westerville, OH, 1991.
15. D. L. Griscom, *J. Ceram. Soc. Jn.*, **99**, 923 (1991).
16. V. Garino-Canina, *C.R.*, **239**, 705 (1954).
17. R. V. Adams and R. W. Douglas, *J. Soc. Glass. Technol.*, **43**, 147 (1959).

18. J. Simon, in *Modern Aspects of the Vitreous State*, Vol. I, J. D. Mackenzie, Ed., Butterworths, London, 1960, p. 138.
19. J. Wong and C. A. Angell, *Glass Structure by Spectroscopy*, Marcel Dekker, New York, 1976.
20. R. J. Bell, P. Dean, and D. C. Hibbins-Butler, *J. Phys.*, **1**, 299 (1968); **3**, 2111 (1970); **4**, 1214 (1971).
21. A. Kats and J. M. Stevels, *Philips Res. Rep.*, **11**, 115 (1956).
22. E. Loh, *Solid State Commun.* **21**, 269 (1964).
23. H. R. Philipp, *Solid State Commun.*, **4**, 73 (1966); *J. Phys. Chem. Solids*, **32**, 1935 (1971).
- 23a. C. Tarrio and S. E. Schnatterly, *J. Opt. Soc. Am.*, **B10**, 952 (1993).
24. A. E. Ruffa, *Phys. Status Solidi*, **29**, 605 (1968).
25. M. H. Reilly, *J. Phys. Chem. Solids*, **31**, 1041 (1970).
26. A. J. Bennett and L. M. Roth, *J. Phys. Chem. Solids*, **32**, 1215 (1971).
27. E. P. O'Reilly and J. Robertson, *Phys. Rev.*, **B27**, 3780 (1983).
28. K. Huber, A. Stern, and E. D. Klinkenberg, *Phys. Status Solidi*, **136**, 211 (1986).
29. B. D. McSwain, N. F. Borrelli, and G. J. Su, *Phys. Chem. Glasses*, **4**, 1 (1963).
30. A. J. Cohen and H. L. Smith, *J. Phys. Chem. Solids I*, **301** (1958).
31. E. Kordes and E. Worster, *Glastech. Ber.*, **32**, 267 (1959).
32. E. R. Lippencott, A. V. Valkenburg, C. E. Weir, and E. R. Bunting, *J. Res. Natl. Bur. Stand.*, **61**, 61 (1958).
33. V. V. Obukhov-Denisov, N. N. Sobolev, and V. P. Chemisinov, *Opt. Spect. (USSR)*, **8**, 267 (1960).
34. M. K. Murthy and E. M. Kirby, *Phys. Chem. Glasses*, **5**, 144 (1964).
35. B. T. K. Chen and G. J. Su, *Phys. Chem. Glasses*, **12**, 33 (1971).
36. J. L. Parsons and M. E. Milberg, *J. Am. Ceram. Soc.*, **43**, 326 (1960).
37. N. F. Borrelli, B. D. McSwain, and G. J. Su, *Phys. Chem. Glasses*, **4**, 11 (1963).
38. E. N. Lotkova, V. V. Obukhov-Denisov, and N. N. Sobolev, *Opt. Spect. (USSR)*, **1**, 772 (1956).
39. J. Krogh-Moe, *Phys. Chem. Glasses*, **6**, 46 (1965); *J. Noncryst. Solids*, **1**, 269 (1969).
40. J. A. Siderov and N. N. Sobolev, *Opt. Spect. (USSR)*, **3**, 560 (1957).
41. J. Goubeau and K. Keller, *Z. Anorg. Chem.*, **272**, 303 (1953).
42. L. A. Kristionsen and J. Krogh-Moe, *Phys. Chem. Glasses*, **9**, 96 (1968).
43. P. E. Jellyman and J. P. Proctor, *J. Soc. Glass Technol.*, **39**, 173 (1955).
44. V. A. Florinskaya and R. S. Pechenkina, *The Structure of Glass*, Consultants Bureau, New York, 1958, p. 55; *J. Struct. Chem. USSR*, **4**, 850 (1963) (English translation).
45. G. J. Su, N. F. Borrelli, and A. R. Miller, *J. Phys. Chem. Glasses*, **3**, 167 (1962).
46. R. Hanna and G. J. Su, *J. Am. Ceram. Soc.*, **47**, 597 (1964).
47. D. Crozier and R. W. Douglas, *Phys. Chem. Glasses*, **6**, 240 (1965).
48. S. A. Brawer and W. B. White, *J. Chem. Phys.*, **63**, 2421 (1975).
49. G. Wilmot, Ph.D. Thesis, Massachusetts Institute of Technology, 1954.

50. W. Bagdage and R. Stolen, *J. Phys. Chem. Solids*, **29**, 2001 (1968).
51. T. Bates, in *Modern Aspects of the Vitreous State*, Vol. 2, J. D. Mackenzie, Ed., Butterworths, London, 1962, p. 195.
52. W. E. Weyl, *Colored Glasses*, Society of Glass Technology, Sheffield, England, 1959.
53. S. Kumar, *Cent. Glass Ceram. Res. Inst. Bull.*, **6**, 99 (1959).
54. K. Bingham and S. Parke, *Phys. Chem. Glasses*, **6**, 224 (1965).
55. S. Kumar and P. Nath, *Trans. Ind. Ceram. Soc.*, **25**, 12 (1966).
56. V. V. Vargeime and T. J. Weinberg, in *IVth Congres Int. Verre*, Imprimerie Chaix, 20, Rue Bergere, Paris, 1957, p. 197.
57. C. R. Kurkjian and E. A. Sigety, *Phys. Chem. Glasses*, **9**, 73 (1968).
58. R. W. Douglas, *10th Int. Congress on Glass*, The Ceramic Soc. of Japan, 1974, Vol. 1, p. 45.
59. M. A. Aglan and H. Moore, *Trans. Soc. Glass Technol.*, **39**, 351 (1955).
60. A. Paul and R. W. Douglas, *Phys. Chem. Glasses*, **8**, 151, 233 (1967).
61. W. H. Turner and J. A. Turner, *J. Am. Ceram. Soc.*, **55**, 201 (1972).
62. M. Yamaga, B. Henderson, K. P. O'Donnell and Y. Gao, *Phys. Rev.*, **B44**, 4853 (1991).
63. J. S. Stroud, *J. Chem. Phys.*, **35**, 844 (1961); **37**, 836 (1962).
64. V. I. Arbuzov and N. B. Belyankind, *Sov. J. Glass Phys. Chem.*, **16**, 327 (1990).
65. E. Antic-Fidancev, J. Holsä, M. Lemaitre-Blaise, and P. Porcher, *J. Phys., Condensed Matter*, **3**, 6829 (1991).
66. E. M. Larson, et al., *J. Noncryst. Solids*, **130**, 260 (1991).
67. B. C. Joshi, M. C. Joshi, and B. D. Joshi, *J. Phys. Chem. Solids*, **52**, 939 (1991).
68. E. L. Demskaya and S. S. Pivovarov, *Sov. J. Glass Phys. Chem.*, **16**, 327 (1990).
69. F. Rasheed, K. P. O'Donnell, B. Henderson and D. B. Hollis, *J. Phys., Condensed Matter*, **3**, 1915 (1991).
70. S. Todoroki, S. Tanabe, K. Hirao, and N. Soga, *J. Noncryst. Solids*, **136**, 213 (1991).
71. M. V. Ramana, P. S. Lakshmi, K. Sivakumar, S. G. Sathyanarayan, and G. S. Sastry, *Phys. Status Solidi*, **A126**, K181 (1991).
72. K. Tonooka, N. Kamata, K. Yamada, *J. Lumin.*, **50**, 139 (1991).
73. K. Hirao, S. Kishimoto, K. Tanaka, S. Tanabe, and N. Soga, *J. Noncryst. Solids*, **139**, 151 (1992).
74. M. A. Marcus and A. Polman, *J. Noncryst. Solids*, **136**, 260 (1991).
75. S. B. Stevens and H. J. Stapleton, *Phys. Rev.*, **B42**, 9794 (1990).
76. P. G. Taylor and Z. V. Vardeny, Eds., *J. Noncryst. Solids*, 141 (1992).
77. R. Zallen, *The Physics of Amorphous Solids*, Wiley, New York, 1983, p. 260ff.
78. N. F. Mott and E. A. Davis, *Electronic Processes in Noncrystalline Materials*, Clarendon Press, Oxford, 1970, p. 237ff.
79. J. Lucas and J.-L. Adams, in D. R. Uhlmann and N. J. Kreidl, Eds., *Optical Properties of Glass*, American Ceramic Society, Westerville, OH, 1991.

80. A. Abdel-Kader, A. A. Higazy, and M. M. Elkholy, *J. Mater. Sci. Mater. Electron.*, **2**, 204 (1991).
81. J. S. Muller, *J. Noncryst. Solids*, **134**, 147 (1991).
82. M. Faraday, *Philos. Mag.*, **14**, 401, 512 (1857).
83. S. D. Stookey, *J. Am. Ceram. Soc.*, **32**, 246 (1949).
84. R. H. Doremus, in *Nucleation and Crystallization in Glasses and Melts*, American Ceramic Society, Columbus, OH, 1967, p. 117.
85. G. Mie, *Am. Phys.*, **25**, 377 (1908).
86. R. H. Doremus, *J. Chem. Phys.*, **40**, 2389 (1964).
87. R. H. Doremus, *J. Chem. Phys.*, **41**, 414 (1965).
88. R. H. Doremus, S.-C. Kao, and R. Garcia, *Appl. Opt.*, **31**, 5773 (1992).
89. C. K. Kao, *Optical Fiber Systems*, McGraw-Hill, New York, 1982.
90. M. A. Newhouse, in D. R. Uhlmann and N. J. Kreidl, Eds., *Optical Properties of Glass*, American Ceramic Society, Westerville, OH, 1991, p. 185.
91. K. J. Beals and C. R. Day, *Phys. Chem. Glasses*, **21**, 5 (1980).
92. R. D. Maurer, *J. Noncryst. Solids*, **47**, 135 (1982).
- 92a. H. Kogelink, *Science*, **228**, 1043 (1985).
93. M. C. Page, R. Oven, and D. G. Ashworth, *Electron. Lett.*, **27**, 2073 (1991).
94. G. Lamouche and S. J. Najafi, *Opt. Eng.*, **30**, 1365 (1991).
95. T. Poszner, G. Schreitner, and R. Muller, *J. Appl. Phys.*, **70**, 1966 (1991).
96. M. J. Weber, *J. Noncryst. Solids*, **123**, 2098 (1990).
97. D. T. Moore, *Ceram. Bull.*, **68**, 1941 (1989).
98. *Applied Optics*, GRIN I (April 1, 1980), GRIN II (March 15, 1982), GRIN III (Feb. 1, 1983), GRIN IV (June 1, 1984), GRIN V (Dec. 15, 1985), GRIN VI (Oct. 1, 1986), GRIN VII (Feb. 1, 1988), GRIN VIII (June, 1990).
99. R. J. Araujo, in *Treatise on Materials Science and Technology*, Vol. 12, M. Tomozawa and R. H. Doremus, Eds., Academic Press, San Diego, CA, 1977, p. 91.
100. R. J. Araujo, in D. R. Uhlmann and N. J. Kreidl, Eds., *Optical Properties of Glass*, American Ceramic Society, Westerville, OH, 1991, p. 185.
101. F. G. K. Bauke and J. A. Duffly, *Chem. Br.*, **21**, 643 (1985).
102. R. B. Goldner et al., *SPIE*, **562**, 32 (1985).
103. N. F. Borrelli and D. W. Hall, in D. R. Uhlmann and N. J. Kreidl, Eds., *Optical Properties of Glass*, American Ceramics Society, Westerville, OH, 1991, p. 87.

AUTHOR INDEX

Index Terms

Links

In most cases only the first edition of an article in a particular chapter is included.

A

<i>Abde, Kader A.</i>	14	120		
<i>Abde, Latifa A. A.</i>	100	104		
<i>Abel, Y.</i>	263	207		
<i>Abercromb, P. P.</i>	233	239		
<i>Abuqawa, T. A.</i>	231	239		
<i>Abuqwa, P.</i>	183	196		
<i>Adam, G.</i>	110	112		
<i>Adam, I.</i>	29	41		
<i>Adams, P. B.</i>	193	197		
<i>Adams, P. V.</i>	198	212	108	11
<i>Adamsen, A.</i>	192	197		
<i>Adigetter, M. A.</i>	10	11		
<i>Agarwal, A.</i>	119	121		
<i>Agarwal, D.</i>	11	120		
<i>Agar, B.</i>	117	148		
<i>Aglio, M. A.</i>	1	19		
<i>Akiba, M. G.</i>	93	97		
<i>Akayemaya, H. T.</i>	109	197		
<i>Albano, P. V.</i>	110	109		
<i>Algra, A.</i>	26	4		
<i>Alexander, G. B.</i>	228	238		
<i>Aljor, F. S.</i>	11	23		

Index Terms

Links

Almeida, R M	40	47		
Alpert, D	126	147		
Alternose, V O	140	148		
Anderegg, F O	156	159		
Anderson, O L	145	149	284	289
Andreev, N S	119	121		
Angell, C A	15	16	23	40
	47	104	106	109
	111	112	285	289
	291	303	304	308
	311	312	318	
Antic-Fidancer, E	315	319		
Antonini, J R	185	193	196	
Appen, A A	297	304		
Araujo, R J	317	320		
Arbuzov, V I	313	315	319	
Arita, J H	85	96		
Armistead, C G	187	196		
Arnold, G W	231	239		
Asequawa, H	40	47		
Augis, J A	83	96		
Avrami, M	16	24	81	96
Awaza, K	202	213		

B

Babcock, C L	10	11	271	288
Babinec, A	222	238		
Babonneau, A F	47			
Bach, H	189	195	219	237

Index Terms**Links**

Bacon, F R	215	237		
Bagdage, W	311	319		
Bagley, B G	44	47		
Bain, D	208	214		
Bakardjico, J	222	238		
Balijustin, A A	247	261		
Banba, T	232	239		
Bansal, N	5	10	11	82
	83	84	94	95
	96	105	111	113
	120	130	148	217
	237	279	289	291
	303	306	317	
Barnes A C	26	44		
Barrer, R M	122	125	132	147
Barry, T J	86	88	89	96
Bartenev, G M	101	111		
Bartholomew, R F	200	212		
Barton, J L	140	148	202	213
	286	290		
Bastress, A W	203	213		
Bates, J K	230	231	239	
Bates, R G	253	261		
Bates, T	313	319		
Baucke, F G K	219	220	224	237
	238	246	257	261
	317	320		
Bauer, G H	39	47		
Beall, G H	68	72	74	75
	81	96		

Index Terms**Links**

Beals, K J	316	320		
Beauchamp, E K	125	147	227	239
Beckman, K H	201	212		
Begeal, D R	125	147		
Bell, R J	31	45	308	318
Bennett, A J	309	318		
Benneff J E	83	96		
Bergeron C G	19	24		
Bermudez, V M	187	195		
Bernal, J D	44	47		
Berry, J P	168	171		
Bestul, A B	55	71	113	120
Bever, M B	8	10	11	
Bhattacharya, G K	178	183		
Bilby, B A	159	170		
Bingham K	313	319		
Biscoe J	32	33	45	46
Blackburn, D H	54	71		
Blau H H	271	288		
Block	58	71		
Blodgetf, K B	203	213		
Bockris, J O	105	112		
Boehm, L	55	71		
Boekenhauer, R	208	214		
Bokov, N A	119	121		
Boksay, Z	217	225	228	233
	237	238	278	289
Bolchakov, O J	140	148		
Bondi, A	43	47	109	112
Borchardt, G	224	238		

Index Terms**Links**

Borisovski, E S	310	311	318	
Borom, M P	278	289		
Borreilli, N F	317	320		
Bottinga, Y	19	23		
Bottom, A E	256	261		
Boulon, G	29	45		
Bouquet, G	217	225	228	237
	538			
Bourcier, W L	231	239		
Boyce, R S	137	148		
Brace, W F	168	171		
Bradley, C R	230	239		
Bradley, J P	230	231	239	
Bradner, T	217	237		
Brady, G W	38	46		
Brady, P V	229	239		
Brandt, W W	147	149		
Brawer, S	29	45	110	112
	116	120	311	318
Bray, P J	37	45	46	285
	290			
Brehardt, G	189	196		
Brehler, B	41	47		
Brennet, P	229	239		
Bresker, R J	297	304		
Breton, J C	300	304		
Brinker, C J	10	11		
Briscoe, J	32	33	45	
Bristow, R H	271	288		
Brodsky M H	15	23		

Index Terms**Links**

Brosset, C	33	46		
Brown, D M	211	214		
Brown, R B	126	143	147	
Bruce, A J	83	84	94	96
Bruckner, R	33	46	199	212
Brund M J D	256	261		
Buchert, R C	39	47		
Buck, R P	256	261		
Bueche F	109	112		
Buff, H	3	11		
Bunker, B C	231	239		
Bunting, E R	310	318		
Bruggraaf, A J	282	289		
Burke, J E	175	183		
Burlitz, R S	126	147		
Burman, C	189	196	217	222
	224	237	238	240
Burn I	135	148		
Burnett, D G	53	54	70	89
	97			
Burt, R	135	148	263	287
Bury, K V	178	183		
Busby, R F	101	111		
Busse, L	119	121		

C

Cable, M	210	214		
Cahn, J W	67	68	72	91
	97			

Index Terms**Links**

Cameron, N M	150	169		
Capella, S	234	239		
Car, R	30	45		
Cargill, G S	44	47		
Cawley, J D	137	148		
Chandan, H C	176	183		
Chandra, D	208	214		
Chang, S S	113	120		
Chao, T S	189	197		
Chapman, J D	33	49	54	71
	191	197		
Charles, R J	53	59	67	68
	71	72	176	180
	183	275	288	295
	304			
Chaudhari, P	32	46		
Chaudhri, M M	159	170		
Chemisinov, V P	310	318		
Chemla, M	270	288		
Chen, B T K	310	318		
Chenylkh, V J	286	290		
Chieux, P	26	44		
Chlebik, A	199	212		
Christ, C L	249	261		
Christensen, P	237	239		
Christian, J W	56	61	71	84
	96			
Chuang, T	181	183		
Chung, K -H	55	71	237	239
Clare, A C	37	46		

Index Terms**Links**

Clark, D E	22	228	238	
Clarke, A R	210	214		
Clemens, K	70	72		
Clinton, D	86	97		
Coenen, M	114	120	293	304
Cohen, A J	310	318		
Cohen, M H	15	20	23	24
	109	112		
Collins J A	29	45		
Colmenero, J	26	44		
Congleton, J	168	171		
Conti, F	256	261		
Cook, R L	109	112		
Cooper, A E	8	11		
Cooper A R	8			
Copley, G J	300	304		
Cordaro J F	285	289		
Cormia, R L	19	23	92	97
	103	111		
Cornelissen, J	282	289		
Cotton, F A	229	239		
Cottrell, A H	56	71		
Covington, A K	256	261		
Coyne D C	177	183		
Cramer, D	17	24		
Crank, J	130	148	267	288
Cranmer, D	82	96		
Crichton, S N	119	120		
Crozier, D	311	318		
Curtis, H L	194	197		

Index Terms

Links

Cushman, K	173	183
Cusumano, J A	191	197
Czandema, W A	189	196

D

Dalton, R N	77	96		
D'Angelo, K	22	238		
Datta, R K	14	23		
Davidge, R W	165	171		
Davies, L B	44	47		
Davis, E A	26	44	314	319
Davis, K	217	237		
Davydov, V Y	185	196		
Day, D E	229	239	279	289
	300	301	304	
Deal, B E	144	149		
Dean, P	31	45	308	318
DeBast, J	118	120		
DeBilly, M	264	287		
DeBolt, M A	119	120		
Deeg E	301	304		
Dejong B H W S	29	45		
Delaney, J R	231	239		
Della Mea, G	224	238		
DeLuca, J P	19	24		
Denskaya, E L	315	319		
Denney, D J	20	24		
DeNordwall, H J	14	23		
DeRiu, L	189	196		

Index Terms**Links**

Dev1 A	193	197		
DeWaal, H	300	304		
DeWet W J	246	261		
Dezsi, J	29	45		
Dick, E	163	170		
Dilmore, M F	222	238		
DiMarcello, F V	150	169		
Dobos, S	217	224	237	238
Dole, M	256	257	261	
Domenici, M	34	46		
Donovan, E P	113	120		
Doody, M	222	238		
Doolittle, A K	109	112		
Douglas, R W	10	11	53	54
	67	70	71	72
	89	97	103	111
	198	204	209	211
	212	213	214	216
	227	229	237	238
	274	288	295	298
	304	308	311	313
	317	318	319	
	10	11	205	213
Douglas, R W	10	11	205	213
Dran J -C	224	238		
Draper, N R	179	183		
Drexhage, M G	14	23	70	72
	94	97	106	112
Drury T	135	148	198	212
Duffy J A	14	23		
Duke, P J	298	304		

Index Terms

Links

Dulaney, E N	168	171		
Dumbgen, G	137	148		
Dunken H H	184	195	196	215
	216	234	237	239
Dupree, R	29	45		
Duwez, P	15	23	44	47
Dyre, J C	291	303	304	

E

Eagan R J	19	24		
Eastal, A J	113	119	120	
Ebbsjo, I	30	45		
Ebstrop'ev, K K	264	279	287	289
Eckersley, M C	26	44		
Eckert, C A	182	183		
Ehrmann, P	264	287		
Eisenberg, A	39	47		
Eisenman, G	243	244	246	247
	249	250	260	282
	289			
el-Bayoum1, O H	55	71		
Elliott, S R	10	11	25	26
	29	39	44	45
	47	285	290	291
	303	304		
Ellis, R C	14	22		
Elmer, T H	70	72	191	197
	228	238		
El-Shamy, T M	227	229	238	

Index Terms

Links

Endo, H	15	23		
Endo, T	14	22		
Engel, J R	270	288		
Equchi, K	70	72		
Erdogan, F	168	171		
Ernsberger, F M	156	158	159	163
	169	170	184	195
	200	212	232	239
	265	282	287	289
Eschbach, H L	140	148		
Ethridge, E C	222	238		
Evans, D L	31	45		
Ewell, R	109	112		
Eyring, H	106	109	112	

F

Faile, S P	14	23	201	212
Fanderlik, J	306	317		
Faraday, M	3	11	194	197
	314	320		
Farman, J	29	45		
Farnum, E G	267	288		
Farooqui, K	208	214		
Fedlman, C	15	23		
Feller, S	208	214		
Ferguson, C	122	147		
Ferrier, R P	15	23		
Ferris, K F	189	197		
Ferry, J D	109	100	111	112

Index Terms**Links**

Feuston, B P	30	45		
Field, J E	159	170		
Filbert, A M	215	237		
Fincham, C J B	208	214		
Findakly, T	283	289		
Finn, A N	22	238		
Finney, J L	44	47		
Finnie, I	150	169		
Firth, E M	210	214		
Fitzgerald, J V	298	304		
Flemming, B A	228	238		
Fletcher, J P	35	46		
Fliegel, W	245	261		
Flinn, O R	245	261		
Flood, E A	191	197		
Florinskaya, V A	311	318		
Folman, M	193	197		
Fontana, E J	19	23	102	111
Fonteneau, G	237	239		
Forry, K E	301	304		
Fowler, R H	126	147		
Frank, F C	66	71	159	170
Frank, R C	123	147		
Frank, S	10	24		
Franz, H	199	212		
Frechette, V D	157	169		
Freed, R L	4	47		
Freiman, S W	158	169		
Frenkel, D	90	97		
Frenkel, J	127	147		

Index Terms

Links

Frerichs, R	14	22		
Friebele, E J	308	317		
Friedman, G S	173	183		
Frischat, H	143	149	189	196
	224	238	267	273
	276	282	283	288
	289			
Frohnsdorff, G J C	191	197		
Fry, D L	126	147		
Fuhs, W	39	47		
Fukumi, K	38	46		
Fulcher, G S	109	112		
Fuller, E R	181	183		
Fulrath, R M	128	147	149	

G

Gaffney, R F	142	149	210	214
Gagliardi, G	189	195		
Galeener, F L	25	38	44	46
Gan Fuxi	14	23		
Garcia, R	95	98	189	195
Garfunkel, H M	245	250	258	261
	281	282	289	
Garino-Canina, V	198	212	308	317
Garofalini, S H	30	45		
Garrels, R M	249	261		
Gaskell, P H	26	28	29	31
	34	44	45	189
	195			

Index Terms**Links**

Gauthier, F R	102	111	164	170
Geddes, S	194	197		
Gee, G	39	47	106	112
Geotti-Bianchini, F	189	195		
Gerber, T	34	46		
Gerth, K	55	71		
Ghezze, M	274	288		
Ghose, A C	120	144		
Gibbs, J W	61	71	110	112
Gieskes, J M	228	238		
Gilard, P	118	120		
Giler, G H	90	93	97	
Gilman, J J	162	165	170	182
	183	184	195	
Gladden, L F	26	45		
Glasser, F P	52	70		
Gobin, P	300	304		
Goldbeck-Wood, G	93	97		
Goldner, R B	317	320		
Goldschmidt, V M	30	45		
Goldstein, M	110	112	276	288
Golub, H R	48	70	167	171
Golubhov, V V	53	70		
Gonser, Y	29	45		
Gonzalez-Oliver, C J R	77	96		
Gottardi, V	215	237		
Gotz, J	199	212		
Goubeau, J	36	46	311	318
Gough, E	264	287	295	304
Graczyk, J F	32	46		

Index Terms

Links

Graham, W A G	43	47		
Granick, S	109	112		
Gravina, S J	37	46		
Greaves, G N	28	29	35	45
	285	290		
Green, R L	202	213	296	304
Greene, C H	142	143	149	210
	212	214		
Greenberg, S A	228	238		
Greenwood, G W	66	72		
Greer, A L	81	195		
Greet, R J	19	24		
Grest, G S	109	112		
Griffith, A A	3	11	155	169
Grimley, D J	25	44	46	
Griscom, D L	308	317		
Groleau, R	217	237		
Grosskopf, K	189	196		
Gruer, R M	158	169		
Grundy, P J	44	47		
Guggenheim, E A	126	147		
Guglielmi, M	189	196		
Gupta, P K	70	72		

H

Hagel, W C	137	148	264	287
Hagen, J T	159	166	170	171

Index Terms**Links**

Hair, M L	33	46	54	71
	185	187	193	196
	197	215	237	
Hakim, R M	278	288	295	304
Hallbrucker, A	15	23		
Haller, W	54	68	71	72
Halloran, J W	137	148		
Hamann, S D	276	288		
Hambleton, F H	187	193	195	197
Hamilton, E H	222	238		
Hammel, J J	48	63	70	71
Hammetter, W F	86	97		
Han, C J	137	148		
Han, W T	158	169	181	183
Handwerker, C A	82	96		
Hanna, R	311	318		
Hansen, J -P	120	121		
Hansen, K W	301	305		
Harding, F L	211	212	214	
Haroon, M A	210	214		
Harrick, N J	201	212		
Harrington, R V	2	4	11	
Hartman, J S	35	46		
Hartwig C M	129	148		
Harvey, K B	238			
Hass, M	31	45		
Haul, R	137	148		
Hauser, C A	232	239		
Haymet, A D	90	97		
Hayward, P J	279	289		

Index Terms**Links**

Heacley, G L	231	239		
Heaton, L	39	47		
Heckman, R W	202	213		
Heinmann, J	270	288		
Helfferich, F	232	239	241	244
	260	280	289	
Helmreich, D	222	238		
Helms, C T	137	148	149	
Hench, L L	219	222	237	238
Hendrickson, J R	285	290		
Hennig, H P	189	196		
Henninger, E H	39	47		
Herbst C A	109	112		
Herd, L R	32	46		
Herman, H	68	72		
Heroux, L	295	304		
Herrell, D J	15	23		
Hertl	187	193	196	197
Hertz, H	159	170		
Hesse, W	109	112		
Heston, W M	228	238		
Hetherington, G	33	46	102	103
	111	198	199	201
	212	282	289	307
	317			
Heurer, A H	89	97		
Heyes, D M	101	111		
Heynes, M S R	105	112		
Hibbins-Butler, D C	308	318		

Index Terms**Links**

Hiemeng, P C	15	23	43	47
	192	197		
Hill, C F	41	47		
Hillig, W B	87	91	93	97
	156	169	175	180
	183			
Hilsch, R	15	23		
Himmel, B	34	46		
Hirao, K	315	319		
Hishinuma, A	82	96		
Hobson, J P	192	197		
Hochstrasser, G	185	193	195	
Hockey, J A	187	193	196	197
Hodkin, F W	210	214		
Hofmaier, G	102	111		
Hogfeldt, E	244	260		
Hollabaugh C M	282	289		
Holland, D	29	45		
Holland, L	184	195		
Holloway, J R	231	239		
Homeny, J	42	47		
Hood, H P	48	70		
Hopkins, J L	298	304		
Horisaka, T	40	47		
Hotta, H	162	170		
Houde-Walter, S N	252	262	283	289
Hubbard, D	194	197	222	238
Huber, K	309	318		
Hughes, K	264	287		
Hulme, R A	25	44		

Index Terms**Links**

Hunt, J D	91	97		
Hunter, C C	283	289		
Husung, R D	222	238		
Hutchins J R	2	4	11	
Hwa, L G	119	121		
Hyde, J M	52	70		
Hyde, J M	285	290	303	305

I

Ihm, S K	18	24		
Iler, R K	228	238		
Imaoka, M	163	170		
Inglis, C E	160	170		
Ingram, M D	14	23	265	283
	285	288	290	291
	304			
Inoue, H	40	47		
Irene, E A	144	149		
Irmann, F	204	213		
Irwin, G R	165	170		
Isard, J O	209	214	264	287
	295	296	304	
Izumitani, T S	10	11	19	195
	197			

J

Jack, J H	33	46	102	111
	199	201	212	282
	289	307	317	

Index Terms**Links**

Jackson, K A	90	91	97	
Jagdt, R	301	304		
Jakus, K	176	177	183	
James, P F	53	70	77	79
	81	96		
Jantzen, C M	235	239		
Jarcho, M	150	169		
Jeanloz, R	26	28	44	
Jelli, A	229	239		
Jellyman, P E	311	318		
Jenckel, E	300	304		
Jewell, J M	200	212		
Jiang, J	29	45		
Johansson, G	256	261		
Johari, G P	15	23		
Johnson, J	135	148		
Johnson, J E	175	183		
Johnson, J R	271	277	288	
Johnson, P A V	37	46		
Johnson, R A	178	183		
Johnson, W C	158	169	181	183
Johnston, J W	150	169		
Johnston, W D	204	213		
Jones, G O	1	11		
Jonscher, A K	291	303		
Jorgensen, P J	126	147		
Joshi, B C	315	319		

Index Terms**Links****K**

Kadone, K	29	45		
Kageyama, H	29	45		
Kalia, R K	30	45		
Kalish, K	176	183		
Kambeyanda, S	208	214		
Kamijo, N	29	45		
Kao, C K	316	320		
Kao, S -C	144	149		
Kaps, C	245	261		
Karreman, G	256	261		
Karsch, K H	300	304		
Karsten, J L	231	239		
Kaschiev, D	66	71		
Kats, A	136	148		
Kauzmann, W	113	115	120	
Kawamoto, Y	40	47	52	70
	72			
Kawazoe H	202	213		
Keaton, S C	133	148		
Keller, A	89	93	97	
Keller, H	36	46		
Keller K	311	318		
Kelton, K F	81	96		
Kemmechi, K	189	197		
Kennan, A G	246	261		
Kennedy, J C	102	111		
Kennedy, J H	14	23		
Kepak, F	194	197		
Kerkhof, F	159	168	170	171
Keshizaki, N	189	196		

Index Terms**Links**

Khar'yuzov, V A	264	287		
Kieth, H D	89	97		
Kim, C	265	288	293	304
King, C B	282	289		
King, H E	109	112		
King, S V	31	45		
Kinton, G L	191	197		
Kirby, E M	310	318		
Kirby, P L	300	304		
Kirkpatrick, R J	35	46		
Kirschner, H P	158	169		
Kiselev A V	185	196		
Kissenger, H E	83	96		
Kitano, J	143	149	210	214
Kitchener, J A	105	112		
Klein, L C	82	96		
Knight, C G	159	170		
Ko, S -H	40	41	47	95
	98	189	196	
Kogelink, H	316	320		
Kohli, J T	125	147		
Kohnstam, G	182	183		
Koike, Y	14	22		
Kolbeck, A G	114	120		
Komatsu, T	14	23		
Kordes, E	310	318		
Koritaka, S.	208	214		
Kornfeld, G	244	250	260	
Kotama, M	265	287		
Kouznetzov, A Ya	194	197		

Index Terms

Links

Kozuka, H K	38	46		
Krause, J T	150	162	170	176
	183	301	304	
Kreidl, N	50	70		
Kriedl, N J	10	12	308	317
Kristionsen, L A	311	318		
Kritz, H M	29	37	45	46
Kroger, C	208	213		
Krogh-Moe, J	36	46		
Krogh-Moe J	36	46	85	97
	310	311	318	
Krutter, K	30	45		
Kugler, G C	256	261		
Kuhl, C	210	214		
Kumar, S.	313	319		
Kurkjian, C R	29	45	103	111
	117	120	150	169
	176	180	183	298
	301	304	313	319
Kushiro, J	105	111		

L

Laberge, N	109	112		
Laborde, P	265	288		
Lacharme, J P	279	289		
LaCourse, W C	157	169		
Ladik, J	162	170		
Laird, J A	19	24		
Laitinen, H A	270	288		

Index Terms**Links**

Lamarche, P	217	237		
Lamouche G	316	320		
Lamparter, P	189	196		
Landel, R F	109	112		
Lanford, W A	189	196	216	217
	220	222	224	238
	240			
Langer, J S	90	97		
Lapham, K E	231	239		
Larsen, E M	315	319		
Laska, H M	126	147		
Laughlin, W T	106	112		
Laursen T	217	237		
Lawn, B R	159	166	170	171
Laws, F A	292	304		
Lay, L A	86	97		
Leadbetter, A J	31	38	41	45
	46	47		
Leblond, M	286	290		
Lee, C L	189	197		
Lee, H A	210	214		
Lee, R W	123	124	126	147
	201	212		
Lee, T F	189	197		
Lee, W E	89	97		
Leeds, R E	202	213		
LeGuillou, J C	60	71		
Lengyel, B	278	289		
Leontewa, A	19	23		
Levengood, W C	158	169		

Index Terms**Links**

Levin, E M	51	58	70	71
Levy, M	60	71		
Lewchuk, R R	48	70		
Lewins, J	227	229	238	
Lewis, G G	14	23		
L ₁ G H	101	111		
L ₁ , P	114	120		
Liebau, F	33	46		
Lifshitz, E M	66	72		
Lillie, H R	164	170		
Lin, X	29	45		
Ling, A C	106	112		
Lippencott, E R	310	318		
Little, L H	185	196		
Lockyer, M W G	29	45		
Loehman, R E	86	97	213	
Loehr, S J	237	239		
Loh, E	308	318		
Lommen, M G W	219	237		
Lotkova, E N	310	318		
Louer, D	40	47		
Low, M J D	190	191	197	
Lucas J	29	40	45	47
	237	239	3	14
	319			
Lummenheim, D	208	213		
Lumsden, J	64	71		
Lundberg, M H	85	97		
Lupis, C H P	204	213	249	261
Lyklema J	258	259	262	

Index Terms

Links

Lyle, A K	211	214
Lyng, S	85	97

M

MacCrone, R K	68	72		
MacDowell, J F	68	92		
Macedo, P B	54	71	103	109
	111	112	114	120
Macfarlane, D R	84	96		
Mackenzie, J D	10	11	12	19
	23	40	47	92
	97	103	105	106
	111	112	137	148
	163	170	264	287
Mader, S R	15	23	44	47
Magill, J D	19	24		
Magonthier, M C	224	238		
Maiden, A	19	24		
Major, L D	137	148		
Mandelkern, L	93	97		
Mando, P A	224	238		
Mansingh, A	296	304		
March, P	189	196		
Marcus, M A	315	319		
Margraf, T	95	98	189	196
Markali, J	85	97		
Markworth, A J	228	238		
Marsh D M	164	170		
Marshall, E	236	239		

Index Terms**Links**

Martin, S W	25	44	104	111
	265	285	288	289
Marx, J W	297	304		
Masaryk, J S	129	148	149	
Matecki, M	84	96		
Materova, E A	246	261		
Matthewson, M J	176	180	183	
Matusita, K	80	83	96	
Matzke, H	135	148		
Maurer, R D	74	77	86	96
	97	140	149	151
	169	316	320	
Mayer, E	15	23		
Mazer, J J	230	239		
Mazurin, O V	10	11	50	53
	70	278	279	289
	298	304		
McCoy, M	89	97		
McCurrie, R A	67	72		
McDonald, R S	185	191	196	197
McGahay, V	59	71		
McMillan, P W	53	54	70	74
	96	199	212	
McMurdie, H F	51	70		
McSwain, B D	310	318		
McTague, J P	90	97		
McVay, G L	267	279	288	289
Means, J L	228	238		
Mecholsky, J J	158	169		
Mehrotra, Y	189	196	217	237

Index Terms**Links**

Meier Zu Kocker, H	208	214		
Meiling, G S	19	24	105	111
Mercer, R A	86	97		
Merzbacher, C J	35	46		
Messier, D R	213			
Meyer, H	39	46		
Michal, E J	204	213		
Micus, G	19	24		
Mieller, E	189	196		
Mikesell, S L	9			
Mikkelson, J C	137	138	148	
Milberg	33	34	46	310
	318			
Miller, A. A	106	112		
Miller, P D	232	239		
Miller, R A	301	305	311	318
Miller, R P	86	97		
Milnes, G C	264	287		
Mitchell, S A	187	196		
Miyaji, F	38	46		
Moak, D	232	239		
Mohr, R K	101	111		
Mohyddin, J	298	304		
Moiseev, V V	245	261		
Montez, B	35	46		
Montrose, L J	101	111		
Moore, D T	252	262	316	320
Moore, H	313	319		
Moorjamı, K	15	23		
Moran, M	140	148	202	213

Index Terms**Links**

Morelock, C R	93	97		
Morey, G W	2	11	100	111
	215	237	263	287
Morgan, A M	191	197		
Moriya, Y	53	71		
Morningstar, O	30	45		
Morrow, B A	193	197		
Mortuza, M G	29	45		
Mott, N F	168	171	314	319
Mould, R E	153	156	169	174
	183			
Moulson, A	198	212		
Moulson, J	135	148	230	239
Moynihan, C T	55	71	94	97
	113	119	120	121
	237	239	302	305
Mozzi, R L	28	30	36	45
	46			
Mukherjee, S P	85	87		
Muller, J S	314	320		
Muller, R L	285	289		
Mullı, R	252	262		
Murahamı, T	224	232	239	
Murphy, D	217	237	240	
Murthy M K	310	318		
Myhra, S	189	196		
Mysen, B O	46			

Index Terms**Links****N**

Nakajuma, H	68	72		
Nakayama G S	125	147		
Nakayama, J	165	171		
Napolitano, A	54	71	103	111
Narayanaswamy, O S	118	120		
Nardy-Szabo, J	162	170		
Nath, P	313	319		
Naudin, F	66	68	72	
Navias, L	296	304		
Neely, J E	163	170		
Neilson, G F	68	72	81	96
Nelson, G G	42	47		
Nemer, L N	143	149		
Neumann, K	19	24		
Newhouse, M A	316	320		
Ngai, K L	116	120	298	303
	304	305		
Nicolsky, B P	246	250	261	
Niekerk, M	246	261		
Niklasson, G A	303	305		
Nofz, M	29	34	45	46
Nordberg, M E	48	70	191	197
	228	238		
North, P	204	213		
Norton, F J	125	137	138	139
	147	148	203	213
Notz, N	256	261		
Nowich, A S	15	23	44	47

Index Terms

Links

O

Oakley, D R	300	304		
Obukhov-Denisov, V V	310	318		
O'Connor, T L	228	238		
Oel, H J	143	149	158	169
	264	287		
Ohlberg, S M	33	46	48	70
	167	171		
Ohta, H	229	239		
O'Keefe, J G	29	37	46	49
Ordway, F	31	45		
O'Reilly, E P	309	318		
Osteryoung, J G	271	288		
Osteryoung, R A	270	288		
Otto, W H	156	169		
Owen, A E	263	264	274	287
	288	291	295	303
	304			
Owen, G D T	39	47		
Oxtoby, D W	90	97		

P

Paccagnella, A	224	238		
Padden, F J	89	97		
Page, N C	316	320		
Palik, E D	306	317		
Panhorst, W	87	97		
Papanikolaou, E	286	290		

Index Terms**Links**

Park, M J	29	37	45	46
Parke, S	313	319		
Parker, J M	26	44		
Parkıale, V E	29	45		
Parks, G A	103	111		
Parks, G S	115	120		
Parrinello, M	30	45		
Parsons, J L	167	171	310	318
Parsons, J M	33	46		
Pask, J A	19	24		
Patano, C G	189	196		
Paul, A	204	205	213	229
	235	239	313	319
Pavelchek, E K	153	155	169	170
	173	180	183	
Pearce, M L	208	213	214	
Pechenkina, R S	311	318		
Pederson, L R	189	197		
Peglar, R J	193	197		
Perera, G	216	218	228	237
	238			
Peri, J B	192	197		
Perkins, W G	123	147		
Petch, N J	168	171		
Peter, K W	159	163	170	
Peters, C R	33	34	46	
Peterson, G L	37	46		
Pethica, B A	187	196		
Petit, J -C	224	238		
Pettifer, R F	29	45		

Index Terms**Links**

Philipp, H R	307	308	318	319
Phillips, J C	31	45		
Pietroneco, L	265	288		
Pike, R G	194	197		
Pincus, A G	58	71		
Platts, D R	212	214		
Plazek, D J	19	24		
Plesset, M S	232	239	280	289
Plodinec, M J	235	239		
Plumat, E	55	71		
Plummer, W A	19	23	102	111
Polk, D E	44	47		
Ponçon, V	29	45		
Porai-Koshits, E A	31	45	48	53
	70			
Portier, J	14	23		
Poszner, T	252	262	316	320
Poulain, M	22	24	84	96
Powell, R E	106	112		
Pozza, F	34	46		
Pradel, A	285	290		
Preston, E	208	213		
Prince, D L	25	44		
Prins J A	2	11		
Priqueler, M	198	212		
Prochazka, S	41	47		
Proctor, B A	150	156	169	175
	183			
Proctor, J P	311	318		
Purdy, G R	85	96		

Index Terms

Links

R

Rajaram, M	213			
Ramana, M V	315	319		
Ramasubramanin, N	190	197		
Ramaswamy, R V	283	289		
Ramsay, M W	282	289	307	317
Rana, M A	217	237		
Randall, J R	202	213		
Raoux, D	28	45		
Rasheed, F	315	319		
Rauch, F	189	196		
Ravaine, D	285	289		
Rawson, H	14	22	58	71
Ray, C S	83	96		
Reau, J -M	14	23		
Rechnitz, G A	256	261		
Reilly, M G	309	318		
Rekhson, S M	101	111	119	120
	121			
Renlund, G M	41	42	43	47
Reugh, J D	115	120		
Reyes, J M	296	304		
Rice, R W	158	169		
Richardson	208	214		
Richet, P	19	23		
Richter, H	168	171		
Richter, T	189	196	244	238
Richter-Mendou, J	189	196		
Rigo, S	137	148	149	

Index Terms**Links**

Rindone, G E	77	96	300	304
Rino, J P	30	45		
Risbud, S. H	35	42	46	47
Ritter, J E	176	177	183	
Riviere, J C	189	196		
Robbins, C R	51	70		
Roberts, G J	135	148	198	212
Roberts J P	135	148	198	199
	212	230	239	
Robinson, M	94	97		
Robinson, P L	14	23		
Rochet, R	137	148	149	
Roesler, F C	159	169		
Rogers, P S	85	96	97	
Rogers, W A	126	131	147	
Rogogine, J V	229	238		
Rotger, H	298	304		
Roth, L M	309	318		
Rothman, S J	276	288		
Rothmund, V	244	250	260	
Rowell, M H	245	261		
Roy, D M	14	23	201	212
Roy, R	22	24	52	70
Ruckenstein E	18	24		
Rudow, H	210	214		
Ruffa, A E	309	318		
Russel, C	270	288		
Ryder, R J	8	212	214	300
	305			

Index Terms

Links

S

Sadler, D M	93	97		
Sager, M	296	304		
Sakaguchi, F	40	47		
Sakaino, T	53	71		
Sakka, S	10	11	38	46
	162	170		
Saloma, R	82	96		
Salomau, R	17	24		
Salsbury, R L	150	169		
Sandhage, K H	8	11		
Sano, N	208	213		
Sarjeant, P T	22	24		
Sarkar, A	53	71		
Sato, T	14	22		
Sawai, I	85	96		
Sayre, E J	14	23		
Schaeffer, H A	264	287		
Scherer, G	10	11	70	72
	100	115	116	118
	120			
Scherrer, S	189	196	224	238
Schiffner, V	87	97		
Schiller, H	286	290		
Schnatter, K H	189	196	219	238
Schnatterly, S E	308	318		
Schnaus, V E	113	120		

Index Terms**Links**

Scholze, H	10	11	198	199
	200	212	217	222
	237	238	297	304
	307	317		
Schonhorn, H	150	169		
Schramm, C M	29	45		
Schreiter, G	252	262		
Schrieber, H D	205	213		
Schroeder J	119	121		
Schuhmann, R	204	213		
Schultz, M M	246	261		
Schulze, F	3	11		
Schulze, G	242	266		
Schwabe, K	256	261		
Schwartz, M	264	287		
Scott, W D	19	24		
Scott, W E	14	29		
Sears, G W	91	93	97	
Sedden, E	271	288		
Service, T E	176	183		
Seward, T P	68	72		
Sewell, P A	191	197		
Shackelford, J F	123	128	129	147
Shand, E B	158	169		
Shardin H	168	171		
Sharma, S K	105	111		
Shartsis, L	55	71	184	196
Shaw, R R	53	70		

Index Terms**Links**

Shelby, J E	122	123	125	126
	129	133	135	139
	147	148	200	212
	301	304		
Shermer, H F	55	71		
Sherriff, B L	35	46		
Shess, M S.	200	212		
Shimada, M	14	22		
Shore, A C	19	24		
Shultz, G	266	288		
Shute, C J	176	183		
Shvaiko-Shvaikovskaya, T P	10	11	105	111
	130	148		
Siderov, J A	310	318		
Sigel, G H	307	309	317	
Sigety, E A	313	319		
Sih, G S	168	171		
Simmons, C J	237	239		
Simmons, J H	53	54	70	71
	74	81	91	96
	97	101	111	237
	239			
Simon, J	308	317		
Sinclair, R N	25	37	44	46
Sitter, H	237	239		
Sivertsen, J M	297	304		
Skinner, S	184	196		
Slavyanskii, V T	210	214		
Slyozov, V V	66	72		
Smekal, A	159	170		

Index Terms**Links**

Smets, B M J	219	224	237	238
Smith, G L	94	98		
Smith, H	179	183		
Smith, H L	310	318		
Sommer, E	158	169		
Sotter, W A	158	169		
Soules, T F	27	29	30	44
	45	101	111	
Souquet, J L	265	283	288	
Southwick, R D	156	169	174	183
Sovolev, N N	310	311	318	
Spaght, M E	103	111		
Sperry, L L	167	171		
Spinosa, E D	228	238		
Srinivasan, G	54	71		
Stanworth, J E	21	24		
Stavely L A K	14	23		
Steinberg, U	29	45		
Steinike, Y	189	196		
Steinkamp, W E	300	304		
Stephenson, G B	68	72		
Stern, K	245	246	261	
Stevels, J M	265	287	291	295
	303	304	308	318
Stevens, S B	315	319		
Stevenson, C M	230	239		
Stewart, A M	189	196		
Stillinger, F	115	120		
Stock, A		14	22	
Stolen, R H	311	319		

Index Terms**Links**

Stone, F G A	43	47		
Stoneham, A M	144	149		
Stookey, S D	74	77	96	200
	212	314	320	
Stosser, R	29	45		
Streltsina, M V	10	11	54	71
	105	111	130	148
Strnad, Z	208	213		
Stroud, J S	77	96	315	319
Stuart, D A	145	149	284	289
Stub, S	189	196		
Studt, P L	128	147		
Su, G J	19	24	114	120
	310	311	318	
Subramanian, R S.	144	149		
Sucov, E W	137	148		
Sugarman, B	169			
Summer, D J	37	46		
Sun, H W	14	23		
Sun, K H	21	23	24	
Suscavage, M J	55	71		
Suschke, H D	256	261		
Suzuki, J	163	170		
Suzuki, Y	229	239		
Swain, M V	159	170	171	
Swain, R A	204	213		
Swartz, E L	212	214		
Swets, D E	123	147		
Swift, H R	88	97		
Symmers, C	169			

Index Terms**Links****T**

Tadros, J F	258	259	262	
Tagliavore, A P	35	46		
Takahasi T	270	288		
Takamori, T	69	72		
Takayangi, M	19	24		
Tallant, D R	231	239		
Tammann, G	3	11	14	22
	109	112		
Tanaka, H	29	45	70	72
Tanguy, B	14	23		
Tappin, G	165	171		
Tarrant, J D	31	45		
Tarrio, C	308	318		
Taylor, E W	163	170		
Taylor, H E	291	303		
Taylor, N W	182	183		
Taylor, P G	314	319		
Tegetmeier, F	3	11		
Testardi, L R	162	170		
Thiel, K	14	23		
Tholen, M G W	224	238		
Thomas, M B	150	169		
Thomas, W F	153	156	169	
Thurston, R N	162	170		
Tippet, E J	271	288		
Titov, A P	53	70		
Tobolsky, A V	39	47		
Tochon, J	282	289		

Index Terms**Links**

Todoroki, S	315	319		
Tolmacheva, T A	246	261		
Tomlinson, J W	105	112		
Tomozawa, M	10	12	50	52
	59	68	69	70
	71	72	158	169
	181	183	200	212
	234	239	265	270
	285	288	289	290
	291	293	303	304
	305			
Tong, H C	182	183		
Tonooka, K	315	319		
Topping, J A	264	287	296	304
Torza, S	150	169		
Totesch, A S	54	71		
Tran, D C	113	120		
Trnovcova, V	264	287		
Tronev, L	283	289		
Tsong, J S T	232	239		
Tsuei, C C	15	23		
Tsukihashi, F	208	213		
Tucker, J	119	120		
Tuller, H L	265	283	288	
Turkalo, A M	32	46	48	70
	78	96	175	183
Turkdogan, E T	208	214		

Index Terms

Links

Turnbull, D	15	16	19	20
	23	24	44	47
	61	68	71	72
	92	93	97	109
	112			
Turner, G L	231	239		
Turner, J A	313	319		
Turner, N H	313	319		
Turner, W E S	48	70	208	210
	213	214	271	288
Turner, W H	313	319		
Tuttle, O F	14	23		
Tweer, H	54	71	109	112
Tyler, A J	187	196		

U

Uhlmann, D R	10	12	16	17
	18	19	22	23
	24	53	68	70
	72	75	81	82
	91	94	97	101
	104	105	106	111
	112	114	120	278
	288	295	304	306
	308	317		
Underwood, S M	71	97		
Ur, H	14	23		
Urbain, G	19	23	102	111
Umes, S	33	46		

Index Terms

Links

V

Valkenburg, A V	310	318		
Van Amerongen, C	295	304		
Van Caugh, L	147	149		
Vander Sande, J B	44	47		
Van Hook, A	19	24		
Van Megan, W	93	97		
Van Ommen,	274	276	288	
Van Reenan, T J	246	261		
Vardar, O	150	169		
Vargeime, V V	313	319		
Varner, J R	158	169		
Vashista, P	30	45		
Vaughn, L	300	304		
Vazirani, H N	150	169		
Veltri, R D	274	288		
Venderovitch, A M	286	290		
Vergano, P J	19	23	92	97
Vermeer, J	286	290		
Verrall, D J	26	45		
Videau, J J	14	23		
Virgo, P	105	111		
Vogel, H	109	112		
Vogel, W	50	53	55	70
	71	97	306	317
Volger, J	295	304		
Volmer, M	19	24		
Vostrov, G A	140	148		
Vuilland, G E	15	23		

Index Terms

Links

W

Wagner, C	66	72	136	148
Wagman, D D	204	213		
Wagstaff, F E	18	23	54	70
	71	92	97	
Wakasugi, T	208	213		
Wall, F T	203	213		
Walters, L C	124	135	147	148
Walther, J V	228	229	238	239
Walton, H F	244	260		
Wang T T	176	183		
Warburg, E	3	11	263	287
Ward, J B	169			
Warren, B E	3	11	28	30
	32	33	36	41
	45	46	47	58
	71			
Warrington, D	53	71		
Warshaw, J	52	90		
Wassick, T A	189	196	217	224
	237	238		
Weaver, E A	202	213		
Weber, M J	316	320		
Weber, M Y	29	45		
Weber, N	276	288		
Weigelt, J	34	46		
Weinberg, M C	144	149		
Weinberg, T J	313	319		
Weir, C E	310	318		

Index Terms**Links**

Weiss, A	14	23		
Wells, A F	39	47		
Weyl, W A	210	214	313	319
White, J To	105	112		
White, W B	35	46	232	239
Whitney, J	150	169	175	183
Wiecker, C	14	23		
Wiecker, W	14	23		
Wihsmann, F G	29	45		
Wikby, A	222	238	256	261
Wilcox, F L	256	261		
Wilder, J A	113	120		
Wilkinson, G	229	239		
Willams, Q	26	44		
Willard, J E	106	112		
Williams, E L	137	148	202	213
Williams, G A	122	147		
Williams, M L	109	110	112	
Williamson, D L	85	96		
Williamson, J	85	93	96	97
Wilmot, G	311	318		
Wilshaw, T R	159	170		
Wilson, H A	91	97		
Winchell, P	265	279	287	289
Winks, F	48	70		
Winter, A	14	22		
Winterberg, A L	232	239		
Wirth, G S	228	238		
Wolf, W W	9	11		
Wollast, B	229	239		

Index Terms**Links**

Wong, J	308	311	312	318
Wood, B J	228	238		
Woodland, A B	231	239		
Woods, K N	122	147		
Worster, E	310	318		
Wright, A C	25	28	32	37
	38	41	44	45
	46	47		
Wright, G B	116	120		
Wustner, H W	122	147		

X

Xu, X J	83	96		
---------	----	----	--	--

Y

Yamaga, M	313	319		
Yamane, M	53	71	94	97
	202	213		
Yannas, J	15	23		
Yasui, I	40	47	163	170
Yazawa, T	70	72		
Yinnon, H	17	24	82	96
Yokota, R	68	72		
Young, G J	185	196		
Young, L	15	23		
Youssefi, A	229	239		
Yurek, G J	8	11		

Index Terms**Links****Z**

Zachariasen, W H	3	11	20	24
	30	45		
Zagar, L	286	290		
Zallen, R	10	11	39	47
	314	319		
Zaman, M S	212	214		
Zarzycki, J	10	11	32	41
	46	47	53	67
	68	72	264	287
Zayonts, L A	229	238		
Zener, C	66	71	146	149
	302	304		
Zhang, H	47	208	214	
Zhang, Z	14	23		
Zhao, X S	119	121		
Zhuravlev, L T	185	196		
Zinn-Justin, J	60	71		
Zotos, B K	228	238		
Zupko, H M	176	183		

SUBJECT INDEX

<u>Index Terms</u>	<u>Links</u>	
A		
Acidic or basic oxides	205	
Acid dissolution in	229	
Adsorption, binary a.	192	
physical	190	
and potentials of glass electrodes	252	
Agglomeration, in phase separation	68	
Alkali silicates - compositions	6	
dense transition	296	
dissolution in water	227	
electrical conductivity	272	
ion exchange selectivity	246	
ionic diffusion in	270	
mechanical loss	400	
optical absorption	11	
phase separation	53	63
properties	6	
structure	43	
surface structure	185	227
viscosity	105	108
Aluminum oxide and alumina, size	201	250
chemical durability	228	
ion exchange selectivity	251	
optical absorption	407	

Index Terms

Links

Aluminum oxide and, anionic size (*Cont.*)

in vitreous silica 33

water solubility 199

Annealing 116

Annealing point 100

Anorthite 17 82

B

Bases, dissolution in 230

Bonding 27

in dissolution in water 228

glass strength 162

in oxidation 204

Books 10

Borate glasses, density 6

heat capacity 114

molecular diffusion in 139

optical absorption 310

phase separation 53 55

structure 35

viscosity 103

Boron oxide anomaly 37

Borosilicates, chemical durability 227

compositions 6

crack propagation 167

crystallization 79

diffusion in 140 282

dissolution in water 227

ion exchange selectivity 245

Index Terms

Links

Borosilicates, chemical durability (*Cont.*)

leaching	223	
mechanical loss	300	
molecular solubility	125	
phase separation	54	
properties	6	
static fatigue	173	177
strength	152	154
surface adsorption	193	
viscosity	100	
Boroxyl groups	36	
Bubbles, diffusion from	142	
in fining	209	
in strength studies	157	

C

Carbon dioxide, in fining	210	
reaction with, glass	208	
glass surface	231	
Chain structure	35	
Chalcogenide glasses		
optical absorption	314	
structure	38	
Chemical durability	215	
crack propagation	181	
testing methods	216	
Chemical reactions, on glass surface	192	
with water	135	
Clearing temperature	52	

Index Terms

Links

Coarsening of a phase	66	68	
Color and sulfates	203		
metallic particles	314		
transition metal ions	313		
Compositions, commercial	6		
Conductivity, electrical	236		
and diffusion	269		
in high fields	285		
measurement	265		
surface	194		
water and	265		
Computer simulation, of structure	29		
of surfaces	90		
Consolute temperature	51	53	
Coordination numbers	31	35	40
of transition metal ions	313		
Correlation in diffusion	210		
Cracks, and energy	165		
in fracture	165		
nucleation of	166		
origins of	167		
propagation of	167	181	
revealed with sodium vapor	158		
stress at	160		
velocity of	160	167	
Crystallite structure	31		
Crystallization	16	19	73
and heat flow	90		
nucleation of	75		
surface	77		

Index Terms

Links

Crystallization (*Cont.*)

theories of

91

velocity

18

90

92

Crystal morphology

88

Crystal structure

30

D

Definitions

1

Delayed failure, *see* Static fatigue

Density

6

Dielectric constant

292

Dielectric loss

291

effect of frequency

293

measurement

291

relation with electrical conductivity

296

theories

301

Diffusion, and chemical reaction

135

and electrical conductivity

269

of gases

122

130

inter ionic

232

279

in ion exchange

229

molecular

135

in phase growth

66

theories

145

284

Dissolution, in melts

8

in water

225

234

Distribution coefficients, in ion exchange

241

244

between two phases

246

DSC, and crystallization

82

Index Terms

Links

E

E Glass composition	6
Einstein Equation	269
Elastic modulus, and crack propagation	167
and molecular diffusion	145
and strength	162

F

Fast ion conductors	283		
Faulting	163		
Fictive temperature	118		
Fiberglass	9		
Fining	209		
Fire-polishing	156		
Flaws, surface, in fracture	165		
Fluoride glasses			
crystallization	94		
reaction with water	218	237	
surfaces	218		
structure	40		
viscosity	106		
Fracture	150		
and crack length	160		
flaw theories	160		
Fragile glasses	109	115	120
Free volume	109	126	
Fused salts, ion exchange with	245		

Index Terms

Links

G

Gases, reaction with glass	198	
solubility in glass	122	
Germanate glasses, infrared absorption	310	
mechanical loss	300	
molecular diffusion in	139	
structure	38	
viscosity	103	
Glass-ceramics	74	
Glass electrodes	252	
Gold particles, diffusion to	140	
optical absorption	314	
Growth rates of, crystals	19	92
phases	66	

H

Hackle	158	
Halogens, on glass surface	193	
Haven ratio	270	
Heat capacity	114	
History	2	
Hopping conduction	285	
Hydrated layer	222	231
Hydrogen, diffusion	135	
reaction with glass	136	201
Hydrogen ions	225	
in interionic diffusion	225	
and mechanical loss	200	

Index Terms

Links

Hydrogen ions (*Cont.*)

from sulfur dioxide 236

Hydronium ion 225

Hydrosilicates 200

Hydroxyl groups, acid ionization constants 193

in diffusion 135

on glass surface 187

from hydrogen 201

infrared, spectra 186

from water 198

I

Immiscibility, *see* Phase separation

Indentation 163

Infrared spectra 186 308 310

Internal friction, *see* Mechanical loss

Ion exchange 220 241

in dissolution 220

equilibrium 244

at glass surface 220

and mechanical loss 202

selectivity 249

with water 225

Ionic distribution and electric conductivity 284

in alkali silicate glasses 33

between melts and glass 244

in vitreous silica 33

Ionic salts 40

viscosity 108

Index Terms

Links

K

Kauzman paradox 115

L

Life prediction 178

Light scattering, and phase separation 52

M

Mechanical loss, alkali ion peak 299

 effect of, composition 300

 frequency and temperature 298

 and hydrogen ions 299

 intermediate peak 299

 measurement 297

 theories 301

Melting 5

Metallic glasses 44

Metallic particles, in nucleation of crystals 77

 optical absorption 314

Mixed-Alkali effect, in electrical conductivity 279

 in mechanical loss 299

Morphology, of crystals 88

 of separated phases 67

N

Narayanaswamy model 119

Nernst-Einstein equation, *see* Einstein equation

Nernst-Planck equations 232

Index Terms

Links

Nitrogen, reaction with glass	207		
Nuclear magnetic resonance	35	38	41
Nucleating agents, in crystallization	85		
impurity particles	77		
mechanisms	86		
metal particles	77		
oxides	86		
in phase separation	55		
Nucleation in glass formation	17		
in crystallization	75		
mechanisms	77		
by phase separation	86		
in phase separation	60		
measurements	64	78	
theory	57	75	
transient	62		

O

Optical spectra	186	307	
Organic liquids	20	44	
viscosity	108		
Organic polymers	42		
crystallization of	93		
Oxidation state, of glass	203		
in fining	211		
of ions	202		
Oxycarbide glass	41		

Index Terms

Links

Oxygen, diffusion	135	137
reaction with, glass	137	202
glass surface	193	

P

Permeation of gases in glass, effect of		
composition	139	
measurement	130	
Phase diagrams	50	
Phase rule	202	
Phase separation	48	
free energy	57	
nucleation of	60	
relation to valence	52	
theories	56	67
Phosphate glasses, electrical conduction in	265	
mechanical loss	301	
structure	37	
ultra-violet absorption	310	
viscosity	103	
Plastic deformation	163	
Polishing	194	
Potential of glass electrode, and ion		
exchange equilibrium	252	
and adsorption	260	
measurement	253	256
theories	254	
Processing	5	

Index Terms

Links

Pyrex glass, *see* Borosilicates
composition

6

R

Radioactive waste disposal	224	236
Random network	24	
Rare earth ions	315	
Reaction layers	231	235
Refractive index	6	306
Regular solution model	54	
and ion exchange selectivity	249	
Relaxation	116	
Rutherford backscattering	218	

S

Sealing	240
Selectivity, and anionic size	246
in ion exchange	247
sequences	248
theories	249
Selenium, structure of	39
Silica, vitreous	
bond angles in	32
chemical adsorption	192
compositions	7
crack propagation	167
crystallization	18
dielectric loss	295
diffusion in	276

Index Terms

Links

Silica, vitreous:

 bond angles in (*Cont.*)

dissolution in, melts	8	
water	227	
electrical conductivity	275	
gas solubility in	122	
ion exchange selectivity	245	
ionic diffusion in	274	276
manufacturers	7	
molecular diffusion in	132	134
optical adsorption	307	310
physical adsorption	190	
reaction with hydrogen	201	
solubility of water in	229	
static fatigue	175	177
strength	156	
structure	27	30
surface structure	185	
viscosity	103	
water in	135	

Silicon, oxidation of

144

Size, anionic, and exchange selectivity

250

 ionic and diffusion

282

 molecular and diffusion

132

146

Soda-Lime glass, composition

6

 crack propagation

167

 density

6

 dielectric loss

296

 electrical conductivity

278

 ion exchange selectivity

245

Index Terms

Links

Soda-Lime glass, composition (*Cont.*)

ionic diffusion in	274	
mechanical loss	299	
molecular diffusion in	141	
phase separation in	49	55
properties	6	
static fatigue	177	
strength	154	
viscosity	100	105

Softening point 100

Sol-gel forming 9

Solubility, carbon dioxide 208

of gas molecules 122

of glass in water 229

hydrogen 124

theories 126

water 135

Spherulites 88

Spinodal decomposition 67

Static fatigue 172

experimental results 174 177

statistics of 177

and surface treatment 176

theories 180

Stokes-Einstein equation 67 273

Strength 154

distribution of 151

testing of 150

theoretical 162

Index Terms

Links

Stress, accelerated reactions	182	
at crack tips	161	181
and ionic diffusion	271	
and molecular diffusion	132	
relaxation	116	
Stress-intensity factors	161	
Sulfur, structure of	39	
Sulfur dioxide, in fining	211	
reaction with glass	209	
Surface conductivity	194	
Surface energy	184	
and strength	165	
Surface experimental techniques	189	
Surface structure	185	

T

Thermal expansion	114	
Thirsty glass	44	190
Transition, glass	113	
and electrical conductivity	272	278
Transition metal ions, coordination numbers	313	
glass-forming tendency	14	
optical absorption	313	
oxidation state	204	
TIT curves	17	

U

Uses of glass	4	
---------------	---	--

Index Terms

Links

V

Viscosity	99			
definition	99			
measurement	101			
theories	109			
Vycor glass	44	48	190	

W

Water, diffusion	135			
effect on electrical conductivity	265			
reaction with glass	135	198	215	
solubility in glass	135			
surface	187			
Weathering	209	231		
Working point	100			

X

X-Ray diffraction	28	31	36	41
small-angle	68			

Z

Zachariasen's Rules for glass formation	21			
-----------------------------------------	----	--	--	--